NASA/CR—2014-218089

Pratt & Whitney/Boeing Engine Validation of Noise Reduction Concepts
Final Report for NASA Contract NAS3-97144, Phase 2

Larry A. Bock, Joseph E. Hauser, Douglas C. Mathews, David A. Topol
United Technologies Corporation, Pratt & Whitney, East Hartford, Connecticut

Gerald W. Bielak, Justin H. Lan, John W. Premo
Boeing Commercial Airplane Group, Seattle, Washington

February 2014

NASA STI Program . . . in Profile

Since its founding, NASA has been dedicated to the advancement of aeronautics and space science. The NASA Scientific and Technical Information (STI) program plays a key part in helping NASA maintain this important role.

The NASA STI Program operates under the auspices of the Agency Chief Information Officer. It collects, organizes, provides for archiving, and disseminates NASA's STI. The NASA STI program provides access to the NASA Aeronautics and Space Database and its public interface, the NASA Technical Reports Server, thus providing one of the largest collections of aeronautical and space science STI in the world. Results are published in both non-NASA channels and by NASA in the NASA STI Report Series, which includes the following report types:

- TECHNICAL PUBLICATION. Reports of completed research or a major significant phase of research that present the results of NASA programs and include extensive data or theoretical analysis. Includes compilations of significant scientific and technical data and information deemed to be of continuing reference value. NASA counterpart of peer-reviewed formal professional papers but has less stringent limitations on manuscript length and extent of graphic presentations.

- TECHNICAL MEMORANDUM. Scientific and technical findings that are preliminary or of specialized interest, e.g., quick release reports, working papers, and bibliographies that contain minimal annotation. Does not contain extensive analysis.

- CONTRACTOR REPORT. Scientific and technical findings by NASA-sponsored contractors and grantees.

- CONFERENCE PUBLICATION. Collected papers from scientific and technical conferences, symposia, seminars, or other meetings sponsored or cosponsored by NASA.

- SPECIAL PUBLICATION. Scientific, technical, or historical information from NASA programs, projects, and missions, often concerned with subjects having substantial public interest.

- TECHNICAL TRANSLATION. English-language translations of foreign scientific and technical material pertinent to NASA's mission.

Specialized services also include creating custom thesauri, building customized databases, organizing and publishing research results.

For more information about the NASA STI program, see the following:

- Access the NASA STI program home page at *http://www.sti.nasa.gov*

- E-mail your question to *help@sti.nasa.gov*

- Fax your question to the NASA STI Information Desk at 443–757–5803

- Phone the NASA STI Information Desk at 443–757–5802

- Write to:
  STI Information Desk
  NASA Center for AeroSpace Information
  7115 Standard Drive
  Hanover, MD 21076–1320

NASA/CR—2014-218089

Pratt & Whitney/Boeing Engine Validation of Noise Reduction Concepts
Final Report for NASA Contract NAS3-97144, Phase 2

Larry A. Bock, Joseph E. Hauser, Douglas C. Mathews, David A. Topol
United Technologies Corporation, Pratt & Whitney, East Hartford, Connecticut

Gerald W. Bielak, Justin H. Lan, John W. Premo
Boeing Commercial Airplane Group, Seattle, Washington

National Aeronautics and
Space Administration

Glenn Research Center
Cleveland, Ohio 44135

February 2014

Acknowledgments

Level of Review: This material has been technically reviewed by NASA technical management OR expert reviewer(s).

Available from

Forward

This report presents results of the work completed in Phase 2 of the Engine Validation of Noise Reduction Concepts (EVNRC) contract. The purpose of the program is to validate, through engine testing, advanced noise reduction concepts aimed at reducing engine noise up to 6 EPNdB and improving nacelle suppression by 50 percent relative to 1992 technology. Phase 1 of the program is completed and is summarized in NASA/CR—2014-218088.

Summary

The EVNRC program was authorized by NASA in August 1997 to validate, through engine testing, noise reduction concepts and technologies that have evolved during the AST program. A team comprised of members from NASA, Pratt & Whitney, Boeing and Goodrich Aerostructures (formerly Rohr) participated in bringing together the concepts, new hardware, software, test equipment and support personnel necessary to complete the program. The program was conducted in two phases on a PW4098 engine on C-11 outdoor test stand at P&W's Florida Test Facility. The test stand is configured and instrumented to FAA noise measurement and data quality standards.

This report covers Phase 2 of the program. Phase 1 was covered by a separate report (see Ref. 1). The major noise reduction concepts tested in Phase 2 were:

1. A 28 vane fan exit guide vane (FEGV) system for demonstrating the noise effects of cut on blade passing frequency (BPF) tone noise and lower broadband noise.
2. An increase in fan blades from 22 to 24 for reduced noise due to aerodynamic loading reductions.
3. The Boeing scarf inlet equipped with a bellmouth lip to reduce flow separation induced BPF noise observed in Phase 1 testing.
4. A primary jet nozzle fitted with acoustic treatment to attenuate turbine noise.

The major results of the testing were:

1. The treated primary jet nozzle showed large reductions in turbine noise, sometimes exceeding 10 dB. This resulted in total engine EPNL reductions of 0.75, 0.75 and 0.5 dB for approach, cutback and sideline flight conditions, respectively. The benefits were observed at almost all low pressure turbine rotor speeds. Testing with this treatment provided more confidence that fan noise changes could be quantified when examining noise data from two configurations having different fan or FEGV designs.
2. The 24 fan blade configuration showed a maximum reduction of 1 dB EPNL at the sideline condition, and about 0.5 dB at most other fan rotor speeds.
3. The 28 acoustically cut on FEGVs resulted in some fan noise components being reduced, relative to the production 60 vanes, despite the unfavorable spacing between the fan and this vane set. Overall though, the EPNL was increased with the 28 vanes, partly because of this decreased spacing.
4. The Boeing scarf inlet with a bellmouth lip showed the expected reduction in BPF noise at low engine powers. Testing at higher powers was precluded by delamination of the inlet acoustic panel.
5. The Boeing microphone array installed in the inflow control device (ICD) and the array mounted in a ring installed immediately forward of the engine's front fan case (Olsen Ring) were both able to measure acoustic differences between the fan blade and FEGV configurations tested. The measurements showed that observed BPF was a combination of modes and was not dominated by a single mode even when the rotor/stator interaction of the direct rotor field was cut on.

A separately funded program managed by the Northrop Grumman Co. in conjunction with Hersh Walker Acoustics (NG/HWCA) was run concurrently with the Phase 2 test. The objective of this program was to evaluate a hybrid, active passive inlet BPF tone reduction system. Hardware problems with amplifier equipment prevented the use of the active noise system during the test. However, the data from the Boeing ICD and Olsen Ring arrays showed very little $m = -6$ BPF tone for the 22 fan blade and 28 cut on FEGV configuration. These data suggest that the active noise control system would have little to control since it was designed to target the $m = -6$ BPF tone.

Contents

Pratt & Whitney/Boeing Engine Validation
of Noise Reduction Concepts
Final Report for NASA Contract NAS3-97144, Phase 2

Larry A. Bock, Joseph E. Hauser, Douglas C. Mathews, and David A. Topol
United Technologies Corporation
Pratt & Whitney
East Hartford, Connecticut 06108

Gerald W. Bielak, Justin H. Lan, and John W. Premo
Boeing Commercial Airplane Group
Seattle, Washington 98124

1.0   Introduction

1.1   Background

Major airports in the world's air transportation systems face a serious problem in providing greater capacity to meet the ever-increasing demands of air travel. This problem could be relieved if airports are allowed to increase their operating time, now restricted by curfews and by relaxing present limits on takeoffs and landings. The key operational issue in extending the present curfews is noise.

In response to these increasing restrictive noise regulations, NASA launched a program in 1997 to validate through engine testing, noise reduction concepts and technologies that have evolved from the Advanced Subsonic Technologies (AST) Noise Reduction Program. The goal of this AST program was to develop and validate technology that reduces engine noise and improves nacelle suppression effectiveness relative to 1992 technology. Contract NAS3-97144 titled "Engine Validation of Noise Reduction Concepts" (EVNRC) was awarded to P&W on August 12, 1997, to conduct full-scale noise reduction tests in two Phases on a PW4098 engine. The following Section 1.2 provides a brief description of the overall program. The remainder of this report provides a detailed documentation of Phase 2 of the program.

1.2   EVNRC Program Description

The EVNRC program is a highly teamed effort involving NASA, Pratt & Whitney (P&W), Boeing, and Goodrich (formerly Rohr). The program duration was from August 1997 to September 2001 and consisted of two phases. The two phases correspond to separate noise test programs in late 1998, and mid-2001 and were conducted with P&W's latest and largest turbofan engine, the PW4098. This engine, which powers growth versions of Boeing's 777 aircraft, has a 112.9-in. diameter fan and generates a rated thrust of 98,000 lb. The tests were planned to validate in full-scale a number of advanced noise reduction concepts identified during the Advanced Subsonic Technology Program.

The program encompassed a very wide range of noise reduction technology such as:

- Advanced noise reduction treatment in a new, novel Boeing inlet
- Advanced noise reduction treatment in P&W's engine cases
- Low noise, cuton FEGVs
- Primary jet nozzle with acoustic lining to attenuate turbine noise

The potential noise reduction from the technologies tested in this program was estimated to be in the 2 to 4 EPNdB range at each condition, relative to the baseline PW4098 engine.

This program offers high potential for technology transfer to commercial product lines. Reduced noise will be an internationally competitive issue, and this program is focused on technologies with a high probability of

cost effective transition into the marketplace for new applications, as well as for retrofit or incorporation into today's production engines. Specific and direct beneficiaries of the technology demonstrated in this proposed program will be the GP7000, the new engine being developed jointly by a P&W/ General Electric (GE) Engine Alliance for installation into future very large Airbus and Boeing aircraft. The program output will also be applicable to the entire PW4000 engine family, to P&W's new PW6000 mid-thrust engine, and to P&W's future family of engines, as well as other manufacturer product lines.

The program cost was reduced because of significant cost sharing by the team members. Boeing supplied the novel low noise inlet, valued at $1.5 million, for the program at no cost. Pratt & Whitney supplied the PW4098 engine and aft nacelle. Noise tests were conducted in conjunction with other planned P&W engine tests to reduce cost. Use of the P&W world-class outdoor C-11 test facilities in Florida, configured and instrumented to FAA noise measurement and data quality standards, also reduced costs.

Phase I of the program has been summarized previously in a NASA Contractor Report (Ref. 1). The purpose of this report is to document the content and results of Phase 2. The structure of the Phase 2 program is described below.

1.2.1 Phase 2

1.2.1.1 Subtask 1.2.1—Concept Selection and Acoustic Design

The noise concepts that were defined by P&W and Boeing in the contract proposal were updated, evaluated and finalized in this subtask. Other concepts that were not in the proposal were also evaluated and selected for testing based on evaluation results.

1.2.1.2 Subtask 1.2.2—Mechanical Design

This subtask provided for the development of working drawings suitable for the fabrication of the 28 vane FEGV and for the acoustic lining treatment of the primary jet exhaust nozzle.

1.2.1.3 Subtask 1.2.3—Fabrication

The fabrication subtask funded construction of the 28 vane FEGV and the acoustically treated primary jet exhaust nozzle.

1.2.1.4 Subtask 1.2.4—Boeing Subcontract

This subtask provided for Boeing's participation to provide overall engineering support and consultation for the Phase 2 program including concept selection, test configuration selection, scarf inlet hardware (at no charge to the program), instrumentation system installation and operation during testing, data analysis, test results and reporting.

1.2.1.5 Subtask 1.2.5—Testing

The testing subtask covered costs associated with full scale PW4098 engine testing at P&W's C-11 Stand Acoustic Test Facility at West Palm Beach, Florida. Test costs were reduced by combining (piggybacking) the NASA funded tests with P&W funded PW4098 FAA Noise Certification Tests.

1.2.1.6 Subtask 1.2.6—Data Analysis

This subtask provided for the analysis of data collected during testing.

1.2.1.7 Subtask 1.2.7—Documentation

Documentation tasks included preparation of test plans, design reviews with NASA, bi-monthly reports and final Contractor Reports.

The report that follows is comprised of contributions from Pratt & Whitney and Boeing authors. Section 2.0 presents the P&W report and Section 3.0, the Boeing report. Conclusions and recommendations from both companies have been listed under separate subheadings in Section 4.0. Figures are in Section 5.0,

followed by the appendices and the references. In these sections, information from both companies is cross-referenced to the appropriate text in the preceding sections.

Phase 2 testing was also run concurrently with a separately funded program managed by the Northrop Grumman Co. in conjunction with Hersh Walker Acoustics (NG/HWA). The objective of this program was to evaluate a hybrid, active passive inlet BPF tone reduction system. References to Northrop Grumman (NG) tests are made in various sections of this report because of the integrated nature of the tests. However results of the NG testing are reported separately in Northrop-Grumman, Vought Aircraft Industries report NSL-RPT-01-051, NASA Contract NAS3-99180. In the Boeing section of this report, certain specific results of the NG configuration tests are reported because of their importance in validating the performance of Boeing's phased microphone array system.

2.0   Pratt & Whitney Report

2.1   Noise Reduction Concepts and Hardware

The noise reduction concepts selected for evaluation in Phase 2 testing are shown in Table 1.

The locations of several of these concepts is shown in Figure 2, while photographs of the 28 vane assembly are shown in Figure 3 and Figure 4.

TABLE 1.—NOISE REDUCTION CONCEPTS FOR PHASE 2 TESTING

1.   P&W 28 vane fan exit guide vane (FEGV) system for acoustically "cut on" BPF tone and for lower broadband noise.
2.   P&W increased fan blade number (+2 blades) for effects of reduced loading on noise.
3.   Boeing scarf inlet with bellmouth lip to reduce flow separation noise at BPF observed in Phase 1 testing.
4.   P&W primary jet nozzle with acoustic lining to attenuate turbine noise.
5.   Northrop Grumman/ Hersh Walker Acoustics (NG/HWA) hybrid active passive inlet BPF tone reduction system. Testing of this concept was performed under separate contract to Northrop Grumman.

In addition to the concepts of Table 1 the following features tested in Phase 1 were included in Phase 2:

- Boeing's Ideal Inlet that incorporated the following:
  - An extended lower lip (scarfing) for noise shielding and noise redirection.
  - Advanced liner design and construction that features triple layer broadband acoustic lining with minimum splice widths.
  - Treatment that extends upstream beyond the inlet throat and hilite.
  - Circumferentially uniform liner close to the fan.
  - No probes and associated hardwalled patches.
- P&W's Engine Fan Case which featured the following:
  - A modified forward fan containment case that allowed testing of the current production liner, a hardwalled liner, and the new advanced linear double layer liner supplied by B.F. Goodrich, with only two circumferential segments separated by narrow hard wall splices.
  - A design to minimize both community and interior buzzsaw noises.

2.1.1   P&W 28 Vane (Cut On) FEGV

As part of EVNRC Phase 2 contract, FEGV noise design studies were undertaken to build two FEGV's for the EVNRC Phase 2 test program. They were to:

- Optimize the vane count to provide lowest noise from a radial FEGV where blade-passing frequency (BPF) is cut on (known in this report as a "cuton FEGV" or "cuton vane count").
- Design a cuton, swept/leaned FEGV that will reduce the fan noise compared to the Bill of Material PW4098.

2.1.1.1   FEGV Noise Design Studies

The swept/leaned FEGV design was not built or tested due to program constraints. However, it will be discussed in this document as a design option that was pursued.

The design method is similar to that used in Reference 5. Instead of using the V072 Rotor Wake/stator interaction code for design, more advanced tone and broadband noise models were used. These are the TFaNS Tone Fan Noise design/prediction System (Refs. 6 to 9) for fan tones, and the BFaNS Broadband Fan Noise design/prediction System (Refs. 10 to 12) for fan broadband, both of these codes having been developed previously under NASA funding. These design systems, when used together, are capable of calculating the inlet and aft fan sound power level spectra.

For the purpose of these studies, only fan noise at subsonic tip speeds (i.e., approach power) has been calculated. Since there are some questions about the rotor self noise predictions, only stator noise predictions were completed. This means that tone noise prediction is limited to rotor wake/stator interaction noise. Broadband noise prediction is limited to rotor tip turbulence/stator interaction noise, rotor hub turbulence/stator interaction noise, and rotor wake turbulence/stator interaction noise.

The relative goodness of each design candidate was based on its predicted total sound power level spectrum. In order to make the selection of a configuration easier; NOY weighting of the sound power level spectrum was performed. Then a "Perceived Noise Level (PNL)" was calculated using the NOY weighted sound power level spectrum. The production PW4098 engine predicted "PNL" was then subtracted from each configuration's "PNL" to obtain a "delta PNL" relative to the bill of material (60 vane) PW4098 engine. Thus, one "delta PNL" level was calculated for each configuration. This allows an evaluation of "delta PNL" versus vane number or "delta PNL" versus vane sweep/lean based on one line plots for each study.

Figure 5 shows the production bill of material PW4098 fan stage geometry. This fan stage has 22 fan blades and 60 non-structural FEGV's. The approach, cutback and sideline operating point tip speeds are also shown in this figure.

In order to design a cuton, radial or a swept/leaned FEGV for the PW4098, there are two geometric constraints as illustrated in Figure 6.

- The vane solidity (chord to pitch) must remain constant.
- The vane trailing edge (t.e.) root cannot be moved.

These constraints were unique to the PW4098 engine, where there already exists a separate row of structural struts downstream of the FEGVs. For this engine, the presence of these fixed struts prevented additional spacing between the cuton blades and vanes that is desirable for low noise. Therefore for a cuton FEGV assembly in the PW4098, as the vane number gets smaller, the constraints mentioned above cause the spacing to be decreased accordingly. However, in a new engine design the cuton vanes would be structural, so there would be no need for two separate rows of vanes. This would allow for larger spacings and lower noise than was possible for the PW4098 engine.

2.1.1.1.1   Vane Number Design Study

To select a vane count for a PW4098 FEGV design where BPF is cut on (cuton FEGV), certain information was considered:

- The optimum vane count predicted by TFaNS and BFaNS.
- Data from past NASA rig tests such as the ADP 22 in. rig tests (Refs. 13 and 14), Allison 22 in. rig test (Ref. 15) and the Source Diagnostic rig test (Ref. 16).
- As part of the PW4098 engine test program, a Northrop Grumman active noise control device was to be tested. For this test, a high enough BPF tone was needed for the active noise control concept to act properly on this tone.
- For the purposes of this vane study, only the vane chord and location were assumed to change.

The optimum vane count was calculated assuming the FEGV trailing edge (t.e.) is at a constant axial location. Delta PNL's were then computed including fan tone and broadband vane generated noise for a range of FEGV numbers that are plotted in Figure 7. Note from this figure that there is a wide range of vane numbers to choose from, ranging roughly from 24 to 36 vanes. A 28-vane count was selected because its noise was reasonably low and because this vane number is consistent with that of the Source Diagnostic rig test (Ref. 16).

Also, as part of this study the broadband delta PNL's were computed to determine the effect of keeping the vane l.e. at a constant axial location as opposed to keeping the vane t.e. at a constant axial location. Results are shown in Figure 8. As expected, the predictions illustrate a greater noise reduction when the vane l.e. axial location is kept constant.

Figure 9 shows the PW4098 engine cross-section with a sketch of the 28 "radial" vanes design. Note that the radial vanes are axially swept slightly 7.7° relative to the radial direction, partly to maximize the spacing in the O.D. region.

The swept/leaned vane study will be discussed in the next section and will further discuss why the radial vane trailing edge is swept slightly.

2.1.1.1.2   Vane Sweep/Lean Design Study

The vane sweep/lean design was not built or tested. However, the design results are shown in this section to document the design that was pursued.

To select the axial sweep and tangential lean for the PW4098 with 28 FEGV's, (where BPF is cut on), certain information was considered:

- The optimum sweep and lean predicted by TFaNS/BFaNS.
- Data from past NASA rig tests such as the Allison 22 in. rig test (Ref. 15) and the Source Diagnostic rig test (Ref. 16).
- As part of the PW4098 engine test program, a Northrop Grumman active noise control device was to be tested. For that test, a high enough BPF tone was needed for the active noise control to act properly on this tone.

Definitions of Sweep and lean are given in Figure 10. Note that positive sweep is in the axial direction downstream while positive lean is opposite the direction of rotor rotation. Both are angles defined in degrees.

To evaluate the impact of sweep and lean, previous Allison 22 in. rig test data (Ref. 15) and V072 Rotor wake/stator interaction predictions (Ref. 5) were used to determine how much sweep and lean are needed to reduce the FEGV generated noise. In addition, the best placement of the vane was attempted in order to keep the fan-to-FEGV spacing as far as possible. The PW4098 FEGV trailing edge at the hub was already moved as far back as it could be as shown in Figure 6. To maximize spacing in the O.D. tip region, It was determined that the FEGV trailing edge at the tip could be moved about 2.91 in. downstream. Thus both the radial and swept FEGV's are designed to have the tip t.e. 2.91 in. downstream of the hub t.e. (Figure 9).

Next, the lowest vane number that could be used on the PW4098 engine assuming a 30° sweep angle is determined mechanically. Figure 11 shows a PW4098 cross-section with a sketch of a 26-swept vane configuration. Note that it is not possible to extend the vane chord any further forward at the root. Thus, for the "worst case" scenario (30° axial sweep), 26 vanes is the lowest number that can be used in this engine given the geometric constraints of this design.

A matrix of the various swept and leaned FEGV designs considered is shown in Table 2.

Note that sweep ranges from 7.7° (as in the 28 "radial" vane design) to 30° (consistent with the Allison and Source Diagnostic 22 in. rigs). Lean is varied from +15° (i.e., leaned 15° in the direction opposite rotor rotation) to −15° (i.e., leaned 15° in the direction of rotor rotation). This gives enough sweep/lean variation to determine which sweep/lean could have been used in the engine test.

TABLE 2.—THE 28 VANE SWEEP AND LEAN STUDY CONFIGURATIONS

Lean	Sweep 7.7	24	26	28	30
+15					x
0	Base	x	x	x	x
-6					x
-12		x			
-13			x		
-14				x	
-15	Recommended				x

Direction of Rotor Rotation

Sweep/lean vane study results use the same method of analysis shown in the vane number study. Figure 12 shows sweep/lean study results relative to 60-vane bill of material PW4098 engine predictions. In this figure the 28 "radial" vane configuration includes a 7.7° axial sweep. This is slightly different from Figure 7 that shows only radial vane (0° sweep) based predictions.

Results show that the "radial" vane configuration is predicted to rise 1.39 dB relative to the bill of material PW4098 configuration. When 28° to 30° of vane axial sweep and 14° to 15° of vane tangential lean (in the direction of rotor rotation) is included in the cuton vane predictions, the swept/leaned FEGV's come within 0.31 dB of the 60 vane bill of material engine.

2.1.1.2 Concluding Remarks

A cuton vane number design study and a cuton vane sweep/lean design study have been shown. Both studies considered only FEGV source acoustic predictions at PW4098 approach power. Noise at cutback and sideline powers could not be reliably predicted and were not calculated. Since the struts downstream of the FEGV's put constraints on the design, all vane axial geometric changes (e.g., chord, sweep) place newly designed vane leading edges closer to the fan. This prevented the noise from being reduced by as much as it might be in a new engine design.

The vane number design study shows the ability to select from a fairly wide range of vane numbers. Since the Source Noise Diagnostic test uses 22 blades, and 28 vanes, 28 vanes was selected to use in the PW4098 EVNRC Phase 2 test.

The vane sweep/lean angle study used the 28-vane configuration as the baseline for its work. Predictions at approach power show that a cuton swept/leaned FEGV set appears feasible that is only 0.31 PNdB higher than the bill of material engine fan noise with 60 cutoff, well spaced, vanes.

2.1.1.3 Mechanical Design

The 28 vane FEGV concept was designed for test purposes and was not flight worthy hardware. Analytical studies were conducted to assure that the vanes and cases were structurally adequate to withstand the aero loads and vibrational stresses predicted for the planned test runs. The material selected for the inner and outer cases was AMS 4312, aluminum alloy, and for the vanes, AMS 4029, aluminum alloy. Figure 3 shows the 28 vane assembly and Figure 4 shows the vane assembly with the outer case. More detail on the test hardware is presented in Section 3.0 and as shown in Figure 15 to Figure 20.

2.1.2 P&W Increased Fan Blade Number

The testing of a 24 fan blade configuration was feasible because of the availability of a 24 slot fan hub from earlier PW4098 development testing. Some modifications to the blade spacers and dampers were necessary to adapt the blades to the 24 slot fan hub. No modifications were made to the blades.

2.1.3   P&W Treated Primary Jet Nozzle

The design features of the noise treatment for the primary jet nozzle outer sleeve (tailpipe) and the and inner plug (tail-cone) are schematically shown in Figure 13 and by photo in Figure 14. The treated parts were fabricated and installed in an existing tailpipe and tail-cone that was available from P&W's test facilities instead of having to order new parts. Astech Mfg. Inc., of Santa Ana, California, completed the detail design and manufacturing of the treated primary jet nozzle.

2.2   Test Program

2.2.1   Test Site Characteristics

The test site has negligible influence on the engine's noise generating processes and, except for known ground surface effects, negligible influence on the propagation of sound from the engine to the microphone. See Figure 21.

2.2.1.1   Overall Site

The C-11 test site is located in an open area having relatively flat terrain that is free of structures and other obstacles that affect farfield sound pressure measurements.

One-third octave band sound pressure levels of ambient noise are sufficiently low so that engine noise measurements are not contaminated by noise from environmental or man made sources.

2.2.1.2   Engine Support Structure and Test Engine Configurations and Objectives

The engine support structure is designed for minimal sound interference characteristics. That is, the structure does not impede sound propagation nor does it have any acoustically reflective surfaces close to noise radiating regions. The engine centerline height above the acoustical arena surface is 15 ft (4.57 m), or no less than one and one half times the fan diameter.

The test engine was a PW4098, X841, build 13. This is a modern high bypass turbofan engine with wide chord shroudless fan blades. The 113 in. diameter bill of material fan stage has 22 rotor blades and 60 FEGV. There are 10 Intermediate Case struts behind the FEGV row including the lower duct bifurcation. The engine as configured for Phase 2 testing is shown on the test stand with a production bill of material inlet, a mini-bellmouth lip at the highlight and the ICD installed (see Figure 22).

Variations from production equivalent hardware for the PW4098 propulsion system during the test included:

- The production inlet had a mini-bellmouth attached to the highlight as shown in Figure 22.
- A modified fan containment case was used throughout the test series to accommodate the installation of two different front fan containment case (FFCC) spool pieces.
- The Active Noise Control (ANC) portion of the test had a special FFCC spool piece to accommodate the ANC system and provide some passive acoustic treatment right in front of the fan. A complete description of this is provided in the contractor's report from Northrop-Grumman, Vought Aircraft Industries, NSL-RPT-01-051, NASA Contract NAS3-99180.

The engine was installed on the test stand with a modified set of 28 closely spaced FEGV.

During the test series the 22 blade rotor and hub assembly was removed and a 24 rotor blade and hub assembly was installed.

The FFCC spool piece used for all non-ANC testing was a modified spool piece and contained the Goodrich supplied R2 acoustic treatment that was used in Phase 1 testing, or it was rendered hardwall with tape.

The primary jet nozzle and centerbody tail-cone were modified with acoustic treatment designed to attenuate low pressure turbine (LPT) noise for all but the last test configuration.

See Table 3 and Figure 1 for a description of every configuration.
Static noise tests in July, August, and September 2001 included:

- A series of tests with an innovative Active Fan Noise Control System provided under separate contract by Northrop-Grumman in partnership with Hersh Walker Acoustics. The system was designed to specifically modify the sound field to reduce blade passage frequency of the 22 blade fan rotor wake—stator interaction with a closely spaced, acoustically cut on radial set of 28 FEGV.
- A back to back comparison of 22 blade fan versus a 24 blade fan with the closely spaced, acoustically cut on radial set of 28 FEGV to investigate the effect of decreased loading on the fan blades
- A modified advanced and innovative scarfed inlet (keel longer than the crown as was used in Phase 1 testing) that had a larger radius highlight than the Phase 1 version of this inlet. The purpose of the more round lip was to see if the vortex generated at the crown in Phase 1 testing could be reduced or eliminated. The 24 blade and 28 FEGV fan stage was used. Two inlet configurations were planned, a hardwall and a treated. A face sheet panel delaminated during the hardwall test and the remainder of testing with this configuration was cancelled. (No configuration 5).
- A back to back comparison of the 24 blade fan with a closely spaced, acoustically cut on radial set of 28 FEGV with an acoustically cut-off set of 60 FEGV with greater axial spacing between fan and FEGV.
- A back to back comparison of an acoustically treated primary jet exhaust centerbody and nozzle sleeve and the production hardwall exhaust nozzle. This test comparison was run with the 24 blade and 60 FEGV fan stage.

2.2.1.3 Acoustical Arena

The acoustical arena is the surface area that extends from beneath the engine to a distance that is at least 25 ft (7.6 m) beyond all microphones.

The area has the following characteristics: Flat with no undulations that cause focusing or scattering of sound or collection of standing water. A slight slope or curvature subtending about 0.25° (4 cm/10 m) has been built in to aid in drainage. A thermally reflective surface of light concrete is used to minimize solar heating and thermal gradients near the ground. The surface is uniformly smooth and hard so as to approximate the acoustical impedance of a perfect sound reflector over the frequency range of interest.

2.2.1.4 Acoustic Barriers

Acoustic barriers were set up for Configurations 3, 4, 5 and 6 to block aft radiated noise from contaminating the inlet radiated noise measured by the farfield microphones. The walls were about 30 ft (9 m) in height and for this test are arranged as shown in Figure 24.

2.2.2 Engine and Noise Measurement

2.2.2.1 Data Acquisition and Reduction System

2.2.2.1.1 Acoustical Data Acquisition and Real Time Analysis System

The acoustic data acquisition system consists of microphones, signal conditioning, transmission components (e.g., preamplifiers, power supplies, and cables), real time data analyzers, and data storage equipment. The objective of this system is to acquire accurate measurements of engine sound pressure levels over the range of one-third octave bands having nominal center frequencies from 50 to 10,000 Hz. Deviations from a uniform frequency response are determined from instrument manufacturer's data, calibrations, or combinations of both.

During data acquisition, one-third octave analysis, narrow-band analysis, and storage of raw signals from up to 48 microphone systems can be performed. Measurements of engine speeds, temperatures,

relative humidity, and wind conditions are recorded at a rate of at least two times per second (2 Hz) during the analysis period. After a test point has been completed the reduced data are stored on the Dell GXA computer hard disk. The reduced data are immediately transmitted via link to the East Hartford Engineering Division acoustic database.

The subcontractor Boeing arranged a special array of 199 dynamic pressure transducers on the ICD. The ICD is a large spherical shaped inflow conditioner mounted in front of the engine during acoustic testing. The ICD is shown in Figure 22. The array was connected to a special data acquisition and analysis system for phased array analysis, mode and source identification. During the test of Configuration 4, the Boeing Ideal Scarf Inlet, a special array of 52 kulites in a ring at "A" flange between the inlet and the engine front fan containment case. The data were recorded and processed by Boeing in their role as a subcontractor. Results are reported in the Boeing sub-contractor's report.

The farfield microphone and related components had the following characteristics: Microphones are located on a 150 ft (45.7 m) radius array. The microphones are ½ in. (1.27 cm) B&K 4192, (pressure type), condenser cartridges and the diaphragm is installed ¼ in. (7 mm) above the acoustic arena ground plane, with symmetrical protective angular grids on. A diagram of the farfield microphone array is shown in Figure 24. The microphone angles measured from forward CL and centered on MARP for this test were: 32 angles 5° to 160° at 5°. The aft acoustic barriers blocked aft radiated noise with the exception of some jet noise "leaking" over the walls and at high power, jet noise radiating around the last barrier and impacting the noise on the last 5 or 6 angles.

The frequency response and stability characteristics were within those specified by the SAE Aerospace Recommended Practice, ARP-1846, February 1990. No windscreens were installed. B&K preamplifiers Type 2669 or equivalent were used. Cables were routed from the microphone location over the surface to central points close by where they were attached to underground cables extending into the control room where they attach to the B&K / Nexus 2690AOS4, Power Supply and Signal Conditioners.

Two dynamic pressure transducers were installed in the diffuser case to measure acoustic signals from the combustor. One was installed in a borescope boss and the other was installed in an igniter boss. A photo of the two installations is shown in Figure 25, Combustion dynamic pressure transducer installation. The data were also recorded on digital tape and provided to NASA GRC for analysis.

2.2.2.1.2   Meteorological Measurement System

The meteorological measurement system consisted of instruments to measure wind speed, wind direction, ambient air temperature, relative humidity and atmospheric pressure. The objective was to monitor meteorological conditions to ensure that static noise tests were conducted within acceptable meteorological limits and to provide information needed for acoustical data normalization to reference meteorological conditions.

Meteorological sensors for wind (speed and direction), air temperature and relative humidity were located in the vicinity of the microphone array over the same surface that extends from the engine to the farfield microphones. Wind speed and direction were measured at approximately engine centerline height, 15 ft (4.6 m). An additional wind speed sensor was placed at 2.5 in. (6 cm) above ground, to measure ground wind speed to provide guidance on wind shear effects on noise radiation. Ambient air temperature was measured at approximate engine centerline height, 15 ft (4.6 m) and about ½ in. (1.27 cm) above the ground surface.

Relative humidity is calculated from measurements of dry bulb air temperature and temperature of the dew point taken at approximately engine centerline height. Ambient atmospheric pressure is measured in the vicinity of the acoustical arena.

2.2.2.1.3   Engine Performance Measurements

Instruments are provided to define the prime engine power setting parameter (e.g., fan rotor speed). The objectives are to ensure that the engine is set at the desired operating condition and is stable when sound pressure signals are recorded. The instruments have the capability of determining the value of the

power setting parameter within an accuracy consistent with a rotor speed measurement accuracy of ±1 percent. A once per rev rotor speed signal was provided for the mode measurement analysis and the blade mounted transducers.

2.2.2.2 Acoustical Calibrations

2.2.2.2.1 Calibrations—General

All components of the test instrumentation were calibrated and certified to comply with the manufacturer's specifications and FAR 36 practices.

2.2.2.2.2 Calibrations—Frequency Response

Calibrations were performed to determine deviations of the entire farfield recording and reproducing and real time data system from a uniform frequency response. The non-uniformity's were determined in terms of time averaged one-third octave band sound pressure levels measured at each preferred one-third octave band center frequency reference signal (250 Hz).

The one-third octave band and narrowband corrections required to adjust the recording and reproducing and real time data systems to a uniform frequency response were applied to the measured data for microphone frequency response, cable losses, analyzer center frequency response and filter shape response.

2.2.2.2.3 Calibrations—Amplitude

Before and after each test period the overall electro-acoustical response of the microphone system was determined by use of a signal from a calibrated acoustical calibrator (pistonphone) generating a known sound pressure level, 124.0 dB at 250 Hz. The level was corrected by the difference in output level of the pistonphone between the calibrated level at standard day barometric pressure and the output level at the barometric pressure when the pistonphone was applied to the microphones.

2.2.2.3 Test Procedures, Engine and Noise Data Acquisition

2.2.2.3.1 General Test and Meteorological Conditions

The acoustic surface was free of extraneous clutter, standing water, or other objects that could alter the nominal acoustical characteristics of the surface. Testing was conducted within certain atmospheric condition limits. Examples of limits for temperature, relative humidity and wind conditions that were used are:

Wind speed:	± 8 kn average	At engine C_L height
	± 10 kn maximum	At engine C_L height
Cross wind:	± 6.5 kn average	At engine C_L height
Surface wind:	± 7 kn maximum	At 2 in. above ground plane
Temperature:	36 to 95 °F (2.2 to 35 °C)	
Temperature gradient:	(Surface temperature -Centerline temperature) ± 7.0 °F (3.9 °C)	
Relative humidity:	20 to 95 percent	
Precipitation:	None permitted	

2.2.2.3.2 Typical Acoustic Test Data Acquisition Procedures

A single frequency acoustic calibration of the microphone systems was performed with Bruel & Kjaer Model 4220 or 4228 pistonphone. The pistonphone output had a current laboratory calibration certificate traceable to the NIST. Immediately before each data recording session, the pistonphone calibrator was applied to each microphone system. The calibrated output level was normalized to a constant output voltage level at the input to the 1/3 octave and narrow band analyzers and the tape recorders and recorded on the pistonphone calibration record. Immediately after each recording session, the pistonphone calibration procedure was repeated (without normalization adjustments) and the system's performance

was accepted if during the acquisition period the sensitivity variation of each microphone system did not exceed ± 0.5 dB.

The electronic equivalent sound pressure reference level sine wave at 250 Hz was applied to all channels of the real time analyzer system and time averaged for a minimum of 30 sec to establish a sound pressure level reference for the analyzers. This was done at the start and end of every data recording session. The reference level in volts with respect to the pistonphone calibration level in dB was noted on the recorder log sheet.

An ICD, designed to minimize inflow distortion and turbulence into the fan was used. It is intended to simulate the clean inflow conditions seen by the engine in flight. It consisted of a support structure that includes the frame, transport wheels, perforated plate and honeycomb panels. The ICD was positioned such that the engine inlet protruded into the ICD. Both the Boeing Production inlet and the Boeing Ideal Scarf inlet were set to similar penetrations into the ICD. A non-porous sailcloth seal was attached to the ICD and the engine to eliminate flow leakage through the annulus between the inlet and the ICD opening. The ICD was inspected for damage and screen blockage prior to testing.

Just prior to engine start up for each data recording session, an ambient noise data record was acquired. The data were acquired on the real time and the tape recording system. The real time data were reviewed immediately prior to engine start up to ensure acceptable ambient noise conditions.

A test matrix of engine speed or power settings was defined prior to conduct of test. The test conditions included rotor speeds typical of the acoustic conditions of sideline, cutback and approach. Configuration descriptions are provided in Table 3, and pictorial representations are shown in Figure 1. A complete list of individual data points by Configuration and Run Number is provided in Appendix A. Selected points were repeated once or twice to establish repeatability or confidence limits based on data scatter. Prior to the first data acquisition of each data recording session, the engine was temperature stabilized for 5 min. For each test condition, before initiating data acquisition, the engine was stabilized such that the engine fan corrected rotational speed did not vary more than ±15 rpm or ±1 percent of the lowest engine speed recorded.

TABLE 3.—ACOUSTIC CONFIGURATION SUMMARY

Test activity	ACOUSDB/ NB	Config. no.	Inlet	Whose	FFC spoolpiece	Active	Fan	FEGV	Primary	Aft	Comments
Contractor	Run no.				Passive		Blade no.	Vane no.	Tailpipe	Walls	
No-Grum	16114GR	1	Prod	NG	HW	HW	22	28	Trt	No	Hardwall baseline
No-Grum	16115GR	2	Prod	NG	Trt	HW	22	28	Trt	No	Insertion loss of passive
No-Grum	16116GR	3	Prod	NG	Trt	m = -6	22	28	Trt	No	On/off ANC with passive
No-Grum	NO DATA	4	Prod	NG	Trt	m = 22	22	28	Trt	No	Same as 3, but m = 22 mode
EVNRC, Ph2	16117GR	1	Prod	BFG	HW	N/A	22	28	Trt	No	FFC spoolpiece change
EVNRC, Ph2	16118GR	2	Prod	BFG	HW	N/A	24	28	Trt	No	Fan hub/blade # change
EVNRC, Ph2	16119GR	3	Prod	BFG	HW	N/A	24	28	Trt	Yes	Walls up
EVNRC, Ph2	16120GR	4	HW Scarf	BFG	HW	N/A	24	60	Trt	Yes	Inlet and FEGV change
EVNRC, Ph2	NO DATA	5	Trt Scarf	BFG	HW	N/A	24	60	Trt	Yes	Untape scarf inlet
EVNRC, Ph2	16121GR	6	Prod	BFG	HW	N/A	24	60	Trt	Yes	Inlet change
EVNRC, Ph2	16122GR	7	Prod	BFG	HW	N/A	24	60	Trt	No	Walls down
EVNRC, Ph2	16123GR	8	Prod	BFG	HW	N/A	24	60	HW	No	Tailpipe change

Real time acoustic data were acquired using an averaging time of 20 sec during which one-third octave data is acquired. Then narrowband data were processed in a second 20 sec data acquisition period. A unique record number identified each data record. (See Appendix A.) All backup acoustic data records on magnetic tape were 60 sec in length.

The low-pressure shaft rotational speed was sampled at a sufficiently high rate such that a continuous representation of this parameter was displayed. The once per rev signal used during Phase 2 testing was fed to the Boeing data analysis system for the ICD mounted data system. Temperature, relative humidity, wind

speed and direction were measured during the period of time when sound pressure signals were being measured, recorded and displayed on-line. The speed signal was also recorded on digital tape with the acoustic signals. The rotational speed during data acquisition was averaged and displayed after the data point acquisition. The data information header also displayed and recorded the maximum and minimum deviations of engine speed from the average speed during the data acquisition and analysis time.

A data point information summary and recorder log was maintained for each data acquisition period. The log contains pertinent information about the test; especially the engine model, engine number, test date, configuration definition, low rotor speed, meteorological conditions, time and date. The same information was also part of each data record as stored on the P&W Acoustic Data Base and was included when the data is transmitted to the customer. A chronological record of the record number, engine low rotor speed, time of data point, outside temperature, relative humidity, and a channel by channel record of the amplifier gain or attenuator settings were also maintained.

At the conclusion of the acoustic data acquisition for each engine condition, the data point was accepted based on meeting all the following criteria: 1) Data acquisition successfully completed and all required acoustical signals appeared good. 2) All weather parameters remained within prescribed limits throughout the acquisition time period. 3) The engine performance was within the prescribed target condition limits. 4) There was no suspected contamination of the signals from aircraft flyovers or other test stands.

2.2.2.4 Test Data Processing Procedures for Farfield Real Time Data

2.2.2.4.1 Data Corrections

Appropriate corrections to the time averaged one-third octave band and narrowband sound pressure levels were applied to account for:

- Microphone pressure response
- Pressure-to-free-field response for 90° incidence, microphone protective grids on
- Pistonphone reference amplitude response
- Microphone system electrical frequency response (not narrowband data)
- Real time data reduction system center frequency response

2.2.2.4.2 Adjustment to Reference Day Atmospheric Conditions

Differences between test and reference day atmospheric absorption coefficients obtained from ARP 866A were applied to each appropriate one-third octave band sound pressure level over the measurement distance.

The reference day conditions are 77 °F (25 °C) and 70 percent relative humidity.

2.3 Test Results—Farfield Data

2.3.1 Configuration Descriptions

Eight EVNRC configuration tests were planned after completion of the four N-G runs as shown in Table 3. Configurations 4 and 5 were planned to evaluate the acoustic benefit of Boeing's treated scarf inlet but configuration 5 was not completed because of delamination of the scarf inlet (see Section 3.5.3.2, Inlet Delamination). Data was collected on Configuration 4 but without the results of Configuration 5 an evaluation of the treated scarf benefits was not possible.

Consequently, results from only six of the eight EVNRC configurations shown in Table 3 were studied. These were configurations number 1 to 3, and 6 to 8. From these six configurations, several objectives were accomplished. First, the noise impact due to several engine hardware changes on both the total, and engine component levels were quantified. These changes consisted of 1) number of fan blades, 2) "cuton" versus "cutoff" FEGVs, and 3) the benefit of primary tailpipe acoustic treatment on the low-

pressure-turbine noise component. A schematic view of the test vehicle used and a summary of the hardware changes can be seen in Figure 2. The acoustical analysis of the data was conducted for both Static, and in-flight projected noise metrics for three FAR 36 noise certification conditions, approach, Cutback, and sideline.

As can be seen from Table 3, configurations number 3 and 6 were tested with aft walls installed on the test stand (Figure 23), in order to block aft radiated noise from contaminating the inlet radiated noise measured by the farfield microphones. In order to conduct a complete and accurate noise analysis, it was imperative that the total noise data be separated into individual component noise sources accurately, and that the inlet and aft radiated noise components were properly defined. The configurations were tested with aft walls, number 3 and 6 were compared to the same engine configuration without aft walls, number 2 and 7, respectively, in order to confirm the validity of Pratt & Whitney's source separation process for inlet and aft radiated noise. Appendix D is dedicated entirely to a comparison of configurations without aft walls to the same engine configuration with aft walls in order to evaluate the source separation process. The results of Appendix D demonstrate that the source separation process does an excellent job in properly defining inlet and aft radiated fan noise from total engine data.

Component noise sensitivity studies were conducted in order to evaluate the importance of each engine component noise source, and it's impact on the total aircraft in-flight projected EPNL. Appendix E has been dedicated to noise component sensitivity studies, and the results of these studies.

The original intent was to test an additional configuration, which was to be representative of the current production engine. The EVNRC configurations studied would have been compared to the baseline engine, so that each hardware change could be assessed relative to the current production engine. The current production engine has 22 fan blades, 60 radial FEGVs, and a hardwall tailpipe. Figure 5 is a schematic view of the production fan geometry that shows the location of the front, and rear fan containment case acoustic treatment.

Since a baseline configuration was not tested, the noise study was conducted by comparing two configurations at a time that differed only by either fan blade quantity, FEGV quantity, or Acoustic treatment in the tailpipe.

2.3.2   Hardware Comparisons

Before a discussion of the hardware changes, the impact on forward fan containment case (FFCC) and rear fan containment case (RFCC) acoustic treatment will be mentioned, since it applies to all of the configurations studied. Figure 15 is a photo showing the inlet acoustic treatment, and it also shows the FFCC acoustic treatment which was made acoustically inactive by the application of clear tape for all configurations. Figure 16 is a photo of the RFCC acoustic treatment and a leading edge view of the 60 FEGVs. The photo also shows that approximately a 2-in. axial section of liner had to be removed prior to the installation of the 28 FEGVs. This section of acoustic treatment was removed around the entire circumference of the rear fan case, and replaced with solid aluminum panels in order to allow assembly of the two cases when the 28 Vanes were installed. This was required since the chord of the 28 Vanes were about 100 percent larger than for the 60 Vane configuration, and thus the leading edge of the 28 Vanes extended approximately 5 to 6 in. across the engine flanges between the fan containment, and rear fan cases. Figure 17 is a photo showing 22 fan blades and 28 FEGVs with the hardwall aluminum panels installed. From this figure, it can be seen that the leading edge of the 28 Vanes overlap the RFCC acoustic treatment panels by approximately 1.5 in. The acoustic treatment section of Figure 16 was replaced when the 60 FEGVs were re-installed. Therefore, the liner section shown on Figure 15 was hardwalled for the 28 FEGV configuration, and treated for the 60 FEGV configuration.

2.3.2.1   22 Fan Blades Versus 24 Fan Blades

From a comparison of configurations number 1 and 2, it can be seen from Table 3 that the fan blade numbers are the only difference. Both configurations were tested with a "cuton" number (i.e., 28) of FEGVs, and a treated tailpipe. A schematic view of the fan geometry for both configurations is shown in

Figure 18. The objective of this data comparison was to quantify the noise reduction due to reduced airfoil loading of the fan blades. Although several key engine performance parameters were measured during the noise tests the performance data for the 24-fan blade configuration was questionable. However, performance data was available from Pratt and Whitney altitude chamber tests that were conducted in 1997 for both fan blades. This data, not supplied in this report, demonstrated that the fan performance for both configurations was essentially equal in efficiency, and flow capacity, at the same corrected low-rotor speeds. The 24 blade configuration did demonstrate a small 0.3 percent higher flow capacity at around 2800 rpm, relative to 22 blades.

A noise benefit for the 24-blade configuration was anticipated, since the loading on the fan blades for the 24-blade configuration is lower than the loading on the 22 bladed fan. Since the fan loading is reduced, the wakes and turbulence from the fan blade trailing edge and also at the leading edge of the FEGVs are reduced relative to the 22-bladed fan, at the same corrected low rotor speeds.

2.3.2.2   "Cuton" Versus "Cutoff" FEGVs

From a comparison of configurations numbers 2 and 7, in Table 3, it can be seen that the only difference is the number of FEGVs. Both configurations were tested with 24 fan blades, and a treated tailpipe. This comparison was conducted to evaluate the noise impact of "cuton" versus "cutoff" FEGVs.

As mentioned in Section 2.2.1.1,there were two design constraints imposed on the "cuton" 28 vane configuration due to the current production fan geometry. Figure 19 is a schematic view of the baseline fan geometry, which shows 22 fan blades and 60 radial FEGVs. From this figure, it can be seen that there are bleed ports at the inside diameter wall of the fan duct close to the trailing edge of the FEGVs. As a result, the axial location of the trailing edge root of the FEGV was constrained for both the "cuton" and "cutoff" configurations. The second constraint was that the FEGV mid-span solidity values had to be approximately equal between both configurations in order to properly turn the flow and to keep the fan/duct performance the same.

Figure 20 is a schematic view of both the "cutoff" and "cuton" configurations. As can be seen from this figure, the mid-span spacing between the fan and FEGV is reduced for the "cuton" configuration due to the constraints mentioned above. In order to maximize the mid-span spacing between the fan and FEGVs as much as possible, the "cuton" FEGVs were slightly swept approximately 7.7°.

2.3.2.3   Treated Versus Hardwall Tailpipe

From a comparison of configuration 7 and 8 in Table 3, it can be seen that the difference is the primary tailpipe configuration. Configuration 7 had acoustic treatment in the tailpipe, which is tuned to attenuate the low-pressure turbine noise component. Both of these configurations were tested with 24 fan blades and 60 FEGVs. Figure 13 describes the tailpipe treatment and Figure 14 is a photo of the acoustic treatment on both the tail-plug, and tailpipe sleeve.

2.3.3   Farfield Test Data Analysis

In order to conduct a complete and accurate noise analysis, it is imperative that the total noise data be separated into individual component noise sources. There are two reasons to "source separate" noise data. One reason is that in order to evaluate impacts of hardware changes, each component must be accurately identified, so that the change in the component noise level can be evaluated. The second reason source separation is required, is that in order to generate the noise certification unit Effective Perceived Noise Level (EPNL), the sea level static data must be projected to a flight condition, and the proper flight effects must be applied to the appropriate components.

The static data was separated into narrowband and broadband components using an automated in-house Pratt & Whitney series of codes (referred to as V673 and U660). These noise components were then "projected" to flight, using an in-house code referred to as U421. The source separation procedure involved first defining, removing, and storing all of the tones from the total narrowband spectra at each angle and engine operating condition. Tones may include fan tones, as well as tones from the low-

pressure compressor and turbine. The remaining broadband portion of the narrowband spectra are then converted to a 1/3rd octave band spectra, using numerical filters that simulate an actual measurement. Conversions done in this manner have been demonstrated to agree extremely well with measured 1/3rd octave band data. Figure 26 shows a typical narrowband spectrum where the tones have been defined. After these tones were defined, removed and stored in their various component data base storage locations, the remainder of the converted 1/3rd octave broadband spectra were then separated into components (e.g., jet noise, combustor noise, fan inlet/aft noise, etc.). Figure 27 shows an example of components separated from a 1/3rd octave broadband spectrum. The flight noise projection procedure was executed at "single point" conditions of approach, cutback, and sideline for two identical engines of a given type, on the Boeing 777 aircraft at its certification altitudes, flight speeds, trajectories, etc. The procedure for these flight noise projections incorporates the latest methodologies to account for atmospheric attenuation, spherical spreading, retarded times, Doppler shifting, grass impedance, etc, and has shown good agreement with similar FAA and JAA approved flight projection methods employed by Boeing and Airbus. A tone correction to the PNL values was also applied per FAA standards, to obtain PNLT and EPNL's.

The resultant in-flight noise information (e.g., component spectra, PNLTs, EPNLs, etc) were generated for each component. These components are defined below and in several cases are combinations of several other components resulting from Pratt & Whitney's automated separation routine. Specifically, the component breakdown is listed below:

INLET NOISE = INLET FAN TONES + INLET FAN BROADBAND + EXTRANEOUS
              BROADBAND + EXTRANEOUS TONES (INCLUDES BUZZ SAW) +LPC
              TONES + SUM TONES
FAN INLET NOISE = INLET FAN TONES + INLET FAN BROADBAND
FAN AFT NOISE = AFT FAN TONES + AFT FAN BROADBAND
JET NOISE = JET
COMBUSTOR NOISE = COMBUSTOR
TURBINE NOISE = TURBINE (tones) + HAYSTACKS

Generally, from this point forward, "component" will refer to the label to the left of the above equals signs. The "sensitivity study" of Appendix E covers tones and broadband as individual components, but it includes sums as well, such as:

TOTAL ENGINE = INLET NOISE + AFT FAN NOISE + JET NOISE + COMBUSTOR NOISE
               + TURBINE NOISE
TOTAL AIRCRAFT = TOTAL ENGINE + AIRFRAME

2.3.4   Test Results

Configuration number 1, 2, 7, and 8 of Table 3 allowed for an independent acoustical evaluation of three separate hardware changes. These are a change in the number of fan blades, "cuton" versus "cutoff" FEGVs, and also the benefit of the primary tailpipe acoustic treatment, tuned for the reduction of low pressure turbine noise.

The results of the hardware changes are presented in this section for static noise metrics, and for the in-flight projected certification unit EPNdB. For a brief discussion of the methodology used to source separate total engine noise data into its respective engine noise components and the procedures used to calculate the noise certification unit EPNdB, refer to the preceding Section 2.3.3.

To minimize the quantity of plots generated, both the static and in-flight projected noise metrics were conducted at three low-rotor speeds typical of approach, cutback, and sideline power conditions for this propulsion system. The comparisons were conducted for both the total engine noise and also the engine component noise sources that changed, as a result of the hardware difference.

2.3.4.1   22 Fan Blades Versus 24 Fan Blades

2.3.4.1.1   Static—Total Measured Comparisons

2.3.4.1.1.1   OAPWL Versus N1C

Figure 28 and Figure 29 show inlet (5° to 80°) and aft (85° to 160°) comparisons, respectively, of total engine overall sound power level versus corrected low-rotor speed. Rotor speeds for App, C/B, and S/L conditions are labeled on the x-axis at 1800, 2400, and 2700 rpm, respectively.

From these figures it can be seen that the 24 fan blade configuration shows approximately 0.5 dB reduction for the inlet comparison at all three power conditions. The aft shows a slight benefit at approach power, and essentially no benefit at C/B or S/L. At approach, the inlet and aft overall sound power levels are comparable in absolute levels, however the aft dominates at both C/B and S/L.

2.3.4.1.1.2   PWL Spectra

Figure 30 and Figure 31, respectively, show inlet (5° to 80°) and aft (85° to 160°) comparisons of total engine sound power level spectra at the approach condition. Figure 32 and Figure 33 are inlet and aft comparisons at C/B, and Figure 34 and Figure 35 are similar comparisons at S/L power.

Due to the increase in fan blade quantity, the 24-blade configuration BPF has shifted one octave band higher than the 22-bladed fan at approach power. The largest benefit can be seen at mid-frequencies for both inlet and aft angles at approach. There is a slight benefit for the inlet at Cutback, however at sideline the spectra is approximately equal for both configurations.

2.3.4.1.1.3   SPL Spectra (60° and 130°)

Figure 36 and Figure 37 are comparisons of total sound pressure level spectra at 60° and 130°, respectively, at approach power. Figure 38 and Figure 39 are comparisons at cutback for 60° and 130°, respectively, and Figure 40 and Figure 41 are similar comparisons at sideline power.

The biggest reduction of sound pressure level for 24 fan blades is seen at both 60° and 130° at the approach power. The reduction is approximately 1 to 2 dB for almost all frequencies. There is also a benefit at 60° for both cutback and sideline powers, but very little difference for the 130° comparison, where the spectra appears to be dominated by jet noise.

2.3.4.1.2   Static—Fan Inlet and Fan Aft Comparisons

Fan inlet noise is the combination of both inlet fan tones and inlet fan broadband. Similarly, fan aft noise is the summation of both aft fan tones and aft fan broadband, as defined by Pratt & Whitney's automated source separation routine. A brief discussion of the source separation system can be found in Section 2.3.3 Farfield Test Data Analysis.

2.3.4.1.2.1   1, 2, and 3-BPF PWL Versus N1C

Figure 42 and Figure 43 are inlet and aft comparisons, respectively, for 1-BPF sound power level versus corrected low rotor speed. Figure 44 and Figure 45 are inlet and aft, respectively, for 2-BPF sound power level versus N1C, and Figure 46 and Figure 47 are inlet and aft 3-BPF sound power level comparisons. Rotor speeds for App, C/B, and S/L conditions are labeled on the x-axis at 1800, 2400, and 2700 rpm, respectively.

From these figures, it can be seen that 1-BPF is the most dominant tone. At approach there appears to be a slight increase in the inlet, and aft 1-BPF sound power levels for 24 fan blades. However, at higher speeds, 1-BPF is much lower than the 22 blade configuration, especially between cutback and sideline power. This reduction is on the order of 1 to 2 dB.

Figure 44 shows an increase in 2-BPF sound power level at high speeds for the 24 bladed fan. However aft 2-BPF (Figure 155) does show a reduction, and a comparison of Figure 44 and Figure 45 shows that aft 2-BPF is dominant at the highest speeds.

From Figure 46 and Figure 47 it can be seen that 24 fan blades has higher 3-BPF sound power levels than the 22 fan blades at both low, and high rotor speeds. But as mentioned earlier 1-BPF power level is the most dominant tone, with the exception of speeds well below the approach power condition.

2.3.4.1.2.2   1 to 3 BPF OAPWL Versus N1C

Figure 48 and Figure 49 are inlet and aft comparisons, respectively, for the total power in the first three harmonics of fan tone noise, plotted 1 to 3BPF versus corrected low rotor speed.

These two figures look very similar to both the inlet and aft 1-BPF sound power level versus speed curves of Figure 41 and Figure 43, respectively, confirming that 1-BPF is the most dominant tone.

2.3.4.1.2.3   Fan Broadband OAPWL Versus N1C

Figure 50 and Figure 51 are inlet and aft comparisons respectively, of fan broadband overall sound power level versus corrected low rotor speed.

Inlet fan broadband is lower for 24 blades than 22 blades at almost all low-rotor speeds. However at sideline power they tend to merge together. From Figure 51, the aft fan broadband is also slightly lower than for 22 blades, but only at speeds below C/B power.

2.3.4.1.3   Flight—Total Aircraft EPNL Comparisons

2.3.4.1.3.1   EPNL Versus N1C

Figure 52 is a comparison of in-flight projected Total EPNL versus corrected low-rotor speed curves, for a typical approach flight path. Figure 53 and Figure 54 are in-flight projected comparisons for typical C/B, and S/L flight paths, respectively. Airframe noise was included for all in-flight noise predictions, approach, C/B, and S/L.

Figure 52 shows a small noise advantage for 24 fan blades relative to 22 blades at around 1800 rpm, and below. Figure 53 shows a reduction of 0 to 0.5 EPNdB for 24 fan blades at all speeds (2100 to 2700 rpm) used for the C/B flight path. The biggest reduction is seen at the sideline flight path of Figure 54. The Total EPNL reduction for 24 blades is almost 1 EPNdB, but mostly at speeds lower than the actual sideline speed of 2700 rpm for this propulsion system.

2.3.4.1.4   Flight—Fan Inlet, and Fan Aft EPNL Comparisons

Fan inlet noise is the combination of both inlet fan tones and inlet fan broadband. Similarly, fan aft noise is the summation of both aft fan tones and aft fan broadband, as defined by Pratt & Whitney's automated source separation routine.

2.3.4.1.4.1   EPNL Versus N1C

Figure 55 and Figure 56 are a comparisons of in-flight projected fan inlet, and fan aft EPNL, respectively, versus corrected low-rotor speed for a typical approach flight path. Figure 57 and Figure 58 are similar, but at a typical cutback flight path and Figure 59 and Figure 60 are for a typical sideline flight path.

Fan inlet EPNL shows a benefit for 24 fan blades relative to 22 blades at all three flight conditions. There is a 0 to 0.5 EPNdB reduction at 1800 rpm for approach, and larger reductions at high rotor speeds for both the Cutback, and sideline flight paths.

Fan aft EPNL shows a slight reduction for 24 blades at 1800 rpm, on the approach flight path. However at higher speeds, the 24 blade configuration does show an increase. At 2000 rpm, the fan inlet and fan aft EPNL values are comparable, but fan aft begins to dominate at higher speeds. From a comparison of Figure 57 to Figure 60, it can be seen that fan aft is more dominant than fan inlet for both cutback and sideline flight paths. There is a reduction in fan aft EPNL for the 24 blade configuration on the sideline flight path at almost all speeds shown, with the exception of 2700 rpm.

2.3.4.1.4.2 PNLT Directivity

Figure 61 and Figure 62 are comparisons of in-flight projected fan inlet and fan aft PNLT directivities, respectively, for the approach flight path at 1800 rpm. Figure 63 and Figure 64 are similar, but for a typical cutback flight path at 2400 rpm. Figure 65 and Figure 66 are also similar, but for a typical sideline flight path at 2700 rpm.

From Figure 61, Figure 63, and Figure 65 it can be seen that the fan inlet peak PNLT is reduced for the 24 blade configuration by approximately 0.5 to 1.0 PNdB at both approach and cutback flight paths. This reduction in fan inlet peak PNLT is much greater at sideline.

From Figure 62 it can be seen that the fan aft peak PNLT is reduced for the 24 blade configuration at approach, similar to the fan inlet reduction. However, the fan aft peak PNLT for the 24 blade configuration is higher at both cutback and sideline flight paths.

2.3.4.1.4.3 SPL Spectra (60° and 130°)

Figure 67 and Figure 68 are comparisons of in-flight projected sound pressure level spectra, for fan inlet (60°), and fan aft (130°), respectively, for the approach flight path at 1800 rpm. Figure 69 and Figure 70 are similar, but for a typical cutback flight path at 2400 rpm. Figure 71 and Figure 72 are also similar, but for a typical sideline flight path at 2700 rpm.

The fan inlet and fan aft spectra at approach, both show a large reduction for 24 fan blades at low to mid frequencies, and a small benefit at high frequencies. Cutback, and sideline flight paths also show a 0 to 2 dB benefit of fan inlet for 24 blades, at low to mid frequencies, but very little reduction of the fan aft component.

2.3.4.2 "Cuton" Versus "Cutoff" FEGVs

2.3.4.2.1 Static—Total Measured Comparisons

2.3.4.2.1.1 OAPWL Versus N1C

Figure 73 and Figure 74 show inlet (5° to 80°) and aft (85° to 160°) comparisons, respectively, of total engine overall sound power level versus corrected low-rotor speed. Rotor speeds for App, C/B, and S/L conditions are labeled on the x-axis at 1800, 2400, and 2700 rpm, respectively.

From these figures, it can be seen that both inlet and aft total engine overall sound power levels are reduced for the "cutoff" configuration by approximately 0 to 0.5 dB, for almost all speeds. At approach, the inlet and aft overall sound power levels are comparable in absolute levels, however the aft dominates at both C/B and S/L.

2.3.4.2.1.2 PWL Spectra

Figure 75 and Figure 76, respectively, show inlet (5° to 80°) and aft (85° to 160°) comparisons of total engine sound power level spectra at the approach condition. Figure 77 and Figure 78 are inlet and aft comparisons at C/B power, respectively, and Figure 79 and Figure 80 are similar comparisons at S/L power.

At approach power, the "cutoff" configuration shows a 1 to 2 dB reduction of 1-BPF PWL, and a reduction in fan broadband sound power level by approximately 0 to 1 dB, for both the inlet, and aft. At cutback power the inlet shows both configurations are "cuton" at this rotor speed of 2400 rpm. The aft comparison shows a large reduction (~ 6 dB) in 1-BPF sound power level for the "cutoff" configuration. The fan broadband reduction for the "cutoff" configuration is approximately 0 to 1 dB for both inlet and aft at C/B power. At S/L power, there is a 0 to 0.5 dB reduction of both inlet and aft fan broadband sound power levels.

2.3.4.2.1.3   SPL Spectra (60° and 130°)

Figure 81 and Figure 82 are comparisons of total sound pressure level spectra at 60° and 130°, respectively, at approach power. Figure 83 and Figure 84 are comparisons at cutback for 60° and 130°, respectively, and Figure 85 and Figure 86 are similar comparisons at sideline power.

The biggest reduction of sound pressure level for the "cutoff" configuration can be seen at both approach, and cutback powers at both 60° and 130° spectra. At sideline power there is very little benefit for the "cutoff" configuration.

At approach power, the "cutoff" configuration shows a 1 to 2 dB reduction of 1-BPF SPL, and essentially no reduction in fan broadband noise, for the both the inlet, and aft.

At cutback power the inlet shows both configurations are "cuton" at this rotor speed of 2400 rpm. The aft comparison shows a large reduction (~ 10 dB) in 1-BPF sound power level for the "cutoff" configuration.

2.3.4.2.2   Static—Fan Inlet and Fan Aft Comparisons

Fan inlet noise is the combination of both inlet fan tones and inlet fan broadband. Similarly, fan aft noise is the summation of both aft fan tones and aft fan broadband, as defined by Pratt & Whitney's automated source separation routine

2.3.4.2.2.1   1, 2, and 3-BPF PWL Versus N1C

Figure 87 and Figure 88 are inlet and aft comparisons, respectively, for 1-BPF sound power level versus corrected low rotor speed. Figure 89 and Figure 90 are inlet and aft, respectively, for 2-BPF sound power level versus N1C, and Figure 91 and Figure 92 are inlet and aft 3-BPF sound power level comparisons. Rotor speeds for App, C/B, and S/L conditions are labeled on the x-axis at 1800, 2400, and 2700 rpm, respectively.

From these figures, it can be seen that 1-BPF is the most dominant tone at all low-rotor speeds for the "cuton" configuration. The biggest increase of tone sound power level can be seen for 1-BPF for the aft at approach and cutback powers for the "cuton" configuration, where as expected the BPF was increased by as much as 10 dB due to the closely spaced cuton FEGV.

This increase can be seen at almost all speeds, but diminishes at high power.

From Figure 89 to Figure 92, it can be seen that there is an increase of both inlet and aft levels of 2-BPF, and 3-BPF sound power levels, for the "cuton" configuration, at approach. This increase was expected due to the tighter spacing between the fan blades and the cuton FEGV assembly.

2.3.4.2.2.2   1 to 3 BPF OAPWL Versus N1C

Figure 93 and Figure 94 are inlet and aft comparisons, respectively, for 1-3BPF overall sound power level versus corrected low rotor speed. Since 1-BPF is the dominant tone at most speeds, these curves mimic the 1-BPF sound power level plots in the previous section.

2.3.4.2.2.3   Fan Broadband OAPWL Versus N1C

Figure 95 and Figure 97 are inlet and aft comparisons respectively, of fan broadband overall sound power level versus corrected low rotor speed.

Both inlet and aft fan broadband overall sound power levels are approximately equal between the "cuton" and "cutoff" FEGVs, at almost all low-rotor speeds.

2.3.4.2.3   Flight—Total Aircraft EPNL Comparisons

2.3.4.2.3.1   EPNL Versus N1C

Figure 97 is a comparison of in-flight projected Total EPNL versus corrected low-rotor speed curves, for a typical approach flight path. Figure 98 and Figure 99 are in-flight projected comparisons for typical

C/B, and S/L flight paths, respectively. Airframe noise was included for all in-flight noise predictions, approach, C/B, and S/L.

From these curves the "cuton" configuration shows an increase in EPNL on the order of 0 to 1 EPNdB at App, and 1 to 2 EPNdB reduction at C/B. However the noise increase varies considerably over the speed ranges shown. The sideline EPNL curve shows that there is essentially no noise penalty for the "cuton" configuration at sideline power (2700 rpm) on the sideline flight path.

2.3.4.2.4   Flight—Fan Inlet, and Fan Aft EPNL Comparisons

Fan inlet noise is the combination of both inlet fan tones and inlet fan broadband. Similarly, fan aft noise is the summation of both aft fan tones and aft fan broadband, as defined by Pratt & Whitney's automated source separation routine.

2.3.4.2.4.1   EPNL Versus N1C

Figure 100 and Figure 101 are a comparison of in-flight projected fan inlet, and fan aft EPNL, respectively, versus corrected low-rotor speed for a typical approach flight path. Figure 102 and Figure 103 are similar, but at a typical cutback flight path and Figure 104 and Figure 105 are for a typical sideline flight path.

Fan inlet EPNL shows very little penalty for the "cuton" configuration at any of the flight conditions.

Fan aft EPNL is increased up to 2 EPNdB for the "cuton" configuration for both approach, and Cutback.

2.3.4.2.4.2   PNLT Directivity

Figure 106 and Figure 107 are a comparison of in-flight projected fan inlet and fan aft PNLT directivities, respectively, for the approach flight path at 1800 rpm. Figure 108 and Figure 109 are similar, but for a typical cutback flight path at 2400 rpm. Figure 110 and Figure 111 are also similar, but for a typical sideline flight path at 2700 rpm.

Figure 108 and Figure 110 both show that the fan inlet peak PNLT is slightly lower for the "cuton" configuration, at both C/B, and sideline flight paths. But for inlet and aft noise at other conditions the cuton noise is higher by as much as 5 PNLT for aft noise at cutback power. Obviously this arises from the increased BPF tone for this cuton design.

2.3.4.2.4.3   SPL Spectra (60° and 130°)

Figure 112 and Figure 113 are comparisons of in-flight projected sound pressure level spectra, for fan inlet (60°), and fan aft (130°), respectively, for the approach flight path at 1800 rpm. Figure 114 and Figure 115 are similar, but for a typical cutback flight path at 2400 rpm. Figure 116 and Figure 117 are also similar, but for a typical sideline flight path at 2700 rpm.

As can be seen from these figures, the biggest penalty for the cuton FEGV is seen for the first harmonic of blade passage frequency (BPF), for fan aft at App, and C/B. The biggest increase in 1-BPF can be seen from Figure 115, where the BPF tone is about 10 dB higher due to cuton and close spacing.

2.3.4.3   Treated Versus Hardwall Tailpipe

The acoustic treatment in the EVNRC tailpipe was tuned to reduce the low-pressure turbine noise component. This primary nozzle treatment was designed and built for two purposes, and was used during the entire program except for the last configuration. The primary objective was to reduce or eliminate turbine noise from the measured spectra so that the effects of various fan noise reduction items (e.g., blade and vane changes) could be seen in the high frequency broadband portion of the spectra. The second objective was to determine how much of the high frequency broadband noise can be attributed to the turbine component. If there were no attenuation, then one could conclude that this noise is coming from the fan, whereas if there is significant attenuation then one could logically conclude that the turbine noise plays an important role.

Figure 14 shows a photo of the tailpipe acoustic treatment.

2.3.4.3.1   Static—Total Measured Comparisons

2.3.4.3.2   OAPWL Versus N1C

Figure 118 and Figure 119 show inlet (5° to 80°) and aft (85° to 160°) comparisons, respectively, of total engine overall sound power level versus corrected low-rotor speed. Rotor speeds for App, C/B, and S/L conditions are labeled on the x-axis at 1800, 2400, and 2700 rpm, respectively.

From these figures it can be seen that there is a reduction of up to 1.0 dB at most engine speeds with acoustic treatment.

2.3.4.3.2.1   PWL Spectra

Figure 120 and Figure 121, respectively, show inlet (5° to 80°) and aft (85° to 160°) comparisons of total engine sound power level spectra at the approach condition. Figure 122 and Figure 123 are inlet and aft comparisons at C/B power, respectively, and Figure 124 and Figure 125 are the same comparisons at S/L power.

A reduction in sound power level can be seen for the Treated tailpipe at approach and cutback flight paths, particularly between 3150 and 10,000 Hz.

There is a small benefit in the aft for the Treated tailpipe, at sideline power.

2.3.4.3.2.2   SPL Spectra (60° and 115°)

Figure 126 and Figure 127 are comparisons of total sound pressure level spectra at 60° and 115°, respectively, at approach power. Figure 128 and Figure 129 are comparisons at cutback for 60° and 115°, respectively, and Figure 130 and Figure 131 are similar comparisons at sideline power.

The biggest reduction for the tailpipe acoustic treatment can be seen at the peak Turbine noise angle of 115°, for both approach, and cutback power. At approach power the treated SPL is reduced by approximately 3 to 5 dB at high frequencies.

2.3.4.4   Static—Source Separated LPT Comparisons

LPT noise is the combination of both Turbine tones, and Turbine broadband noise (referred to as LPT "haystack" noise), as defined by Pratt & Whitney's automated source separation routine.

2.3.4.4.1   Low-Pressure Turbine OAPWL Versus N1C

Figure 132 is a comparison of the low-pressure turbine noise component for both the Treated and Hardwall tailpipe.

From this figure it can be seen that the LPT (Tones + Haystack) noise power is significantly reduced for the Treated tailpipe for all corrected low-rotor speeds. The reduction in overall sound power level is on the order of 3 to 5 dB, at all speeds.

2.3.4.4.2   Flight—Total Aircraft EPNL Comparisons

2.3.4.4.2.1   EPNL Versus N1C

Figure 133 is a comparison of in-flight projected Total EPNL versus corrected low-rotor speed curves, for a typical approach flight path. Figure 134 and Figure 135 are in-flight projected comparisons for typical C/B, and S/L flight paths, respectively. Airframe noise was included for all in-flight noise predictions, approach, C/B, and S/L.

From these curves it can be seen that the total EPNL is reduced by about 0.75 EPNdB for App and C/B, and and about 0.5 EPNdB at S/L.

2.3.4.4.3   Flight—Low-Pressure Turbine Comparisons

2.3.4.4.3.1   EPNL Versus N1C

Figure 136 is a comparison of in-flight projected LPT EPNL versus corrected low-rotor speed for the approach flight path. Figure 137 is a similar comparison for a typical cutback flight path, and Figure 138 is a comparison for the sideline flight path.

All of these figures show a substantial LPT EPNL component reduction, on the order ~ 5 EPNdB, for the treated tailpipe at all flight path three flight path conditions.

2.3.4.4.3.2   PNLT Directivity

Figure 139 shows a comparison of in-flight projected low-pressure turbine PNLT directivities, at the approach flight path for 1800 rpm. Figure 140 shows the comparison at the cutback flight path for 2400 rpm. Figure 141 shows the comparison at the sideline flight path for 2700 rpm.

These curves show a substantial noise reduction for LPT PNLT directivity at all three noise flight paths. The reduction for the treated tailpipe is on the order of 5 to 10 PNdB at all conditions.

2.3.4.4.3.3   SPL Spectra (60° and 115°)

Figure 142 and Figure 143 are comparisons of in-flight projected sound pressure level spectra, for the low-pressure turbine component at 60° and 115°, respectively, for approach flight path at 1800 rpm. Figure 144 and Figure 145 are similar, but for a typical cutback flight path at 2400 rpm. Figure 146 and Figure 147 are also similar, but for a typical sideline flight path at 2700 rpm.

These curves show a large reduction of in-flight LPT sound pressure levels at the peak LPT angle of 115° at all three flight conditions.

3.0   Boeing Report

3.1   Introduction

3.1.1   P&W/NG Test Objectives

The overall purpose of the Engine Validation Noise Reduction Concepts (EVNRC) testing was to demonstrate the effectiveness of engine and nacelle related noise reduction concepts developed as part of the NASA Advanced Subsonic Technology (AST) airplane noise reduction technology program. This program began in 1994 with NASA, U.S. industry and academia participating. The subject testing was Phase 2 of the PW4098 testing conducted in 2001. Phase 1 was conducted in two stages, Part A in 1998 and Part B in 1999 (Ref. 1). The noise reduction concepts planned to be evaluated in the Phase 2 testing are shown in Table 4.

TABLE 4.—NOISE REDUCTION CONCEPTS PLANNED FOR PHASE 2 TESTING

- Northrop Grumman/ Hersh Walker Acoustics (NG/HWA) hybrid active passive inlet BPF tone reduction system. Testing of this concept was performed under separate contract to Northrop Grumman.
- P&W lower number EGV system for cut on subsonic tip speed BPF and lower broadband noise.
- P&W increased blade number fan (+2 blade) for reduced loading noise.
- Boeing scarf inlet with bellmouth lip to reduce flow separation noise observed in Phase 1 testing.
- P&W primary nozzle with acoustic lining to attenuate turbine noise.

Boeing had two subcontracts with P&W for this testing. The first was to provide hardware, instrumentation and consultation for the entire EVNRC Phase 2 test. The second was specifically related to data collection in support of the separate NG/HWA active noise control testing. The work statements for these contracts were as follows.

3.1.1.1 The Boeing Statement of Work (SOW) for EVNRC Phase 2 Test

Boeing shall provide the ideal acoustic inlet and the certification test production inlet for testing at no cost to the program.

In addition, Boeing shall assist and consult with P&W on all aspects of the program from concept selection and design to test planning, testing, data analysis and final report preparation. Boeing shall also apply its phased array microphone and mode measurement experience from Phase 1 to maximize the success in Phase 2 of isolating the fan and jet source reduction mechanisms, separating inlet and aft radiated fan noise contributions, and measuring the spatial distribution of jet noise.

Boeing will reinstall the ICD microphone array and associated instrumentation, similar to that used in Phase 1, to be used for the Phase 2 testing and for the NASA active noise control test to follow the Phase 2 test. Boeing will also assist P&W to design, fabricate and install an aft noise array aimed at understanding jet and aft-radiated fan noise effects of tested noise reduction concepts.

Boeing shall operate the array data collection instrumentation during engine noise tests and provide consultation during testing to optimize the data acquisition. Data analysis shall be performed at Boeing during and after test completion to determine mode and source changes related to the specific noise reduction concepts tested. Finally, Boeing shall prepare a report containing the results of this analysis.

Additionally, in support of the Active Noise Control Test, Boeing will use the ICD array to measure the $m = 22$ rotor locked BPF tone at cutback power. Boeing will consult with Northrop Grumman/Hersh Walker Acoustics and supply predictions of the propagation of the BPF tone to their error microphone locations to improve the performance of their active control system. Boeing will also modify the "A" flange adapter ring to hold 56 microphones and collect spinning mode data with it during the $m = 22$ mode testing.

3.1.1.2 The Boeing SOW for the Active Noise Control Test

Task 1 Support the design of the NGC pressure transducer-mounting configuration on the Boeing inlet lip. Provide drawings of the Boeing inlet and bellmouth to support the design of the control microphones.

Task 2 Support the development of and review NGC supplied test plan. Provide inputs and recommendations to the NGC supplied test plan.

Task 3 Review NGC supplied installations to the inlet lip.

Task 4 delete

Task 5 Provide a PW4098 acoustic certification bellmouth, which consists of production inlet with a small bellmouth, attached from the throat forward.

Task 6 Support instrumentation operation and data acquisition of the Boeing Phased Array measurement system for the engine operating conditions listed below. The Phased Array system shall provide the radiated sound power level for a specified BPF and target circumferential mode, which will be in the frequency range 600 to 800 Hz. Within a reasonable level of effort, a circumferential mode order breakdown of the radiated BPF tone is desired, as would a full spectrum of the total radiated noise. The reference sound power for the reported levels may be arbitrary and undisclosed, as long as the same reference power is used for all measurements. The engine will be operated over a selected range of rpm's for the following anticipated NGC fan case liner configurations:

- Active system operating
- Active system off, selected segments of active system off (assume four conditions)
- Active segment of liner hardwalled (on-site modification using tape)

At a minimum, the Phased Array system shall provide radiated sound power level (with arbitrary but consistent reference power) for total BPF and for target circumferential spinning mode order (probably $m = -6$). BPF will be in the range of 600 to 800 Hz.

Task 7 A baseline passive treatment configuration will be selected for evaluation of the performance of the active hybrid system. Provide results of phased array measurement of baseline

3.1.2 Boeing Objectives

Boeing had specific objectives for the Phase 2 EVNRC test in some cases beyond the contracted work statements. These were as follows:

Further develop the Boeing process for using the ICD microphone array in conjunction with the duct propagation code CDUCT to relate the ICD measurements to the noise field at the fan. It was hoped that the acoustic drivers installed to provide the cancellation sound for the active control system could be used to generate specific modes at a frequency slightly shifted from the BPF while the engine was operating. In this way the ICD measurements at this frequency would provide the "steering vector" data needed to properly decompose the BPF data accounting for with flow 3D propagation effects. These steering vectors could then be compared to those calculated by CDUCT for verification of the CDUCT code.

Determine if the data measured on the ICD could be related to the 150 ft polar arc microphone data.

Determine if transient ICD data measured during a uniform engine acceleration could be related to the steady state data.

Determine if a bellmouth lip on the scarf inlet would eliminate the unexpectedly high BPF tone level and (hardwall inlet) buzz saw noise observed during the Phase 1 testing.

Determine if a bellmouth lip on the scarf inlet would result in the expected high frequency acoustic lining attenuation at higher engine power conditions in contrast to the results from the Phase 1 testing.

3.2 Boeing Instrumentation

3.2.1 Overview of the Test Setup

The EVNRC Phase 2 test was conducted at the P&W C11 outdoor engine test stand in West Palm Beach, Florida, with the same PW4098 engine used for the Phase 1 test. Figure 148 is a photo of the engine on the test stand with the Boeing production inlet installed. This was the inlet used for most of the Phase 2 testing except for the scarf inlet test. As reported in Reference 1, there is a 150 ft polar arc ground microphone array used for the standard farfield noise measurement. The scarf inlet was tested with aft barriers as shown in Figure 149 and Figure 150. Most of the other test configurations did not use the barriers. A linear microphone array in the aft region was used to help separate aft engine noise from inlet noise as well as primary nozzle noise from fan nozzle noise Figure 151.

The phased array instrumentation used for this test can be broadly categorized into four groups. The first group is associated with the ICD mounted mode measurement hardware Figure 152 including the transducers, cabling and power supplies. The second is associated with the "Olsen Ring" Figure 154, spinning mode measurement instrumentation. The third group contains the farfield linear array instrumentation as well as the P&W primary nozzle Kulite transducers. The final group includes all the hardware necessary for the data acquisition process.

3.2.2 ICD Microphone Array

The mode array instrumentation covers all the instrumentation needed to produce the voltage signals from the mode array. The mode array instrumentation consists of the mode array transducers, the mode array cables, and The Boeing Company's bridge-balance power supplies.

3.2.2.1 ICD Array Pressure Transducers

The ICD array was designed to separate the inlet noise into spinning and radial mode information to better understand the BPF noise suppression for the Active Noise portion of the test. The suppression provided by the Active Noise transducers for a particular set of modes could have been masked at the farfield polar microphones by uncontrolled modes. The ICD array consisted of 199 transducers located on the ICD in 11 rings as shown in Figure 155. The transducers in each ring are uniformly spaced, which is

in contrast to the previous Phase 1 ICD array Figure 156 that clustered transducers to one side of the ICD. The overall placement of the transducers was designed to maximize the orthogonality of different modes propagated from the fan to the ICD array as predicted by the CDUCT propagation code. This improves the ability of the array to distinguish between the different modes.

Kulite MIC-093 transducers were used for the ICD array. The Kulites are friction fit into a specially designed holder that can be quickly and securely attached to the ICD perforated plate. Figure 157 shows a holder attached to an ICD panel. The holder consists of a hollow 3/16-in. diameter, 1 13/16-in. long nylon rod threaded onto a 4-40 by 1/2-in. set screw. A slot is cut into the top of the rod in order to accommodate the Kulite wire and vent tube. A small bent piece of 0.059-in. diameter music wire is soldered into a hole drilled into one end of the setscrew. The music wire hook is inserted into the ICD perforated plate and two 18-8 stainless steel nuts are threaded onto the set screw to provide a way of tightening the holder to the perforated plate.

In order to initially position the transducers on the ICD, the Kulite locations were marked on full size paper templates of the individual ICD panels. The full size paper templates were printed from a three-dimensional CATIA model of the ICD. The paper templates were then placed on the correct ICD panel and a Kulite holder was placed at the marked locations. Figure 158 shows a sample paper template. This initial positioning method provides a quick and easy way to place the Kulites on the ICD.

Accurate locations of the ICD transducers are required for phased array applications. This was accomplished with a photogrammetry survey. Photogrammetry is a method of extracting accurate position information from photographs. A nylon cap with a ½-in. photo-reflective target is placed on each transducer (Figure 159). The target reflects a large percentage of a camera flash's light that allows the point to be easily distinguished from the background (Figure 160). Multiple pictures are taken from different angles, and the target positions are processed and triangulated through a Boeing designed software package to determine the relative positions. A Kodak DCS420 1.5 Mpixel, black and white, digital camera is used for all survey pictures. The survey pictures were taken at night, which provided maximum contrast between the background and targets (Figure 161). An absolute scale is established through the use of specially built scale bars with calibrated targets seen in Figure 161, as two linear rows of eight lights in the night photograph, and Figure 162. A coordinate system relative to the engine is established by surveying the ICD in its installed position around the engine and placing a few targets in known locations on the "A-prime" engine flange.

3.2.2.2 Cables

A schematic diagram of the instrumentation cables is shown in Figure 163. The ICD transducer cables were routed from the transducer to the power supplies along the ICD panel joints. Aluminum tape was used to securely attach the cables to the ICD. The 95 ft lengths of 0.050-in. diameter low capacitance Gore cables were used to allow the signal to travel from the most distant transducer to the power supply with enough slack such that the power supplies could be located away from the ICD cart when testing without barrier walls. This minimizes possible extraneous acoustic reflections from the presence of the power supply enclosures.

3.2.2.3 Bridge-Balance Power Supplies

Boeing built Dual Purpose Power Supplies (DPPS) were used to power and condition the analog signals from the ICD Kulite transducers. The 16-channel DPPS units (capable of powering either dynamic bridge transducers or microphones on a per channel basis) were used in the dynamic bridge transducer (DBT) mode. The very low noise DPPS units provided the flexibility required delivering high quality analog signals to the data acquisition system.

In DBT mode, the DPPS units provide manual bridge balance capability via a trim-pot that enables removal of any DC offset inherent in the sensors. The ability to balance the bridge was necessary for this application because of the need to introduce substantial gain to optimize the dynamic range of the

measurement system. Without a balanced bridge, the gain would have caused the output of the power supply to overload. The DPPS units also provided the excitation voltage to the transducers.

The DPPS units are equipped with two-stage gain circuitry. There is 40 dB of input gain and 40 dB of output gain possible with a vernier attenuator at the output. This setup is extremely flexible because it allows the gains to be set such that the output between different channels can be matched for a given transducer input. The amount of gain for each set of sensors was chosen to maximize the analog signal level (without risk of overload).

The DPPS units have excellent channel-to-channel phase matching. The primary component of mismatch is due to the addition of vernier attenuation, which causes a linear phase shift with frequency. However, the channel-to-channel phase matching of the DPPS units remains within ±0.5° up to 57.5 kHz when vernier attenuation settings are within 3.0 dB of each other.

The power supplies were connected to the P&W infrastructure cables in a blockhouse near the engine stand (the SADAR Room). The signals were then broke out of the infrastructure cables inside the Control Room and were connected to the Boeing (DDS5) acquisition and channel monitoring system.

3.2.3   "Olsen Ring" Microphone Array

The "Olsen Ring" was originally made for the second entry of Phase 1 EVNRC testing to mount the scarf inlet to the production case spool. For the Phase 2 test the ring was modified to hold up to 52 equally spaced pressure transducers around the circumference. The ring of transducers was added to Phase 2 of the EVNRC test with the addition of the Active Noise m = 22 testing. It was thought that a measurement of the source spinning orders near the fan would be helpful in understanding m = 22 control.

Figure 153 is a schematic of the ring with the microphone locations. The array was composed of 52 equally spaced transducers located between the inlet and the fan case (STA 121). Figure 154 shows the location of the ring just upstream of the forward fan case. The 52 Kulite transducers are mounted in tubes and held with Swage-Loc fittings. The Swage-Loc fittings are airtight to insure that leaking air next to the fan generates no noise.

Special pressure transducers were used, which had very little phase variations between transducers. These transducers were developed to measure broadband modes for the NASA Source Diagnostic Test completed in March of 2000. The transducers are a slight variation of Kulite Model XCQ-125B-093-15A having an RTV layer over the diaphragm instead of a protective screen. The piezo-resistive transducers are capable measuring the pressure without the need for a phase calibration between the sensors at frequencies up to 50 kHz.

The transducers were wired through the strut above the engine and connected to 150 ft extension cables to the power supplies in the SADAR room. The output of the bridge/balance power supplies was coupled into the P&W infrastructure cables to the Control Room. In the Control Room, adapter cables were used to connect the signals to the acquisition system.

3.2.3.1   Pressure Transducers

The pressure transducers used in the ring array were originally selected for a model scale circumferential array application. The description below refers to the requirements for the model scale application, which are much more stringent than the full-scale application. It does show the ultimate capability of these transducers however.

The model scale system design, including the pressure transducers, provided a challenging set of constraints. The transducers couldn't disturb the flow and needed to have a relatively large dynamic range. However, the most difficult requirement was a maximum deviation in amplitude and phase response of 1.0 dB and 5° to 50 kHz, respectfully. This was required to assure the signal to noise ratio (SNR) of the mode arrays would remain near 40 dB.

Piezo-resistive transducers were chosen as the best solution to these constraints. Other designs required expensive and difficult calibrations that might change with time. The piezo-resistive design only requires a level correction at a single frequency.

The final design required careful consideration of not only the sensors themselves, but also the cabling between the sensors and the power supplies. The amplitude and phase variation requirements translate into a requirement that the first resonance of the transducer be above 150 kHz and that the change in the resistance/line capacitance product be less than 17 percent.

Several tests were conducted to verify the design and are described in the mode measurement section of Reference 2. These tests showed that the transducers met their design requirements and prove that the ring measurement system should give a SNR near 40 dB.

3.2.4   Aft Farfield Linear Microphone Array

As part of the EVNRC contract, Boeing agreed to work with P&W to field, acquire and analyze a farfield, linear array. Boeing performed a number of up-front parametric studies to help define a suitable array within the channel count and location constraints of the test. The output of the studies provided recommendations for size/aperture of the arrays as well as the number of microphones. Ultimately, a 25-ft long, 30-microphone array was chosen 50 ft from the engine at 120°. This array is shown schematically in Figure 164 and a picture is included in Figure 165.

The Boeing Noise Engineering Lab defined the coordinates for the final array. This array is unconventional in design, having closer microphone spacing near the edges of the array instead of the center. This decreases the width of the point-spread function (improving the arrays ability to discern two closely spaced sources) without making the array too large. However, the spacing makes it much more difficult to use a subset of the microphones at high frequencies where aperture is not usually required. Table 5 gives the coordinates of the microphones in the array.

TABLE 5.—FARFIELD LINEAR ARRAY MICROPHONE LOCATIONS

Microphone no.	X, in.	Microphone no.	X, in.	Microphone no.	X, in.
1	-149.00	11	-71.90	21	65.61
2	-143.93	12	-59.89	22	76.92
3	-138.39	13	-46.79	23	87.68
4	-132.36	14	-32.52	24	97.94
5	-125.79	15	-16.96	25	107.71
6	-118.63	16	0.00	26	117.01
7	-110.82	17	14.43	27	125.87
8	-102.31	18	28.18	28	134.31
9	-93.03	19	41.27	29	142.35
10	-82.92	20	53.73	30	150.00

The microphones, cabling and power supplies were provided by P&W. The microphones were a combination of B&K 4192 and 4134 ½ in. microphones that were available from older inventories. P&W designed and tested the support structure holding the microphones using a crossbar with holes. Figure 166 shows the crossbar with microphones installed as well as one of the metal locating pins that was put over the top of marks surveyed onto the tarmac by P&W. This system worked well for maintaining exact inter-microphone spacing and allowed the array to easily be positioned for testing each day.

The linear phased array was designed to allow the following questions to be answered during the test:

1. Determine if the low frequency noise peak (near 500 Hz) in the PW4098 spectra is coming from the primary or fan nozzle (i.e., is it combustor related noise or does it come from the fan).
2. At higher powers (e.g., cutback and sideline), clarify the relative contributions of jet noise and aft fan broadband noise as a function of frequency.

3. For fan tones and broadband noise at a number of inlet and aft angles, define the relative contributions of inlet and aft-radiated noise. An ability to do this could eliminate the need for barrier testing.
4. In the 3000 to 8000 Hz range at aft angles, determine the relative contributions from turbine noise (haystacks) and fan broadband noise.

Boeing used their DDS5 acquisition system and P&W used a 32-channel Sony SIR-1000 recorder to acquire the data. The plan was that Boeing and P&W would compare processed results to help P&W establish this technique and for P&W to report the final results.

3.2.5 Additional Sensors

3.2.5.1 Once Per Revolution Signal

A *short tooth* gear was used as the trigger signal for data acquisition and pulse-synchronized averaging.

Figure 167 is a typical trace of the trigger signal as measured by the data acquisition system. Table 6 provides details of the trigger signal.

TABLE 6.—DETAILS OF THE TRIGGER SIGNAL

	587 rpm		1833 rpm	
	Rise	Fall	Rise	Fall
Edge slope, V/ms	113.6	-122.8	108.5	-111.0
Edge width, ms	0.0417 ms	0.0417 ms	0.0417 ms	0.0417 ms
Edge width, deg.	0.147°	0.147°	0.46°	0.46°
Pulse width, sec	0.792 ms		0.604 ms	
Pulse width, deg.	2.79°		6.64°	

3.2.6 Data Acquisition System

Boeing's Digital Data Acquisition System 4 (DDS4) was used to acquire acoustic data from the ICD array (199 channels), the mode ring (52 channels), and a once-per-rev pulse. In addition, DDS5 was configured during the test to acquire acoustic data from the aft farfield array (30 channels) and the primary nozzle Kulites (2 channels). Either data system can support nearly 400 simultaneous channels of continuous data acquisition at sample rates of up to 196k samples/sec per channel. These are custom data acquisition systems built primarily from Agilent (formerly Hewlett Packard Test and Measurement Division) data acquisition VXI hardware. The host computer for the VXI data acquisition hardware is a HP E1497A V743 embedded controller (a HP UNIX workstation on a single-slot VXI card). HP E1433B 8-channel VXI input data acquisition modules provided the digital data acquisition. The E1433B input modules provide the analog anti-aliasing filters, programmable gain, and analog-to-digital conversion with simultaneous sampling necessary to acquire high-quality digital data. The input modules provide inherent channel-to-channel phase matching within 2° at 88 kHz. The system architecture required to configure the high-channel-count system provided by Boeing introduces additional, but predictable and repeatable time delays between groups of input modules. Boeing book keeps these time delays with the sampled data and accounts for them during downstream data processing to insure 2° phase matching at 88 kHz across all channels.

DDS4 achieves high-channel-count, high-bandwidth data acquisition by coupling sets of E1433B input modules with HP E1562E dual SCSI disk modules using HP's proprietary local bus. A separate local bus is dedicated to each E1562 module and the set of E1433B modules that feed it. Data is streamed from the FIFO buffers of the input modules over the high-speed local buses to the E1562 disk modules. Each E1562 module has two 9-Gbyte SCSI disk drives attached that together are capable of consuming data at the rate produced by the input modules that feed them. The system architecture is scaleable upwards of 400 channels with no software changes.

3.2.7 Conversion of Input Voltages to Engineering Units

Time series data were acquired and stored with associated information that enables conversion of the raw sampled values to engineering units. The data acquisition software requires the operator to enter a calibration value for each acquisition channel in the form of a 1-V equivalent. The 1-V equivalent is defined as the dB SPL value that is required to produce 1 V rms (0 dB re 1 Vrms) at the data acquisition system input. The per-channel 1-V equivalent values are used by the data system software, along with several other data-system-internal values, to produce a scale factor for each channel. When the raw sampled values are multiplied by the scale factor, the resultant values correspond to instantaneous pressure in units of microPascals.

One-Volt equivalent values were determined by placing a calibrator with a known Sound Pressure Level (SPL) over each sensor and recording the voltage level at the input to the data acquisition system. Note that this calibration method captures the instrumentation system sensitivity end-to-end (from the transducer to the data system input) and not just the sensitivity of the transducer. In actuality, many of the instrumentation system channels were purposely adjusted to the same sensitivity using the vernier gain capability of the Boeing Dual Purpose Power Supplies. The primary reason for adjusting to the same sensitivity is that it simplifies signal monitoring and range setting during data acquisition.

During instrumentation setup, the power supply gains were adjusted to provide the best possible signals to the inputs of the data acquisition system (given of course the inherent constraints of setup such as cable lengths, equipment location, and electrical environment). The input ranges of the data system were manually set in order to ensure high quality digital data. That is, the ranges were set as low as possible (avoiding data system input overloads) so that the maximum dynamic range could be achieved from the 16-bit analog-to-digital converters.

3.2.7.1 Calibration of Mode Sensors

Two types of sensor calibrations were used during testing. Boeing built an attachment that allowed the sensors to be calibrated with a pistonphone source. The pistonphone has a cavity of a predefined volume with a plunger that changes the volume and thus changes the pressure. This type of calibration required placing the transducer in the calibrator with an adapter. Boeing pistonphones are calibrated within ±0.2 dB absolute.

In addition, a "Kulite Calibrator" was used as a calibrator. This type of calibrator uses a feedback circuit and a microphone in a cavity to adjust the driver to give a specific level. This type of calibrator has the advantage that it can be used while the transducer is mounted in-situ. The Kulite Calibrator gives levels ±0.5 dB absolute.

A short test was run at Boeing to help understand the errors associated with each of these calibration methods. The data show that the pistonphone was superior in absolute calibration and day-to-day repeatability to the Kulite calibrator when corrected for barometric pressure differences. However, the Kulite calibrator did give very repeatable levels within a day and between samples. In other words, the accuracy of the Kulite calibrator was somewhat less than the pistonphone, but both were very precise.

It was decided that the best way to use the calibrators was to use the pistonphone to set initial absolute levels. The in-situ Kulite calibrator was then used to verify that the relative levels remained constant and that all the sensors worked properly before starting testing. This strategy worked well for testing and resulted in few modifications to the levels after the initial setup.

3.3 Data Processing

The array data were processed in several ways to better understand the noise sources. The specific processing depended on whether or not the data was pulse-synchronous resampled using the once per revolution signal. Most the data shown in this report was pulse-synchronous resampled because these data are much better suited for analyzing and removing tones.

This section describes each type of processing used in the analysis of the data. These types of processing include average and standard deviations of pressure traces, auto-spectra, Olsen Ring mode plots and ICD mode plots.

3.3.1 Data Sampling

Almost all the data are analyzed by first re-sampling the data at specific angular locations of the rotor using the once-per-revolution pulse. This process requires using a digital linear-phase finite impulse response (FIR) filter to first remove frequencies above the new Nyquist frequency in the data. A simple interpolation procedure can then be used to resample the data without significant errors since the data are over-sampled by a factor of approximately eight.

3.3.2 Average and Standard Deviation Pressure Traces

By averaging the individual pressure traces for each rotation, an average pressure trace representing one rotation of the rotor was produced. Ten seconds of data was used for averaging which represented approximately 360 rotations at N1C = 1620 rpm and 475 rotations at N1C = 2800 rpm.

The average and standard deviation could then be measured for a microphone as a function of rotor position. Figure 168 shows the average and standard deviations measured near the rotor in the inlet at 2000 N1C. These measurements show the average pressures are much larger than the unsteady pressures associated with the standard deviation at this tip speed. At lower tip speeds or locations farther from the rotor, the unsteady pressures may be higher than the average pressures.

3.3.3 Power Spectra

Two types of power spectra were generated for the pulse-synchronized data. Taking the average of the individual Fourier transforms of the pressure traces for each rotation or equivalently the FFT of the averaged pressure traces generates the so-called *pulse-synchronized averaged or average* spectrum. The averaging process reduces the non-rotor-locked sources by 10*LOG10 (# averages) in decibels. There were approximately 360 revolutions at the lowest power of N1C = 1620 rpm and approximately 475 revolutions at the highest power of N1C = 2800 rpm.

The other power spectrum calculated is equivalent to the typical spectrum, the average of the magnitudes of the FFT's of the individual pressure traces for each rotation, and is called the *total* spectrum. This spectrum includes all the energy measured at the transducer including the non-rotor-locked energy. Figure 169 shows both these spectra computed for the same condition. Note that the total spectrum is greater than the average spectrum at all frequencies.

The pulse-synchronized averaging process can dramatically reduce the non-synchronous noise and improve the ability to view "pure" tones. In this context, pure tones are tones that are completely deterministic and therefore have infinitesimally small bandwidth.

The difference between the two processing methods is particularly apparent in the broadband levels where one would expect the spectra to be dominated by non-synchronous sources. There is approximately a 17 dB difference between the two processing methods for the N1C = 1620 condition which corresponds to $10*LOG_{10}$ (number of averages).

3.3.4 ICD Array Data

The ICD array data was processed in several ways. First, average and total-spectra were generated to view the steady state SPL distributions on the ICD. The total spectra data were compared to the farfield microphone data as discussed below. The steady state ICD data were compared to data collected while the engine was slowly accelerated as well. These distributions compared well with the engine acceleration data at BPF. However, the primary use of the ICD array data was to decompose the sound field into spinning and radial source modes.

3.3.4.1   Steady State SPL Distributions

The steady state SPL distributions were generated by plotting the average and total spectra levels at the measurement locations on the ICD. An interpolation scheme was then used to estimate distributions over the ICD. An example for the BPF total spectrum level is shown in Figure 170. Note that the BPF tone SPLs can change dramatically on the surface of the ICD. These differences in level are caused by the interference pattern of the sound as it propagates through the inlet onto the ICD.

Figure 171 shows the same ICD SPL distributions with pulse-synchronized averaged spectra. Note that the valleys are lower because the pulse-synchronized averaged data only includes energy that is deterministic.

3.3.4.2   Accell SPL Distributions

Acceleration data was acquired for several configurations during the testing to compare with steady-state data and to provide more engine operating power points for tone data. These data were acquired by running the engine from N1C = 1600 rpm to N1C = 2700 rpm in 40 sec.

Figure 172 shows the acceleration data for 10 averages for a subsonic tip speed. Note that the acceleration data matches the steady state data very well. Therefore, acceleration data can be used to obtain data at any engine power point without the need to stabilize the engine at that power point and sample over a finite time interval.

3.3.4.3   Spinning and Radial Modes

The primary purpose of the ICD array was to measure the spinning and radial inlet source modes. For this type of processing, pulse synchronized averaged data was used to determine the relative amplitudes and phases of the BPF and BPF harmonics at each transducer location on the ICD.

The Boeing CDUCT propagation code was used to propagate each cut-on mode through the inlet and to the ICD transducer locations in order to predict the pressure magnitude and phase. These data are normalized by their L2-norm and represent the "steering vectors" used for the modal decomposition.

The transducer locations were selected in such a way that the steering vectors were as normal to each other as possible. This can be shown by pre-multiplying the matrix of steering vectors by the complex conjugate transpose of the matrix of steering vectors. Each row of the resulting matrix is normalized such that the diagonal is 0 dB. Figure 173 shows an example orthogonality plot for 1800 N1C at BPF. This plot gives an indication of the signal-to-noise ratio (SNR) capabilities of the array and how well the different modes can be distinguished from each other. The displayed value in each square is taken from the lower left corner in this "corner" contour plot. At BPF for 1800N1C, there are 33 cut-on circumferential modes at the first radial, 23 modes at the second radial, 17 modes at the third radial, 11 modes at the fourth radial, and 7 modes at the fifth radial which corresponds to index numbers 1 to 33, 34 to 56, 57 to 73, 74 to 84, and 85 to 91, respectively. For a perfect ICD array, the off-diagonal terms will be very small. From the example orthogonality plot, the SNR of the ICD array design is 9 dB or greater for circumferential modes. In general, the SNR is approximately 4dB between the first and second radials and fourth and fifth radials. However, the SNR drops to 1.4 dB at certain circumferential modes (m = –11 or 11).

3.3.5   Olsen Ring Array Spinning Mode Charts

The ring array pressure signals can be used to generate mode charts by applying a discrete Fourier transform (DFT) in both frequency and space (or angular position). The resulting spectra separate the pressure signals into frequencies and acoustic spinning modes. Figure 174 shows an example of a typical mode plot for the production inlet at 1800 N1C. The ordinate shows the frequency, and the abscissa contains the spinning orders or m-orders. Several horizontal lines are noticeable representing the BPF and harmonics. There is a measured BPF tone at approximately 620 Hz, although it is theoretically cut-off at this low operating condition.

Modes near cut-off propagate down the duct very slowly and give increased pressure amplitudes at the wall transducers. This phenomenon generates a "V" in the plot which originates at the m = 0 mode at

zero frequency. Cut-off for this particular figure at the BPF is at m = 16. Another artifact of the data is the preponderance of co-rotating modes for the broadband noise. This is consistent with earlier work of Joppa (Ref. 3).

3.4   Boeing Hardware

3.4.1   Boeing Scarf Inlet with Bellmouth Lip

The Boeing scarf inlet was first tested during Phase 1 of the PW4098 EVNRC testing (Ref. 1). Although the significant acoustic benefits of the scarf inlet with complete coverage of triple layer acoustic treatment were demonstrated by this test, certain unexpected results showing higher noise levels than expected were observed. These were: higher BPF and 2BPF tone levels than for the production inlet at the subsonic fan tip speed conditions, higher buzz noise for the "hardwalled" scarf inlet than for the "hardwalled" production inlet at the cutback power condition, and high frequency acoustic lining attenuation falling off monotonically as engine power increased. As a result of the Phase 1b diagnostic testing, utilizing blade mounted microphones and a circular ring array of microphones at the engine "A" flange, it was concluded the scarf inlet with the flight lip was giving rise to unsteady flow separation even at low engine power conditions (Ref. 1). The length scales of the resulting flow distortions entering the fan were such as to cause the fan to generate BPF and 2BPF tones very similar to what occurs when an engine is run statically without an ICD for dissipating atmospheric eddies.

Estimated inlet wall Mach number profiles for the scarf inlet operating statically with the flight lip are shown in Figure 175. As a result of the Phase 1 test results, it was decided to build and install a bellmouth lip on the scarf inlet for the Phase 2 test. Figure 176 shows a schematic of the bellmouth lip shape compared to the flight lip. Figure 177 shows a photo of the resulting bellmouth. It is seen that significant reduction of the peak wall Mach numbers were expected with the bellmouth lip such that there was confidence that there would be no flow separation for the scarf inlet with the bellmouth lip during static noise testing.

3.5   Measurement Results and Discussion

Olsen Ring and ICD data were acquired for the configurations shown Table 7. These configurations include three configurations for the Active Noise testing, one configuration where the active drivers were run without the engine operating, and four configurations for the EVNRC test.

TABLE 7.—TEST CONFIGURATIONS FOR OLSEN RING AND ICD DATA

Configuration	Date	Run	Description
NG1	07/28/01	16114	BOM Trt inlet, NG ANC Active HW, Passive HW, 22B/28V, Trt T/p, No Walls
NG2	08/04/01	16115	BOM Trt inlet, NG ANC Act-Trt Pass, 22B/28V, Trt T/p, No Walls
	08/07/01	Active	BOM Trt inlet, NG ANC, Active Control on at Static Engine
NG3	08/08/01	16116	BOM Trt inlet, NG ANC, Trt Act-HW Pass, 22B/28V,Trt T/p, ICD, No Walls
EVNRC1	08/10/01	16117	BOM Trtd inlet, HW BFG R2 Spool, 22B/28V, TrTrt T/P, ICD, no Walls, Baseline
EVNRC2	08/21/01	16118	BOM Trtd inlet, HW BFG R2 Spool, 24B/28V, TrTrt T/P, ICD, no Walls
EVNRC3	08/22/01	16119	BOM Trtd inlet, HW BFG R2 Spool, 24B/28V, TrTrt T/P, ICD, Walls
EVNRC4	08/27/01	16120	Scarf HW inlet, HW BFG R2 Spool, 24B/60V, TrTrt T/P, ICD, Walls

A list of the data taken for each configuration is included in Appendix B. The EVNRC and NG/HAE Active Noise test operated the engine at different corrected powers than those used for the EVNRC testing which reduced the ability to compare these configurations. A standard power line was defined for the EVNRC configurations and tested for each condition. In addition, an acceleration condition was also recorded for each EVNRC configuration except the first. The operating points acquired for the ENVRC mode data are shown in Table 8. The only point in common with the NG/HAE Active Noise testing was at 1800 rpm.

TABLE 8.—DATA ACQUISITION OPERATING
POINTS FOR THE EVNRC DATA

Point	N1C	Description
1	1620	Lowest power
2	1800	Low approach
3	2000	Approach
4	2200	Low cutback
5	2450	High cutback
6	2700	Full power
7	accel	40 sec acceleration

3.5.1 Olsen Ring Array

The Olsen Ring array was added to the test with the addition of work statement supporting the m = 22 active control. Active control of the rotor-locked, m = 22 mode with 24 pairs of speakers in a ring could have led to increased levels in the m = –2 mode. The Olsen Ring array, by virtue of its regular spacing, has improved signal to noise ratio (SNR) over the ICD array for measuring spinning modes. This allows the Olsen ring to measure spinning modes when other spinning orders of appreciable level are present.

3.5.1.1 Olsen Ring Array—Active Noise Control Test

The first engine configuration tested (NG1) with the Olsen Ring consisted of 22 fan blades and 28 exit guide vanes with the active transducers and fan case liner completely hardwall (HW) taped. Unfortunately, none of the three tachometers were recorded for this configuration due to a wiring problem. This prevented any pulse-synchronized resampling of the data. However, conventional analysis of the non-resampled data could still be performed and a plot of the modal decomposition of the data is shown in Figure 178. This plot shows the SPL level as a function of spinning mode number and frequency as discussed in Section 3.3, Data Processing.

The active noise system was setup to control a strong m = –6 mode from the cut-on rotor/stator design. The rotor/stator design consisted of 22 blades and 28 vanes which results in an expected m = 22 – 28 = –6 mode. Unfortunately, this combination of the rotor and stators did not generate a strong m = –6 tone. In Figure 178 the BPF is at approximately 670 Hz and a dominating m = –6 mode is not observed. However, the 2xBPF interaction of the rotor and stator at m = 2 × 22 – 28 = 16 is clearly apparent in the data and dominates the 2xBPF frequency in level. Figure 179 shows the BPF line of the contour plot on an XY plot. Again the m = –6 is not dominating in this plot. Instead, the modes near m = ±15 dominate. Recall that modes near cutoff dominate these wall measured mode results and that the measurements do not correspond directly to radiated modal energies. Note also, some HW tape came off near the fan during this test which could cause mode scattering, but it was unknown how early in the run that this happened.

The second configuration (NG2) uncovered the passive liner section near the fan, but left the active noise Helmholtz transducers covered. The passive liner was designed to attenuate the cut-on BPF to levels that could be controlled. Unfortunately, this liner was made of wire mesh and was clogged with tape promoter. The promoter partially blocked the liner in places, which creates random impedance near the fan. Comparison of the curves in Figure 180 shows that these impedance discontinuities greatly increased the wall SPL at the mode ring. Note that the levels at BPF are on the order of 10 dB greater for certain spinning orders.

These data show the potentially large BPF SPL effect that impedance discontinuities near the fan can cause. Some work was done to remove the promoter from the lining. However, these attempts failed and it was decided that the forward fan case passive liner section would be hardwalled for future runs by applying a polyurethane coating to the wire mesh.

A test of the active control Helmholtz transducers was attempted without the engine running. This configuration had foam over the blades to absorb back-reflected energy. Unfortunately, the active

Helmholtz transducer's power supply started to have a problem at this point in the test. The power supply could only drive one of the four rows of transducers. A single data point was acquired with the transducers operating for Row D and is shown in Figure 181.

These data show that the single row of transducers was very successful in generating the target, m = –6, mode and that little m = 18 energy was generated. The output levels at the mode ring were on the order of 110 dB at 651 Hz for the m = –6 spinning order. This is considered a successful demonstration of the drivers, although it does not demonstrate the performance of the active noise control system.

The last active noise configuration, NG3, consisted of the hardwalled forward fan case passive liner and uncovered active noise driver section with the screen over each hole in the Helmholtz resonators cut out. Data for this configuration showed a very strong m = –2 mode which was probably due to the 22 blade direct rotor field interacting with the 24 sets of transducers as seen in Figure 180.

3.5.1.2   Olsen Ring Array—ENVRC Test

The first configuration for the EVNRC portion of testing, called EVNRC1, consisted of a hardwall production fan case instead of the longer active noise hardware of the before mentioned configurations. Figure 182 shows the mode plot for this configuration at the lowest engine power at the BPF. Note that the cuton, m = –6, mode is still not apparent in the data. Figure 183 shows the data for a range of operating conditions.

For the EVNRC2 configuration, a 24-blade fan replaced the 22-blade fan with the 28-vane stator set. A comparison of the mode plots for the EVNRC1 and EVNRC2 configurations is shown in Figure 184. Note that the levels at the "Olsen ring" are basically equivalent at BPF for these configurations. However, the rotor/stator interaction at, m = 24 – 28 = –4, is now apparent, but is not dominant.

Configuration EVNRC3 was a repeat of EVNRC2 except for the addition of aft noise barriers. Figure 185 shows a comparison of these two configurations at the lowest power. Note that the addition of the barriers did not change the in-duct measured modes appreciably. Of course, one would not expect the modes to change with the addition of the walls.

The final configuration for which mode data was acquired was EVNRC4. This configuration had the Boeing Scarf Inlet attached instead of the production inlet. The results for this testing are discussed below with the other scarf inlet results.

3.5.2   ICD Array

3.5.2.1   Active Noise Test Spinning and Radial Mode Estimates

Spinning and radial mode estimates at the blade-passage-frequency (BPF) were made with the ICD array for the Active Noise Control configurations at several power settings. The first configuration (NG1) consisted of taped hardwall active segment liner and passive liner sections. Unfortunately, no tachometer signal was recorded due to a data cabling error and therefore the standard data processing was not possible.

The second configuration (NG2) consisted of the tape being removed from the passive liner section. Figure 186 to Figure 194 show the ICD mode plots at different power settings where the integer symbols represent the radial modes and the T-symbol represents the total log-sum of the radial modes at each spinning mode. Note that only propagating modes are accounted for in the ICD data processing. The ICD mode plots do not show the expected dominant m = –6 mode (predicted from standard Tyler-Sofrin theory with a 22 blades/28 vanes cut-on design). This result is consistent with the Olsen ring array which also does not show a dominant m = –6 mode (Figure 180). It is likely that the rotation of the fan reflects a large portion of the energy in the counter-rotating m = –6 towards the aft. It was also discovered during inspection of the passive liner that the wire mesh was non-uniformly blocked with tape adhesive and/or adhesive promoter. This non-uniform impedance in the forward fan-case greatly increases the BPF levels due to scattering of the rotor locked field and also gives rise to a somewhat random distribution of modes. All attempts to clean the wire mesh failed. There were several repeat power settings; three of which were processed (Figure 192 to Figure 194). In general, the mode distributions for the repeat power settings are

similar to the first set of results. There are some differences that may be explained by the fact that tape was coming off at several locations on the active noise liner section, which may cause modal scattering. It is also observed that the mode distribution is generally skewed toward co-rotating positive spinning modes.

It was discovered that the active noise control system was not operating properly, possibly due to humidity related malfunction of the amplifier/power supply system. The third data set acquired tested the active noise drivers in an engine-off configuration. Since the face sheet covering in the duct segment containing the active control drivers was also non-uniformly blocked with tape adhesive and/or adhesive promoter, the wire mesh covering the Active Helmholtz Resonator (AHR) portholes were cut out. The forward fan case passive liner section was made uniformly hardwall with several coats of liquid polyurethane. Figure 195 shows a layer of Sonex foam, which was attached to the fan blades in order to minimize scattering of the sound radiating from the active noise drivers. One row of active noise drivers was activated with an input spinning mode of $m = -6$ at a normalized frequency of 640 Hz. Data from the ICD and Olsen ring arrays was acquired. Figure 196 shows the ICD mode results which indicates a strong $m = -6$ mode. This is consistent with the Olsen ring array which also shows a strong $m = -6$ (Figure 181).

The third configuration (NG3, active noise port holes cut out, uniform hardwall passive liner) was tested in order to provide a baseline even though the malfunctioning active noise control system was not immediately repairable. This configuration allows the possibility of testing the active noise control system with the compromise that flow over the exposed portholes may cause distortions into the fan. Figure 197 to Figure 202 show the ICD mode plots for all the tested power settings except idle. The ring data are shown in Appendix C for these same power settings. The first three power settings (N1C 1745, 1800, 1909) show a strong $m = -2$ mode. The next two power settings (N1C 2045 and 2182) show a strong $m = -3$ and $m = -4$, respectively. The highest power setting (N1C 2318) once again shows a strong $m = -2$ mode. The Olsen ring array also shows the presence of the $m = -2$ mode, which dominates for all power settings. The source of the $m = -2$ mode is believed to be the interaction of the 22 fan blade pressure field with 24 discontinuities. The likely source of discontinuities is that there are 24 hardwall sections between the 24 active noise control drivers. An impedance discontinuity was created when the tape was removed from the active noise control drivers and the mesh covering the portholes was removed (Figure 195). The overall levels from the ICD mode results are generally lower for this hardwall passive liner configuration than the previous configuration with the non-uniformly blocked passive liner configuration. This is consistent with the idea that it is desirable to minimize discontinuities in front of the fan. The sources of the $m = -3$ and $m = -4$ modes are not known, though it is noted that the two power settings (N1C 2045 and 2182) result in a near sonic tip speed. It is interesting to observe that as the power setting increases, the Olsen ring array also shows an overall broadening of mode amplitudes slightly negative of the peak at $m = -2$ which suggests that there is an increase in mode power at $m = -3$ and $m = -4$ (see Appendix C). It is speculated that any blade-to-blade variations at a near-sonic tip speed can vary the source due to variations in shock structure emanating from the blades. In general, the ICD mode results are consistent with the Olsen ring array results, except as noted.

3.5.2.2   EVNRC Test Spinning and Radial Mode Estimates

The fourth configuration (EVNRC1) consisted of replacing the active noise control forward fan case with a slightly shorter taped hardwall fan case (BFG R2 spool). Figure 203 to Figure 206 show the ICD mode results for the first four acquired power settings (Points 1,2,4,5). Once again, the ICD mode plots do not show the expected strong $m = -6$ mode from the 22 blades/28 vanes configuration. This result is consistent with the Olsen ring array which also does not show a dominant $m = -6$ mode (Figure 183). A direct comparison between the ICD and Olsen ring array results at the lowest power setting (N1C 1620) shows some similarities at $m = -12, -3, 3, 9, 13$ though it is difficult to interpret since the Olsen ring array only indicates wall pressures which may emphasize modes which are closer to cut-off. The sources of the indicated modes are not known. At the highest analyzed power setting (N1C 2455), the ICD array shows a large number of modes. A rotor locked mode ($m = 22$) should be cut-on for the highest analyzed power setting but it is not shown in the ICD mode result (Figure 206).

The fifth configuration (EVNRC2) consisted of replacing the 22-blade fan with a 24-blade fan. Figure 207 to Figure 211 show the ICD mode results for the first five power settings above idle (Points 1 to 5). At the lowest power setting (N1C 1620), the ICD mode plot shows the expected spinning mode $m = -4$ and an unexpected $m = 4$ mode along with a peak at $m = 0$. The Olsen ring array also shows peaks at $m = -4, 0,$ and 4 though the levels indicate that the $m = -4$ mode is not as strong as expected (Figure 184). It is likely that the transmission through the fan is not very efficient for the $m = -4$ mode. It is speculated that the $m = 4$ mode is a result of an interaction between the 24-blades/28-vanes and 9 struts. The struts are arranged at the following clock angles: 0°, 45°, 90°, 135°, 165°, 195°, 225°, 270°, and 315°. This arrangement results in primarily an eight interaction since the struts are essentially spaced as if there are eight struts where the strut at 180 has been replaced with the struts at 165 and 195. The $m = -4$ mode interacts with the essentially eight struts and produces an $m = 4$ mode which can propagate forward through the fan. At N1C = 1800, the ICD mode plot shows a strong $m = 4$ and weaker modes at $m = -9$ and $m = -4$. The Olsen ring array results, from Appendix C, show peaks at $m = -4$ and 4 though there are several additional peaks at $m = -8, 6, 9, 11$ that are not consistent with the ICD mode results. These additional peaks may be a result of only wall pressures being measured. At higher power settings, the ICD and Olsen ring results are not very consistent.

The sixth configuration (EVNRC3) was the same as the fifth except that the aft barrier walls were installed. The ICD penetration depth was slightly less to accommodate the ICD septum wall. Figure 212 through Figure 216 show the ICD mode results for the first five power settings above idle (Points 1 to 5). The results are similar to those from the fifth configuration. The presence of the aft barrier walls does affect the measurements at the ICD, which will be discussed in the next section. At N1C = 1620, the ICD mode plot shows the $m = -9, -4,$ and 4 modes which are consistent with peaks in the corresponding Olsen ring array results (Figure 185). At higher power settings, the ICD and Olsen ring results are not very consistent.

The ICD mode data from the scarf inlet testing (EVNRC4) is discussed below in the section on the scarf inlet.

3.5.2.3   ICD SPL Distributions

An unstructured mesh whose nodes are the locations of the 199 ICD Kulite sensors was created in order to show the SPL spatial distribution on the ICD at a given frequency. Figure 217 and Figure 218 show the SPL distribution at frequencies without a tone (1008 and 5904 Hz, respectively) for configuration EVNRC3, Run 11907 (N1C = 1800). The unstructured mesh is shown as black triangles and every intersection (node) corresponds to the location of a Kulite. The high levels near the bottom of the ICD correspond to a ground reflection. In general, the azimuthal variation around the ICD is small for these broadband frequencies. For the same configuration and run, Figure 219 and Figure 220 show the SPL distribution at BPF and 2BPF, respectively. It is observed that the azimuthal variation for these tones is quite large. At 2BPF, the SPL on the side closest to the farfield polar microphones are larger than on the opposite side. Figure 221 shows the SPL distribution at 2528 Hz, which corresponds to the difference tone of the second harmonic of the first stage low-pressure compressor (LPC) and the first harmonic of the fan. It is interesting to note the strong circular band of SPL contours at the most forward angle (around the area of no data) that indicates a strongly cut-on mode. The SPL on the side closest to the farfield polar microphones are larger than on the opposite side. Furthermore, the pattern of SPL contours on the side of the ICD closest to the farfield polar microphones suggests the existence of additional radial modes. Figure 222 shows the SPL distribution at 2800 Hz, which corresponds to the first harmonic of the second stage LPC. The prominent circular band of SPL contours indicates a strongly cut-on spinning mode with a minimum of radial modes. The interference pattern in the circular band indicates the presence of several spinning modes, though the dominant spinning mode is likely an $m = 7$ which is obtained from the LPC blade counts. Figure 223 shows the SPL distribution at 4752 Hz, which corresponds to the sum tone of the second harmonic of the first stage LPC and the second harmonic of the fan. The prominent band of SPL contours around the bottom of the ICD indicates the presence of a strongly cut-on mode, and the

interference of additional modes cause the break-up of the circular SPL pattern on the top of the ICD. It is noted that the shape of the contours can be greatly affected by the interpolation between data points.

A preliminary method of projecting the ICD data to the farfield polar microphones has been developed. Figure 224 shows the ICD data relative to the farfield microphones. Straight lines connect an assumed source point location at the inlet hilite plane to the farfield microphones. Figure 225 shows a magnified view of the ICD data. At the intersection of each line with the ICD data, the SPL is projected to the corresponding farfield microphone by correcting for spherical divergence and atmospheric absorption. Figure 226 shows the comparison of the farfield narrowband spectra data and the projected ICD data at a few angles for configuration EVNRC3, Run 11907 (N1C = 1800). The assumed source point location is at the inlet hilite plane on the engine axis. At low frequencies the farfield data appears to contain jet noise (despite the presence of the aft barrier walls), which the ICD array does not show. At larger angles the projected ICD data over predicts the farfield levels. In general, the projected ICD data is within 8 dB of the farfield data. Figure 227 and Figure 228 show the directivity comparison for two frequencies without tones (1008 and 5904 Hz, respectively). At these two frequencies, the error is within 3 or 4 dB. Figure 229 shows the directivity comparison for BPF = 736 Hz. The assumed source point has been moved 50 in. in the positive Y-direction from the engine axis at the inlet hilite plane in order to match the location of the first peak at 30°. The error in the projected ICD data is fairly large (up to 8 dB at some angles). Furthermore, the projected ICD data misses the location of the second peak by 5°. Figure 230 shows the directivity comparison for 2BPF = 1472 Hz. The assumed source point has been moved 40 in. in the negative Y-direction from the engine axis at the inlet hilite plane in order to match the location of the first peak at 30°. The error in the projected ICD data is in the range of 3 to 5 dB. It is noted that wind and atmospheric turbulence are not accounted for in this current method of projecting the ICD data to the farfield. It is also noted that the data at the point of intersection on the ICD relies on interpolation and the density of Kulite sensors. In general, the projected ICD data compares favorably with the farfield data taking into account the simplistic nature of the projection method.

In order to explore the effect of the aft barrier walls on the ICD data, the SPL difference for the ICD data between Configuration EVNRC2 (Run 11810) and EVNRC3 (Run 11907) at a frequency of 208 Hz is shown in Figure 231. On the side closest to the farfield microphones, the difference between the configurations is minimal. However, on the side of the ICD facing away from the farfield microphones, the difference is significant. Figure 232 shows a spectral comparison at a Kulite located on the side facing away from the farfield microphones. It is observed that the low frequencies increase with the presence of the walls on the side facing away from the farfield microphones. Figure 233 shows a spectral comparison at a Kulite located on the top of the ICD, which shows a large increase in frequencies below BPF with the presence of the walls. It is speculated that aft noise is being reflected off the aft barrier walls, and it affects the ICD Kulites located on top and to the unshielded side of the ICD.

Figure 234 shows the ICD SPL distribution for the third data set, which tested the active noise drivers at a normalized frequency of 640Hz in an engine-off configuration. It is observed that despite the strong m = –6 mode (Figure 181 from mode ring and Figure 196) the SPL distribution does not exhibit any dominant circular band, which would occur for a single dominant mode. The observed SPL pattern is a result of the interference of the dominant mode along with other modes.

The amplitude and phase of each mode is determined from the ICD array modal analysis. This data can be re-combined with the CDUCT calculated steering vectors to generate a synthesized complex pressure distribution on the ICD. A comparison of the synthesized pressure to the synchronized Kulite data can give an indication of the error in the steering vector calculations. Figure 235 shows the comparison of the synthesized real part of the pressure to the real part of the pressure from the synchronized data for the active noise engine-off configuration. Figure 236 and Figure 237 show the magnitude of the complex pressure for the synthesized data and the synchronized data from two different viewing angles. The locations of the higher level red contours in the far forward angle (near white pentagon) compare favorably. In general the red contour levels do not compare well at higher angles. This result is consistent with the small-angle approximation in the CDUCT propagation code (Ref. 4), which is accurate at small angles and possesses phase errors at higher angles. The array design also leads to errors in these

comparisons since modal energy may spill over into other modes and the existence of extraneous modes are not properly accounted for in the synthesized pressures. Essentially, the current ICD modal analysis does not perfectly decompose the sound field into spinning and radial modes, though it still does detect dominant spinning modes. Improvements to the steering vector calculations should improve the accuracy of the modal analysis.

3.5.3   Scarf Inlet

3.5.3.1   Measured Versus Expected Wall Mach Numbers

Static pressure taps were located on the scarf inlet crown in the throat region to verify the expected bellmouth lip flow Mach numbers. Figure 175 shows the resulting measured wall Mach number data compared the pre-test predictions for the bellmouth lip and for the flight lip used for the Phase 1 testing. This comparison is shown for the approach condition only because no test data was measured for the cutback and higher conditions. It is clear that the desired reduction of lip wall Mach numbers was obtained with the bellmouth.

3.5.3.2   Inlet Delamination

As stated above no test data was measured for the cutback and higher engine power conditions. Because of a severe delamination of the inlet acoustic panel, acoustic data was only obtained for five test conditions for the full hardwall configuration. No data was obtained for the scarf inlet with the acoustic treatment exposed. The delamination was due to failure of the face sheet bond to the honeycomb core. Small areas of delamination had been observed after the Phase 1 testing but were judged not to be a problem. With hindsight it is now believed that the "room temperature" adhesive used for manufacturing the scarf inlet did not result in a lasting bond. High temperature adhesives are used for flight worthy production inlets but the tooling approach used to manufacture the ground test scarf inlet would not allow for the high temperature curing process needed for these adhesives. The Phase 1 and 1b testing cycles apparently were the limit for the scarf structure. Some photos of the resulting delamination are shown in Figure 238 and Figure 239.

3.5.3.3   Farfield BPF Comparisons to Previous Data

Figure 240 to Figure 244 show 1/3 octave spectra comparisons of the hardwall scarf inlet with the bellmouth lip data from the Phase 2 test with hardwall scarf inlet and production inlet data from the Phase 1 testing. These plots are for 150 ft polar arc and the data is corrected to free field by subtracting 6 dB from each 1/3 octave SPL. Data is shown for the five engine power conditions tested from nominal N1C of 1600 to 2000 rpm, respectively. Another view of the same data, showing 1/3 octave SPL directivities for selected frequency bands is shown in Figure 245 to Figure 249. A number of observations are made from the directivity plots.

- The lower frequency broadband inlet fan noise, as represented by band 26 (400 Hz) shown in Figure 245, was unaffected by the changing the scarf inlet lip. The shielding effect of the scarf inlet relative to the production inlet is clearly seen at band 26.
- The BPF and 2BPF 1/3 octave band SPLs were significantly lowered with the bellmouth lip on the scarf inlet relative to the flight lip as shown in Figure 246 and Figure 247. When compared to the production inlet data the shielding effect of the scarf inlet is clearly seen with the scarf bellmouth lip data for these frequency bands as well.
- For higher frequency bands, represented by Figure 248 and Figure 249 for bands 34 and 37, the scarf effect appears to be enhanced with the bellmouth lip compared to the flight lip. There was a slight increase in scarf angle (13.2° versus 13°) and inlet length (7 in.) with the bellmouth lip, which may account for the increased shielding although these changes seem fairly small. There was an expectation that the bellmouth lip would tend to focus sound to forward angles and therefore reduce the levels at the higher angles (90°) relative the flight lip levels. While there is a

reduction at the higher angles as stated above, the concurrent increase in levels at the lower angles (40°) is not seen in the data.

3.5.3.4 Olsen Ring Spinning Mode Measurements

Only three operating power points were acquired with the Olsen ring and ICD arrays for the scarf inlet configuration before vibration problems ended running and delamination in the inlet left the inlet unusable. Figure 250 compares the Olsen ring BPF mode data for the production and scarf inlets with 24 blades at the lowest operating condition. These data show that the production and scarf inlets have very similar, but slightly different BPF levels at propagating spinning modes. Small differences in boundary layer thickness or circumferential differences in Mach number are likely causes for the small differences.

3.5.3.5 ICD Array Spinning and Radial Modes Measurements

The ICD mode plots for the hardwall scarf inlet configuration are shown in Figure 251 to Figure 253 for power setting points 1, 2, 3. This configuration has a more conventional "cut-off" fan stage design with 24-blades/60-vanes. At N1C = 1620, the strongest mode is at m = 8 which is not clearly observed in the Olsen ring array results (Figure 250). The source of the m = 8 is not known. At N1C = 1800, the ICD mode plot shows peaks at m = –13, –11, –7, 0, 1, 10, 15, 17. There are some similar peaks in the Olsen ring array results, especially at m = –7 and 17. At the highest power setting (N1C = 2000), shown in Appendix C, the ICD mode plot does not indicate a dominant mode. The m = 9 peak does correspond to a large peak in the Olsen ring array results.

3.5.3.6 ICD Array SPL Distribution

The SPL contours on the ICD for the production inlet (EVNRC3) and the scarf inlet (EVNRC4) are compared in Figure 254 at N1C = 1800 and a frequency of 5440 Hz. The scarf shielding effect can be clearly observed by the location of the lower level blue contours. It is interesting to note that the higher level red contours are angled in such a manner that is consistent with the inlet geometry. The production inlet beams noise toward the keel side while the scarf inlet beams noise toward the crown side. Only one frequency is shown, but the results are similar at frequencies higher than 1000 Hz. Note that for the production inlet, a ground reflection effect is observed for some Kulites on the keel side. The scarf inlet was tested with the keel pointed toward the farfield polar arc microphones and therefore the Kulites affected by the ground are located on the opposite side of the figure.

4.0   Conclusions and Recommendations

4.1   P&W Conclusions

Eight configurations were planned under the Engine Validation Noise Reduction Concept (EVNRC) Phase 2 program. Due to a hardware problem, Boeing's treated scarf inlet was not tested. Therefore, seven of the eight planned configurations were tested. All configurations are shown in Table 3.

A detailed analysis was conducted for the six configurations that were tested with the current production inlet. Of these six, two configurations were tested with aft walls installed on the test stand in order to block aft radiated noise from contaminating the inlet. The data for the two configurations that were tested with aft walls were compared to the same engine configuration tested without aft walls, in order to evaluate the validity of Pratt & Whitney's noise component source separation routine. The conclusion of Appendix D, confirms that Pratt & Whitney's source separation routine is doing a good job of separating inlet, and aft, radiated noise. Appendix E is dedicated to engine component noise sensitivity studies. This is the study of Total EPNL change as a result of engine component noise level changes. The result of this study revealed that the inlet broadband noise was most influential on Total EPNL at the approach condition for all engine configurations. Aft broadband noise at the cutback and sideline condition was the most influential on Total EPNL, with the exception of the "cuton" configuration. The

"cuton" configuration aft fan tones (primarily the cuton BPF tone) were more influential on Total EPNL than aft broadband.

From Table 3, it can be seen that noise data was acquired for three engine hardware changes. These consisted of a change in the number of fan blades and FEGVs, as well as the incorporation of acoustic treatment located in the tailpipe, tuned to attenuate low-pressure turbine noise. The results have been presented for both Static, and in-flight noise for two configurations at a time, which differed by only one hardware component change. These noise component comparisons have been presented for only the source separated noise component that changed as a result of the hardware change.

Results of the acoustic analysis of the EVNRC Phase 2 data showed that all three hardware changes can be effective in the reduction of the Total aircraft in-flight noise levels. Specifically:

1. The treated primary jet nozzle showed large reductions in turbine noise, sometimes exceeding 10 dB. This resulted in total engine EPNL reductions of 0.75, 0.75 and 0.5 dB for approach, cutback and sideline flight conditions, respectively. The benefits were observed at almost all low pressure turbine rotor speeds. Testing with this treatment provided more confidence that fan noise changes could be quantified when examining noise data from two configurations having different fan or FEGV designs.
2. The 24 fan blade configuration showed a maximum reduction of 1 EPNdB at the sideline condition, and about 0.5 dB at most other fan rotor speeds.
3. The 28 acoustically cut on FEGVs resulted in some fan noise components being reduced, relative to the production 60 vanes, despite the unfavorable spacing between the fan and this vane set. Overall though, the EPNL was increased with the 28 vanes, partly because of this decreased spacing.

4.2   Boeing Conclusions

The ICD and Olsen Ring arrays were shown to give high quality measurements of the inlet noise sources for the PW4098 test engine. The data from both arrays showed very little $m = -6$ BPF tone for the 22 fan blade/28 cuton stator design. These data suggest that the active noise control system would have had little to control since it was designed to target the $m = -6$ BPF tone. The mode and ICD arrays showed that the forward passive liner section that was contaminated with tape adhesive promoter, introducing circumferential wall acoustic impedance discontinuities, generated significant BPF noise. These data were responsible for the decision to hardwall the passive liner section in the active noise actuator ring.

Contamination by the tape adhesive required the face sheet mesh to be cut out from in front of the noise cancellation drivers (configuration NG). The resulting circumferential discontinuities again caused an increase in blade passing frequency noise manifested in a strong $m = -2$ spinning order mode at low and high power settings (22 blades/24 discontinuities). At transonic power settings the $m = -3$ and -4 spinning modes were found to dominate the ICD data for this configuration.

Hardware problems prevented the use the active noise system during the test. Unfortunately, these problems also prevented the acquisition of the "training tone data", which was to be used to improve the ICD array performance. One transducer ring, however, was run at static conditions (engine not running) and showed high levels of the $m = -6$ mode with little energy in the $m = 18$. These data suggest that the actuator rings operated as designed, but did not verify the control system.

The arrays were also used to measure the EVNRC configurations tested after the active noise portion of the test. These configurations included a change in the number of fan blades and stators. The ICD and Olsen Ring instrumentation was able to measure the acoustic differences between these configurations. These measurements showed that the BPF was a combination of modes and was not dominated by a single mode even when the rotor/stator interaction or the direct rotor field was cut on. In general there was not complete agreement between the ICD array mode results and the Olsen ring results. Usually the primary features were similar (peak amplitude modes) but differences in the secondary mode peaks as

well as amplitude differences were often seen. To some degree this was expected since the Olsen ring only measures the wall pressures near the fan, which may emphasize modes that are closer to cut-off.

The mode data showed similar BPF noise levels for the 22 and 24 blade fans with 28 FEGV's with the ICD array indicating that the 24-blade fan was slightly noisier. The energy distribution within the modes showed some significant differences however. Whereas a dominant –6 mode was not observed for the 22-blade/28-vane system the –4 mode was clearly seen for the 24-blade/28-vane system. An $m = +4$ mode was also seen with the 24 blade/28 vane system which may be due to scattering of the –4 mode with the engine strut system which has an $m = 8$ spacing.

The spatial SPL distributions on the ICD showed evidence of contamination from reflection from the ground at the bottom portion of the array. A simulation study showed the effect of this contamination on the modal decomposition to be small. Circular spatial SPL patterns consistent with dominant spinning modes were clearly seen for many tones as were large azimuthal variations presumably due to interactions of two or more spinning modes. An attempt to extrapolate the ICD SPL distribution to the farfield met with limited success when compared to the measured farfield data. The agreement was close enough to suggest refinements in the extrapolation process will eventually be successful but further development is necessary.

The modal decomposition of the ICD data relies on the CDUCT code to supply accurate "steering" vectors, which act as modal basis vectors to decompose the measured data. Since the CDUCT code uses a parabolic approximation to the wave equation, it's accuracy is limited for modes closer to cut off which propagate to higher radiation angles. This reduces the ability to identify these modes and possibly introduces spill over effects into more cut-on modes.

The Boeing Company supplied a scarf inlet with a bellmouth lip for this test. The earlier test of this scarf inlet included a flight lip and was believed to have a partial flow separation problem that generated increased BPF and multiple pure tone noise. Static pressure taps were located on the inlet crown in the throat region to verify the expected bellmouth lip flow Mach numbers. At the lower engine powers, the scarf inlet with the bellmouth lip showed the expected reduction in BPF noise. Unfortunately, no test data was measured for the cutback and higher engine power conditions because of a severe delamination of the inlet acoustic panel. The delamination was due to failure of the face sheet bond to the honeycomb core.

Olsen Ring data show that the production and scarf inlets have very similar, but slightly different levels at propagating spinning modes. Small differences in boundary layer thickness or circumferential differences in Mach number are likely causes for the small differences.

The ICD data clearly show the scarf inlet effect on radiation by showing additional shielding at the keel.

4.3   Boeing Recommendations

Measure steering vectors.

As part of the active noise testing it was planned to use the active noise control system to generate specific modes at frequencies close to engine tones of interest with the engine operating. This would allow measurement of the so-called "steering vectors" for these modes, which could be used to verify the CDUCT calculations. This is still believed to be an important need and should be considered as part of a future engine or fan rig test.

Implement CDUCT wide angle and flow improvements.

It is recognized that the CDUCT calculated steering vectors for higher order modes are incorrect and result in incorrect estimates of the energy contained in these modes with the ICD mode measurement process. For example this may explain the relatively low levels measured for the rotor locked BPF mode ($m = 22$) at supersonic fan tip sped engine powers. It is therefore recommended that enhancements to the CDUCT code to improve the accuracy be defined and implemented. In addition, the current CDUCT code assumes one dimensional "plug" flow. This limitation should be corrected to allow the effects of three-dimensional flow to be evaluated.

Conduct a steering vector study using Eversman code.

Estimates of the CDUCT errors should be determined by comparison of steering vectors calculated with CDUCT and the Eversman code. The Eversman code is an axisymmetric code, whereas the CDUCT analysis used in the current study was a 3D analysis that included the effect of the inlet droop. However steering vectors calculated with CDUCT for the axisymmetric assumption and compared to steering vectors calculated with the Eversman code would give insight into the errors introduced because of the parabolic approximation, plug flow assumption and approximations used for the propagation from the inlet to the ICD. This study should also be used to further understand the relationship of the sound field at the ICD to the sound at the farfield microphones.

Improve ICD array optimization for radial modes.

Future ICD microphone arrays should require better isolation of radial modes. The array for the EVNRC Phase 2 test essentially consisted of equally spaced asymuthal ring arrays optimized for the first radial mode for all cut on BPF spinning modes at subsonic tip speeds for the 22 blade/28 vane fan configuration. More consideration needs to be given to defining an array that better isolates more radial modes. This may require more microphones and/or different polar arc spacing.

Conduct source and propagation studies to understand why in general a large number of modes were observed.

It is unclear why the modal energy was spread over a large range of BPF spinning modes for the Phase 2 test configurations. Many modes not attributable to blade/vane interactions, scattering from known circumferential discontinuities or 3D effects such and inlet droop were observed. It may be that CDUCT deficiencies result in more scattering effects than predicted. Also inflow distortions observed during the Phase 1b diagnostic testing with blade-mounted transducers may be responsible. Fan noise generation and propagation studies using the measured inflow distortion data with a fan distortion noise code together with a linearized Euler CAA code to account for 3D inlet geometry and flow effects are needed to understand these results.

Fix scarf inlet and retest.

Because of the scarf inlet face sheet delamination structural failure, data was not measured for the transonic and supersonic fan tip speeds for the hardwall scarf inlet configuration and for any engine conditions for the acoustically treated scarf inlet configuration. As a result it was not determined if the bellmouth lip resulted in lower buzzsaw noise as expected or increased the high frequency lining attenuation at higher engine power conditions. This data is very important for verifying the noise benefits of the scarf inlet at takeoff power conditions. It is therefore recommended that the scarf inlet be repaired and retested on the PW4098 engine. It was estimated that the cost to repair the scarf inlet would be fairly modest at about 1/10 the original cost to construct it. The engine test could also incorporate a refined ICD array designed with the improved CDUCT code recommended above and an active control system tuned for the –4 spinning mode which was observed with the 24 fan blade/28 vane system. This would also allow direct measurement of the $m = -4$ steering vector as described above.

5.0 Figures
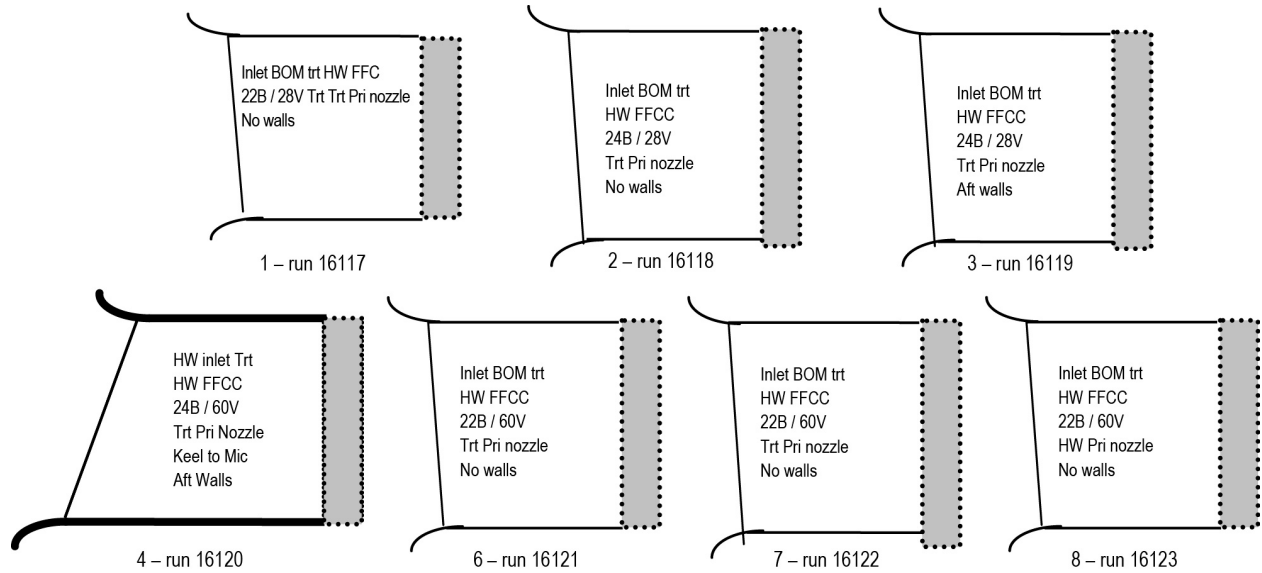
Figure 1.—EVNRC—Phase 2 inlet configuration diagrams.
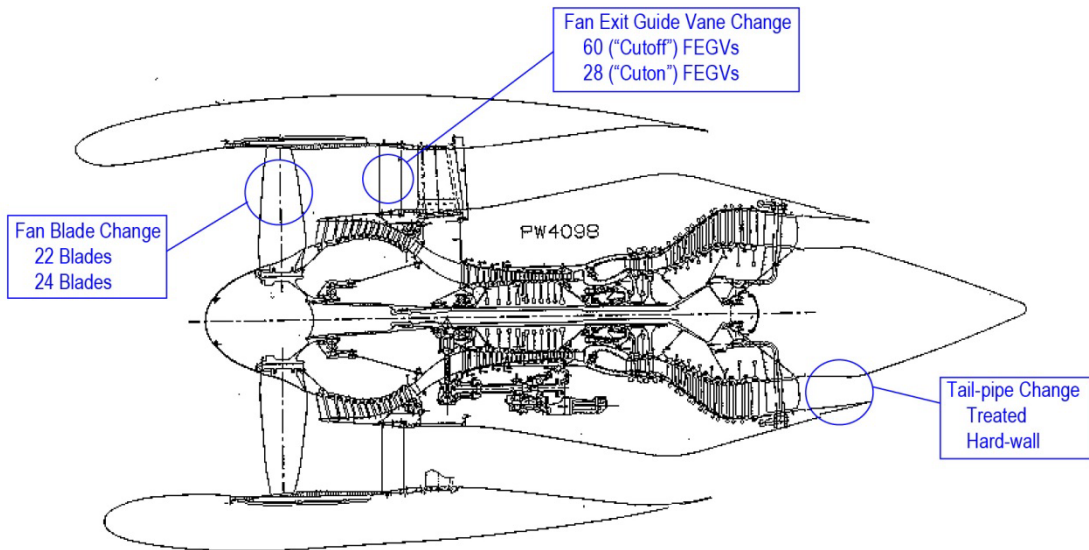
Figure 2.—Schematic of PW4098 showing Phase 2 noise reduction concepts.
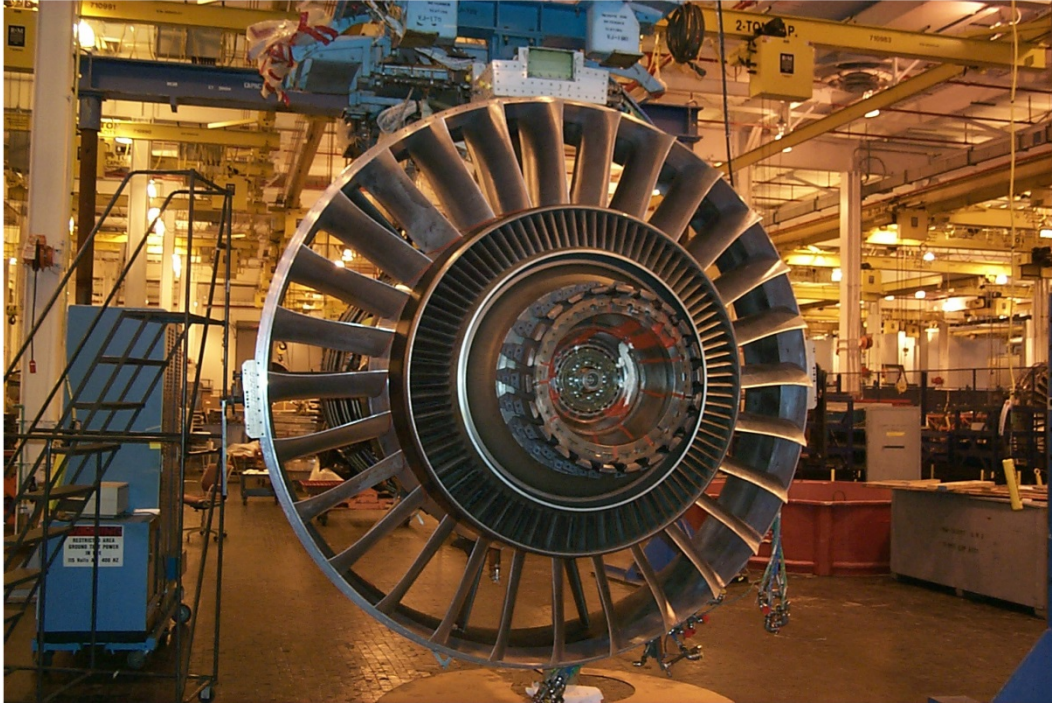
Figure 3.—The 28 vane FEGV assembly.

Figure 4.—The 28 vane FEGV with outer case.

FFCC Treatment

RFCC Treatment

60 Vanes nonstructural

113-in. diameter

22 blades

Acoustic operating points:
Approach: 871 fps
Cutback: 1256 fps
Sideline: 1409 fps
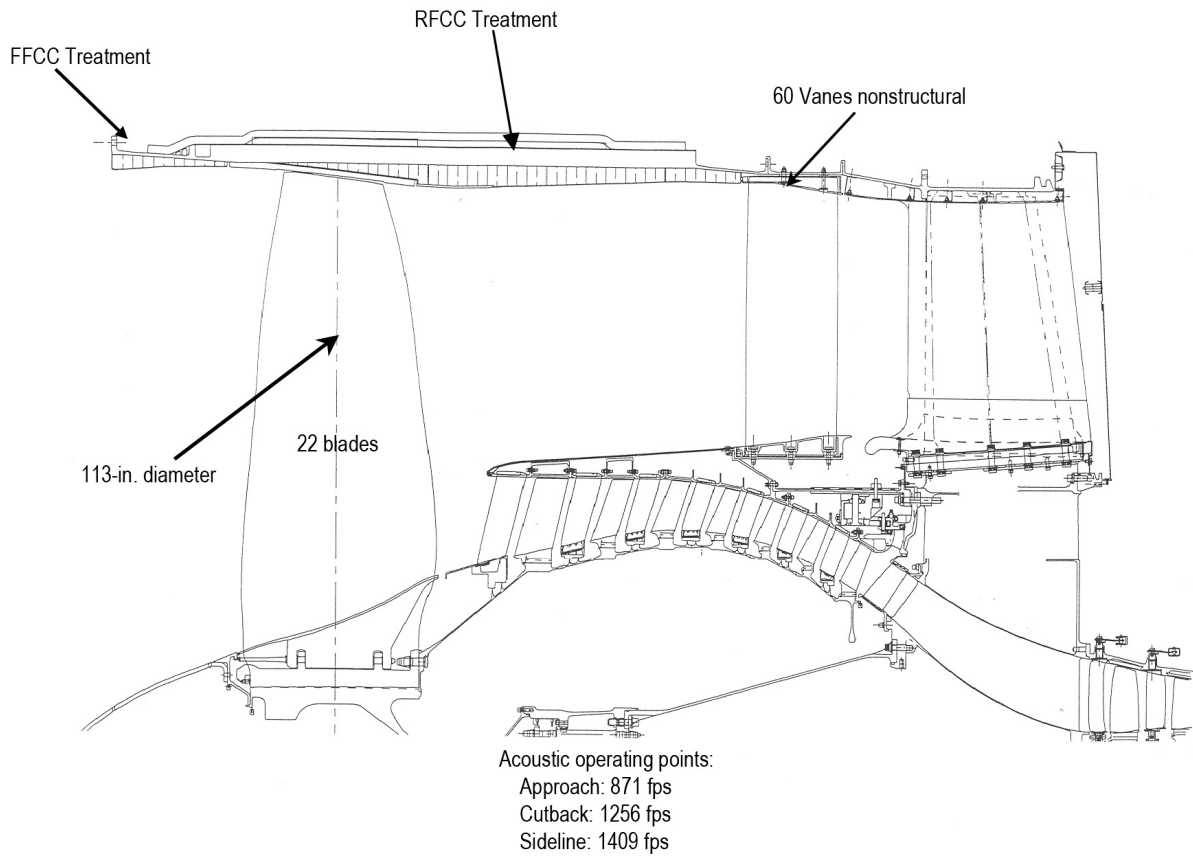
Figure 5.—Bill of material fan section.

Vane solidity must
be kept constant

Vane t.e. root cannot be moved
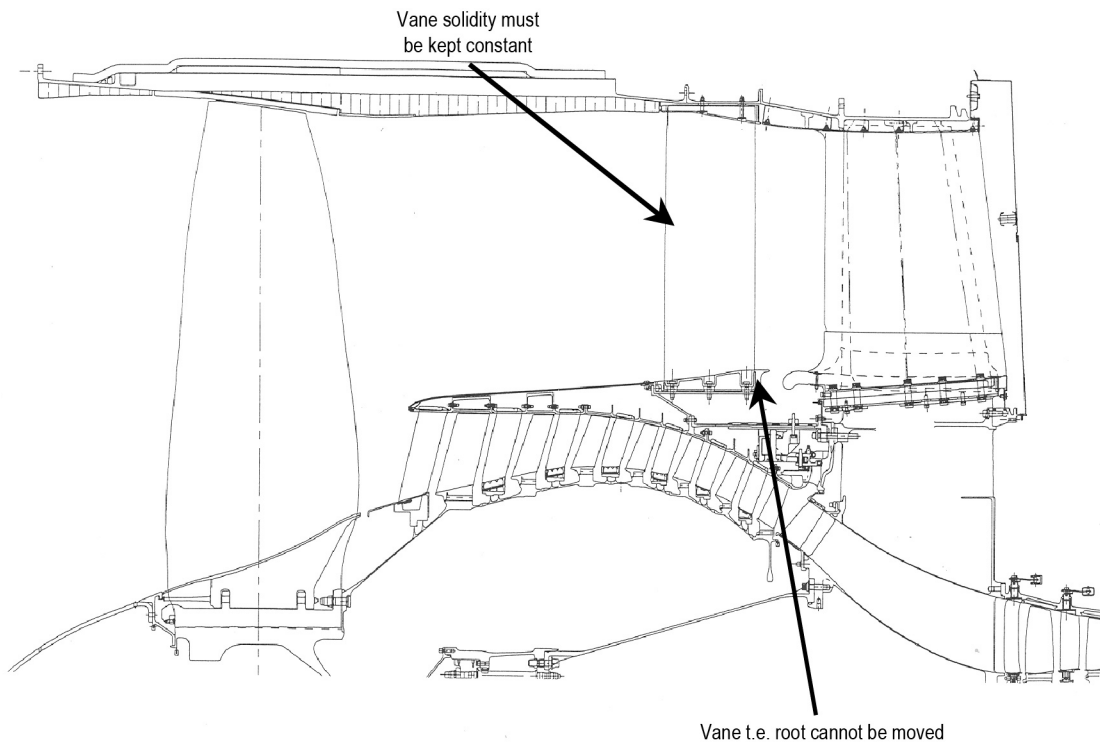
Figure 6.—Vane number study constraints.
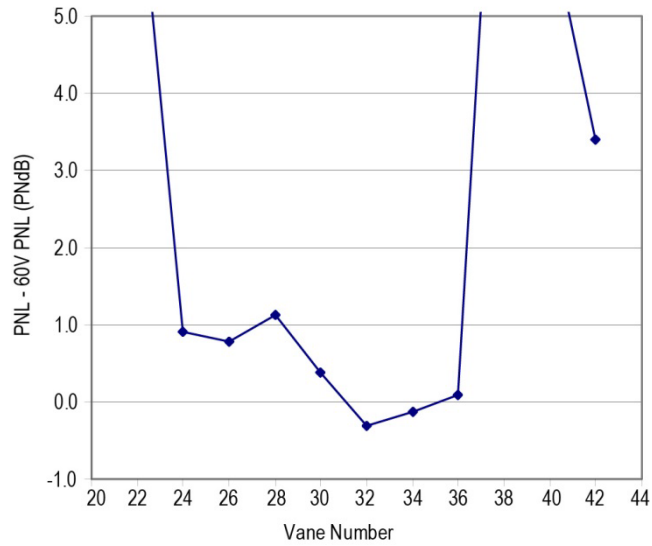
Figure 7.—Vane number study predictions (assuming a radial vane, relative to PW4098 bill of material, 60 Vane (60V) predictions).
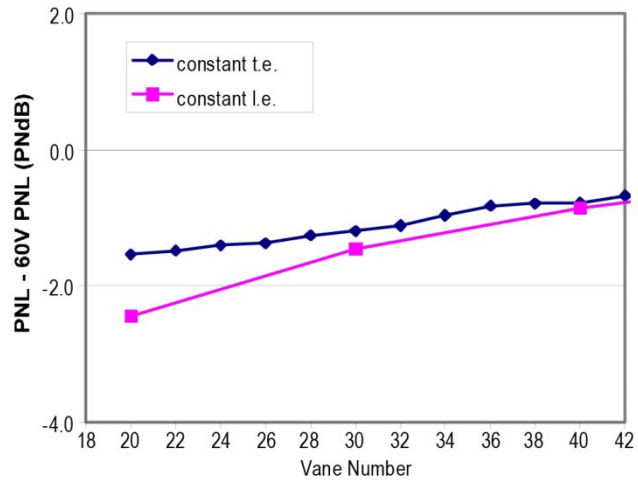
Figure 8.—Impact on PW4098 broadband noise of keeping the FEGV t.e. constant versus keeping the FEGV l.e. constant.

Use 28 vanes for radial cut-on design
(slightly swept 7.7°)
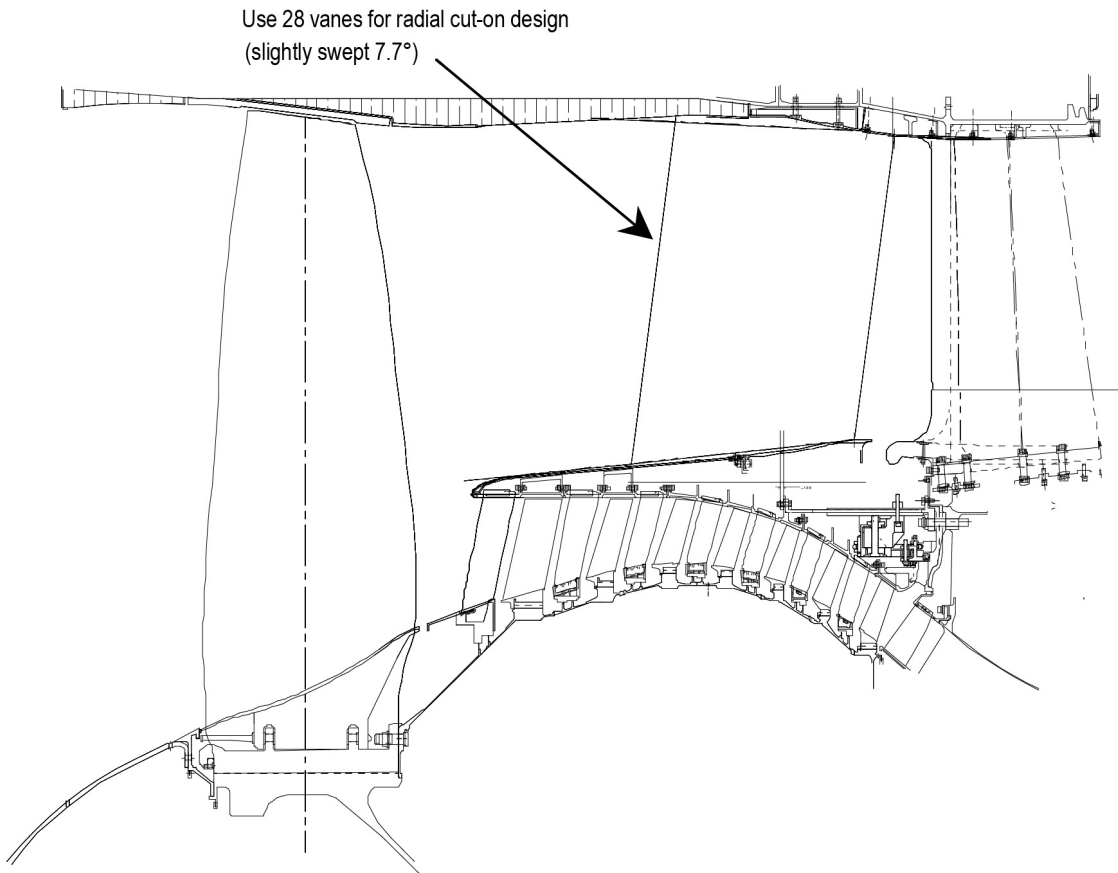
Figure 9.—PW4098 engine cross section with a sketch of the 28 "radial" FEGV design.

Radial Direction

Direction of Rotor Rotation

Lean

Circumferential Direction

Radial Direction

Axial Flow

Sweep

Axial Direction
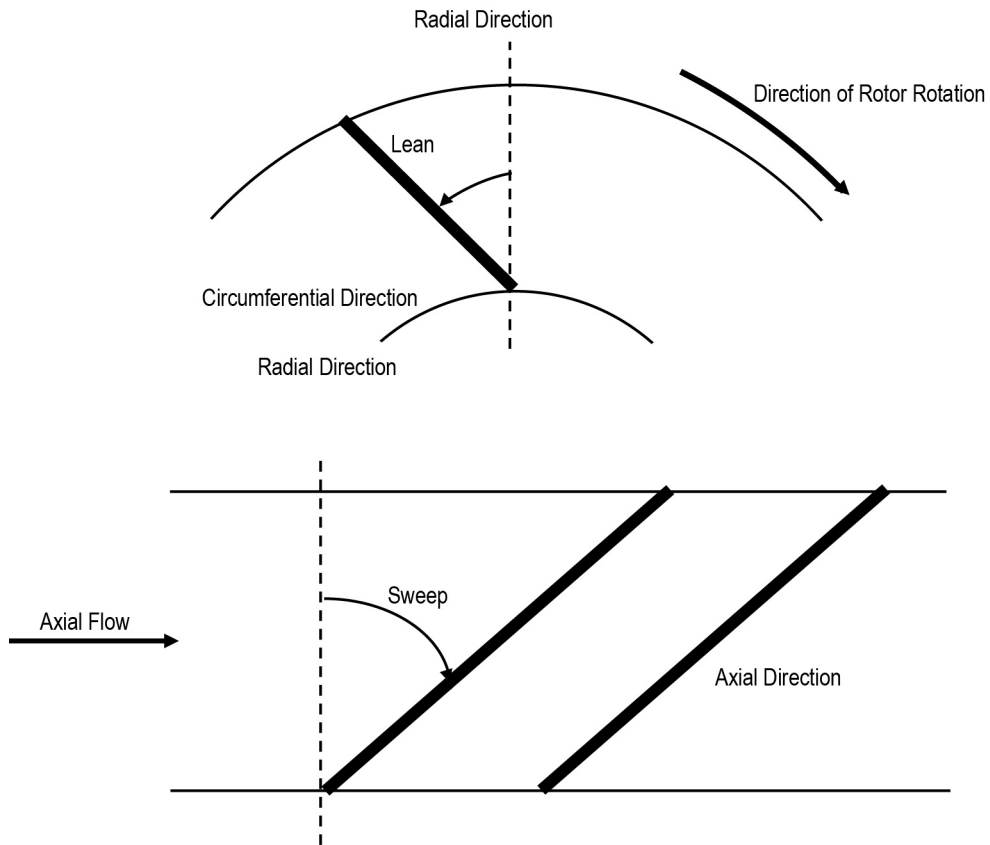
Figure 10.—Definition of positive sweep and lean.

Vane t.e. tip can be moved
2.91 in. downstream

30° sweep is achievable
with 26 vanes or more
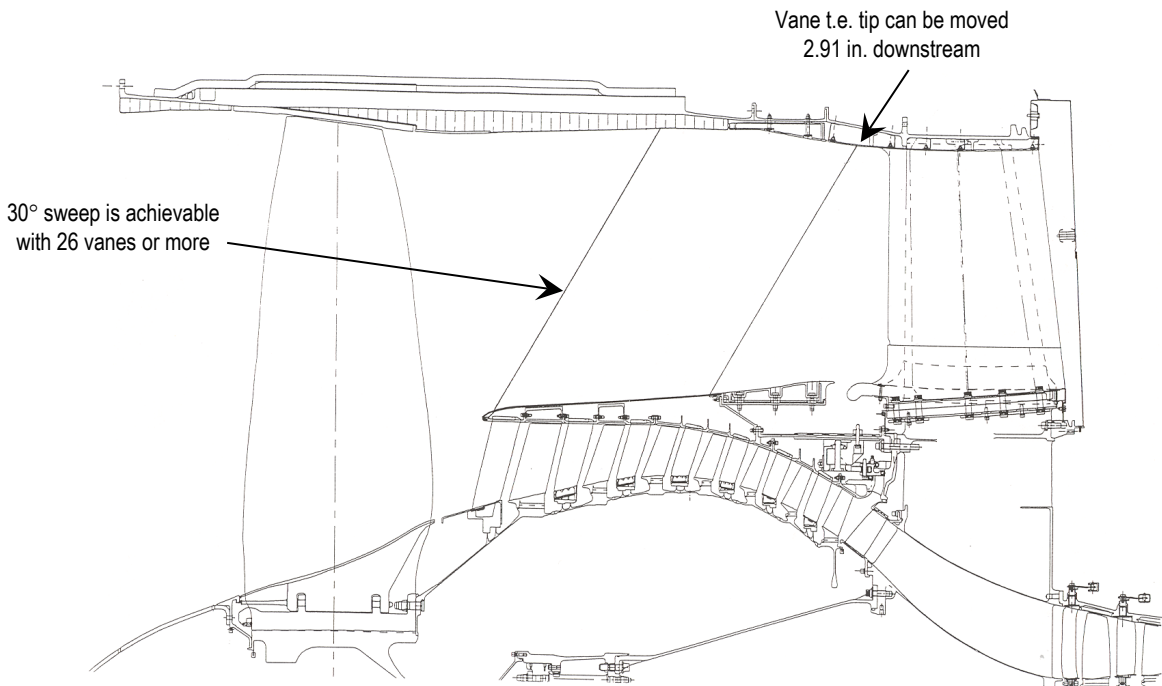
Figure 11.—Sweep study design constraints.
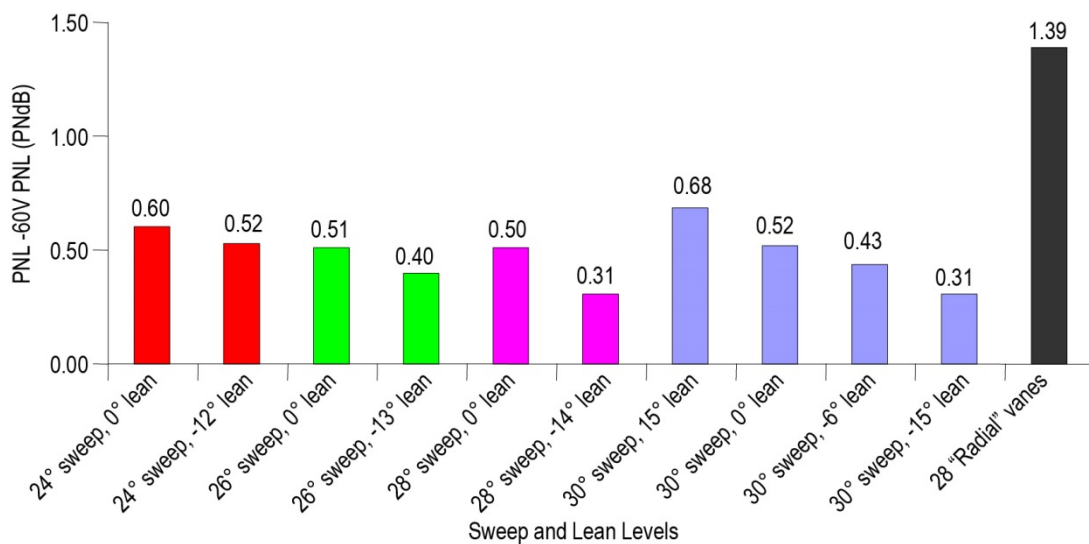
Figure 12.—Sweep/lean study predictions relative to PW4098 bill of material, 60 Vane (60V) prediction.

Primary Exhaust Nozzle Liner
Inner Face Sheet Thickness 0.023 in. with 5% Open
Area Perforate and 0.050 in. diameter holes.
Core Depth 0.500 in.
Foil Thickness 0.005 in.
Outer Face Sheet Thickness 0.014 in.
Effective Area 18.4 ft^2
Material—Beta 21—S Titanium

Primary Exhaust Nozzle Plug Liner
Outer Face Sheet Thickness 0.018 in. with 5% Open Area Perforate
and 0.050 in. diameter holes.
Core Depth 0.500 in.
Foil Thickness 0.005 in.
Inner Face Sheet Thickness 0.016 in.
Effective Area 12.6 ft^2
Material—Beta 21—S Titanium

Figure 13.—Description of Treatment in Primary Jet Nozzle.

Figure 14.—Photo of tailpipe acoustic treatment.
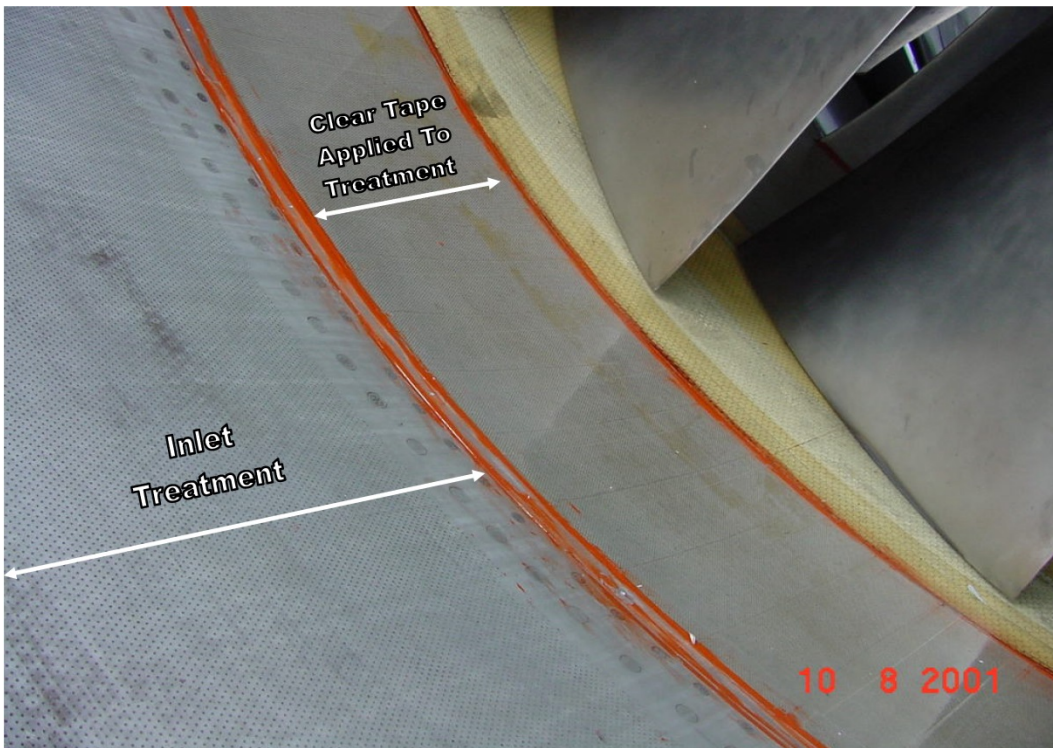
Figure 15.—Photo of inlet treatment, and taped front fan containment case (FFCC) treatment.

Figure 16.—Rear fan containment case (RFCC) liner section removed to accommodate 28 FEGV.

Figure 17.—Photo of 22 fan blades with 28 "cuton" FEGVs.

Hardwall for test (clear tape)

28

22

2 in. liner removed about circumference (28V only)

Reduced air-foil loading (relative to 22 blades)

28

24

Slightly swept (~ 8°) to increase fan-FEGV spacing
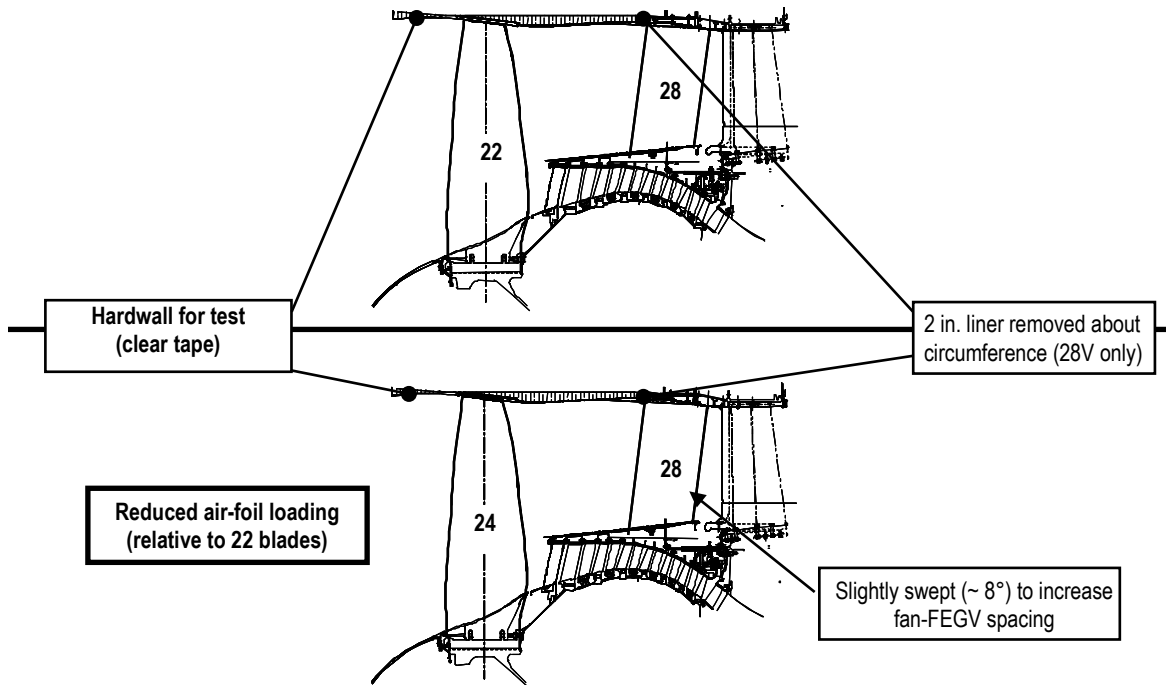
Figure 18.—Schematics of 22, and 24 fan blades with "cuton" FEGVs.

2 in. liner must be removed to accommodate 28 V

Vane solidity (1.585) must be kept ~ constant

Vane t.e. root cannot be moved (bleeds)
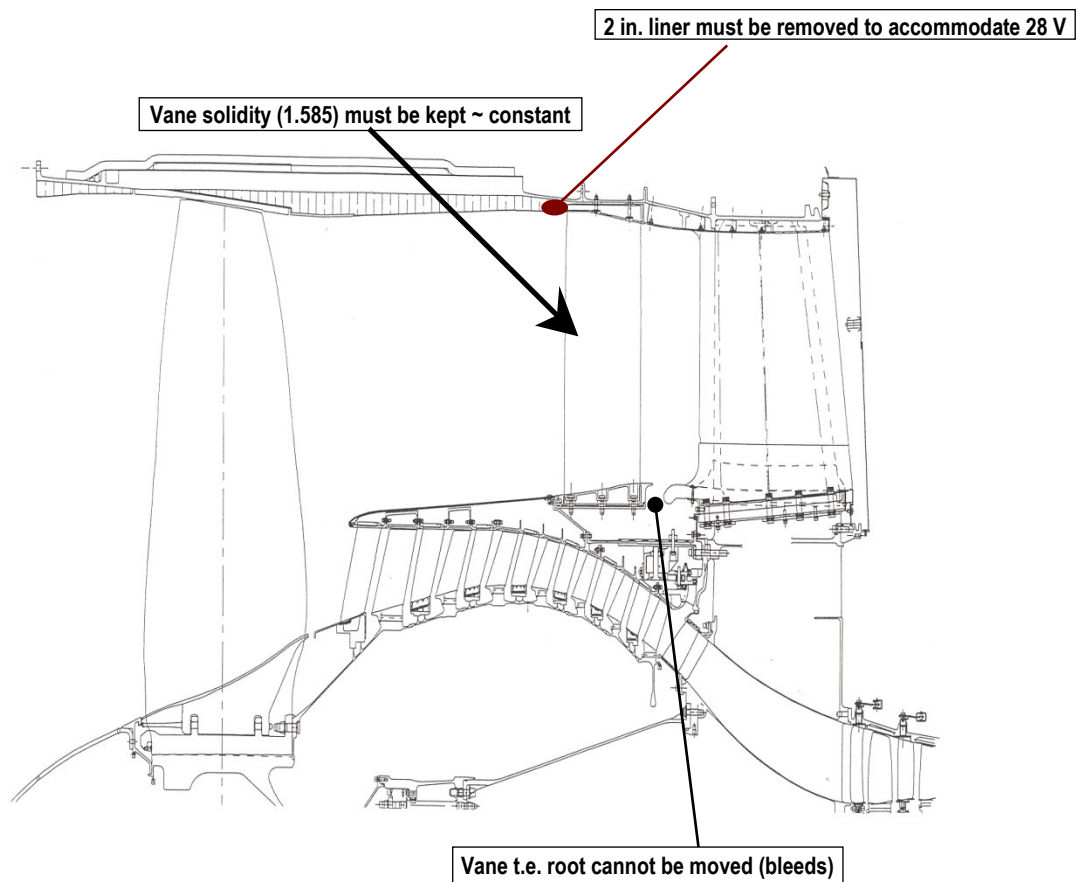
Figure 19.—Schematic showing design constraints for "cuton" FEGVs.

"Cut-off" FEGV

FEGV solidity = 1.585

60

24

Hardwall for test (clear tape)

FEGV solidity = 1.591

28

24

"Cut-on" FEGV

2 in. liner removed about circumference (28V only)

Slightly swept (~ 8°) to increase fan-FEGV spacing
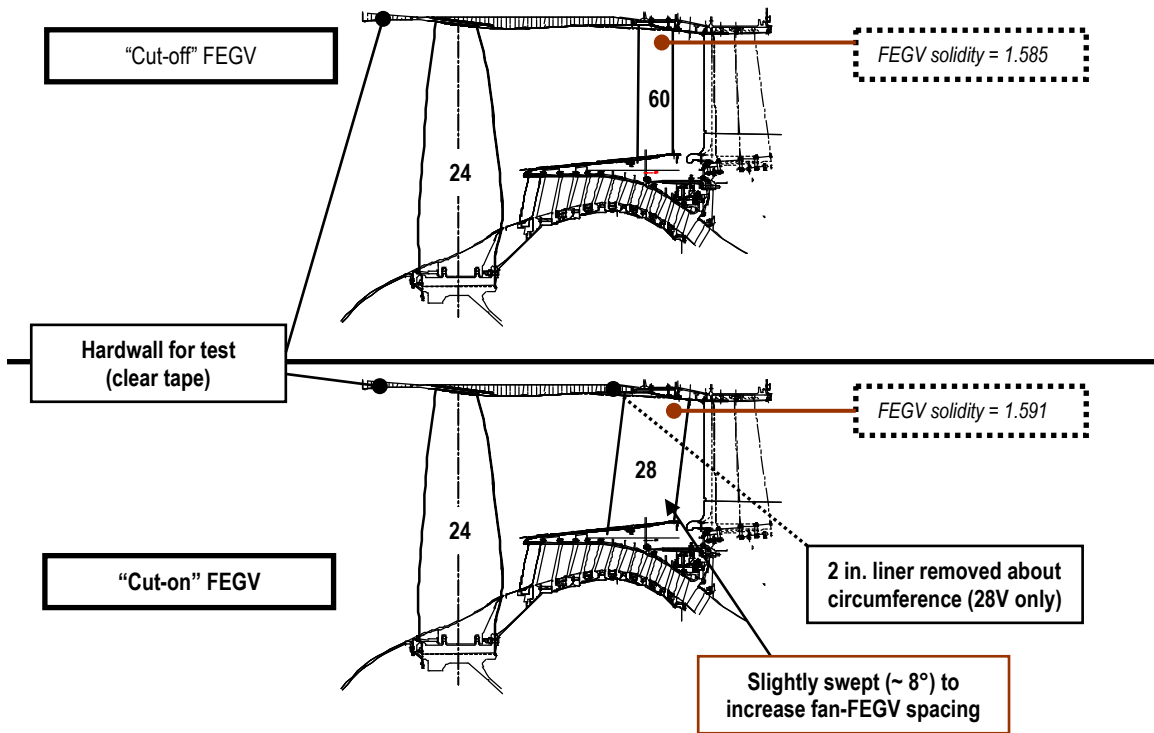
Figure 20.—Schematic of "cutoff", and "cuton" FEGVs.

Figure 21.—Overall view of P&W C11 stand farfield acoustic arena.

Figure 22.—PW4098 test engine with production flight inlet and ICD.
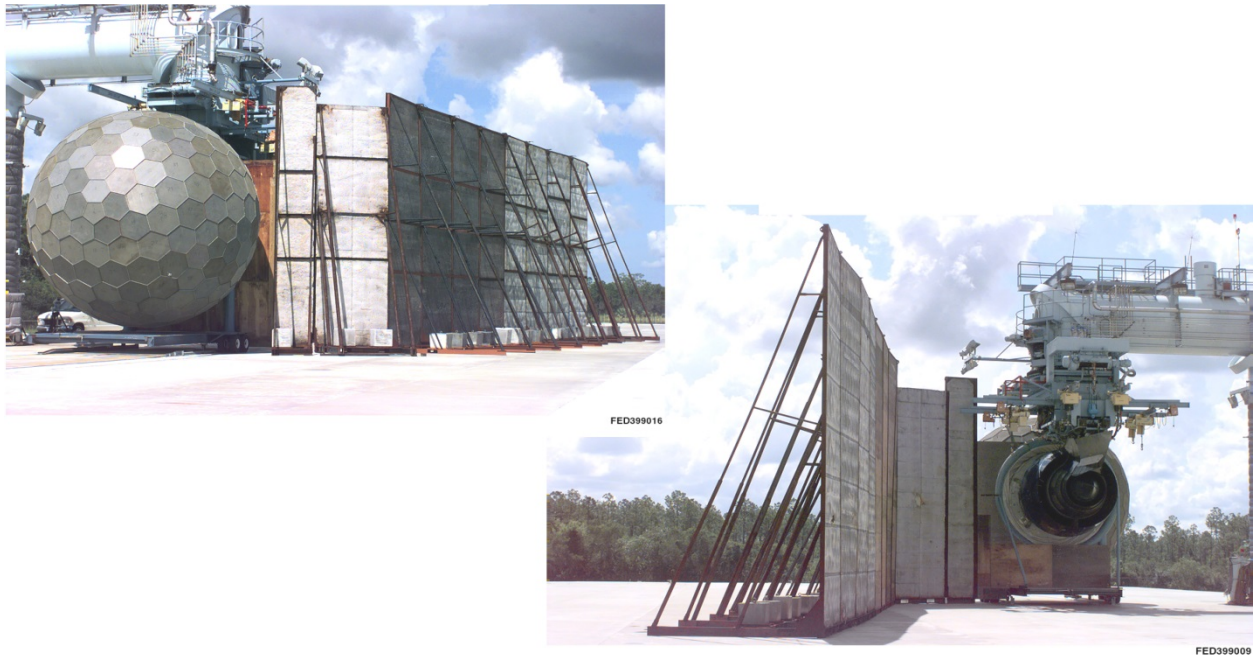
Figure 23.—Photos of aft walls to isolate inlet noise, configurations 3 to 6.
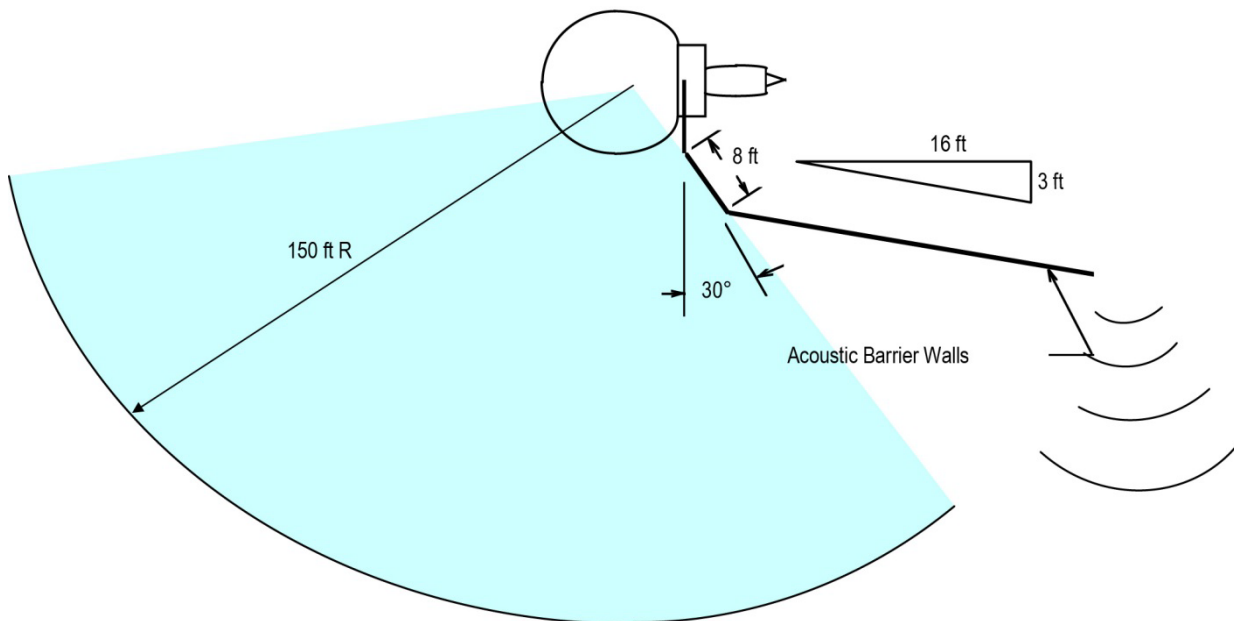
Figure 24.—Farfield mic array with aft acoustic barriers.
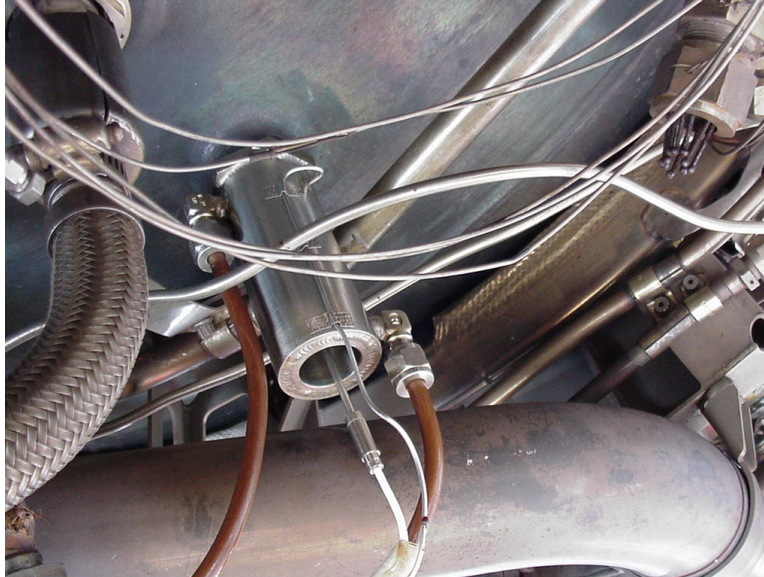
Installation at 127°, CCW, aft looking forward

Installation at 337°, CCW, aft looking forward

Figure 25.—Combustion dynamic pressure transducer installation.

Narrow Band Tone Removal and Storage
(Mid-Power, 80° Inlet Angle)
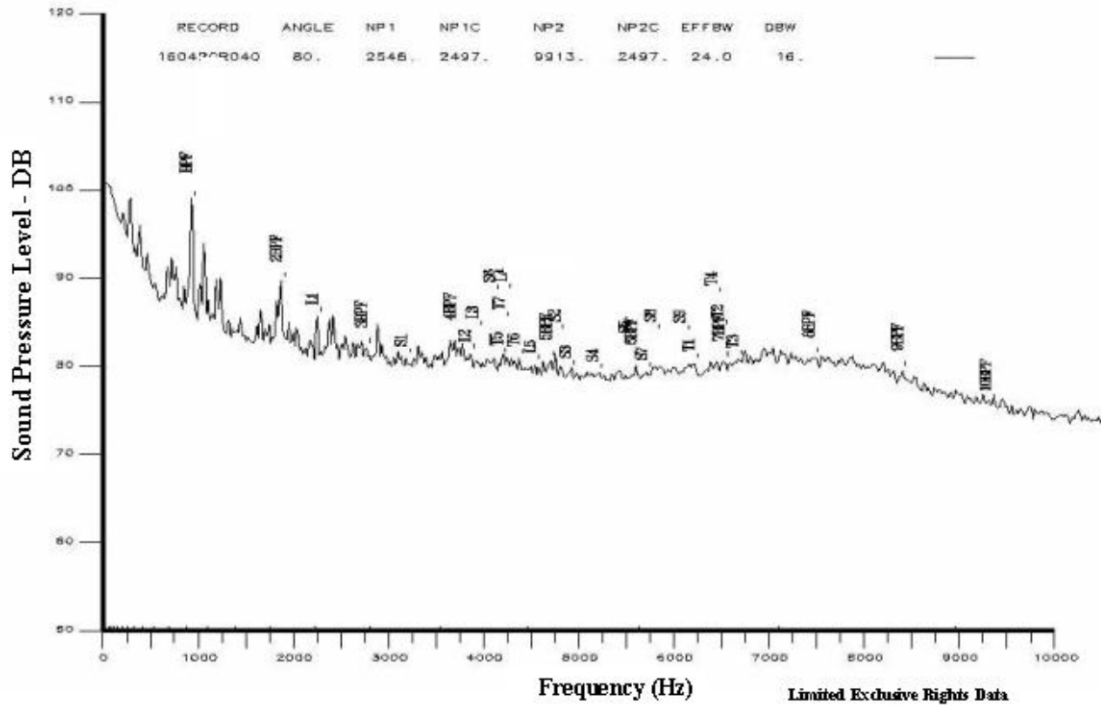
Figure 26.—Sample narrowband engine noise spectra with tones identified for removal and storage.

1/3 Octave Band Noise Source Separation
(Mid-Power, 80° Inlet Angle)
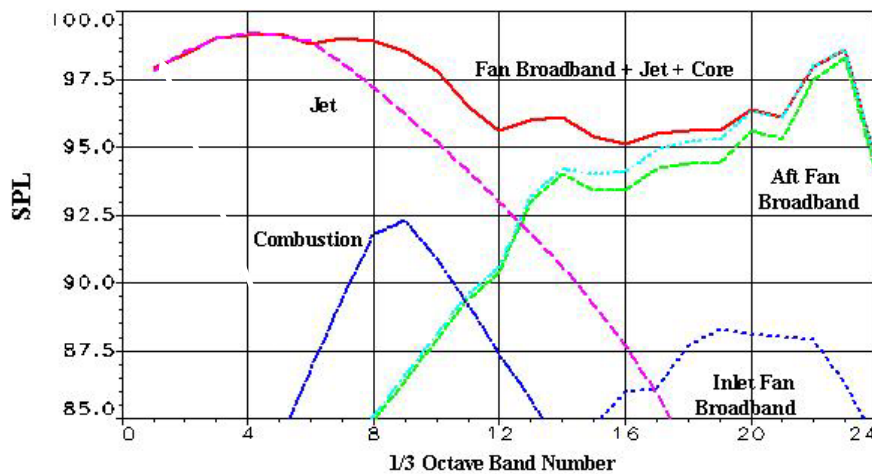
Figure 27.—Sample of 1/3 octave band engine noise spectra with broadband components identified and separated.
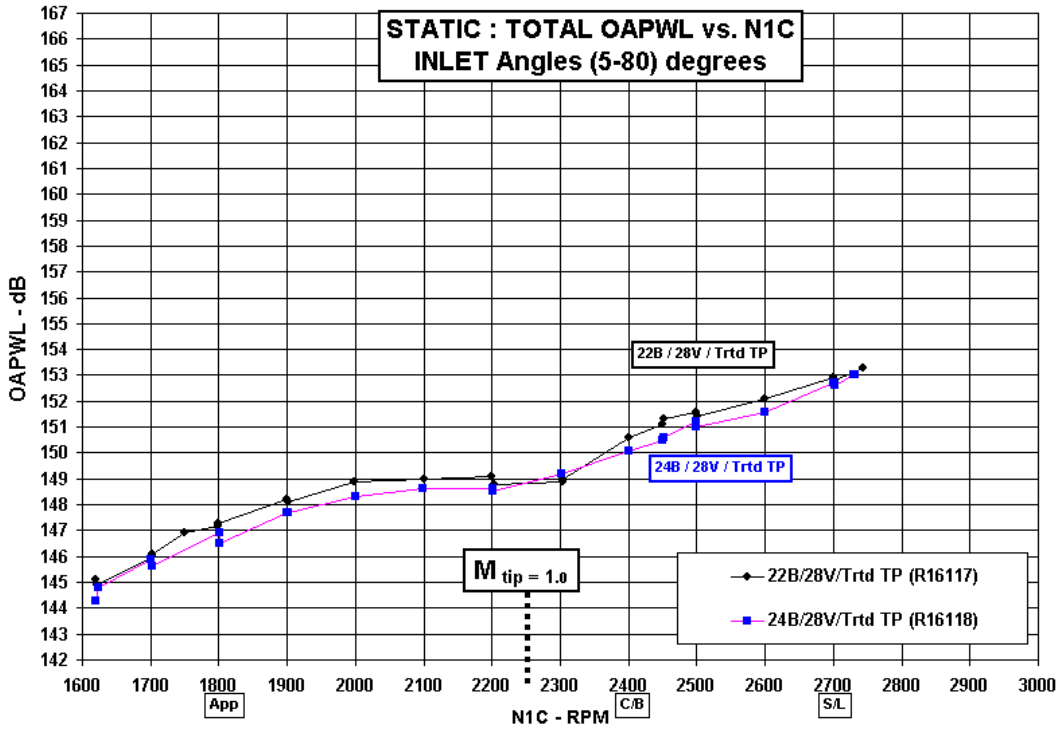
Figure 28.—Effect of fan blade number on static total OAPWL versus N1C—inlet angles (5° to 80°).
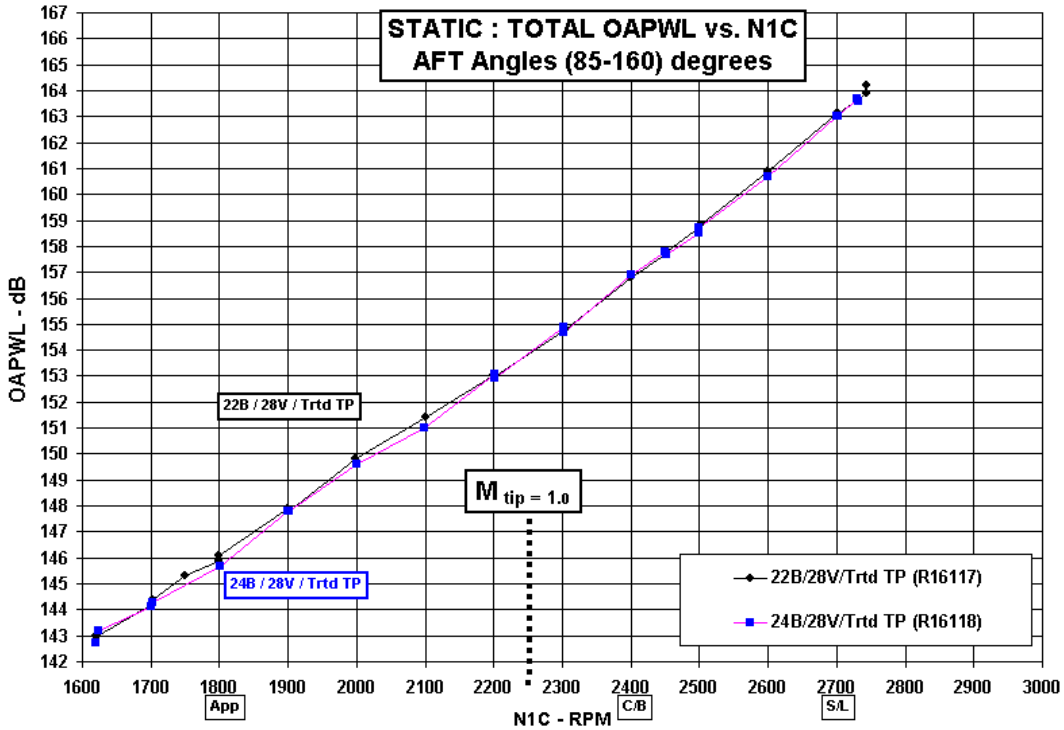
Figure 29.—Effect of fan blade number on static total OAPWL versus N1C—aft angles (85° to 160°).
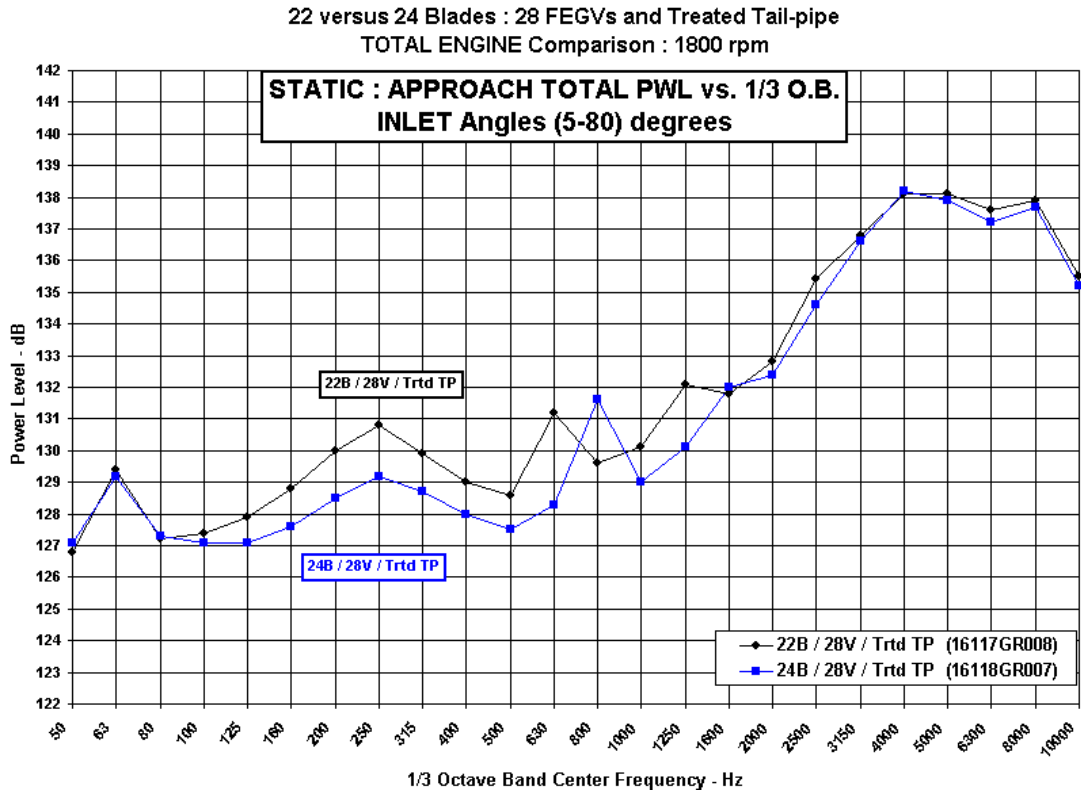
Figure 30.—Effect of fan blade number on static total PWL spectra (inlet angles 5° to 80°)—approach power.

Figure 31.—Effect of fan blade number on static total PWL spectra (aft angles 85° to 160°)—approach power.

Figure 32.—Effect of fan blade number on static total PWL spectra (inlet angles 5° to 80°)—cutback power.
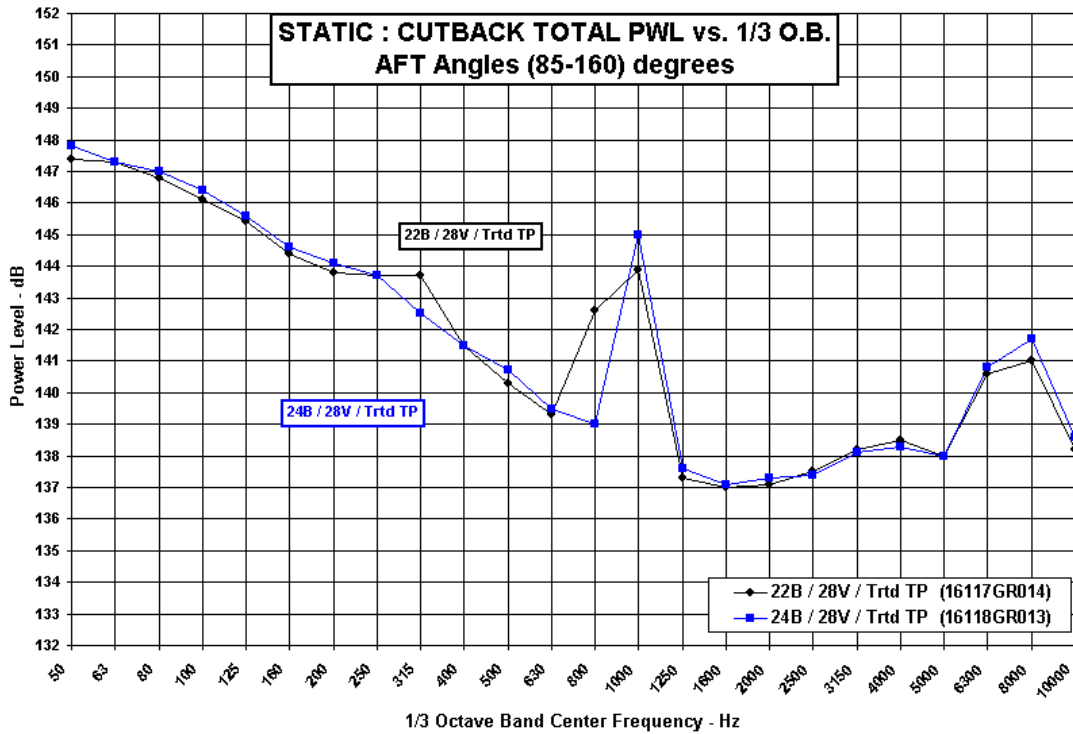
Figure 33.—Effect of fan blade number on static total PWL spectra (aft angles 85° to 160°)—cutback power.
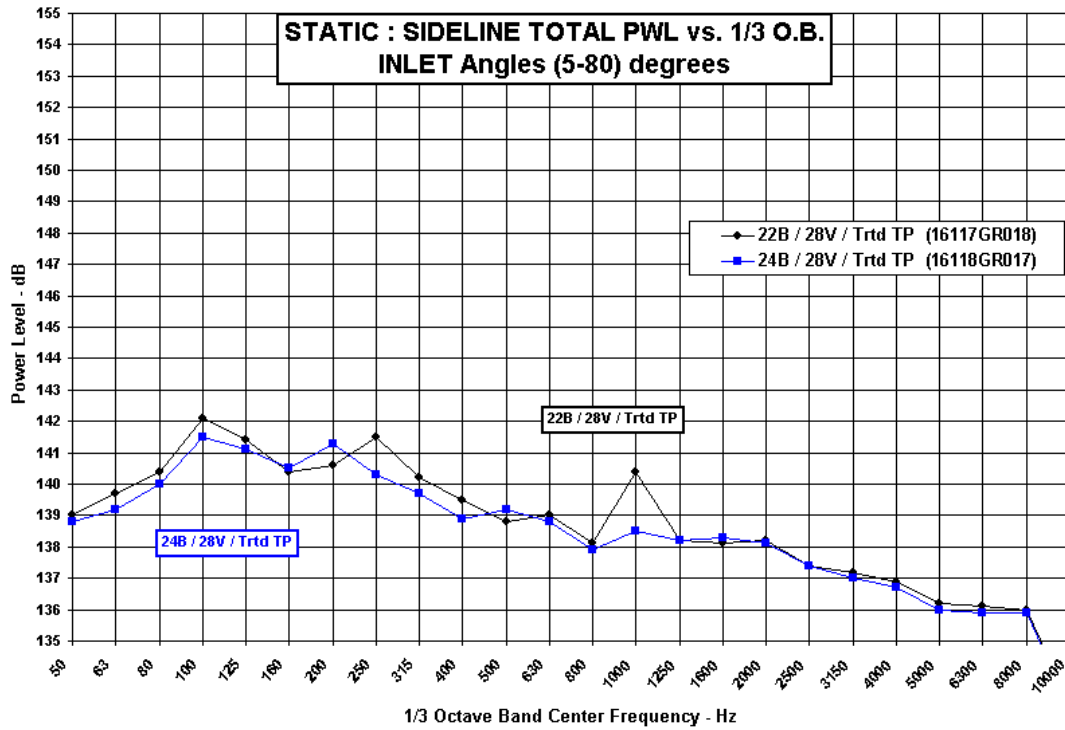
Figure 34.—Effect of fan blade number on static total PWL spectra (inlet angles 5° to 80°)—sideline power.

Figure 35.—Effect of fan blade number on static total PWL spectra (aft angles 85° to 160°)—sideline power.

Figure 36.—Effect of fan blade number on static total SPL spectra at 60°—approach power.
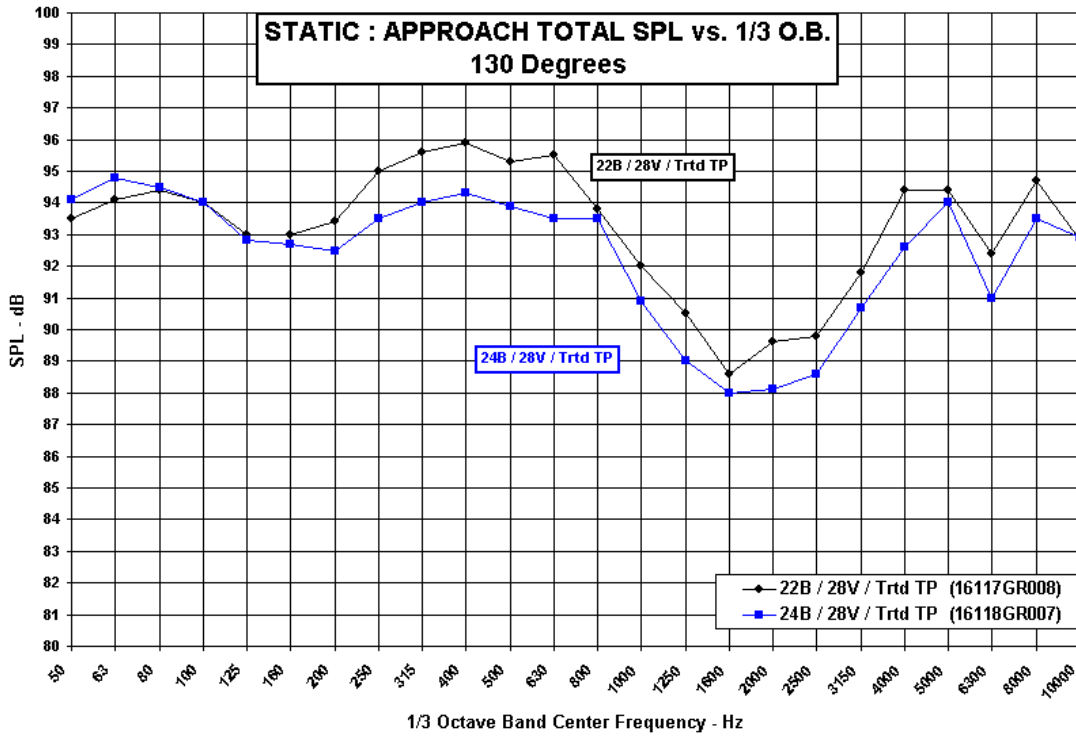
Figure 37.—Effect of fan blade number on static total SPL spectra at 130°—approach power.
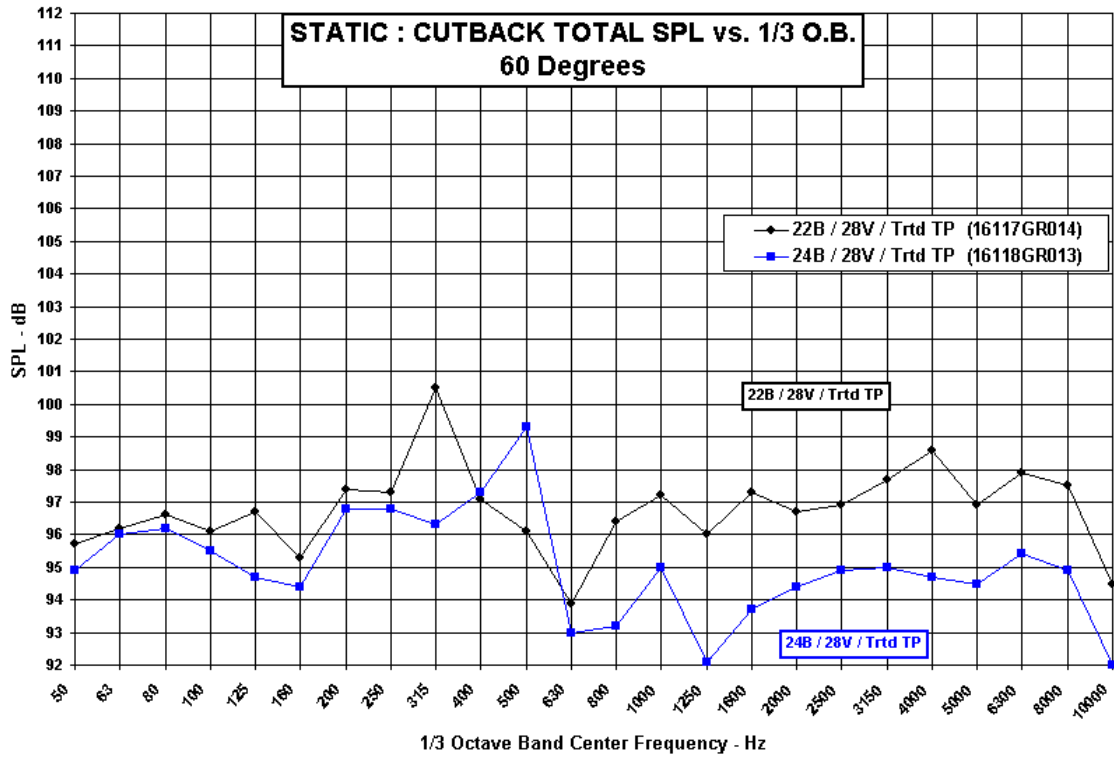
Figure 38.—Effect of fan blade number on static total SPL spectra at 60°—cutback power.
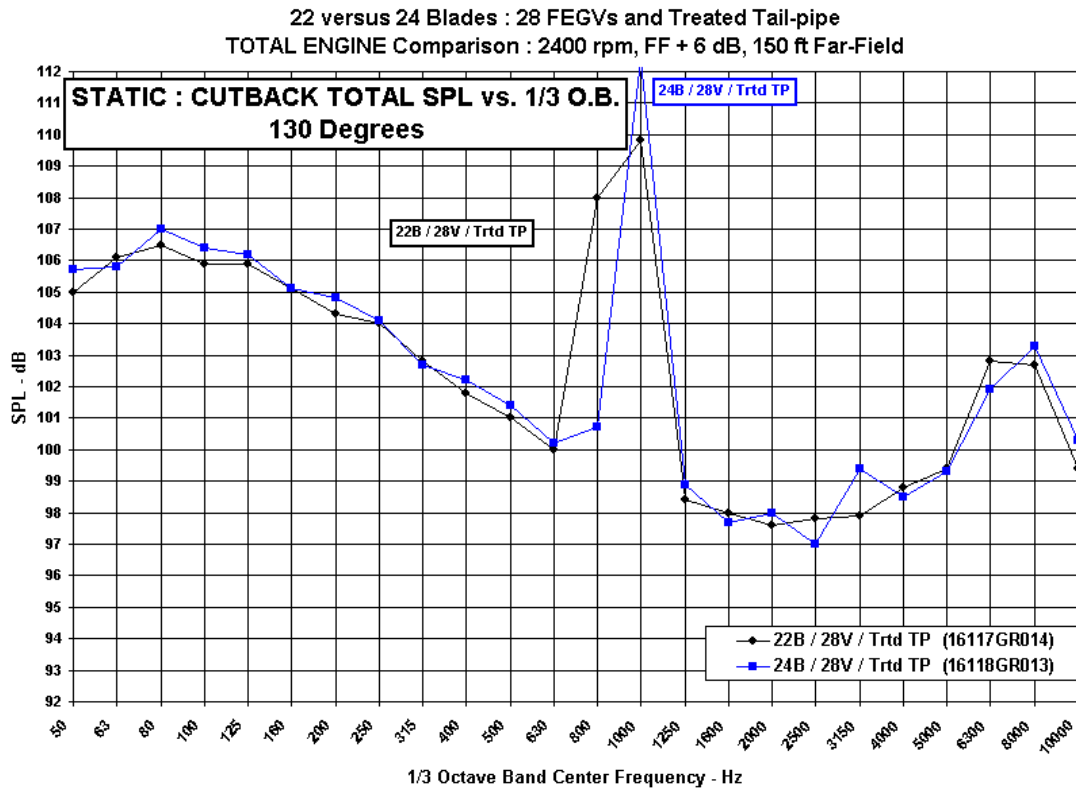
Figure 39.—Effect of fan blade number on static total SPL spectra at 130°—cutback power.
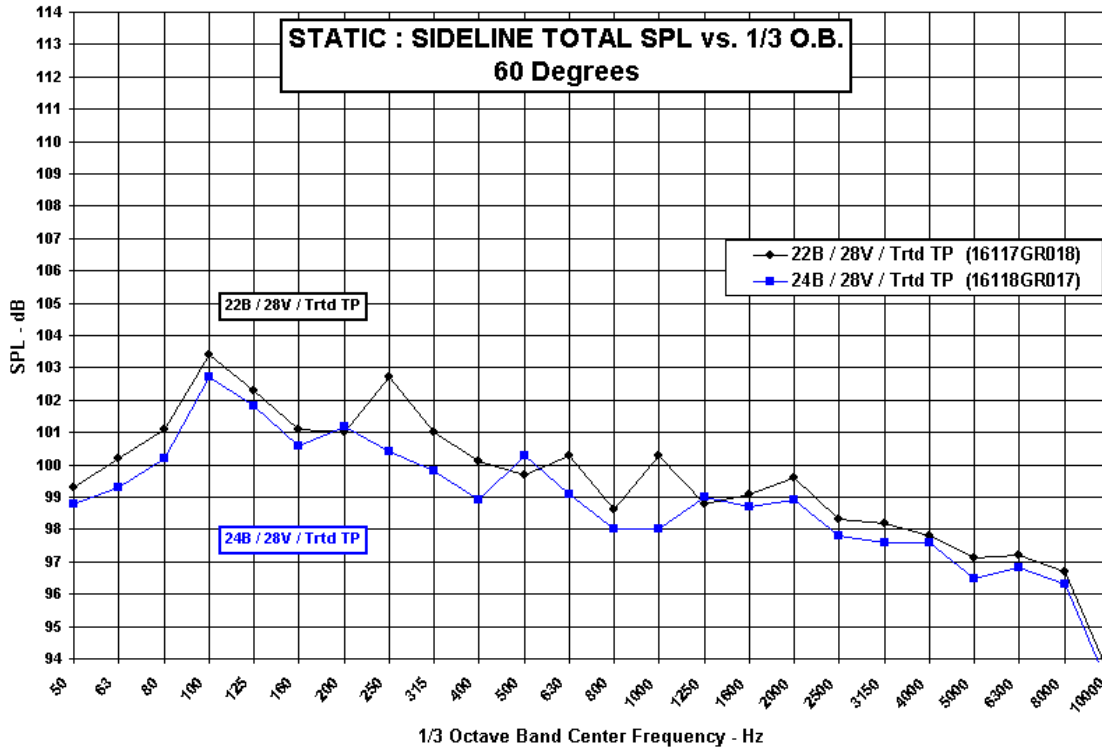
Figure 40.—Effect of fan blade number on static total SPL spectra at 60°—sideline power.
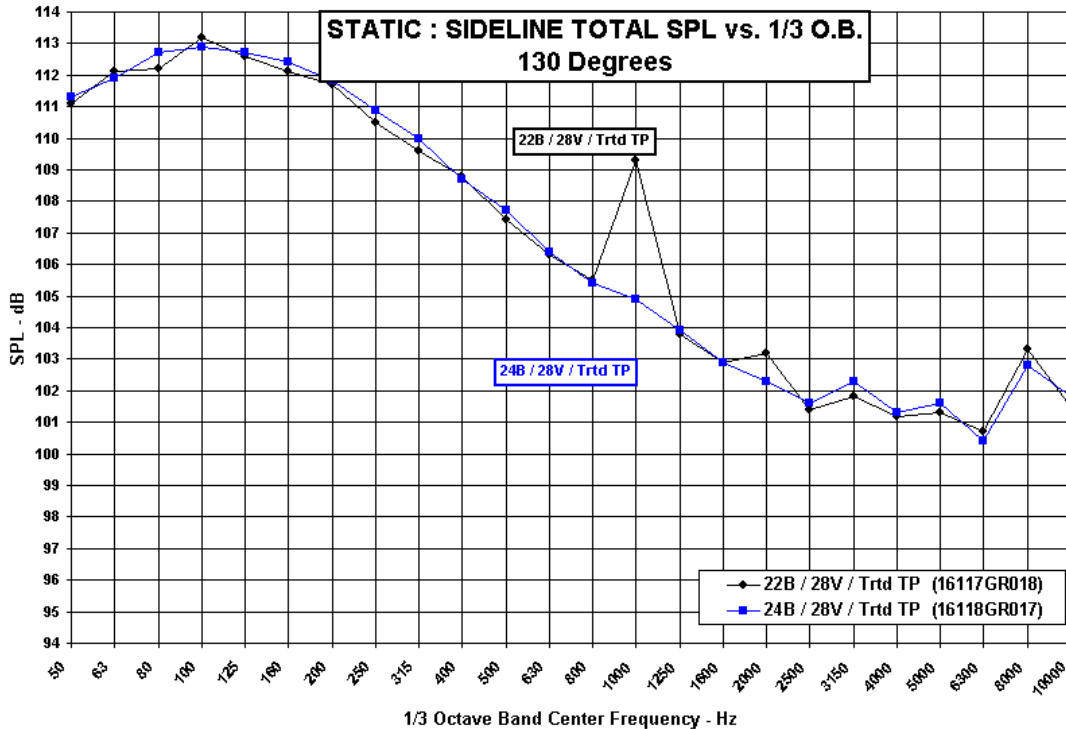
Figure 41.—Effect of fan blade number on static total SPL spectra at 130°—sideline power.
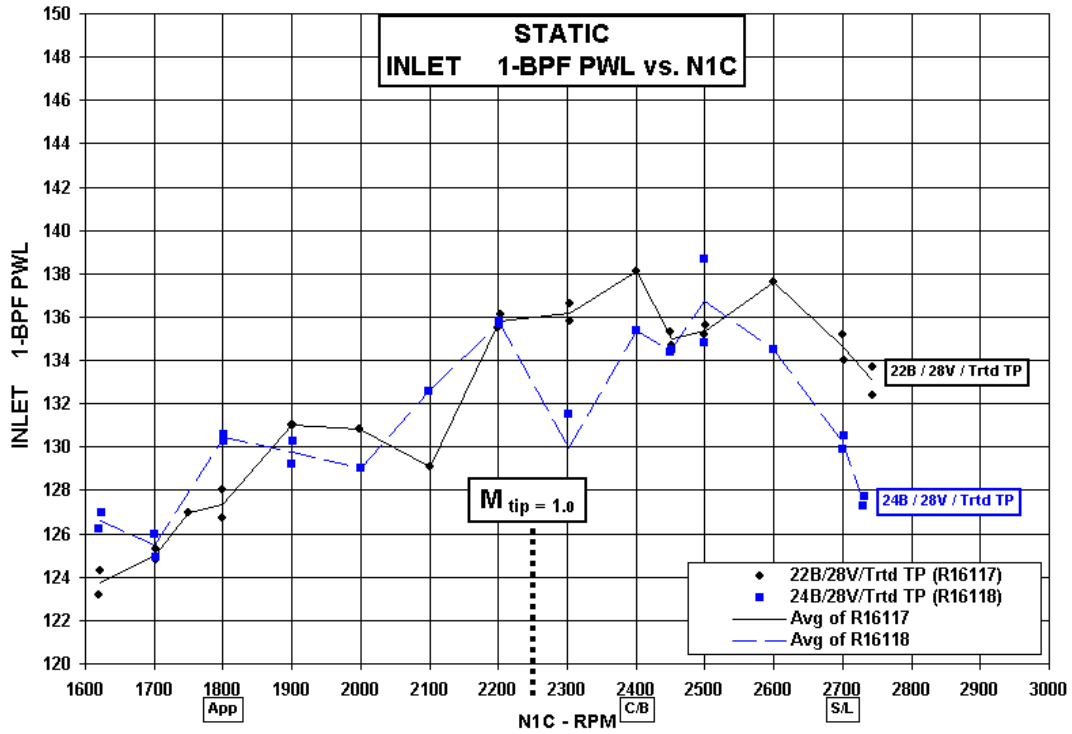
Figure 42.—Effect of fan blade number on static inlet 1-BPF PWL versus N1C.
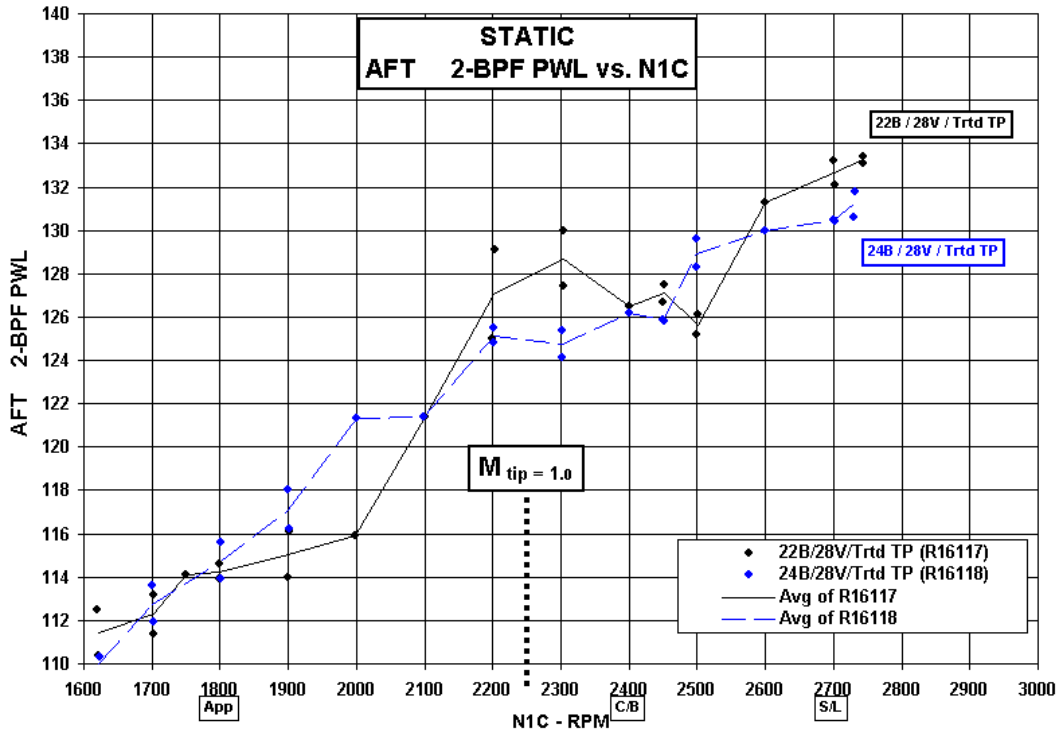
Figure 43.—Effect of fan blade number on static aft 1-BPF PWL versus N1C.
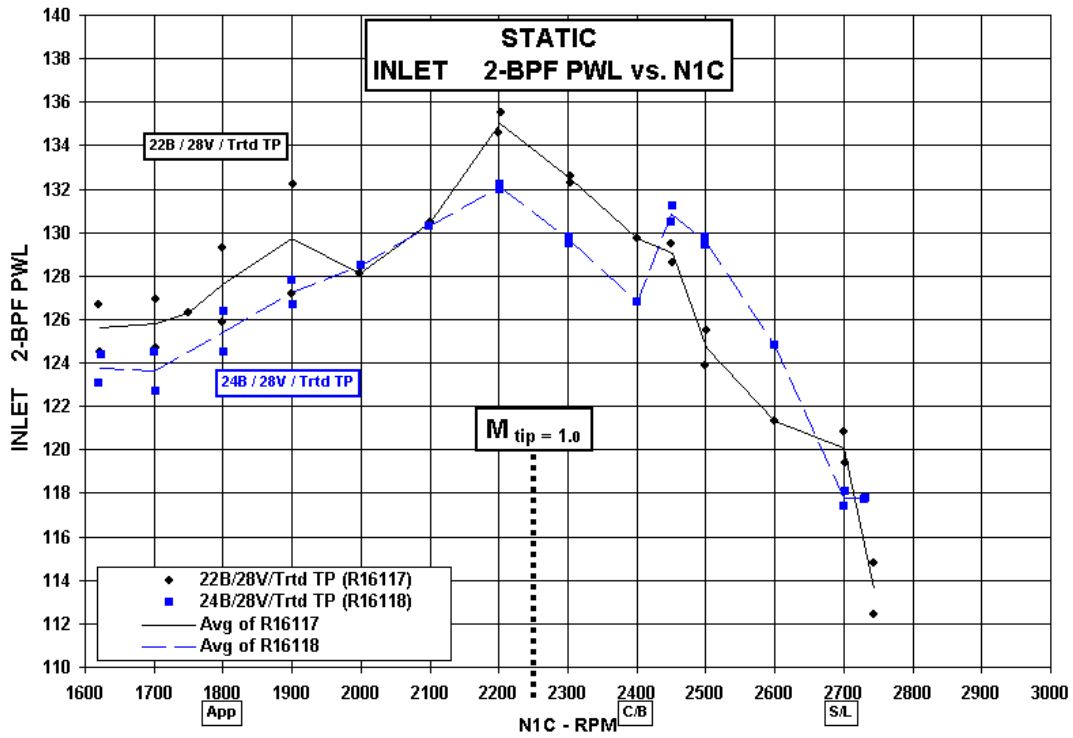
Figure 44.—Effect of fan blade number on static inlet 2-BPF PWL versus N1C.
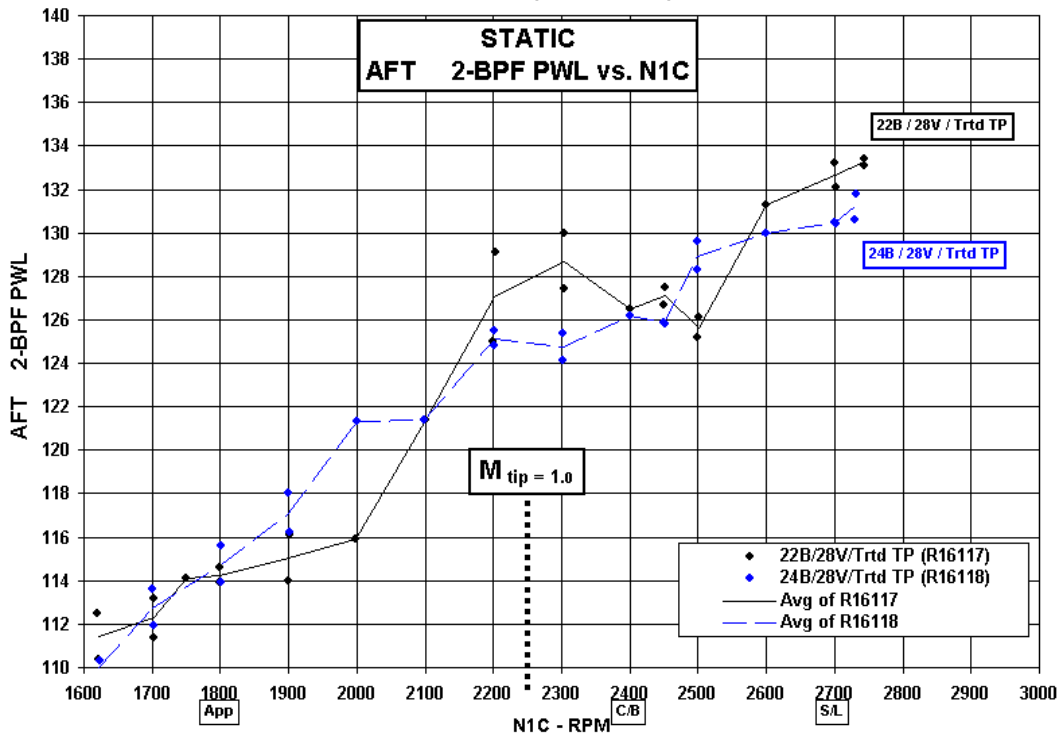
Figure 45.—Effect of fan blade number on static aft 2-BPF PWL versus N1C.
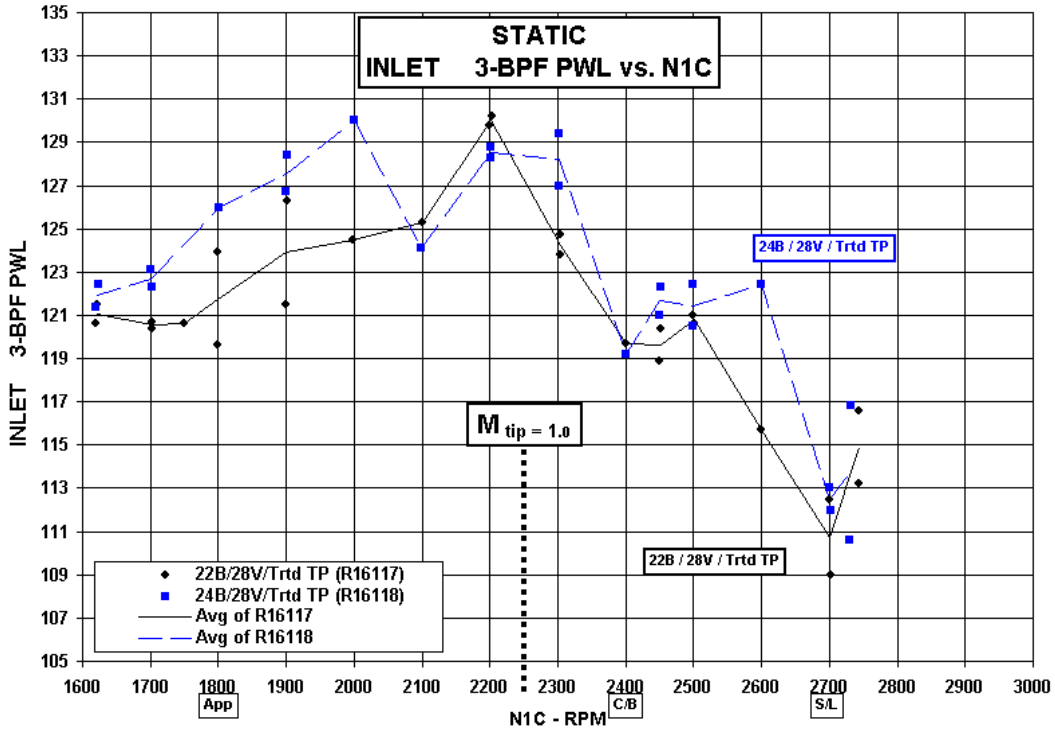
Figure 46.—Effect of fan blade number on static inlet 3-BPF PWL versus N1C.
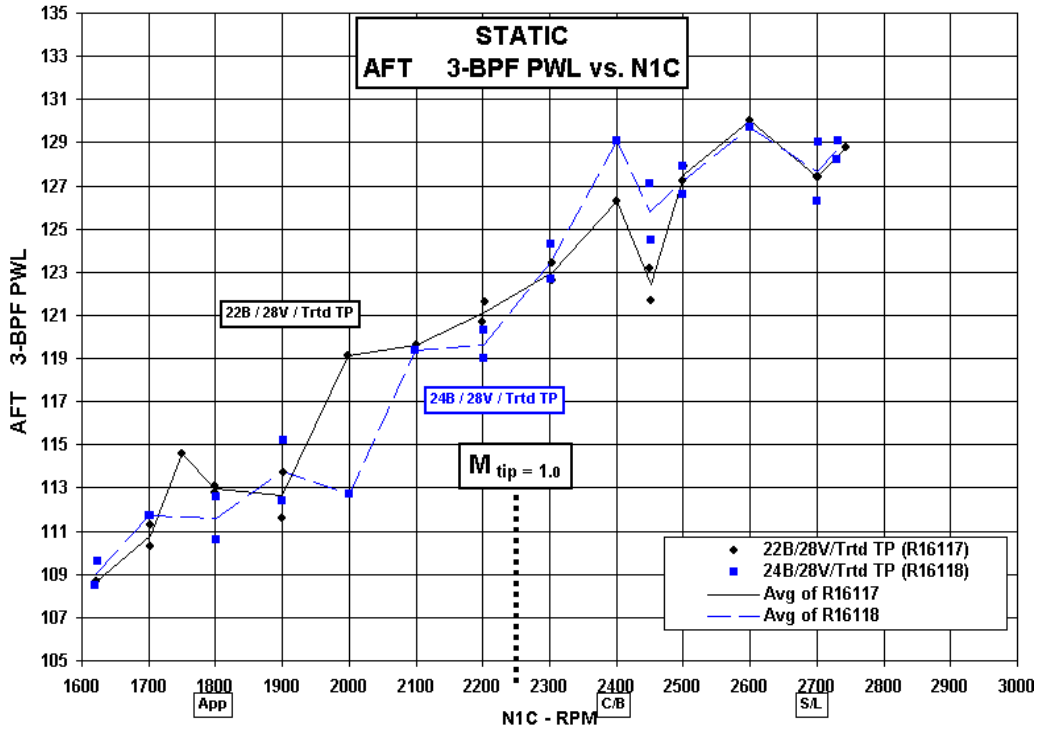
Figure 47.—Effect of fan blade number on static aft 3-BPF PWL versus N1C.
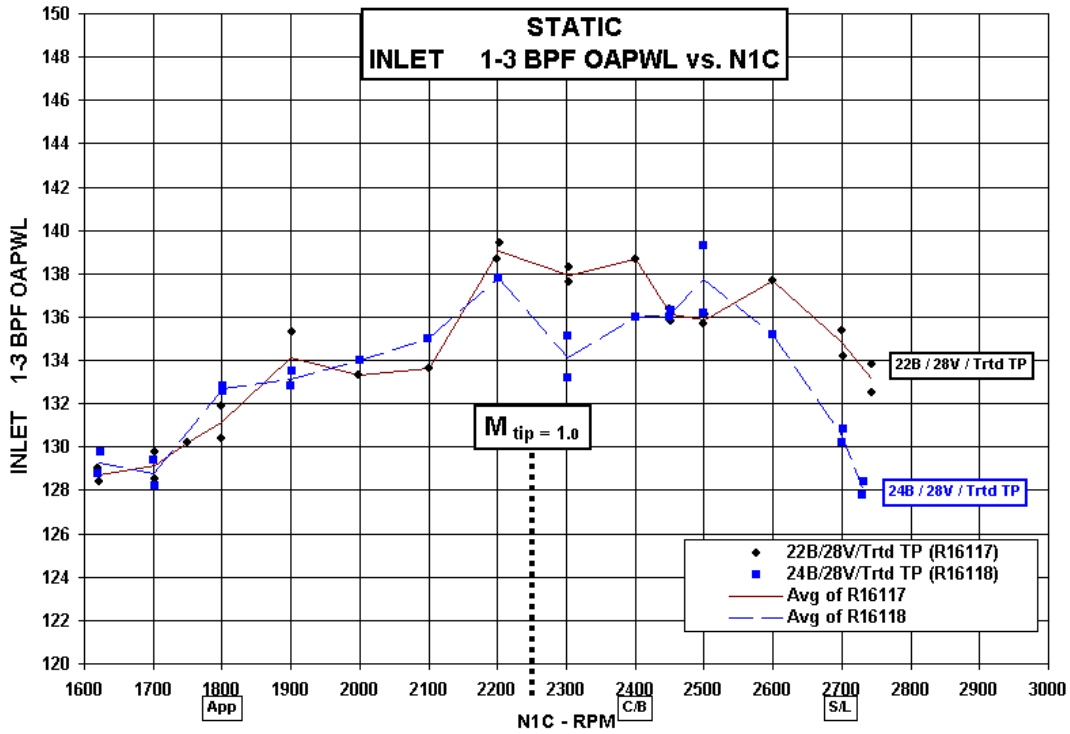
Figure 48.—Effect of fan blade number on static inlet 1-3 BPF OAPWL versus N1C.
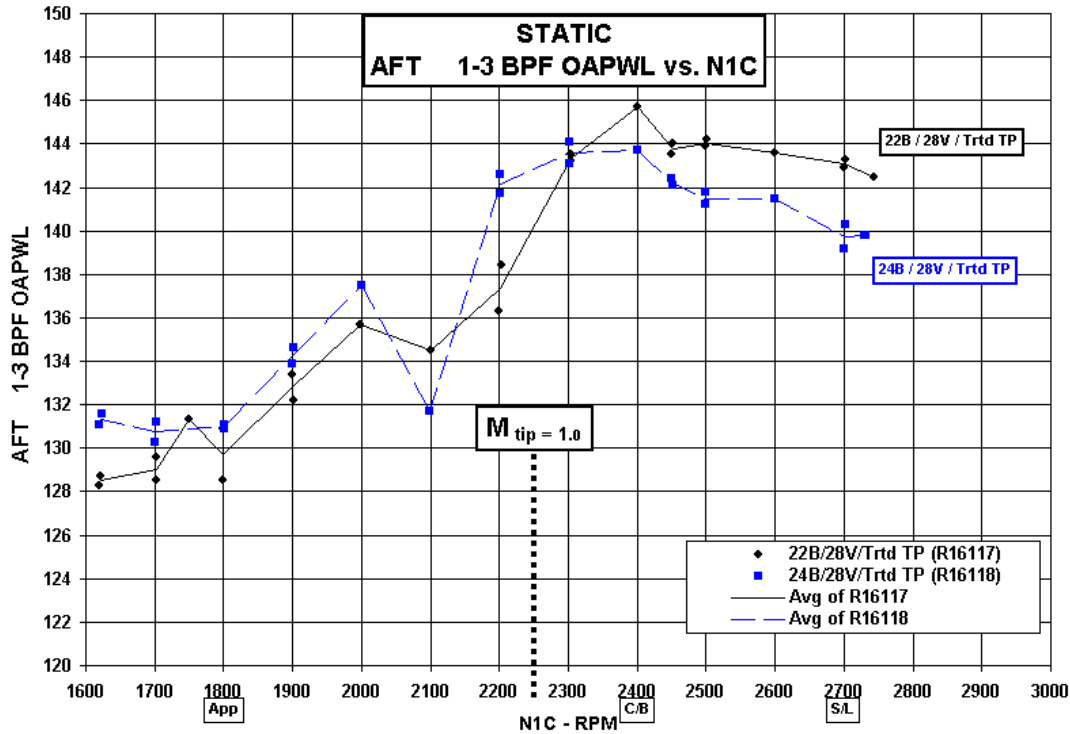
Figure 49.—Effect of fan blade number on static aft 1-3 BPF OAPWL versus N1C.
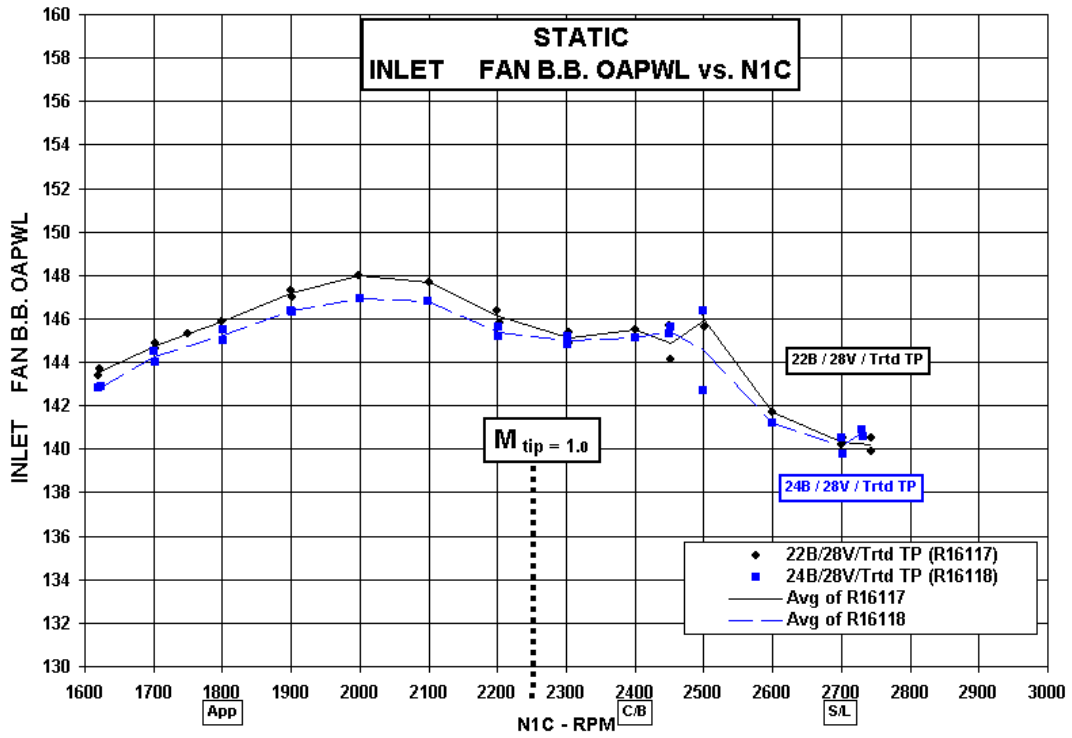
Figure 50.—Effect of fan blade number on static inlet fan B.B. OAPWL versus N1C.
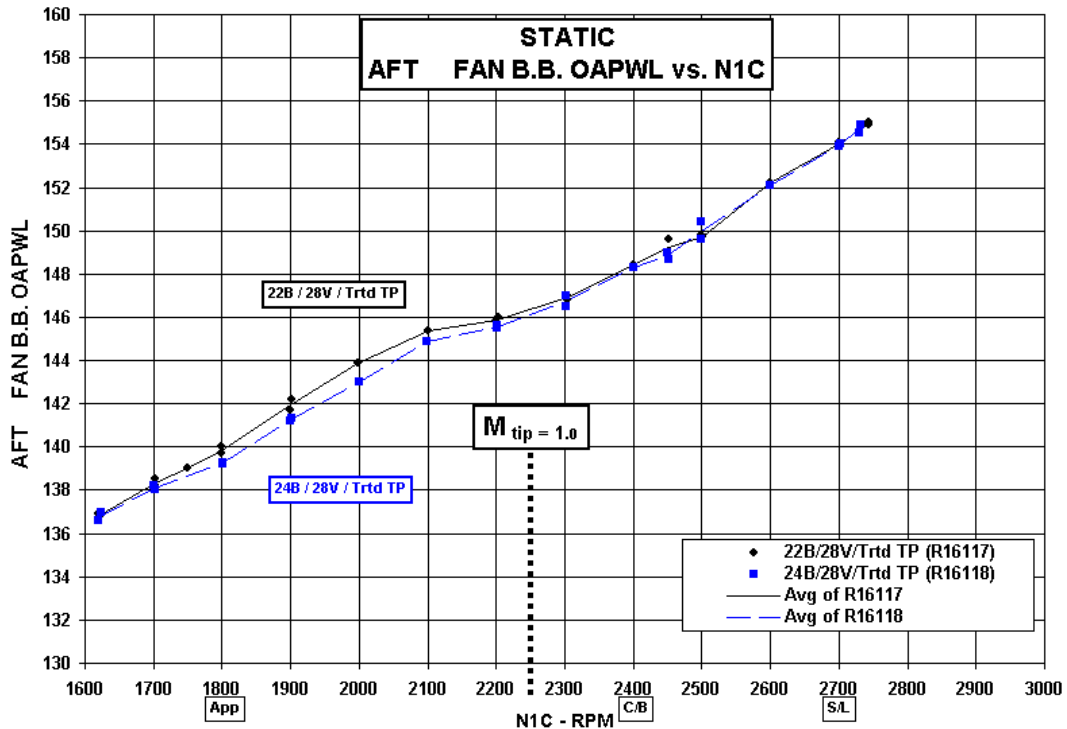
Figure 51.—Effect of fan blade number on static aft fan B.B. OAPWL versus N1C.
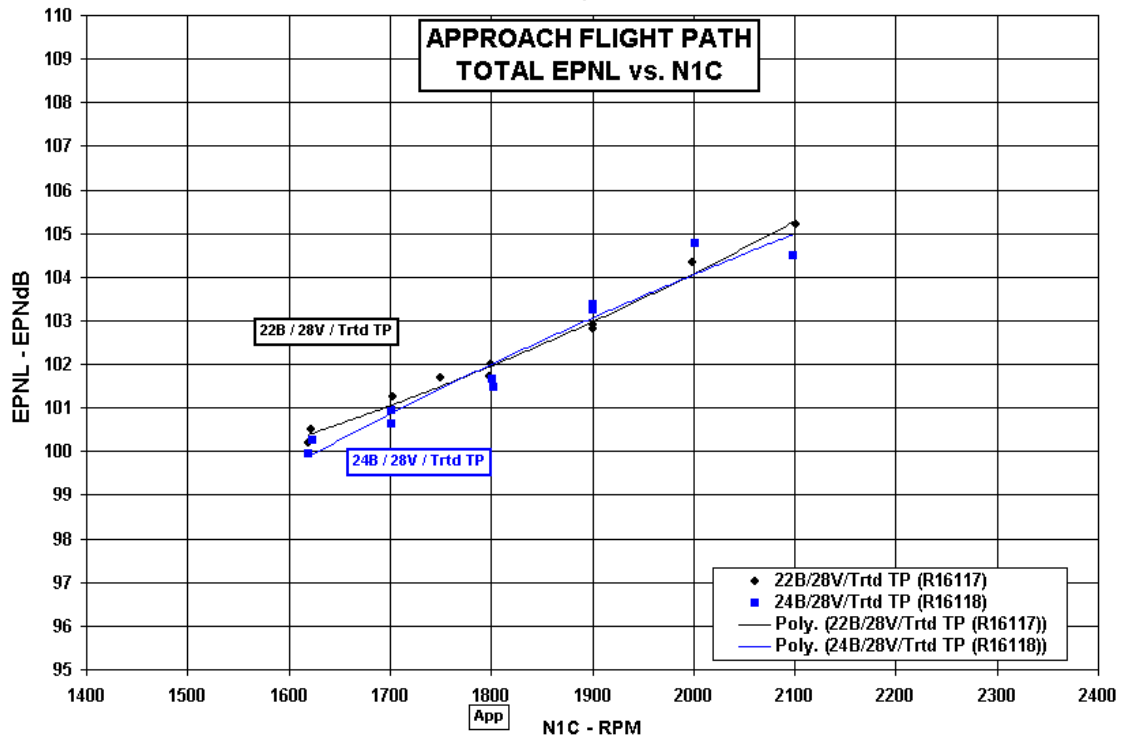
Figure 52.—Effect of fan blade number on total EPNL versus N1C—approach flight path.
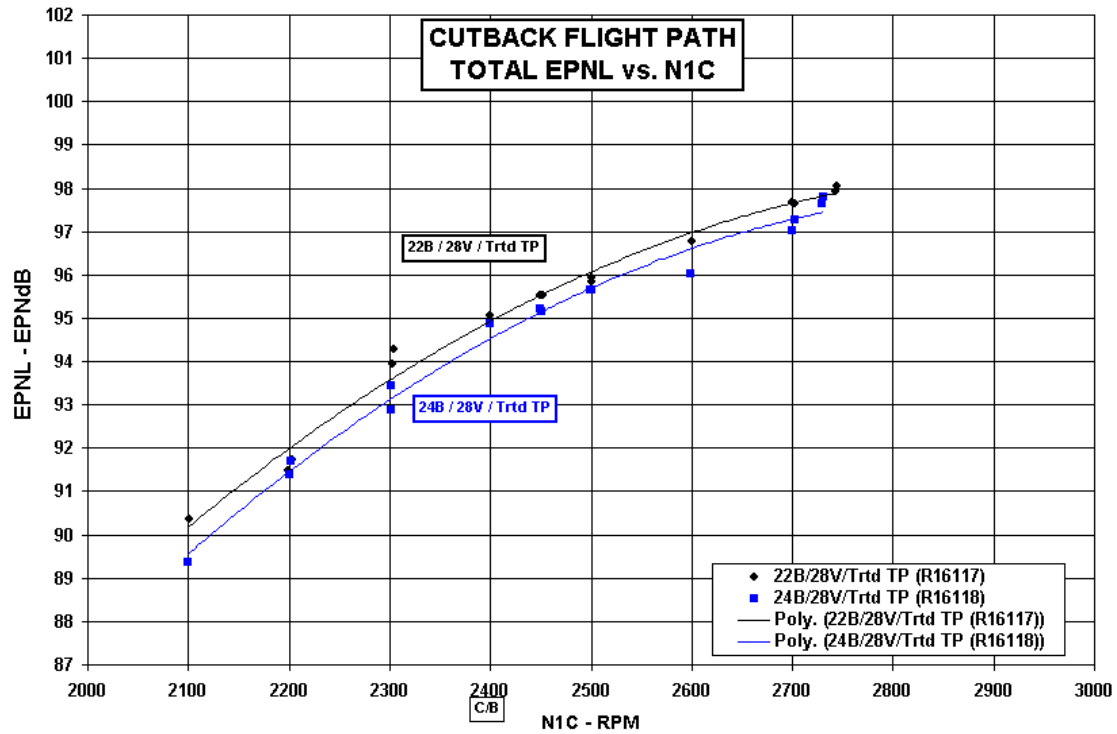
Figure 53.—Effect of fan blade number on total EPNL versus N1C—cutback flight path.
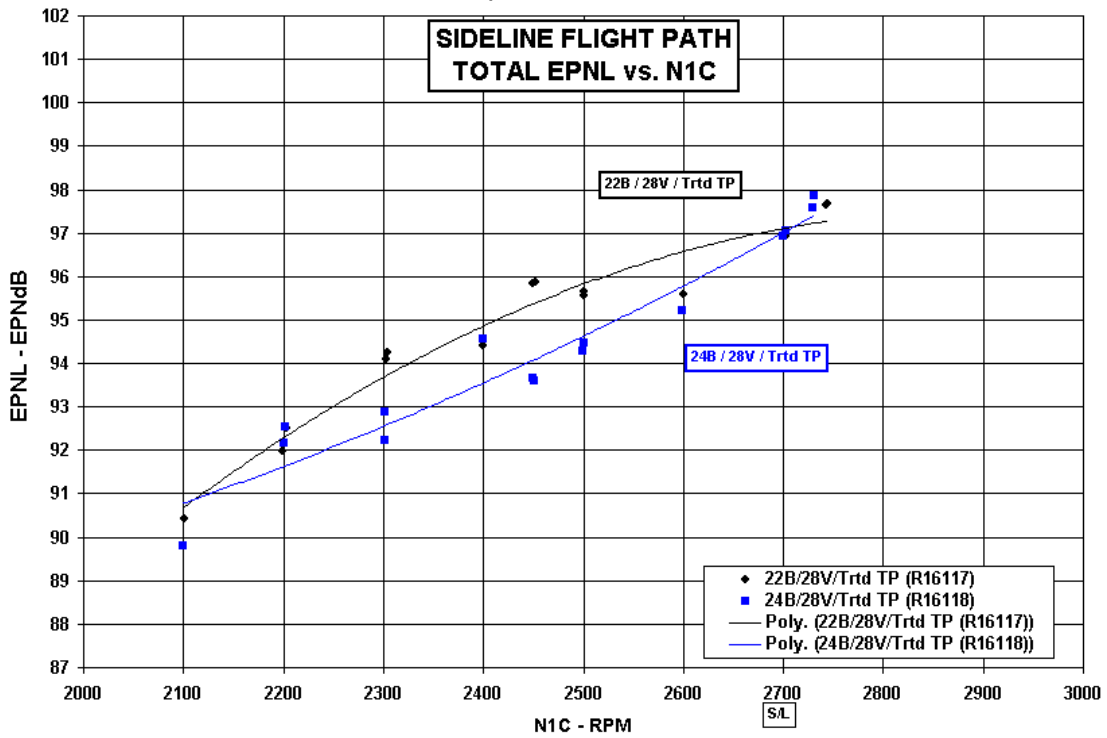
Figure 54.—Effect of fan blade number on total EPNL versus N1C—sideline flight path.
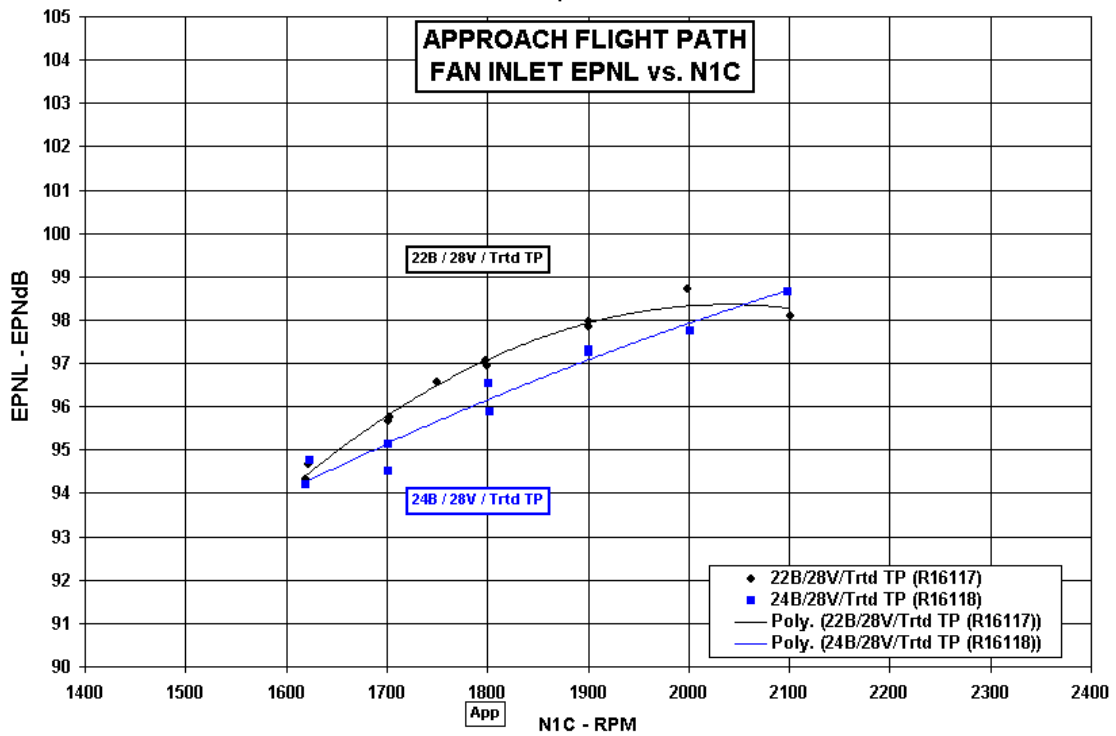
Figure 55.—Effect of fan blade number on fan inlet EPNL versus N1C—approach flight path.
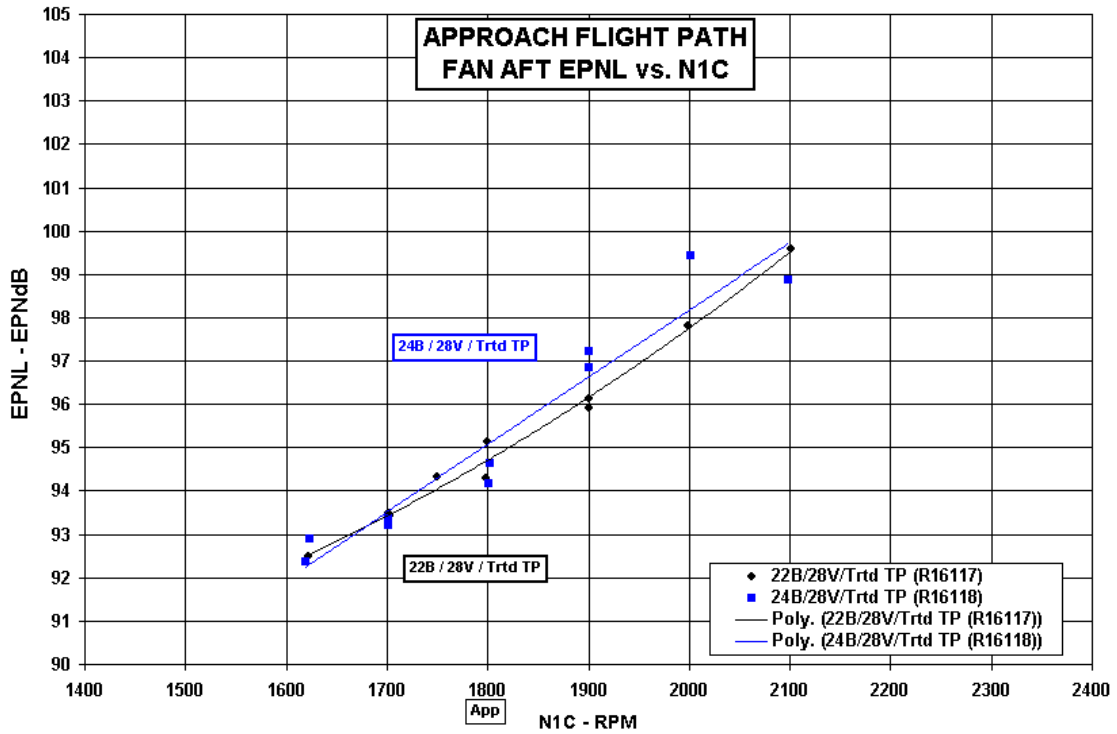
Figure 56.—Effect of fan blade number on fan aft EPNL versus N1C—approach flight path.

Figure 57.—Effect of fan blade number on fan inlet EPNL versus N1C—cutback flight path.
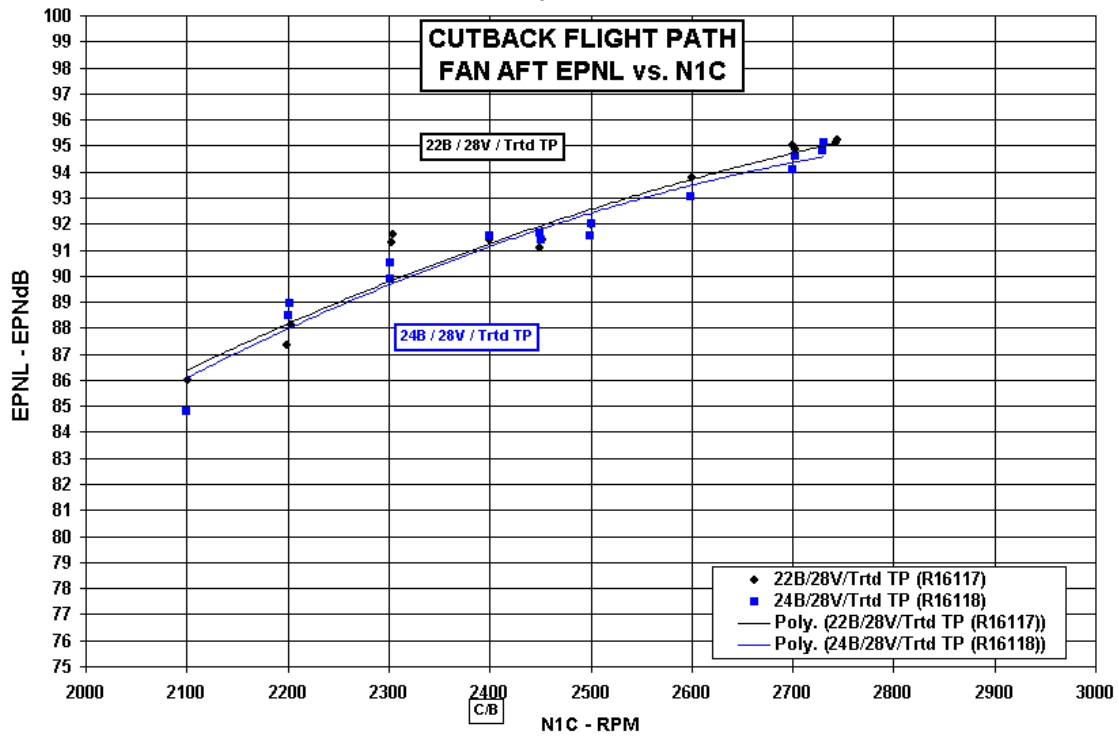
Figure 58.—Effect of fan blade number on fan aft EPNL versus N1C—cutback flight path.
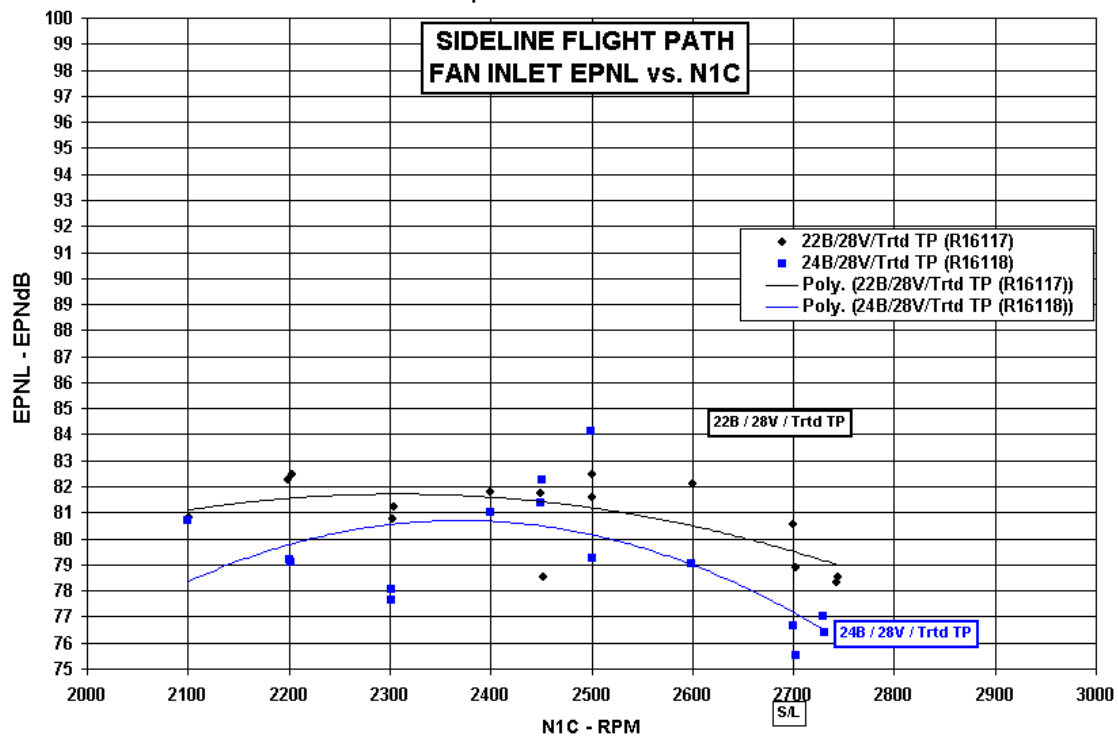
Figure 59.—Effect of fan blade number on fan inlet EPNL versus N1C—sideline flight path.

Figure 60.—Effect of fan blade number on fan aft EPNL versus N1C—sideline flight path.

Figure 61.—Effect of fan blade number on in-flight fan inlet PNLT directivity—approach power.
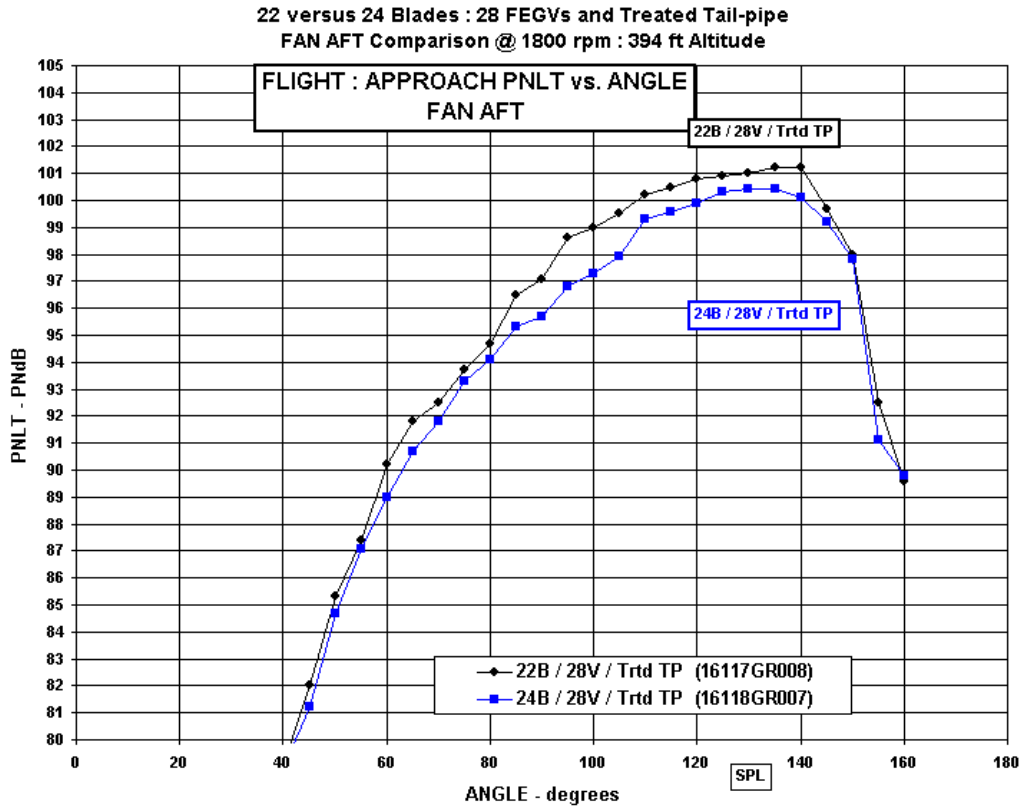
Figure 62.—Effect of fan blade number on in-flight fan aft PNLT directivity—approach power.
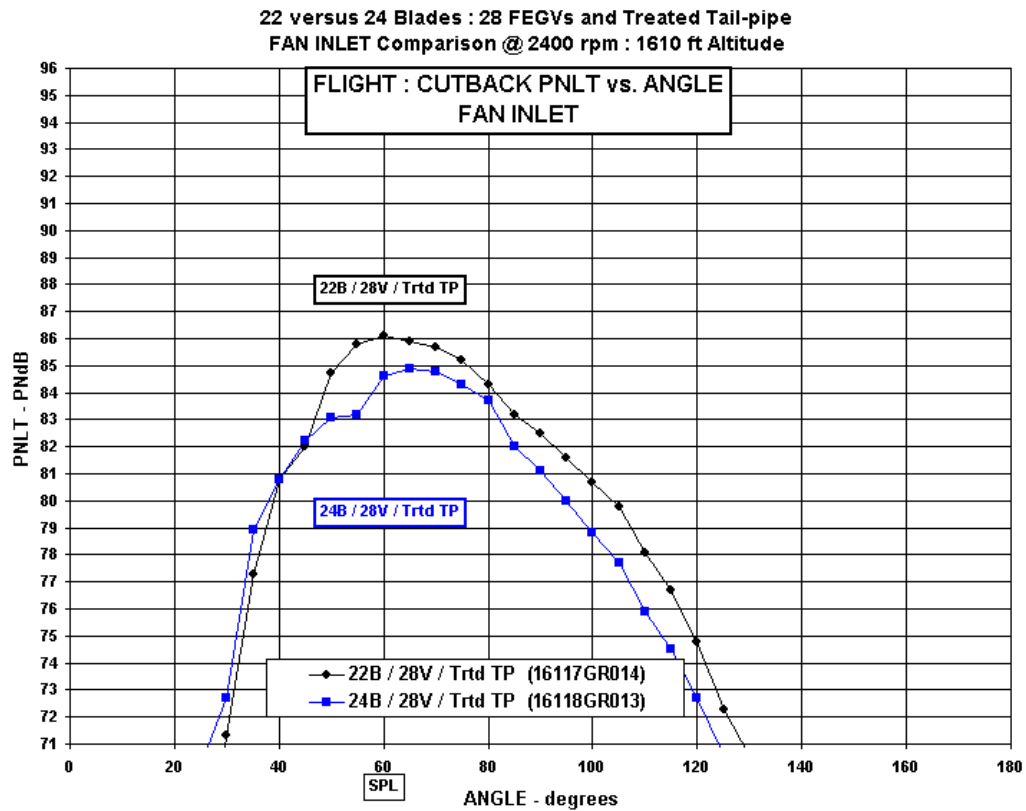
Figure 63.—Effect of fan blade number on in-flight fan inlet PNLT directivity—cutback power.
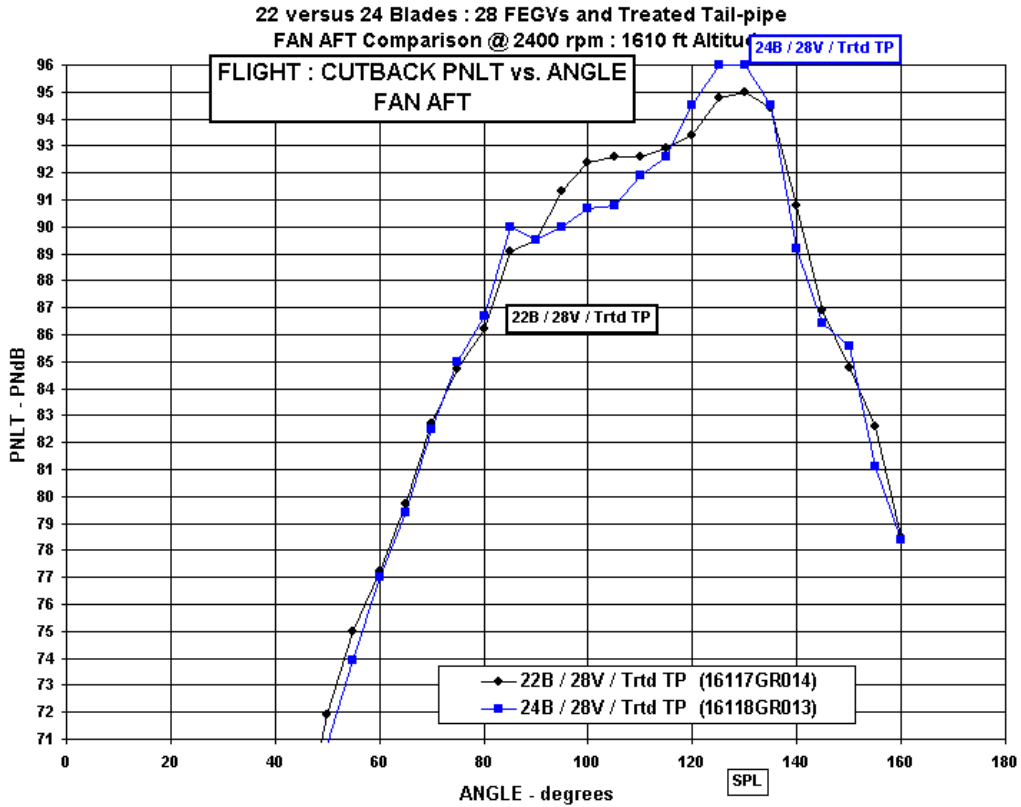
Figure 64.—Effect of fan blade number on in-flight fan aft PNLT directivity—cutback power.
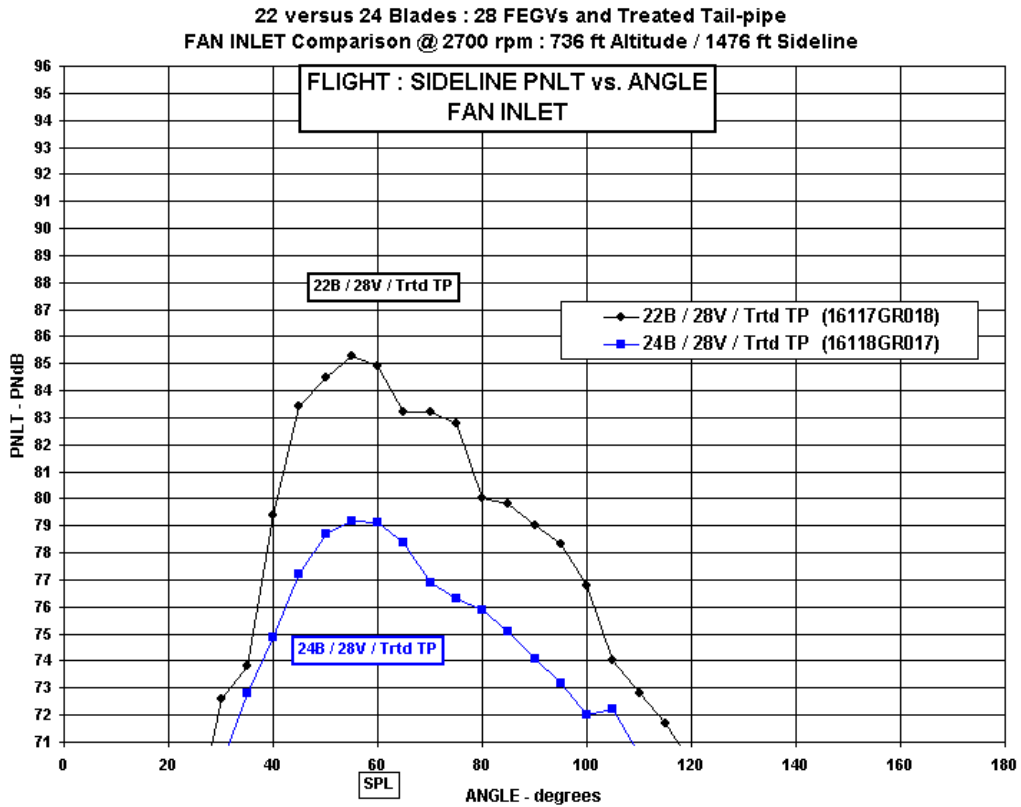
Figure 65.—Effect of fan blade number on in-flight fan inlet PNLT directivity—sideline power.

22 versus 24 Blades : 28 FEGVs and Treated Tail-pipe
FAN AFT Comparison @ 2700 rpm : 736 ft Altitude / 1476 ft Sideline
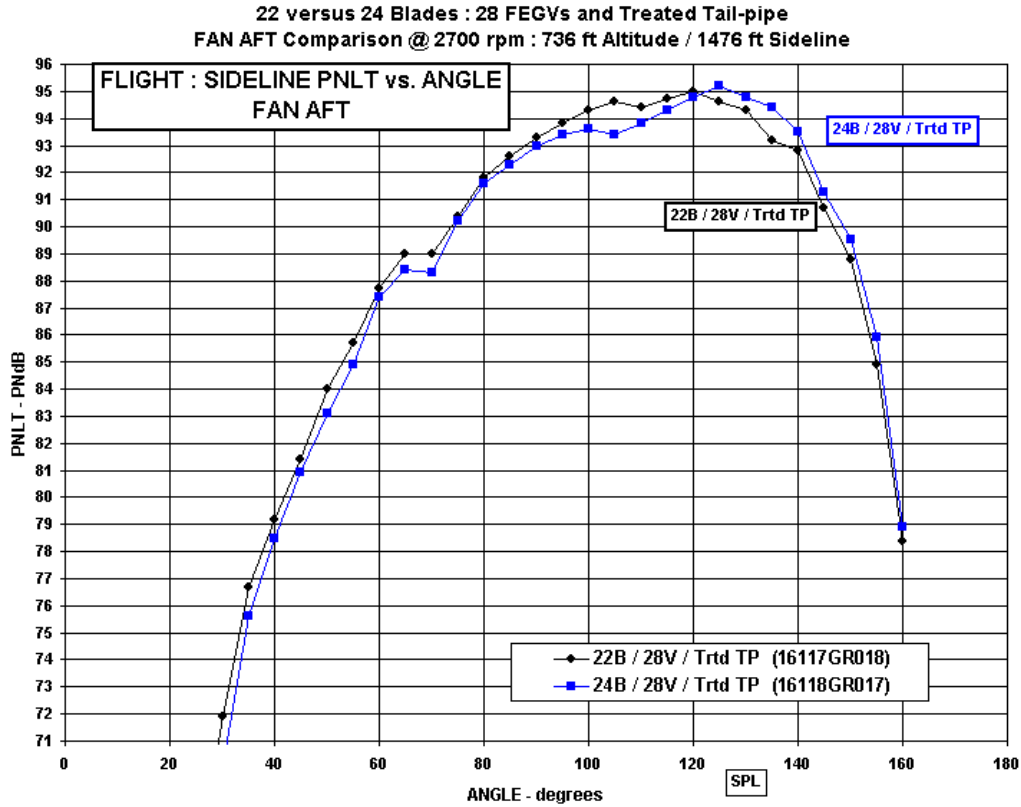
Figure 66.—Effect of fan blade number on in-flight fan aft PNLT directivity—sideline power.

22 versus 24 Blades : 28 FEGVs and Treated Tail-pipe
FAN INLET Comparison @ 1800 rpm : 394 ft Altitude
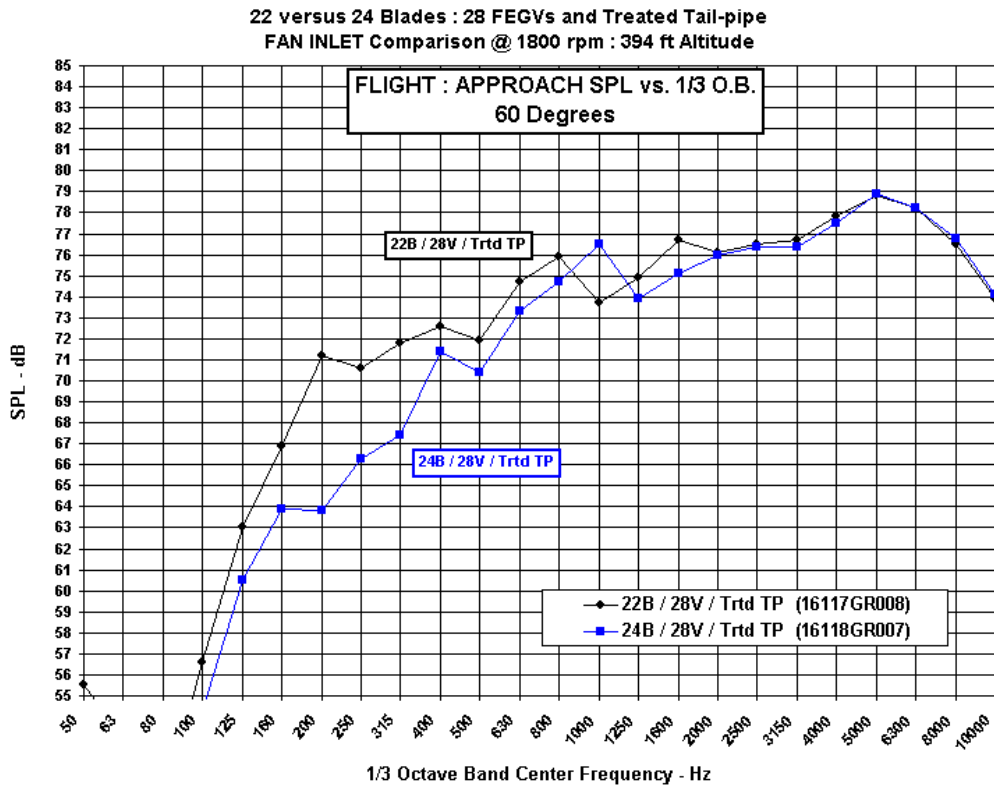
Figure 67.—Effect of fan blade number on in-flight fan inlet SPL spectra at 60°—approach power.

22 versus 24 Blades : 28 FEGVs and Treated Tail-pipe
FAN AFT Comparison @ 1800 rpm : 394 ft Altitude

FLIGHT : APPROACH SPL vs. 1/3 O.B.
130 Degrees

22B / 28V / Trtd TP

24B / 28V / Trtd TP

SPL - dB

22B / 28V / Trtd TP (16117GR008)
24B / 28V / Trtd TP (16118GR007)

1/3 Octave Band Center Frequency - Hz
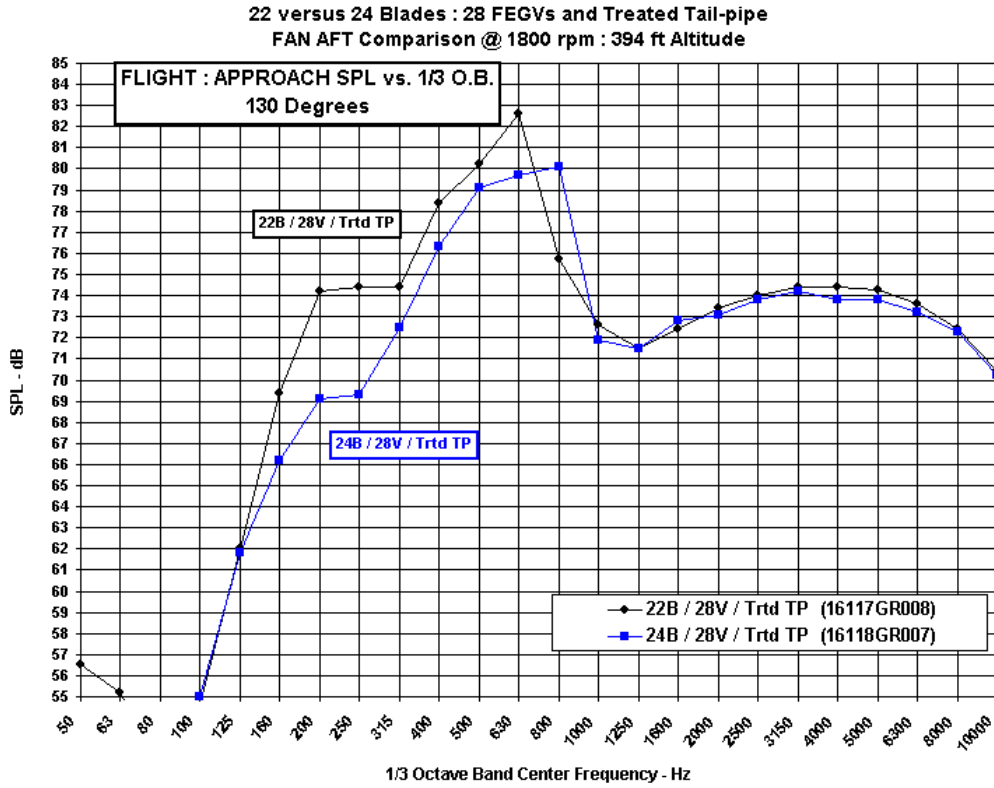
Figure 68.—Effect of fan blade number on in-flight fan aft SPL spectra at 130°—approach power.

22 versus 24 Blades : 28 FEGVs and Treated Tail-pipe
FAN INLET Comparison @ 2400 rpm : 1610 ft Altitude

FLIGHT : CUTBACK SPL vs. 1/3 O.B.
60 Degrees

22B / 28V / Trtd TP (16117GR014)
24B / 28V / Trtd TP (16118GR013)

22B / 28V / Trtd TP

24B / 28V / Trtd TP

SPL - dB

1/3 Octave Band Center Frequency - Hz
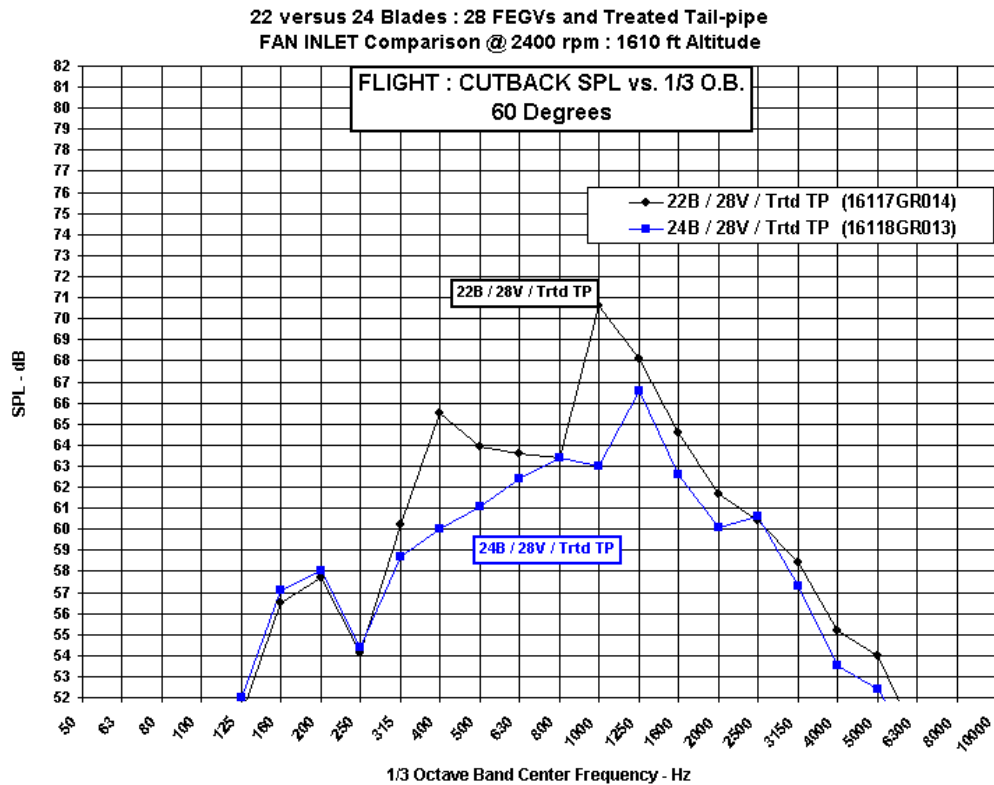
Figure 69.—Effect of fan blade number on in-flight fan inlet SPL spectra at 60°—cutback power.
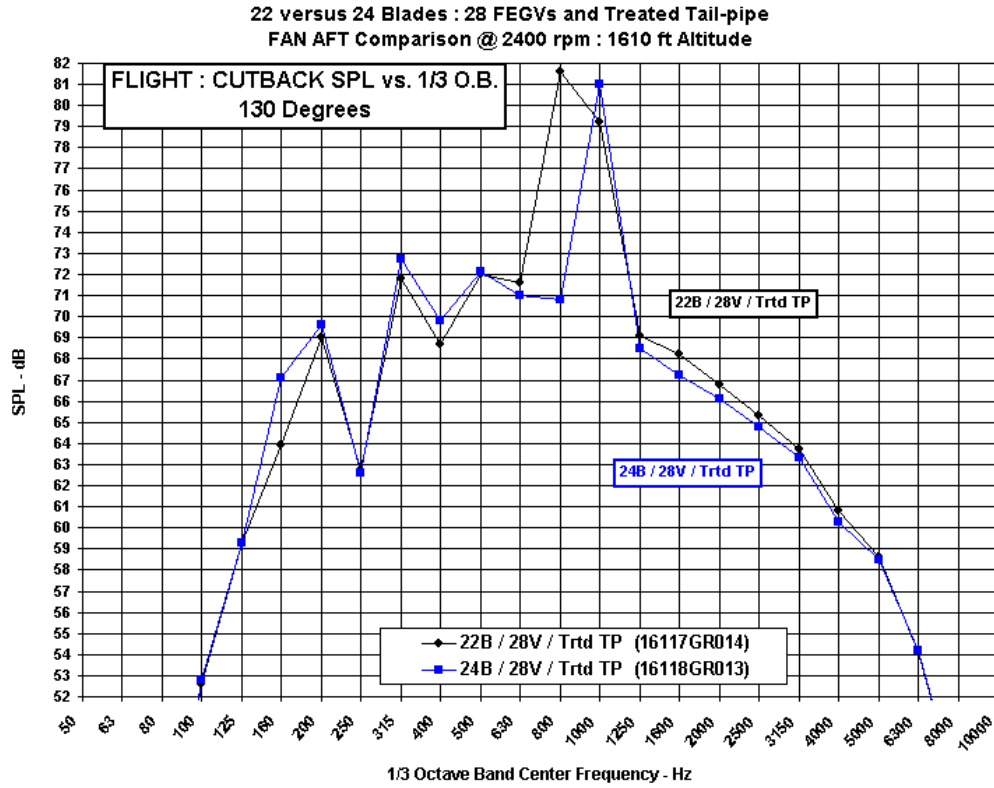
Figure 70.—Effect of fan blade number on in-flight fan aft SPL spectra at 130°—cutback power.
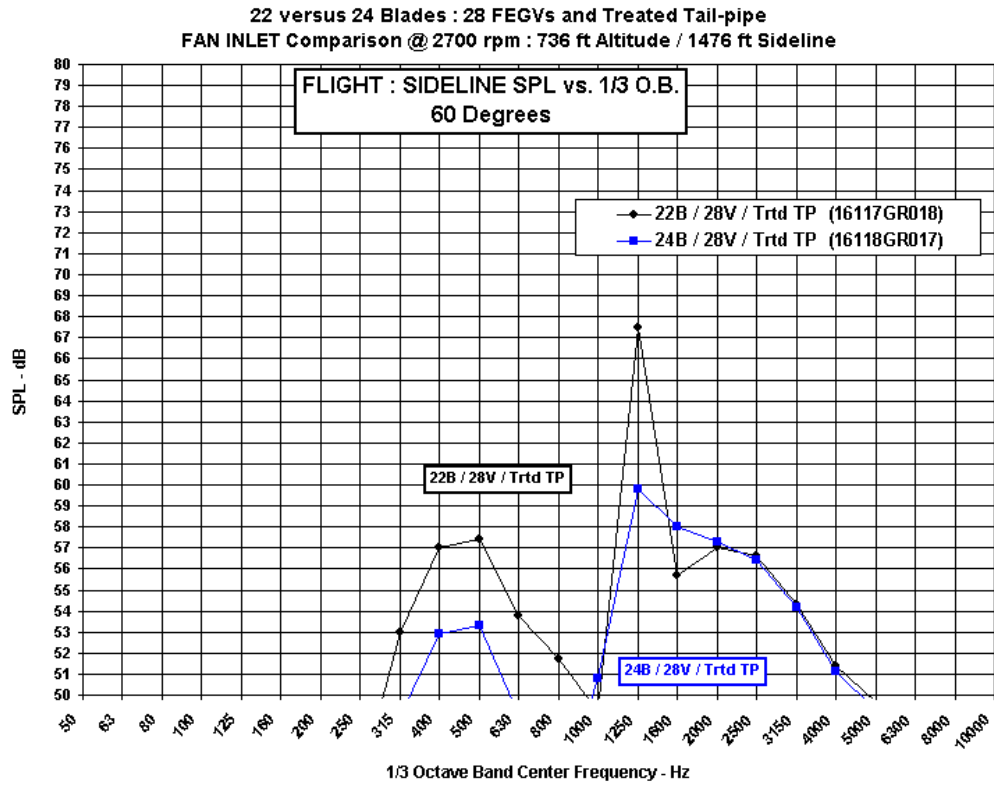
Figure 71.—Effect of fan blade number on in-flight fan inlet SPL spectra at 60°—sideline power.
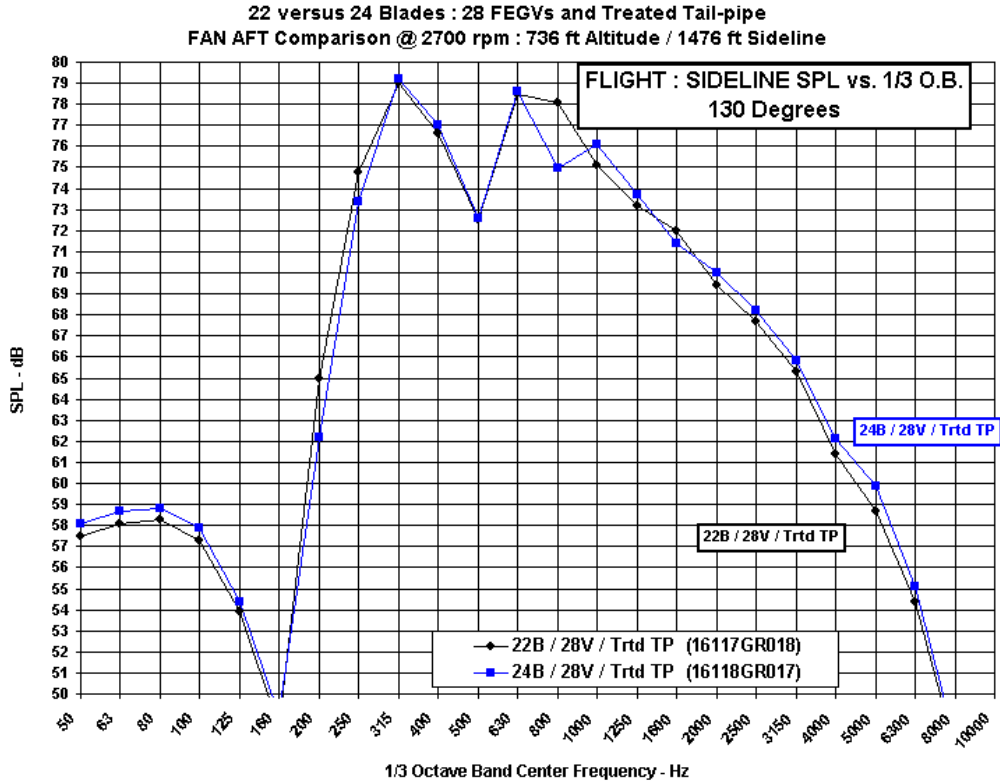
Figure 72.—Effect of fan blade number on in-flight fan aft SPL spectra at 130°—sideline power.
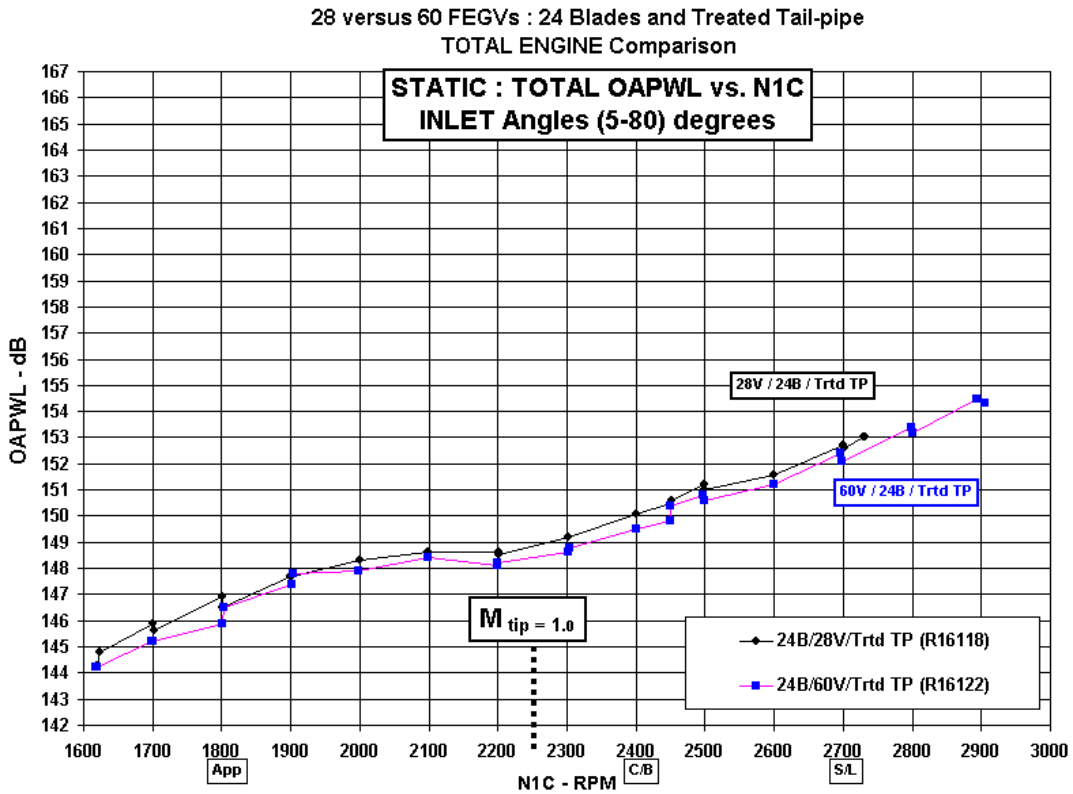
Figure 73.—Effect of FEGV number on static total OAPWL versus N1C—inlet angles (5° to 80°).

28 versus 60 FEGVs : 24 Blades and Treated Tail-pipe
TOTAL ENGINE Comparison
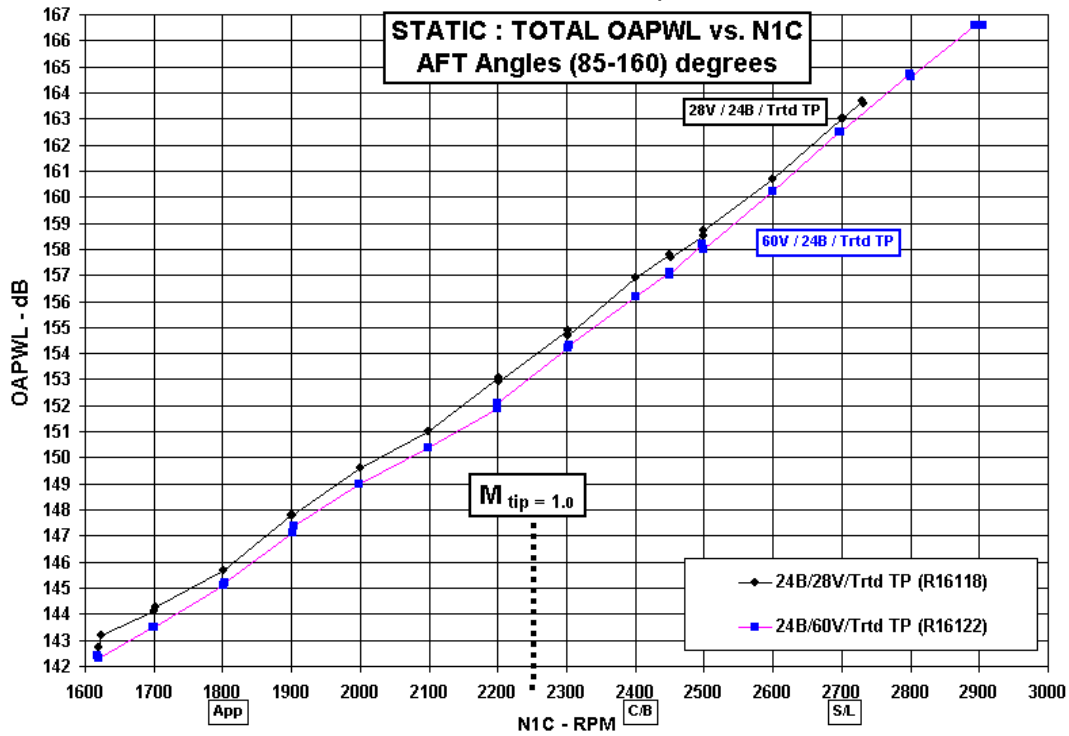
Figure 74.—Effect of FEGV number on static total OAPWL versus N1C—aft angles (85° to 160°).

28 versus 60 FEGVs : 24 Blades and Treated Tail-pipe
TOTAL ENGINE Comparison : 1800 rpm
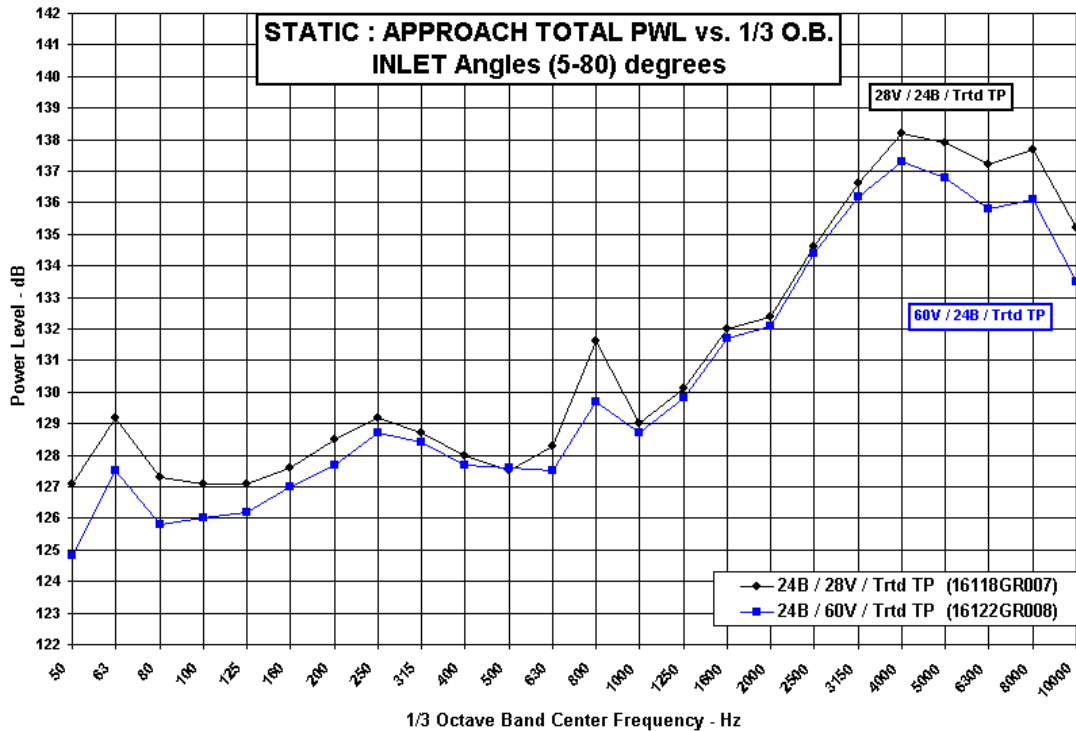
Figure 75.—Effect of FEGV number on static total PWL spectra (inlet angles 5° to 80°)—approach power.
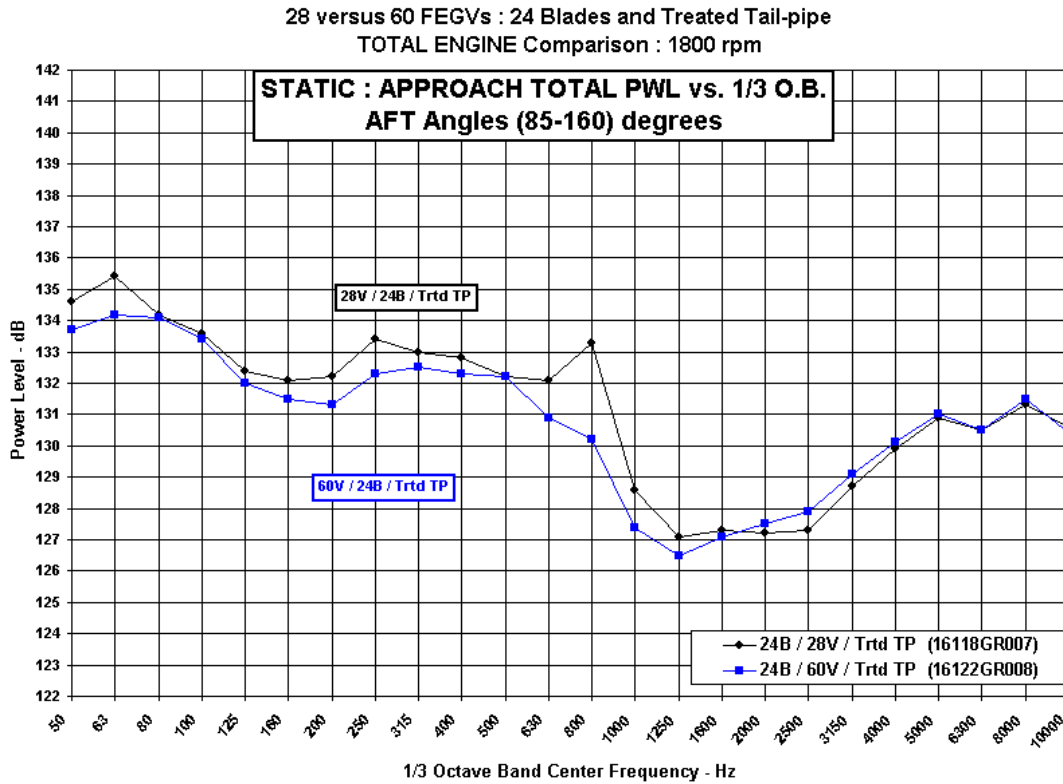
Figure 76.—Effect of FEGV number on static total PWL spectra (aft angles 85° to 160°)—approach power.
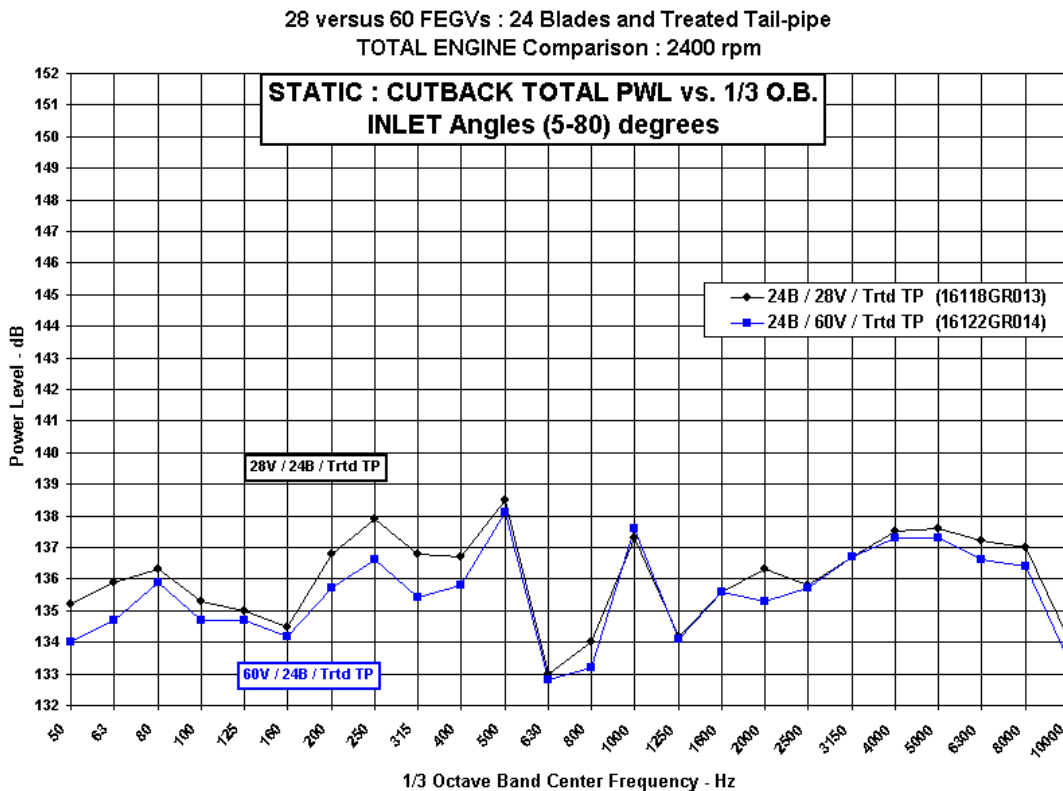
Figure 77.—Effect of FEGV number on static total PWL spectra (inlet angles 5° to 80°)—cutback power.

28 versus 60 FEGVs : 24 Blades and Treated Tail-pipe
TOTAL ENGINE Comparison : 2400 rpm
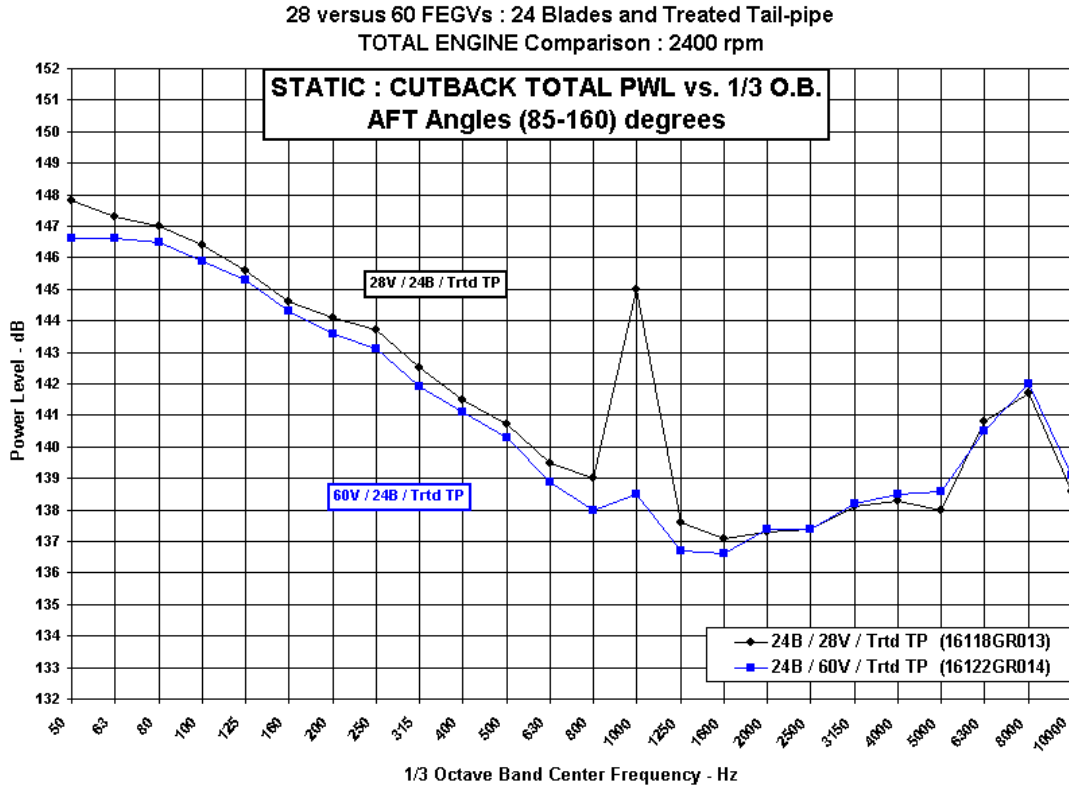
Figure 78.—Effect of FEGV number on static total PWL spectra (aft angles 85° to 160°)—cutback power.

28 versus 60 FEGVs : 24 Blades and Treated Tail-pipe
TOTAL ENGINE Comparison : 2700 rpm
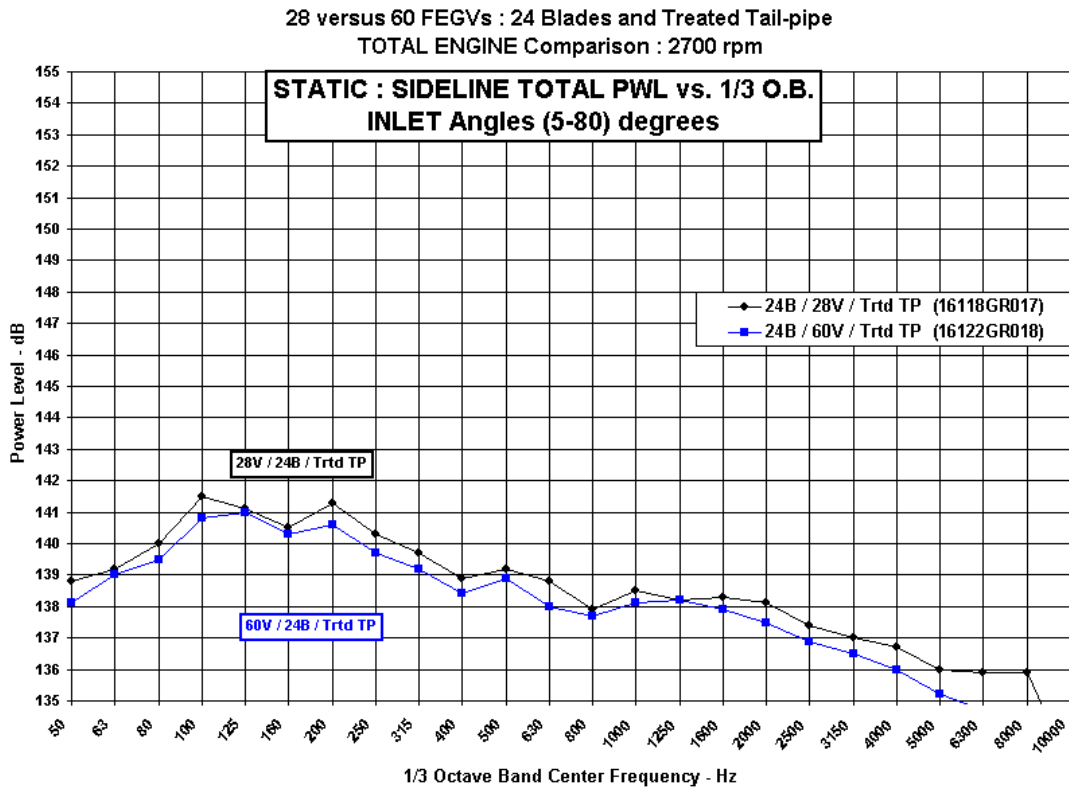
Figure 79.—Effect of FEGV number on static total PWL spectra (inlet angles 5° to 80°)—sideline power.
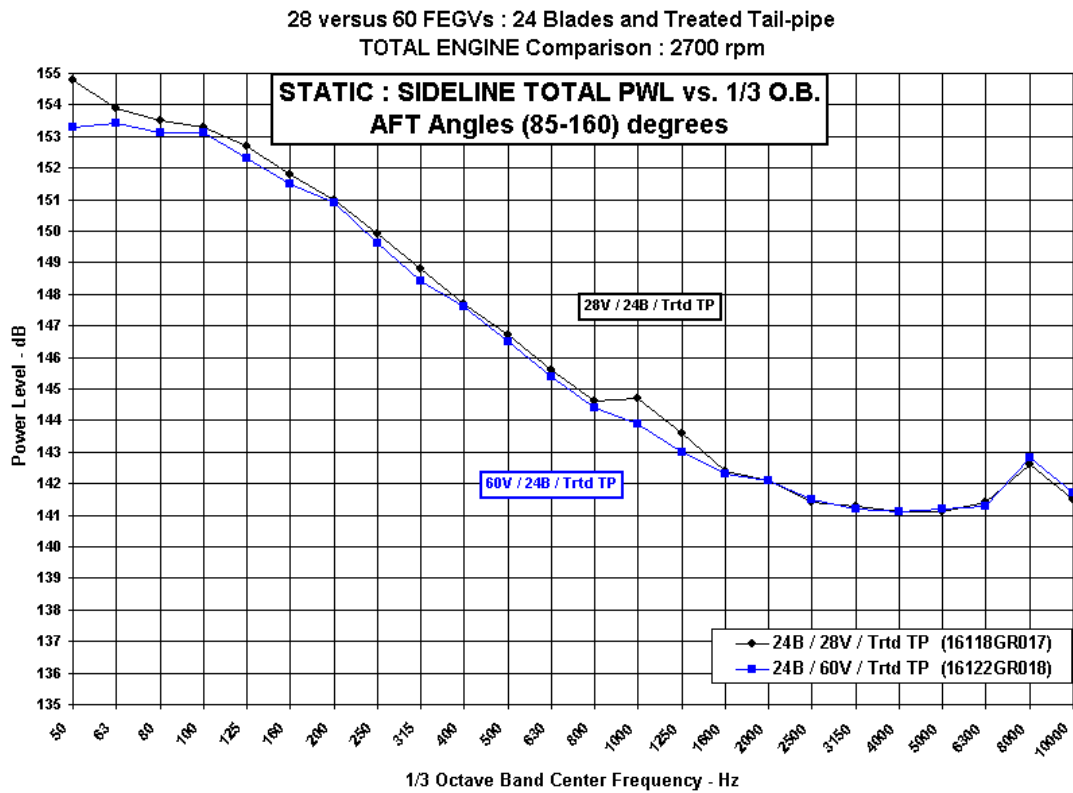
Figure 80.—Effect of FEGV number total PWL spectra (aft angles 85° to 160°)—sideline power.
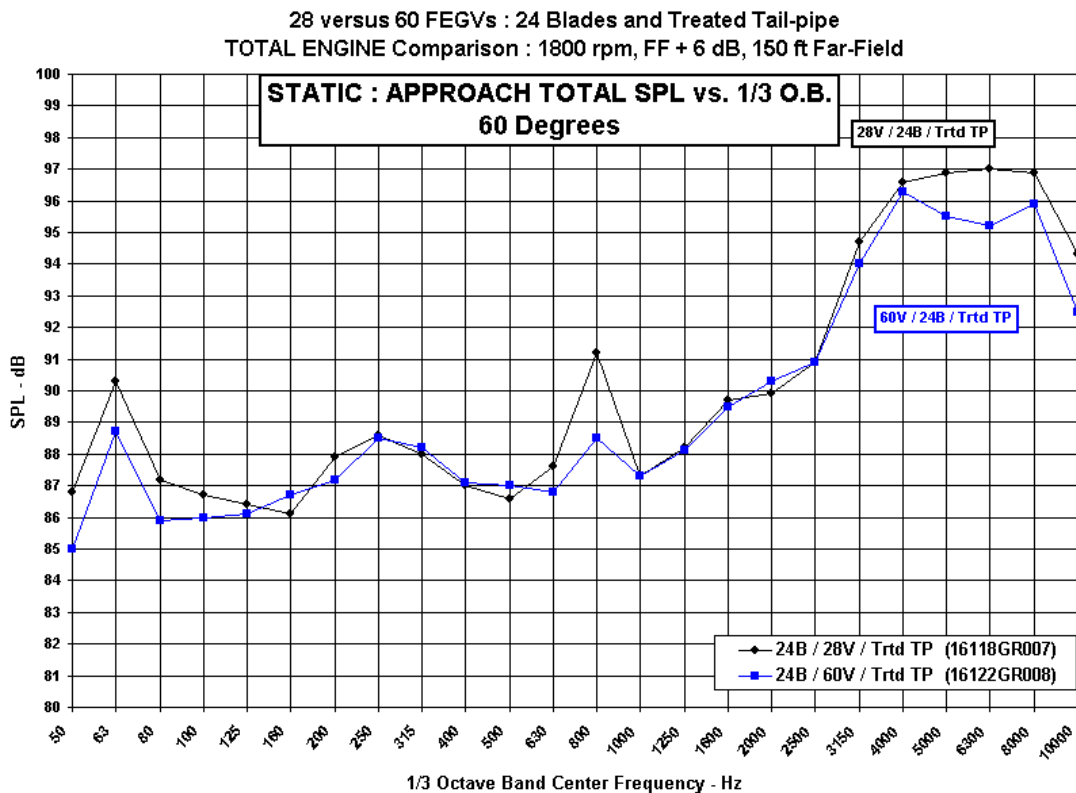
Figure 81.—Effect of FEGV number on static total SPL spectra at 60°—approach power.

Figure 82.—Effect of FEGV number on static total SPL spectra at 130°—approach power.
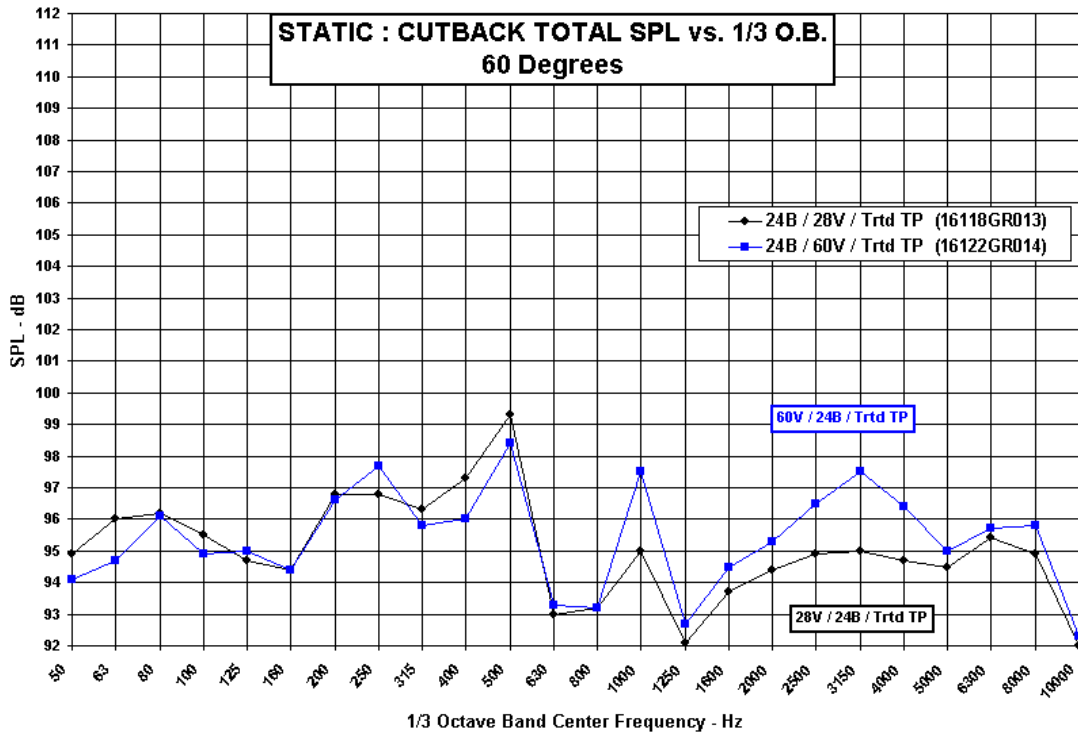
Figure 83.—Effect of FEGV number on static total SPL spectra at 60°—cutback power.
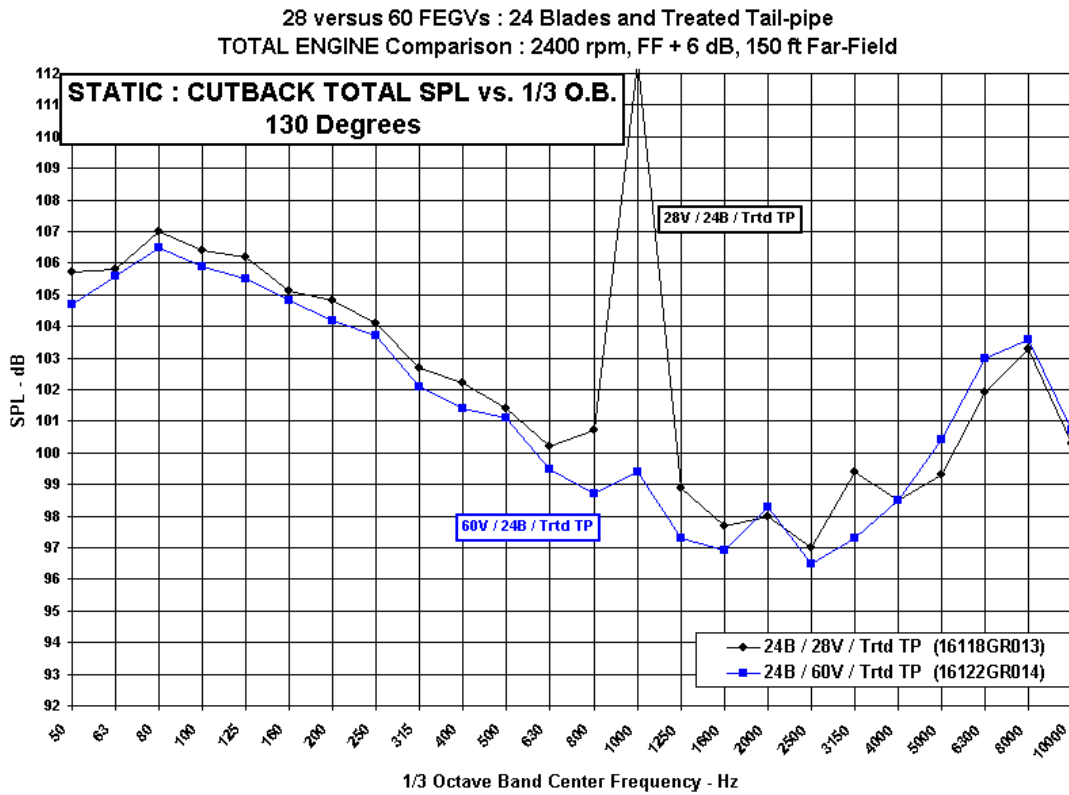
Figure 84.—Effect of FEGV number on static total SPL spectra at 130°—cutback power.
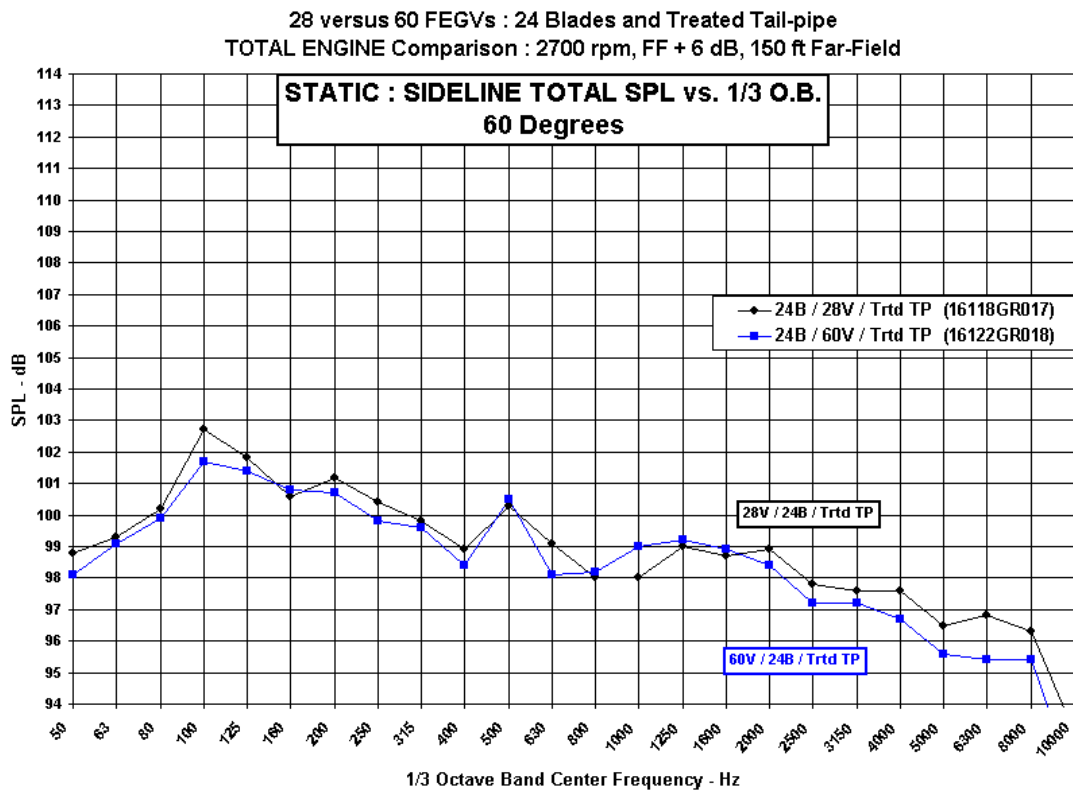
Figure 85.—Effect of FEGV number on static total SPL spectra at 60°—sideline power.
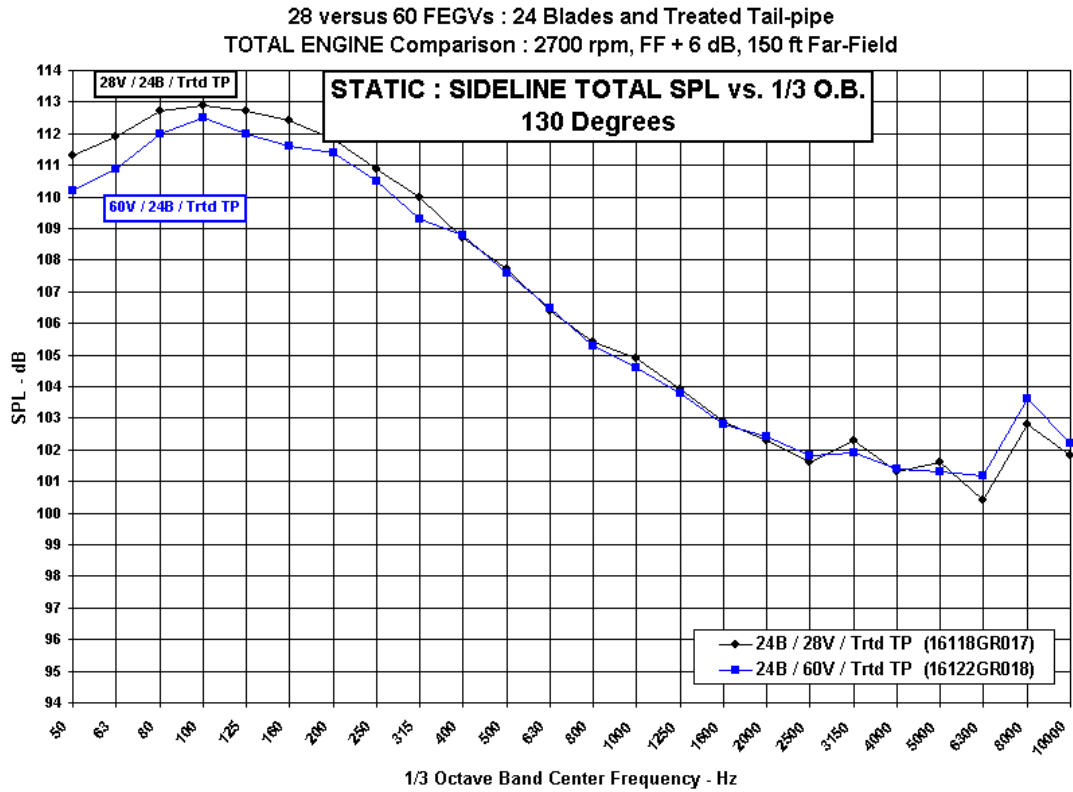
Figure 86.—Effect of FEGV number on static total SPL spectra at 130°—sideline power.
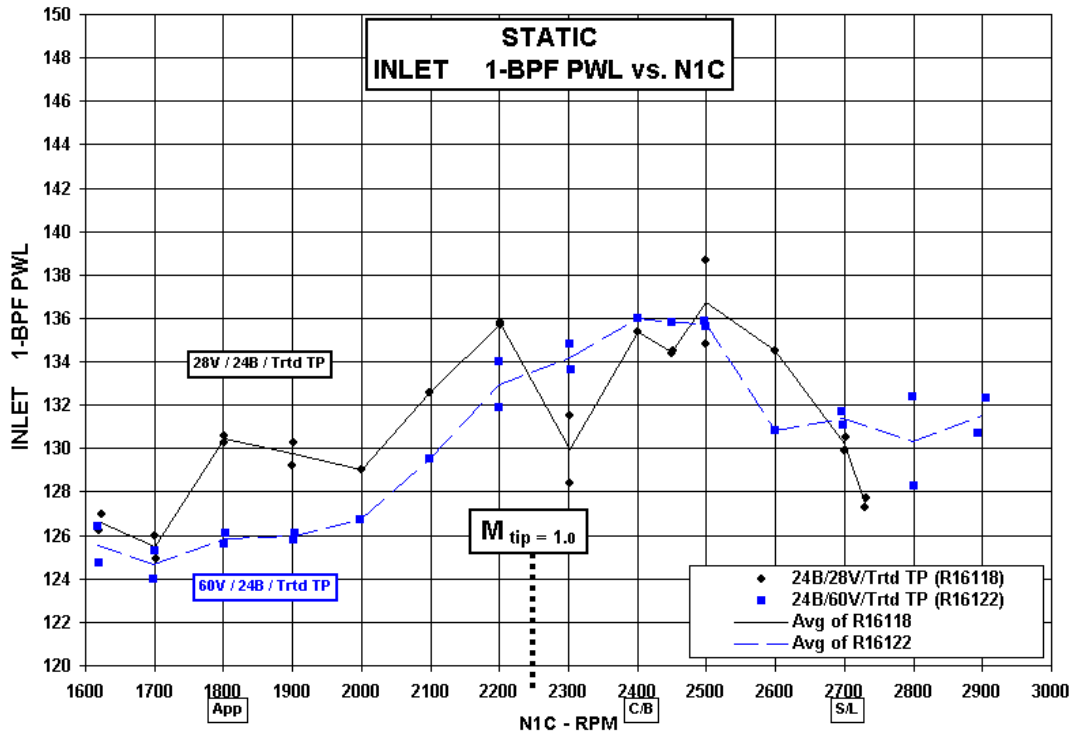
Figure 87.—Effect of FEGV number on inlet 1-BPF PWL versus N1C.
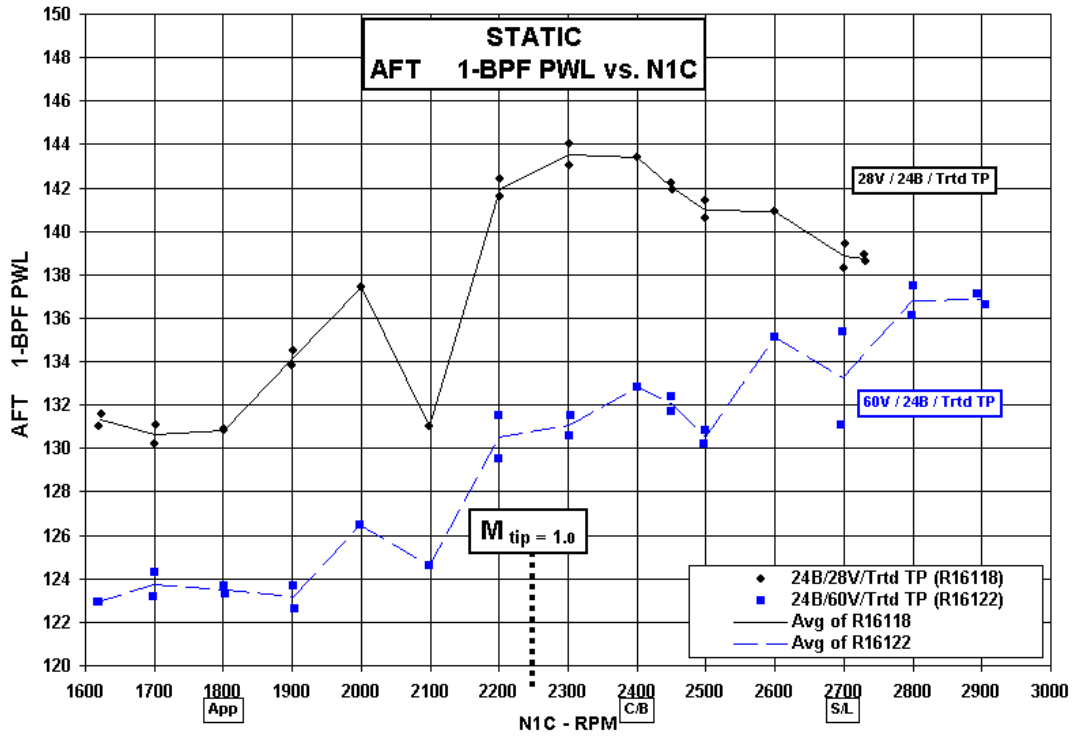
Figure 88.—Effect of FEGV number on static aft 1-BPF PWL versus N1C.
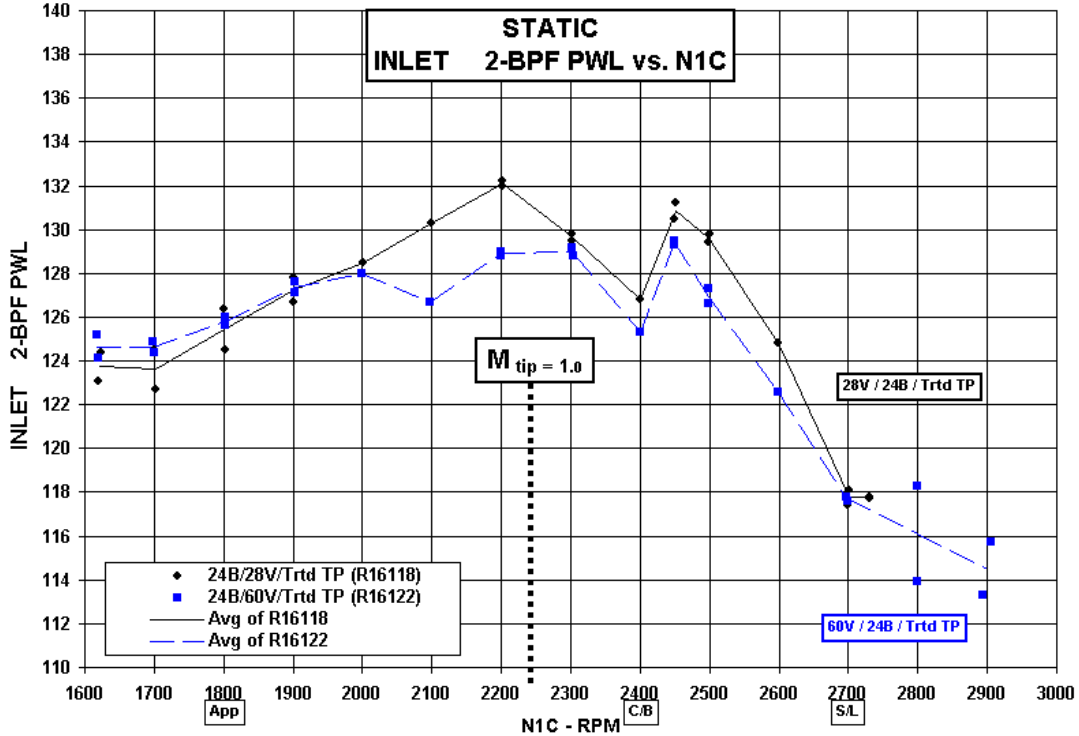
Figure 89.—Effect of FEGV number on static inlet 2-BPF PWL versus N1C.
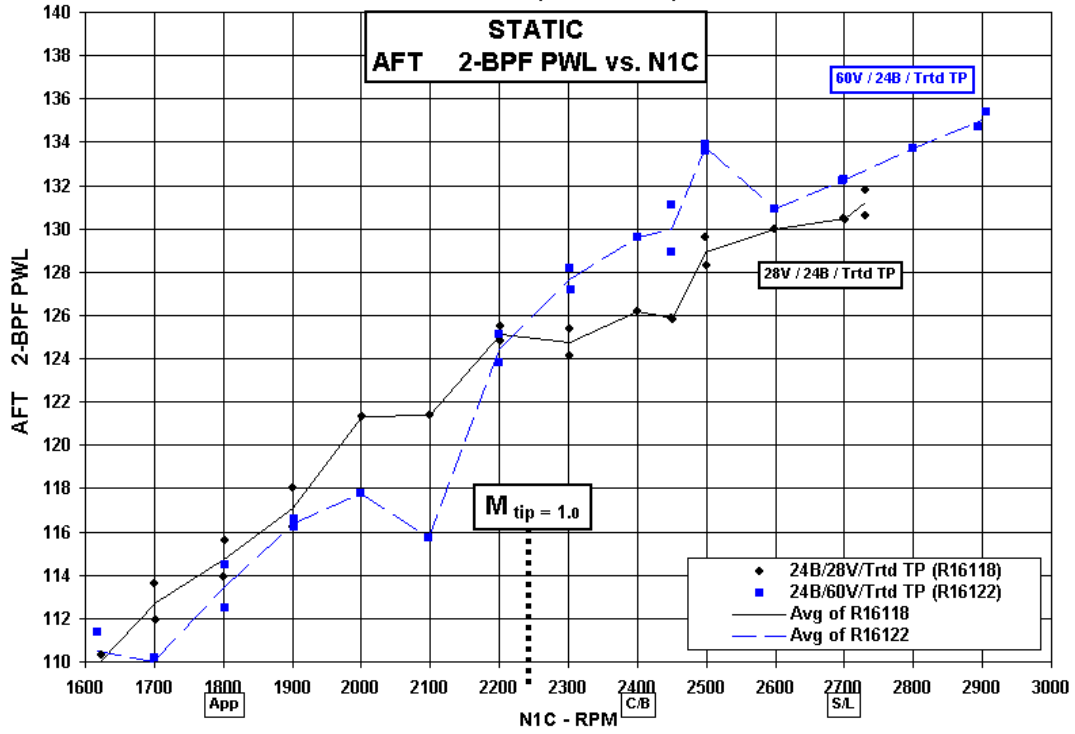
Figure 90.—Effect of FEGV number on static aft 2-BPF PWL versus N1C.
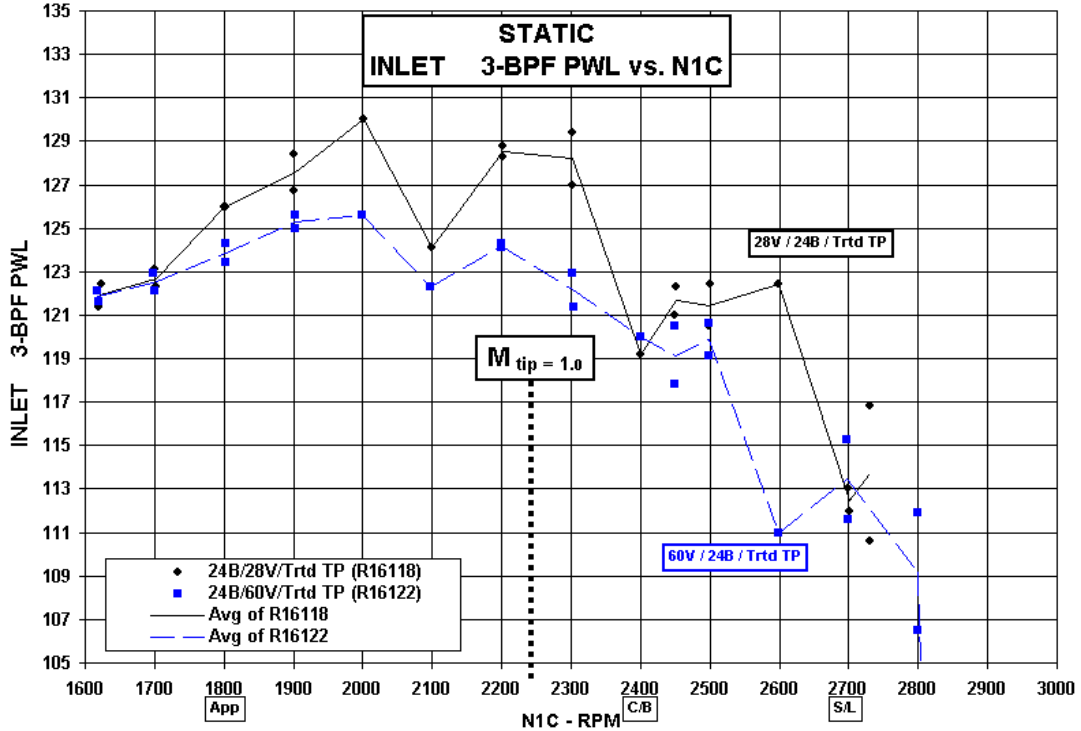
Figure 91.—Effect of FEGV number on static inlet 3-BPF PWL versus N1C.
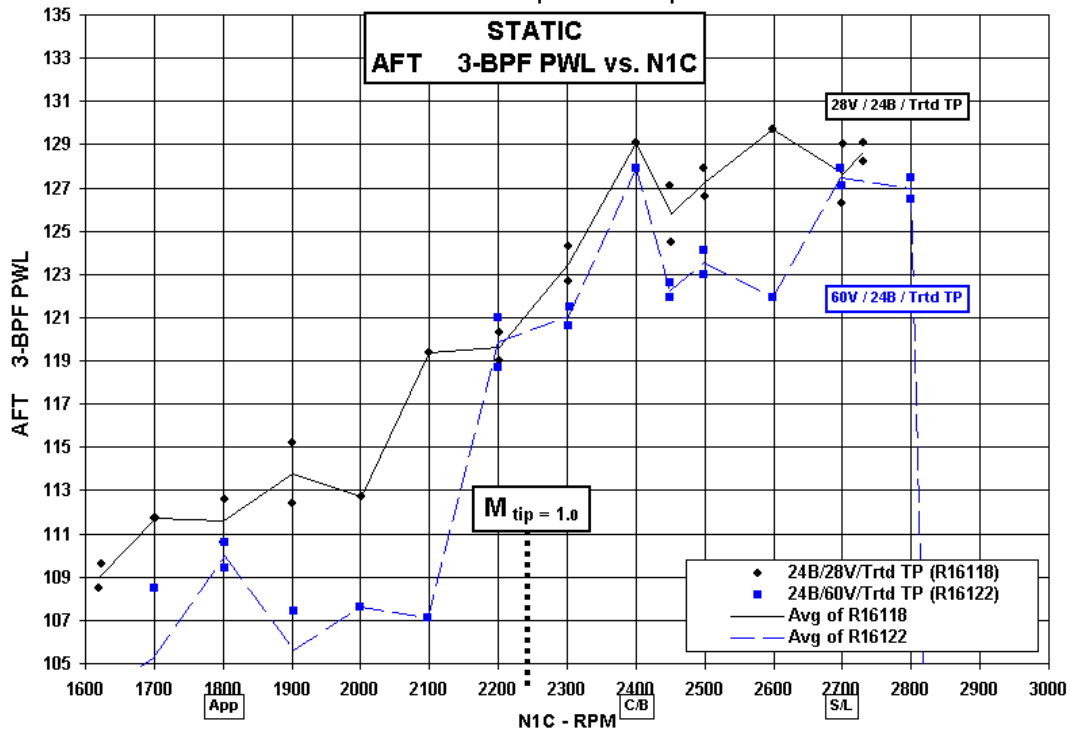
Figure 92.—Effect of FEGV number on static aft 3-BPF PWL versus N1C.
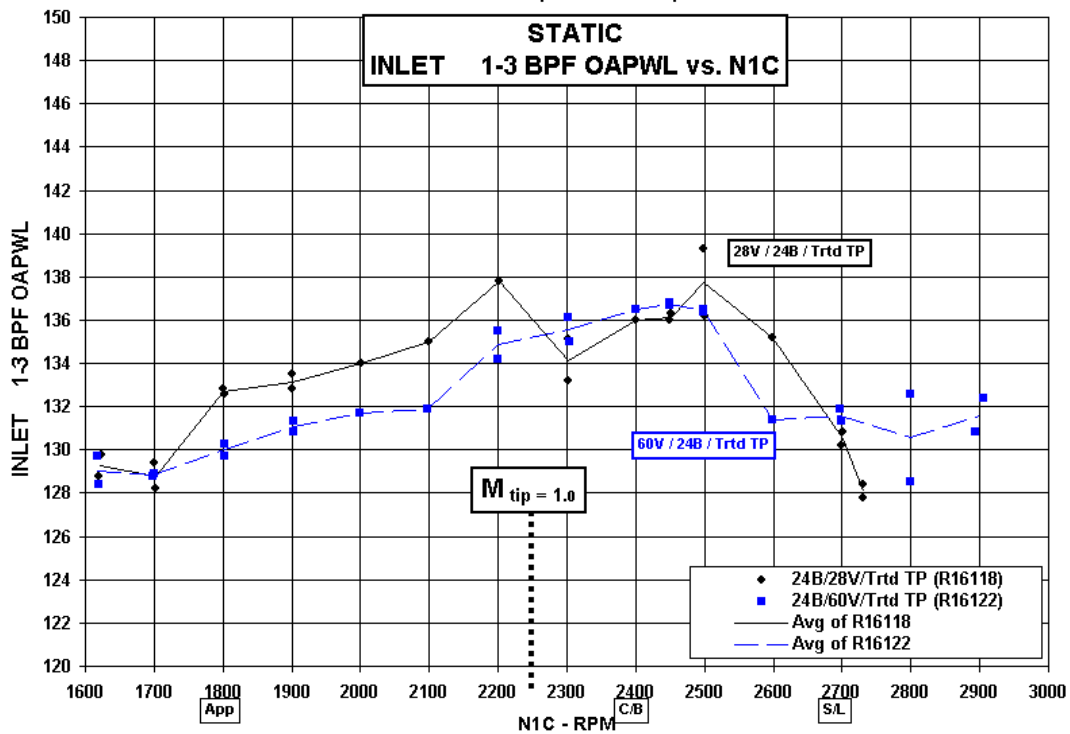
Figure 93.—Effect of FEGV number on static inlet 1-3 BPF OAPWL versus N1C.
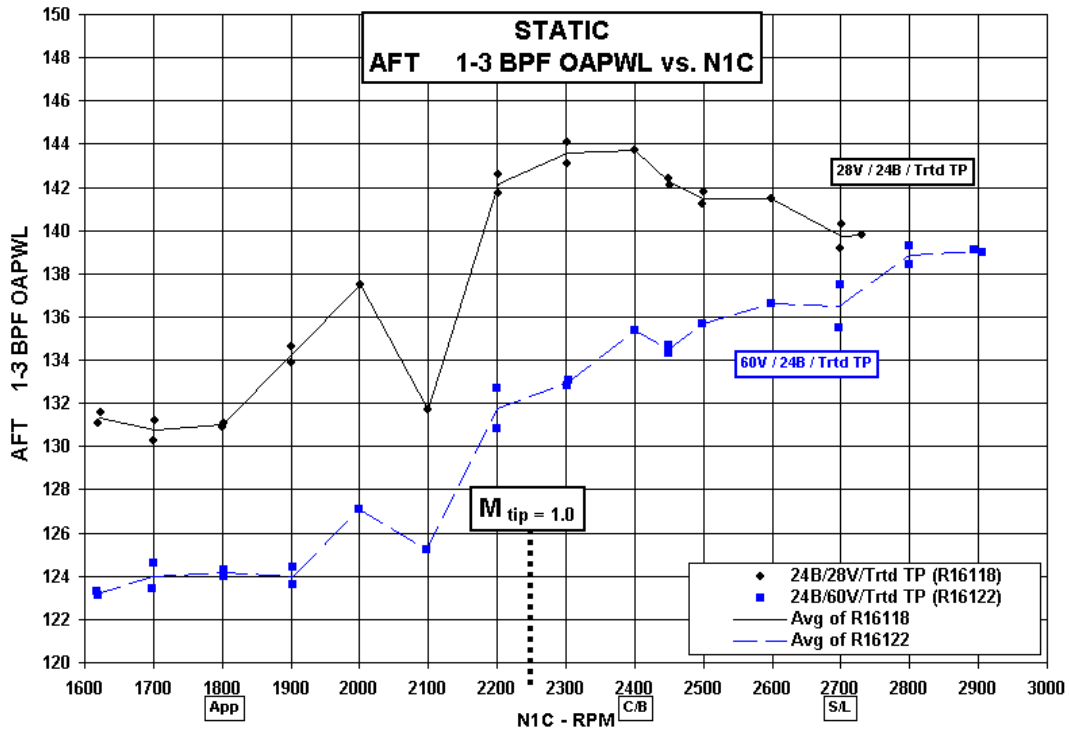
Figure 94.—Effect of FEGV number on static aft 1-3 BPF OAPWL versus N1C.
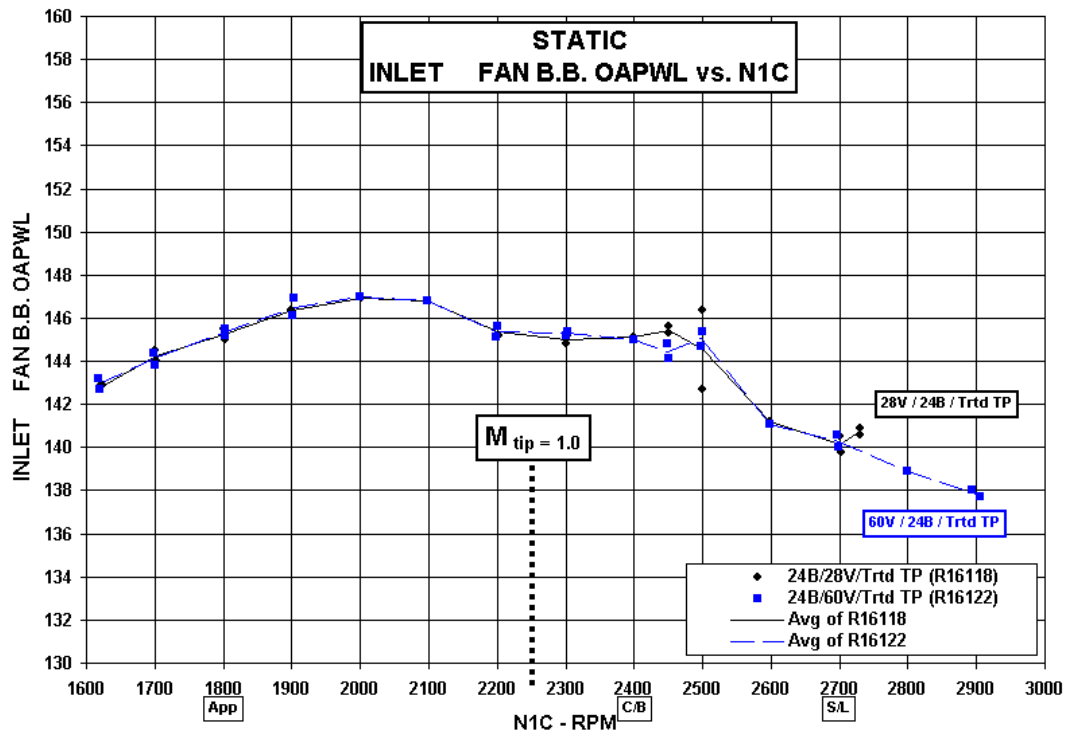
Figure 95.—Effect of FEGV number on static inlet fan B.B. OAPWL versus N1C.
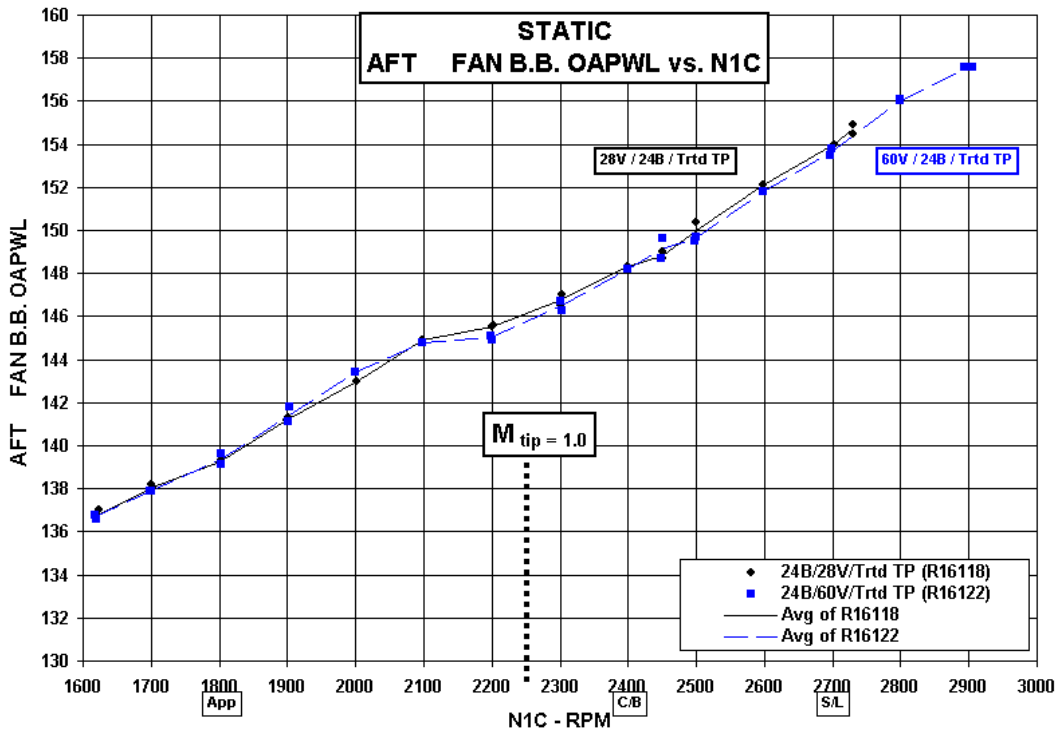
Figure 96.—Effect of FEGV number on static aft fan B.B. OAPWL versus N1C.
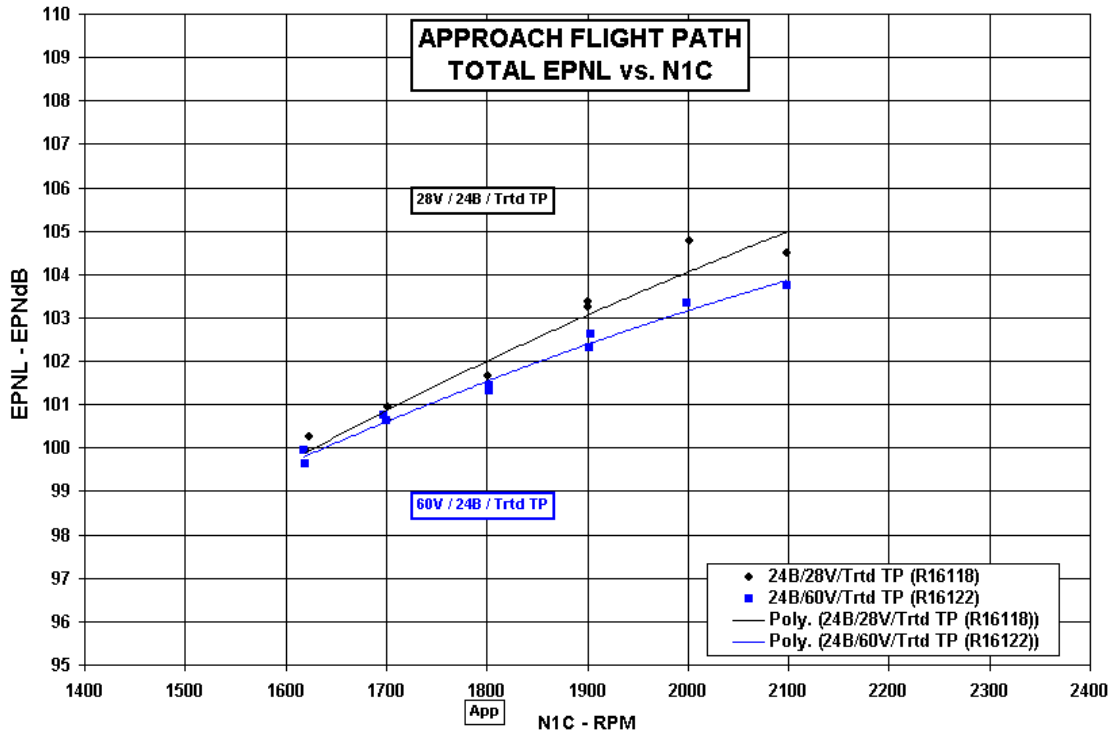
Figure 97.—Effect of FEGV number on total EPNL versus N1C—approach flight path.
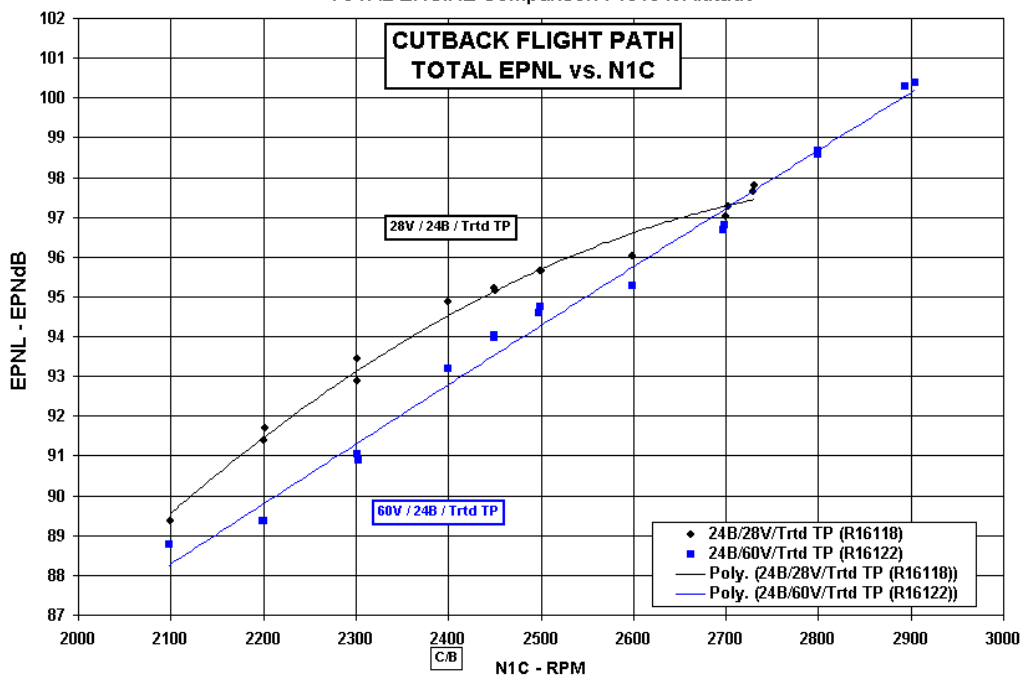
Figure 98.—Effect of FEGV number on total EPNL versus N1C—cutback flight path.
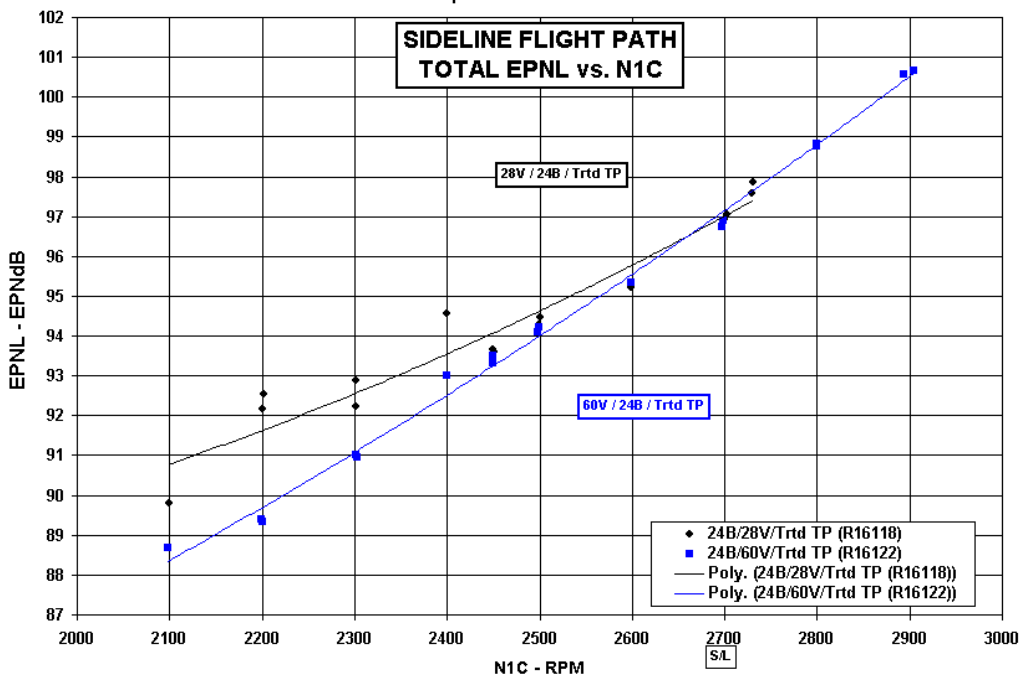
Figure 99.—Effect of FEGV number on total EPNL versus N1C—sideline flight path.

Figure 100.—Effect of FEGV number on fan inlet EPNL versus N1C—approach flight path.
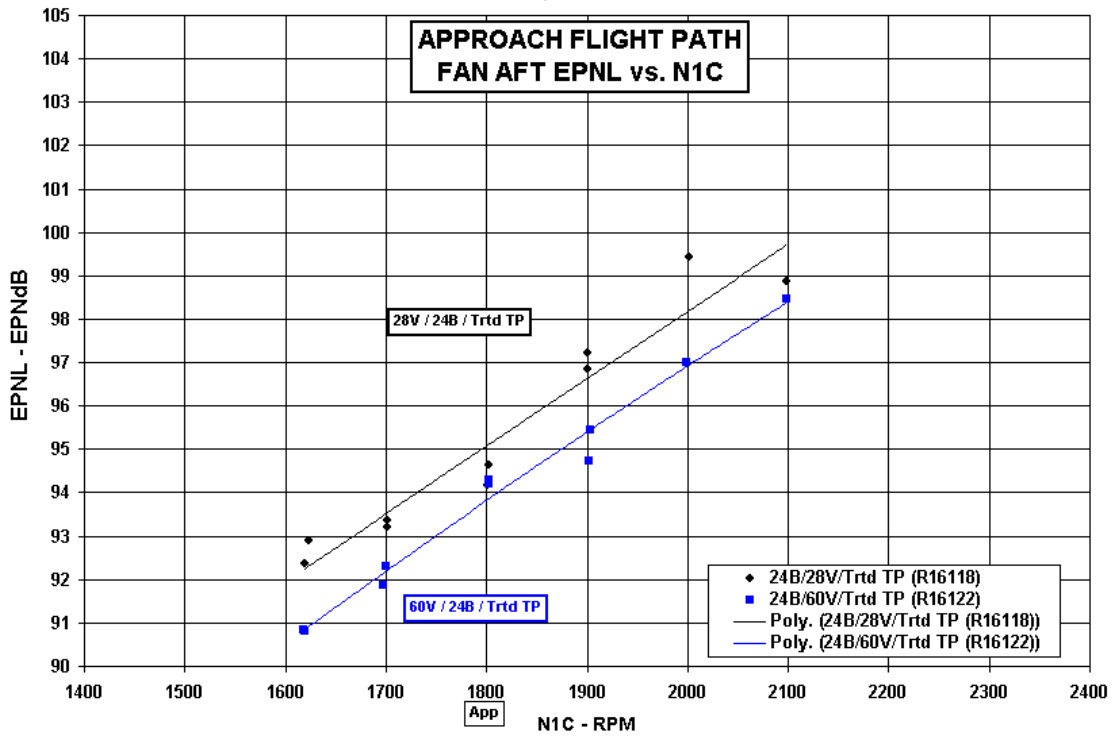
Figure 101.—Effect of FEGV number on fan aft EPNL versus N1C—approach flight path.
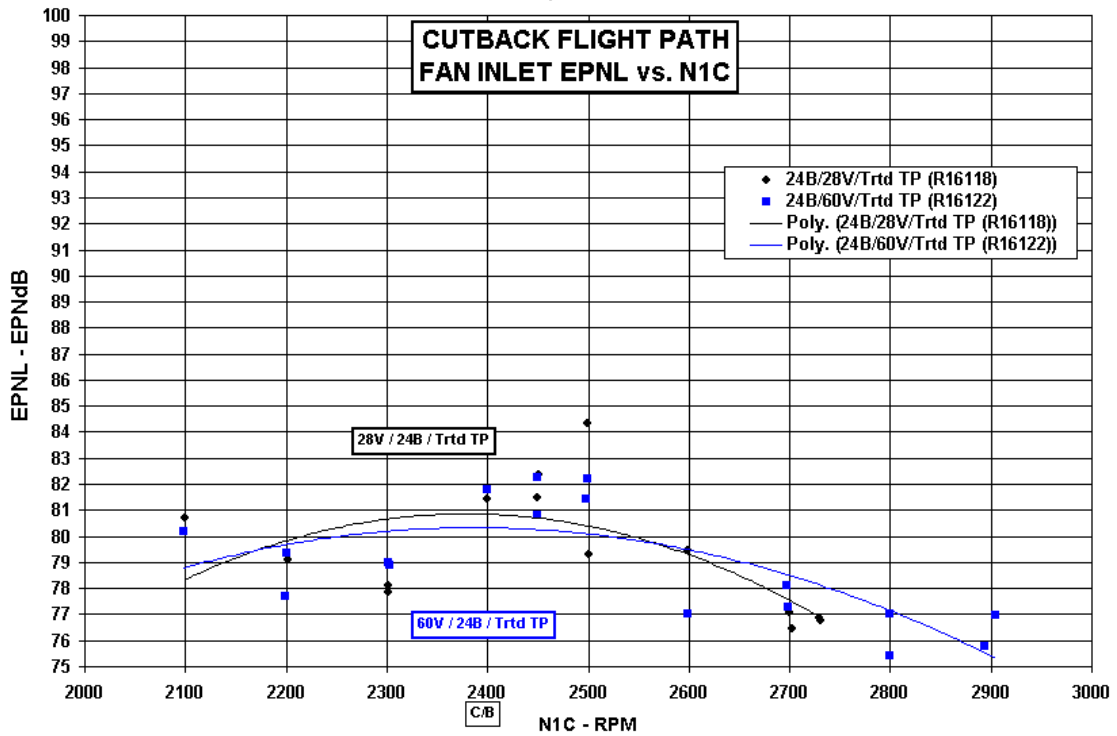
Figure 102.—Effect of FEGV number on fan inlet EPNL versus N1C—cutback flight path.

Figure 103.—Effect of FEGV number on fan aft EPNL versus N1C—cutback flight path.

28 versus 60 FEGVs : 24 Blades and Treated Tail-pipe
FAN INLET Comparison : 736 ft Altitude / 1476 ft Sideline
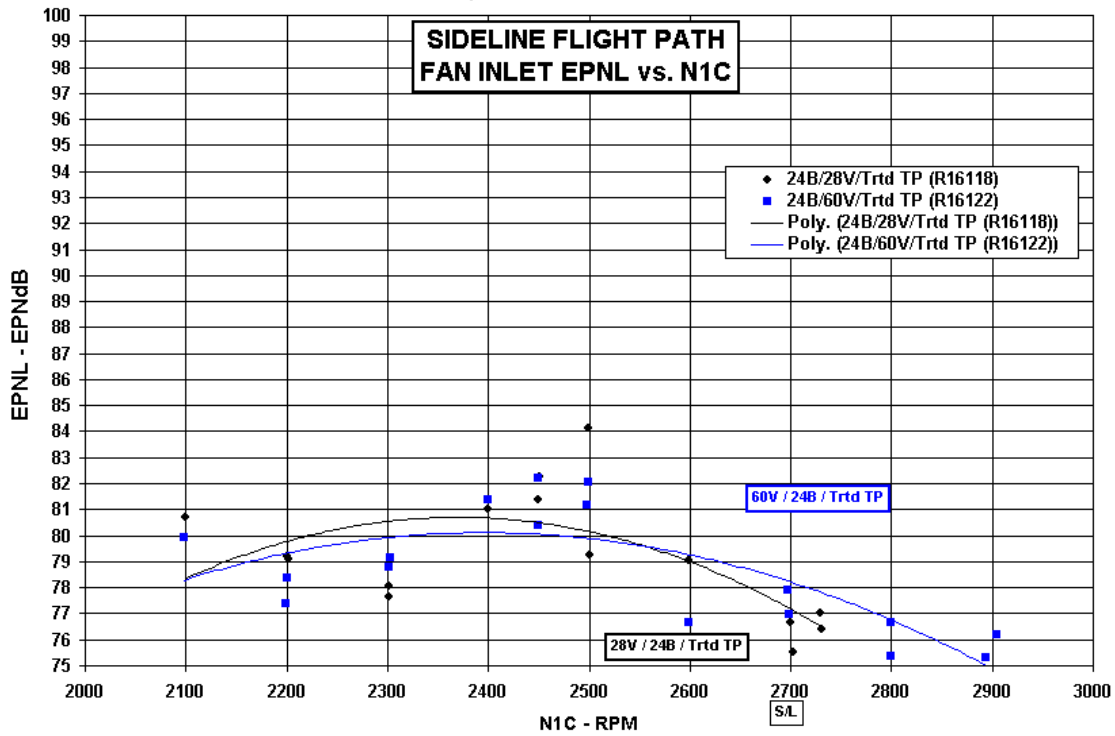
Figure 104.—Effect of FEGV number on fan inlet EPNL versus N1C—sideline flight path.

28 versus 60 FEGVs : 24 Blades and Treated Tail-pipe
FAN AFT Comparison : 736 ft Altitude / 1476 ft Sideline
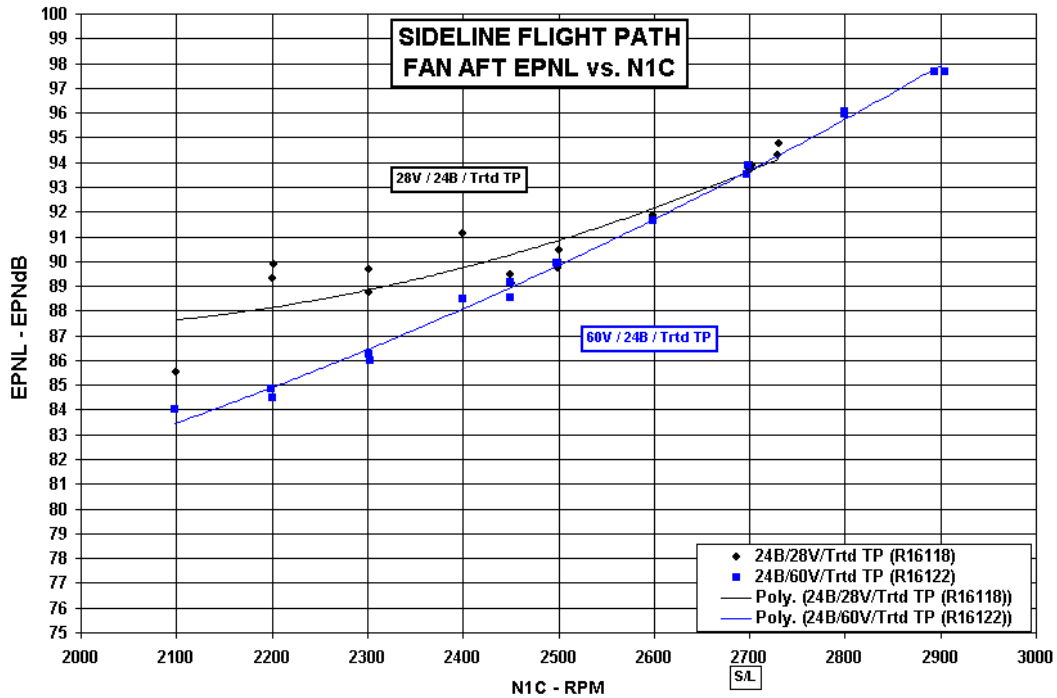
Figure 105.—Effect of FEGV number on fan aft EPNL versus N1C—sideline flight path.
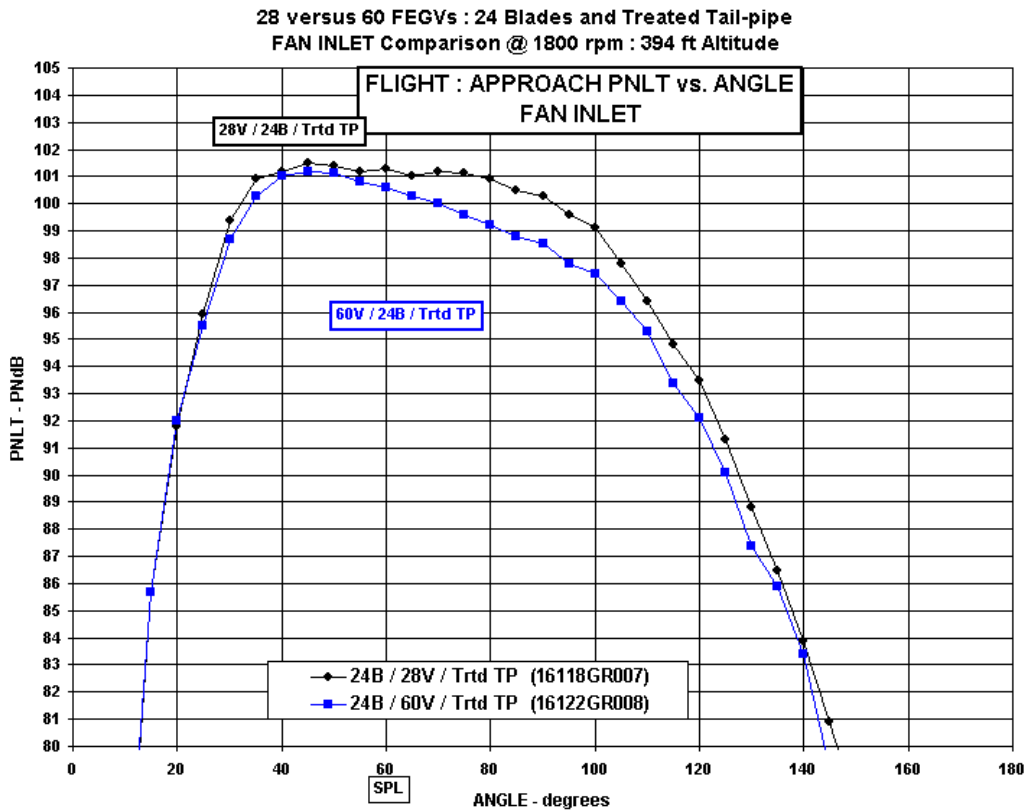
Figure 106.—Effect of FEGV number on in-flight fan inlet PNLT directivity—approach power.
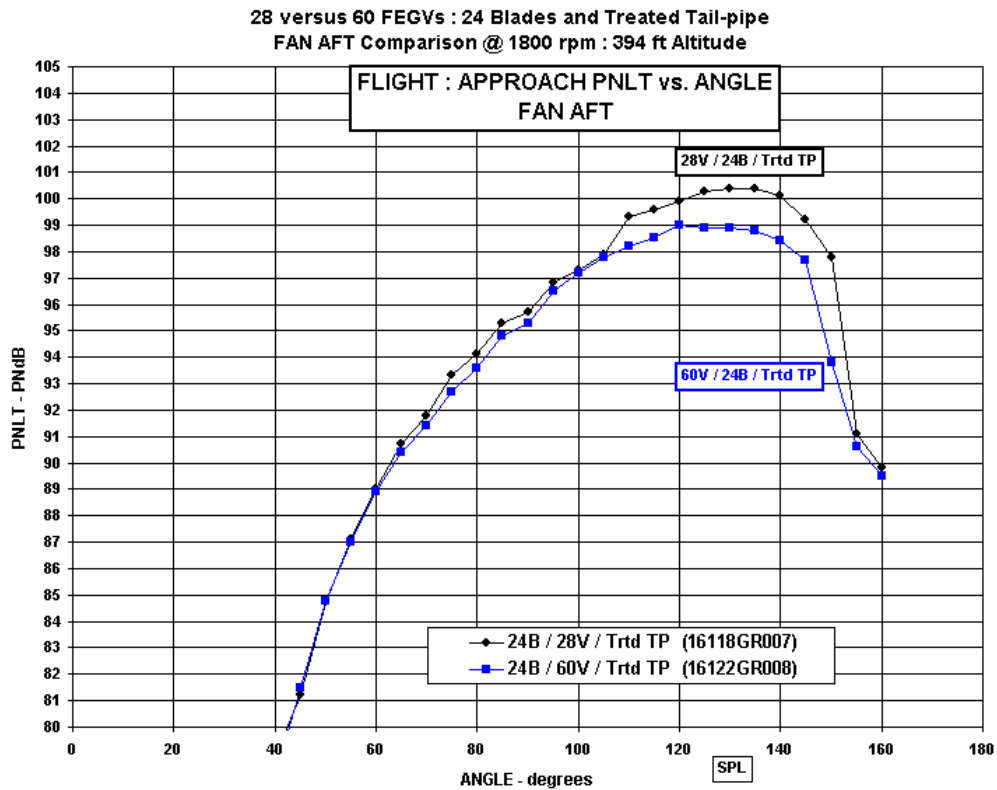
Figure 107.—Effect of FEGV number on in-flight fan aft PNLT directivity—approach power.
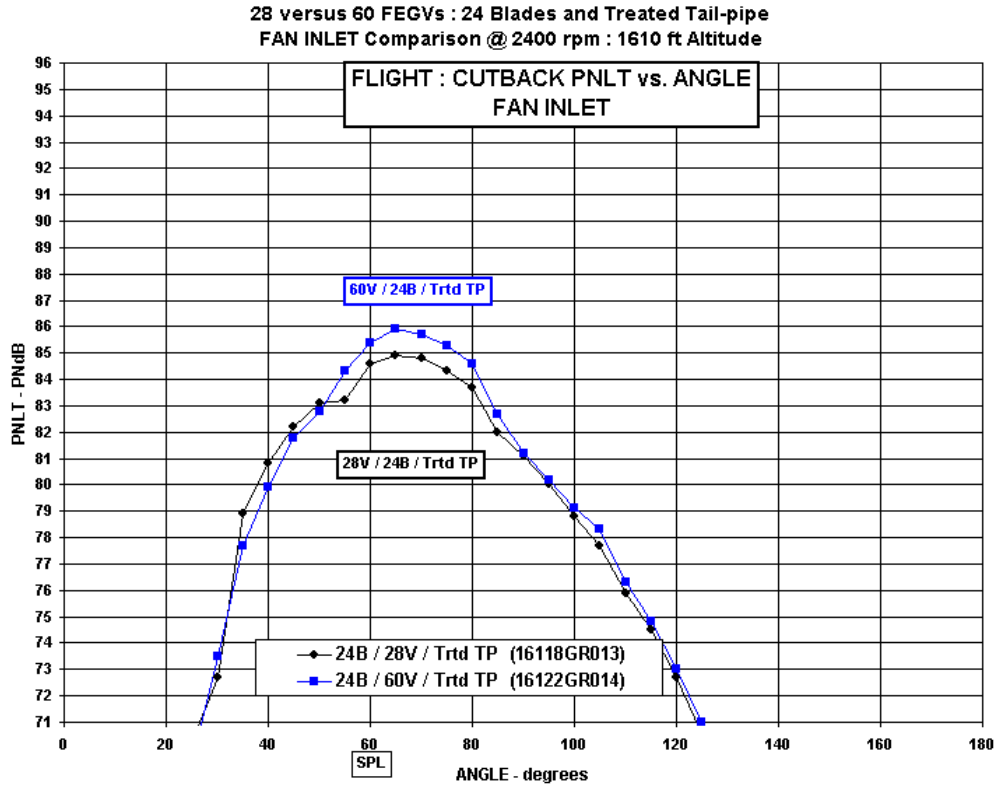
Figure 108.—Effect of FEGV number on in-flight fan inlet PNLT directivity—cutback power.
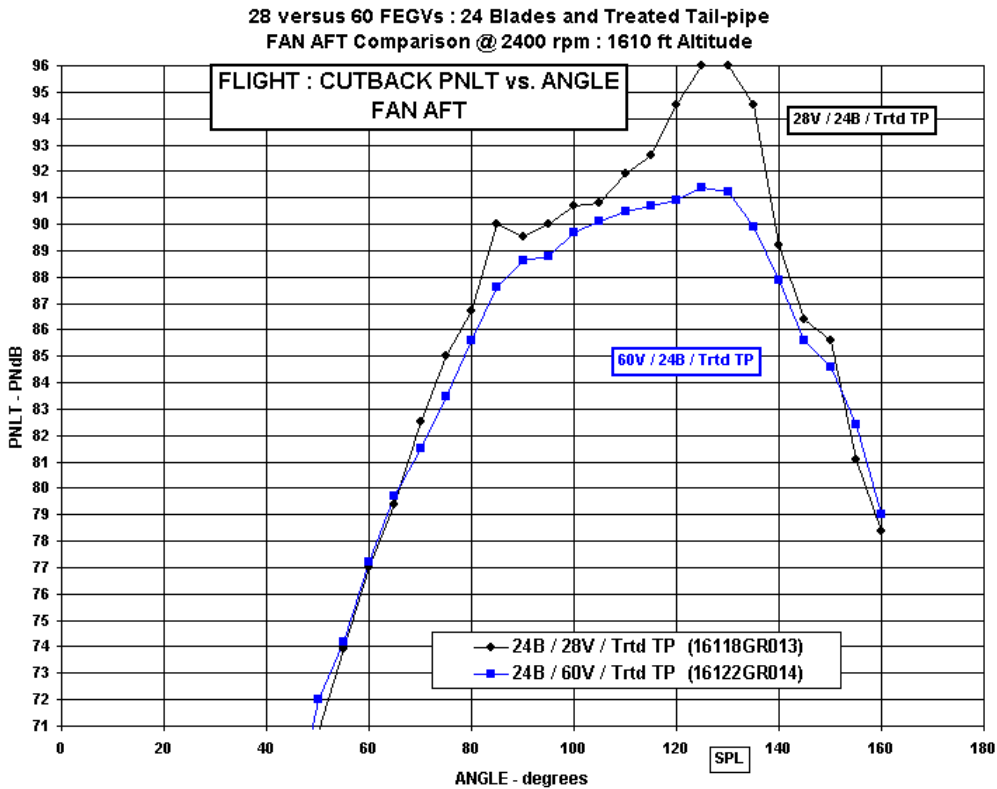
Figure 109.—Effect of FEGV number on in-flight fan aft PNLT directivity—cutback power.
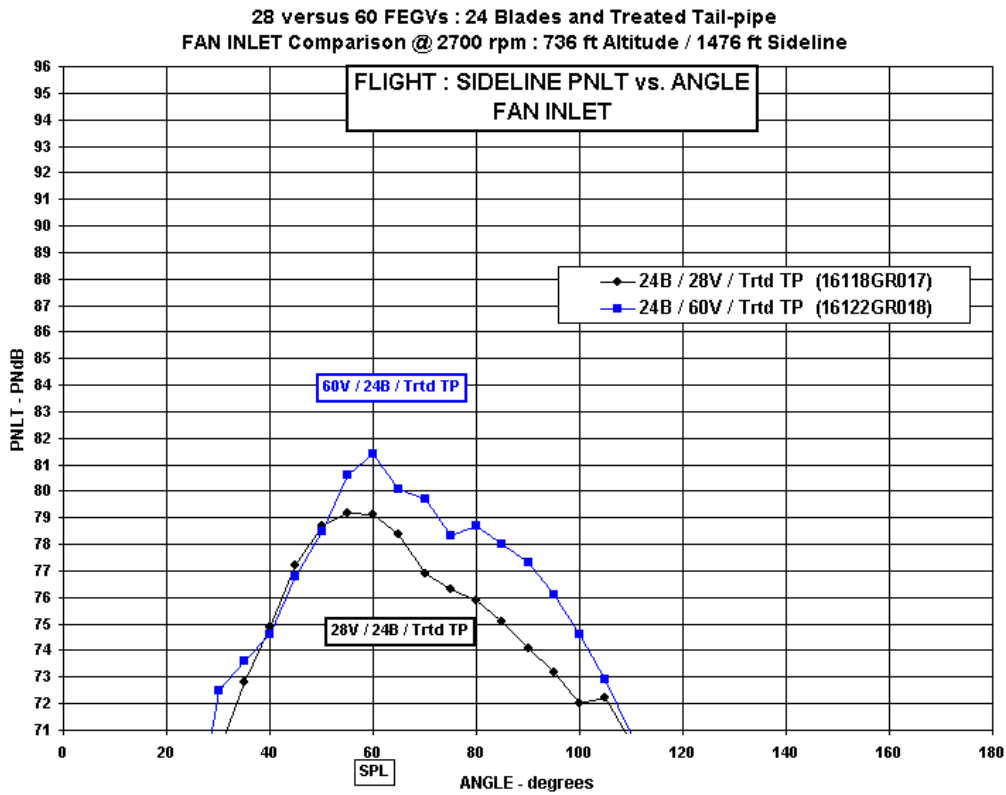
Figure 110.—Effect of FEGV number on in-flight fan inlet PNLT directivity—sideline power.
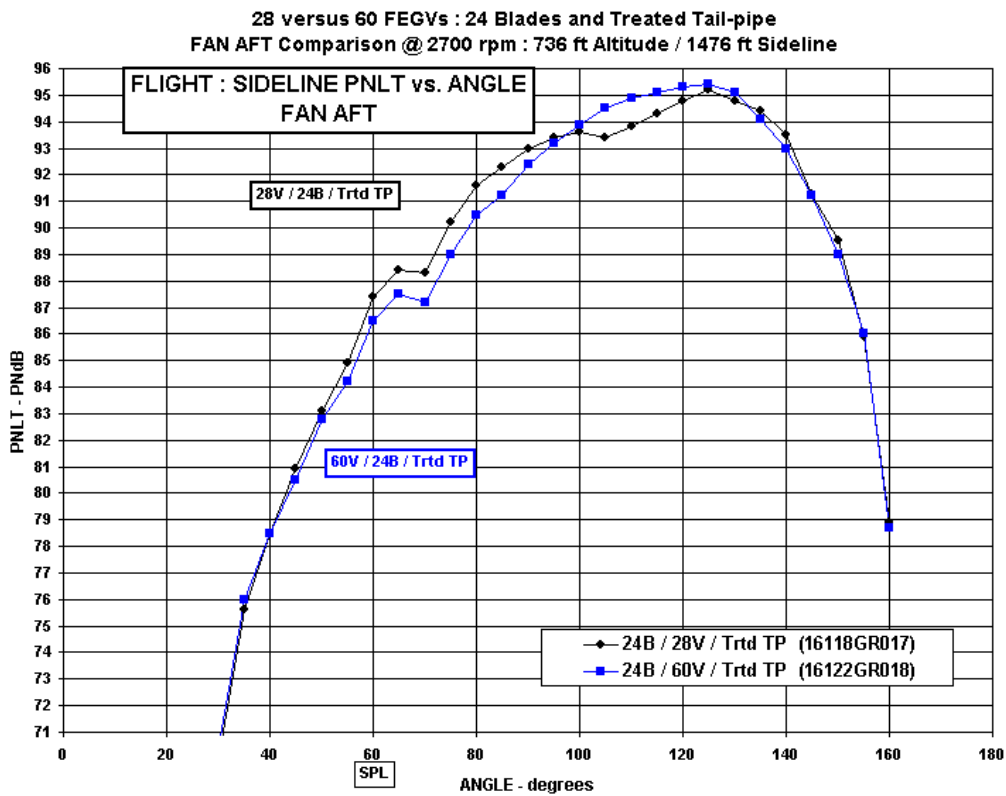
Figure 111.—Effect of FEGV number on in-flight fan aft PNLT directivity—sideline power.
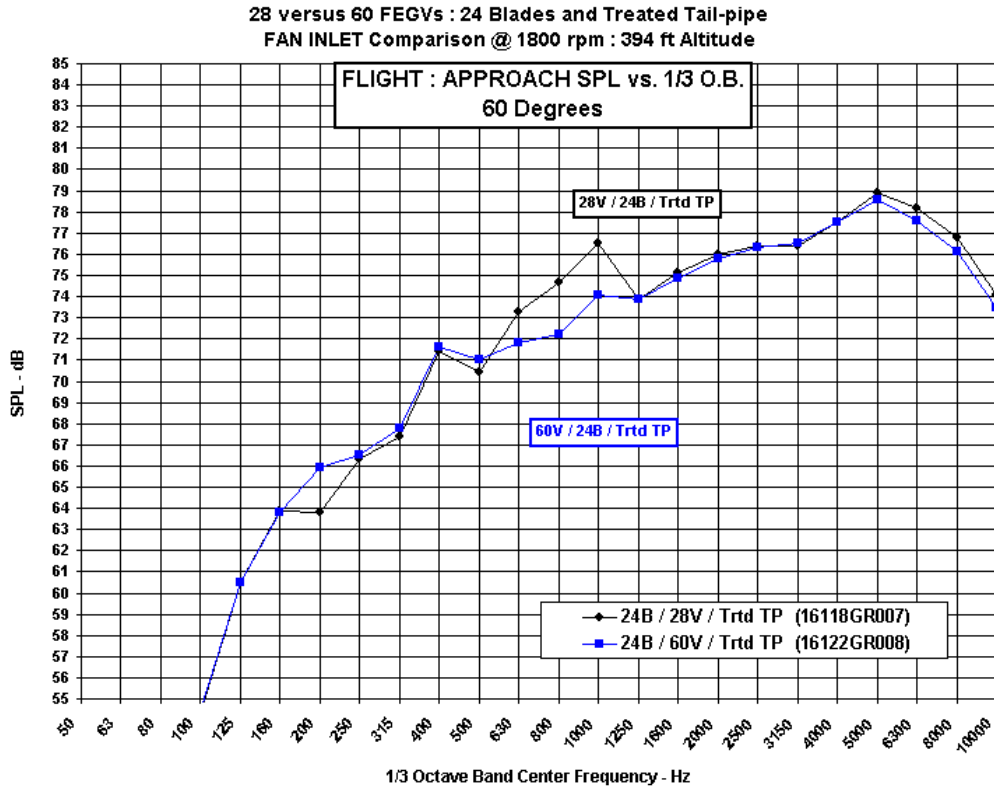
Figure 112.—Effect of FEGV number on in-flight fan inlet SPL spectra at 60°—approach power.
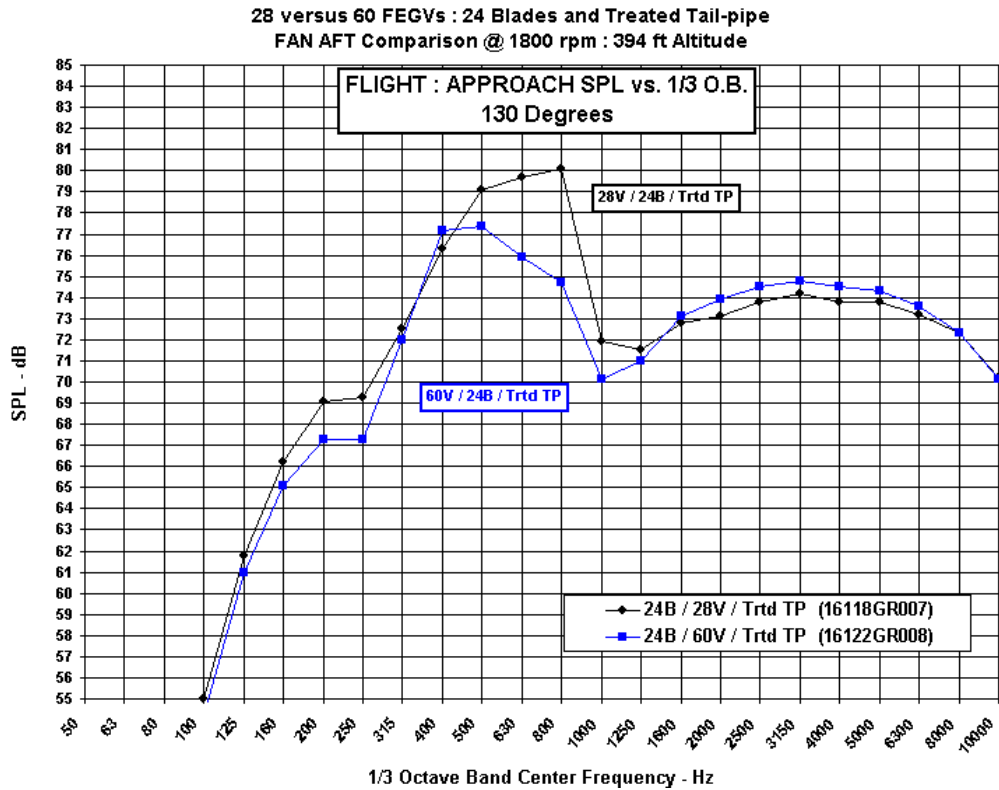
Figure 113.—Effect of FEGV number on in-flight fan aft SPL spectra at 130°—approach power.
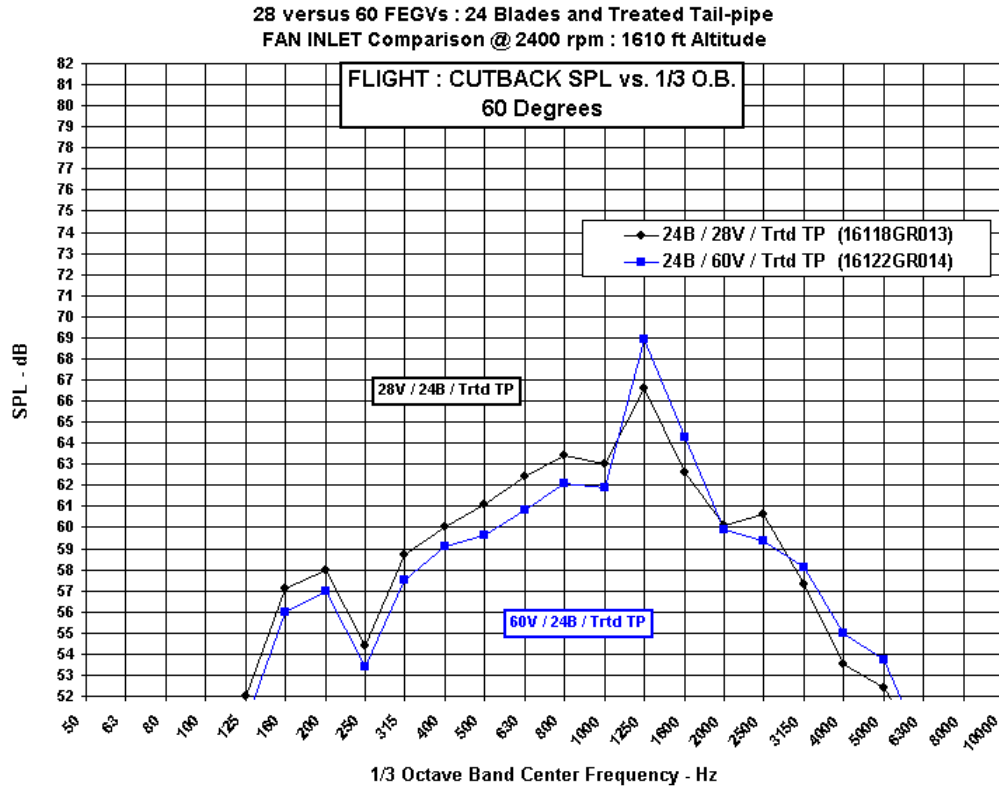
Figure 114.—Effect of FEGV number on in-flight fan inlet SPL spectra at 60°—cutback power.
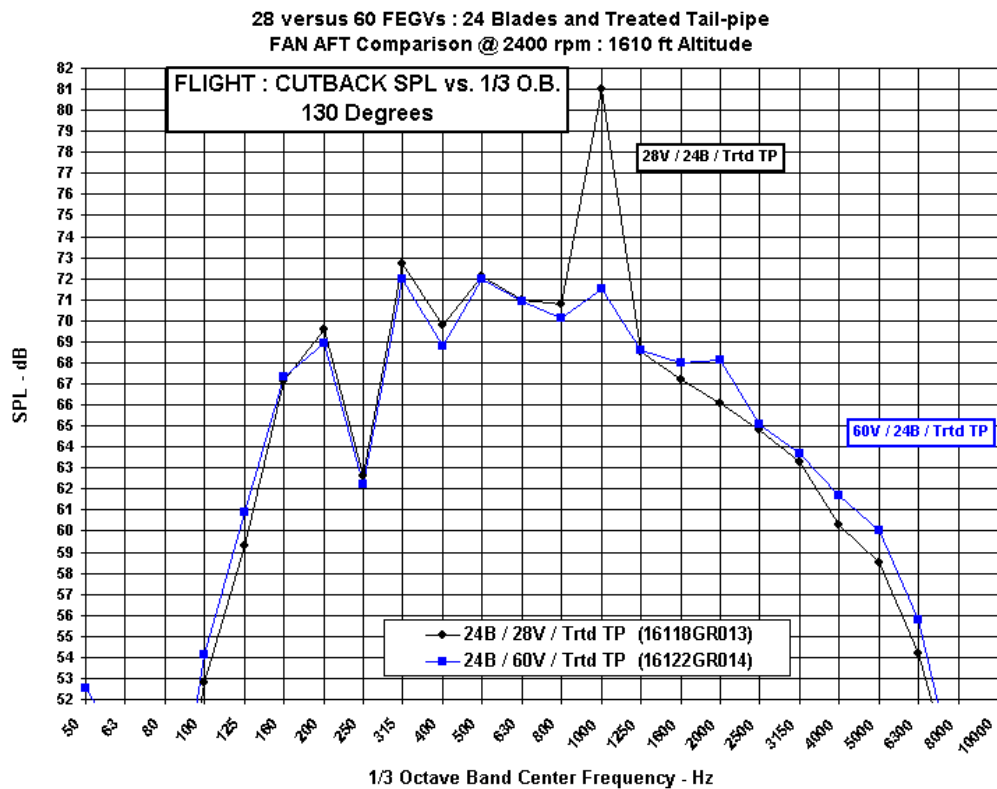
Figure 115.—Effect of FEGV number on in-flight fan aft SPL spectra at 130°—cutback power.
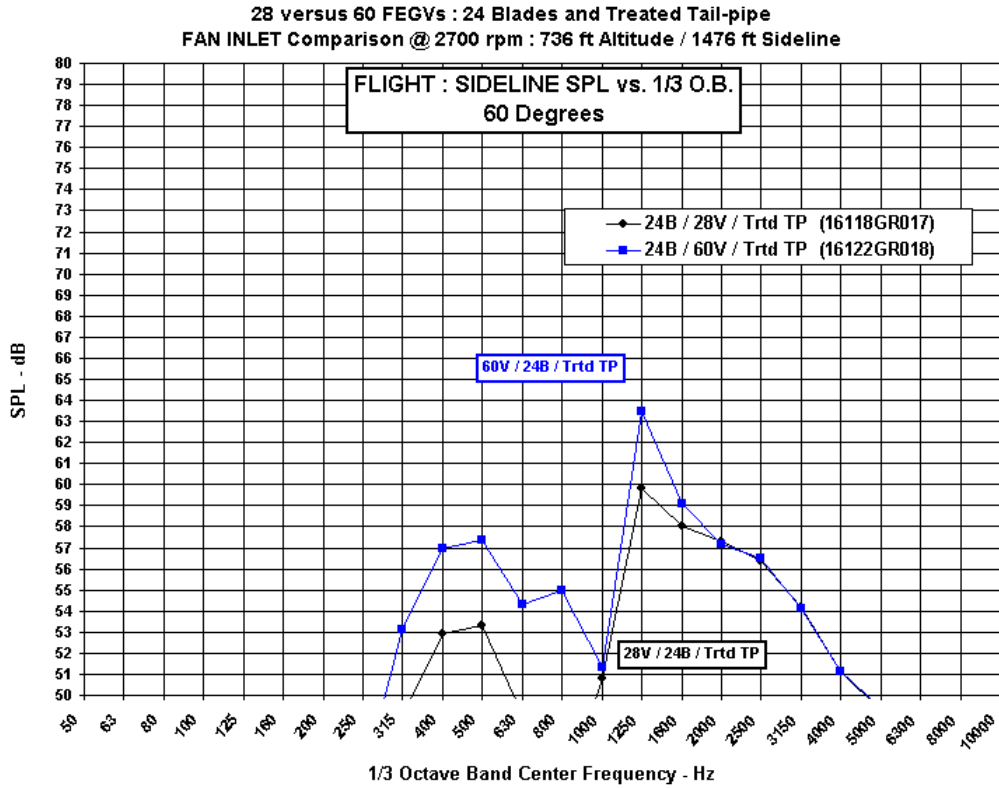
Figure 116.—Effect of FEGV number on in-flight fan inlet SPL spectra at 60°—sideline power.
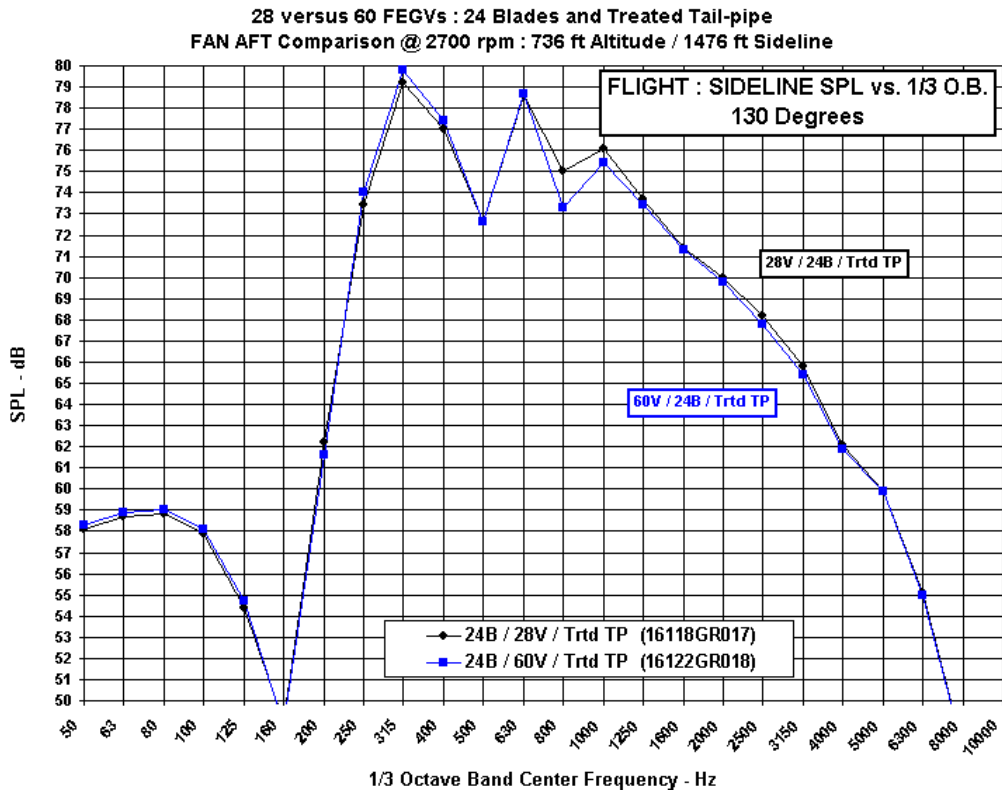
Figure 117.—Effect of FEGV number on in-flight fan aft SPL spectra at 130°—sideline power.
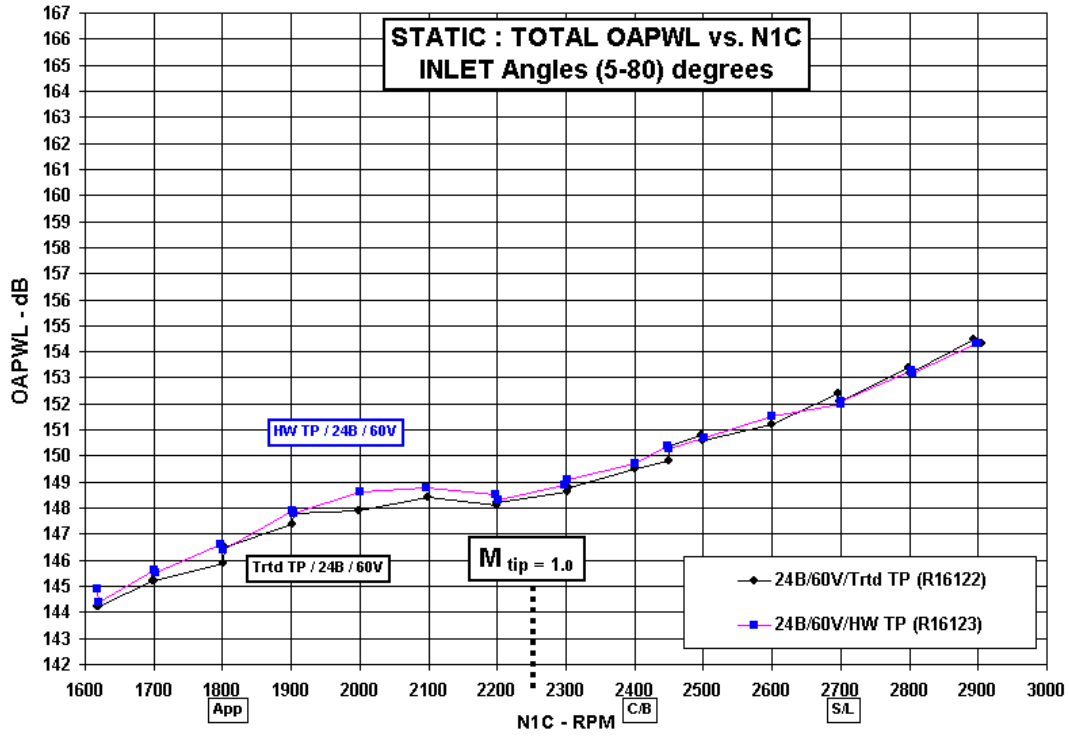
Figure 118.—Effect of tailpipe acoustic treatment on static total OAPWL versus N1C—inlet angles (5° to 80°).
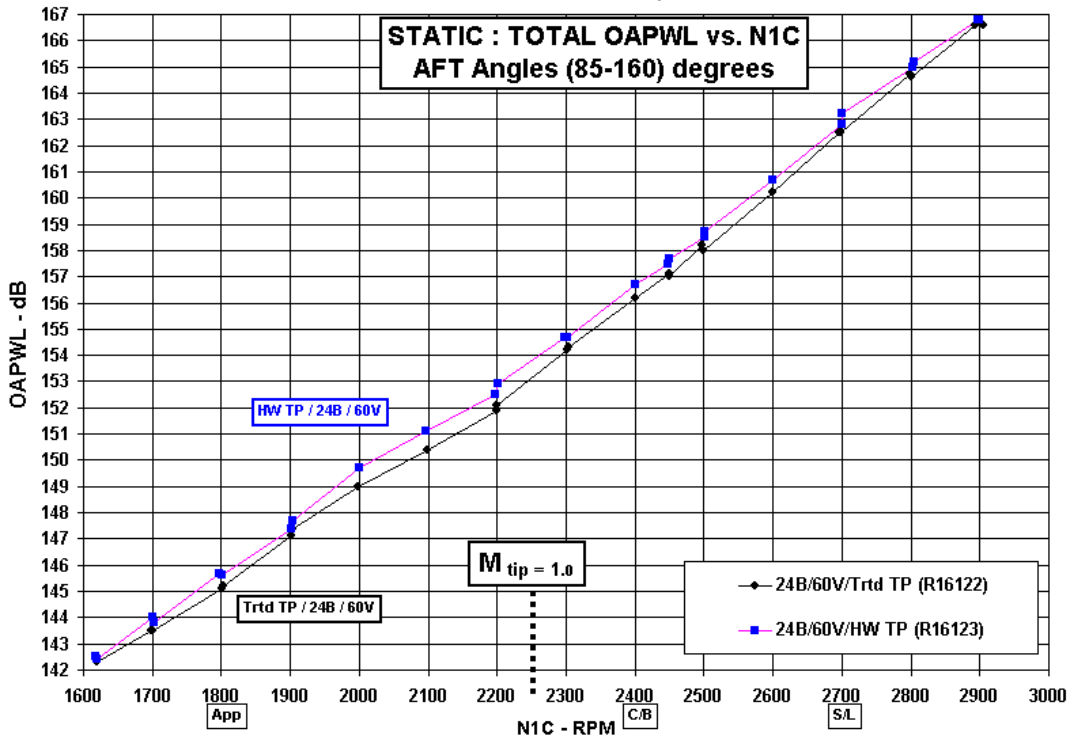
Figure 119.—Effect of tailpipe acoustic treatment on static total OAPWL versus N1C—aft angles (85° to 160°).
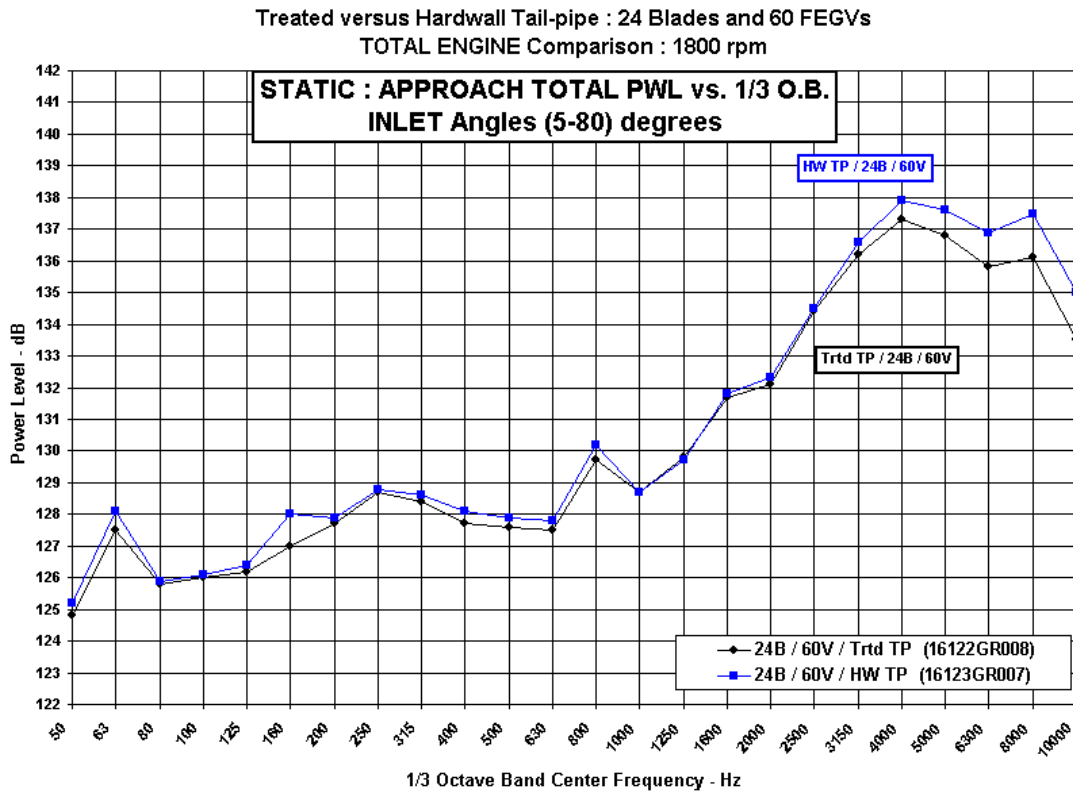
Figure 120.—Effect of tailpipe acoustic treatment on static Total PWL spectra (inlet angles 5° to 80°)—app power.
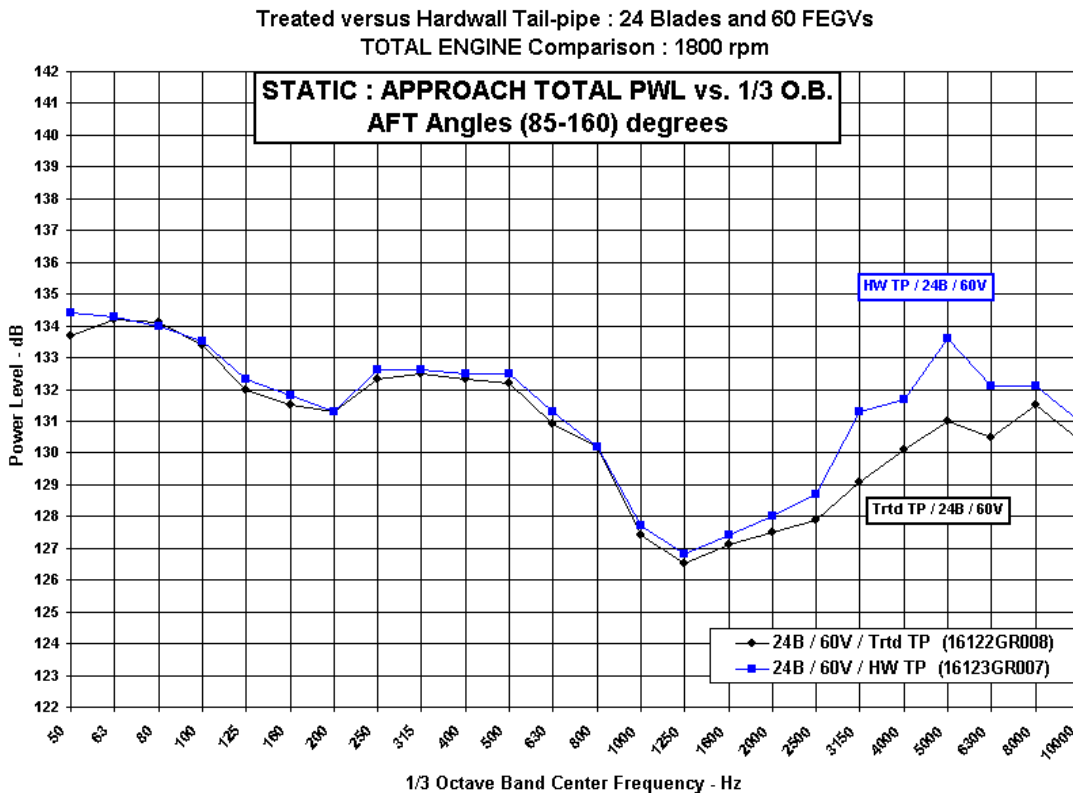
Figure 121.—Effect of tailpipe acoustic treatment on static total PWL spectra (aft angles 85° to 160°)—app power.
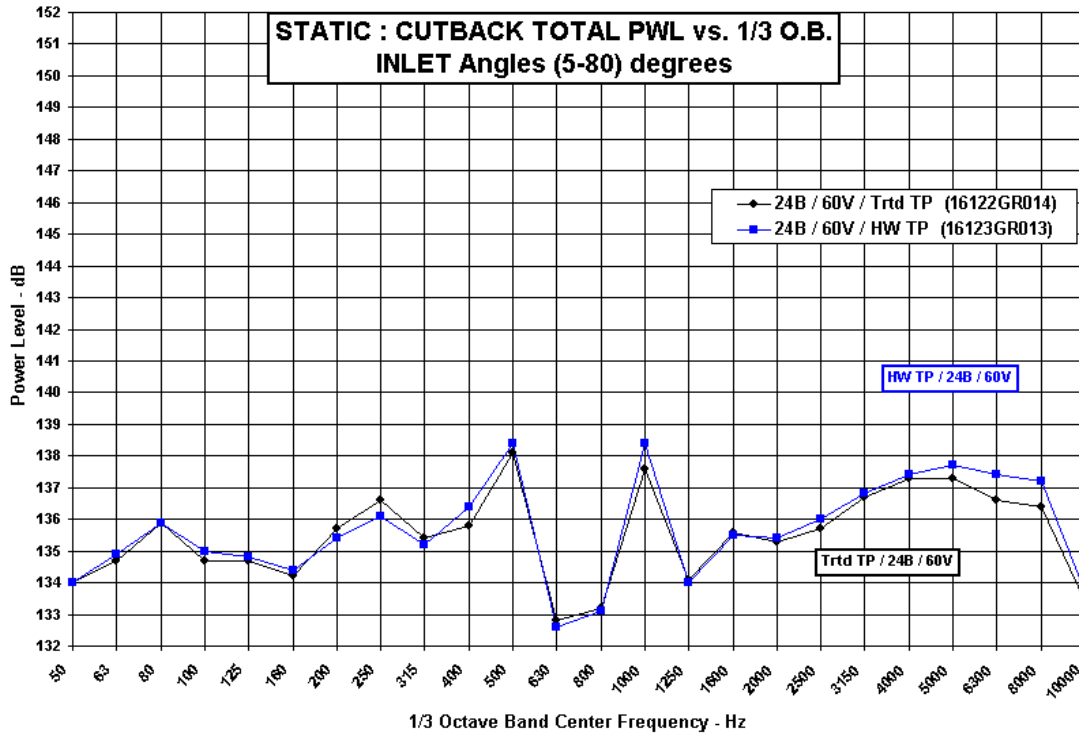
Figure 122.—Effect of tailpipe acoustic treatment on static total PWL spectra (inlet angles 5° to 80°)—C/B power.
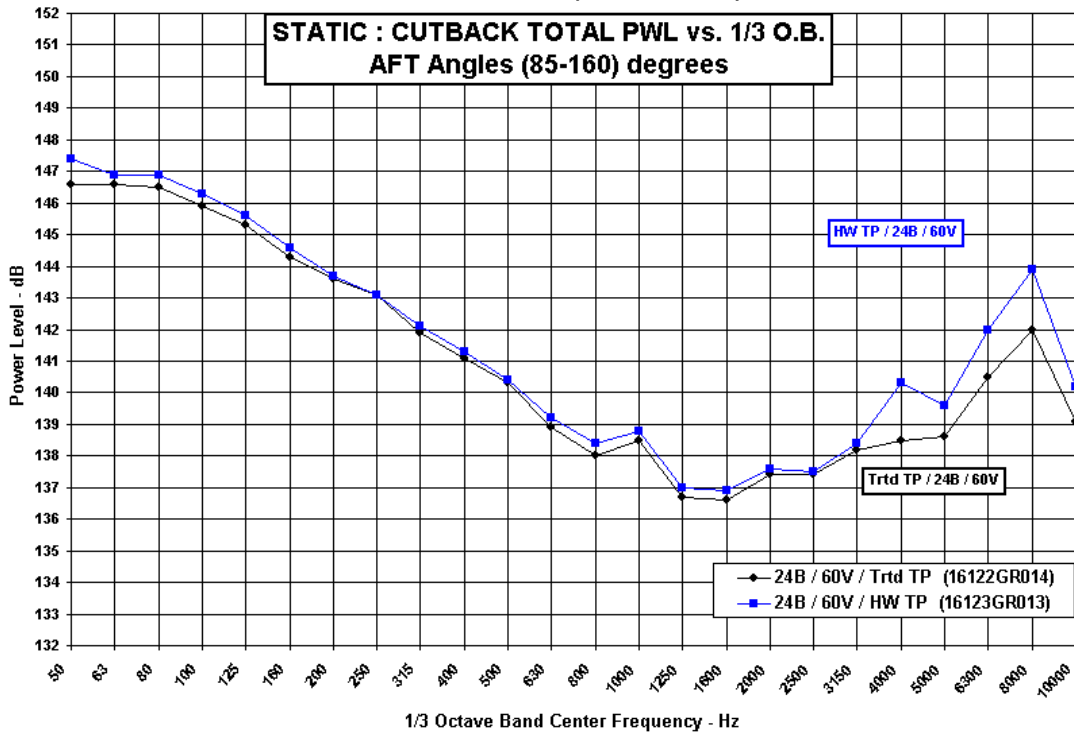
Figure 123.—Effect of tailpipe acoustic treatment on static total PWL spectra (aft angles 85° to 160°)—C/B power.

Treated versus Hardwall Tail-pipe : 24 Blades and 60 FEGVs
TOTAL ENGINE Comparison : 2700 rpm

STATIC : SIDELINE TOTAL PWL vs. 1/3 O.B.
INLET Angles (5-80) degrees

Legend:
- 24B / 60V / Trtd TP (16122GR018)
- 24B / 60V / HW TP (16123GR017)

Trtd TP / 24B / 60V
HW TP / 24B / 60V

Y-axis: Power Level - dB
X-axis: 1/3 Octave Band Center Frequency - Hz
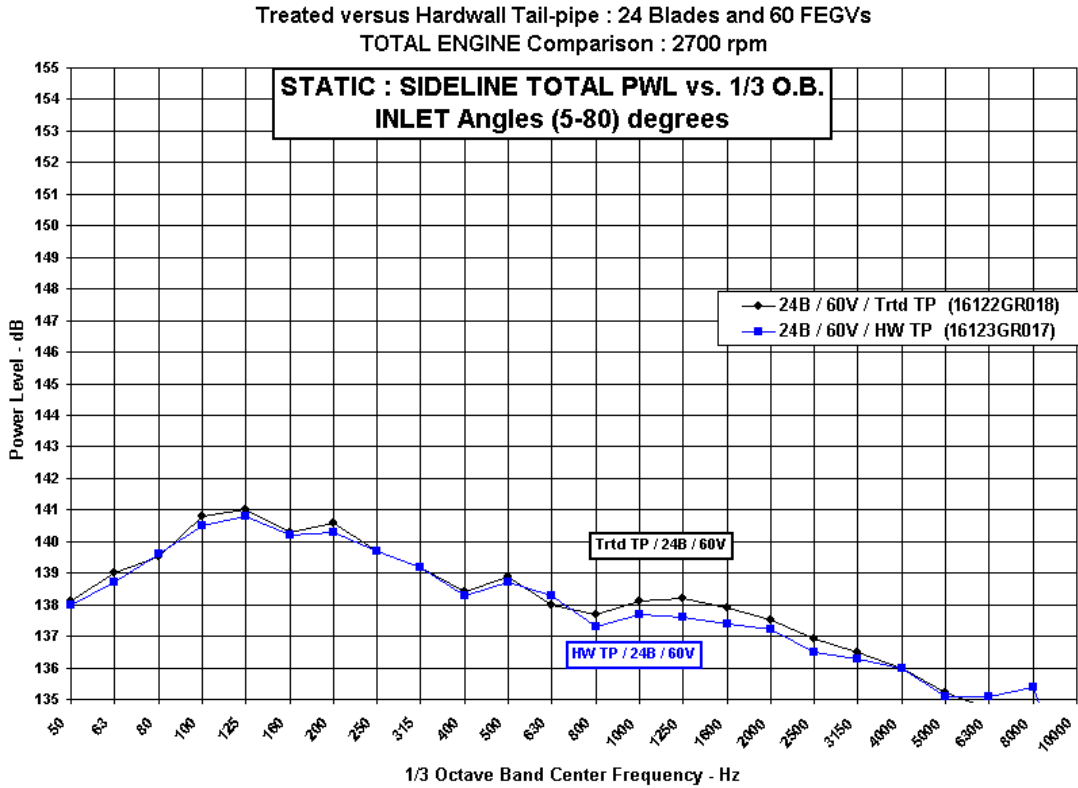
Figure 124.—Effect of tailpipe acoustic treatment on static total PWL spectra (inlet angles 5° to 80°)—S/L power.

Treated versus Hardwall Tail-pipe : 24 Blades and 60 FEGVs
TOTAL ENGINE Comparison : 2700 rpm

STATIC : SIDELINE TOTAL PWL vs. 1/3 O.B.
AFT Angles (85-160) degrees

HW TP / 24B / 60V
Trtd TP / 24B / 60V

Legend:
- 24B / 60V / Trtd TP (16122GR018)
- 24B / 60V / HW TP (16123GR017)

Y-axis: Power Level - dB
X-axis: 1/3 Octave Band Center Frequency - Hz
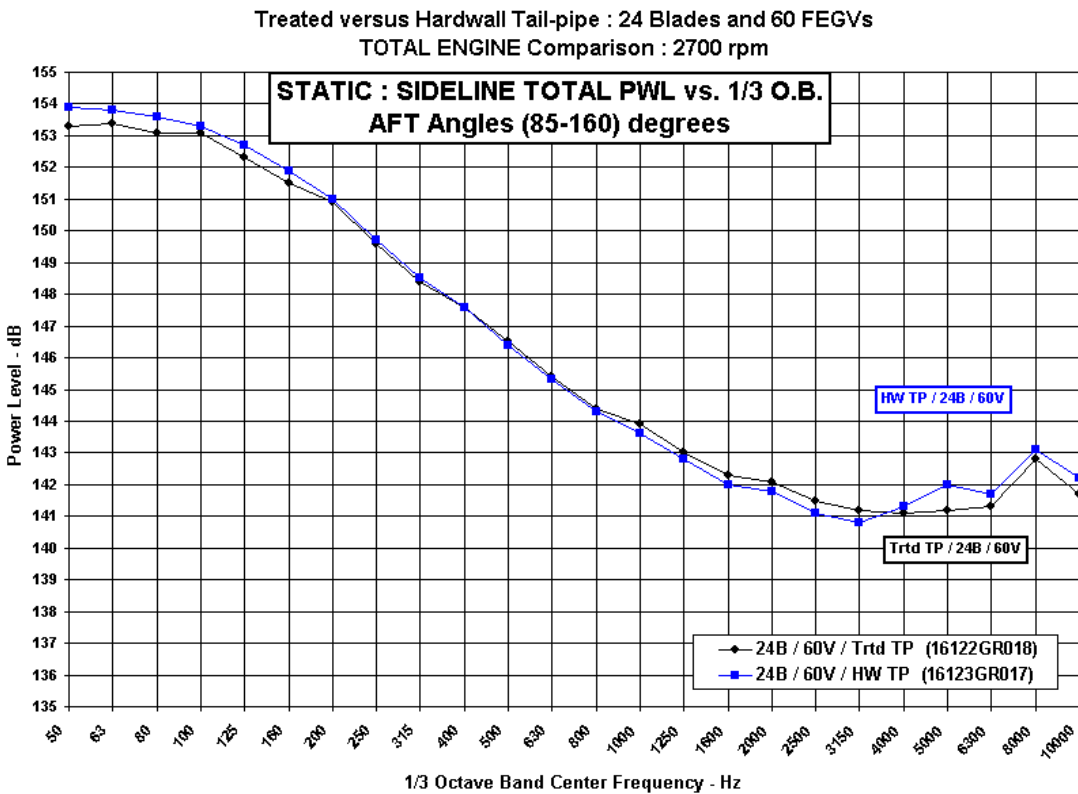
Figure 125.—Effect of tailpipe acoustic treatment on static total PWL spectra (aft angles 85° to 160°)—S/L power.
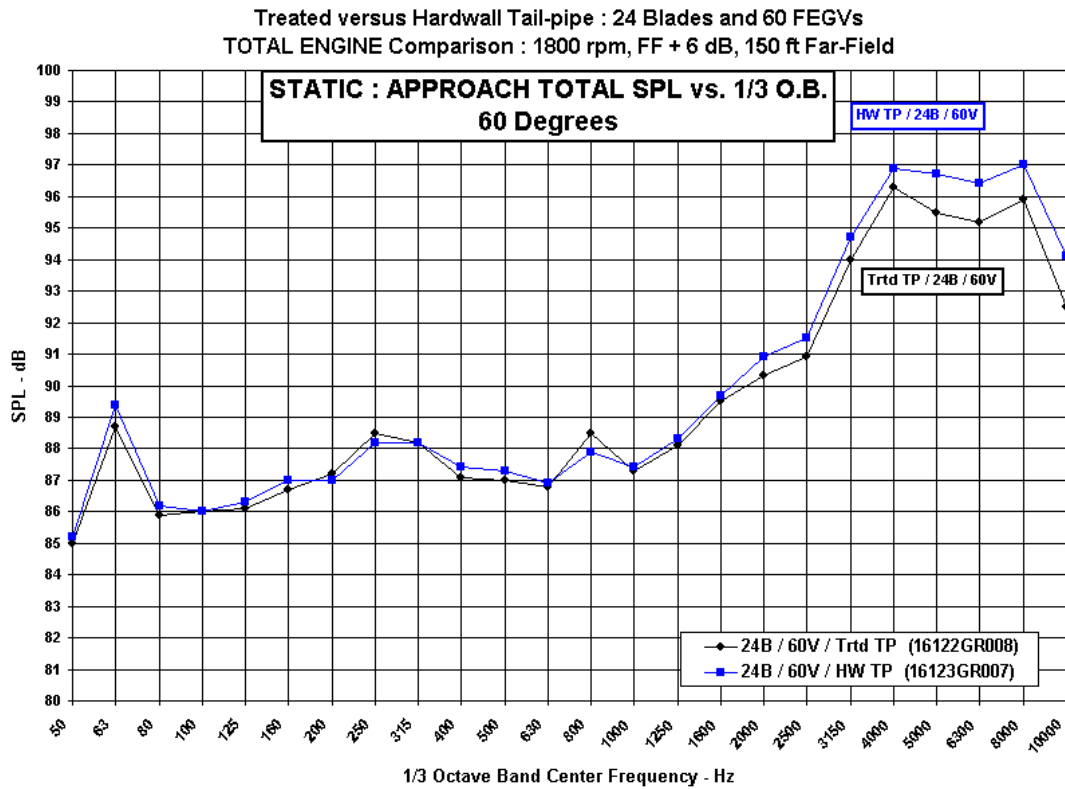
Figure 126.—Effect of tailpipe acoustic treatment on static total SPL spectra at 60°—app power.
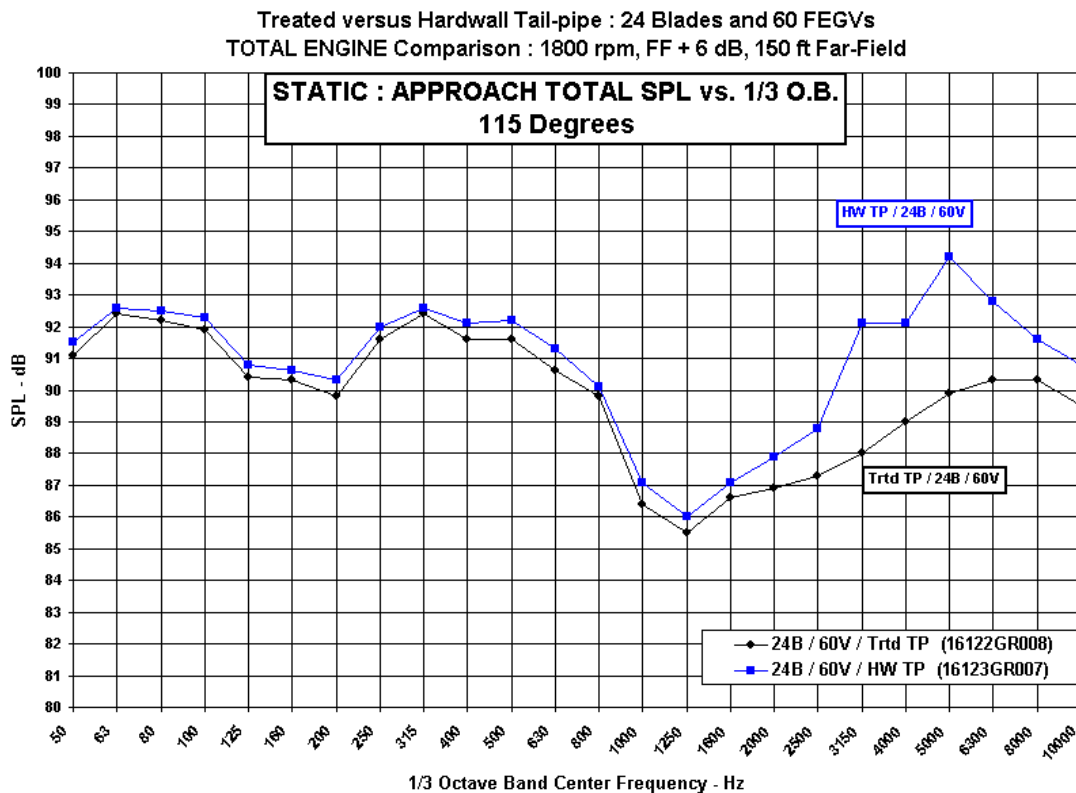
Figure 127.—Effect of tailpipe acoustic treatment on static total SPL spectra at 115°—app power.

Treated versus Hardwall Tail-pipe : 24 Blades and 60 FEGVs
TOTAL ENGINE Comparison : 2400 rpm, FF + 6 dB, 150 ft Far-Field

STATIC : CUTBACK TOTAL SPL vs. 1/3 O.B.
60 Degrees

- 24B / 60V / Trtd TP (16122GR014)
- 24B / 60V / HW TP (16123GR013)

HW TP / 24B / 60V

Trtd TP / 24B / 60V

SPL - dB

1/3 Octave Band Center Frequency - Hz
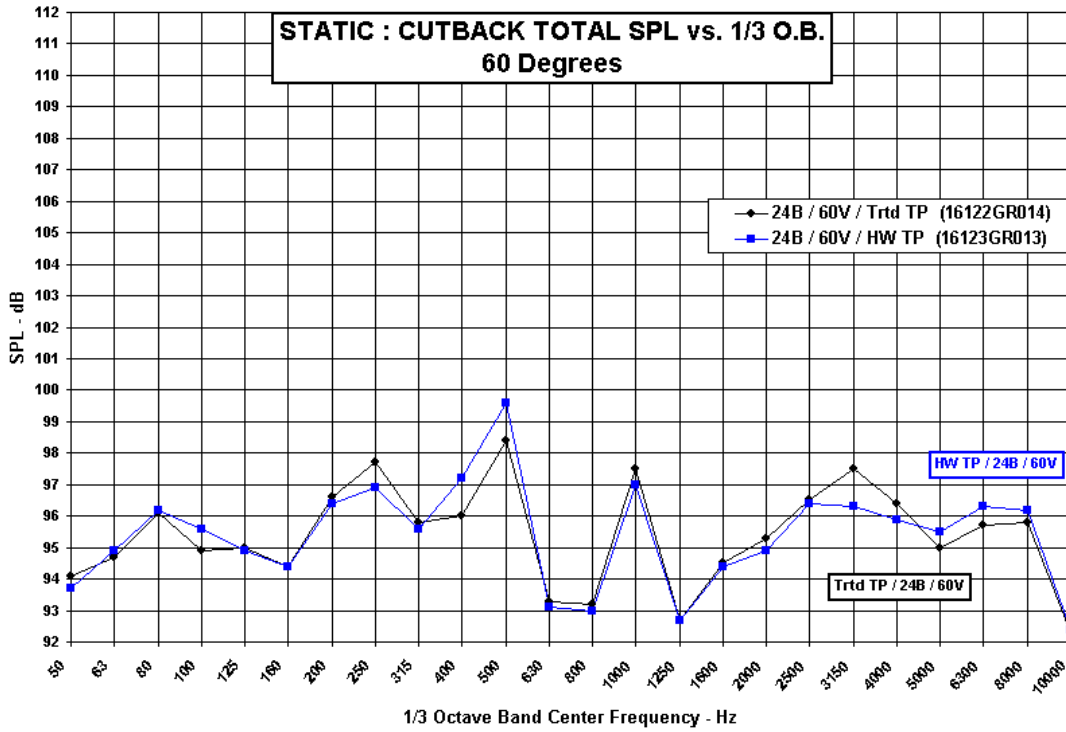
Figure 128.—Effect of tailpipe acoustic treatment on static total SPL spectra at 60°—C/B power.

Treated versus Hardwall Tail-pipe : 24 Blades and 60 FEGVs
TOTAL ENGINE Comparison : 2400 rpm, FF + 6 dB, 150 ft Far-Field

STATIC : CUTBACK TOTAL SPL vs. 1/3 O.B.
115 Degrees

HW TP / 24B / 60V

Trtd TP / 24B / 60V

- 24B / 60V / Trtd TP (16122GR014)
- 24B / 60V / HW TP (16123GR013)

SPL - dB

1/3 Octave Band Center Frequency - Hz
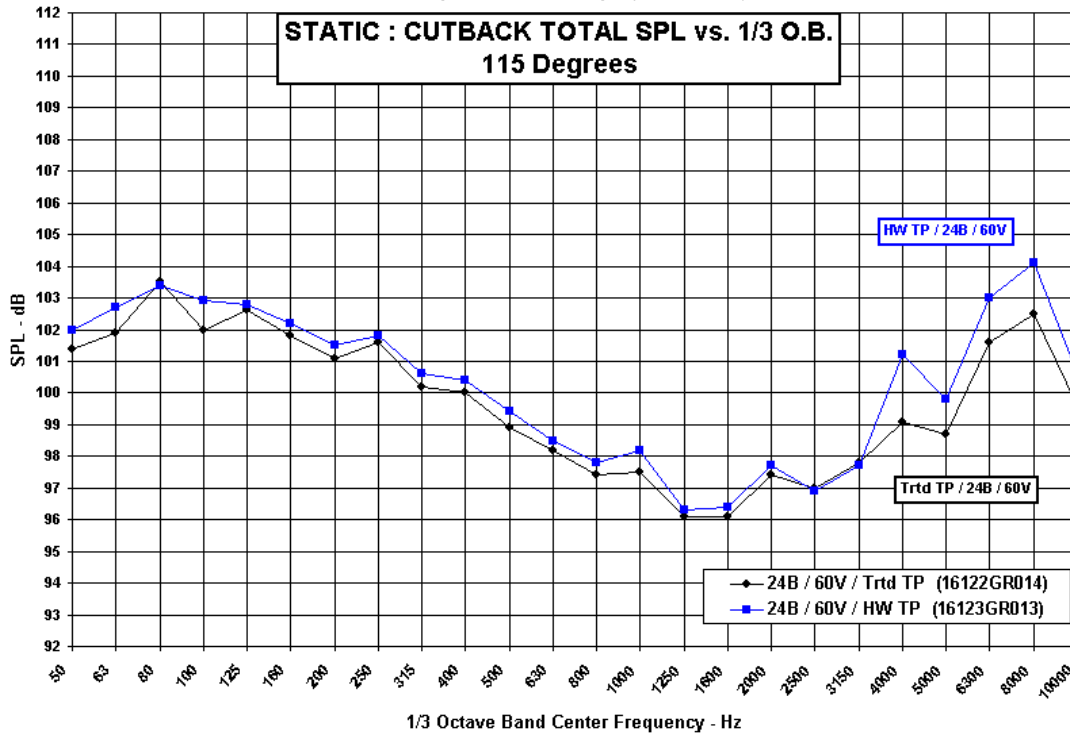
Figure 129.—Effect of tailpipe acoustic treatment on static total SPL spectra at 115°—C/B power.
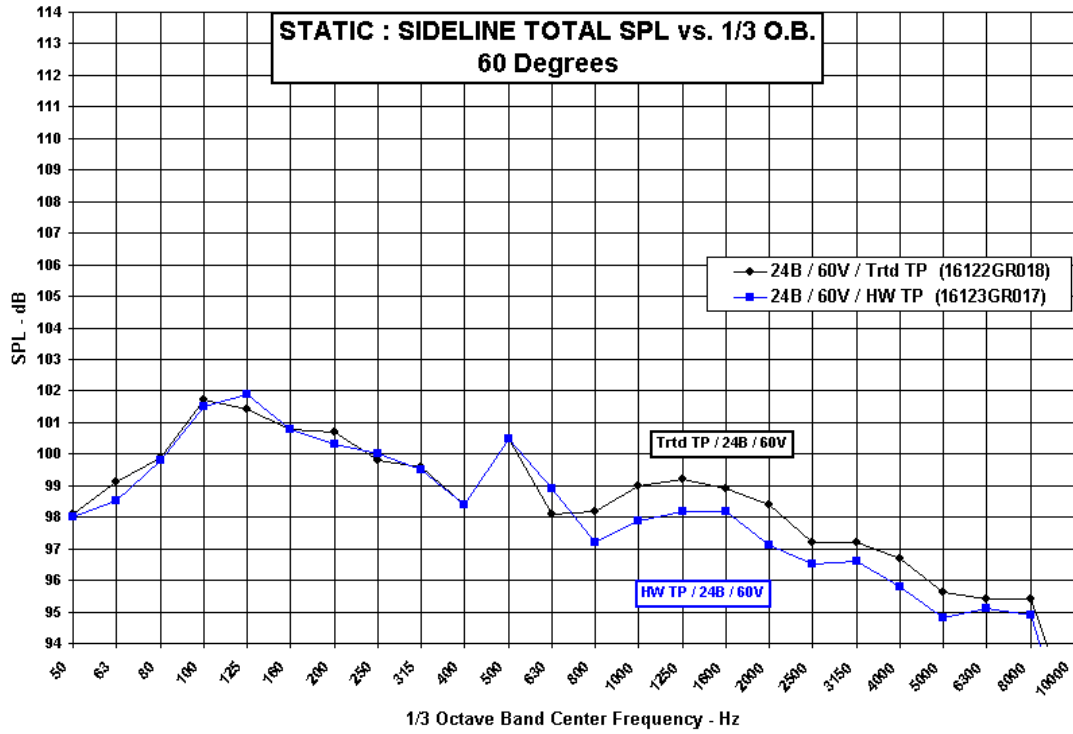
Figure 130.—Effect of tailpipe acoustic treatment on static Total SPL spectra at 60°—S/L power.
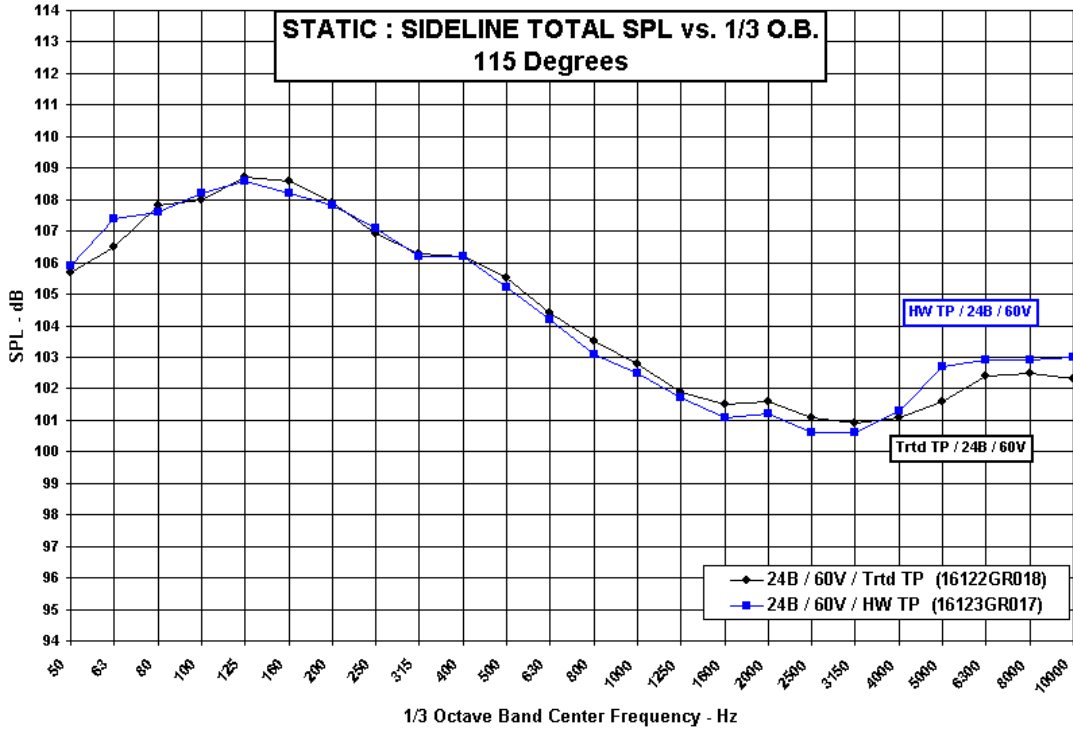
Figure 131.—Effect of tailpipe acoustic treatment on static total SPL spectra at 115°—S/L power.
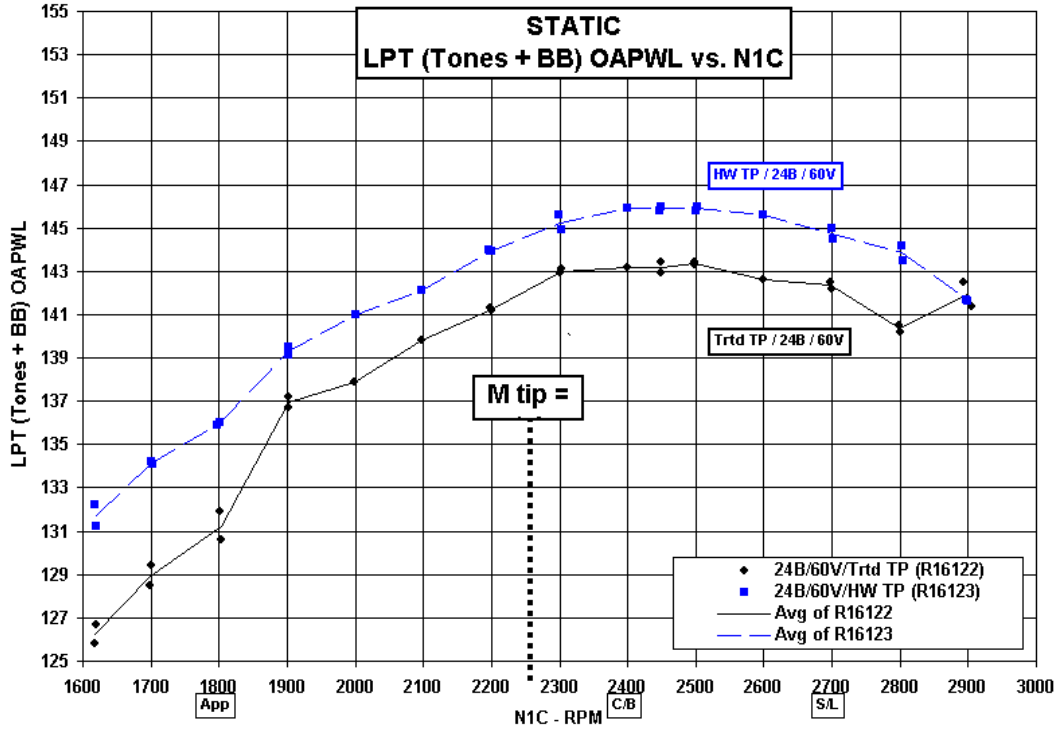
Figure 132.—Effect of tailpipe acoustic treatment on static LPT OAPWL versus N1C.
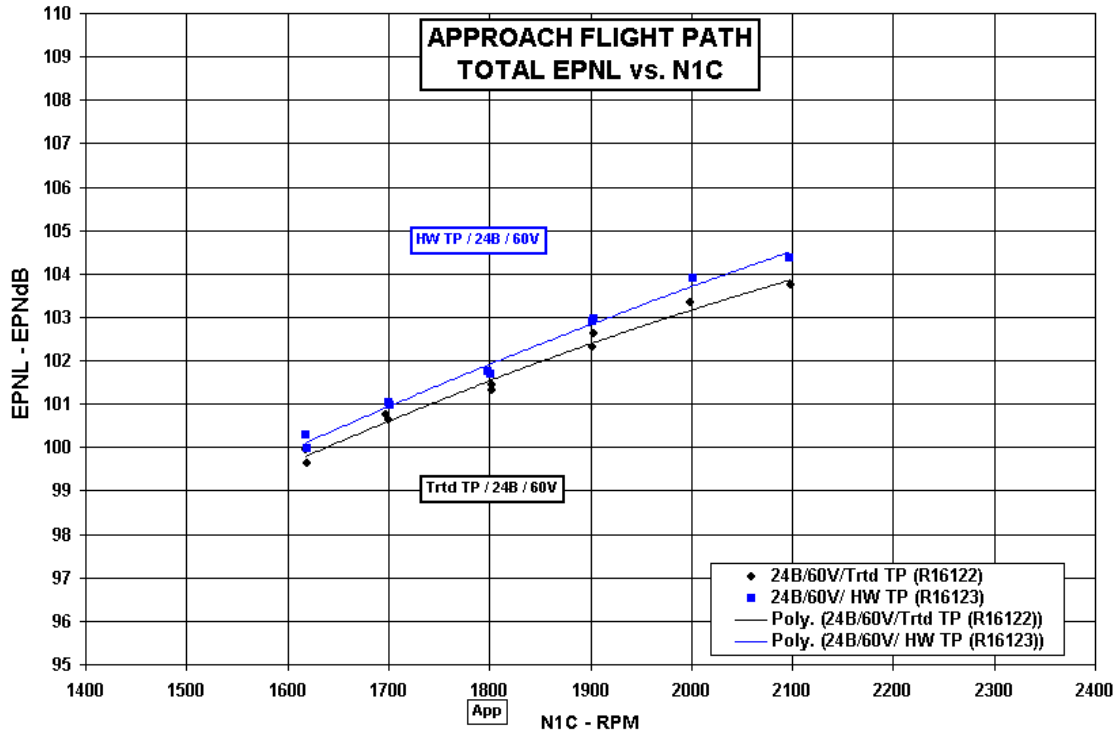
Figure 133.—Effect of tailpipe acoustic treatment on total EPNL versus N1C—approach flight path.
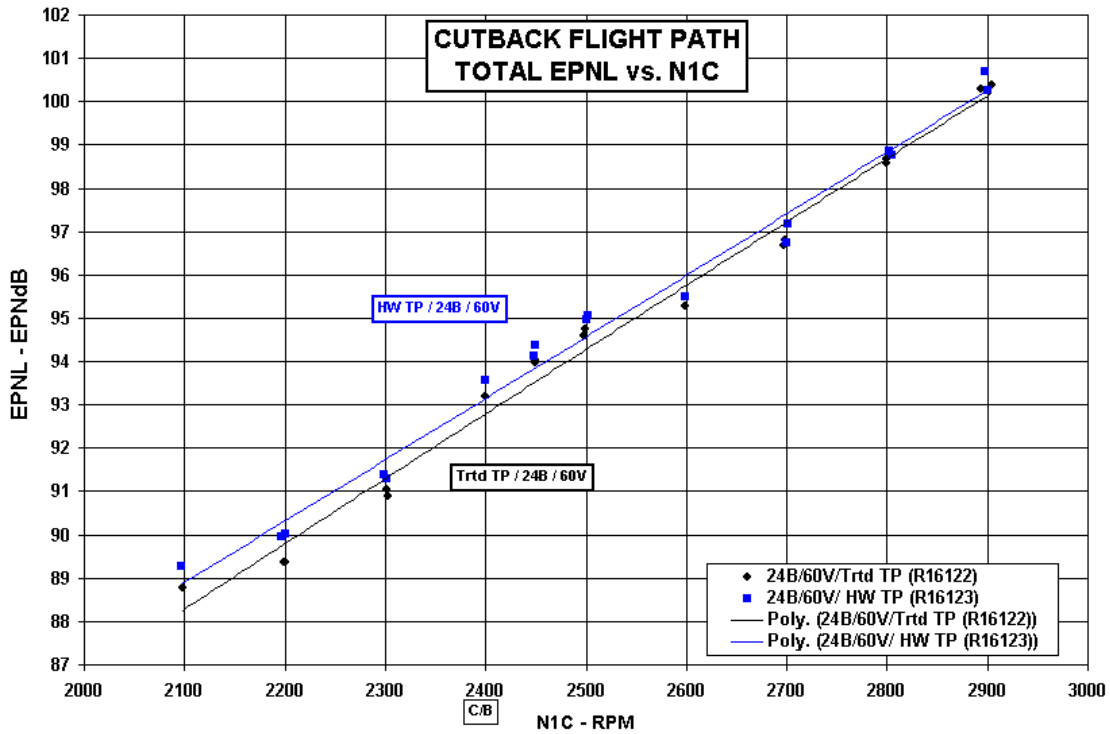
Figure 134.—Effect of tailpipe acoustic treatment on total EPNL versus N1C—cutback flight path.
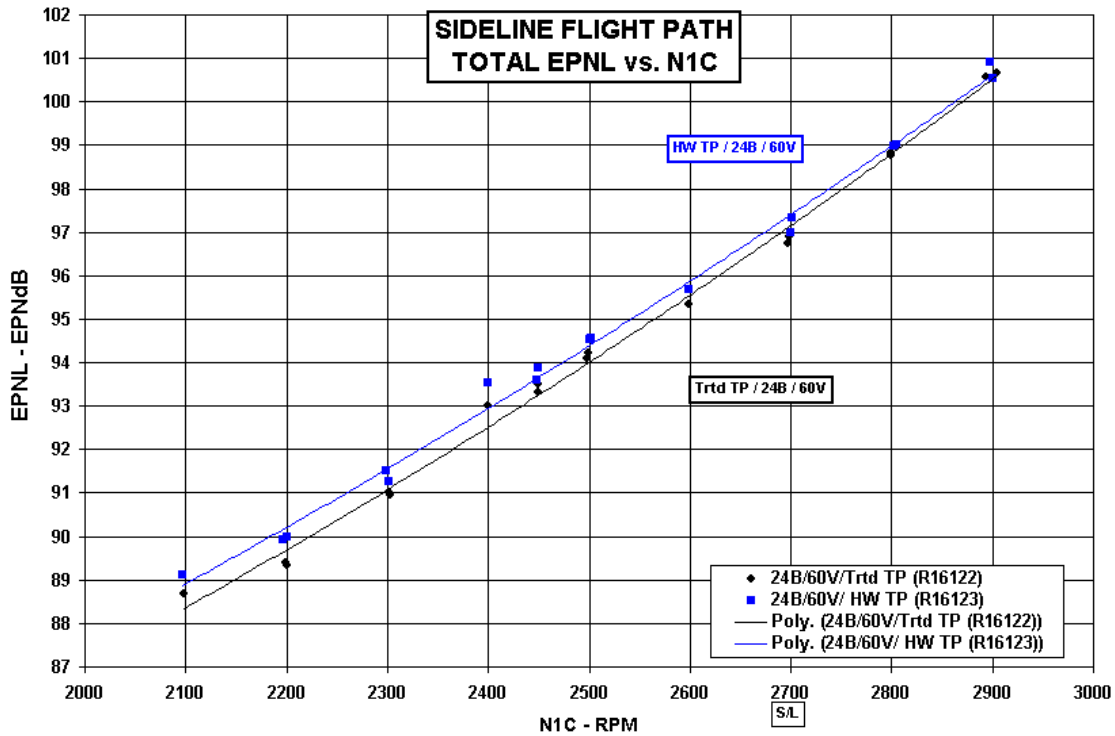
Figure 135.—Effect of tailpipe acoustic treatment on total EPNL versus N1C—sideline flight path.
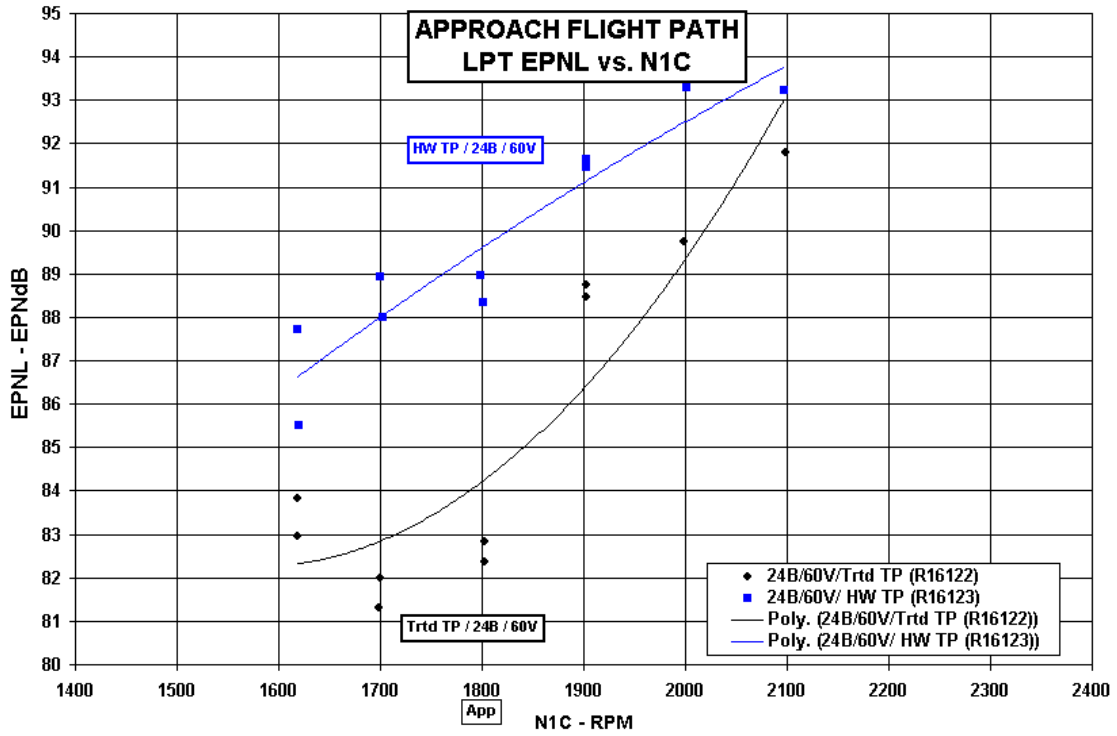
Figure 136.—Effect of tailpipe acoustic treatment on LPT EPNL versus N1C—approach flight path.
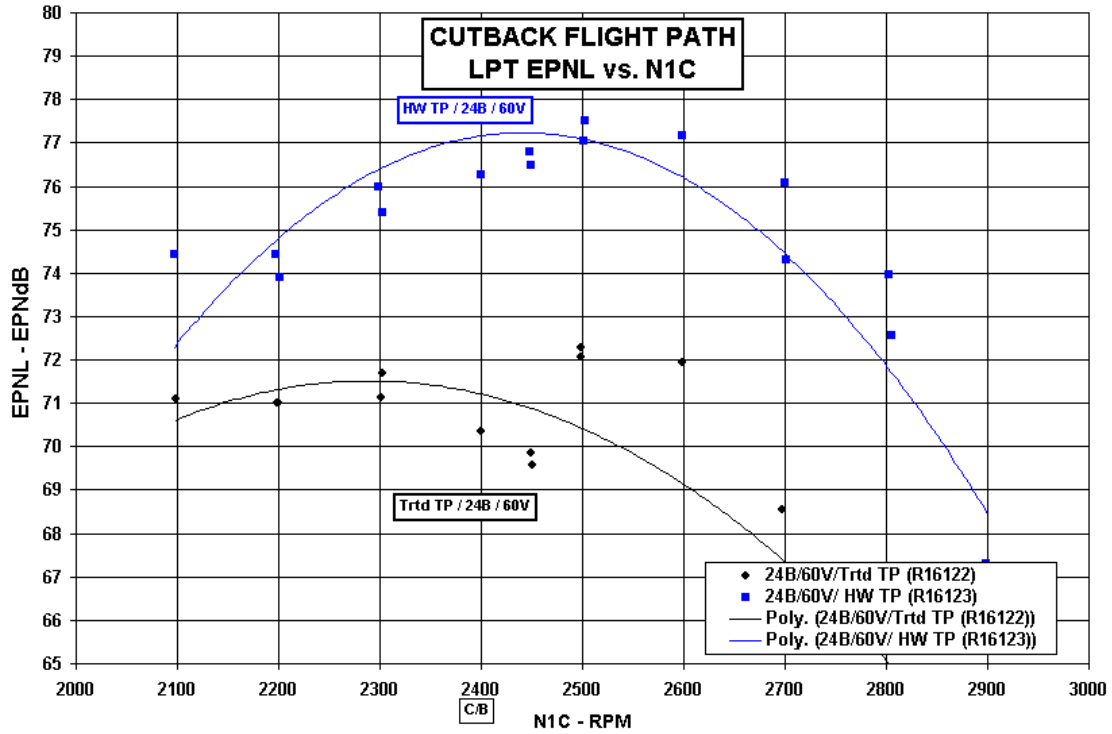
Figure 137.—Effect of tailpipe acoustic treatment on LPT EPNL versus N1C—cutback flight path.
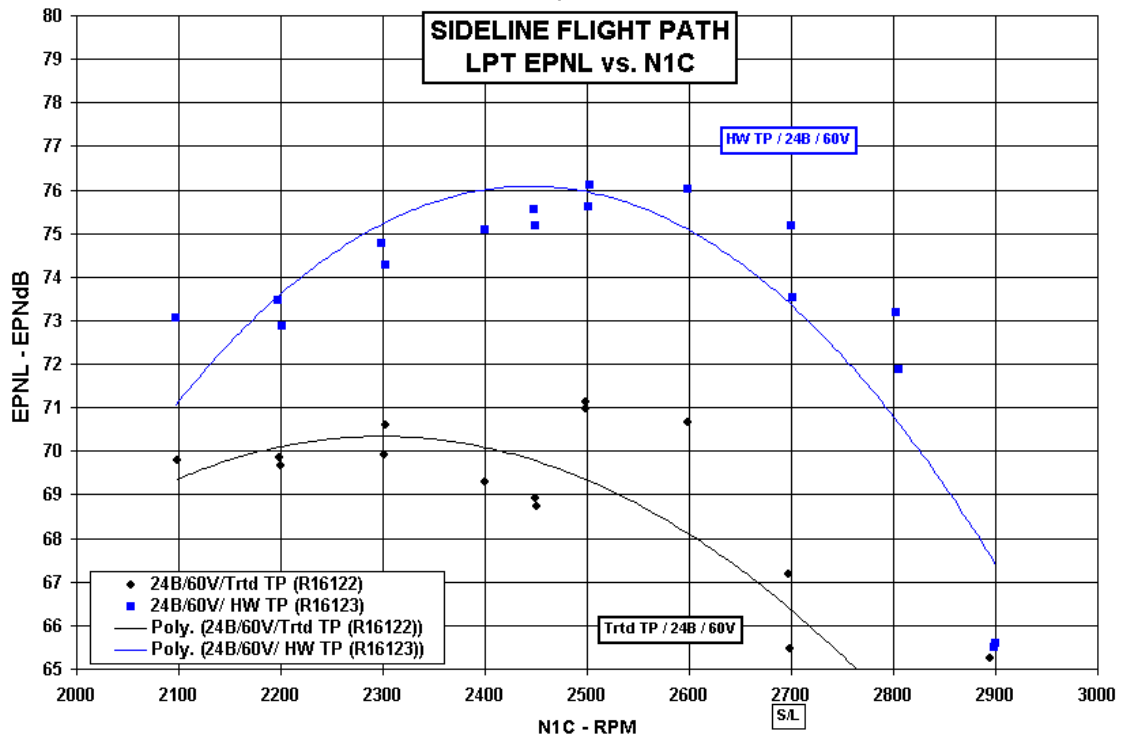
Figure 138.—Effect of tailpipe acoustic treatment on LPT EPNL versus N1C—sideline flight path.
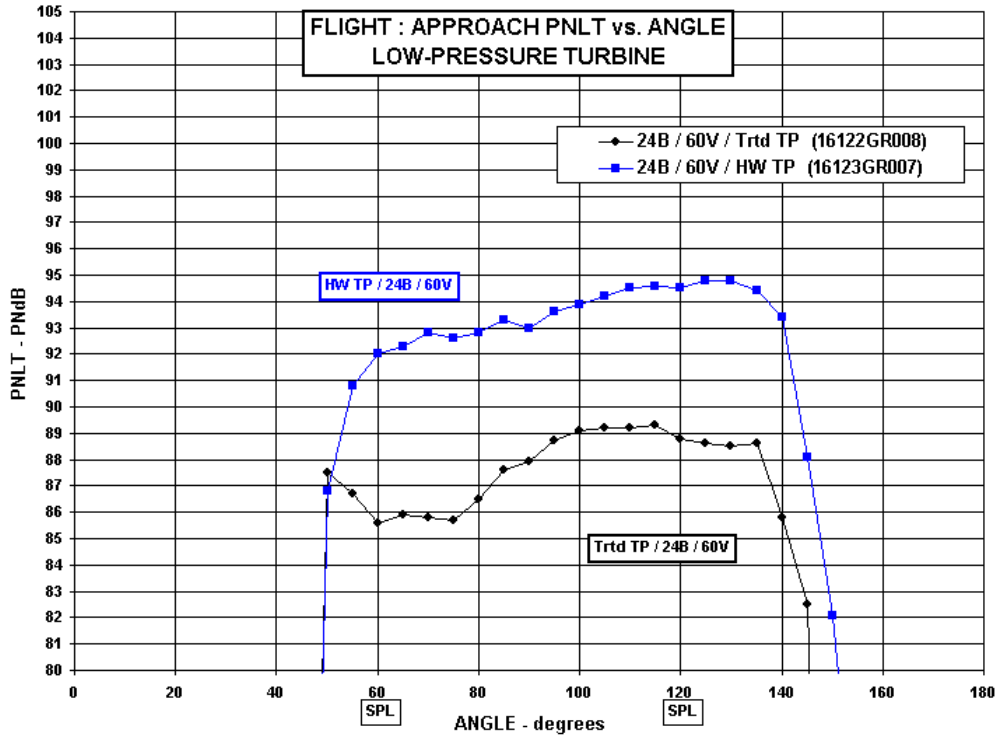
Figure 139.—Effect of tailpipe acoustic treatment on in-flight LPT PNLT directivity—app power.
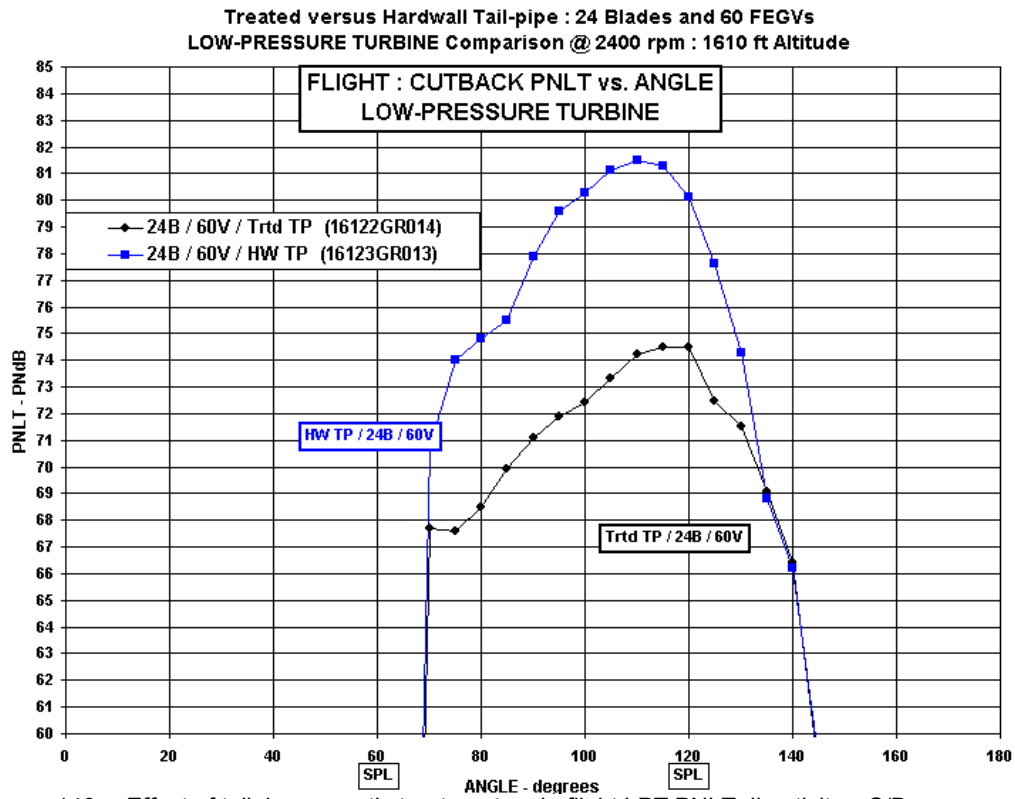
Figure 140.—Effect of tailpipe acoustic treatment on in-flight LPT PNLT directivity—C/B power.
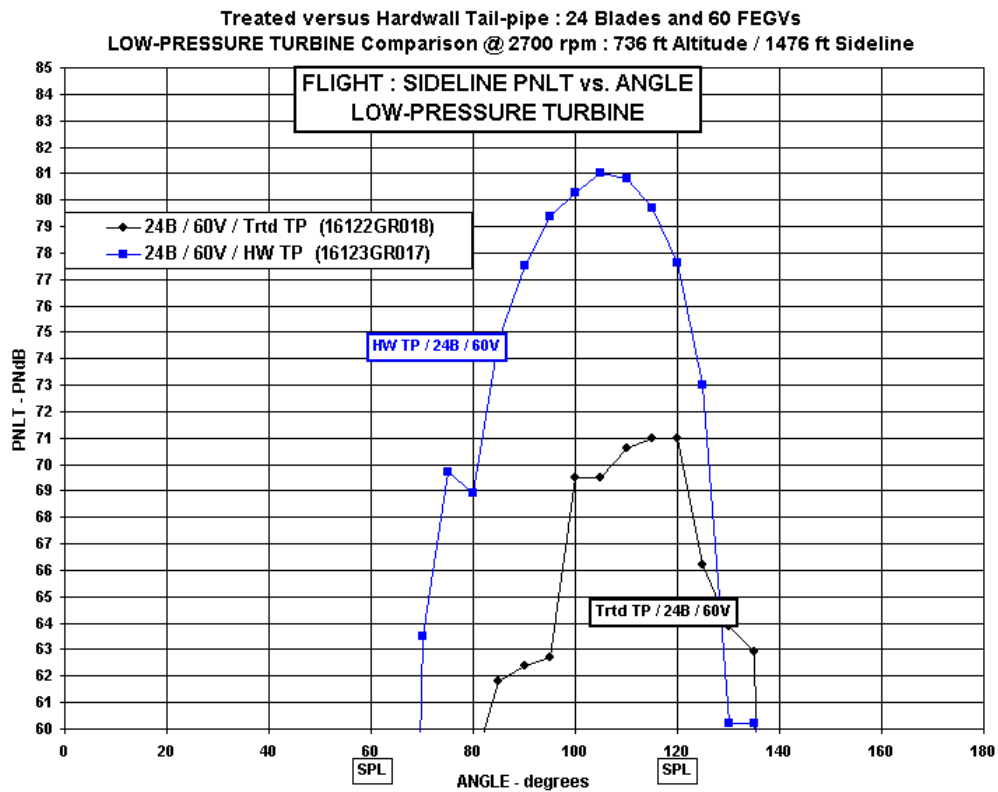
Figure 141.—Effect of tailpipe acoustic treatment on in-flight LPT PNLT directivity—S/L power.
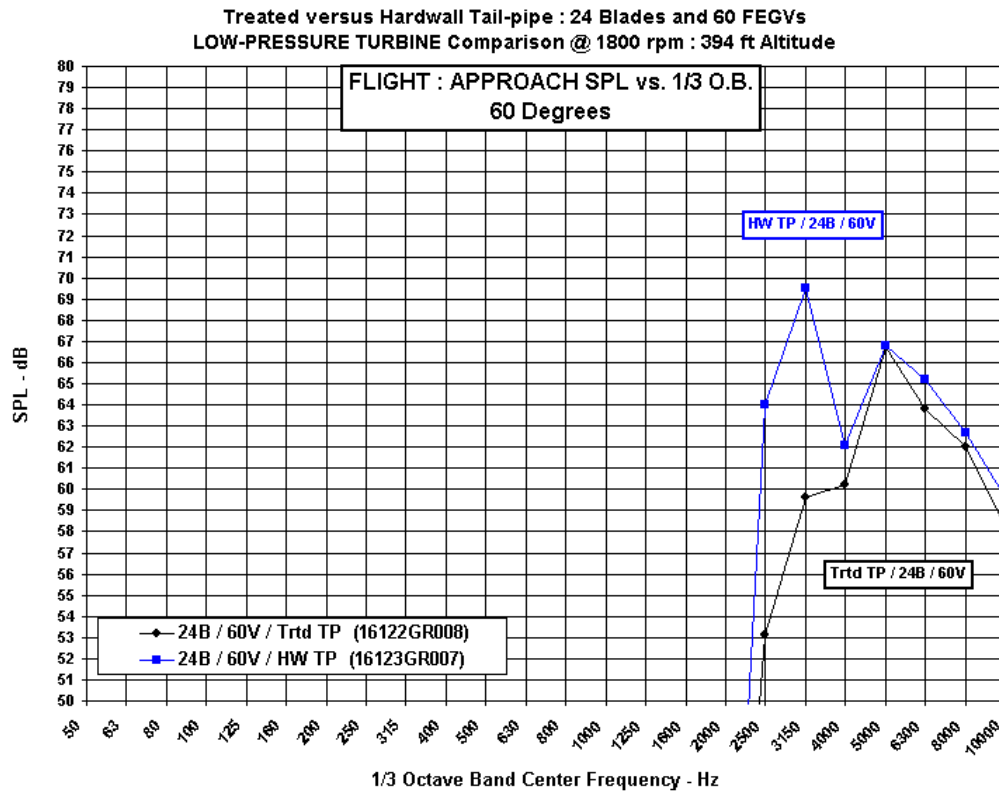
Figure 142.—Effect of tailpipe acoustic treatment on in-flight LPT SPL spectra at 60°—app power.
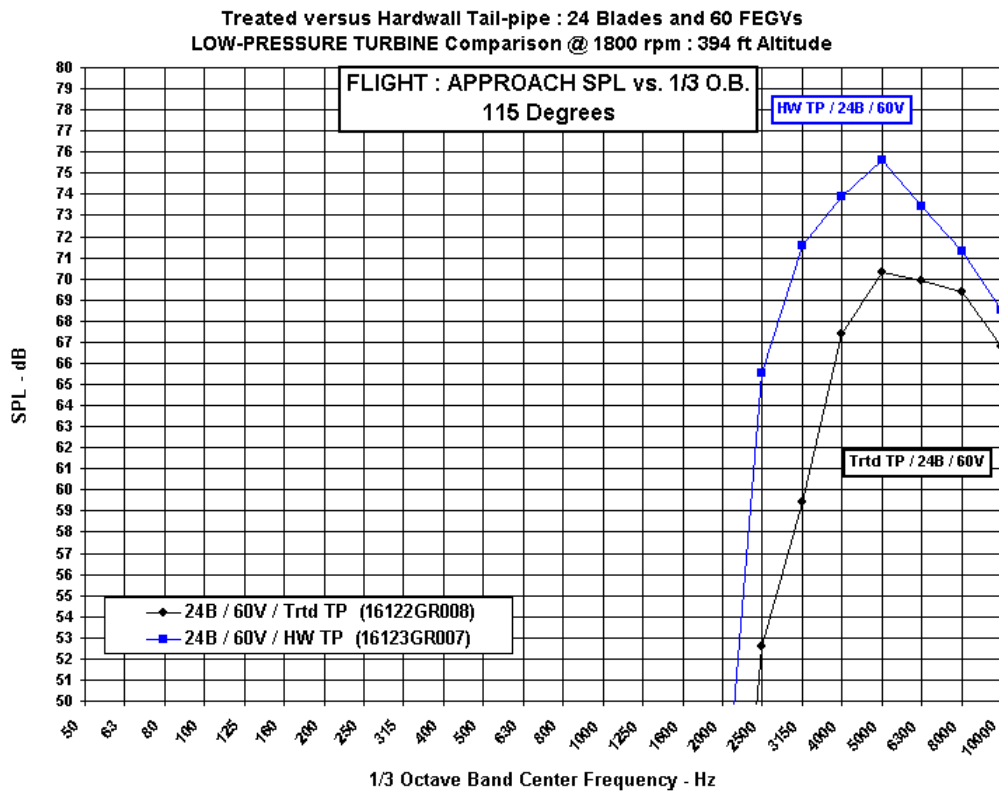
Figure 143.—Effect of tailpipe acoustic treatment on in-flight LPT SPL spectra at 115°—app power.
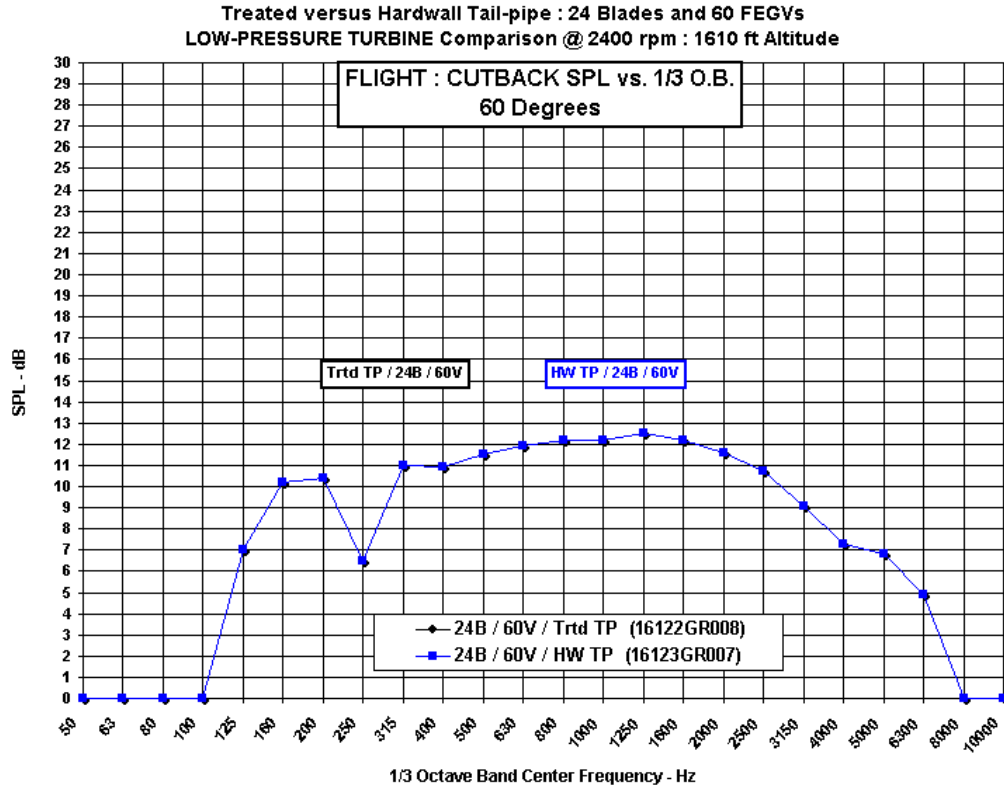
Figure 144.—Effect of tailpipe acoustic treatment on in-flight LPT SPL spectra at 60°—C/B power.
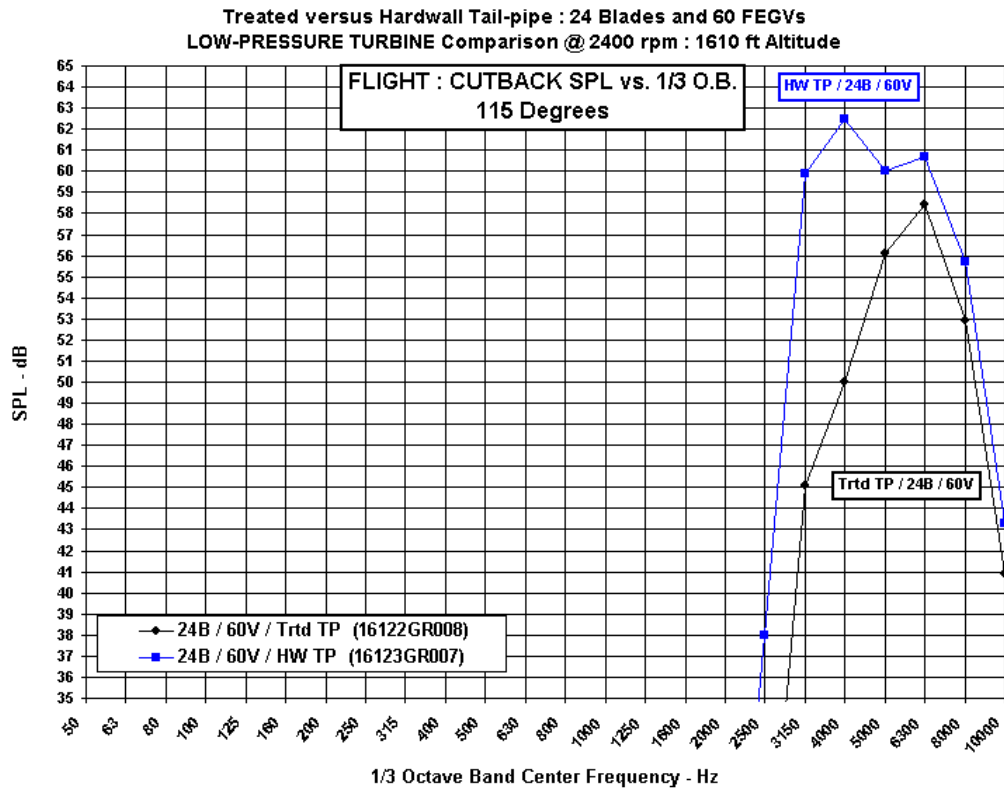
Figure 145.—Effect of tailpipe acoustic treatment on in-flight LPT SPL spectra at 115°—C/B power.
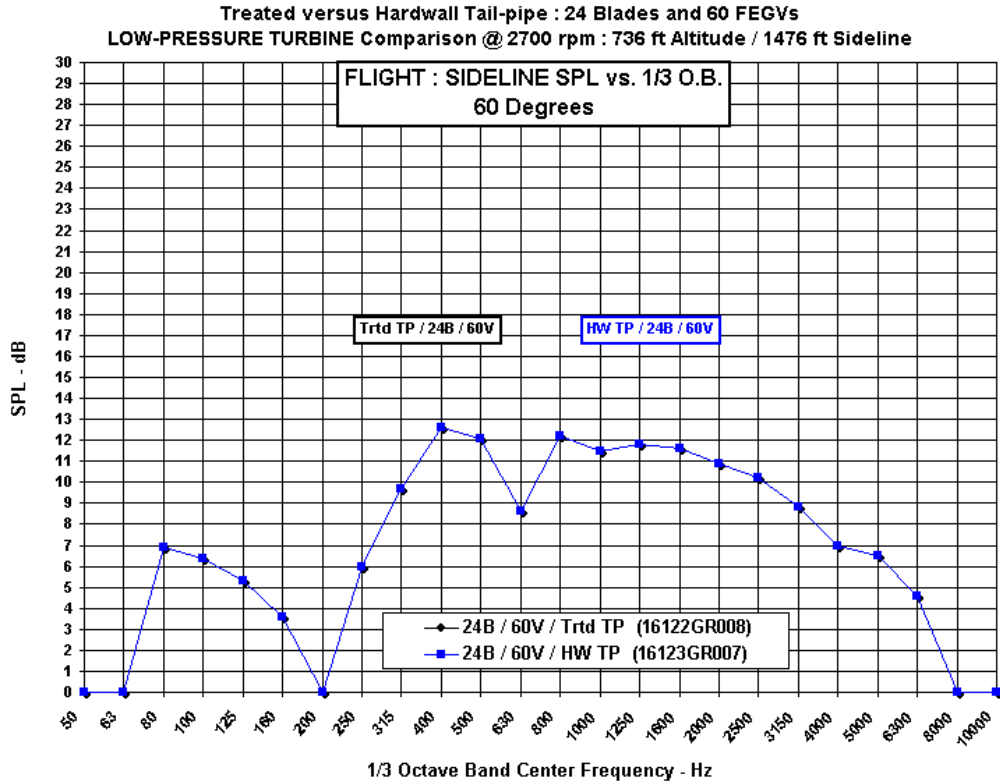
Figure 146.—Effect of tailpipe acoustic treatment on in-flight LPT SPL spectra at 60°—S/L power.
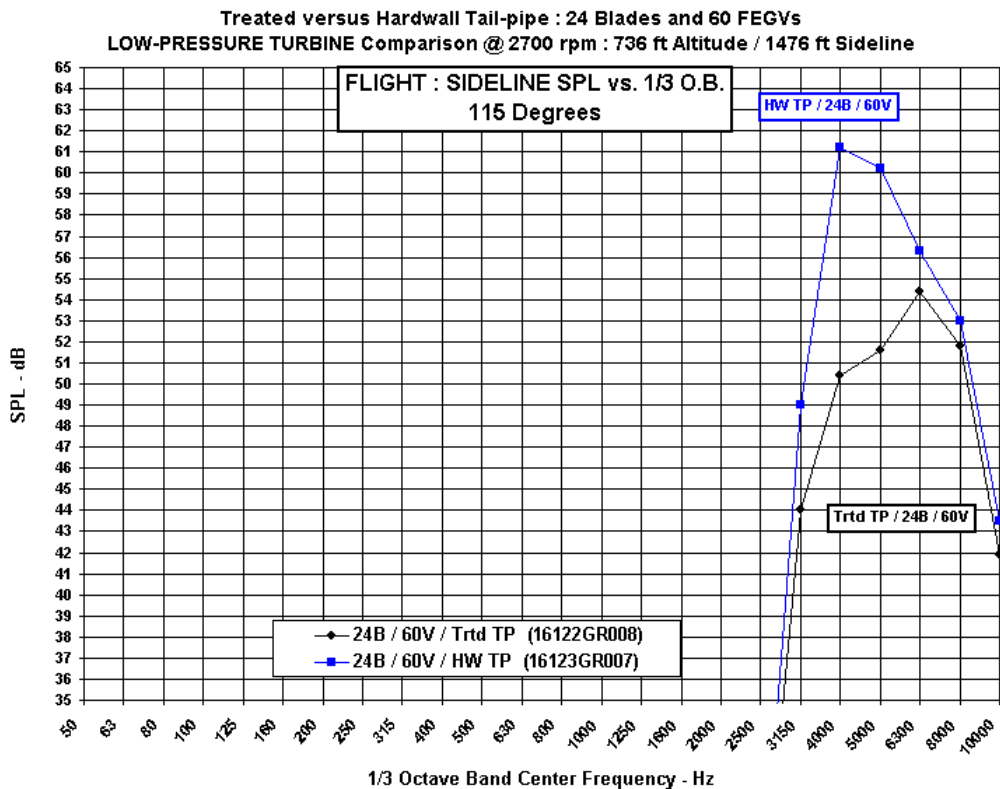
Figure 147.—Effect of tailpipe acoustic treatment on in-flight LPT SPL Spectra at 115°—S/L Power.

Figure 148.—Production inlet installed on PW4098 engine.

Figure 149.—Scarf inlet, taped hardwall, installed on PW4098 engine.

Figure 150.—Scarf inlet installed on PW4098 engine with ICD and aft barriers.

Figure 151.—Aft linear microphone array.

Figure 152.—ICD with phased array microphones installed.
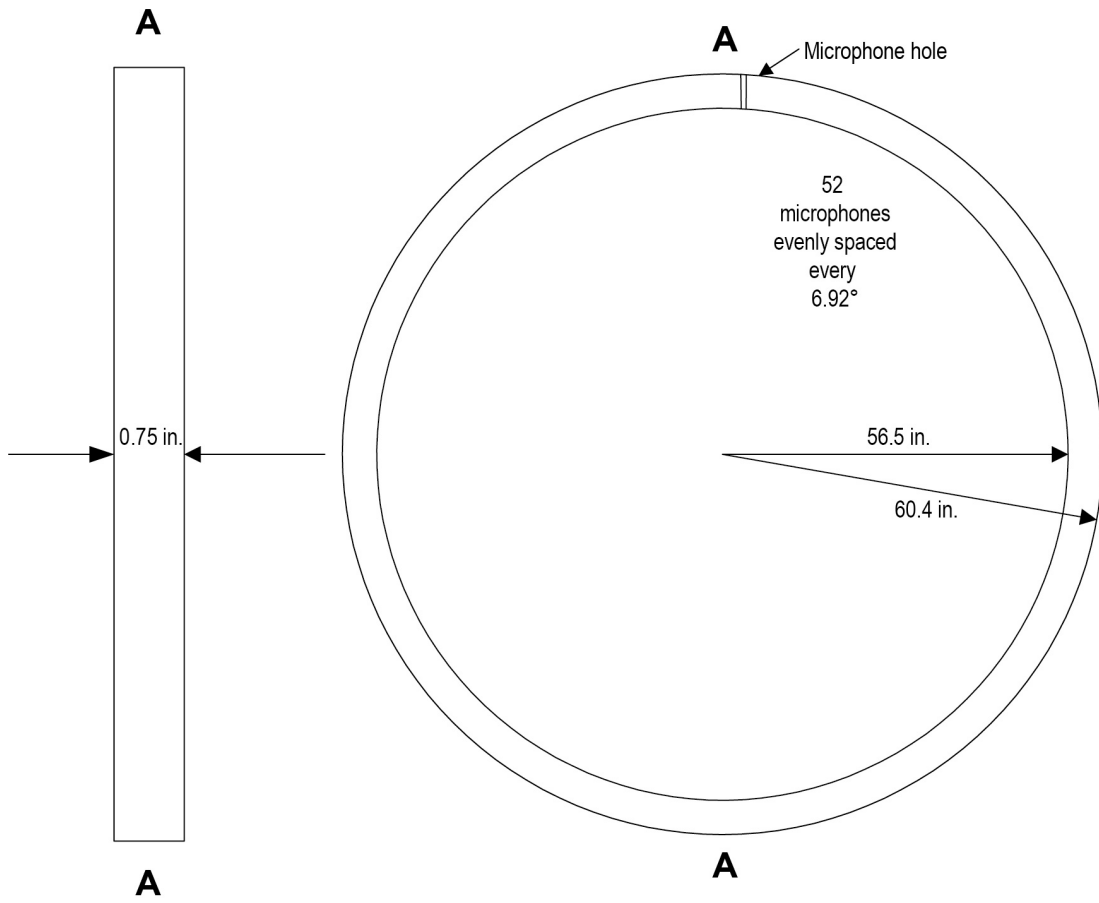
Figure 153.—Schematic of "Olsen Ring" used to hold circular array of microphones located between forward fan case and inlet.
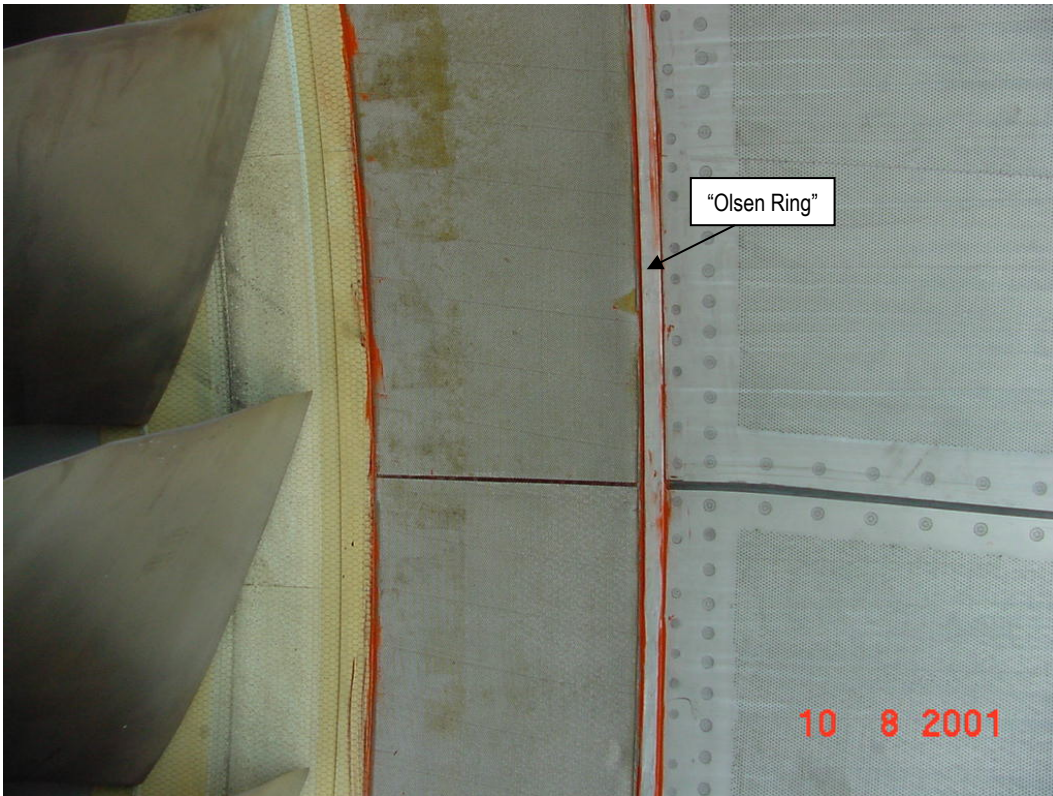
Figure 154.—"A" flange adaptor ring modified to hold 52 Kulite microphones (Olsen Ring).

Front   **Side**
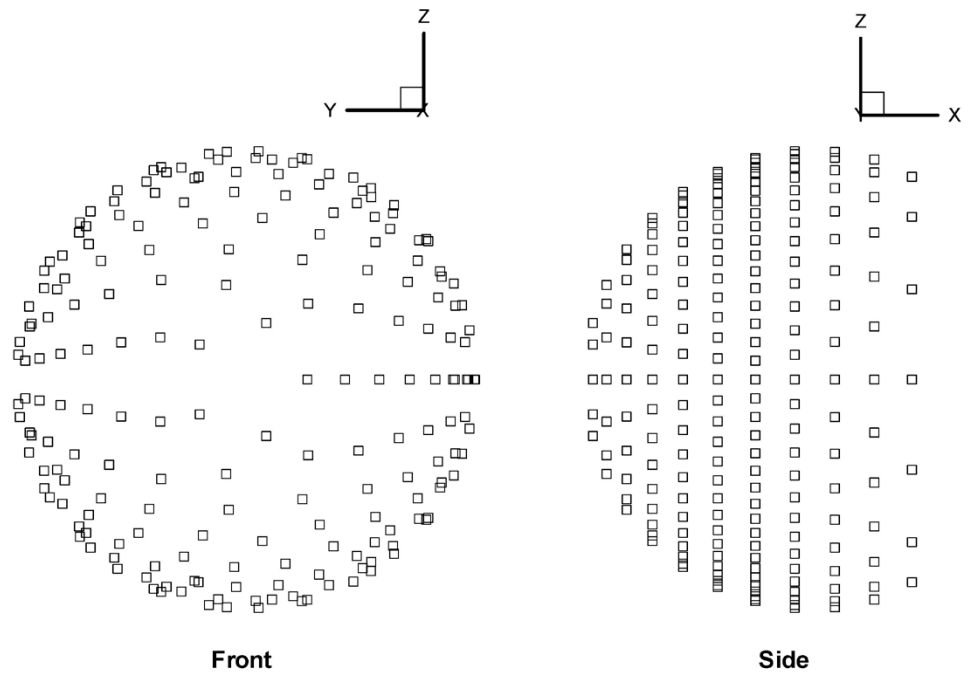
Figure 155.—New Phase 2 ICD array design.

Front   Side
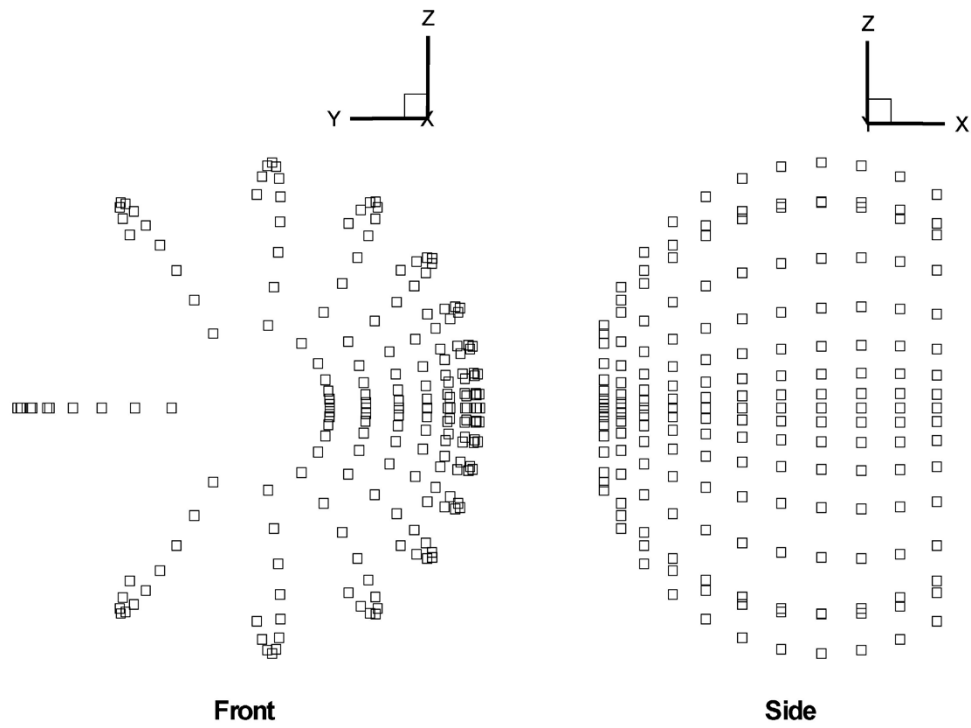
Figure 156.—Old Phase 1 ICD array design.
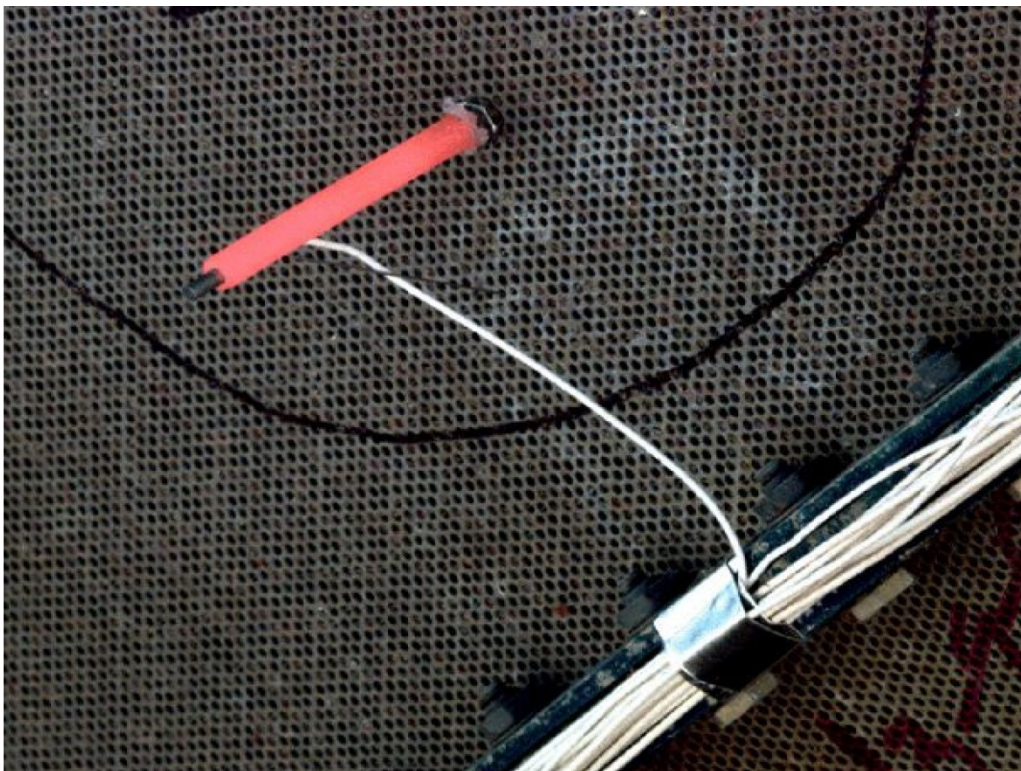
Figure 157.—Kulite holder attached to ICD panel.

Figure 158.—Paper template for initial Kulite placement.
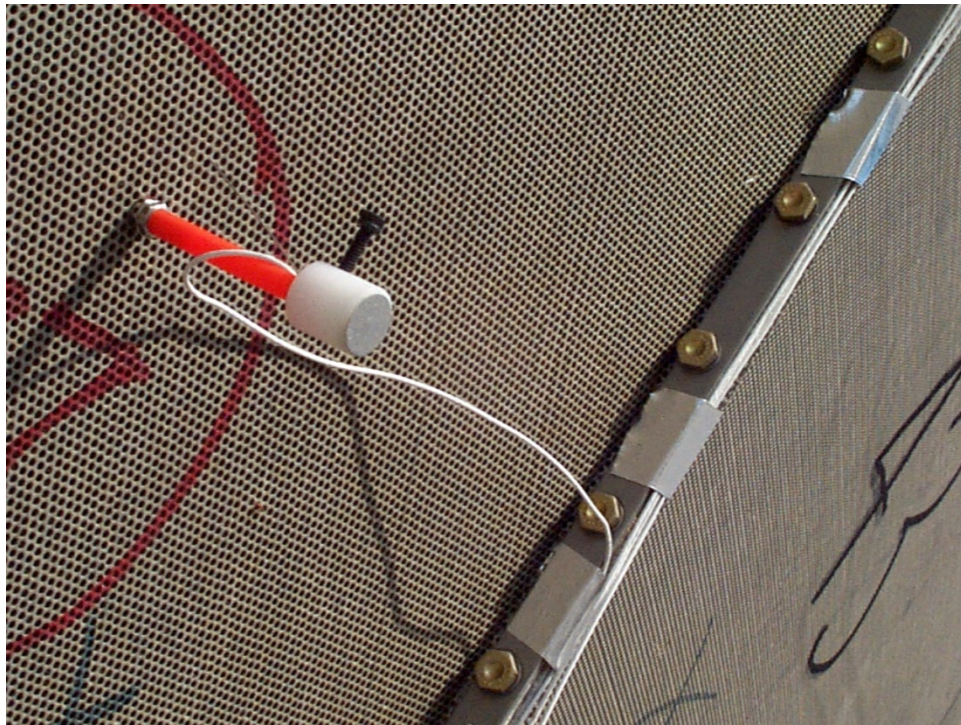
Figure 159.—Photoreflective target installed on Kulite holder.
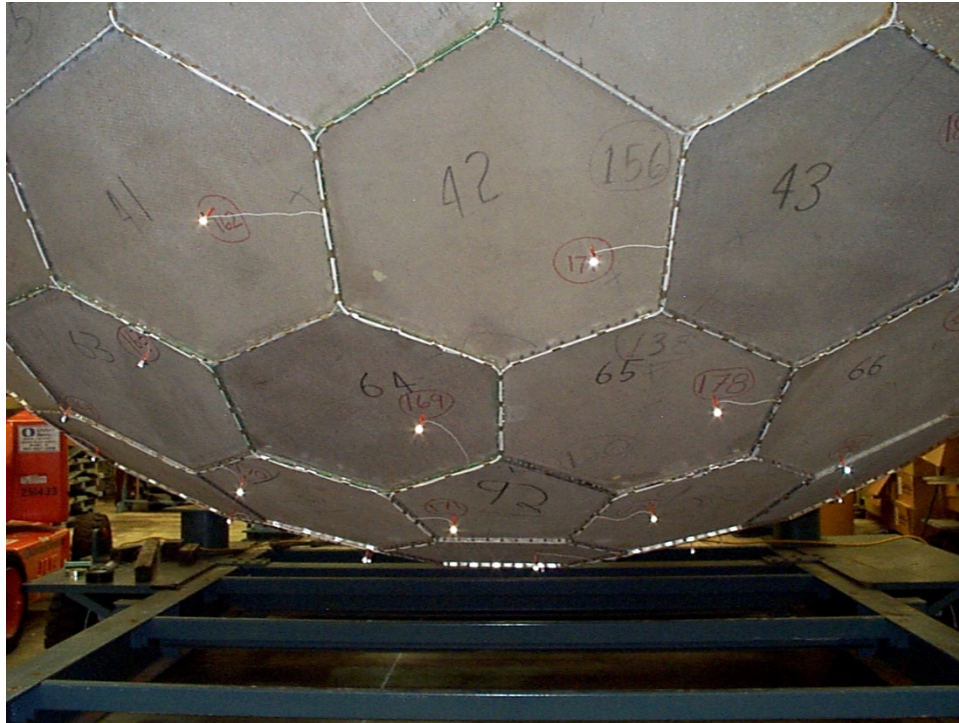
Figure 160.—Light from camera flash reflecting from photoreflective targets.
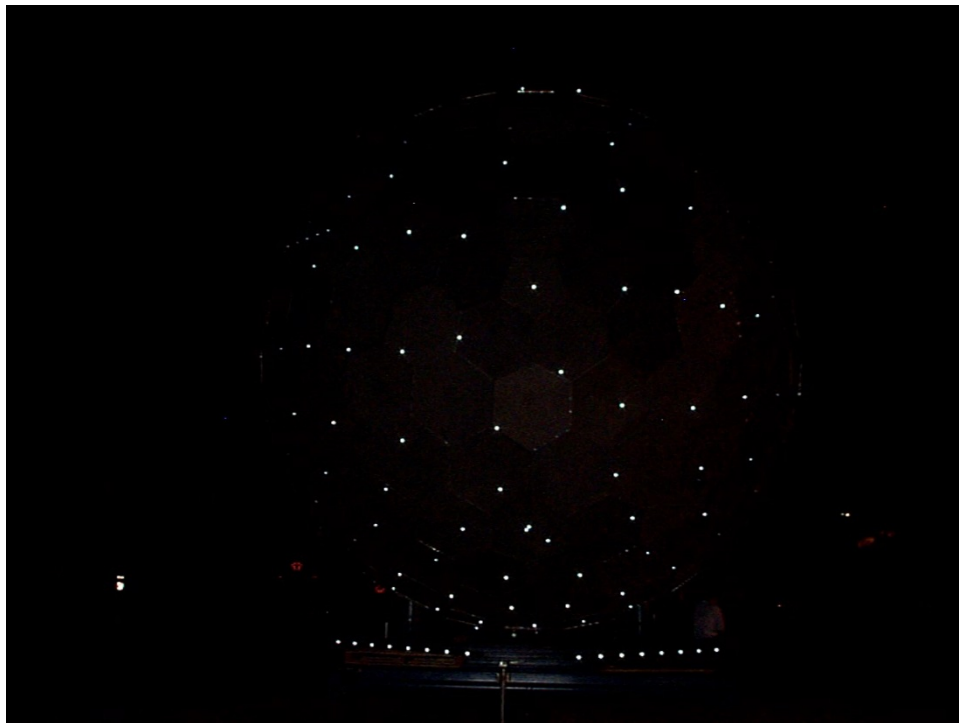
Figure 161.—Photogrammetry survey at night.
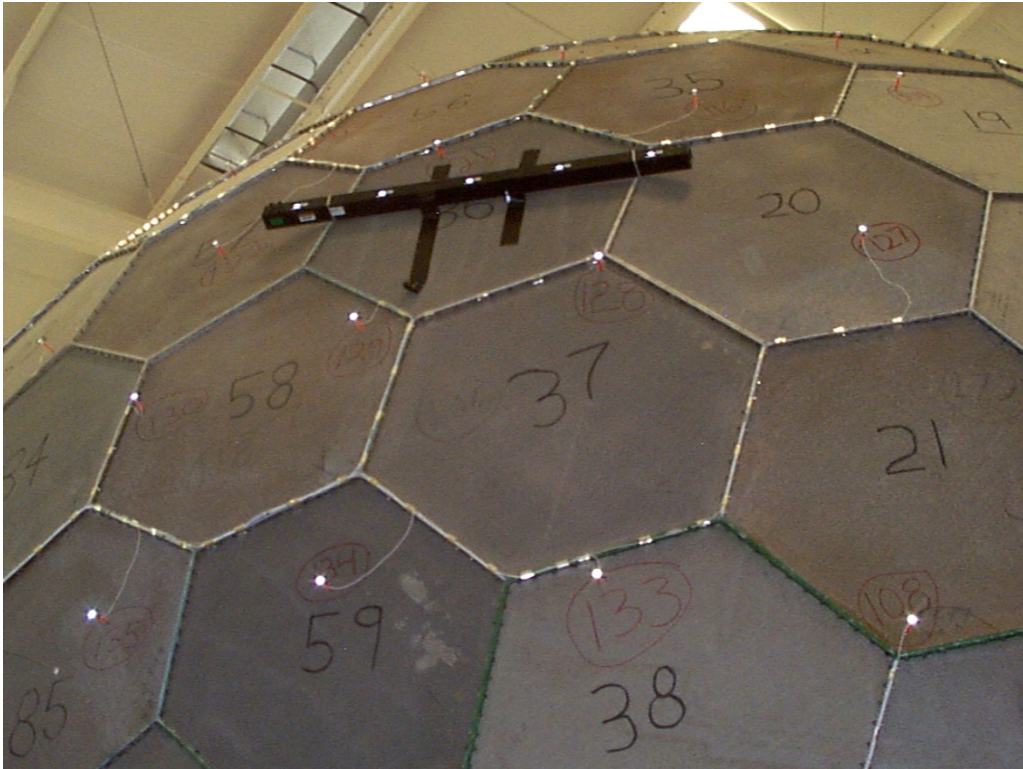
Figure 162.—Reference scale bar for photogrammetry survey.

52 ea. in-duct Kulites with integral Teflon cable and female flat pack connector (#1-52)

52 ea. 21.5 ft male flat pack to male LEMO Teflon cable (ch #1-52)

52 ea. 100 ft orange LEMO to LEMO cable (ch #1-52)
Note: Bring additional 52 ea. in case need 200 ft

Boeing DPPS 14-17 (ch # 1-52)

1 ea. 40-ft 61-pin female connector to 20 male BNC (ch # 1-20 / 201-220)
Note: Use cable numbered 191-210

Supplied by P&W

1 ea. 25-ft BNC to BNC (ch # 200) [in-duct array ch # 1]

1 ea. 15-ft. BNC to BNC (ch # 200)

1 ea. 61-pin male connector to 61-pin connector (ch # 201-220) [in-duct array ch # 2-21]

1 ea. 15-ft 61-pin female connector to 20 male BNC (ch # 1-20 / 201-220)
Note: Use cable numbered 191-210

9 ea. 25-ft 6-pin male connector to 2 male BNC (ch # 21-38 / 221-238) [in-duct array ch # 22-39]

SADR to control room infrastructure cable

9 ea. 20-ft 6-pin female connector to 2 male BNC (ch # 21-38 / 221-238)

16 ea. 40-ft male BNC to terminal strip (ch # 239-254)

1 ea. 25-ft 55-pin male connector to 16 male BNC (ch # 239-254) [in-duct array ch # 40-52, 3 spares]

Patch panel inside SADR

Control Room Patch panel

ch #200

SW2

Out   128 CHMUX

ch #201-251

SW3

RG174 coax 12 ft BNC to BNC Cables (ch #200-251) (Green bundles)

DDS4

Pre-connect Tees

ch #200-251

JRU - 03/27/01

Figure 163.—ICD microphone instrumentation cable diagram.
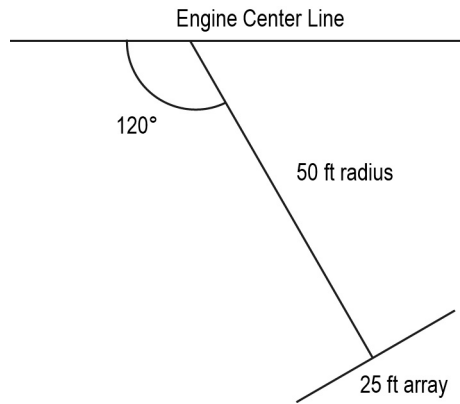
Figure 164.—Schematic of farfield linear array.

Figure 165.—Farfield linear array.

Figure 166.—Farfield linear array installation and locating pin.
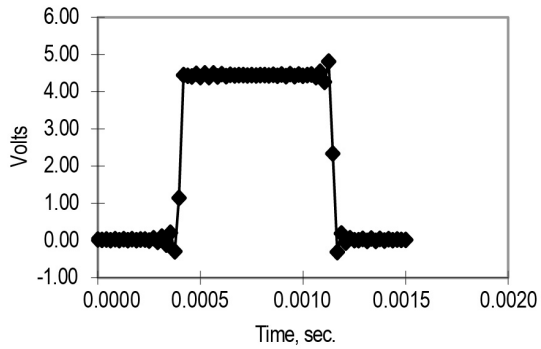
(a) 587 rpm
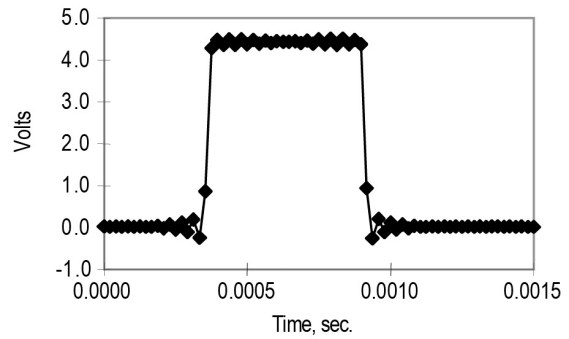
(b) 1833 rpm
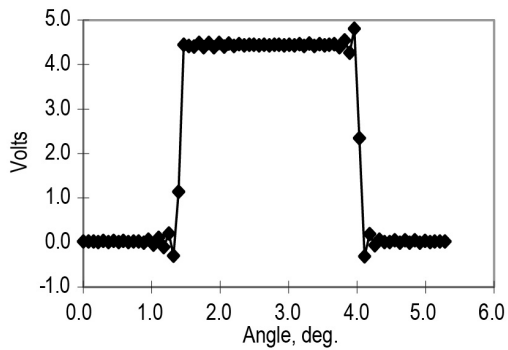
(c) 587 rpm
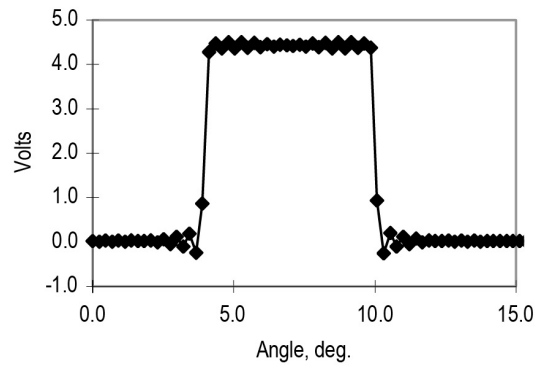
(d) 1833 rpm

Figure 167.—Typical trace of trigger signal, (a) 587 rpm Volts versus Time, (b) 1833 rpm Volts versus time, (c) 587 rpm Volts versus angle, and (d) 1833 rpm Volts versus angle.
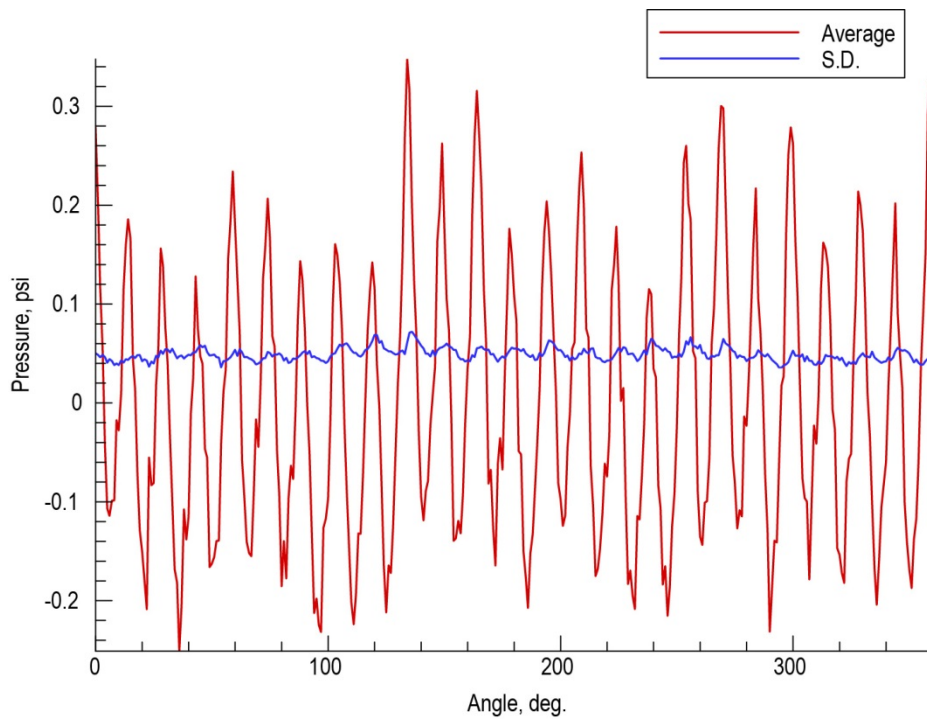
Figure 168.—Average and standard deviation of an Olsen Ring Kulite.
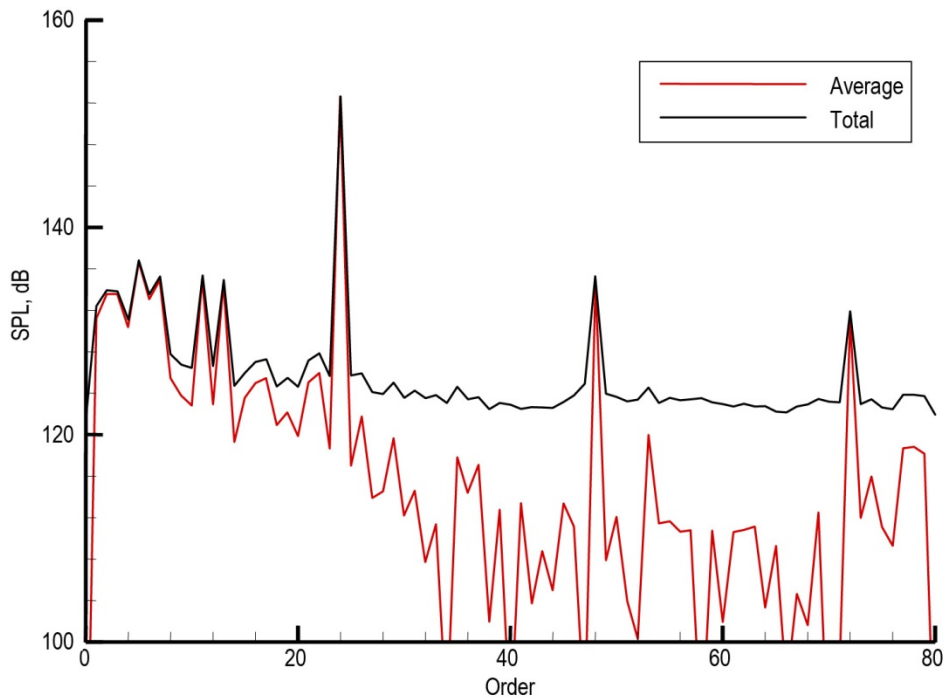
Figure 169.—Average and total spectra of a Olsen Ring Kulite.
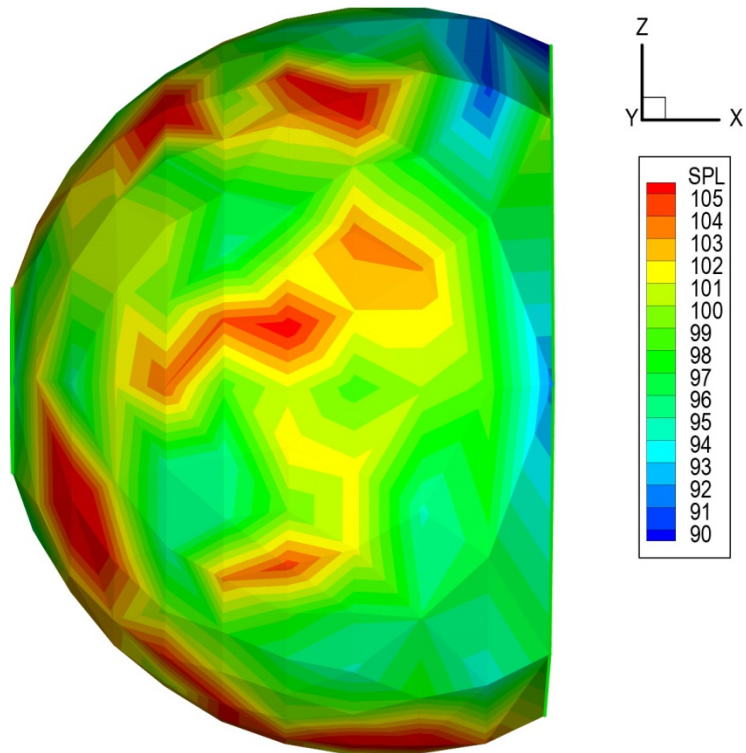
Figure 170.—Total BPF tone SPLs on the ICD.
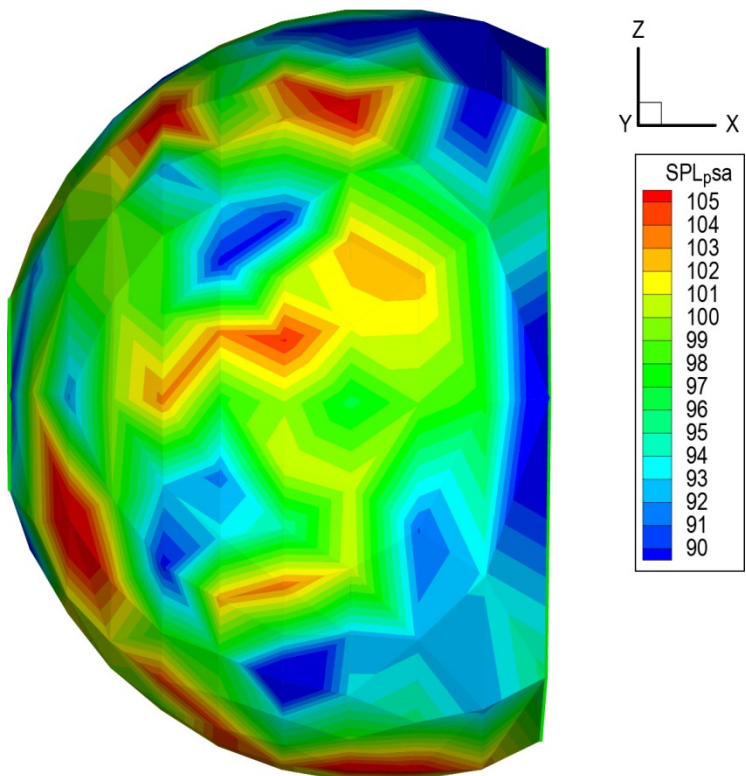
Figure 171.—Average BPF SPLs on the ICD.
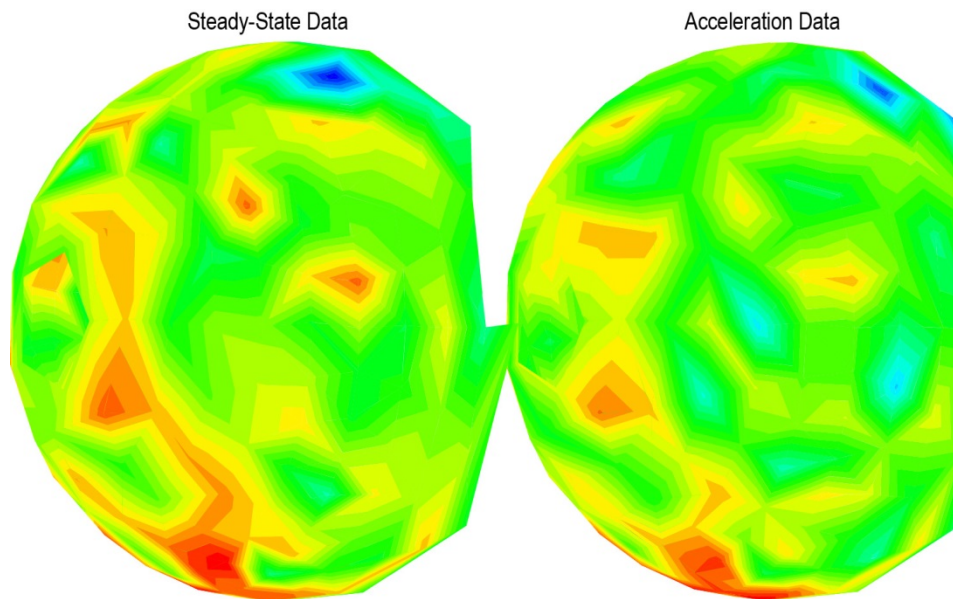
Figure 172.—Steady and acceleration data at BPF for a subsonic tip speed.

1st Rad = 1 -> 33
2nd Rad = 34 -> 56
3rd Rad = 57 -> 73
4th Rad = 74 -> 84
5th Rad = 85 -> 91

1 -> 33 = > m= -16 to 16
34 -> 56 = > m = -11 to 11
57 -> 73 = > m = -8 to 8
74 -> 84 = > m = -5 to 5
85 -> 91 = > m = -3 to 3
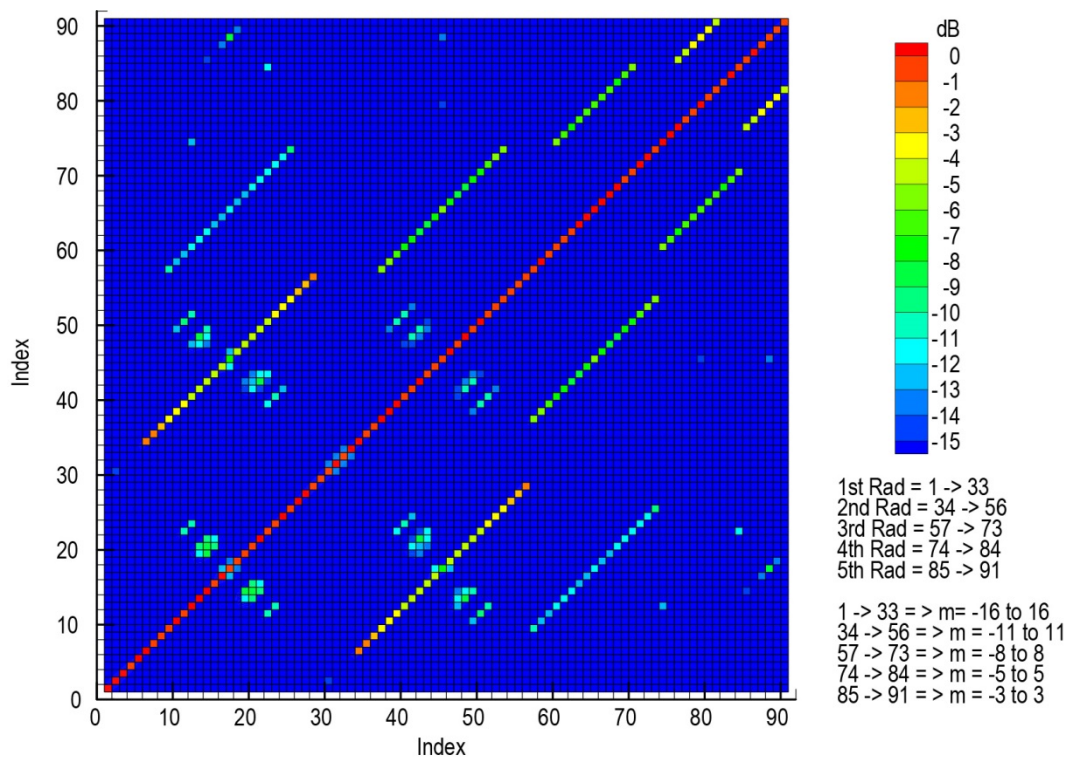
Figure 173.—Example orthogonality plot, 1800N1C, BPF.
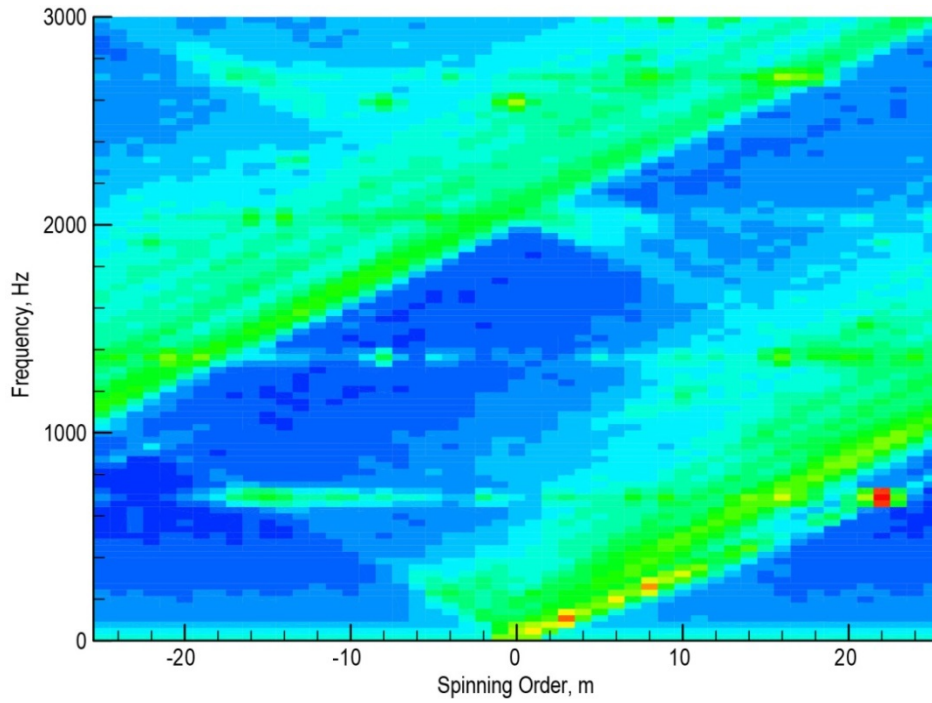
Figure 174.—Mode measurement plot from EVNRC1 at 1800 N1C.
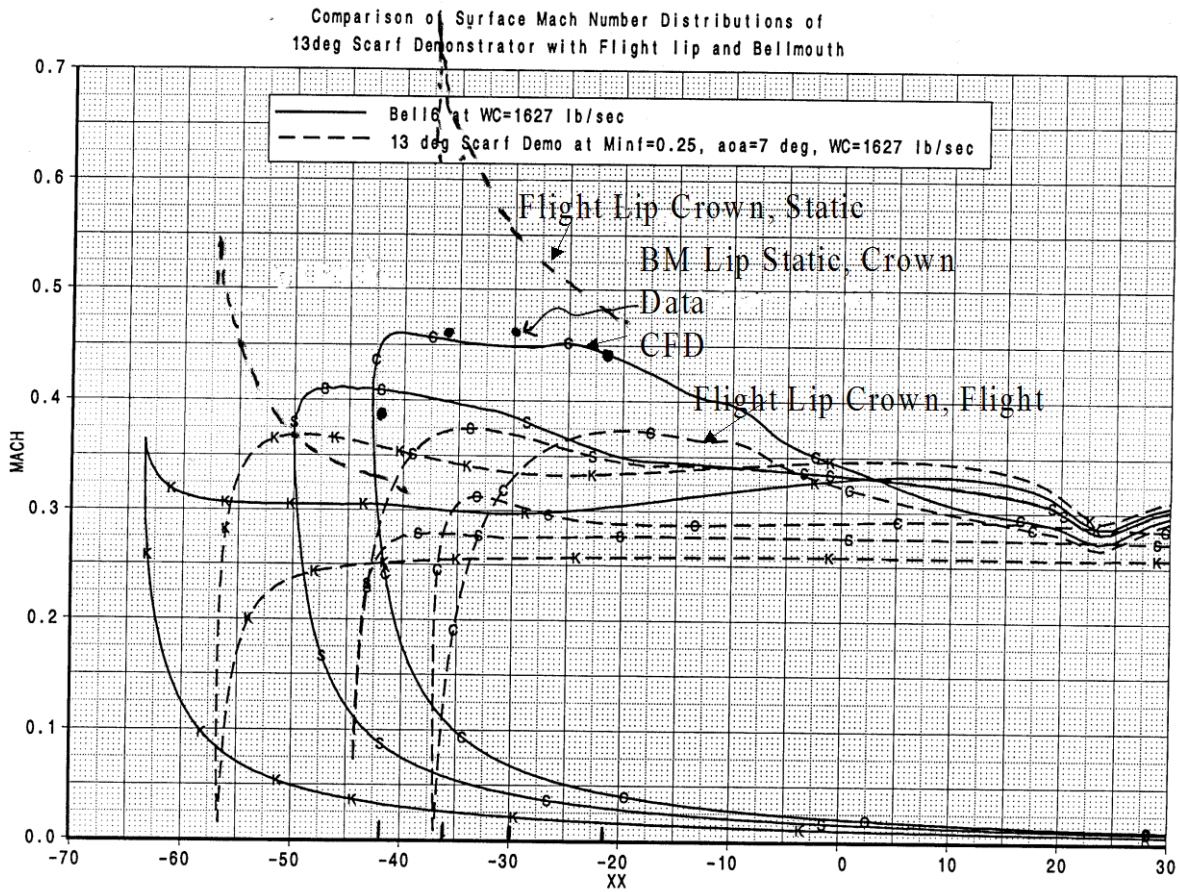
Figure 175.—Scarf inlet wall mach number profiles at approach power.
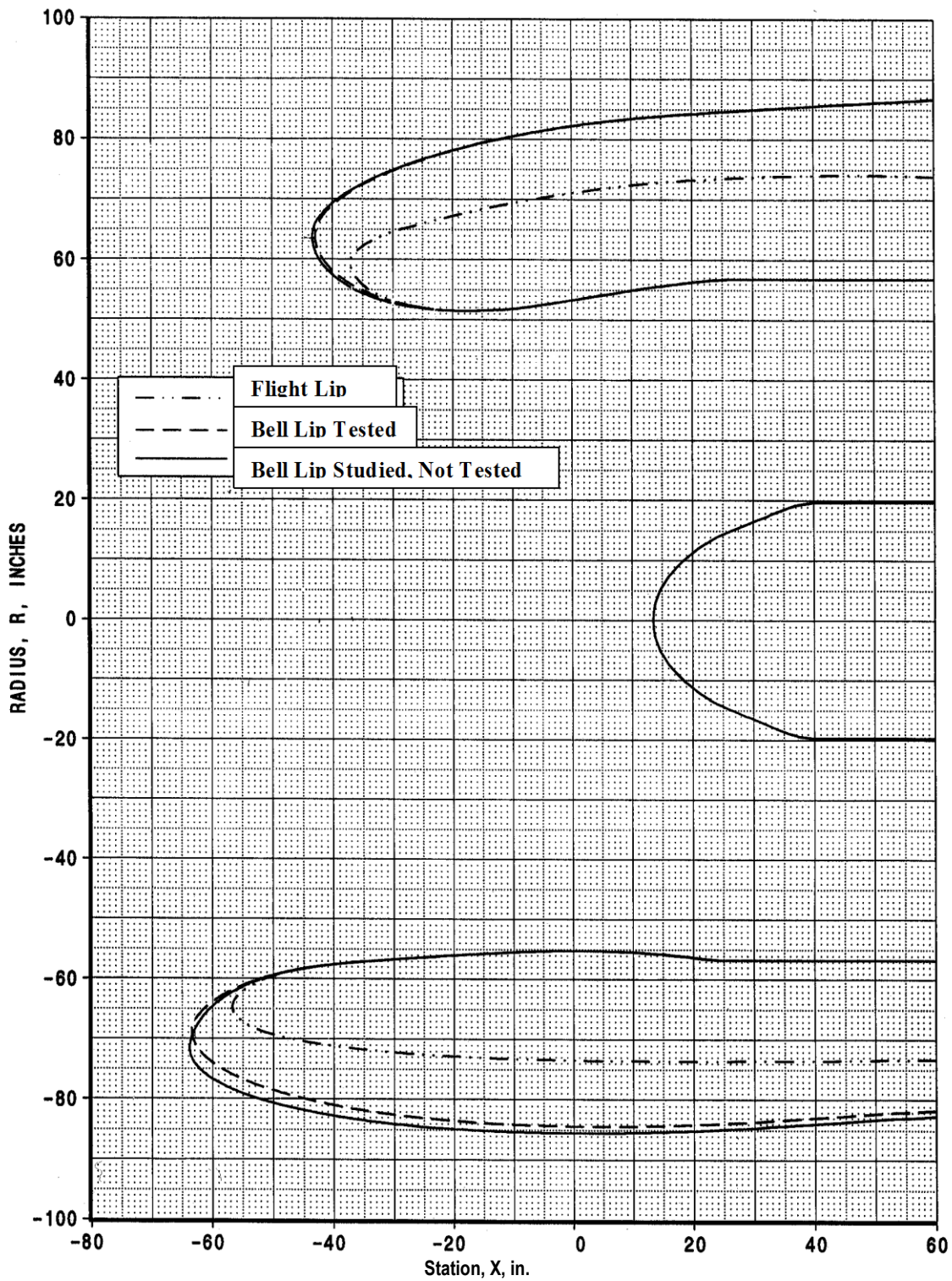
Figure 176.—Schematic of scarf inlet with flight lip and bellmouth lip.
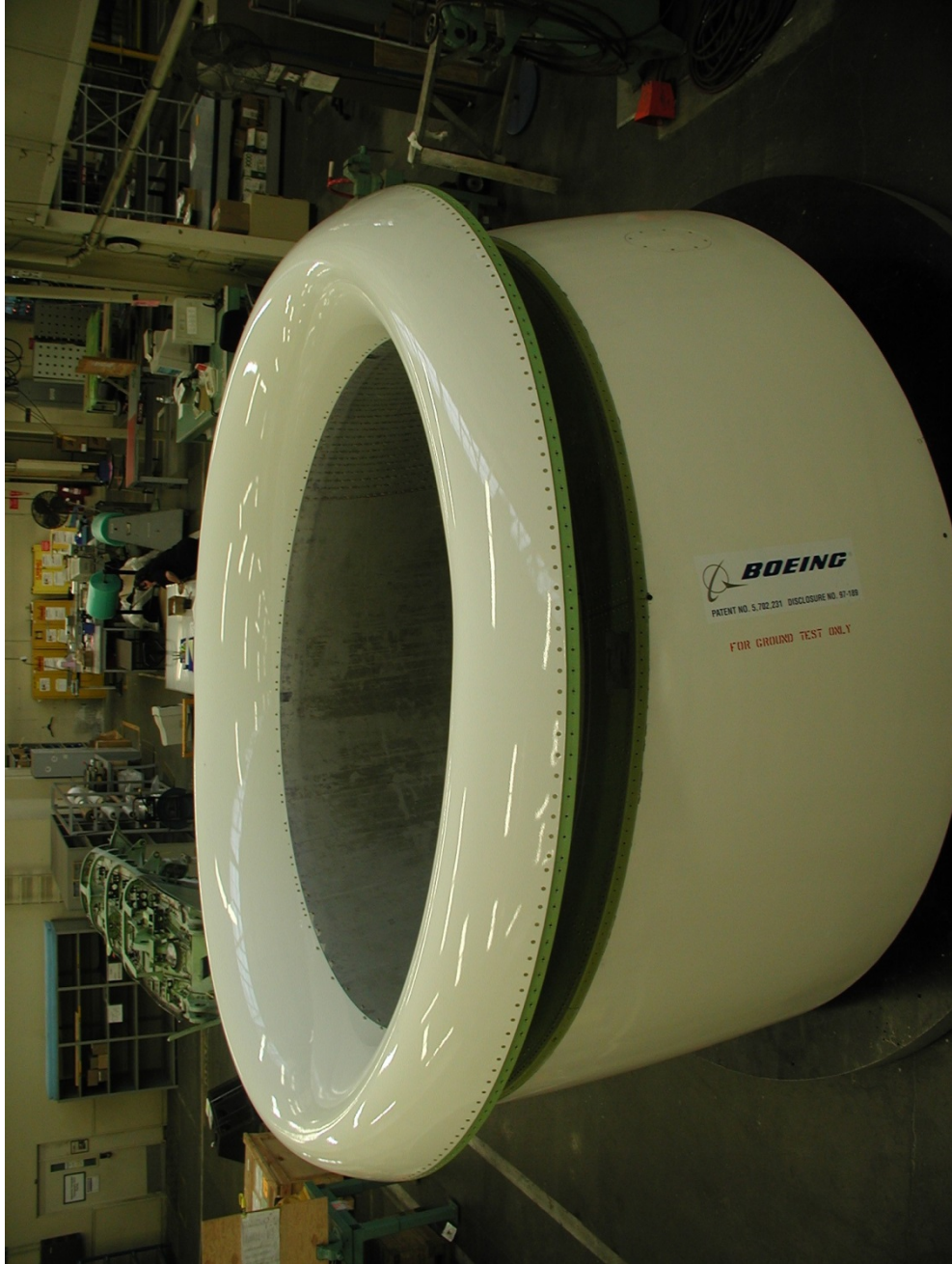
Figure 177.—Scarf inlet with bellmouth lip.
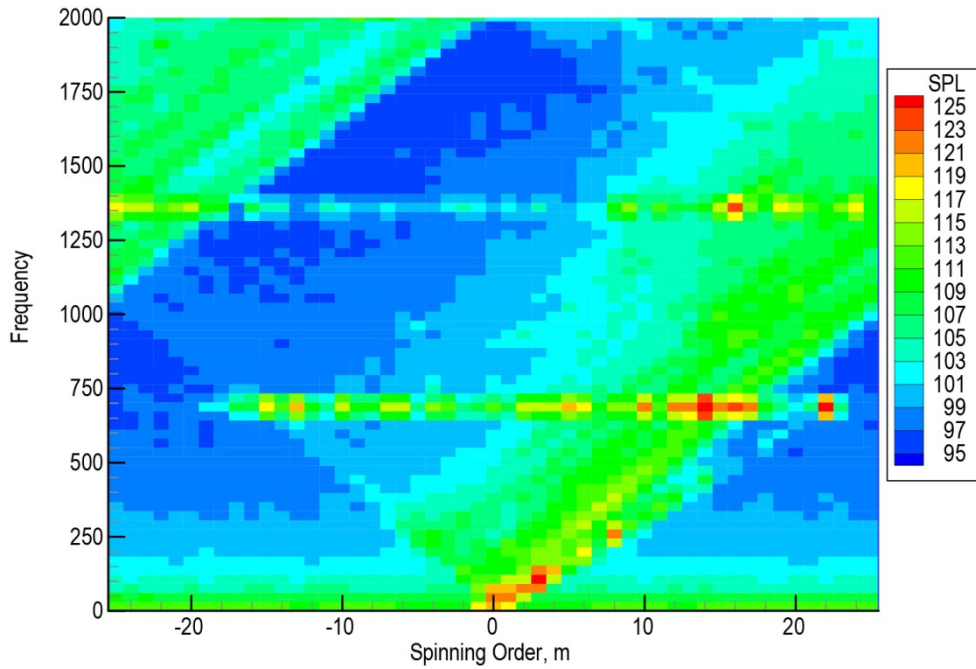
Figure 178.—Mode plot for configuration NG1 at N1C = 1800 rpm.
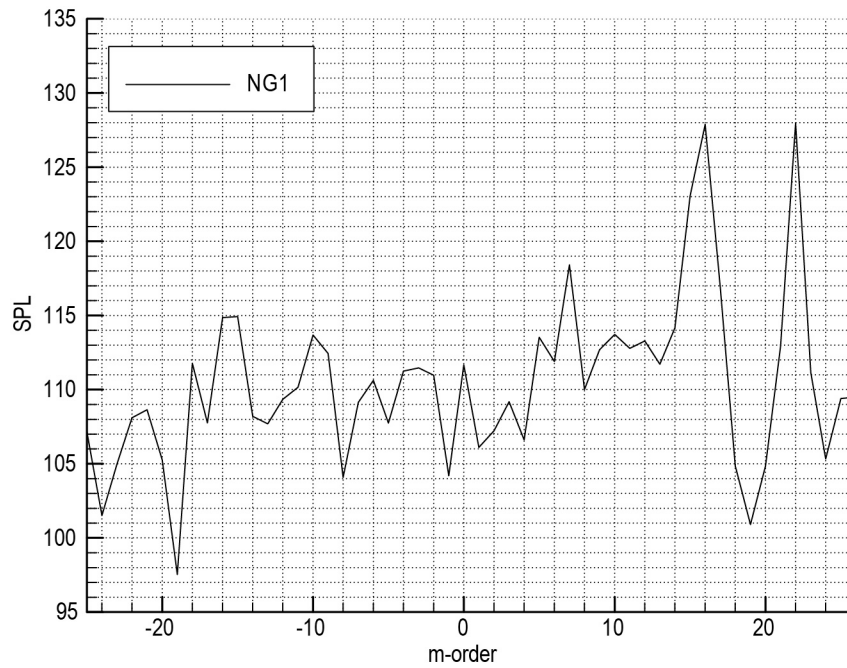
Figure 179.—Blade passage tone versus m-Order for NG1 at N1C = 1800 rpm.
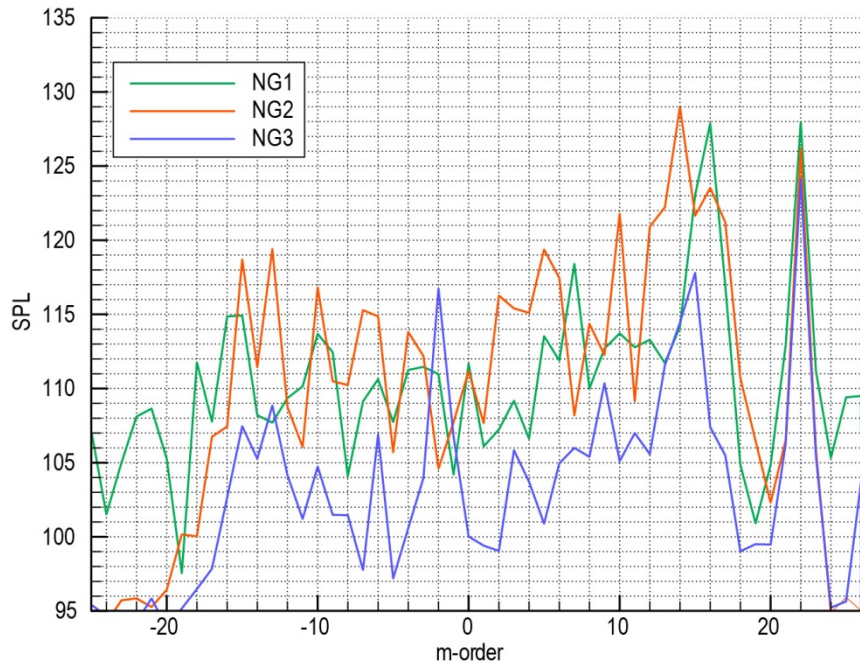
Figure 180.—Comparison of the active configurations at N1C = 1800 rpm.
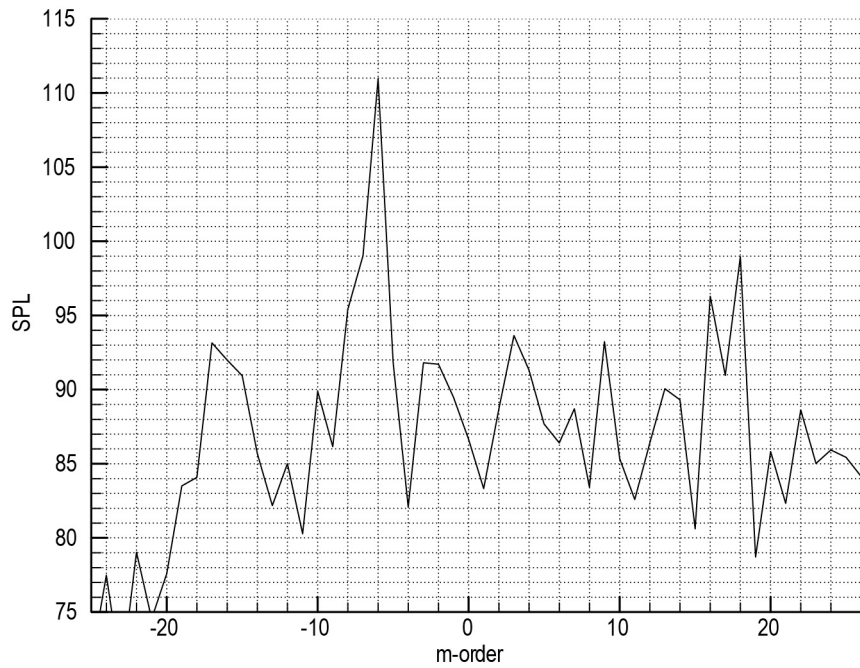
Figure 181.—Static engine with one row of transducers for m = –6 mode.
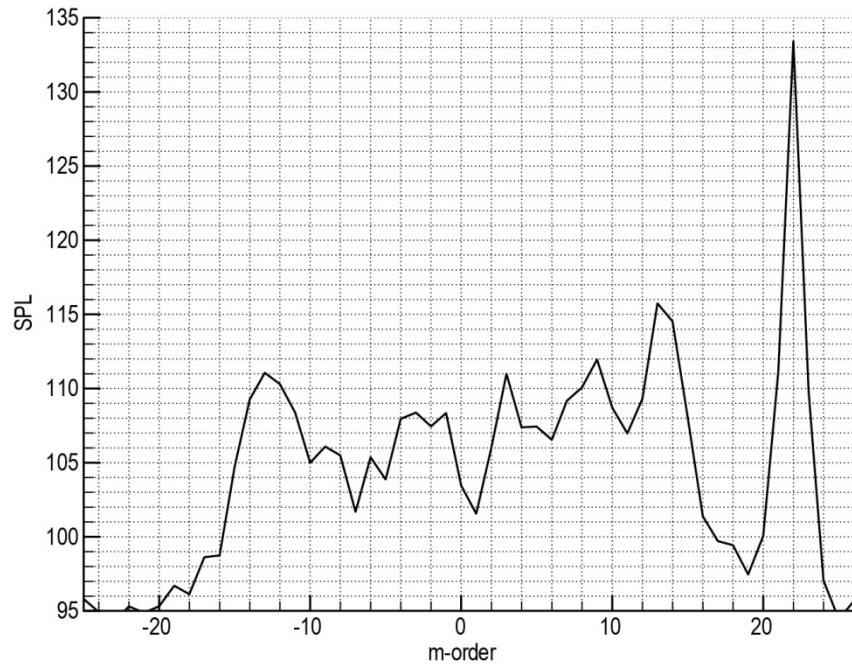
Figure 182.—Configurations EVNRC1 at N1C = 1620 rpm.
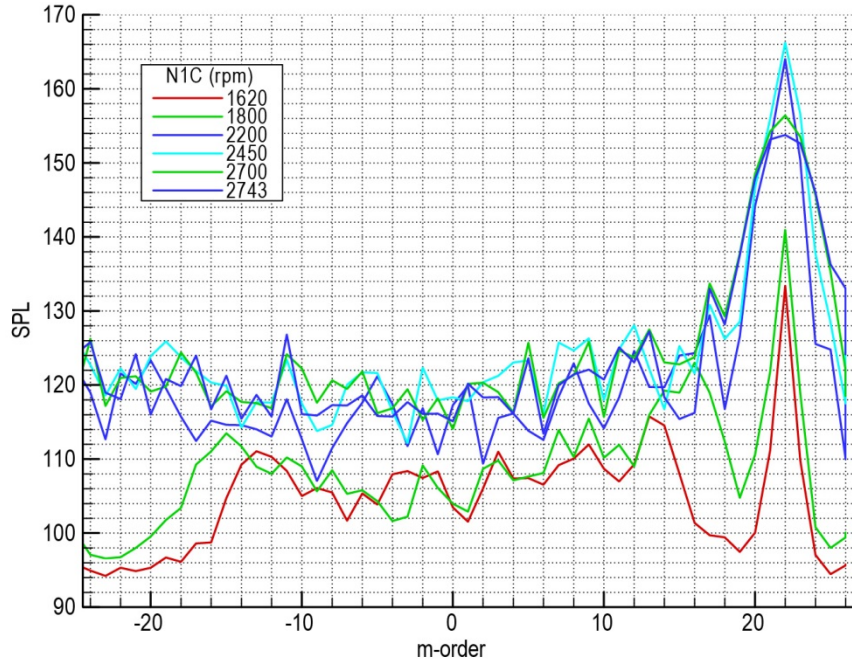
Figure 183.—Powerline for EVNRC1 at BPF.
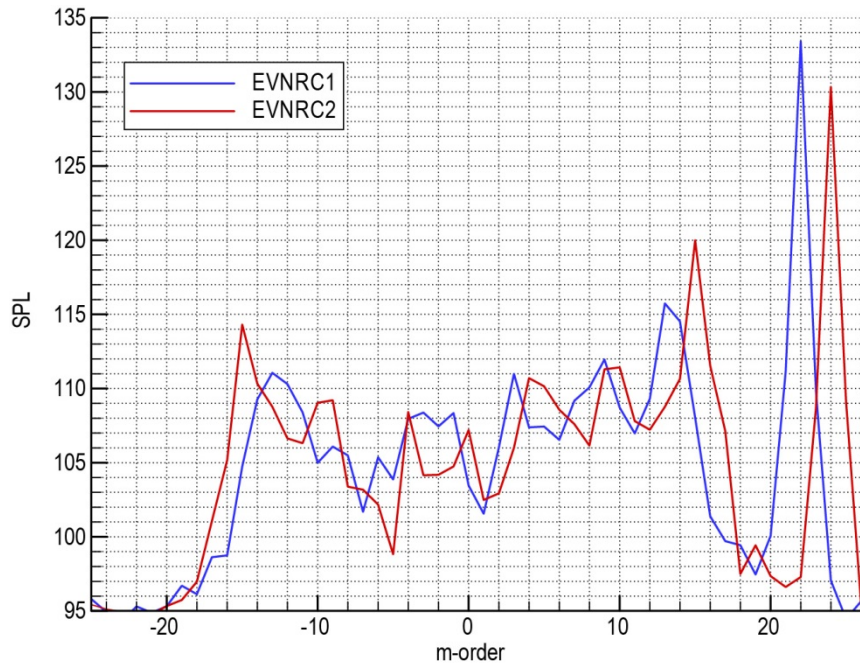
Figure 184.—Comparison of 22 versus 24 blades at N1C = 1620 rpm
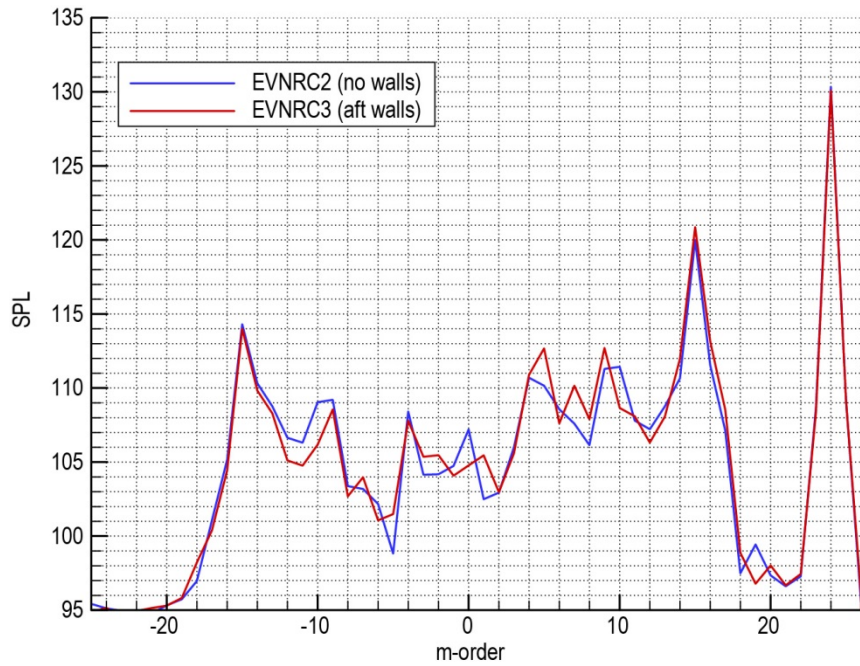
Figure 185.—Effect of aft barriers on BPF noise at N1C = 1620 rpm.

Production Inlet, Northrup-Grumman Spool Piece
Exposed Passive, Taped Active
Run 11509b, N1C = 1745, BPF, 22 Blades, 28 Vanes
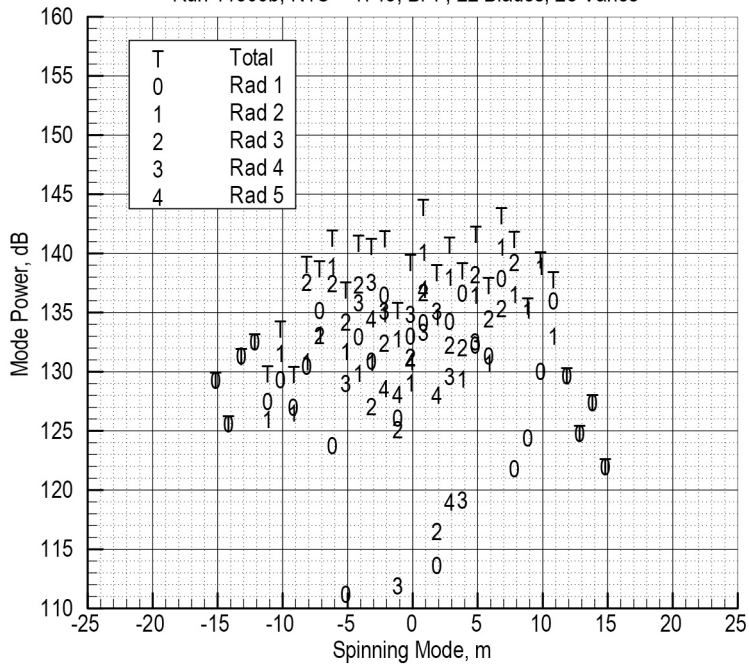
Figure 186.—ICD array, NG2, N1C1745.

Production Inlet, Northrup-Grumman Spool Piece
Exposed Passive, Taped Active
Run 11510, N1C = 1800, BPF, 22 Blades, 28 Vanes
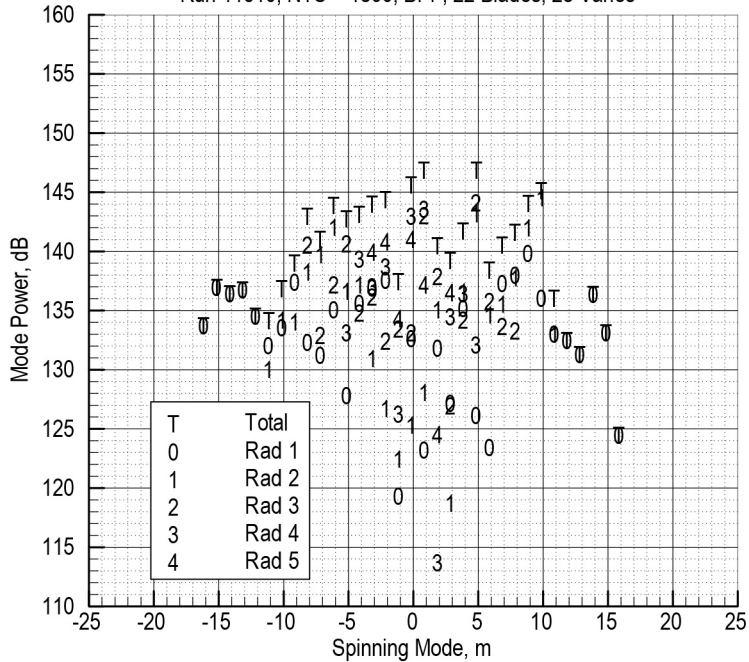
Figure 187.—ICD array, NG2, N!C1800.

Production Inlet, Northrup-Grumman Spool Piece
Exposed Passive, Taped Active
Run 11512, N1C = 1909, BPF, 22 Blades, 28 Vanes
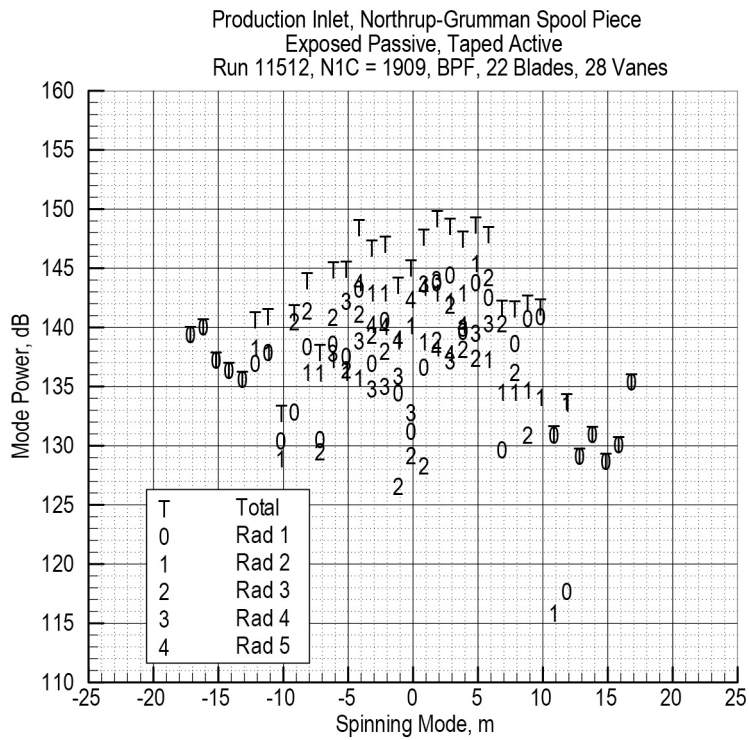
Figure 188.—ICD array, NG2, N1C1909.

Production Inlet, Northrup-Grumman Spool Piece
Exposed Passive, Taped Active
Run 11514a, N1C = 2045, BPF, 22B lades, 28 Vanes
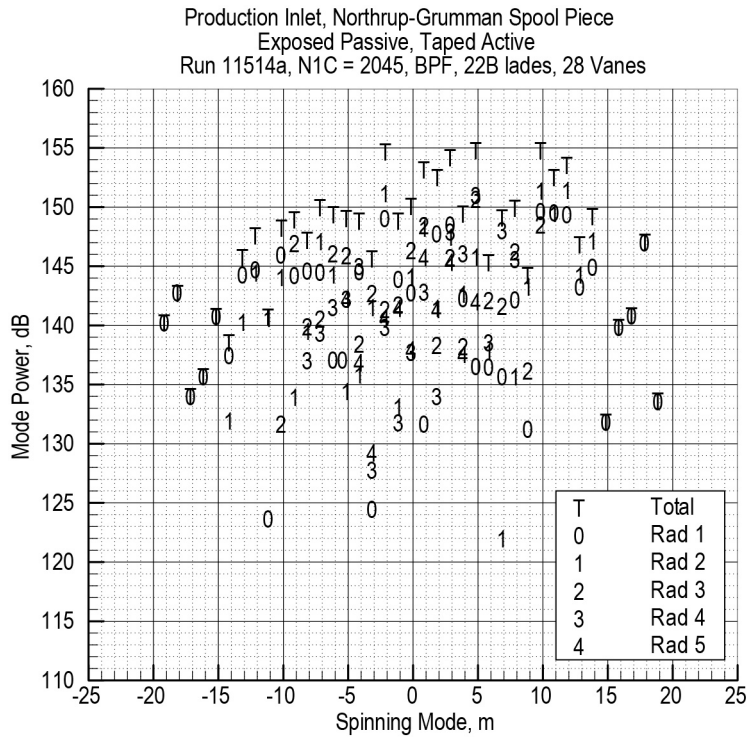
Figure 189.—ICD array, NG2, N1C = 2045.

Production Inlet, Northrup-Grumman Spool Piece
Exposed Passive, Taped Active
Run 11516, N1C = 2182, BPF, 22 Blades, 28 Vanes
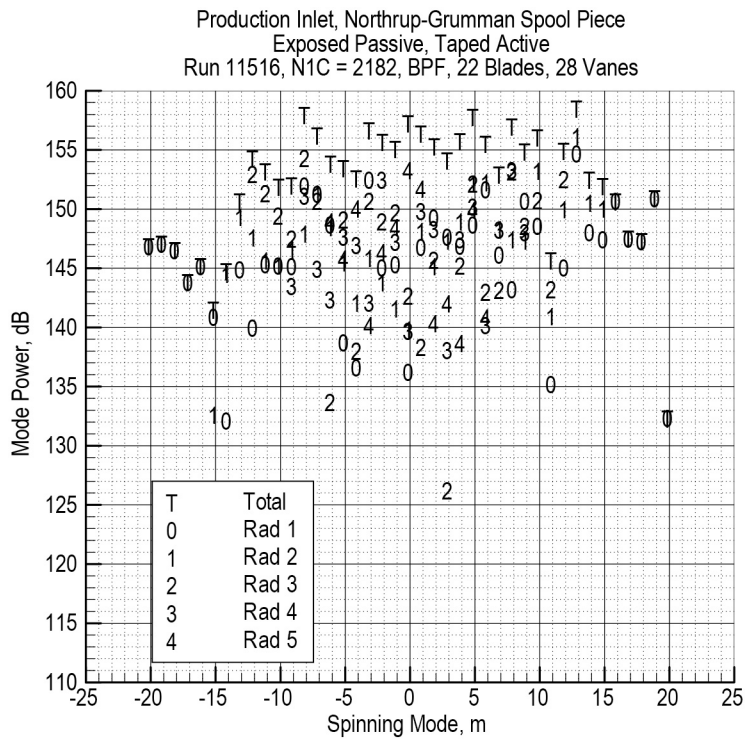
Figure 190.—ICD array, NG2, N1C2182.

Production Inlet, Northrup-Grumman Spool Piece
Exposed Passive, Taped Active
Run 11518, N1C = 2318, BPF, 22 Blades, 28 Vanes
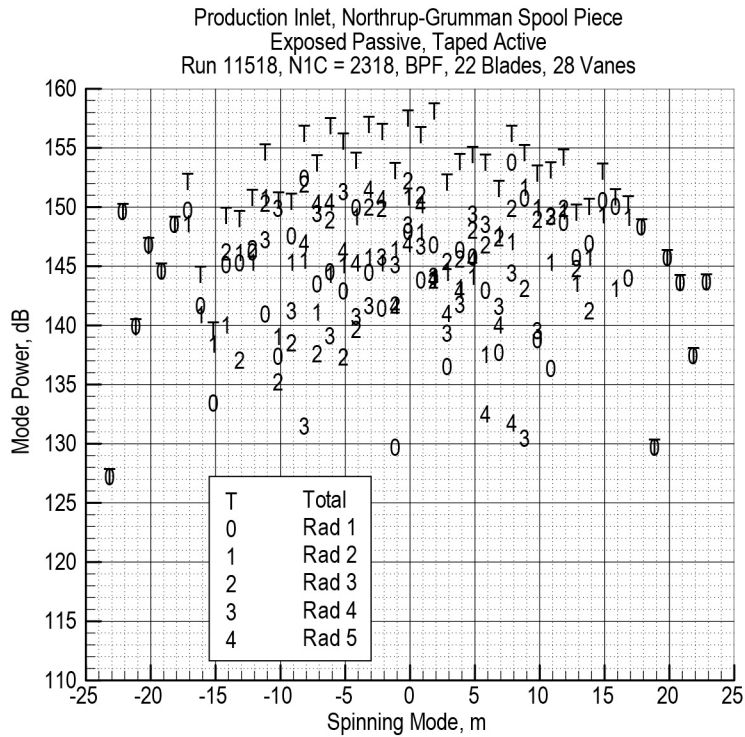
Figure 191.—ICD array, NG2, N1C2318.

Production Inlet, Northrup-Grumman Spool Piece
Exposed Passive, Taped Active
Run 11520, N1C = 1745, BPF, 22 Blades, 28 Vanes
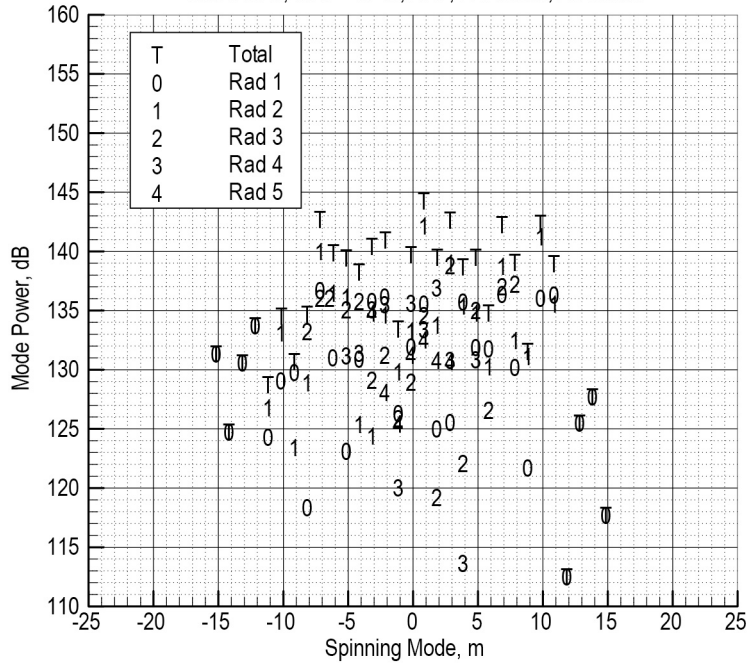
Figure 192.—ICD array, NG2, N1C1745 repeat

Production Inlet, Northrup-Grumman Spool Piece
Exposed Passive, Taped Active
Run 11521, N1C = 1909, BPF, 22 Blades, 28 Vanes
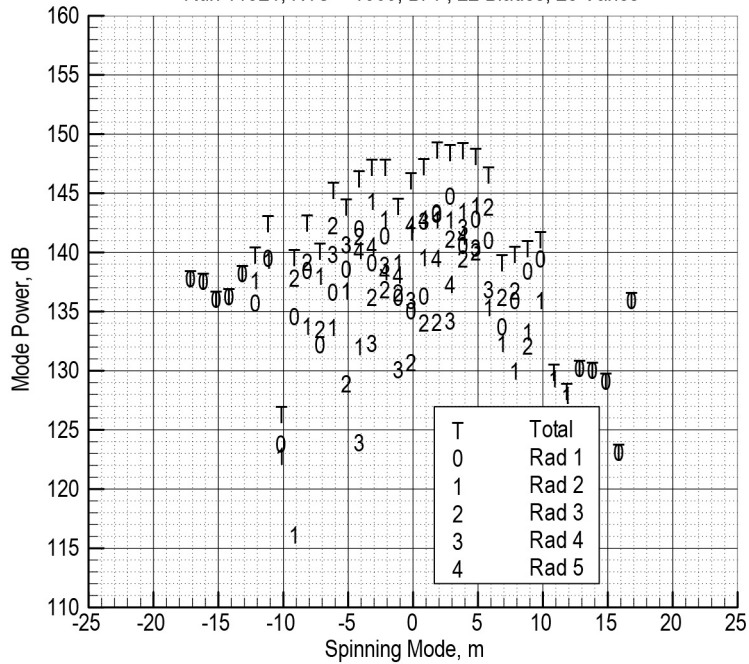
Figure 193.—ICD array, NG2, N1C1909 repeat.
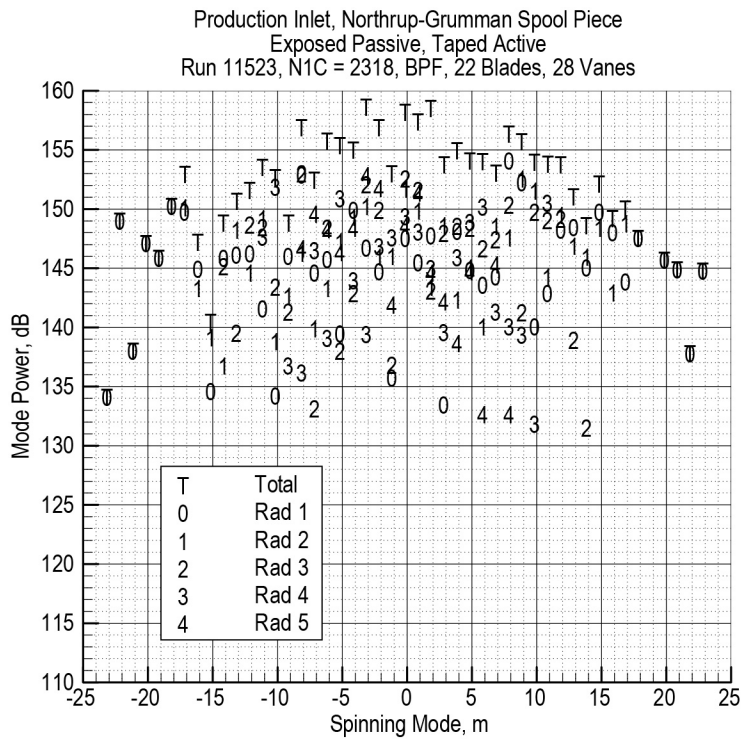
Figure 194.—ICD array, NG2, N1C2318 repeat.

Figure 195.—Foam attached to fan blades during no flow test.

Production Inlet, Northrup-Grumman Spool Piece
Painted Hardwall Passive, Holes Cut Out Active
Static Run, Active Ring D Input m = -6, Frequency = 640 Hz
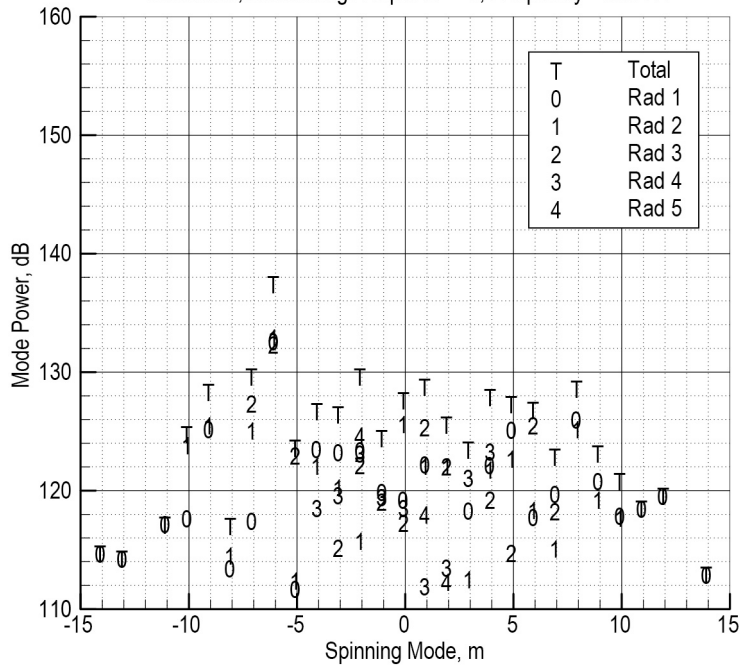
Figure 196.—ICD array, no flow test showing –6 mode.

Production Inlet, Northrup-Grumman Spool Piece
Painted Hardwall Passive, Holes Cut Out Active
Run 11606, N1C = 1745, BPF, 22 Blades, 28 Vanes
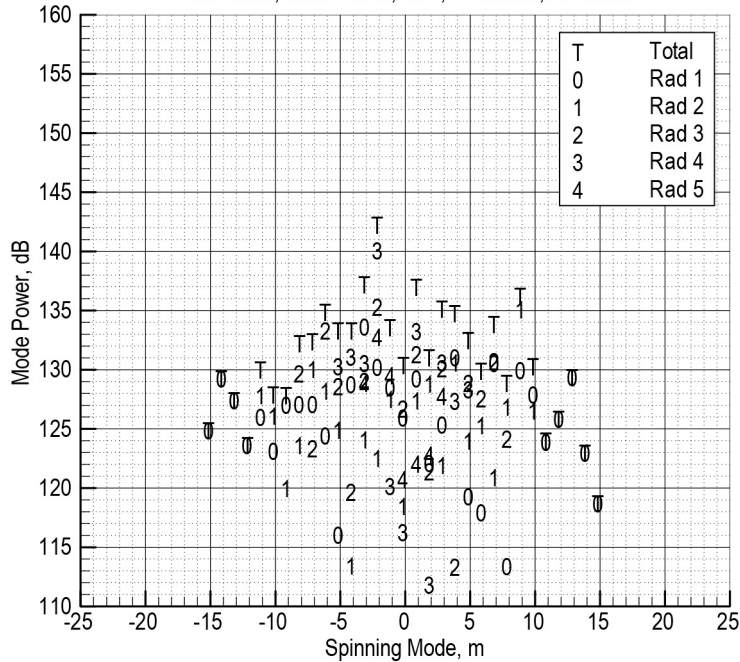
Figure 197.—ICD array, NG3, N1C1745.

Figure 198.—ICD array, NG3, N1C1800.

Figure 199.—ICD array, NG3, N1C1909.
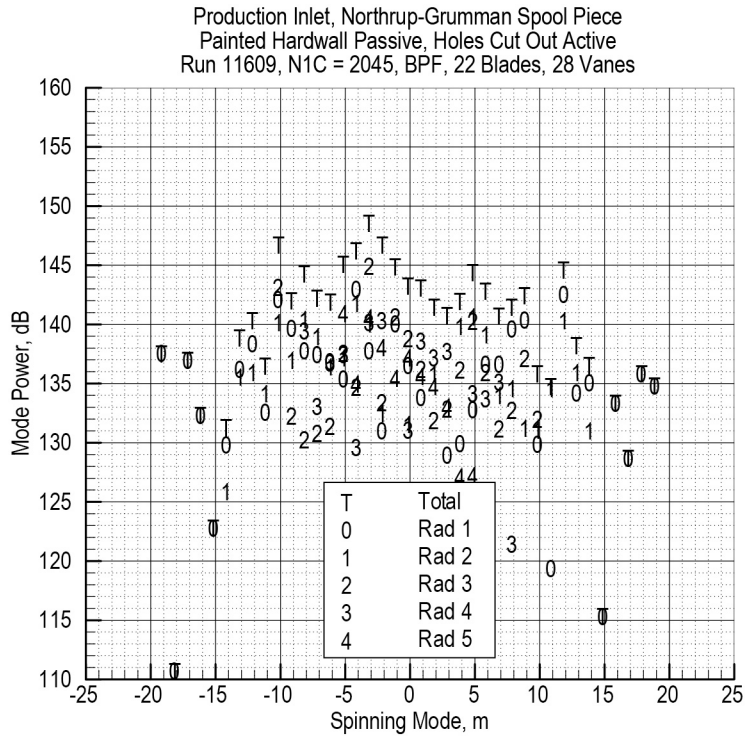
Figure 200.—ICD array, NG3, N1C2045.
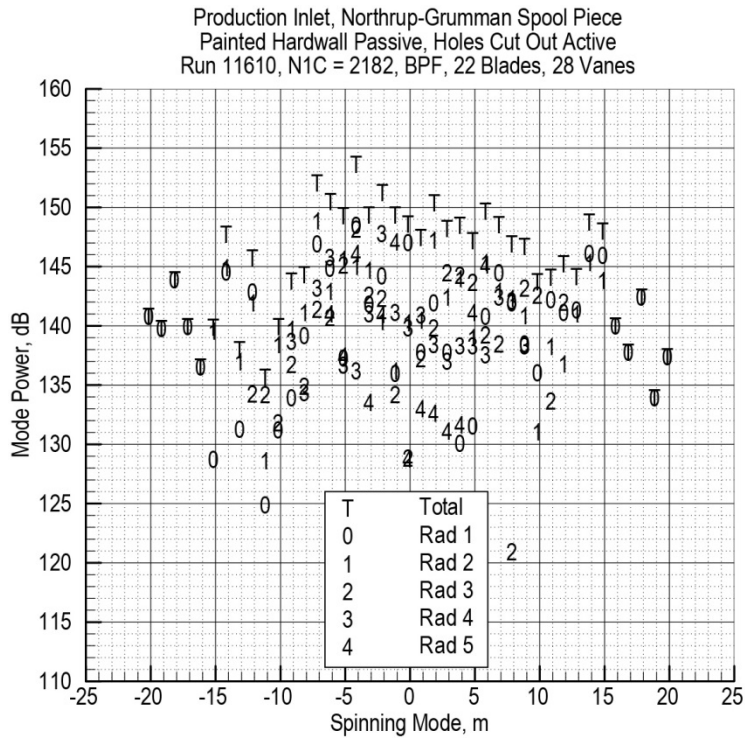
Figure 201.—ICD array, NG3, N1C2182.

Production Inlet, Northrup-Grumman Spool Piece
Painted Hardwall Passive, Holes Cut Out Active
Run 11611a, N1C = 2318, BPF, 22 Blades, 28 Vanes

T	Total
0	Rad 1
1	Rad 2
2	Rad 3
3	Rad 4
4	Rad 5
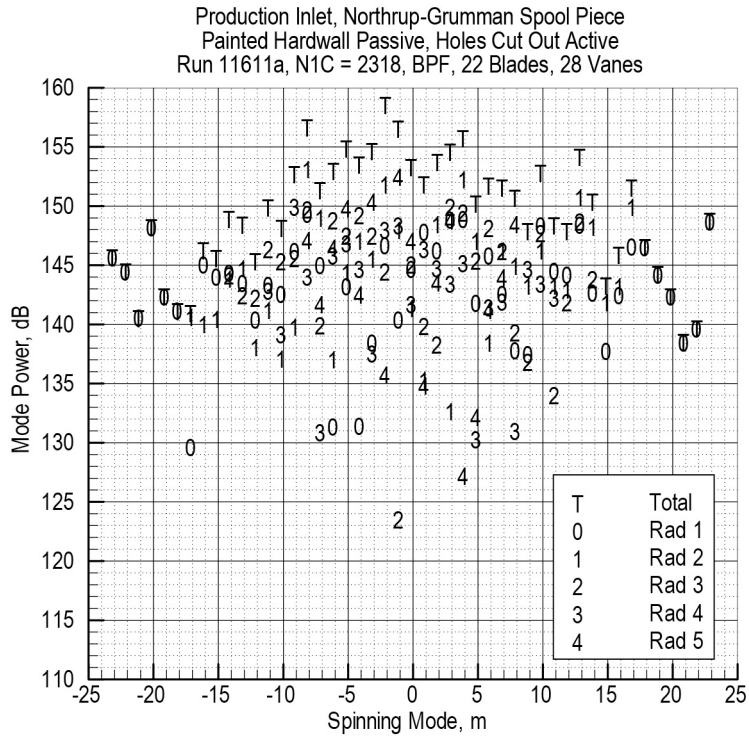
Figure 202.—ICD array, NG3, N1C2318.

Production Inlet, Taped Rohr Spool Piece
Run 11705a, N1C = 1620, BPF, 22 Blades, 28 Vanes

T	Total
0	Rad 1
1	Rad 2
2	Rad 3
3	Rad 4
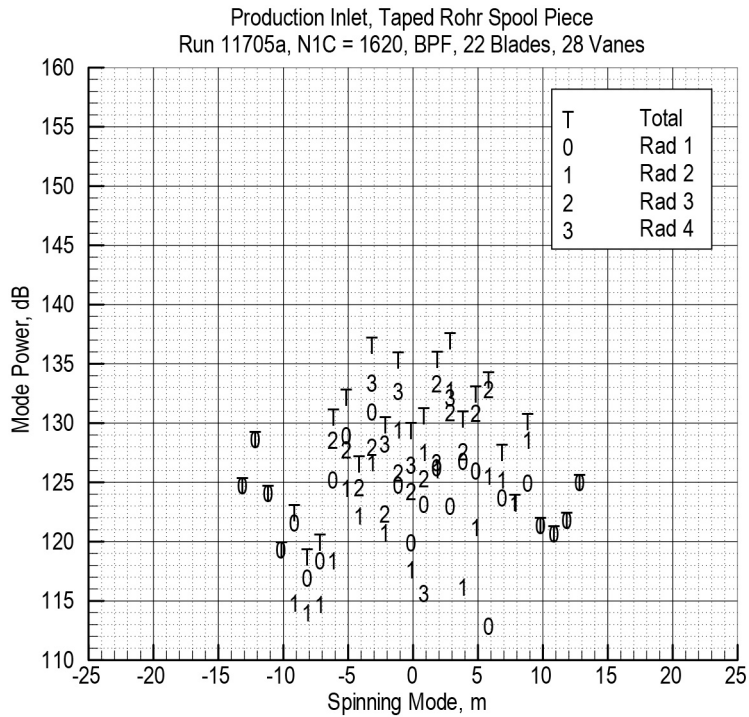
Figure 203.—ICD array, EVNRC1, N1C1620.

Figure 204.—ICD array, EVNRC1, N1C1800
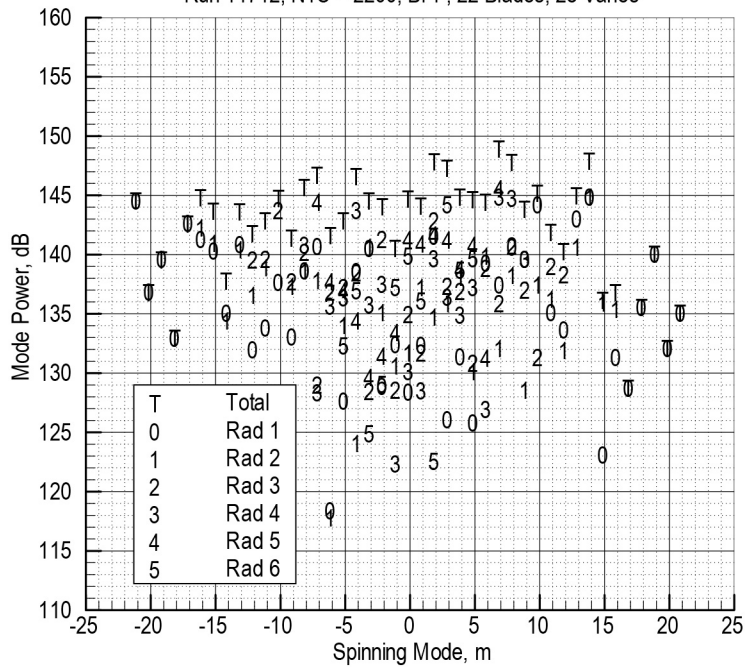
Figure 205.—ICD array, EVNRC1, N1C2200.
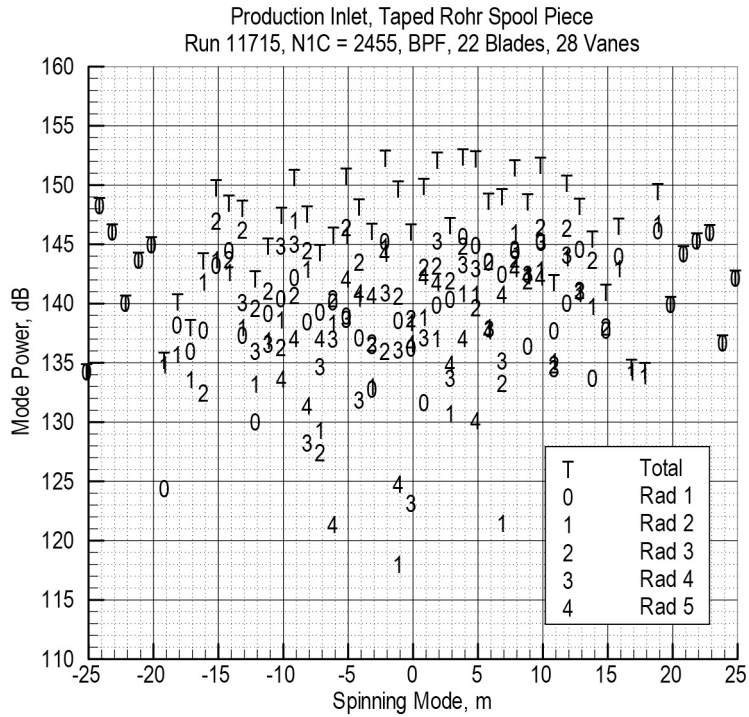
Figure 206.—ICD array, EVNRC1, N1C2455.
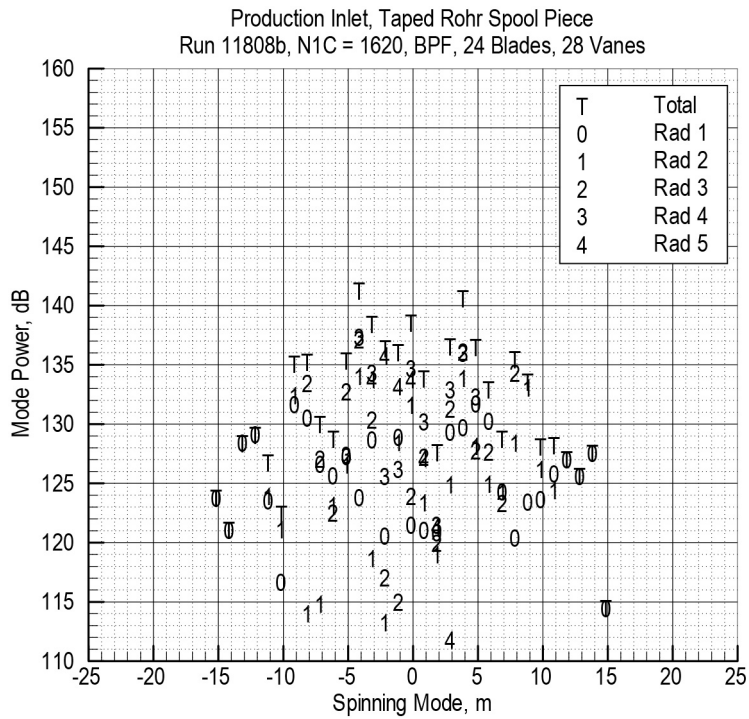
Figure 207.—ICD array, EVNRC2, N1C1620.
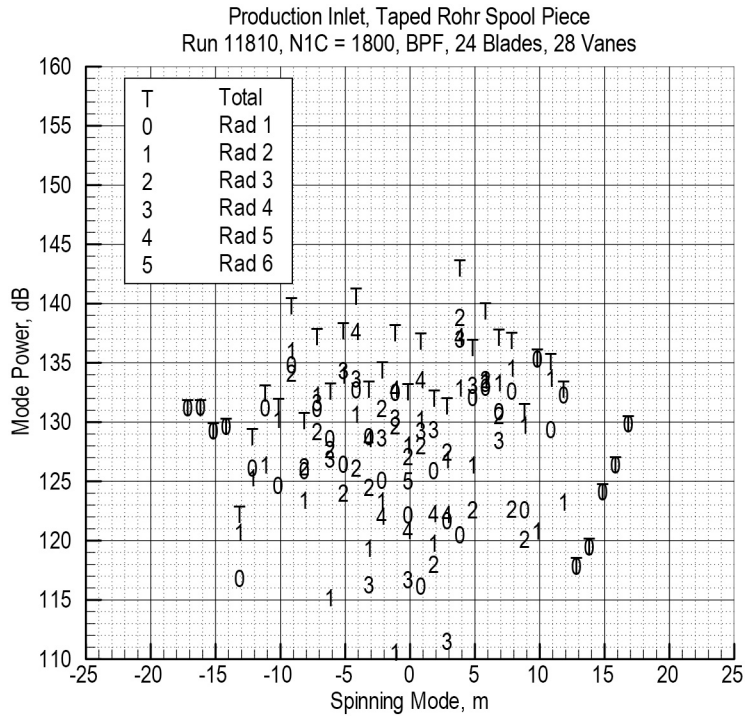
Figure 208.—ICD array, EVNRC2, N1C1800.
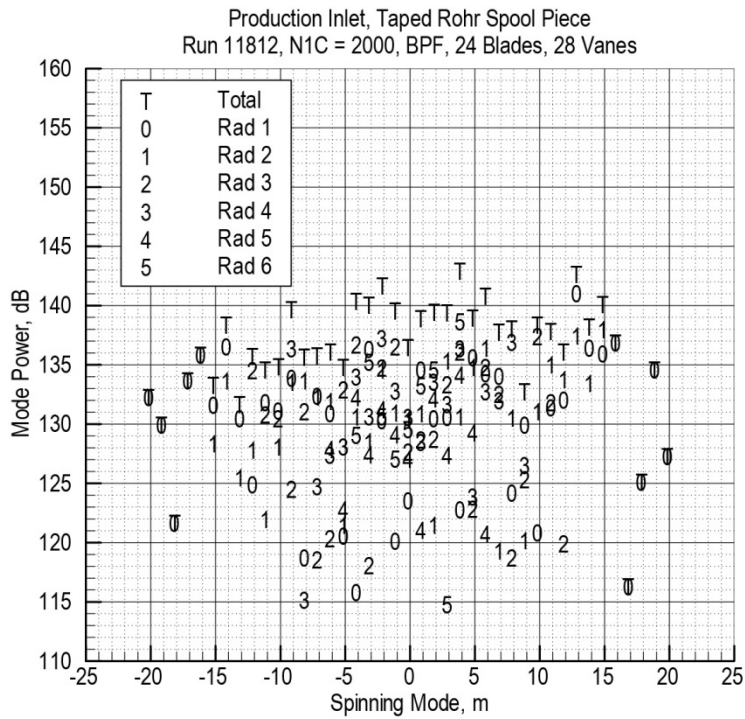
Figure 209.—ICD array, EVNRC2, N1C2000.
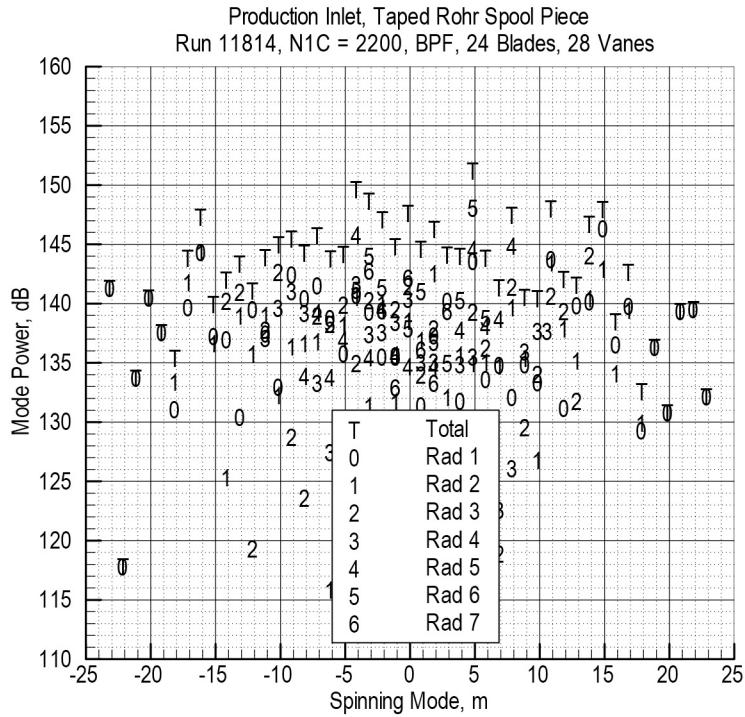
Figure 210.—ICD array, EVNRC2, N1C2200.
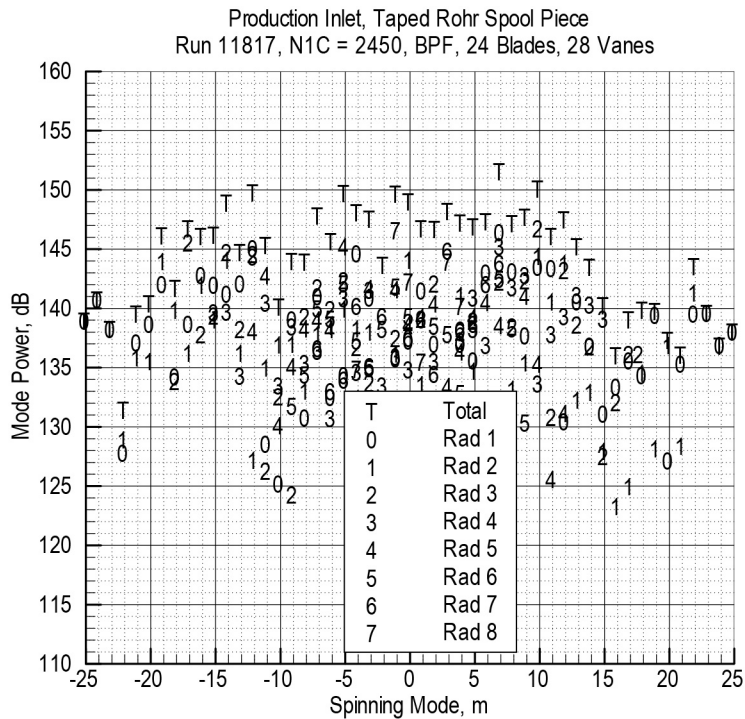
Figure 211.—ICD array, EVNRC2, N1C2450.

Production Inlet, Taped Rohr Spool Piece
Run 11905, N1C = 1620, BPF, 24 Blades, 28 Vanes
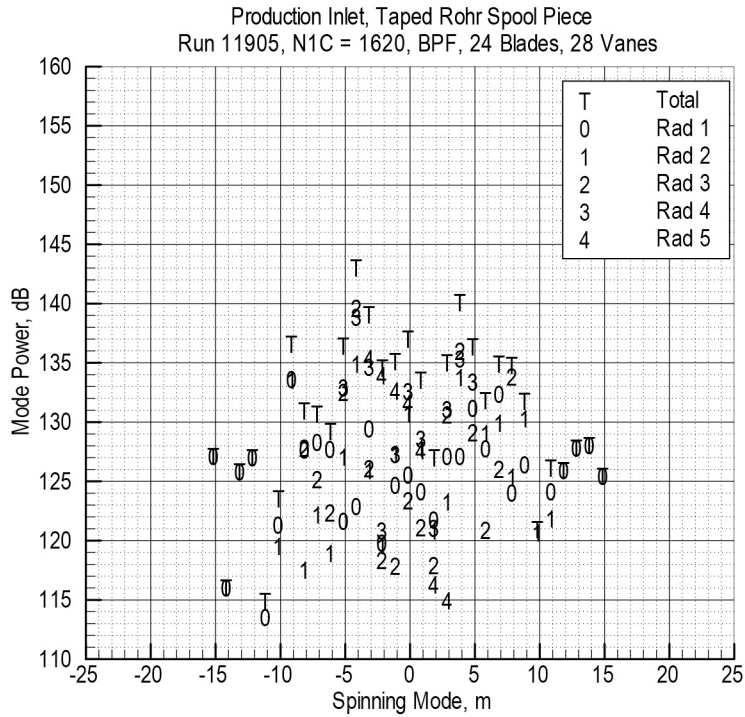
Figure 212.—ICD array, EVNRC3, N1C1620, aft barrier walls.

Production Inlet, Taped Rohr Spool Piece
Run 11907, N1C = 1800, BPF, 24 Blades, 28 Vanes
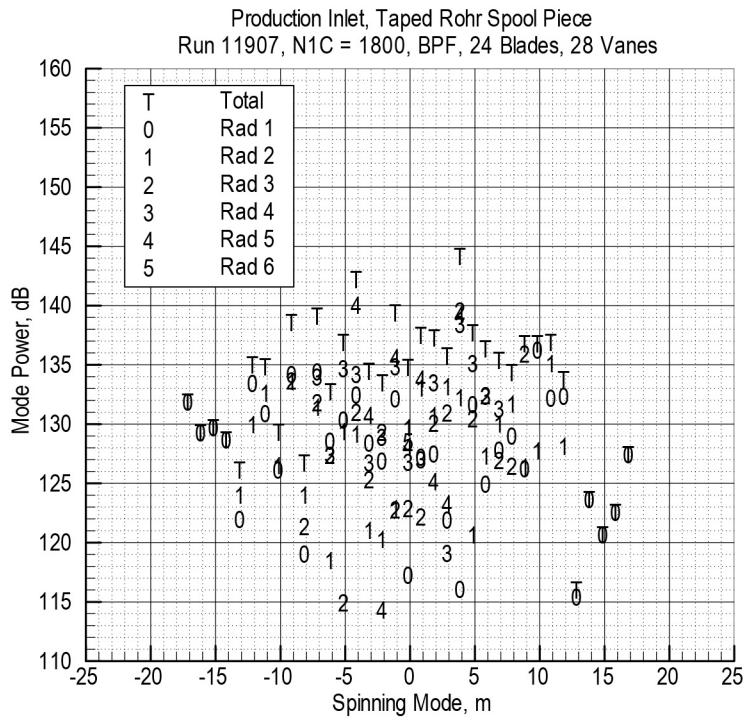
Figure 213.—ICD array, EVNRC3, N1C1800, aft barrier walls.
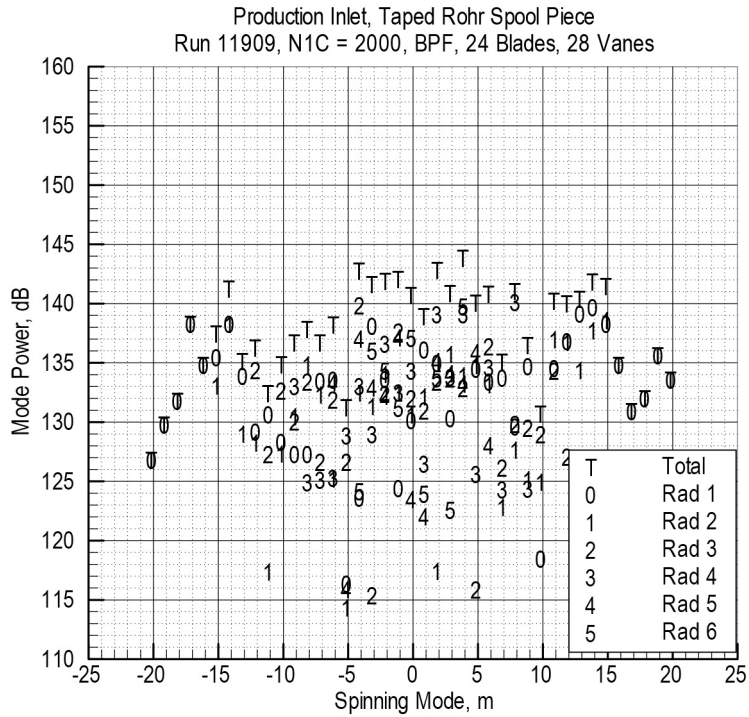
Figure 214.—ICD array, EVNRC3, N1C2000, aft barrier walls.
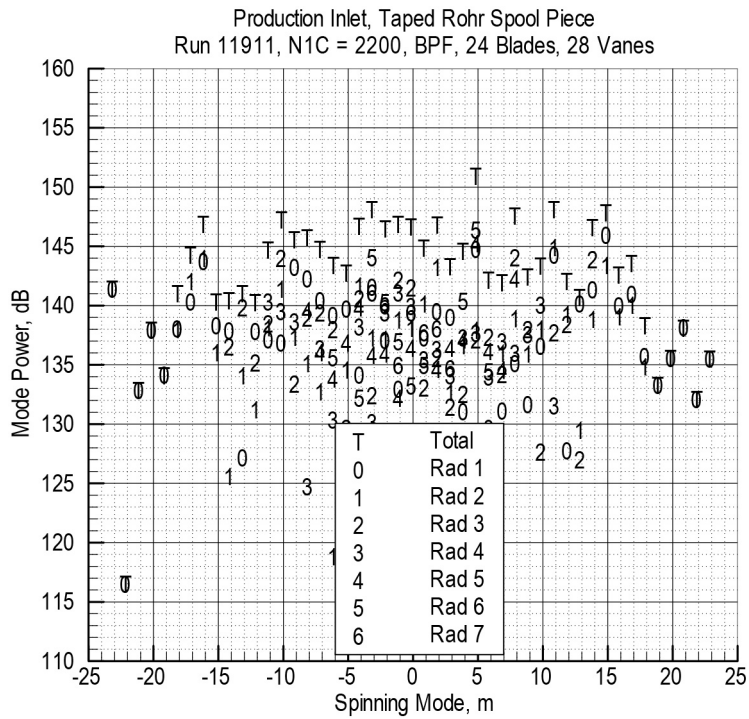
Figure 215.—ICD array, EVNRC3, N1C2200, aft barrier walls.
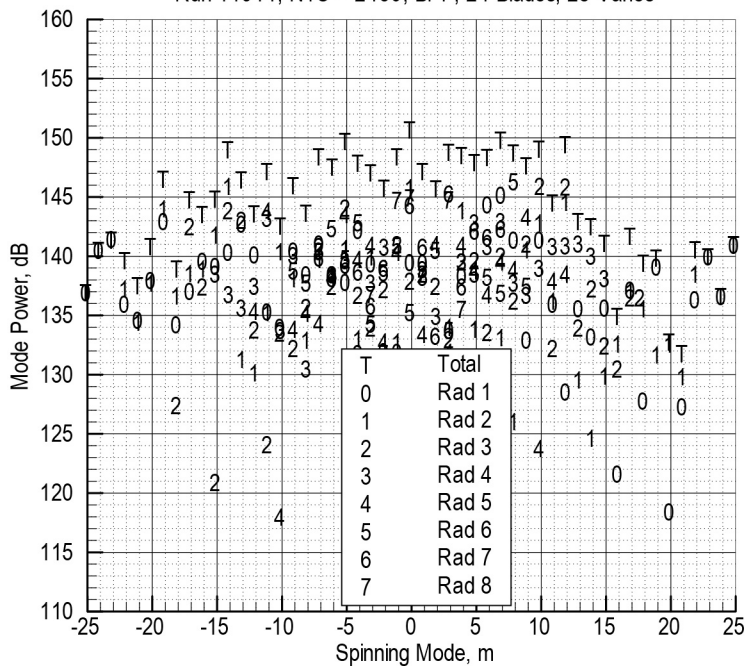
Figure 216.—ICD array, EVNRC3, N1C2450, aft barrier walls.
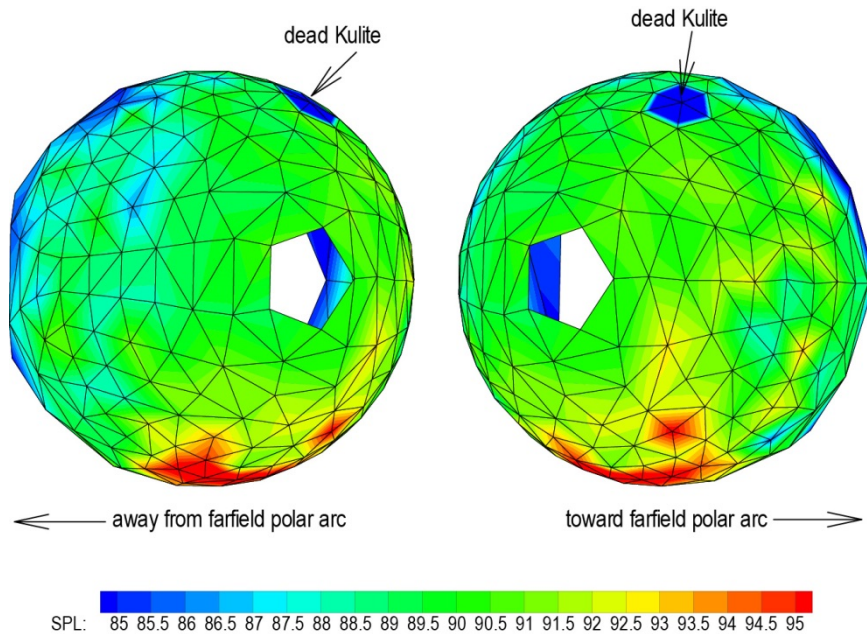
Figure 217.—ICD SPL distribution at 1008 Hz, EVNRC3, N1C1800.
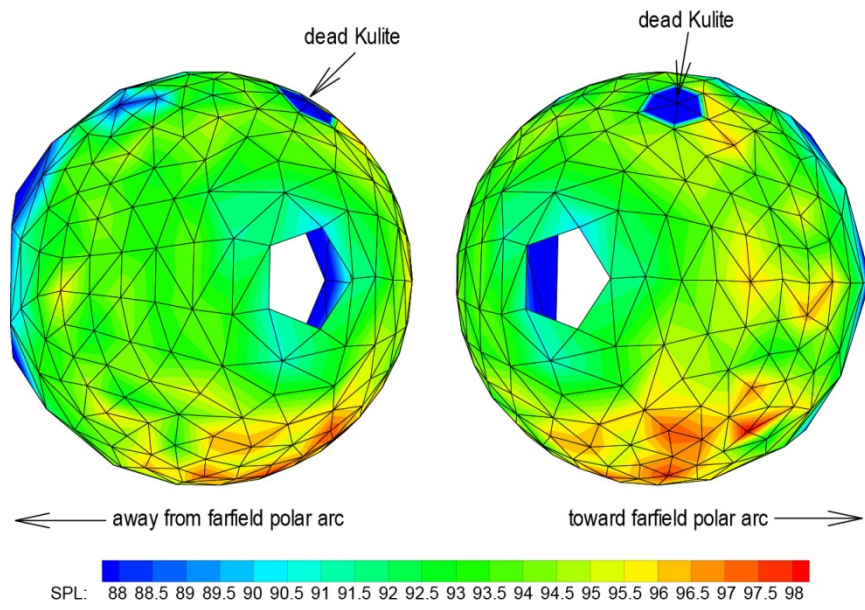
Figure 218.—ICD SPL distribution at 5904 Hz, EVNRC3, N1C1800.
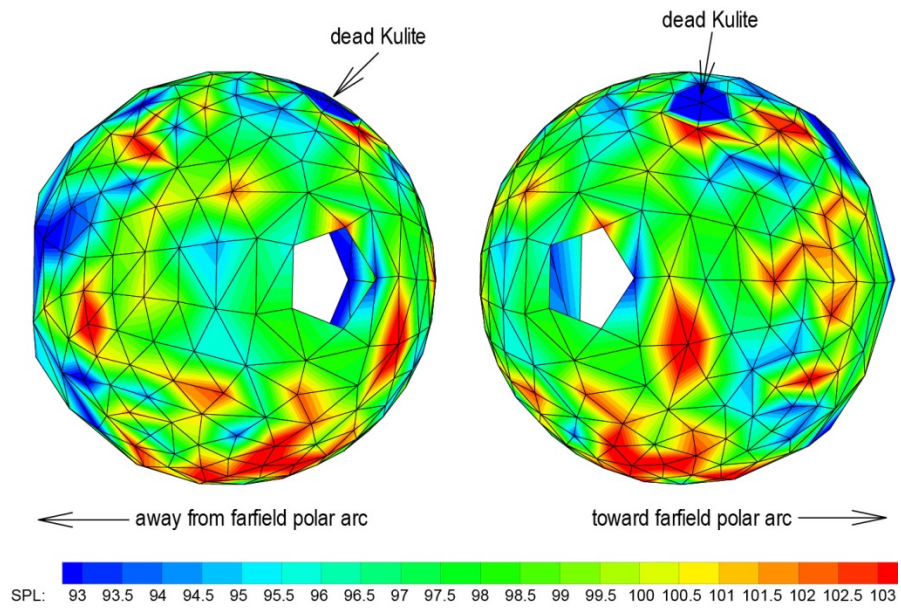
Figure 219.—ICD SPL distribution at BPF, EVNRC3, N1C1800.
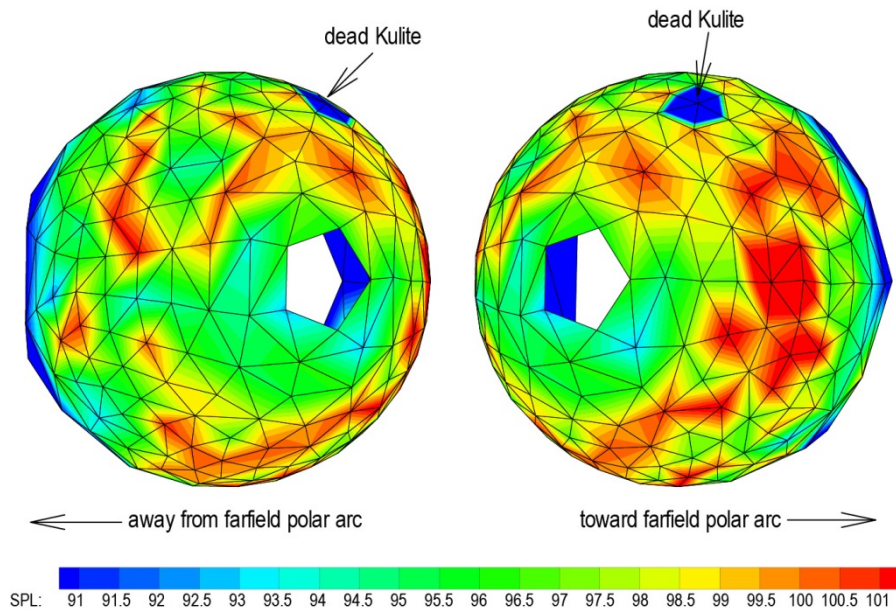
Figure 220.—ICD SPL distribution at 2BPF, EVNRC3, N1C1800.
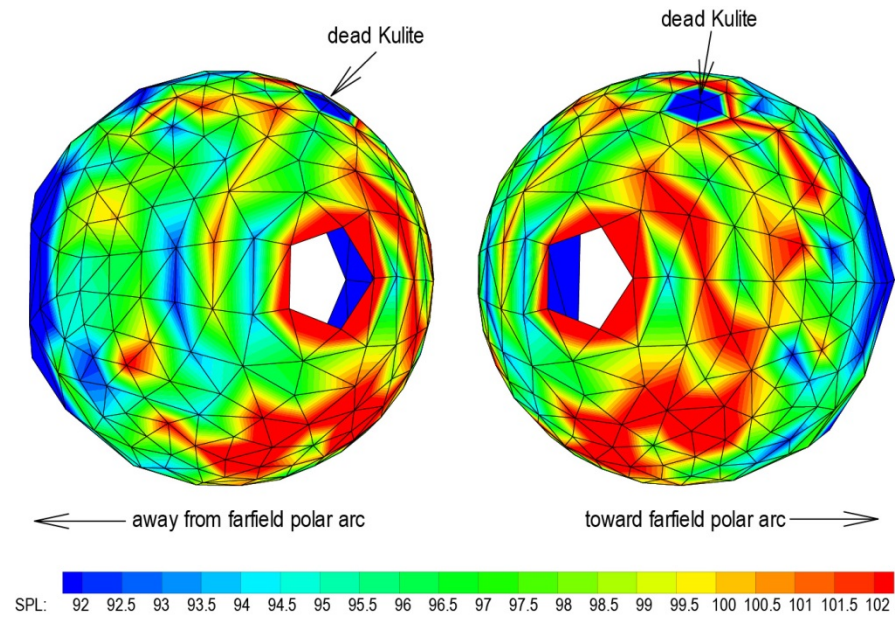
Figure 221.—ICD SPL distribution at 2528 Hz, EVNRC3, N1C1800.
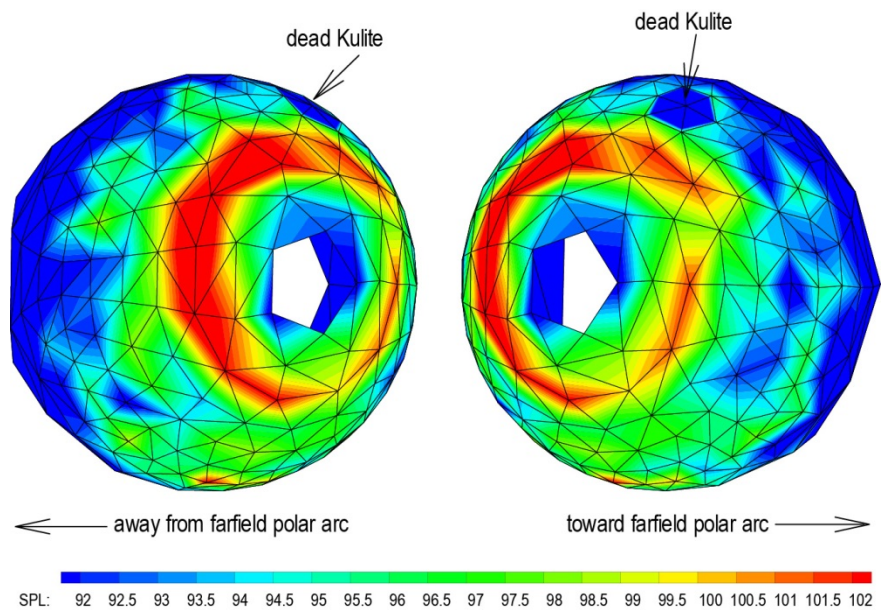
Figure 222.—ICD SPL distribution at 2800 Hz, EVNRC3, N1C1800.
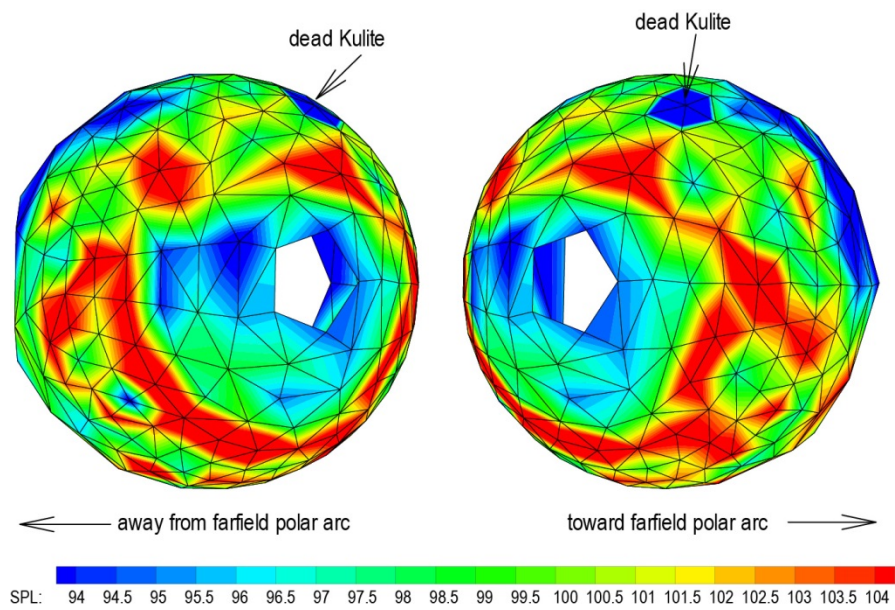
Figure 223.—ICD SPL distribution at 4752 Hz, EVNRC3, N1C1800.
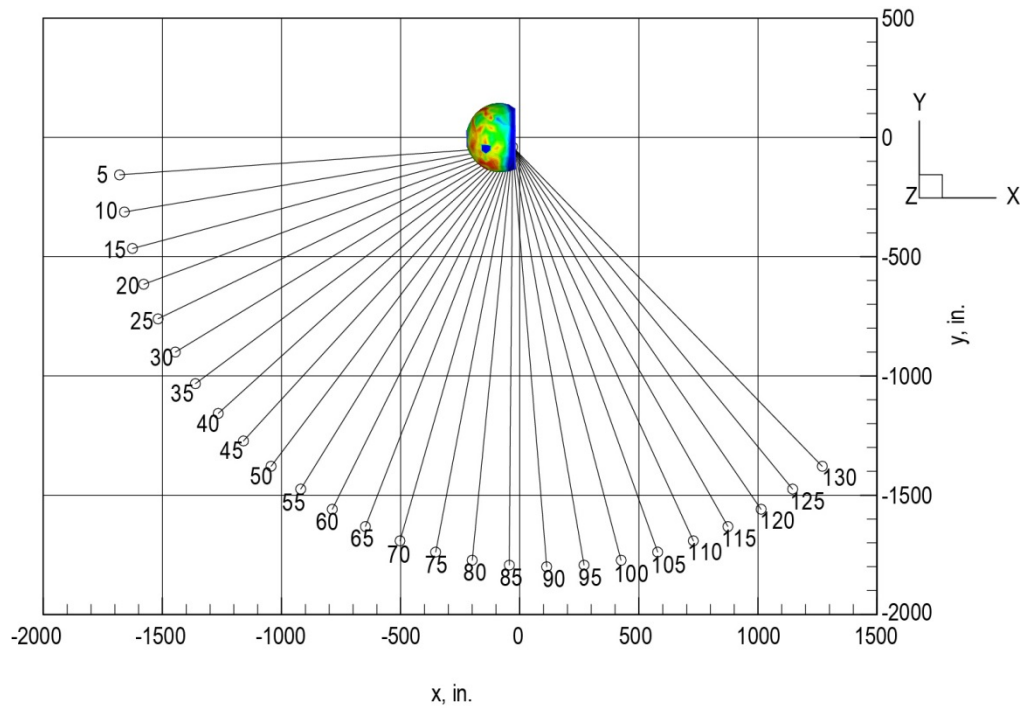
Figure 224.—ICD data relative to farfield polar microphones.
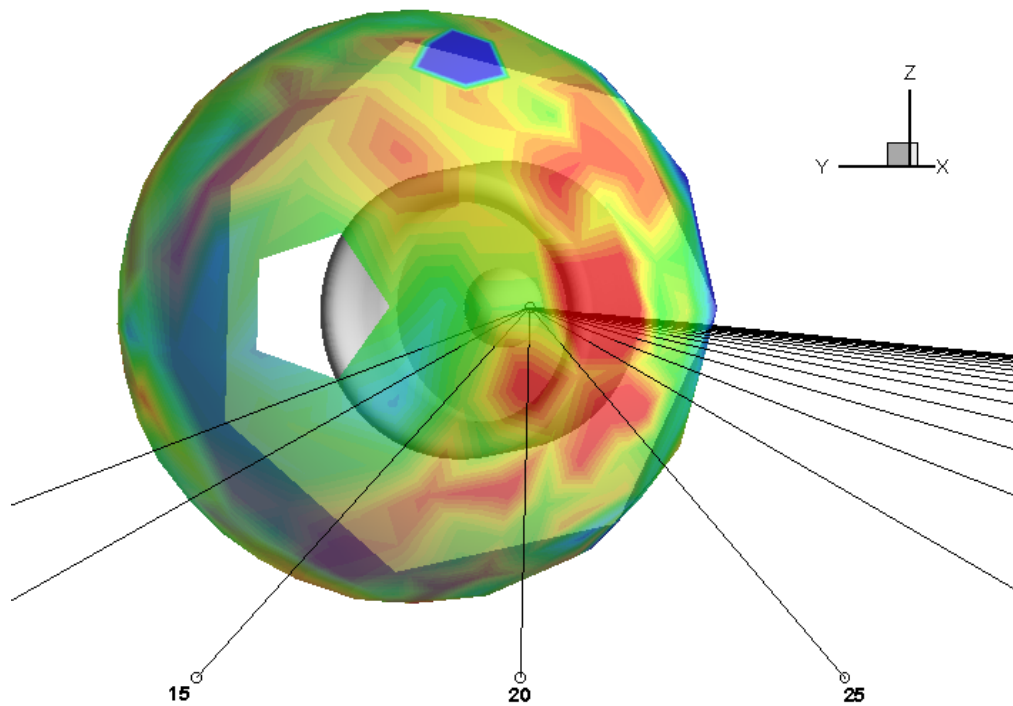
Figure 225.—Magnified view of ICD data relative to farfield polar microphones.
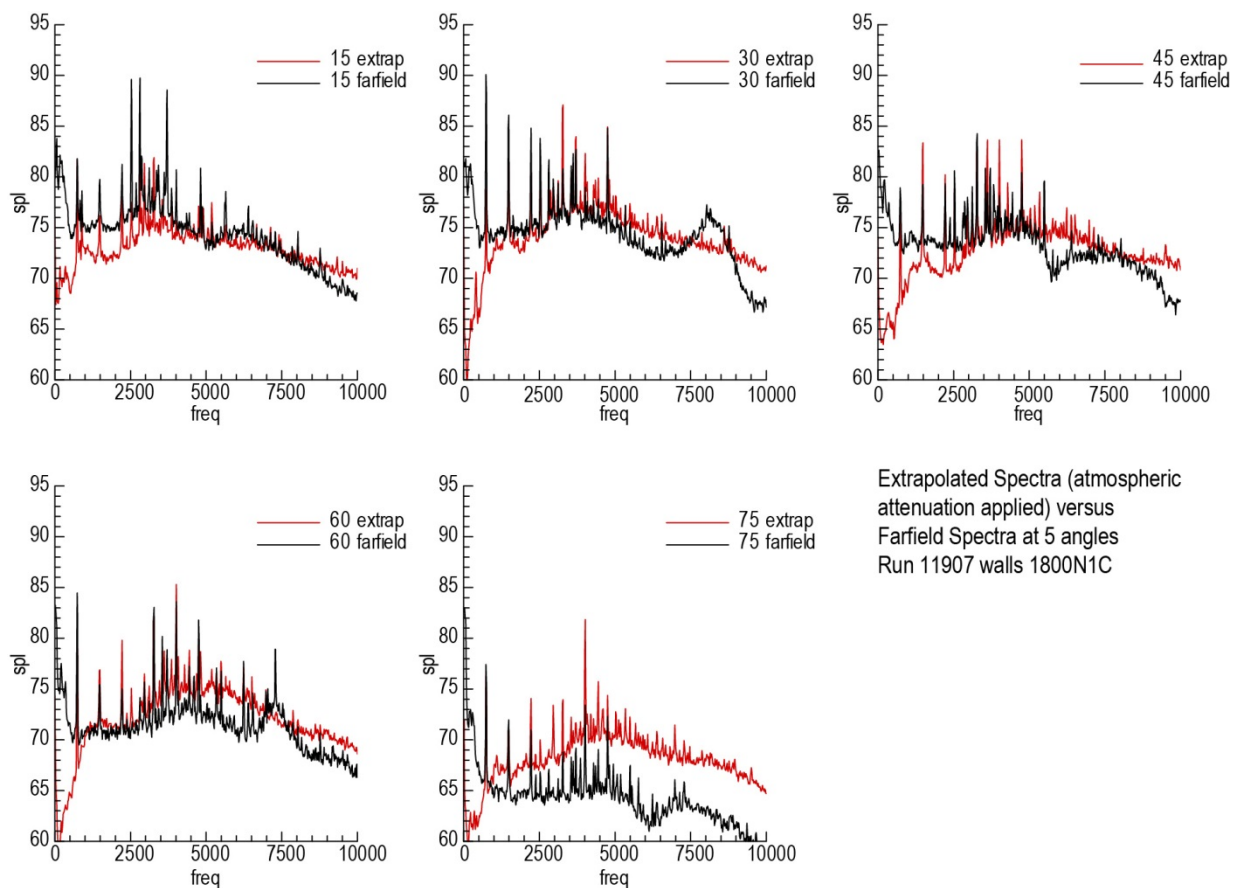
Figure 226.—Comparison of farfield spectra and ICD extrapolated spectra.
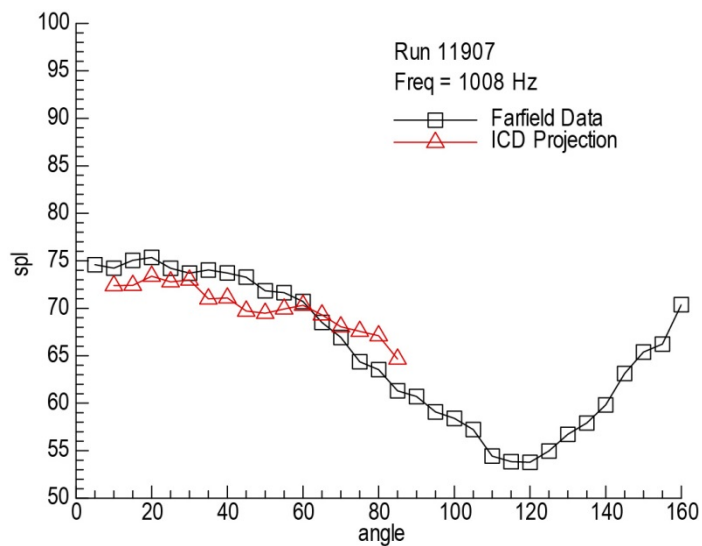
Figure 227.—Directivity Comparison at 1008 Hz.
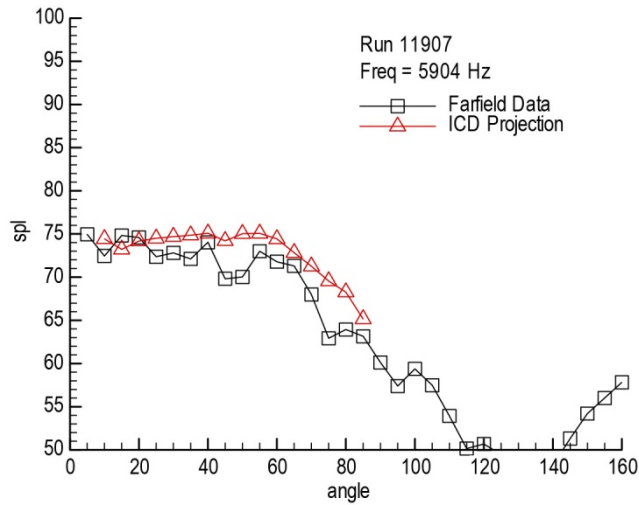
Figure 228.—Directivity Comparison at 5904 Hz.
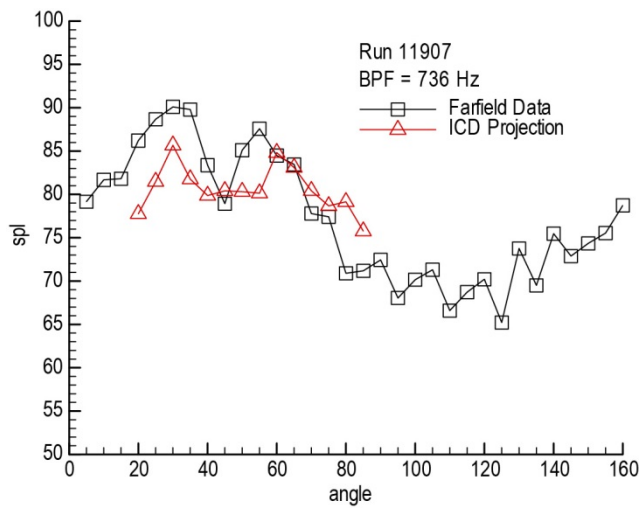
Figure 229.—Directivity comparison at BPF.
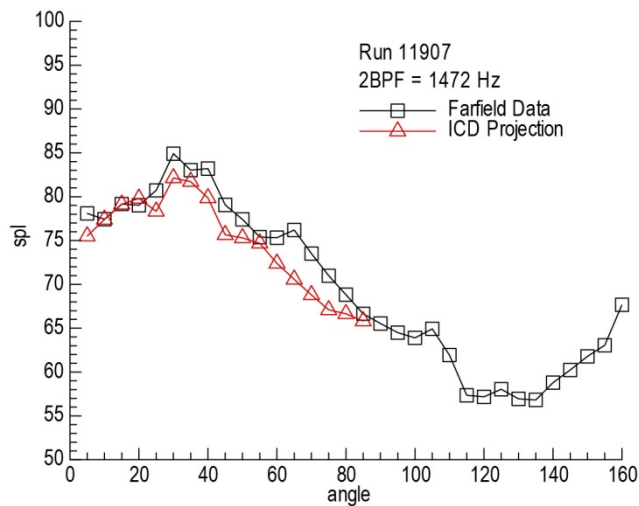
Figure 230.—Directivity Comparison at 2BPF.

← away from farfield polar arc   toward farfield polar arc →

SPL difference, dB   0 1 2 3 4 5 6 7 8 9 10 11 12 13 14 15 16
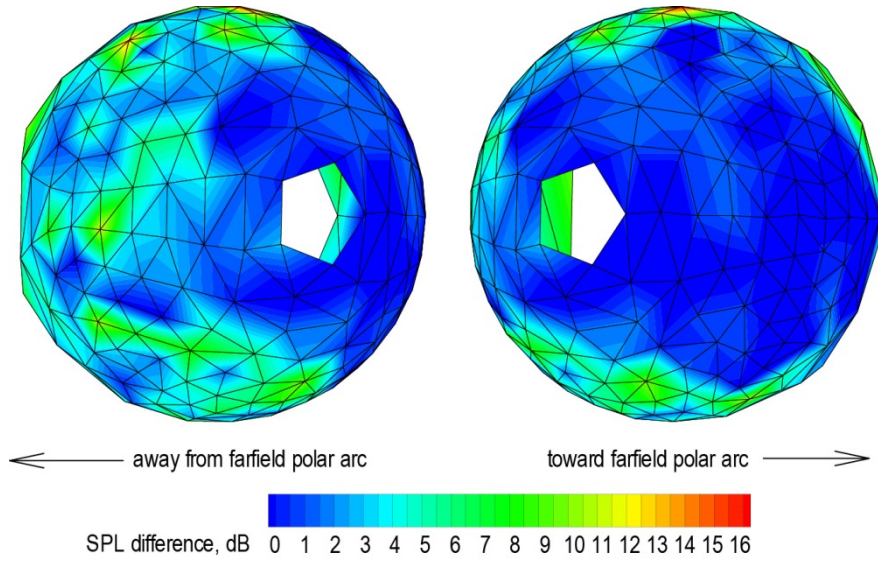
Figure 231.—Aft barrier wall effect on the ICD SPL data at 208 Hz.
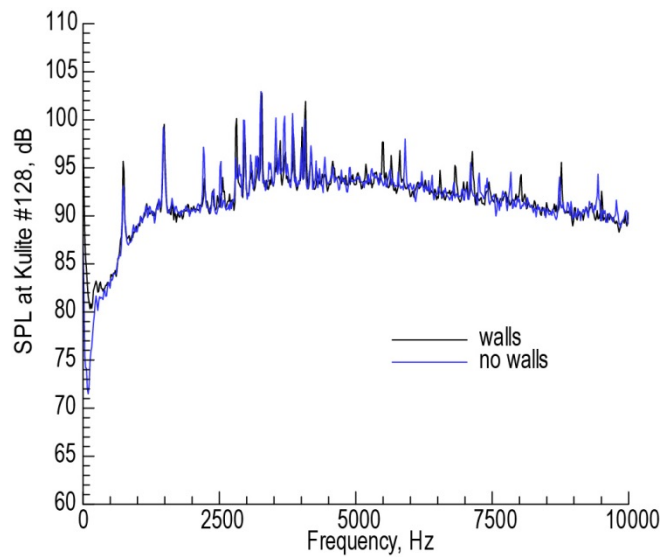
Figure 232.—Spectral comparison at a ICD Kulite on the
side facing away from farfield polar microphones showing
wall effect.
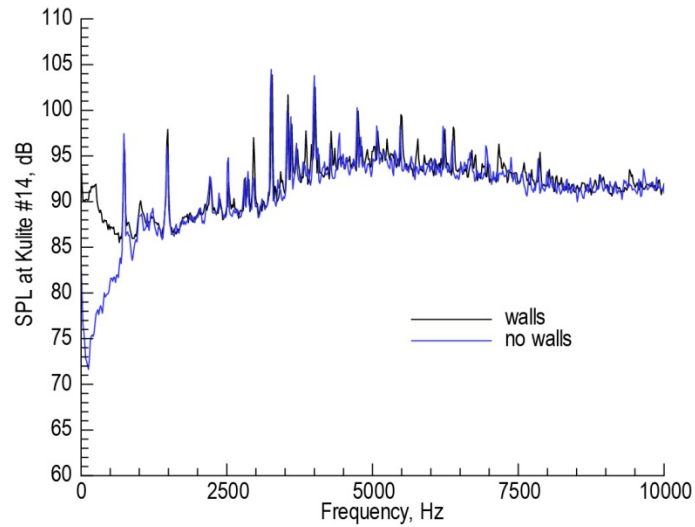
Figure 233.—Spectral comparison at a Kulite on top of the ICD showing wall effect.

⟵ away from farfield polar arc   toward farfield polar arc ⟶

SPL: 83 83.5 84 84.5 85 85.5 86 86.5 87 87.5 88 88.5 89 89.5 90 90.5 91 91.5 92 92.5 93
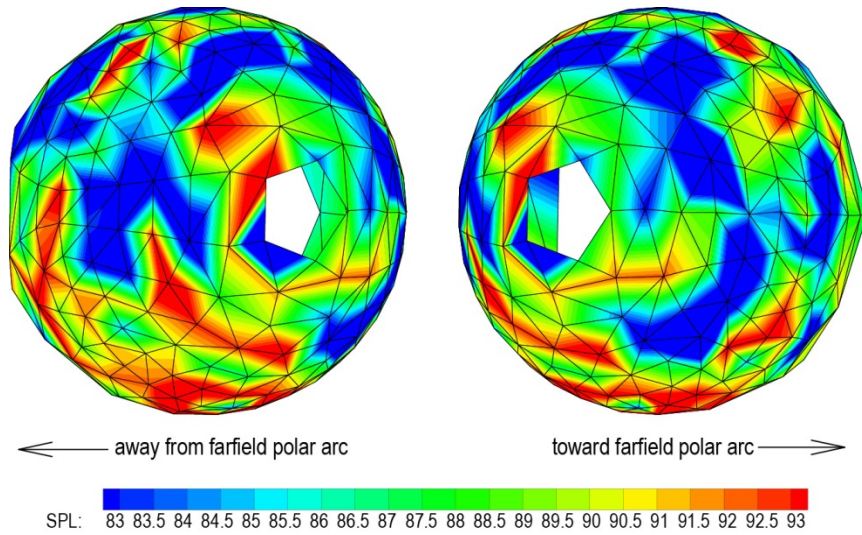
Figure 234.—ICD SPL distribution at 640 Hz for no flow test.

Synthesized, Real Part of Pressure   Sync Data, Real Part of Pressure
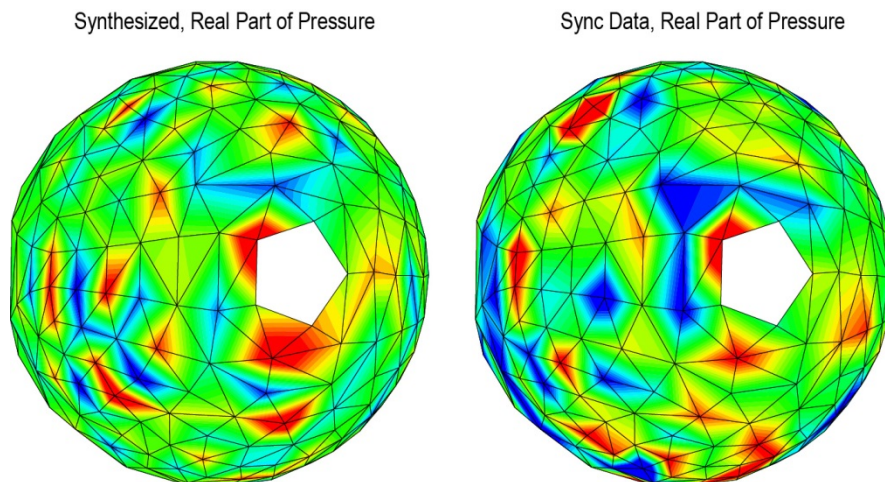
Figure 235.—Comparison between synthesized real part of pressure and synchronized Kulite data.

Synthesized Pressure Magnitude   Synchronized Pressure Magnitude

SPL: 100 101 102 103 104 105 106 107 108 109 110 111 112 113 114 115 116 117 118 119 120 121 122 123 124 125
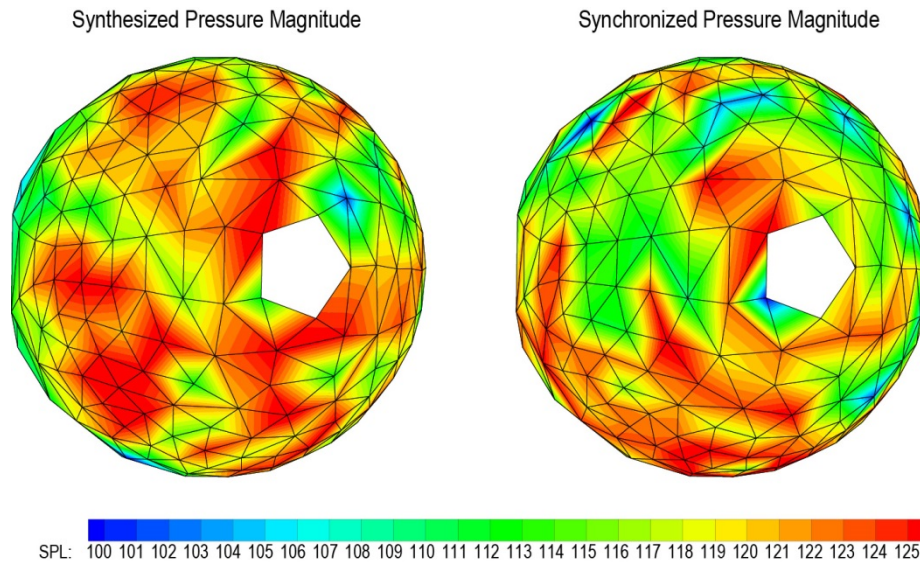
Figure 236.—Comparison between synthesized SPL and synchronized Kulite data .

Synthesized Pressure Magnitude   Synchronized Pressure Magnitude

SPL: 100 101 102 103 104 105 106 107 108 109 110 111 112 113 114 115 116 117 118 119 120 121 122 123 124 125
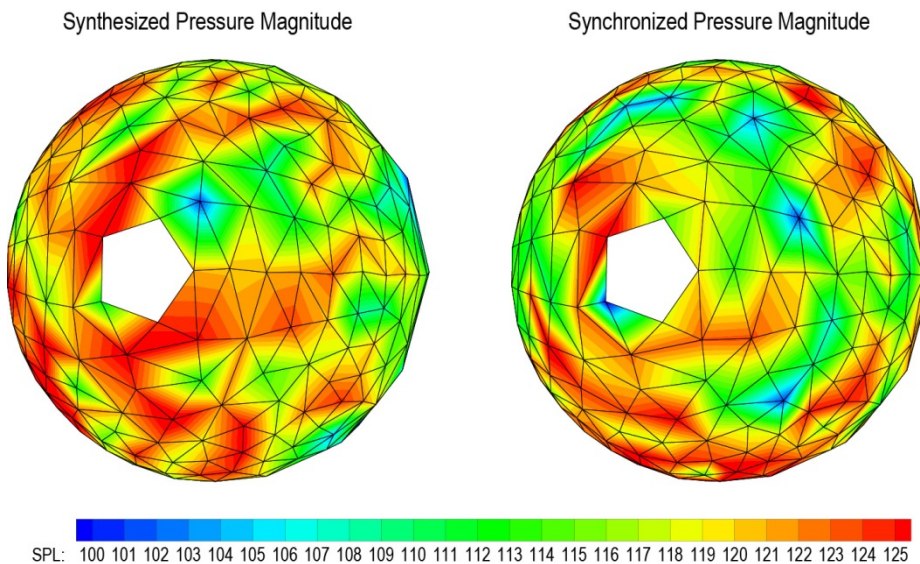
Figure 237.—Comparison between synthesized SPL and synchronized Kulite data, viewed from side closest to farfield polar microphones.
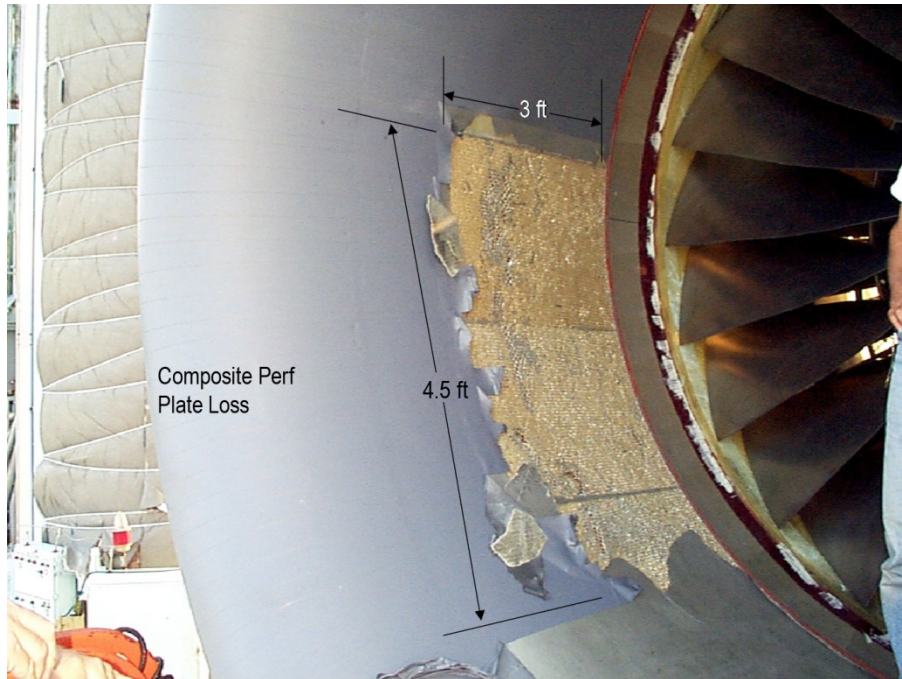
Figure 238.—Scarf inlet face sheet delamination—View 1.

Figure 239.—Scarf inlet face sheet delamination—View 2.
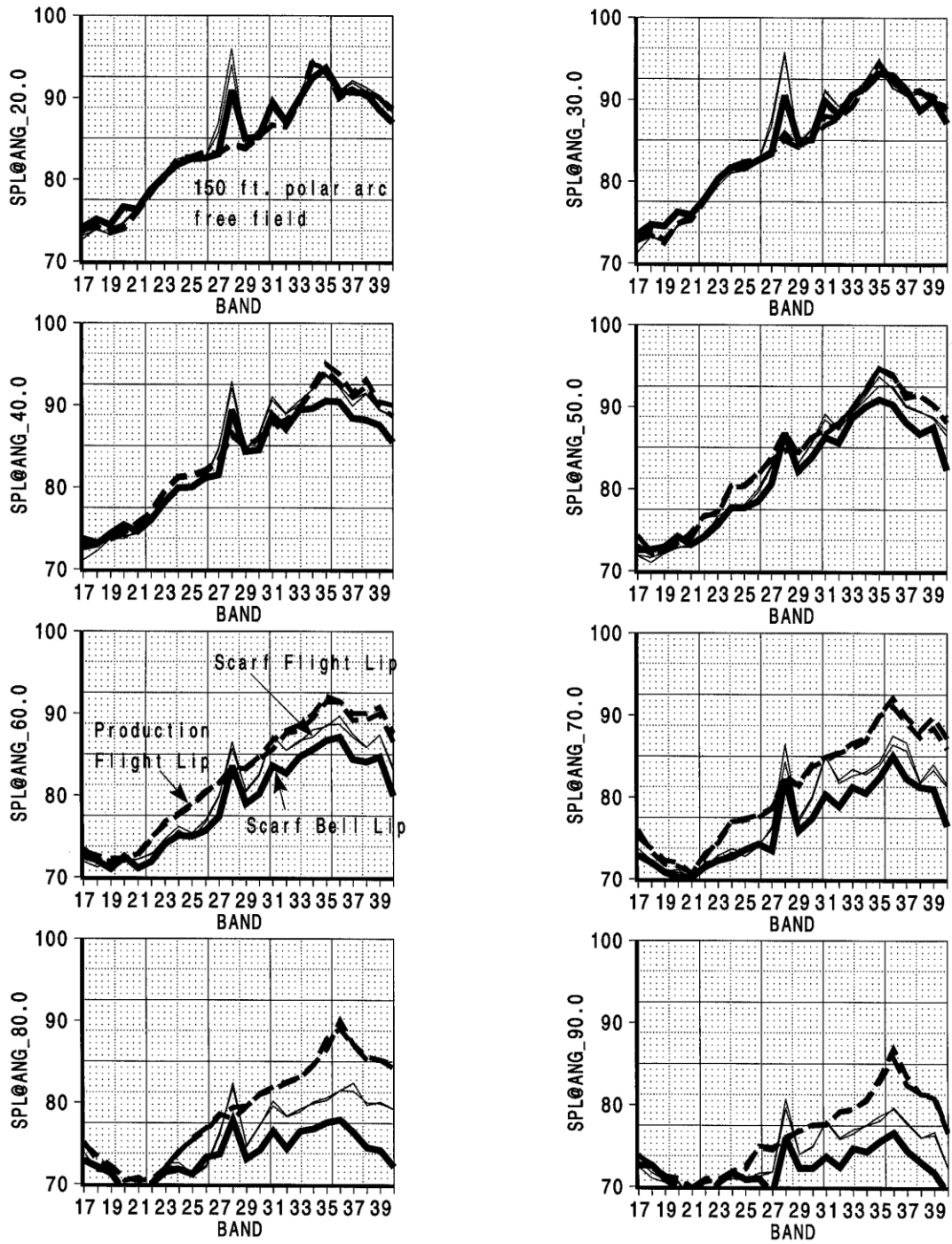
Figure 240.—Production flight lip, scarf flight lip, bellmouth lip, hardwall, 1600 rpm.
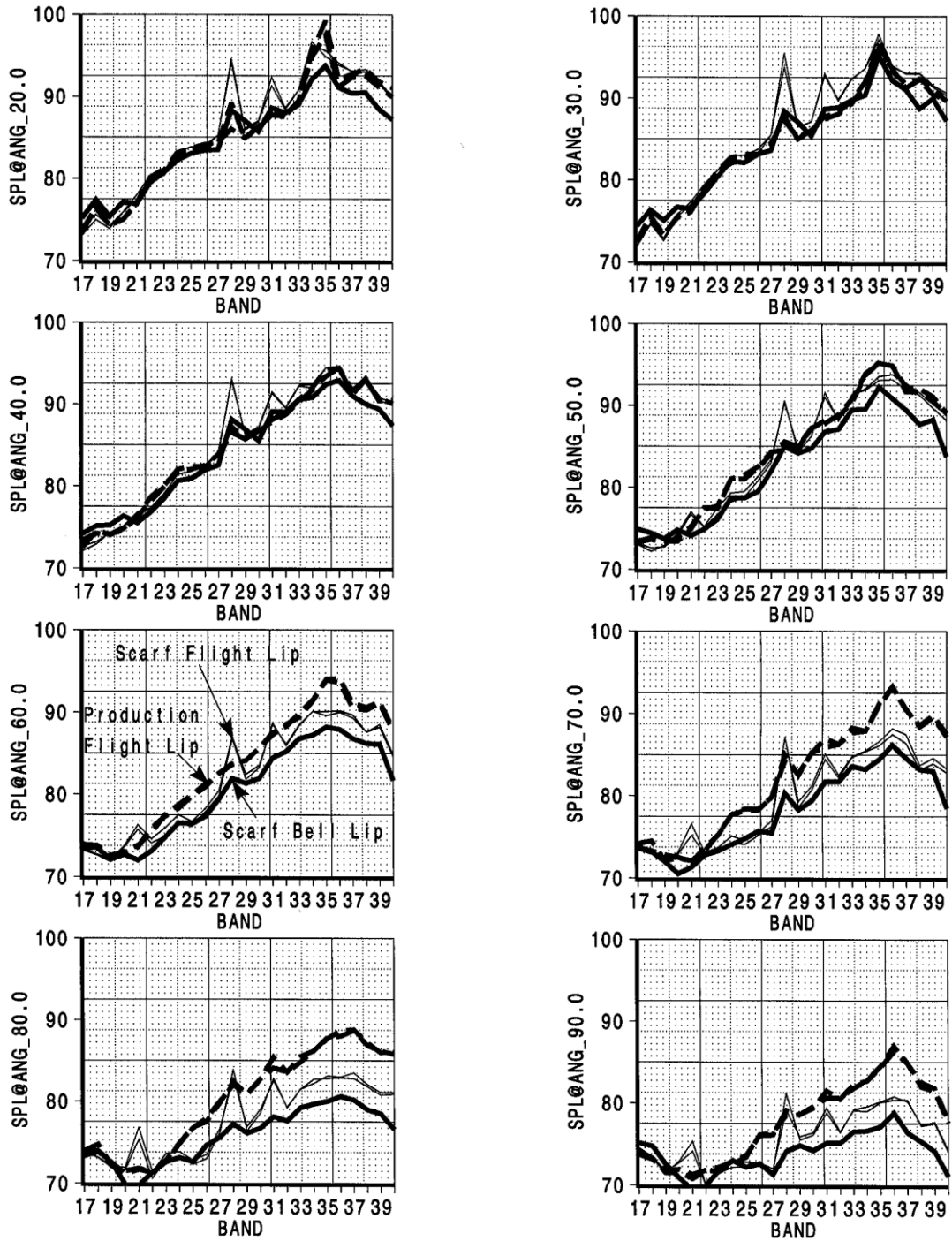
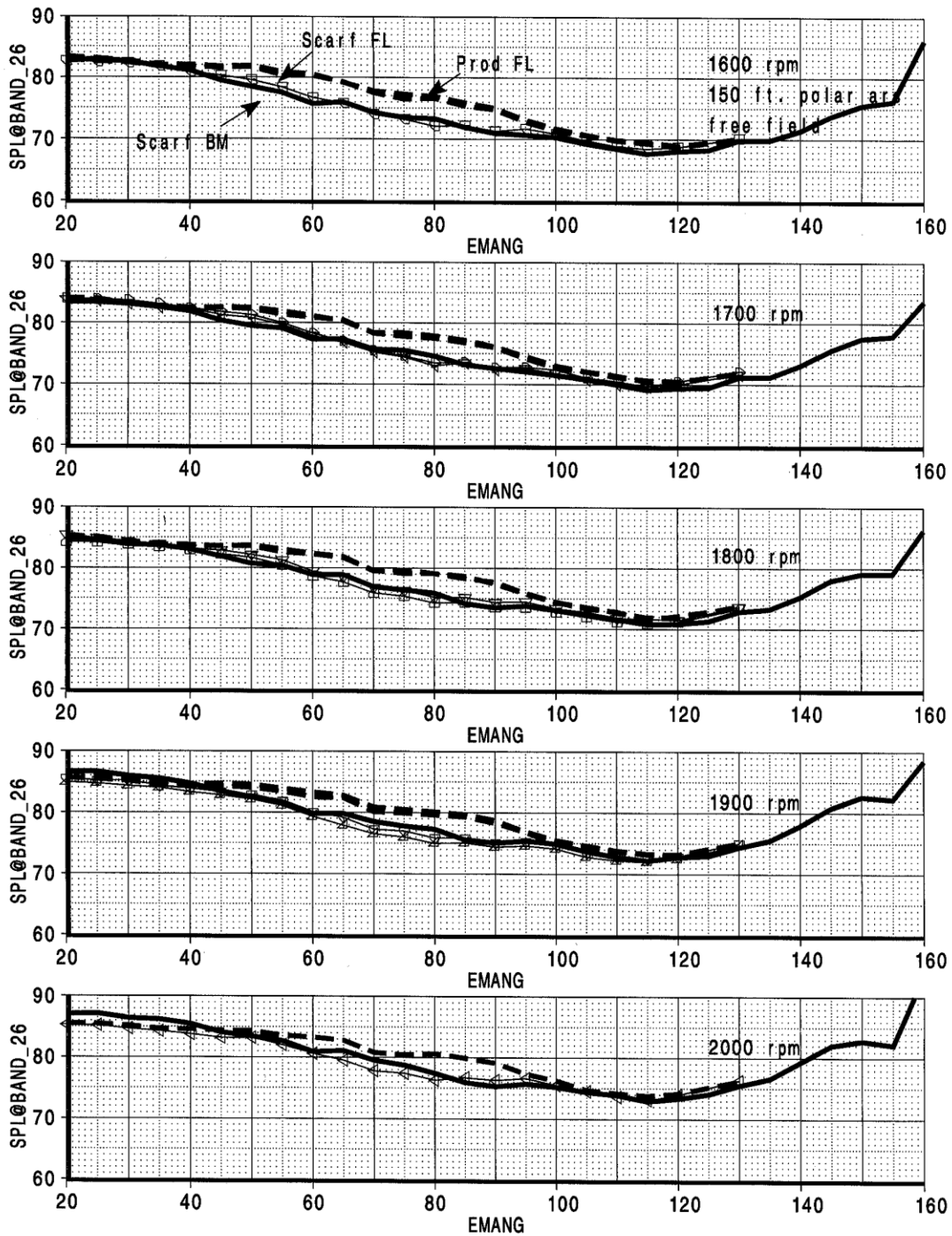Figure 241.—Production flight lip, scarf flight lip, bellmouth lip, hardwall, 1700 rpm.
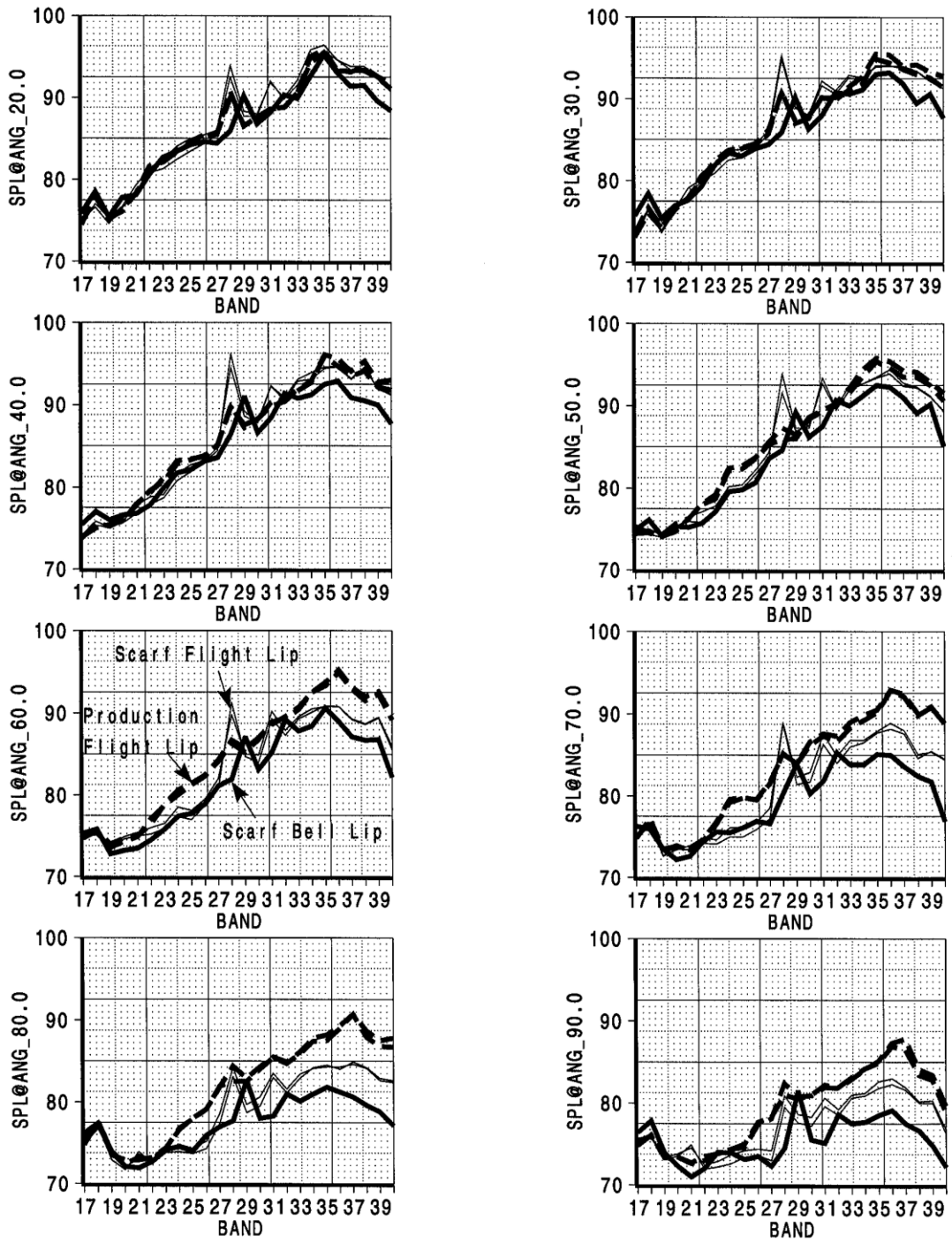
Figure 242.—Production flight lip, scarf flight lip, bellmouth lip, hardwall, 1800 rpm.
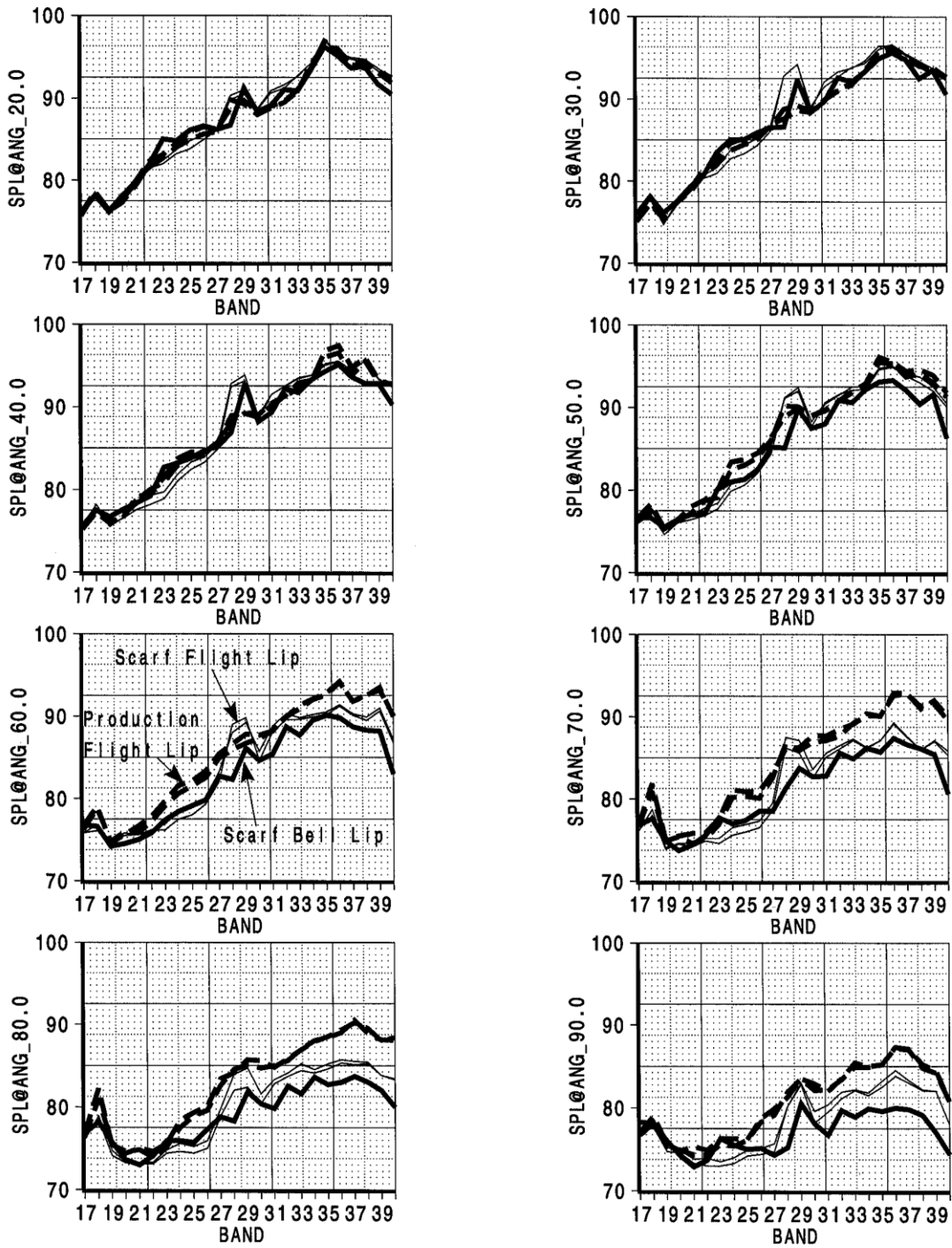
Figure 243.—Production flight lip, scarf flight lip, bellmouth lip, hardwall, 1900 rpm.
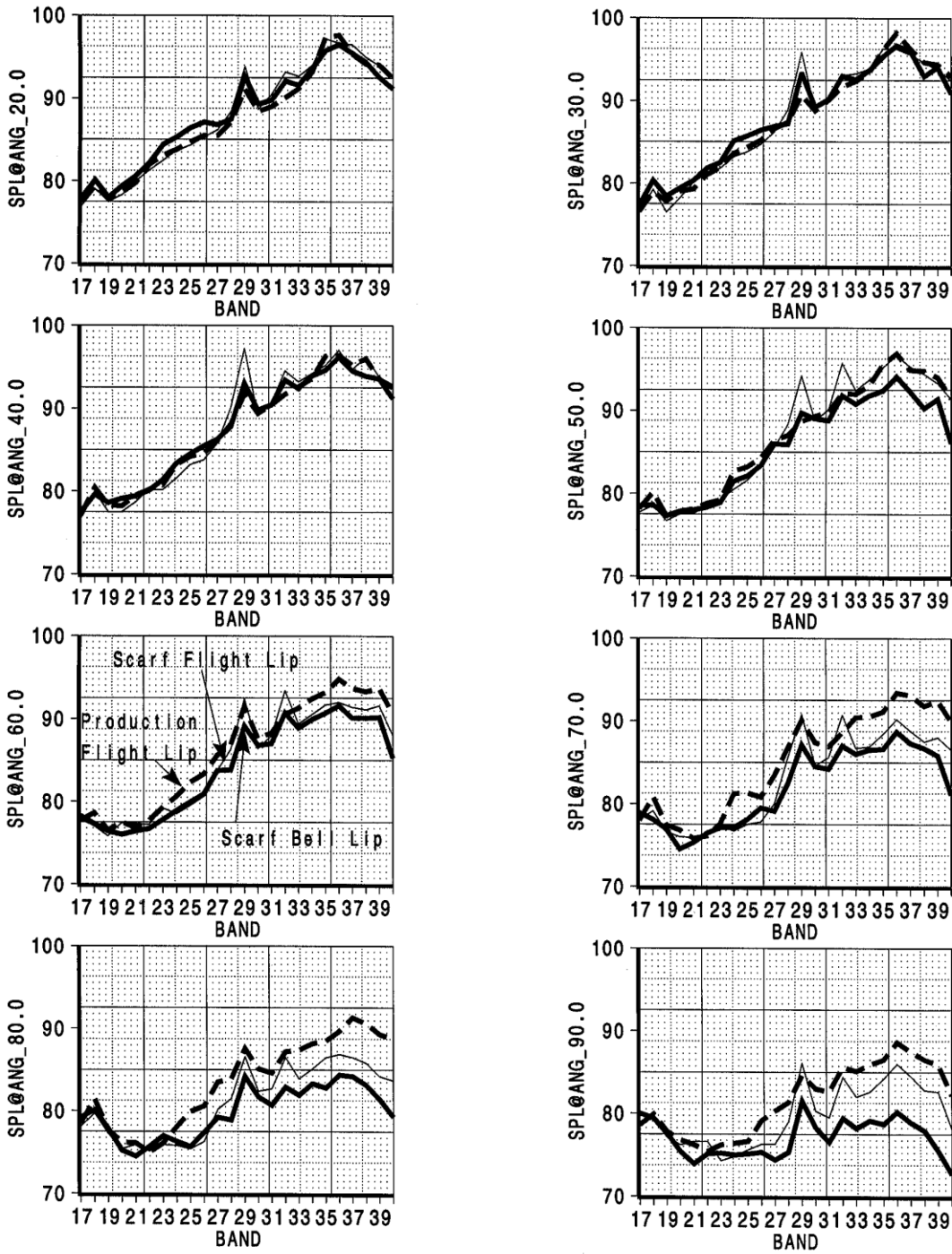
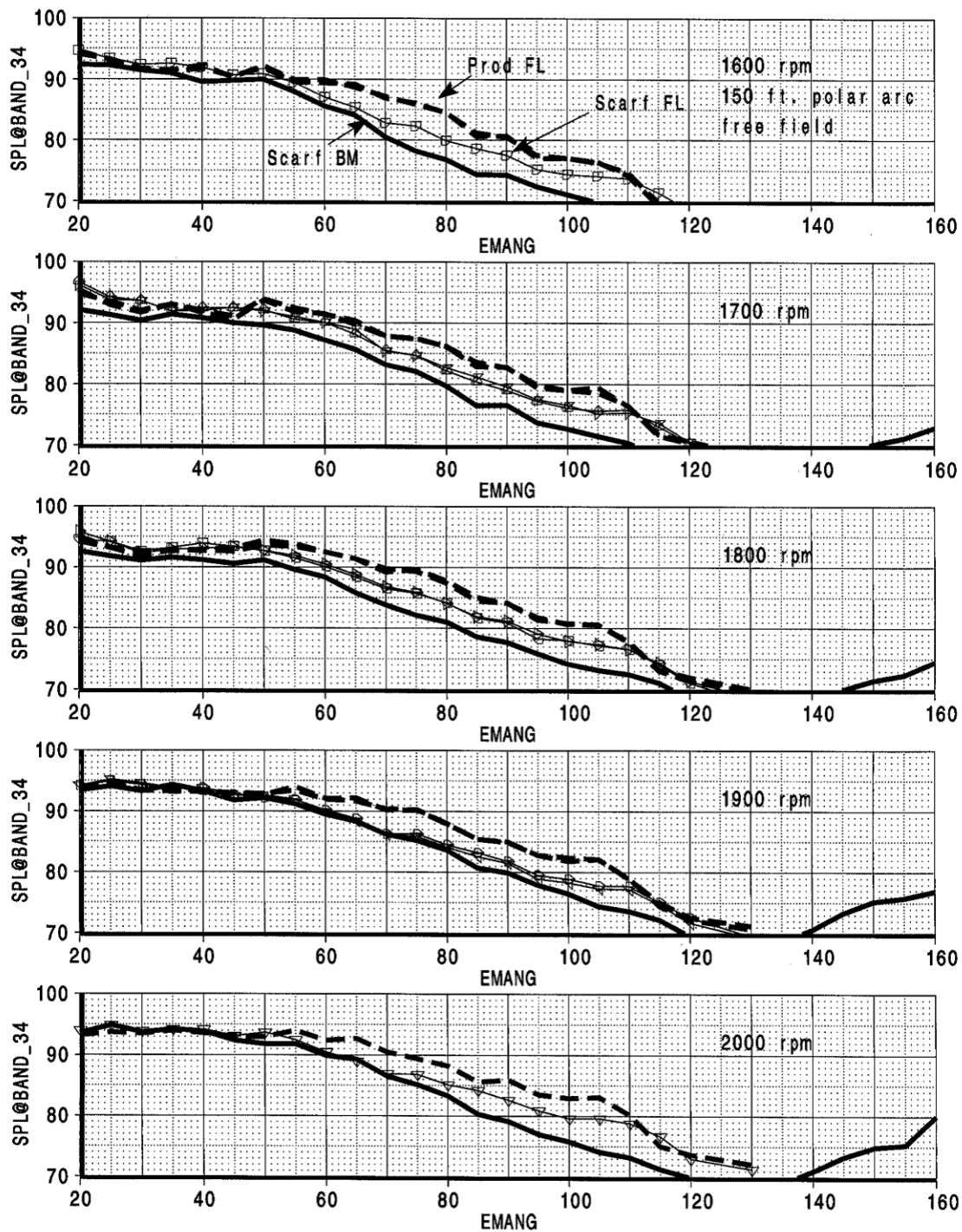Figure 244.—Production flight lip, scarf flight lip, bellmouth lip, hardwall, 2000 rpm.

Figure 245.—Band 26 (400 Hz) 1/3 octave directivity—production flight lip, scarf flight lip, scarf bellmouth lip—hardwall.
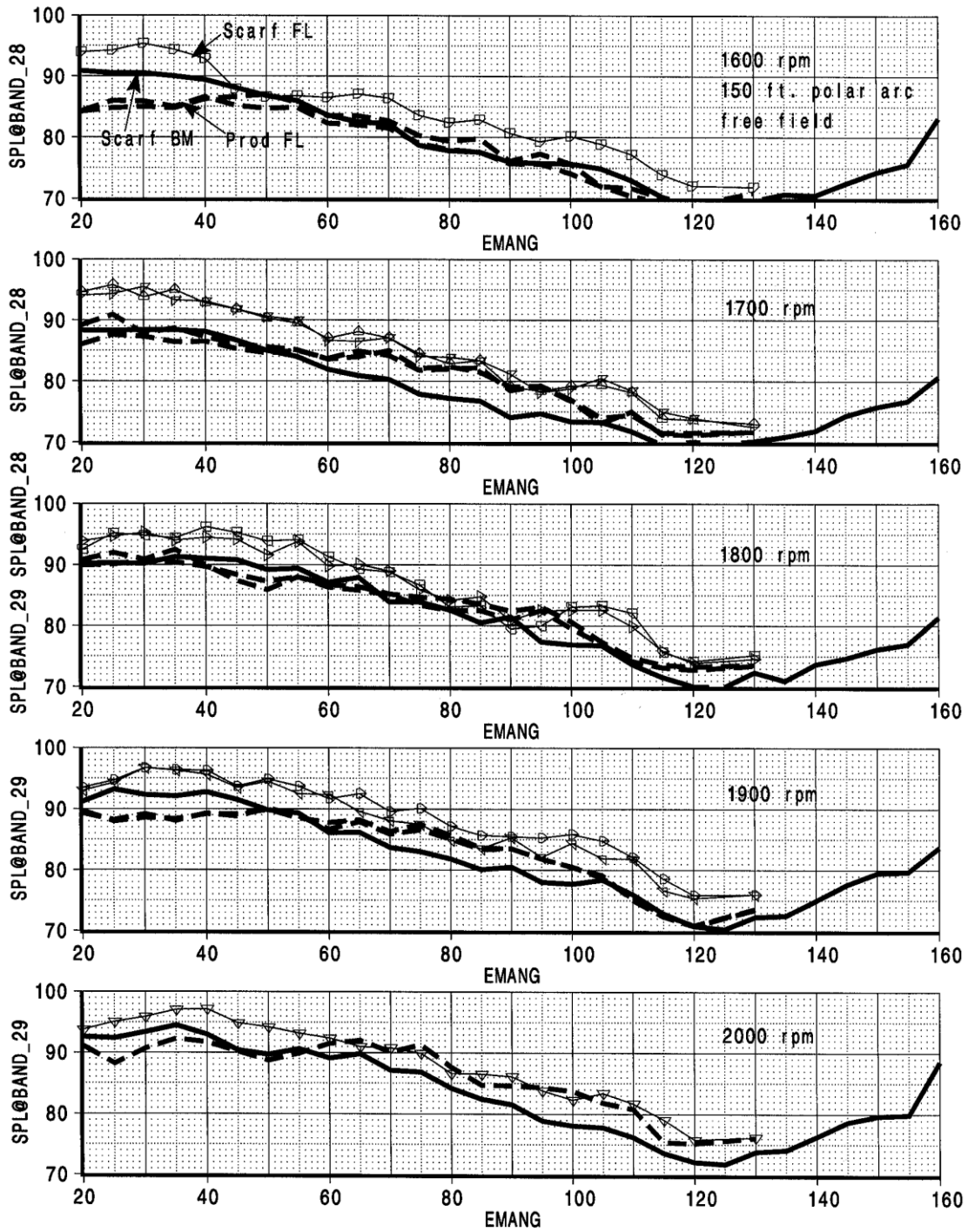
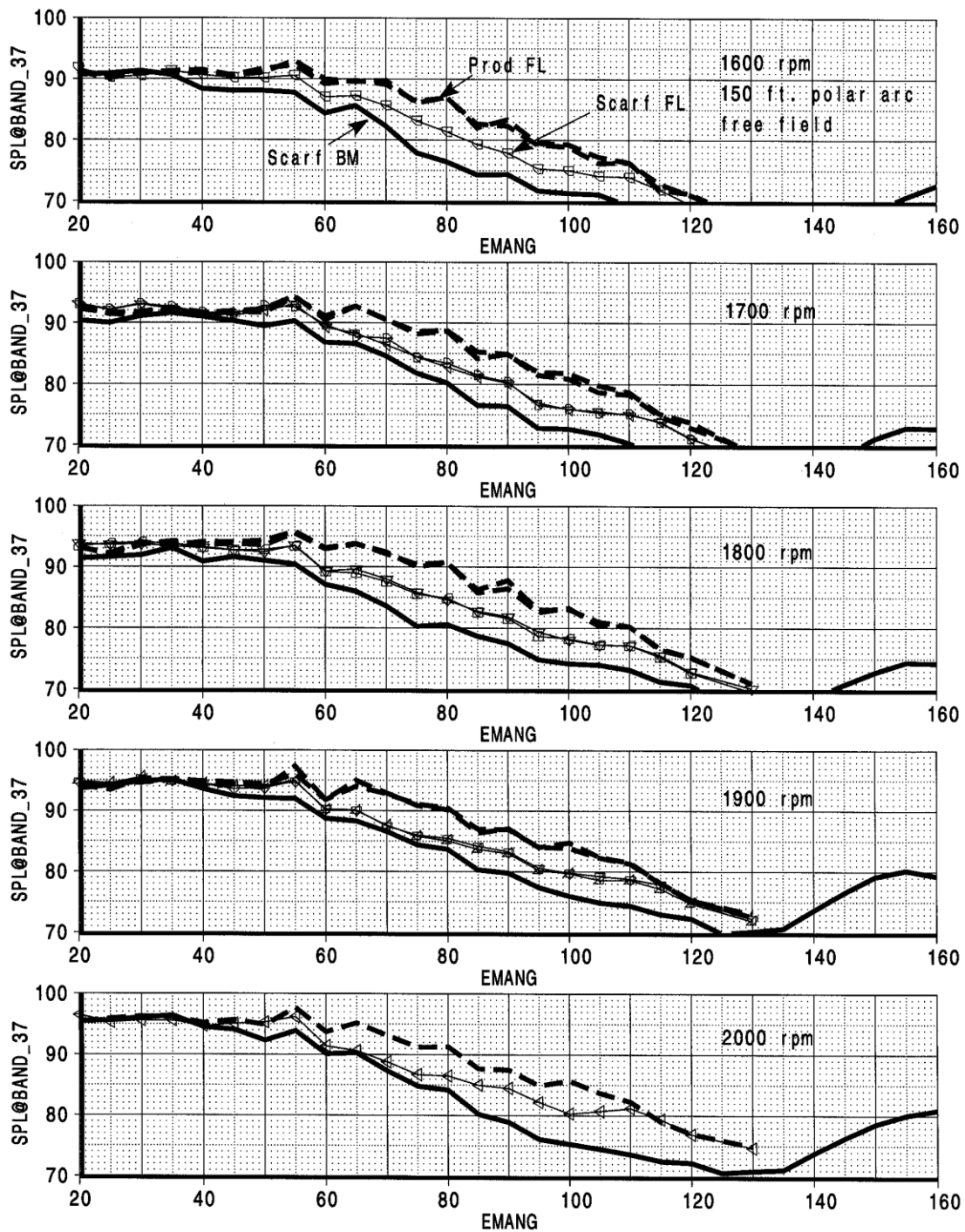Figure 246.—BPF 1/3 octave directivity—production flight lip, scarf flight lip, scarf bellmouth lip—hardwall.
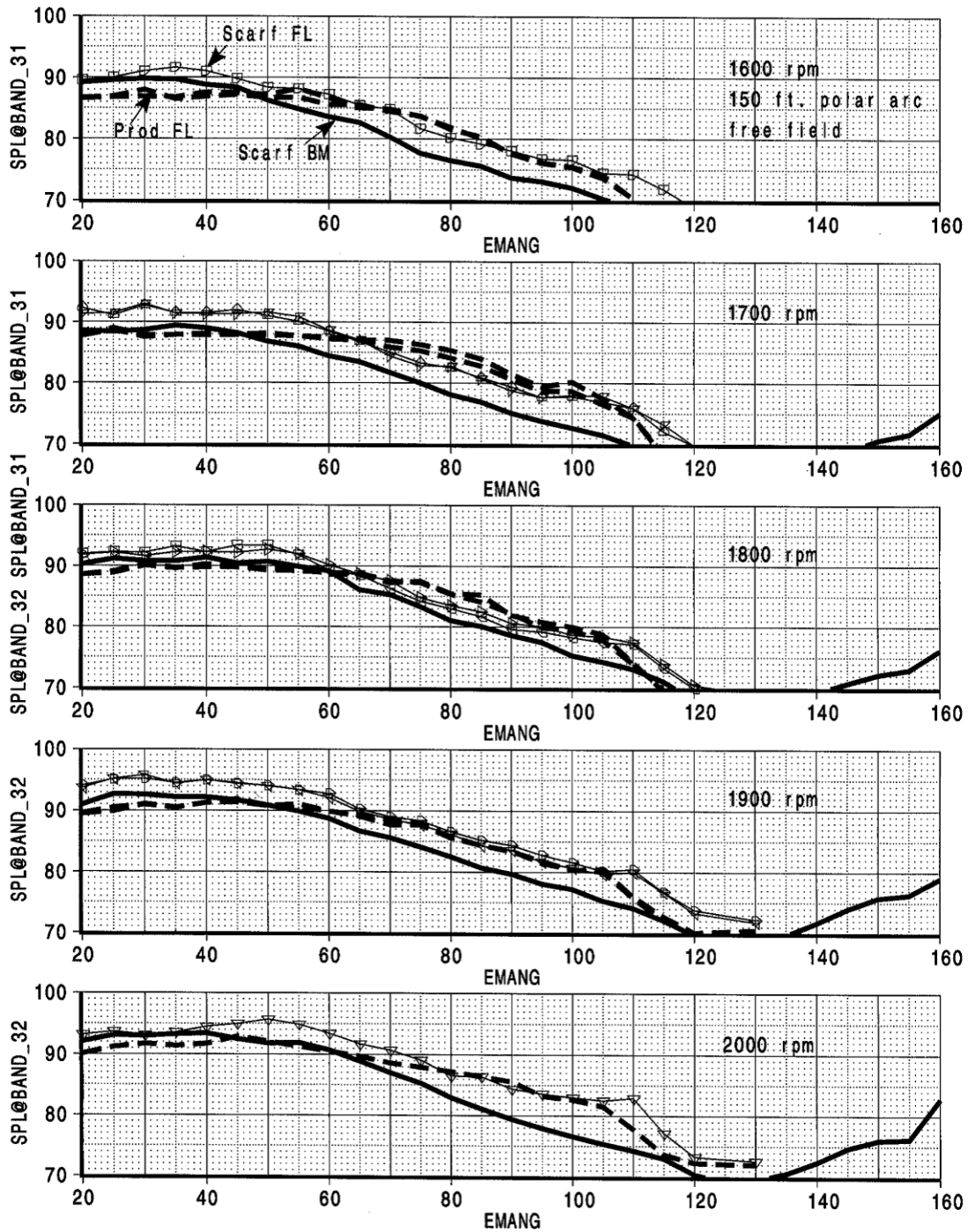
Figure 247.—2BPF 1/3 octave directivity—production flight lip, scarf flight lip, scarf bellmouth lip—hardwall.

Figure 248.—Band 34 (2.5 kHz) 1/3 octave directivity—production flight lip, scarf flight lip, scarf bellmouth lip—hardwall.

Figure 249.—Band 37 (5 kHz) 1/3 octave directivity—production flight lip, scarf flight lip, scarf bellmouth lip—hardwall.
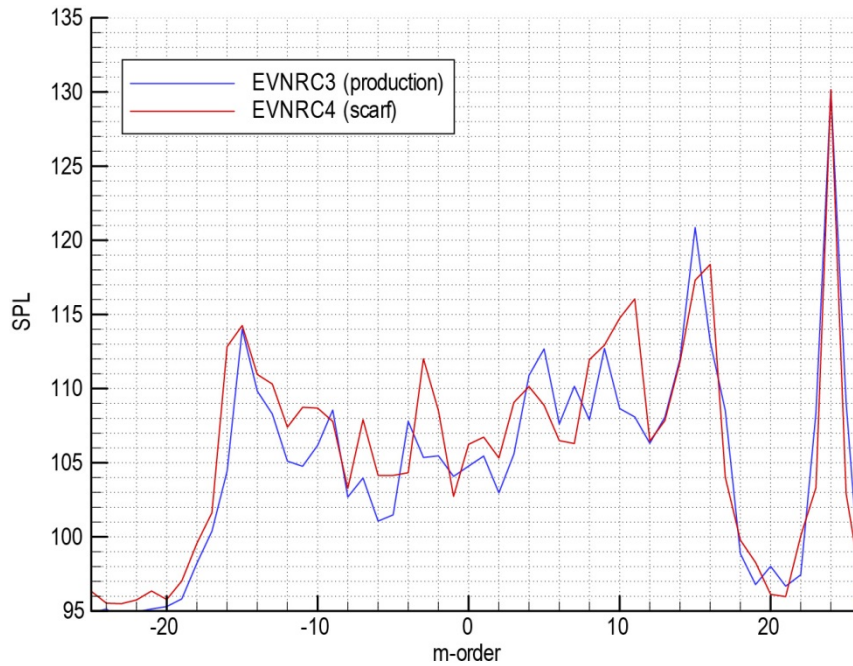
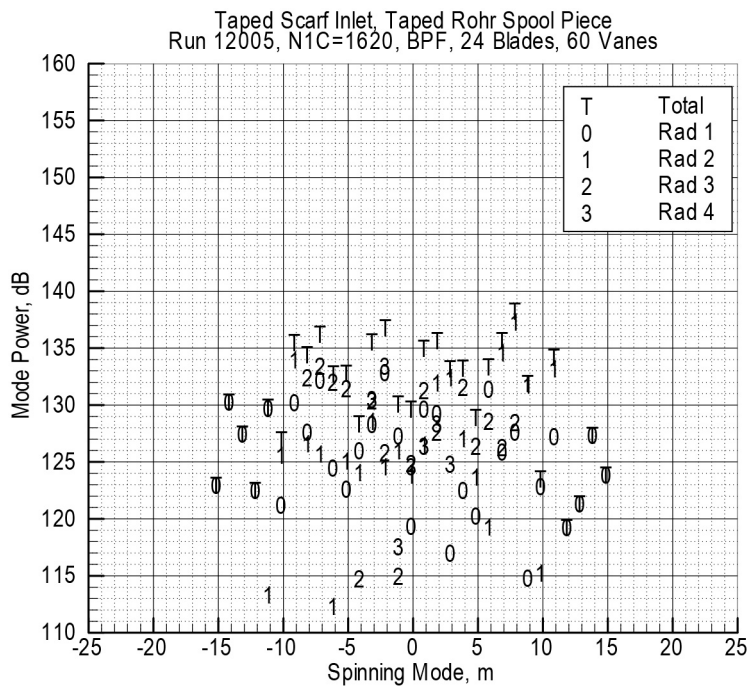Figure 250.—Comparison of the production and scarf inlets for BPF Noise at N1C = 1620 rpm.

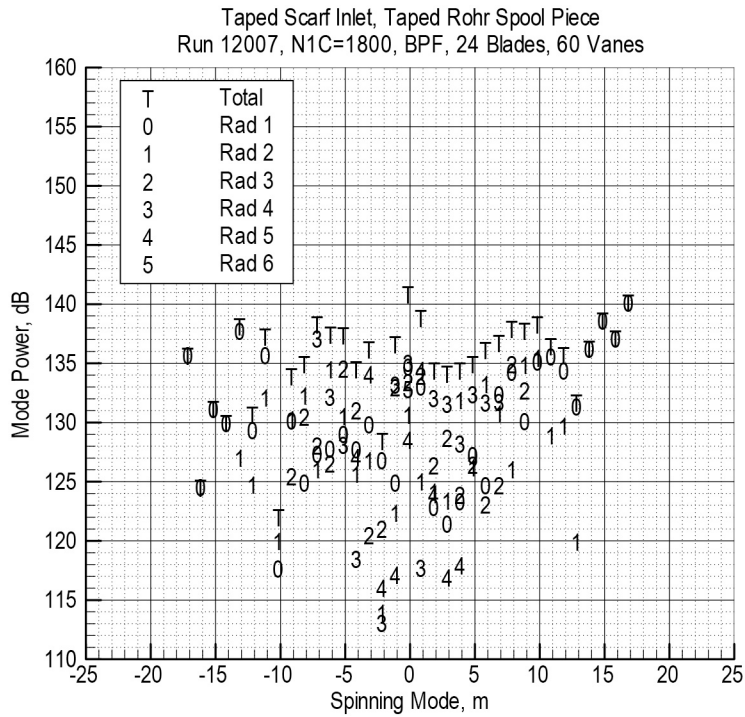Figure 251.—ICD array, EVNRC4 hardwall scarf, N1C1620.

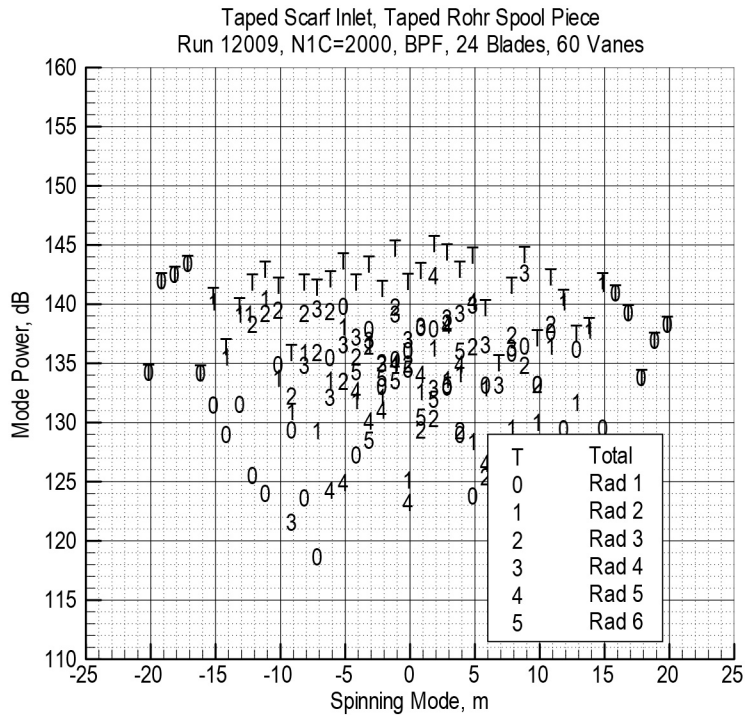Figure 252.—ICD array, EVNRC4 hardwall scarf, N1C1800.

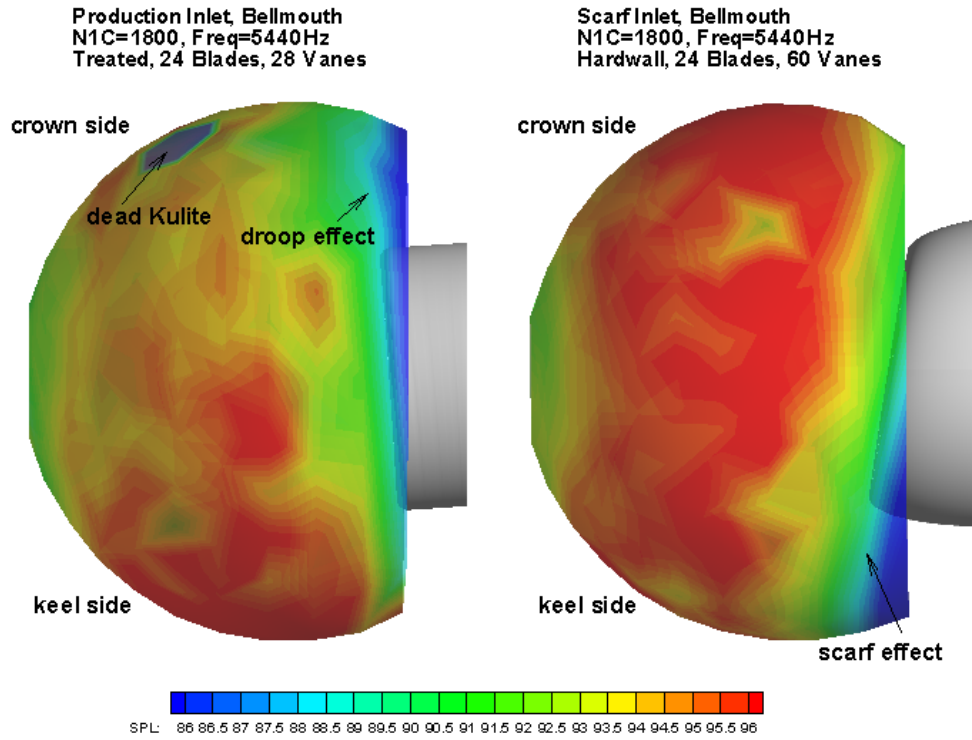Figure 253.—ICD array, EVNRC4 hardwall scarf, N1C2000.

Figure 254.—ICD SPL contours showing scarf shielding at 5440.

Appendix A.—P&W Data

A Complete listing of data records by Configuration, Run Number, Microphone Type and Analysis Bandwidth

A.1   Convention to Data Record ID (Database ID)

RRRRRMMXXX

RRRRR = 5 digit run number.   A unique run number is assigned for every configuration. A configuration represents a hardware or test set up change.

MM = Microphone type code and is either GR or KI
GR = Microphone type code where GR means a ground plane microphone as part of a radial array

KI = Microphone type code and KI means a dynamic pressure transducer, e.g., a Kulite

XXX = An index counter, a new index is given to each data point acquired within a run number

Database ID for one third octave band data = Database ID for constant bandwidth, BW = 16Hz data = Data base ID for the burner location kulite transducers

The following list of Database IDs will serve as the list for one third octave band and constant bandwidth data as well as ground plane microphone and
kulite data.

RUN 16114: ACOUSDB (1/3 OB) & ACOUSNB (Constant BW = 16Hz); Kulite = KI
BOM Trt Inlet, N-G ANC all HW fan case baseline, 22B/28V,trt T/P,ICD,no walls

*** SORTED BY N1C ***

RECORD ID	No. of ANGLES	N1CORR	N1OBS	DATE	TIME
16114GR001	32	0.	0.	072701	145607
16114GR002	32	0.	0.	072701	145936
16114GR004	32	0.	0.	072801	211439
16114GR005	32	0.	0.	072801	212225
16114GR006	32	0.	0.	072801	213211
16114GR003	32	1.	0.	072801	133823
16114GR007	32	581.	592.	072801	222444
16114GR008	32	1750.	1782.	072801	223804
16114GR009	32	1804.	1837.	072801	224142
16114GR010	32	1857.	1891.	072801	224450
16114GR011	32	1909.	1942.	072801	224736
16114GR012	32	1976.	2012.	072801	224945
16114GR013	32	2046.	2082.	072801	225321
16114GR014	32	2111.	2149.	072801	225555
16114GR015	32	2182.	2221.	072801	225935

RUN 16115: ACOUSDB (1/3 OB) & ACOUSNB (Constant BW = 16Hz); Kulite = KI
BOM Trt Inlet,N-G ANC 2, HW, Passive,Trt FC, 22B/28V, Trt T/P,ICD, no walls

*** SORTED BY N1C ***

RECORD ID	No. of ANGLES	N1CORR	N1OBS	DATE	TIME
16115GR001	32	0.	0.	073001	124810
16115GR002	32	0.	0.	073001	125115
16115GR004	32	0.	0.	080101	082036
16115GR005	32	0.	0.	080301	080112
16115GR006	32	0.	0.	080301	095425
16115GR003	32	1.	0.	080101	081317
16115GR007	32	2.	0.	080401	090139
16115GR008	32	583.	594.	080401	100746
16115GR025	32	712.	726.	080401	110650
16115GR020	32	1743.	1775.	080401	105531
16115GR009	32	1745.	1777.	080401	102256
16115GR010	32	1802.	1834.	080401	103447
16115GR011	32	1857.	1890.	080401	103637
16115GR012	32	1910.	1945.	080401	103818
16115GR021	32	1911.	1946.	080401	105721
16115GR013	32	1976.	2013.	080401	103955
16115GR014	32	2044.	2082.	080401	104135
16115GR015	32	2113.	2152.	080401	104424
16115GR016	32	2181.	2221.	080401	104559
16115GR017	32	2249.	2291.	080401	104822
16115GR022	32	2250.	2291.	080401	105933
16115GR018	32	2318.	2361.	080401	105021
16115GR023	32	2319.	2363.	080401	110136
16115GR024	32	2385.	2429.	080401	110311
16115GR019	32	2387.	2432.	080401	105204

RUN 16116: ACOUSDB (1/3 OB) & ACOUSNB (Constant BW = 16Hz); Kulite = KI
BOM Trt Inlet,N-G ANC 2,Trt ,Trt FC, 22B/28V, Trt T/P,ICD, no walls,ANC,m= -6

*** SORTED BY N1C ***

RECORD ID	No. of ANGLES	N1CORR	N1OBS	DATE	TIME
16116GR001	32	0.	0.	080401	131542
16116GR002	32	0.	0.	080401	131722
16116GR003	32	0.	0.	080701	212210
16116GR004	32	2.	0.	080801	135921
16116GR005	32	581.	598.	080801	143428
16116GR006	32	1745.	1795.	080801	144621
16116GR007	32	1801.	1853.	080801	144948
16116GR008	32	1909.	1963.	080801	145231
16116GR009	32	2045.	2099.	080801	165251
16116GR010	32	2182.	2239.	080801	170012
16116GR011	32	2319.	2380.	080801	170306

RUN 16117: ACOUSDB (1/3 OB) & ACOUSNB (Constant BW = 16Hz); Kulite = KI
BOM Trt Inlet, HW BFG R2, 22B/28V, Trt T/P,ICD, no walls, baseline.

*** SORTED BY N1C ***

RECORD ID	No. of ANGLES	N1CORR	N1OBS	DATE	TIME
16117GR001	32	0.	0.	081001	084213
16117GR002	32	0.	0.	081001	084414
16117GR003	32	0.	0.	081001	194050
16117GR031	32	0.	0.	081001	220523
16117GR032	32	0.	0.	081001	220731
16117GR004	32	582.	594.	081001	200552
16117GR030	32	583.	594.	081001	215700
16117GR020	32	1620.	1654.	081001	212207
16117GR005	32	1622.	1656.	081001	201302
16117GR021	32	1702.	1737.	081001	212528
16117GR006	32	1703.	1739.	081001	202514
16117GR007	32	1750.	1787.	081001	202817
16117GR022	32	1799.	1836.	081001	212859
16117GR008	32	1800.	1838.	081001	203216
16117GR009	32	1900.	1940.	081001	203644
16117GR023	32	1901.	1940.	081001	213112
16117GR010	32	1999.	2041.	081001	203953
16117GR011	32	2101.	2145.	081001	204232
16117GR012	32	2199.	2245.	081001	204510
16117GR024	32	2203.	2248.	081001	213403
16117GR025	32	2303.	2350.	081001	213632
16117GR013	32	2304.	2352.	081001	205118
16117GR014	32	2400.	2450.	081001	205413
16117GR015	32	2450.	2501.	081001	205727
16117GR026	32	2452.	2503.	081001	213859
16117GR016	32	2500.	2552.	081001	205955
16117GR027	32	2501.	2551.	081001	214210
16117GR017	32	2600.	2654.	081001	210348
16117GR018	32	2700.	2756.	081001	210654
16117GR028	32	2702.	2758.	081001	214440
16117GR019	32	2743.	2800.	081001	211147
16117GR029	32	2744.	2800.	081001	214719

RUN 16118: ACOUSDB (1/3 OB) & ACOUSNB (Constant BW = 16Hz); Kulite = KI
BOM Trt Inlet, HW BFG R2, 24B/28V, Trt T/P,ICD, no walls, baseline.

*** SORTED BY N1C ***

RECORD ID	No. of ANGLES	N1CORR	N1OBS	DATE	TIME
16118GR001	32	0.	0.	081701	141923
16118GR002	32	0.	0.	081701	142116
16118GR030	32	0.	0.	082101	140244
16118GR031	32	0.	0.	082101	140434
16118GR003	32	1.	0.	082101	102242
16118GR004	32	581.	594.	082101	104131
16118GR019	32	582.	597.	082101	113142
16118GR020	32	1619.	1659.	082101	113625
16118GR005	32	1624.	1663.	082101	105210
16118GR006	32	1701.	1742.	082101	110012
16118GR021	32	1702.	1743.	082101	113802
16118GR007	32	1801.	1844.	082101	110208
16118GR022	32	1802.	1847.	082101	113940
16118GR008	32	1900.	1946.	082101	110427
16118GR023	32	1901.	1949.	082101	114118
16118GR009	32	2001.	2050.	082101	110608
16118GR010	32	2099.	2152.	082101	110845
16118GR011	32	2201.	2256.	082101	111037
16118GR024	32	2202.	2258.	082101	114334
16118GR012	32	2301.	2358.	082101	111311
16118GR025	32	2302.	2360.	082101	114507
16118GR013	32	2400.	2460.	082101	111456
16118GR014	32	2450.	2511.	082101	111643
16118GR026	32	2451.	2513.	082101	114732
16118GR027	32	2499.	2563.	082101	114920
16118GR015	32	2500.	2563.	082101	112001
16118GR016	32	2599.	2665.	082101	112155
16118GR028	32	2700.	2769.	082101	115122
16118GR017	32	2702.	2769.	082101	112332
16118GR029	32	2730.	2800.	082101	115256
16118GR018	32	2731.	2800.	082101	112606

RUN 16119: ACOUSDB (1/3 OB) & ACOUSNB (Constant BW = 16Hz); Kulite = KI
BOM Trt Inlet, HW BFG R2, 24B/28V, Trt T/P,ICD, with Aft walls, baseline.

*** SORTED BY N1C ***

RECORD ID	No. of ANGLES	N1CORR	N1OBS	DATE	TIME
16119GR001	32	0.	0.	082201	122840
16119GR002	32	0.	0.	082201	123034
16119GR028	32	0.	0.	082201	152807
16119GR029	32	0.	0.	082201	153024
16119GR003	32	580.	596.	082201	134704
16119GR019	32	588.	603.	082201	144153
16119GR005	32	1620.	1662.	082201	141151
16119GR020	32	1621.	1664.	082201	144551
16119GR006	32	1699.	1746.	082201	141617
16119GR021	32	1700.	1746.	082201	144732
16119GR022	32	1799.	1848.	082201	144906
16119GR007	32	1803.	1853.	082201	141756
16119GR008	32	1900.	1951.	082201	141935
16119GR023	32	1902.	1955.	082201	145058
16119GR009	32	2002.	2053.	082201	142122
16119GR010	32	2099.	2154.	082201	142339
16119GR024	32	2200.	2261.	082201	145316
16119GR011	32	2201.	2260.	082201	142522
16119GR012	32	2300.	2362.	082201	142709
16119GR025	32	2302.	2365.	082201	145457
16119GR013	32	2396.	2462.	082201	142850
16119GR004	32	2449.	2514.	082201	135903
16119GR014	32	2451.	2517.	082201	143029
16119GR026	32	2500.	2568.	082201	145718
16119GR015	32	2501.	2566.	082201	143344
16119GR016	32	2601.	2668.	082201	143534
16119GR017	32	2699.	2769.	082201	143722
16119GR027	32	2701.	2772.	082201	145917
16119GR018	32	2729.	2800.	082201	143928

RUN 16120: ACOUSDB (1/3 OB) & ACOUSNB (Constant BW = 16Hz); Kulite = KI
HW ideal Scarf Inlet, HW BFG R2, 24B/60V, Trt T/P,ICD, with Aft walls.

*** SORTED BY N1C ***

RECORD ID	No. of ANGLES	N1CORR	N1OBS	DATE	TIME
16120GR001	32	0.	0.	082701	100232
16120GR002	32	0.	0.	082701	100410
16120GR003	32	1.	0.	082701	141958
16120GR004	32	580.	594.	082701	145152
16120GR005	32	1621.	1662.	082701	145912
16120GR006	32	1701.	1744.	082701	150113
16120GR007	32	1804.	1849.	082701	150255
16120GR008	32	1899.	1946.	082701	150518
16120GR009	32	1999.	2048.	082701	150704

RUN 16121: ACOUSDB (1/3 OB) & ACOUSNB (Constant BW = 16Hz); Kulite = KI
BOM Treated Inlet, HW BFG R2, 24B/60V, Trt T/P,ICD, with Aft walls.

*** SORTED BY N1C ***

RECORD ID	No. of ANGLES	N1CORR	N1OBS	DATE	TIME
16121GR001	32	0.	0.	082901	081754
16121GR002	32	0.	0.	082901	081954
16121GR032	32	0.	728.	083001	115355
16121GR033	32	0.	727.	083001	115528
16121GR003	32	1.	0.	083001	105127
16121GR004	32	580.	595.	083001	105838
16121GR020	32	587.	603.	083001	112800
16121GR005	32	1621.	1663.	083001	110223
16121GR021	32	1626.	1670.	083001	113123
16121GR022	32	1699.	1745.	083001	113253
16121GR006	32	1704.	1750.	083001	110405
16121GR007	32	1801.	1850.	083001	110534
16121GR023	32	1802.	1851.	083001	113438
16121GR008	32	1898.	1950.	083001	110714
16121GR024	32	1904.	1955.	083001	113605
16121GR009	32	2002.	2057.	083001	110843
16121GR010	32	2100.	2157.	083001	111019
16121GR011	32	2199.	2260.	083001	111201
16121GR025	32	2201.	2261.	083001	113819
16121GR012	32	2300.	2365.	083001	111334
16121GR026	32	2301.	2362.	083001	114016
16121GR013	32	2399.	2465.	083001	111518
16121GR027	32	2448.	2513.	083001	114224
16121GR014	32	2451.	2517.	083001	111701
16121GR015	32	2500.	2566.	083001	111854
16121GR028	32	2501.	2569.	083001	114449
16121GR016	32	2599.	2667.	083001	112035
16121GR029	32	2698.	2774.	083001	114652
16121GR017	32	2699.	2769.	083001	112216
16121GR018	32	2799.	2872.	083001	112406
16121GR030	32	2800.	2877.	083001	114835
16121GR019	32	2897.	2972.	083001	112543
16121GR031	32	2902.	2982.	083001	115022

RUN 16122: ACOUSDB (1/3 OB) & ACOUSNB (Constant BW = 16Hz); Kulite = KI
BOM Treated Inlet, HW BFG R2, 24B/60V, Trt T/P,ICD.

*** SORTED BY N1C ***

RECORD ID	No. of ANGLES	N1CORR	N1OBS	DATE	TIME
16122GR001	32	0.	0.	083001	202231
16122GR002	32	0.	0.	083001	202507
16122GR003	32	1.	0.	083001	202851
16122GR004	32	2.	0.	083101	141455
16122GR033	32	3.	0.	083101	162836
16122GR005	32	580.	598.	083101	142010
16122GR021	32	589.	606.	083101	145247
16122GR006	32	1618.	1667.	083101	142650
16122GR022	32	1619.	1665.	083101	145650
16122GR023	32	1698.	1748.	083101	145823
16122GR007	32	1700.	1751.	083101	142829
16122GR008	32	1802.	1855.	083101	143005
16122GR024	32	1803.	1855.	083101	145959
16122GR009	32	1902.	1960.	083101	143148
16122GR025	32	1903.	1960.	083101	150144
16122GR010	32	1999.	2060.	083101	143317
16122GR011	32	2098.	2161.	083101	143454
16122GR012	32	2199.	2265.	083101	143627
16122GR026	32	2200.	2264.	083101	150346
16122GR013	32	2301.	2370.	083101	143759
16122GR027	32	2303.	2371.	083101	150528
16122GR014	32	2400.	2471.	083101	143953
16122GR015	32	2449.	2522.	083101	144148
16122GR028	32	2450.	2521.	083101	150733
16122GR029	32	2498.	2572.	083101	150918
16122GR016	32	2499.	2572.	083101	144337
16122GR017	32	2599.	2676.	083101	144525
16122GR030	32	2697.	2779.	083101	151137
16122GR018	32	2699.	2779.	083101	144710
16122GR031	32	2799.	2884.	083101	151333
16122GR019	32	2800.	2882.	083101	144849
16122GR032	32	2894.	2982.	083101	151523
16122GR020	32	2905.	2989.	083101	145030

RUN 16123: ACOUSDB (1/3 OB) & ACOUSNB (Constant BW = 16Hz); Kulite = KI
BOM Treated Inlet, HW BFG R2, 24B/60V, HW T/P,ICD.

*** SORTED BY N1C ***

RECORD ID	No. of ANGLES	N1CORR	N1OBS	DATE	TIME
16123GR001	32	0.	0.	090401	171913
16123GR002	32	0.	0.	090401	172409
16123GR032	32	0.	0.	090501	134159
16123GR033	32	0.	0.	090501	134350
16123GR003	32	1.	0.	090501	111129
16123GR004	32	581.	596.	090501	112936
16123GR020	32	586.	602.	090501	121359
16123GR005	32	1618.	1662.	090501	114508
16123GR021	32	1620.	1665.	090501	121741
16123GR006	32	1700.	1746.	090501	114738
16123GR022	32	1702.	1749.	090501	121938
16123GR007	32	1798.	1845.	090501	114912
16123GR023	32	1801.	1850.	090501	122132
16123GR024	32	1902.	1954.	090501	122403
16123GR008	32	1903.	1953.	090501	115049
16123GR009	32	2001.	2053.	090501	115222
16123GR010	32	2097.	2153.	090501	115456
16123GR025	32	2197.	2257.	090501	122628
16123GR011	32	2201.	2259.	090501	115639
16123GR012	32	2299.	2360.	090501	115741
16123GR026	32	2302.	2366.	090501	122824
16123GR013	32	2400.	2464.	090501	115938
16123GR027	32	2448.	2518.	090501	123049
16123GR014	32	2449.	2514.	090501	120127
16123GR028	32	2501.	2573.	090501	123253
16123GR015	32	2502.	2570.	090501	120311
16123GR016	32	2599.	2671.	090501	120503
16123GR017	32	2700.	2777.	090501	120657
16123GR029	32	2701.	2779.	090501	123620
16123GR030	32	2802.	2883.	090501	123837
16123GR018	32	2805.	2885.	090501	120911
16123GR031	32	2898.	2980.	090501	124026
16123GR019	32	2900.	2984.	090501	121132

Appendix B.—Boeing Data

Boeing ICD and In-Duct Acquisition Log Sheet
Engine Validation of Noise Reduction Concepts Test
NG Configuration #1: ANC HW Baseline
BOM Trt Inlet, NG ANC Active HW, Passive HW, 22B/28V, Trt T/p, No Walls

Run: 16114
Date: 07-28-01

Filename	Time	Target N1C	N1C	N1O	Temp	RH (%)	Inlet	Case	Walls (Y/N)	Notes
114007	22:24	580	581	591	78	91	P	AHW	N	
114008	22:37	1745	1750	1782	78	90	P	AHW	N	
114009	22:40				78	91	P	AHW	N	
114010	22:43	1800	1804	1836	78	92	P	AHW	N	
114011	22:47	1855	1857	1889	78	93	P	AHW	N	
114012	22:48	1909	1909	1942	78	94	P	AHW	N	
114013	22:52	2045	2047	2082	78	94	P	AHW	N	
114014	22:55	2114	2112	2149	78	94	P	AHW	N	
114015	22:58	2182	2183	2221	78	95	P	AHW	N	

General Notes: Rhino tape to hardwall the active noise spool piece for both the active and passive sections.
Tape tore off much of the liner near the fan. Channels 248-255 are bad (includes all tachs).

Boeing ICD and In-Duct Acquisition Log Sheet
Engine Validation of Noise Reduction Concepts Test
NG Configuration #2: ANC HW, Treated ANC Passive
BOM Trt Inlet, NG ANC Act-Trt Pass, 22B/28V, Trt T/p, No Walls

Run: 16115
Date: 08-04-01

Filename	Time	Target N1C	N1C	N1O	Temp	RH (%)	Inlet	Case	Walls (Y/N)	Notes
11508	22:04	580	583		78	87	P	A	N	
11509	22:22	1745	1745	1777	78	87	P	A	N	
11510	22:26	1800	1802	1834	78	87	P	A	N	
11511	22:30	1855	1857	1890	77	88	P	A	N	
11512	22:38	1909	1910	1945	78	86	P	A	N	
11513	22:40	1977	1976	2013	78	87	P	A	N	
11514	22:41	2045	2044	2082	78	86	P	A	N	
11515	22:44	2114	2113	2152	78	85	P	A	N	
11516	22:46	2182	2181	2221	78	85	P	A	N	
11517	22:48	2250	2249	2291	78	86	P	A	N	
11518	22:50	2318	2318	2361	78	86	P	A	N	
11519	22:52	2386	2387	2432	79	86	P	A	N	
11520	22:55	1745	1743	1775	79	86	P	A	N	
11521	22:57	1909	1910	1946	79	86	P	A	N	
11522	22:59	2250	2249	2291	79	87	P	A	N	
11523	23:01	2318	2319	2363	79	86	P	A	N	
11524	23:02	2386	2385	2429	79	86	P	A	N	

General Notes: The tape was removed from the NG Passive portion of the liner. Note that the liner was
already damaged from the tape and generated considerable BPF noise. Some tape came off the drivers, too.

Boeing ICD and In-Duct Acquisition Log Sheet
Engine Validation of Noise Reduction Concepts Test
NG Configuration #3: ANC Open (Cutout holes), HW ANC Passive
BOM Trt Inlet, NG ANC, Trt Act-HW Pass, 22B/28V, Trt T/p, ICD, No Walls

Run: 16116
Date: 08-08-01

Filename	Time	Target N1C	N1C	N1O	Temp	RH (%)	Inlet	Case	Walls (Y/N)	Notes
11605	14:35	580	581	598	88	60	P	A	N	
11606	14:46	1745	1745	1795	89	57	P	A	N	
11607	14:49	1800	1801	1853	89	57	P	A	N	
11608	14:52	1909	1909	1963	89	60	P	A	N	
11609	16:53	2045	2045	2099	87	64	P	A	N	
11610	17:00	2182	2182	2239	87	64	P	A	N	
11611	17:02	2318	2319	2380	87	63	P	A	N	

General Notes: Tested after the passive active liner was hardwalled with paint with no tape
on the active drivers. Also, the holes for the drivers were cut out because some were clogged.

Boeing ICD and In-Duct Acquisition Log Sheet
Engine Validation of Noise Reduction Concepts Test

Run: static
Date: 08-07-01

Filename	Time	Target N1C	N1C	N1O	Temp	RH (%)	Inlet	Case	Walls (Y/N)	Notes
static01.dat										All rings (not working correctly)
static02d.dat										Ring D (working)
										(Frequency set at 652 Hz)

General Notes: Note that there was tape on all the transducers in the lower half of the duct. These were
roughly numbers 15 to 38. The active power supply was failing and made it impossible to get a lot of data.

Boeing ICD and In-Duct Acquisition Log Sheet
Engine Validation of Noise Reduction Concepts Test
EVNRC Configuration 1
BOM Trtd Inlet, HW BFG R2 Spool, 22B/28V, TrTrt T/P, ICD, no Walls, Baseline

Run: 16117
Date: 08-10-01

Filename	Time	Target N1C	N1C	N1O	Temp	RH (%)	Inlet	Case	Walls (Y/N)	Notes
11705	20:12	1620	1622	1656	81	79	P	HWP	N	
11708	20:31	1800	1800	1838	81	79	P	HWP	N	
11712	20:44	2200	2199	2245	81	81	P	HWP	N	
11715	20:56	2450	2450	2501	81	80	P	HWP	N	
11718	21:06	2700	2700	2756	81	82	P	HWP	N	
11719	21:11	2743	2743	2800	81	82	P	HWP	N	
accel	22:00	accel	accel	accel	81	81	P	HWP	N	

General Notes: Tape started coming up at the backside near the fan on a couple places. However, not that much tape really came up.

Boeing ICD and In-Duct Acquisition Log Sheet
Engine Validation of Noise Reduction Concepts Test
EVNRC Configuration 2
BOM Trtd Inlet, HW BFG R2 Spool, 24B/28V, TrTrt T/P, ICD, no Walls

Run: 16118
Date: 08-21-01

Filename	Time	Target N1C	N1C	N1O	Temp	RH (%)	Inlet	Case	Walls (Y/N)	Notes
11807	10:41	580	581	594	83.5	82				
11808	10:52	1620	1624	1663	84.6	77.3				
11810	11:02	1800	1801	1844	84	81				
11812	11:06	2000	2001	2050	84.4	80.2				
11814	11:10	2200	2201	2256	85.2	79.4				
11817	11:16	2450	2450	2511	85	75.4				
11820	11:23	2700	2702	2769	85.1	74.8				
11821	11:26	2731	2731	2800	85.5	73.9				
118aca	11:57	N/A	N/A	N/A	86.1	71.1				

General Notes:

Boeing ICD and In-Duct Acquisition Log Sheet

Engine Validation of Noise Reduction Concepts Test
EVNRC Configuration 3
BOM Trtd Inlet, HW BFG R2 Spool, 24B/28V, TrTrt T/P, ICD, Walls

16119
8/22/2001

Filename	Time	Target N1C	N1C	N1O	Temp	RH (%)	Inlet	Case	Walls (Y/N)	Notes
11904	13:57	2450	2449	2514	86.9	66	P	HWP	Y	Repeat of 16118 but with walls
11905	14:10	1620	1620	1662	86.5	67.3	P	HWP	Y	blocking aft noise.
11907	14:16	1800	1803	1853	88	65.3	P	HWP	Y	
11909	14:19	2000	2002	2053	86.1	72.6	P	HWP	Y	
11911	14:23	2200	2201	2260	87.3	64.7	P	HWP	Y	
11914	14:28	2450	2451	2517	87.5	67.6	P	HWP	Y	
11917	14:35	2700	2699	2769	86.4	66.2	P	HWP	Y	
119acc	14:59	N/A			86.6	64.8	P	HWP	Y	

General Notes: This configuration had 0.5" less penetration than the previous configurations.

Boeing ICD and In-Duct Acquisition Log Sheet

Engine Validation of Noise Reduction Concepts Test
EVNRC Configuration 4
Scarf HW Inlet, HW BFG R2 Spool, 24B/28V, TrTrt T/P, ICD, Walls

16120
8/27/2001

Filename	Time	Target N1C	N1C	N1O	Temp	RH (%)	Inlet	Case	Walls (Y/N)	Notes
12005	14:59	1620	1621	1662	85.7	60.9	S	HWP	Y	Hardwall scarf with walls
12007	15:03	1800	1804	1849	85.2	61.8	S	HWP	Y	
12009	15:07	2000	1999	2048	85	61.3	S	HWP	Y	

General Notes: This configuration had 0.5" less penetration than the previous configurations.

Appendix C

EVNRC Test Mode Ring Results
ACTIVE3: BOM Trtd Inlet, HW Passive, Uncovered Drivers
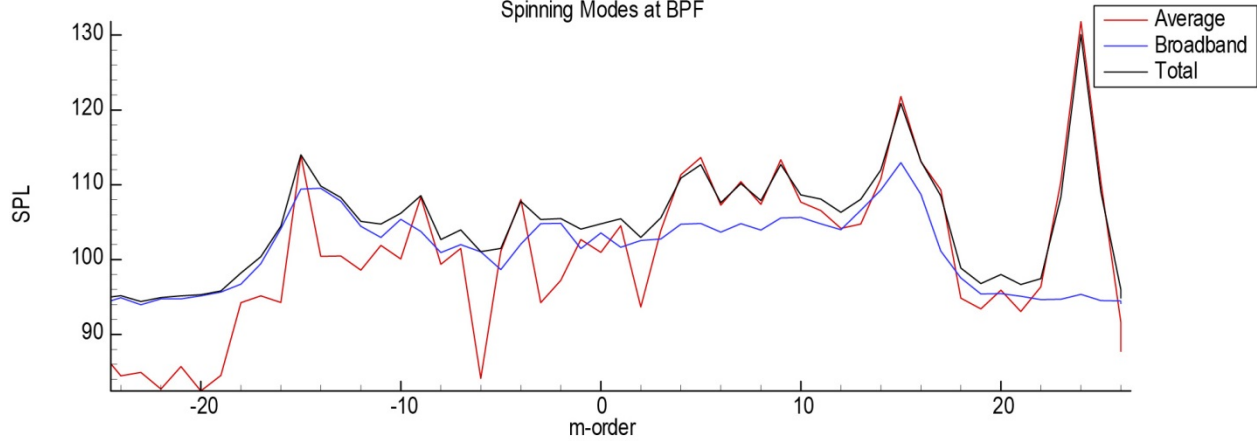(Run 11606, N1C=1745 rpm)

Mean and Standard Deviation of a Transducer

Autospectra Versus Rotation Order

Spinning Modes at BPF

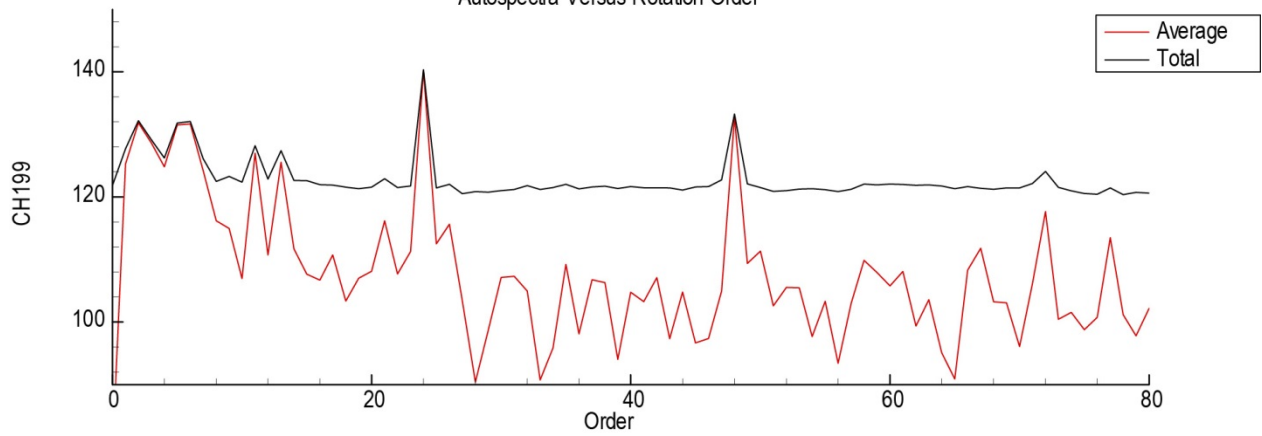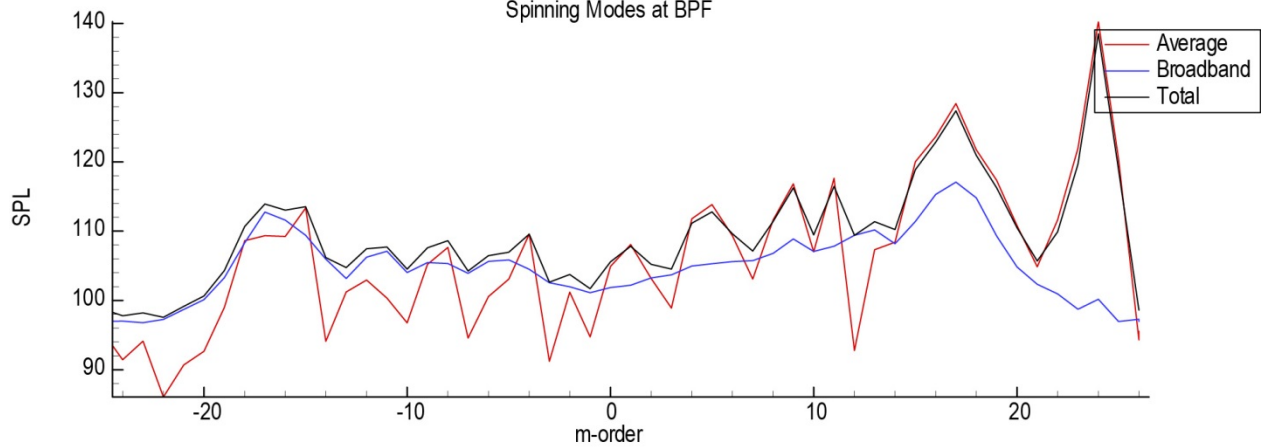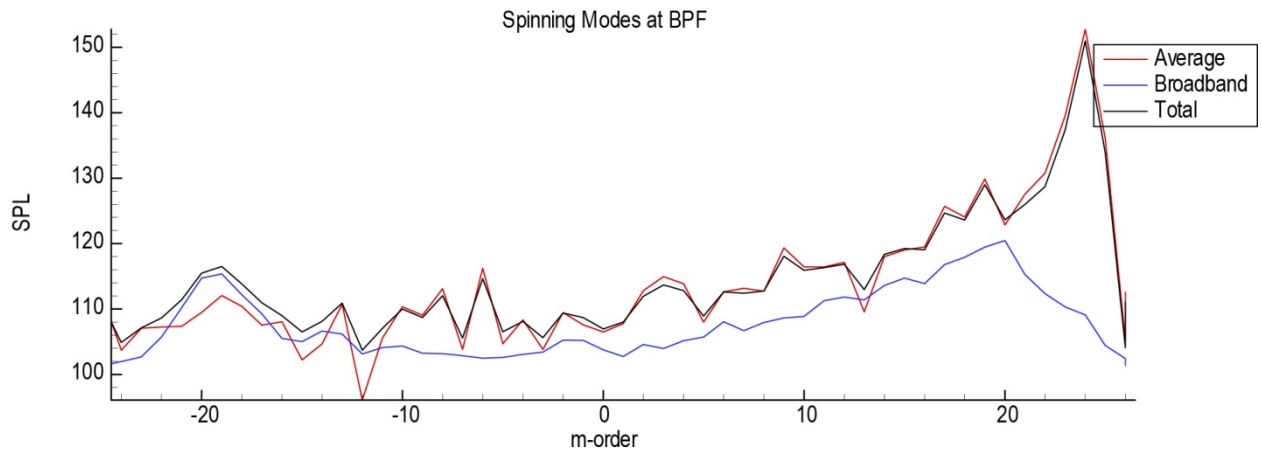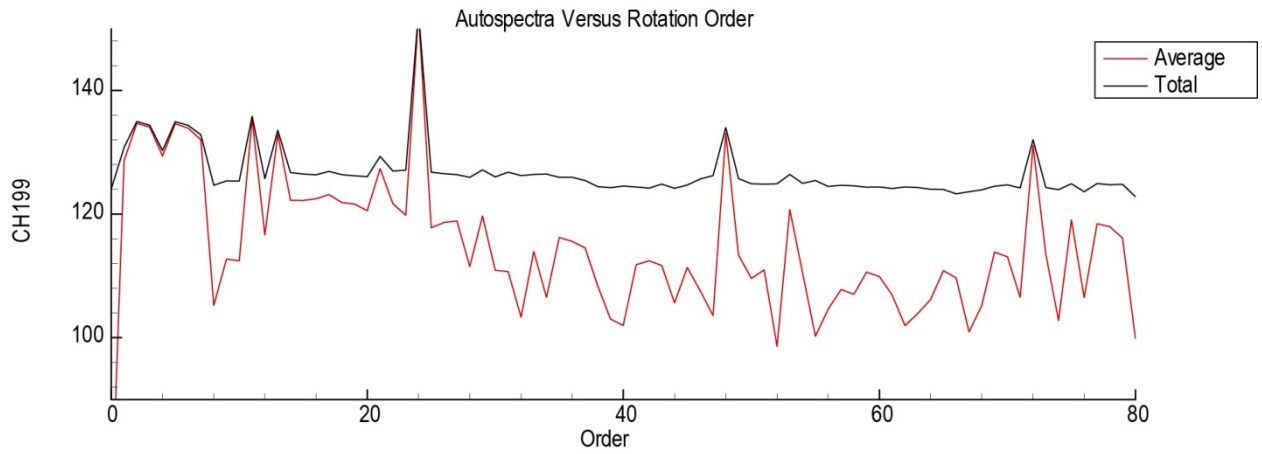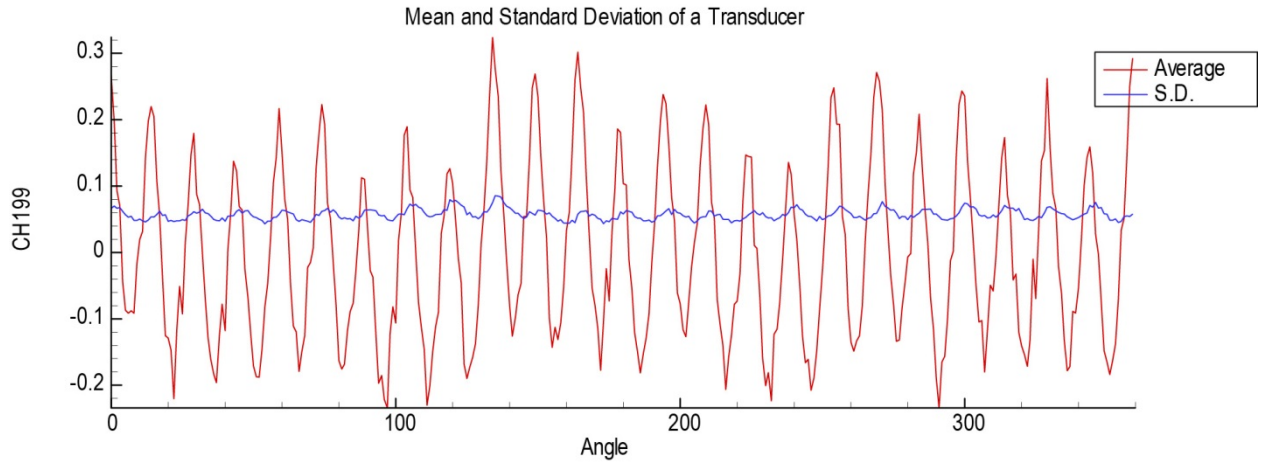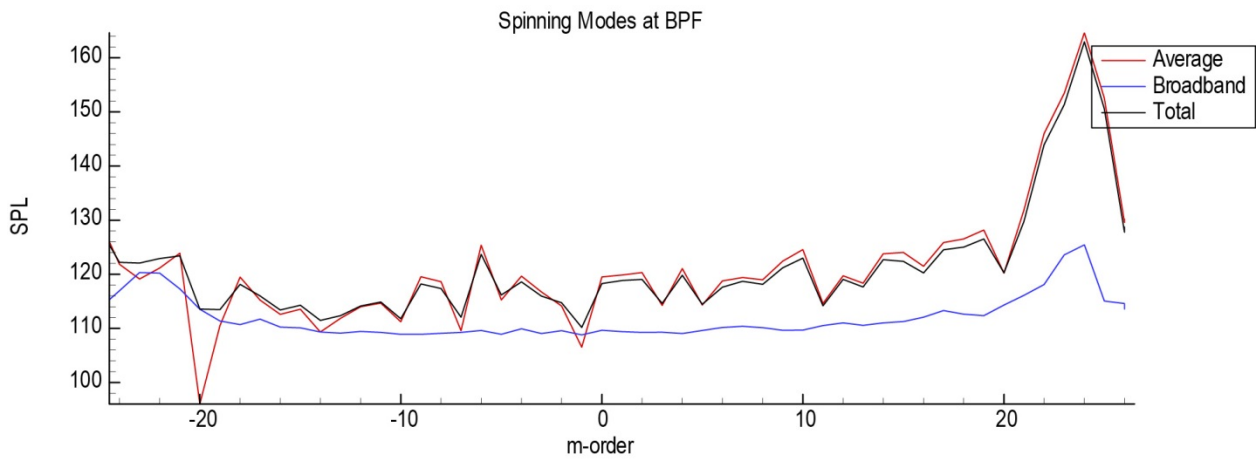## EVNRC Test Mode Ring Results
ACTIVE3: BOM Trtd Inlet, HW Passive, Uncovered Drivers
(Run 11606, N1C=1745 rpm)

Mean and Standard Deviation of a Transducer

Autospectra Versus Rotation Order

Spinning Modes at BPF
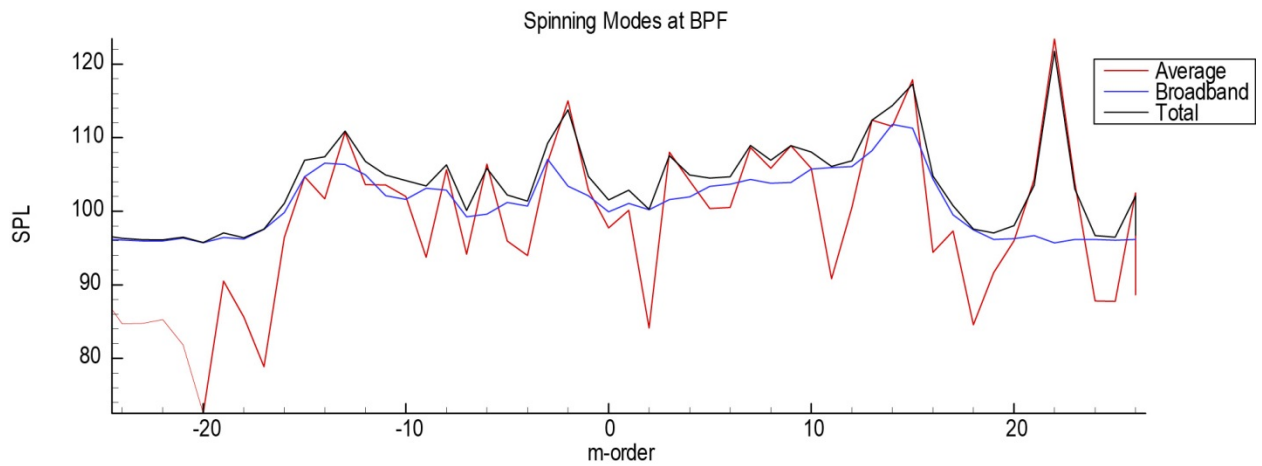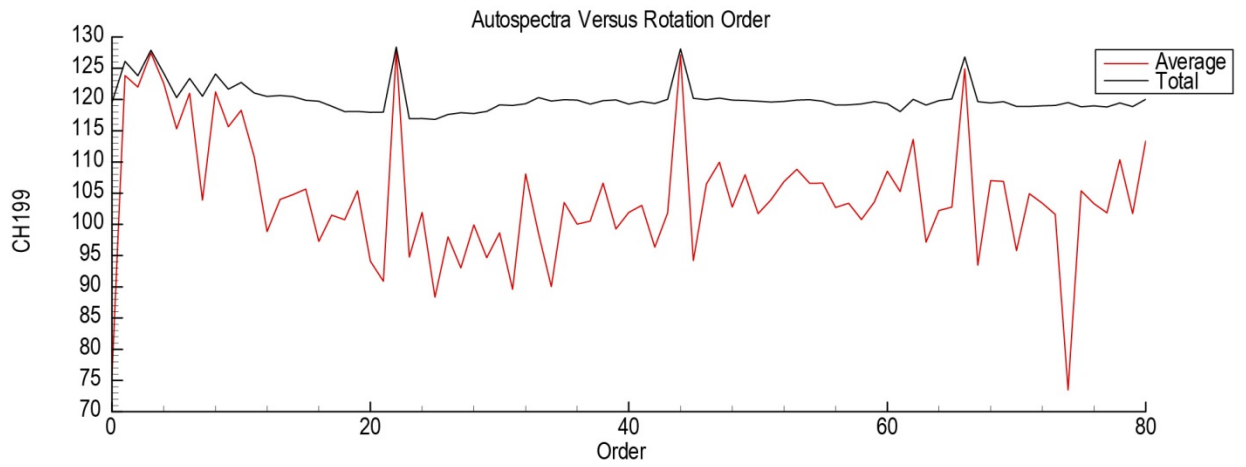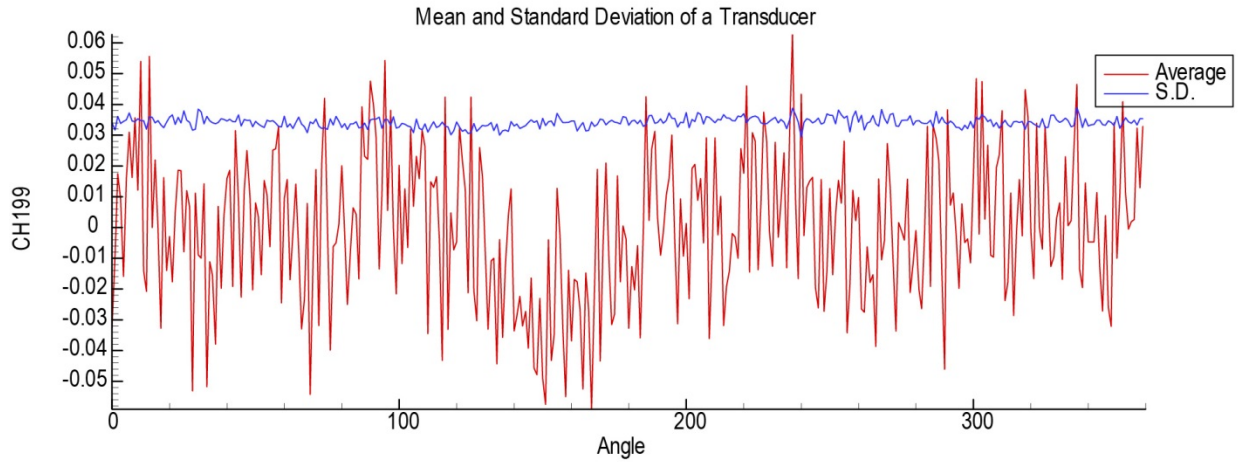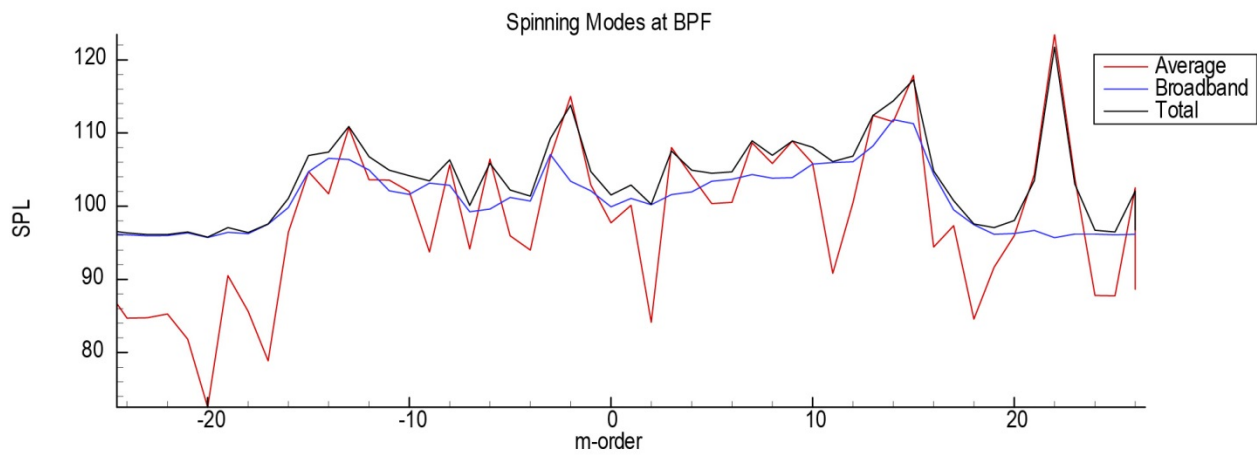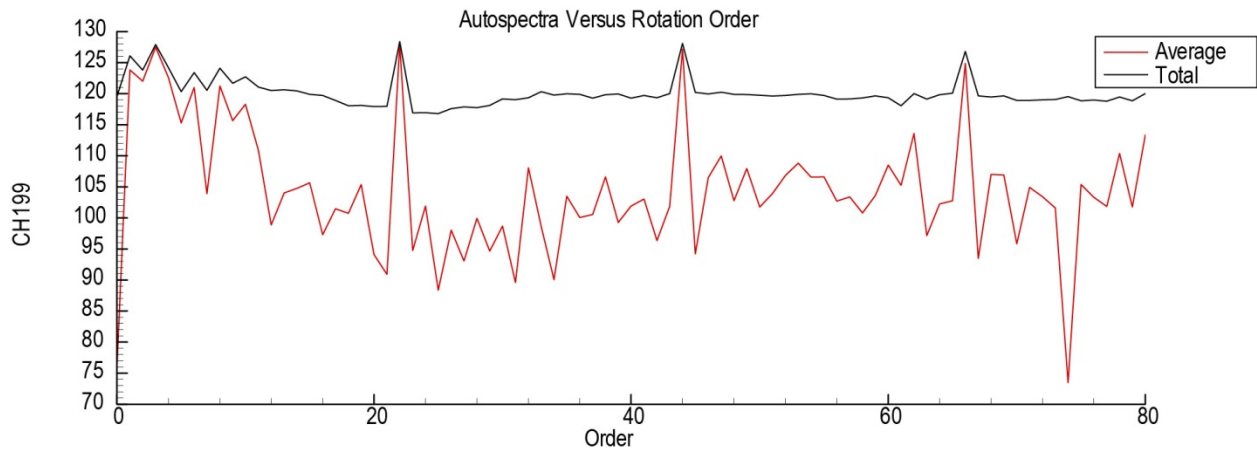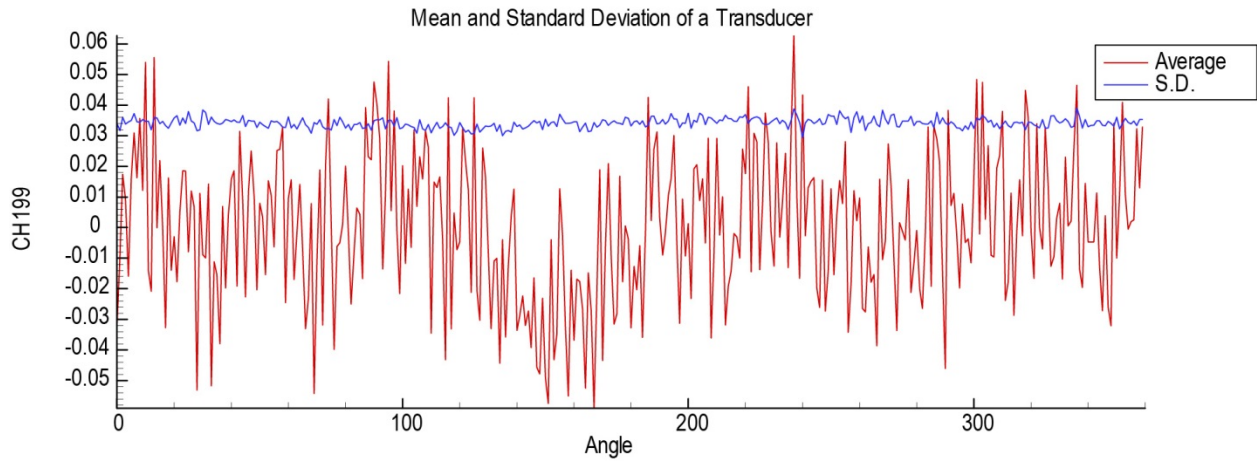
EVNRC Test Mode Ring Results
ACTIVE3: BOM Trtd Inlet, HW Passive, Uncovered Drivers
(Run 11607, N1C=1800 rpm)

Mean and Standard Deviation of a Transducer

Autospectra Versus Rotation Order

Spinning Modes at BPF
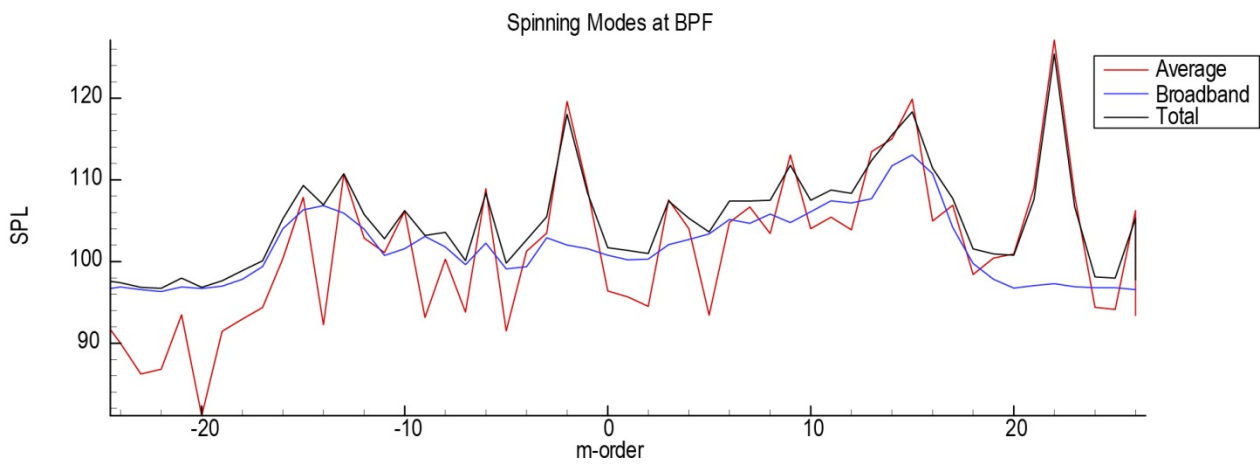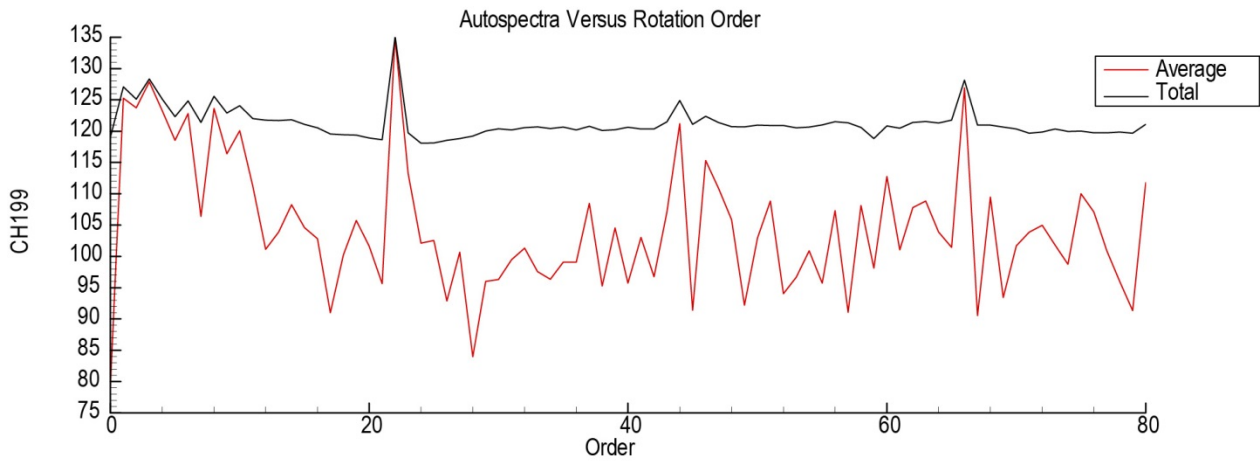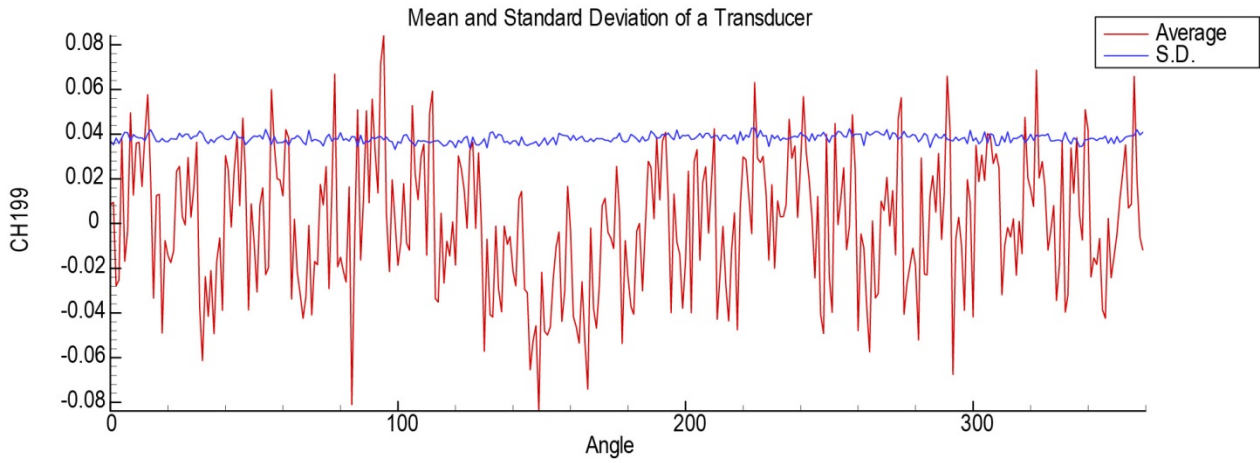
EVNRC Test Mode Ring Results
ACTIVE3: BOM Trtd Inlet, HW Passive, Uncovered Drivers
(Run 11608, N1C=1909 rpm)

Mean and Standard Deviation of a Transducer

Autospectra Versus Rotation Order

Spinning Modes at BPF
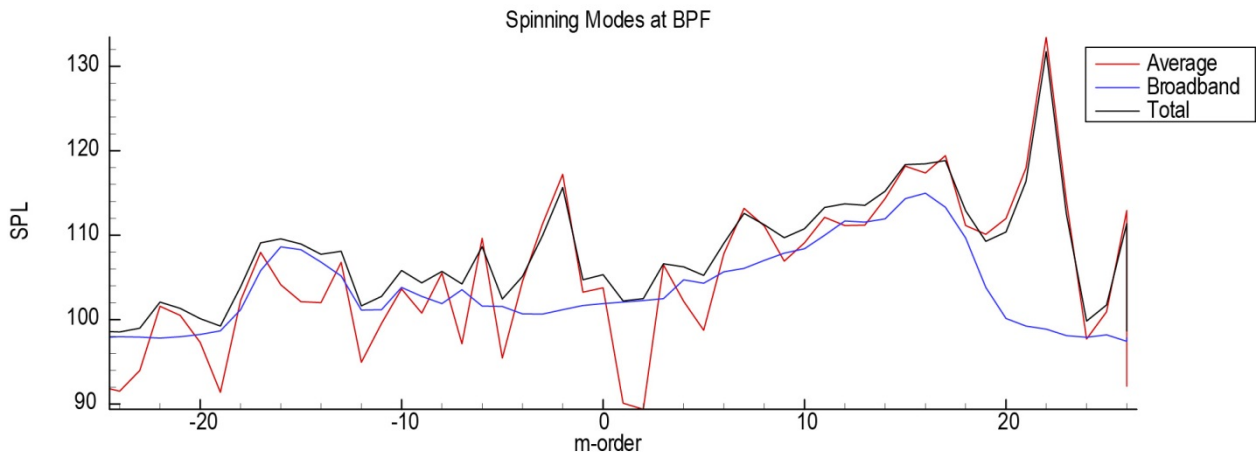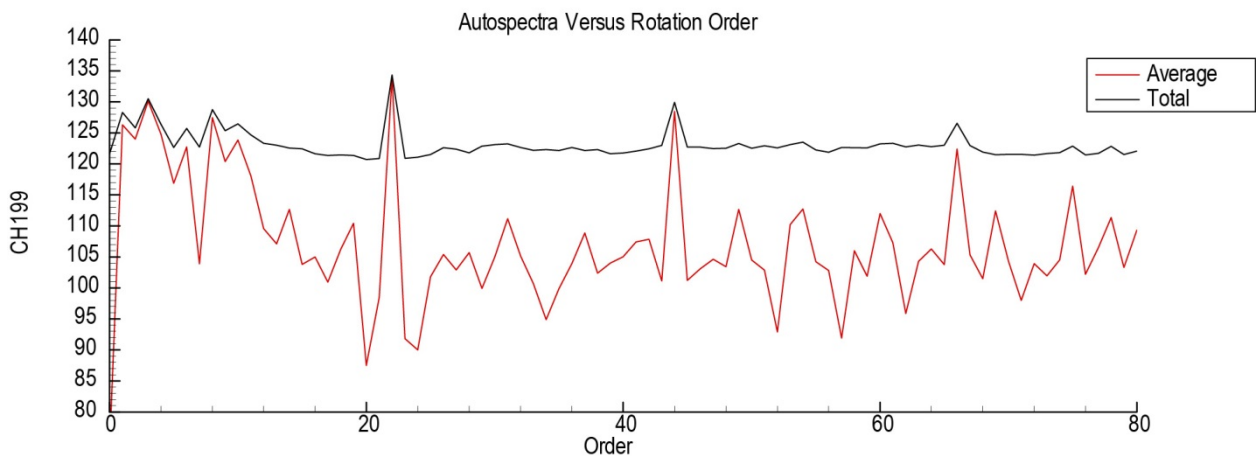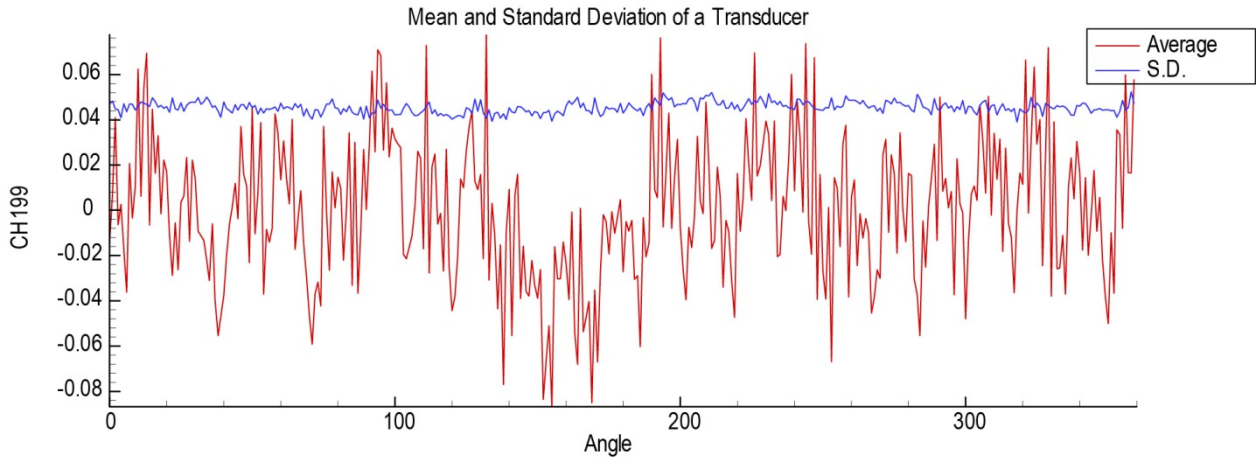
EVNRC Test Mode Ring Results
ACTIVE3: BOM Trtd Inlet, HW Passive, Uncovered Drivers
(Run 11609, N1C=2045 rpm)
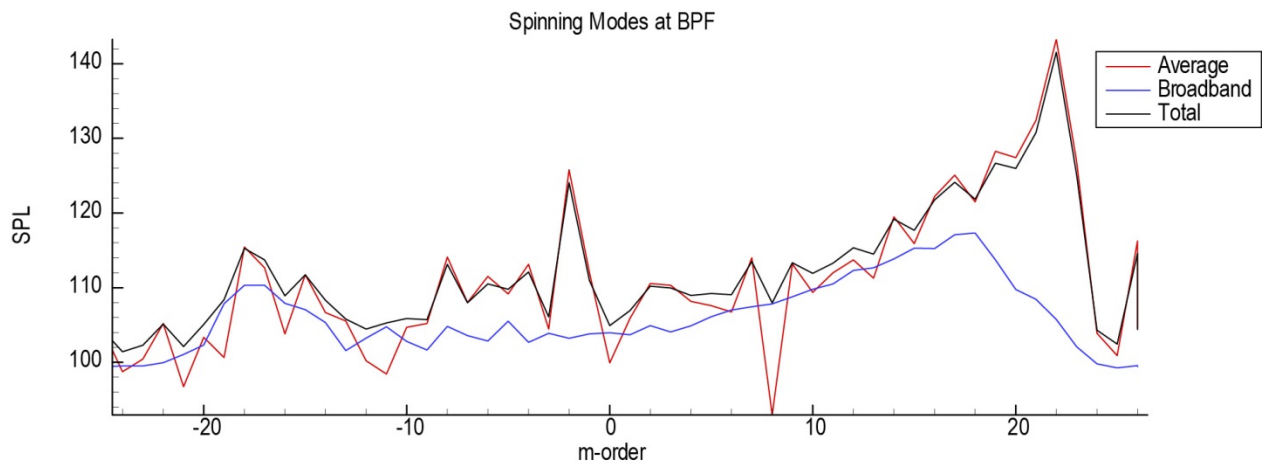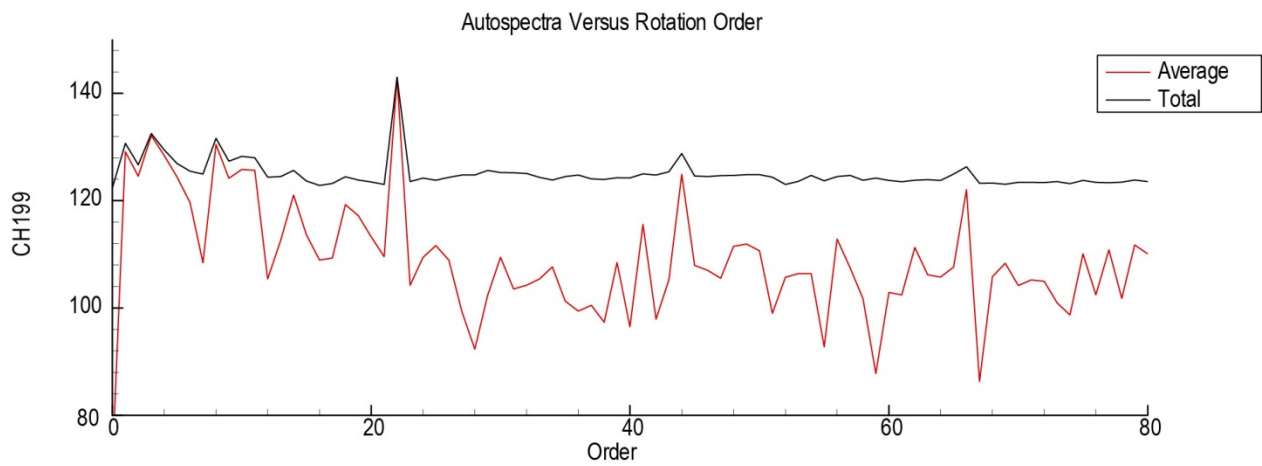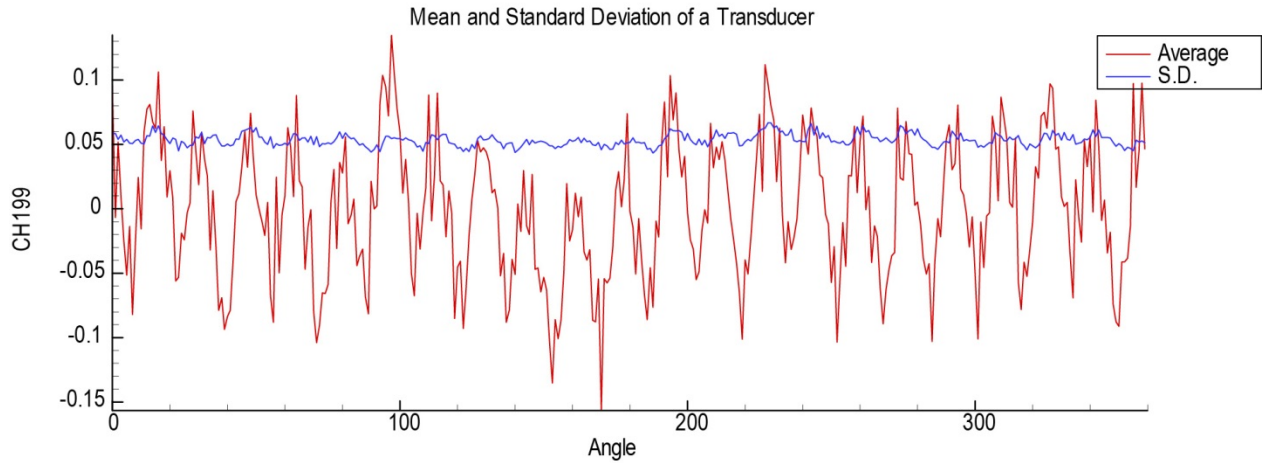
EVNRC Test Mode Ring Results
ACTIVE3: BOM Trtd Inlet, HW Passive, Uncovered Drivers
(Run 11610, N1C=2182 rpm)

Mean and Standard Deviation of a Transducer

Autospectra Versus Rotation Order

Spinning Modes at BPF
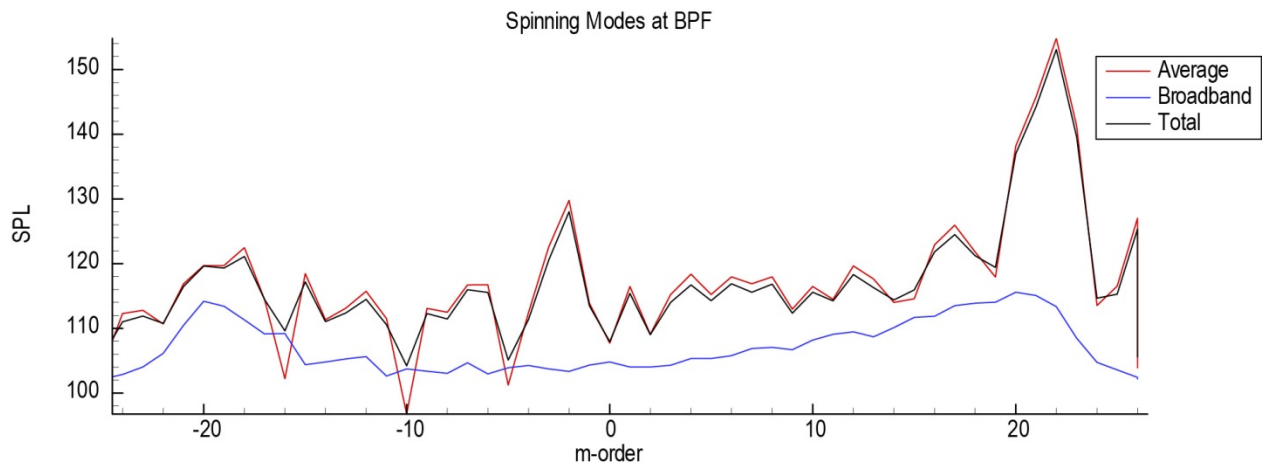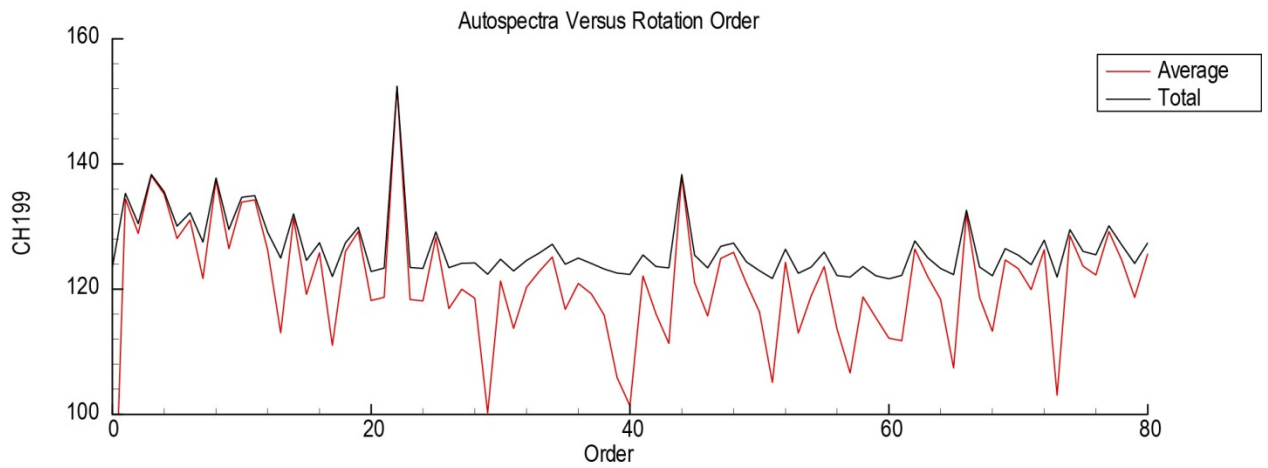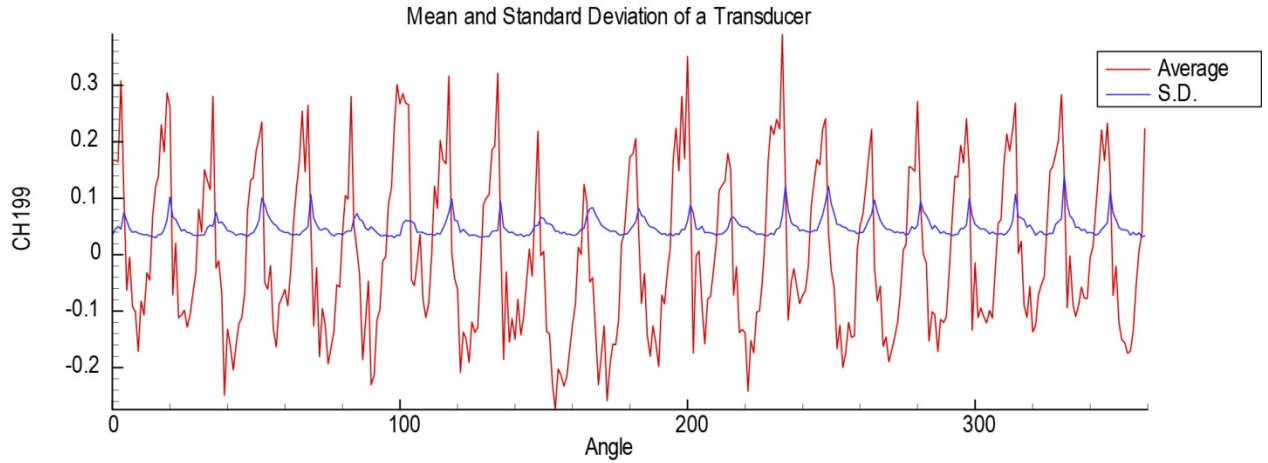
EVNRC Test Mode Ring Results
ACTIVE3: BOM Trtd Inlet, HW Passive, Uncovered Drivers
(Run 11611, N1C=2318 rpm)

Mean and Standard Deviation of a Transducer

Autospectra Versus Rotation Order

Spinning Modes at BPF
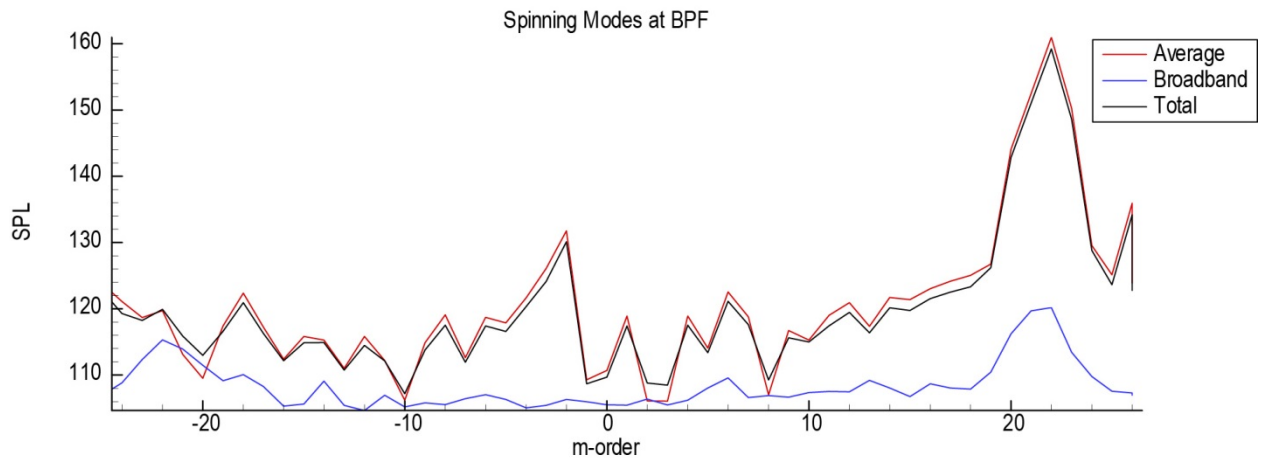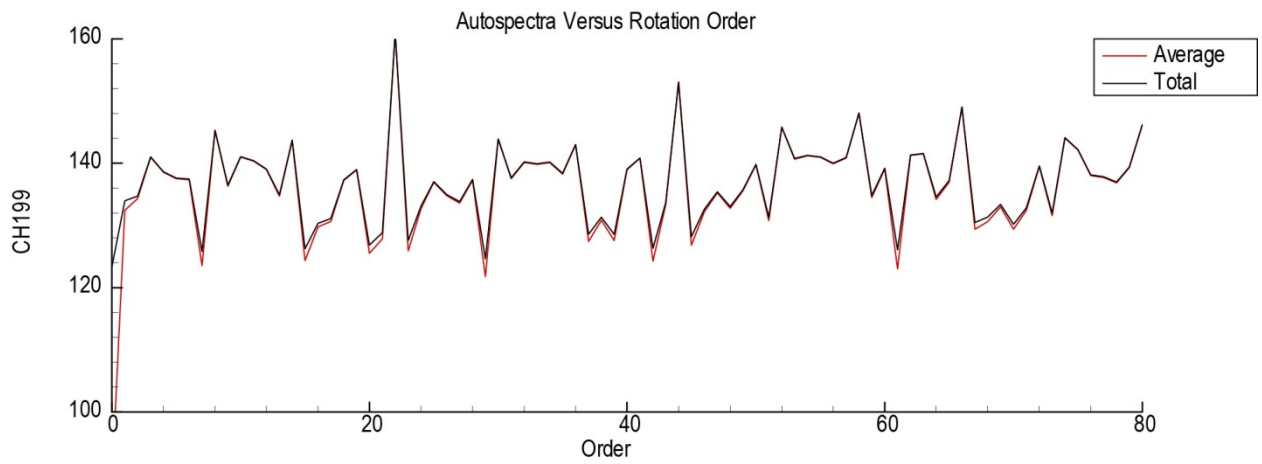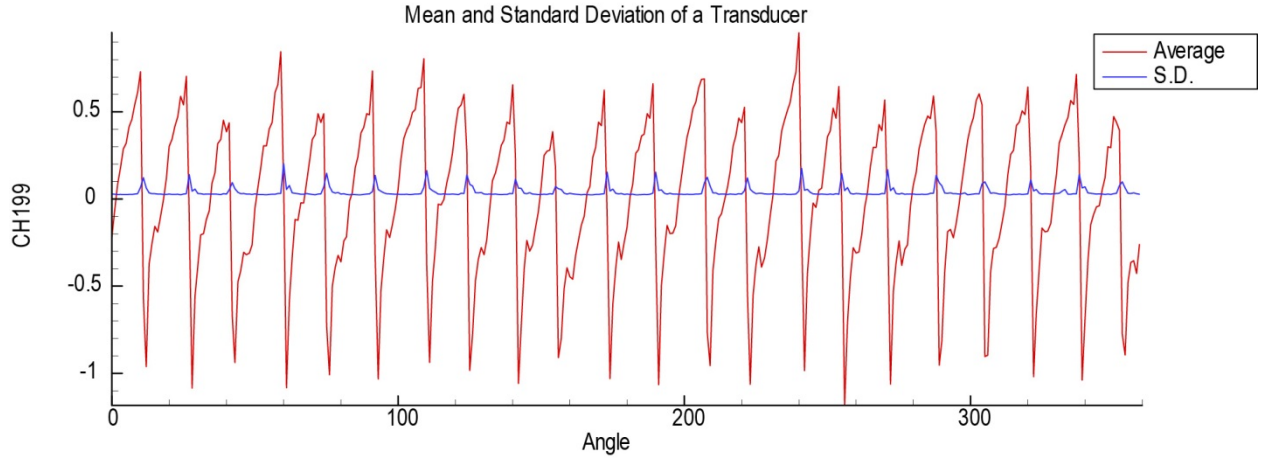
EVNRC Test Mode Ring Results
EVNRC1: BOM Trtd Inlet, HW Spool, 22B,28V
(Run 11705, N1C=1620 rpm)
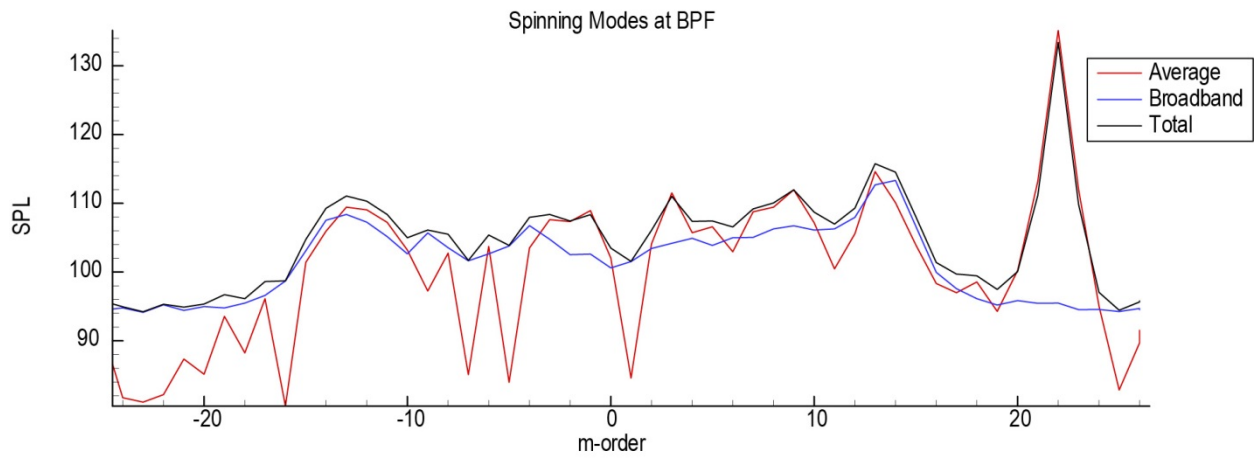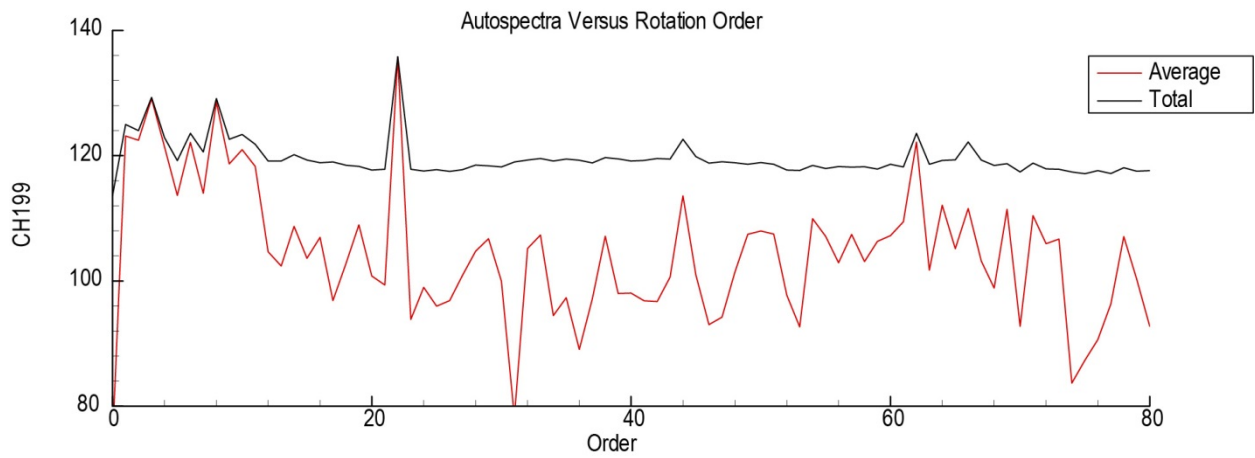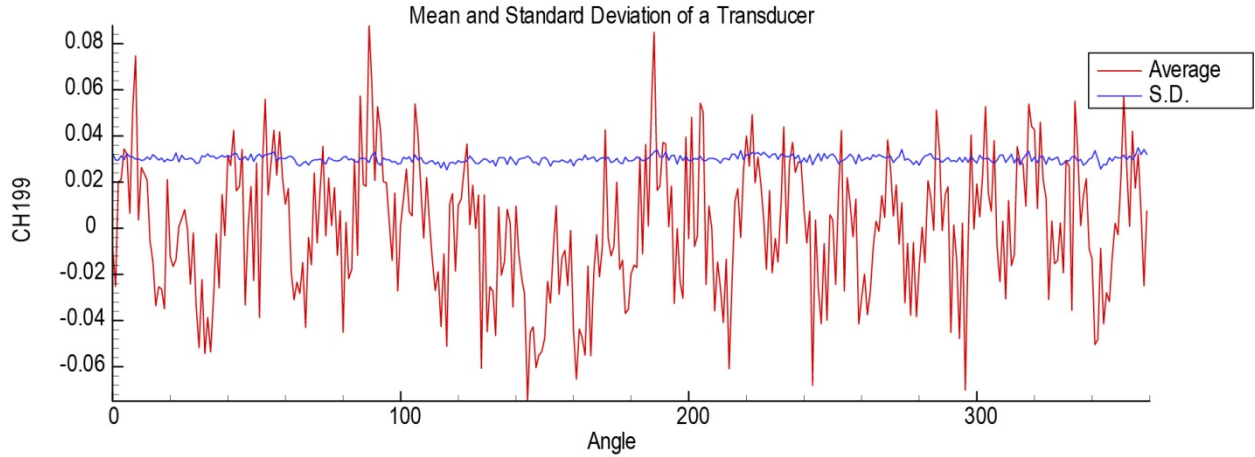
EVNRC Test Mode Ring Results
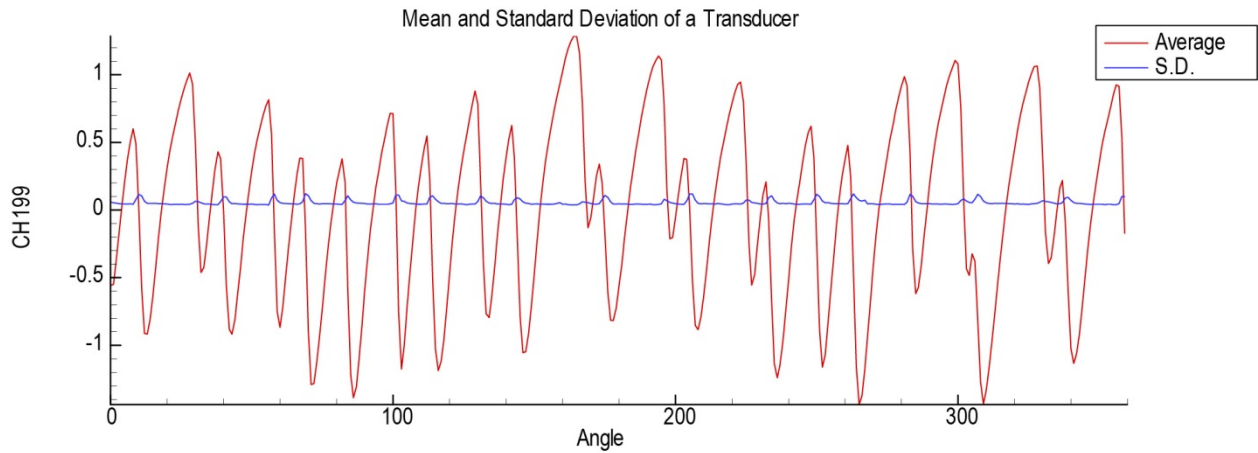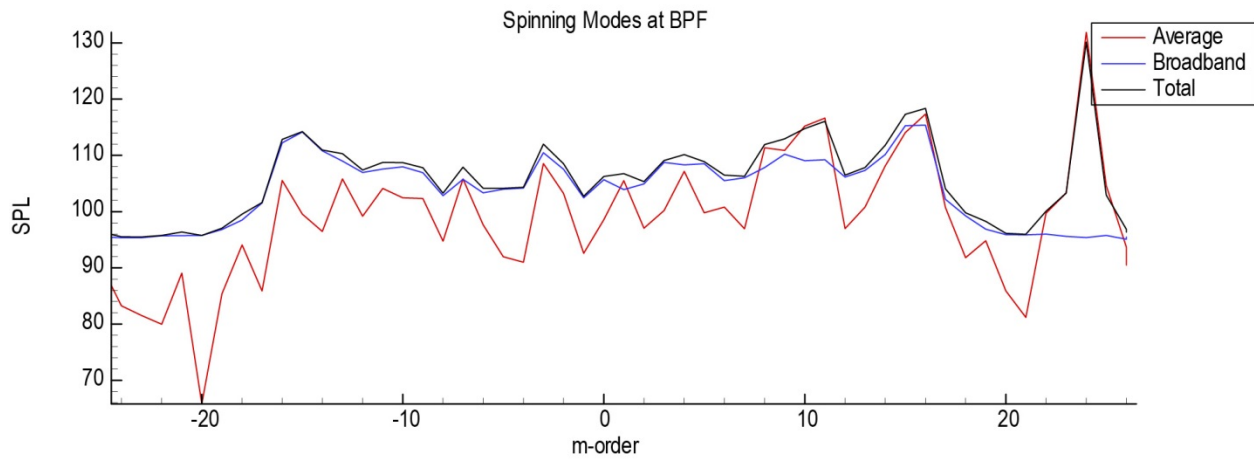EVNRC1: BOM Trtd Inlet, HW Spool, 22B,28V
(Run 11708, N1C=1800 rpm)
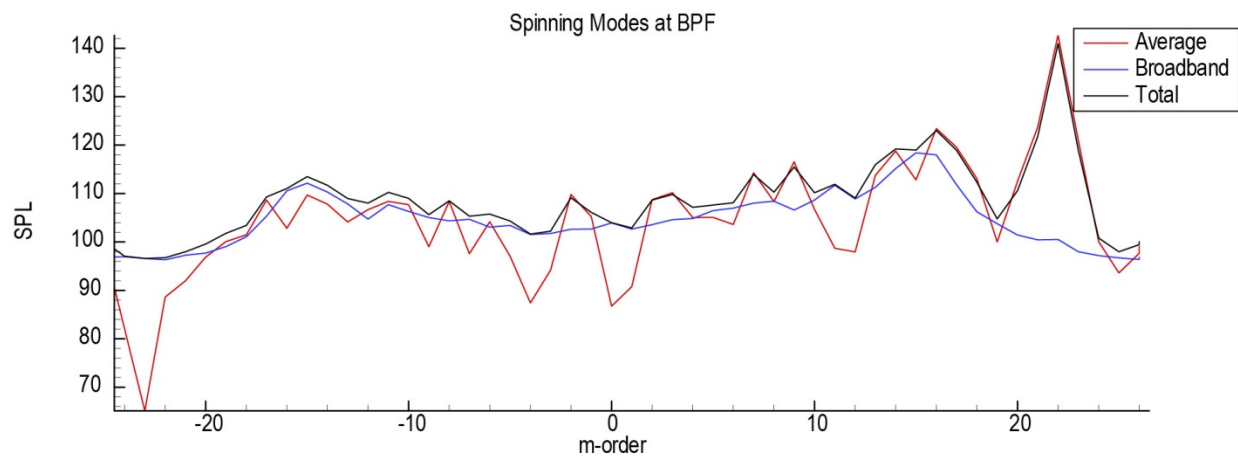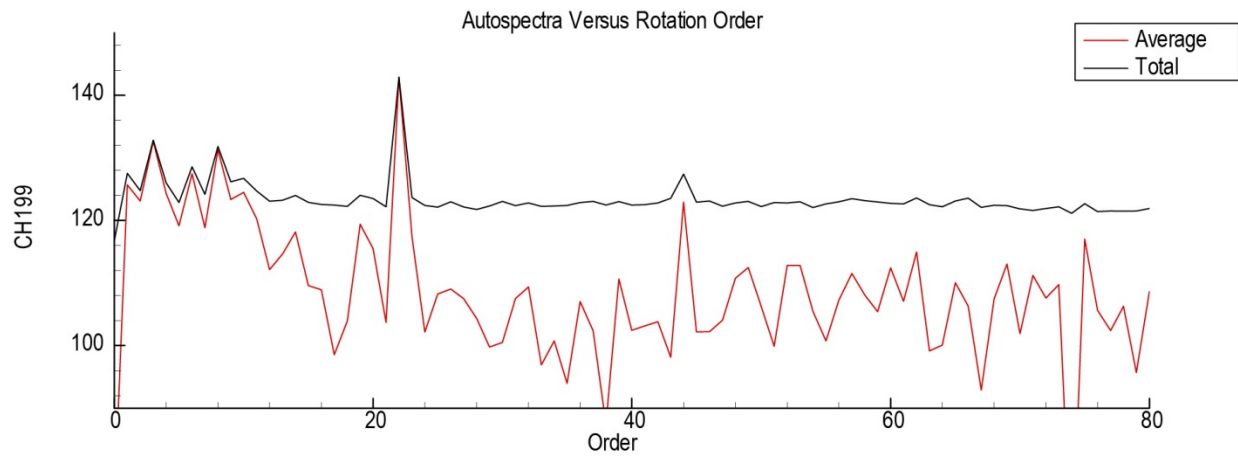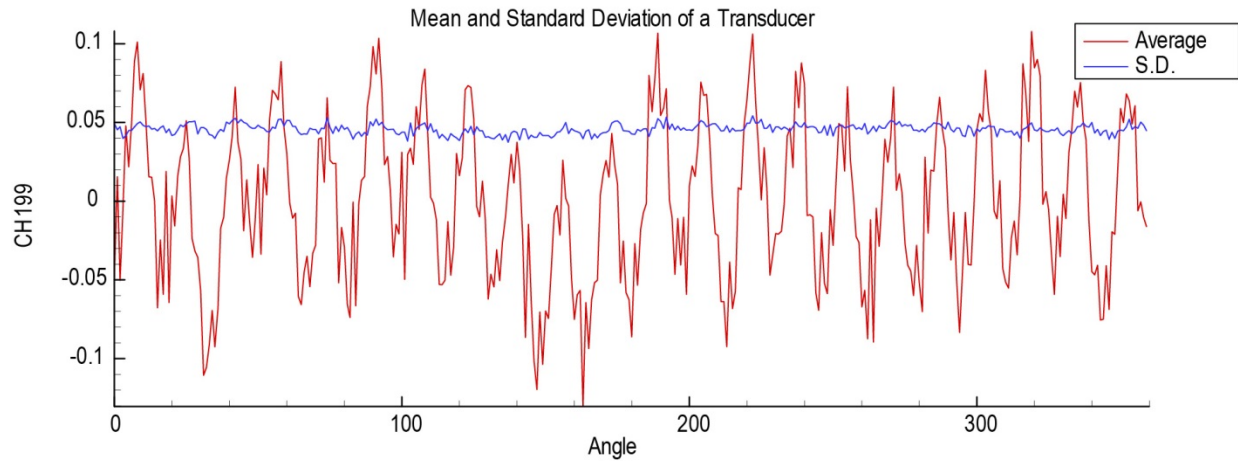
EVNRC Test Mode Ring Results
EVNRC1: BOM Trtd Inlet, HW Spool, 22B,28V
(Run 11712, N1C=2200 rpm)

Mean and Standard Deviation of a Transducer

Autospectra Versus Rotation Order
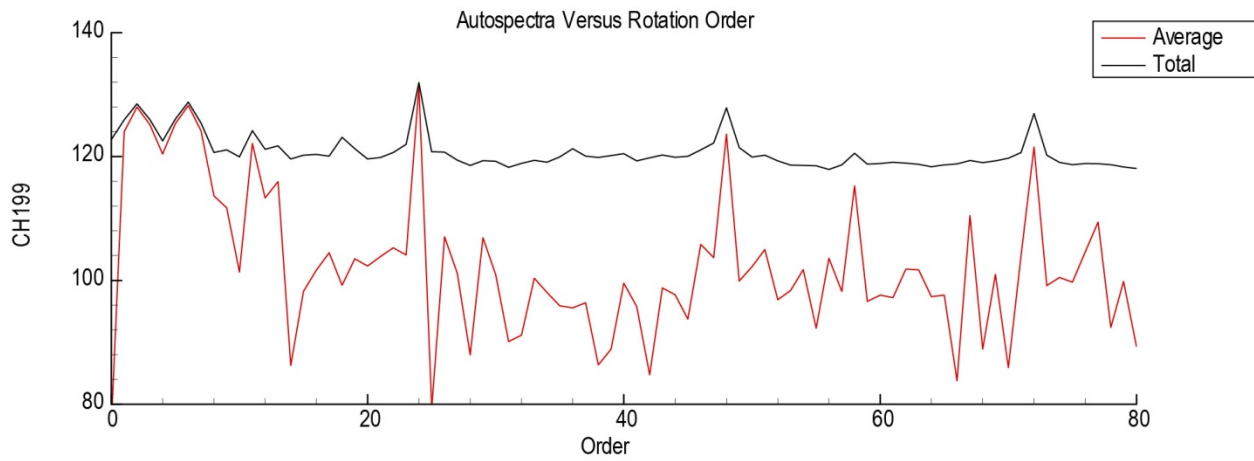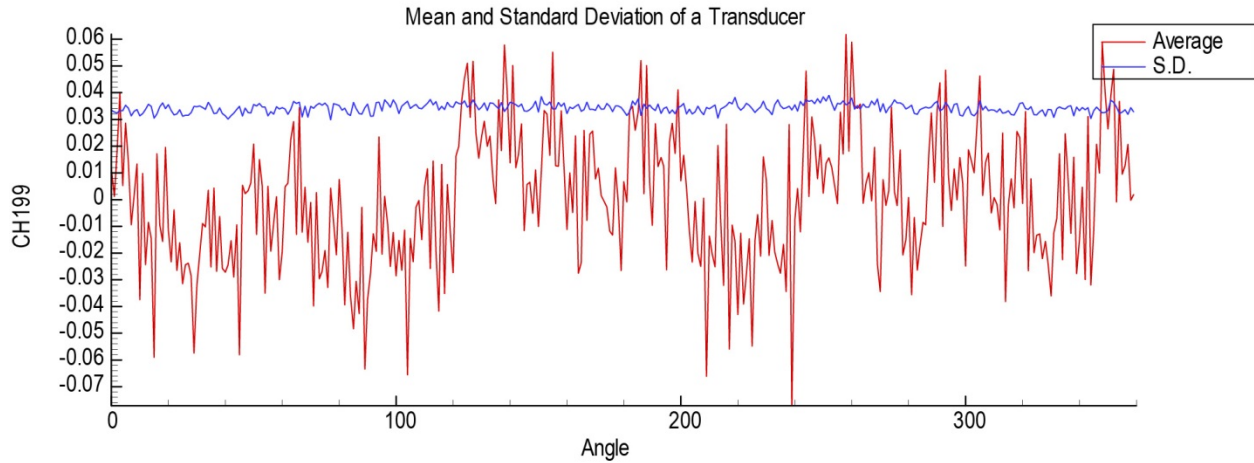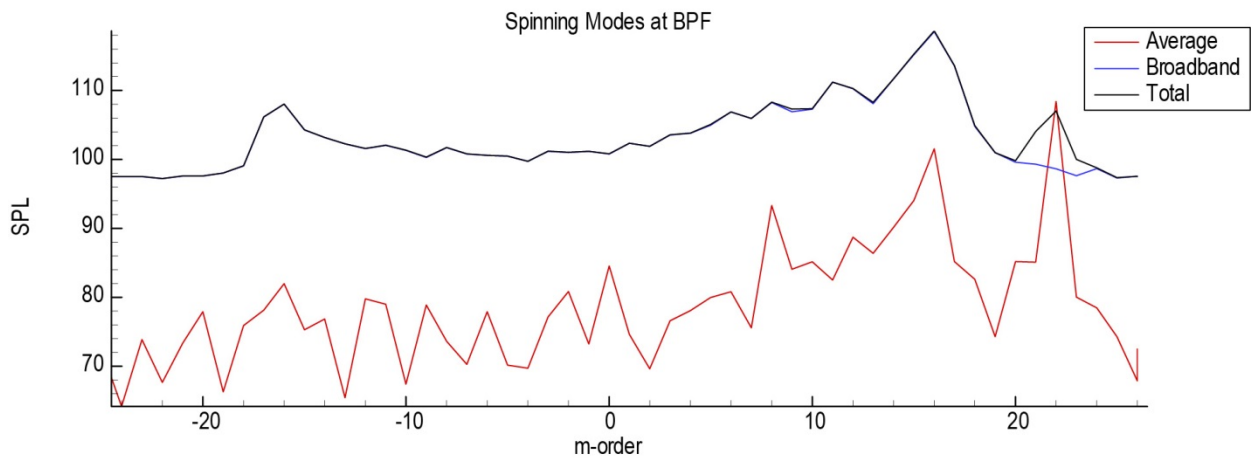

Spinning Modes at BPF
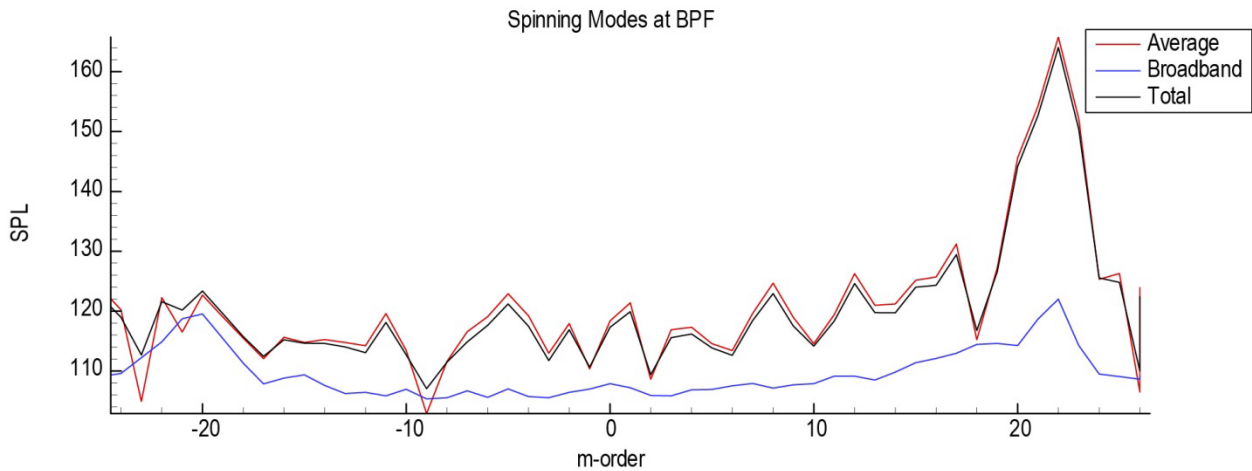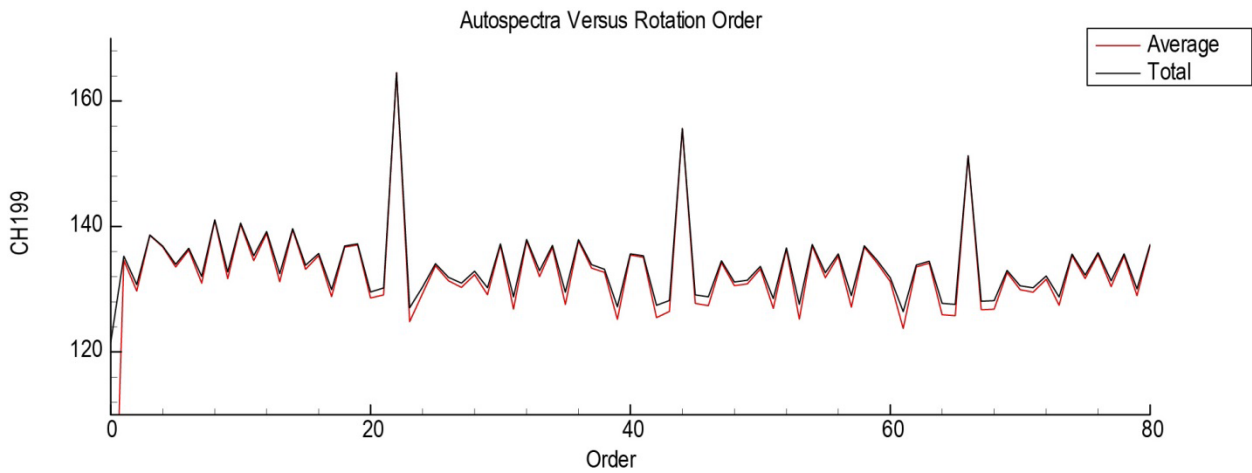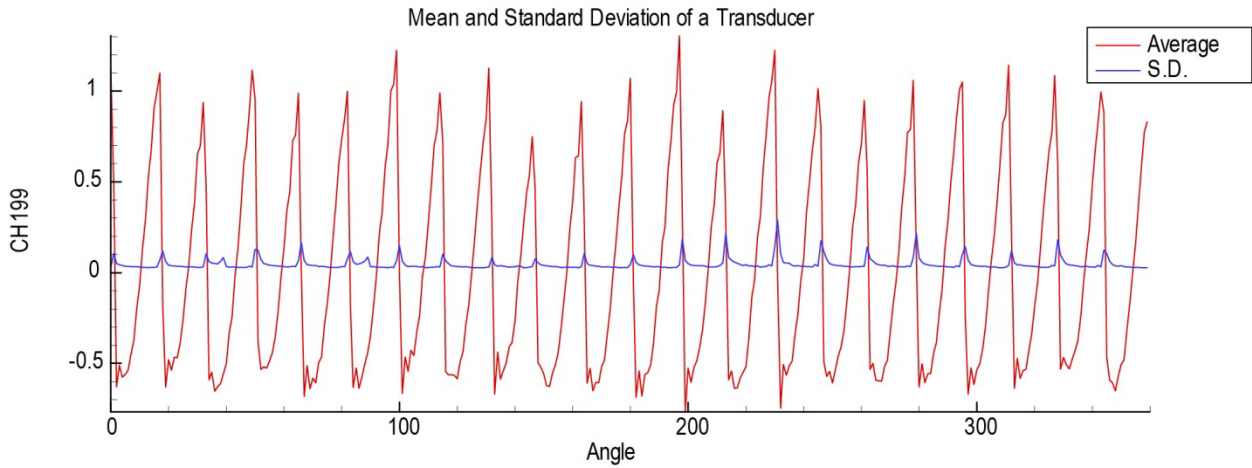
EVNRC Test Mode Ring Results
EVNRC1: BOM Trtd Inlet, HW Spool, 22B, 28V
(Run 11715, N1C=2450 rpm)
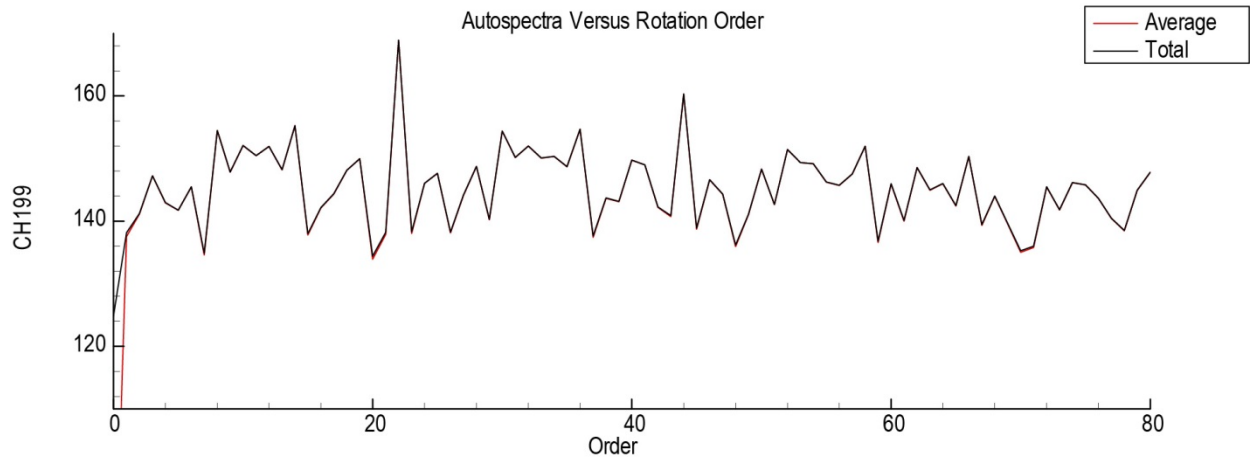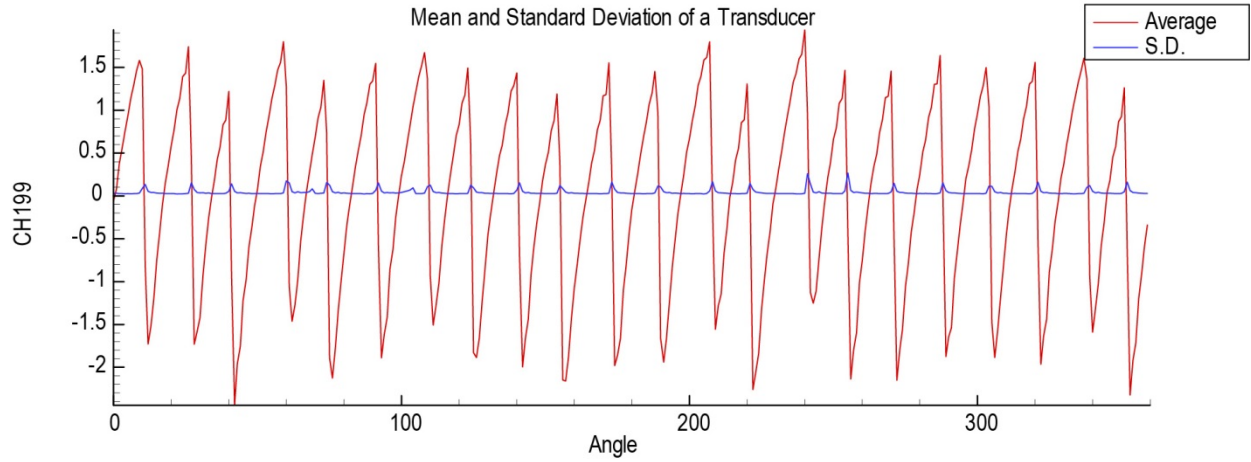
EVNRC Test Mode Ring Results
EVNRC1: BOM Trtd Inlet, HW Spool, 22B, 28V
(Run 11718, N1C=2700 rpm)

Mean and Standard Deviation of a Transducer

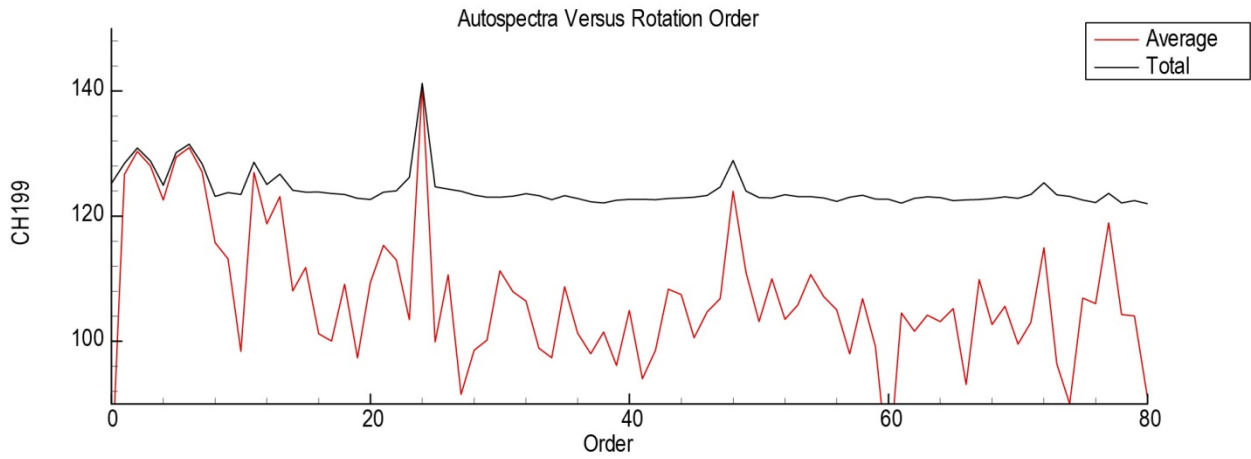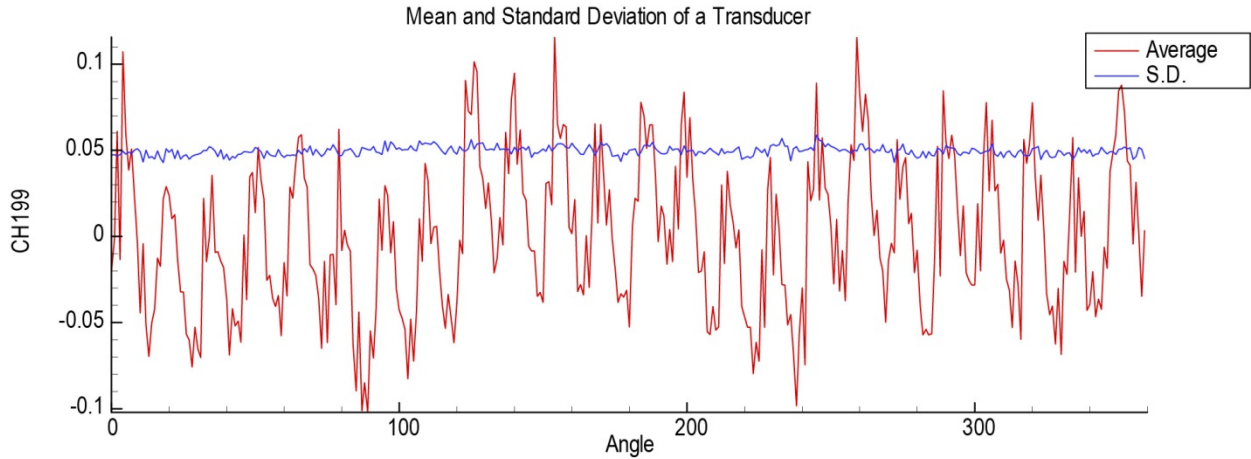Autospectra Versus Rotation Order

Spinning Modes at BPF
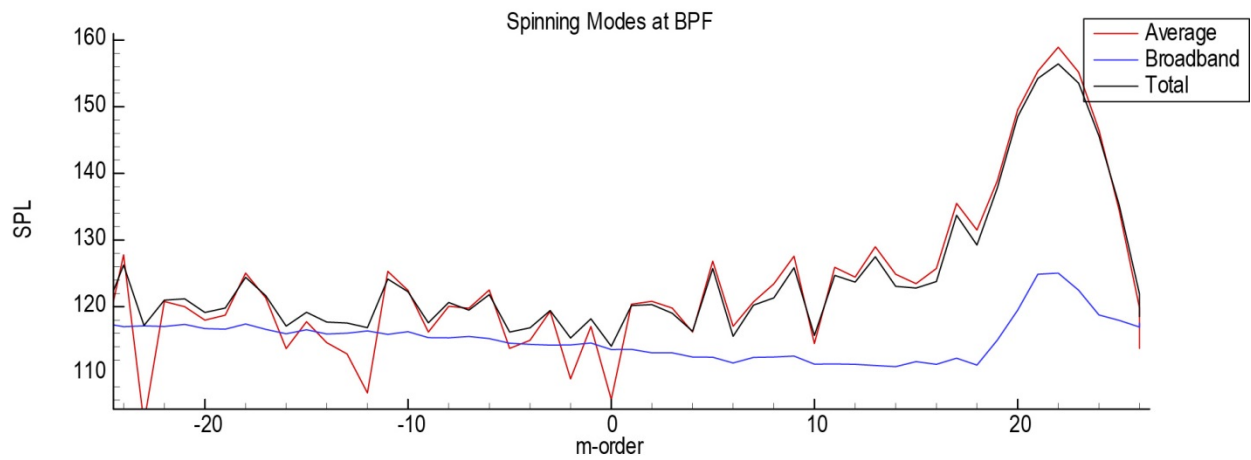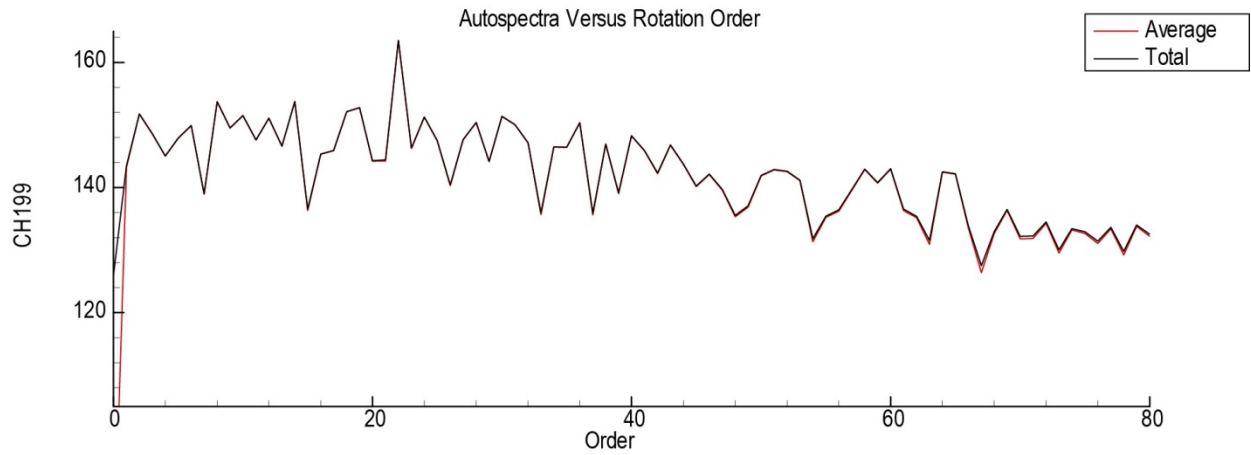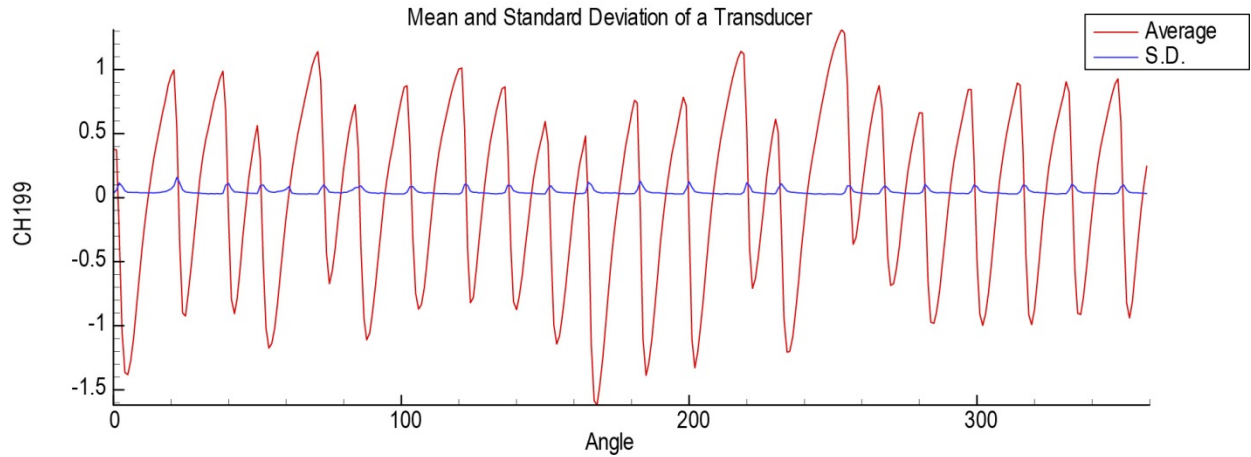
EVNRC Test Mode Ring Results
EVNRC1: BOM Trtd Inlet, HW Spool, 22B, 28V
(Run 11719, N1C=2743 rpm)

Mean and Standard Deviation of a Transducer

Autospectra Versus Rotation Order

Spinning Modes at BPF
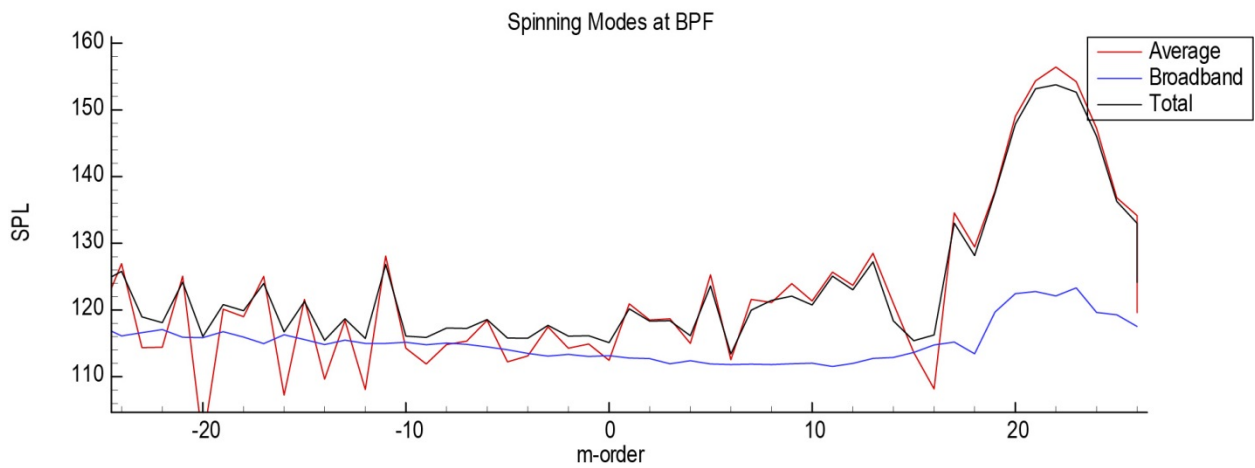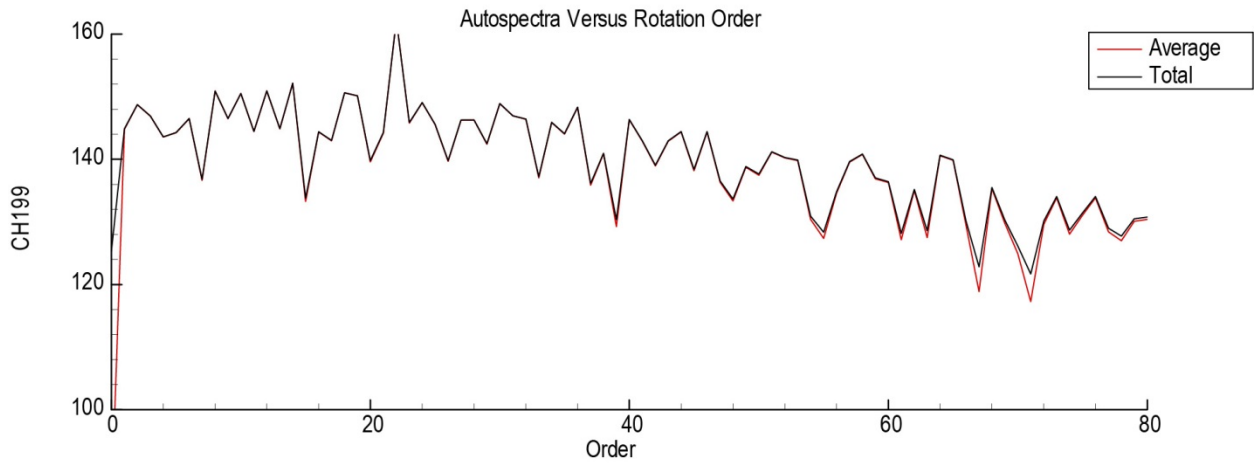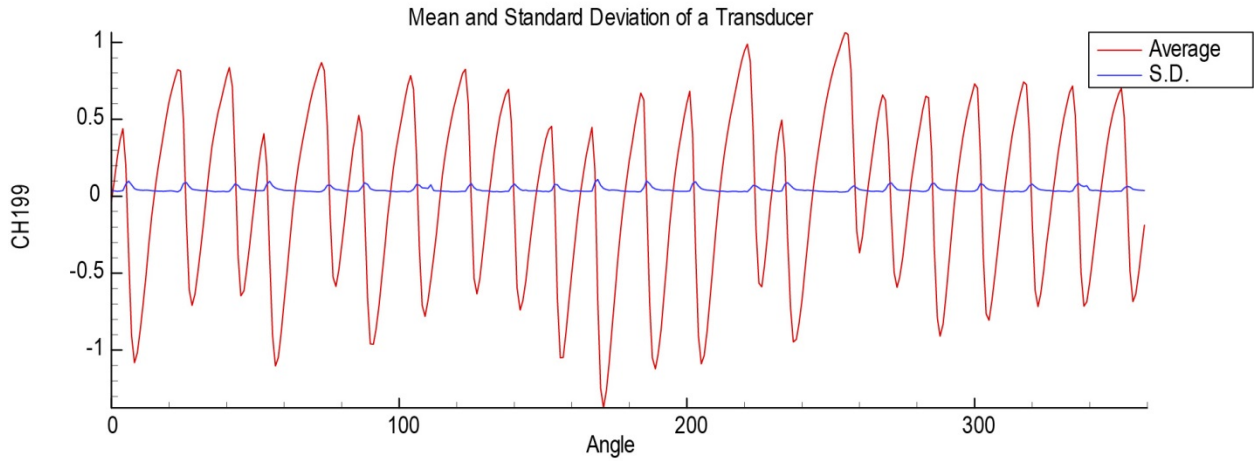
EVNRC Test Mode Ring Results
EVNRC2: BOM Trtd Inlet, HW Spool, 24B, 28V
(Run 11807, N1C=580 rpm)

Mean and Standard Deviation of a Transducer

Autospectra Versus Rotation Order

Spinning Modes at BPF
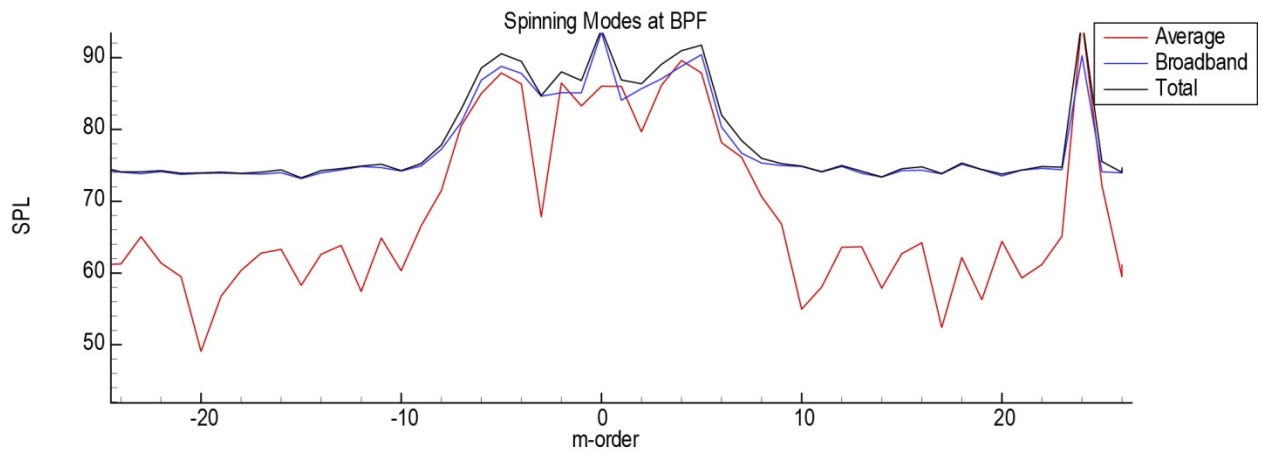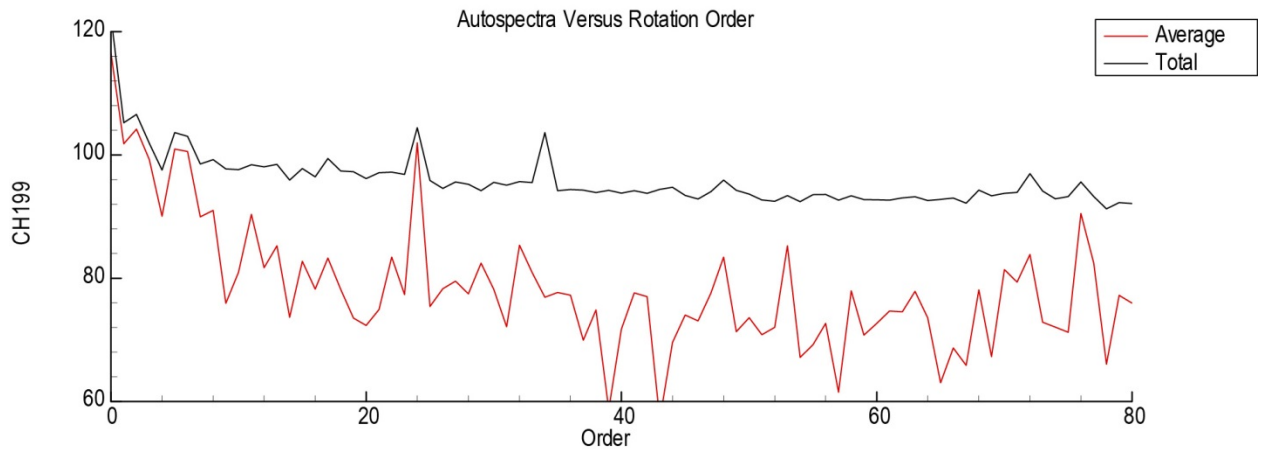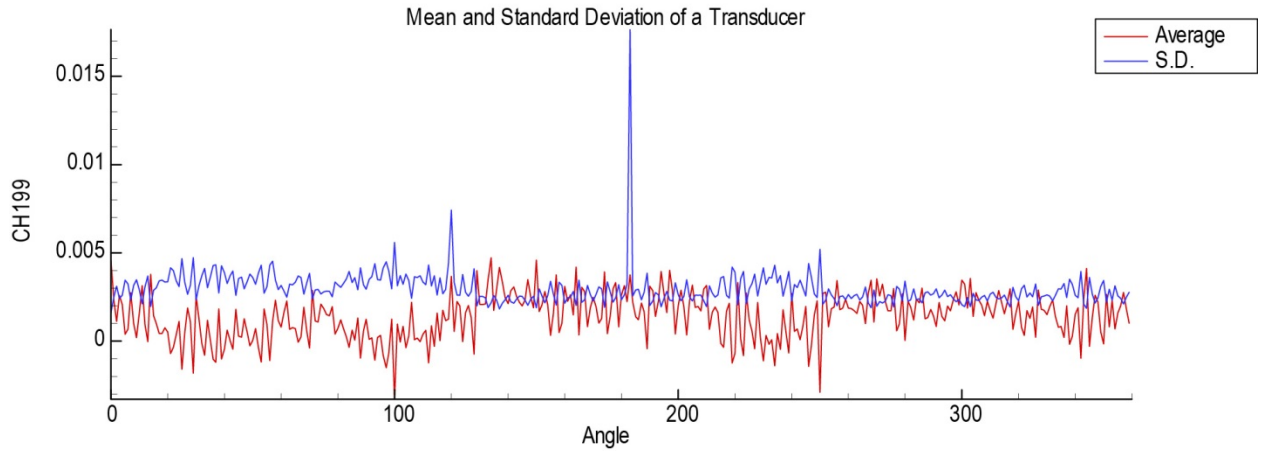
EVNRC Test Mode Ring Results
EVNRC2: BOM Trtd Inlet, HW Spool, 24B, 28V
(Run 11808, N1C=1620 rpm)

Mean and Standard Deviation of a Transducer

Autospectra Versus Rotation Order

Spinning Modes at BPF
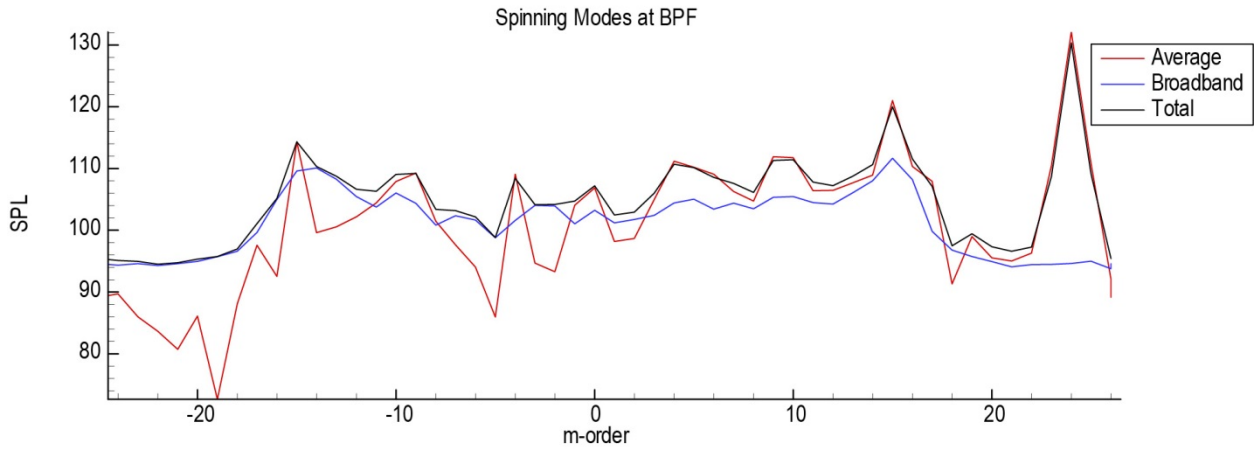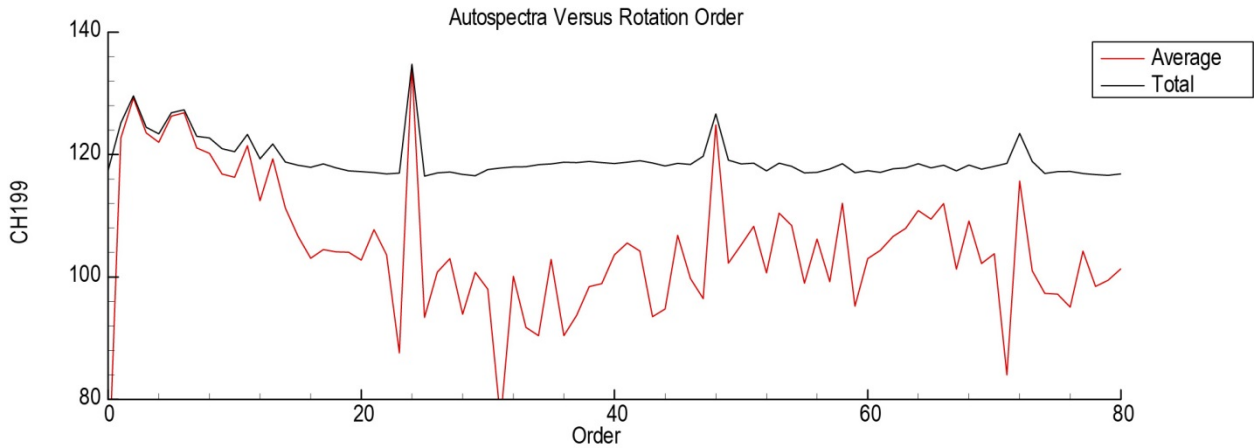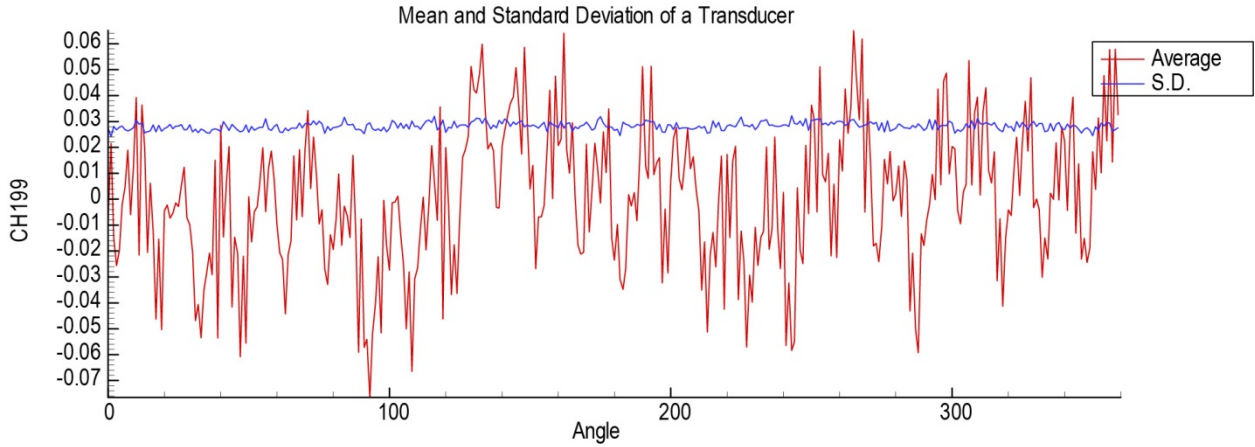
EVNRC Test Mode Ring Results
EVNRC2: BOM Trtd Inlet, HW Spool, 24B, 28V
(Run 11810, N1C=1800 rpm)

Mean and Standard Deviation of a Transducer

Autospectra Versus Rotation Order

Spinning Modes at BPF
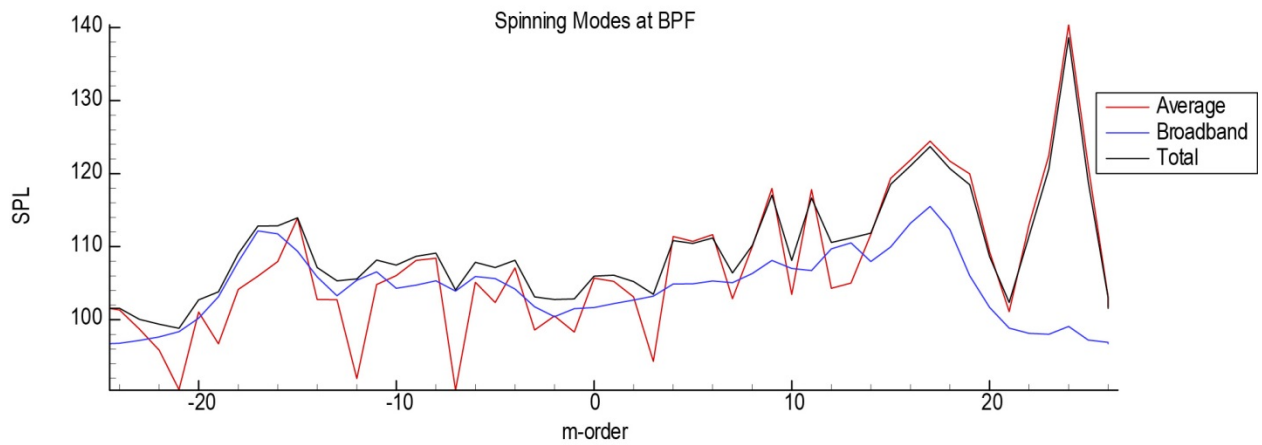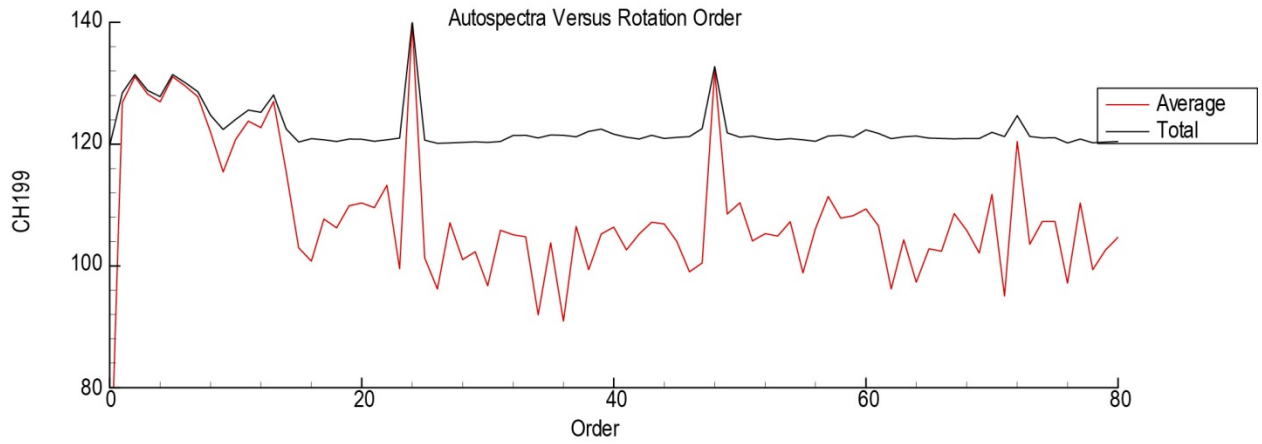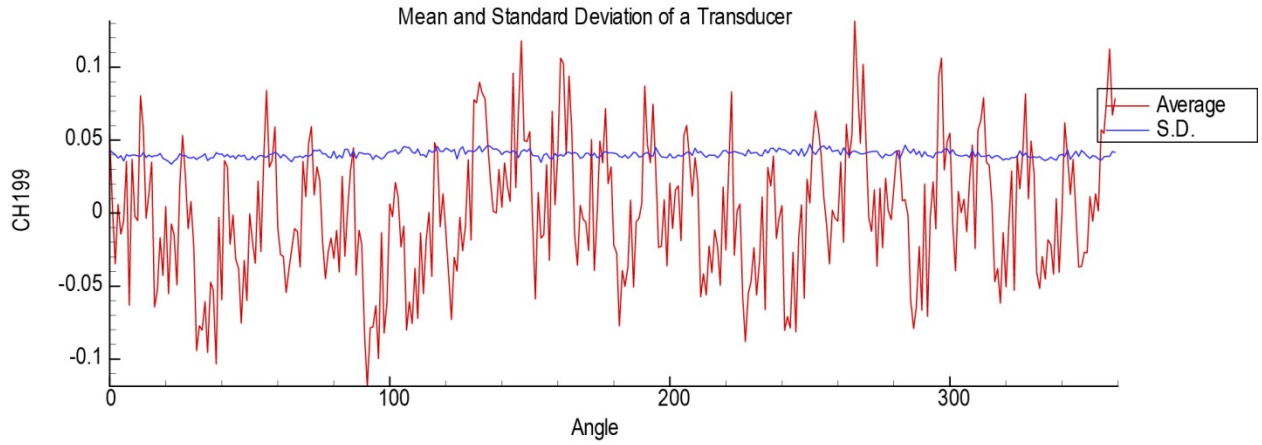
EVNRC Test Mode Ring Results
EVNRC2: BOM Trtd Inlet, HW Spool, 24B, 28V
(Run 11812, N1C=2000 rpm)

Mean and Standard Deviation of a Transducer

Autospectra Versus Rotation Order

Spinning Modes at BPF
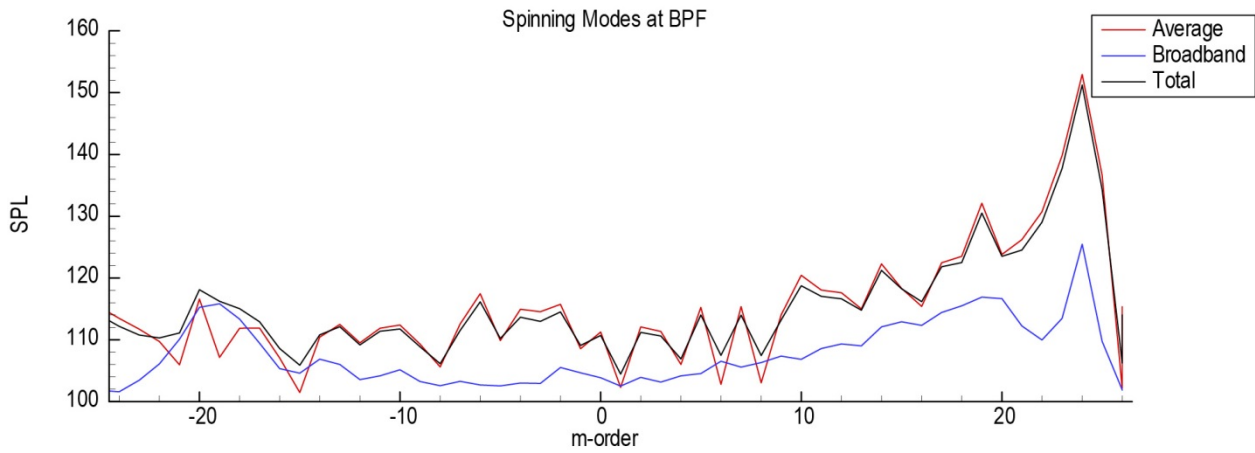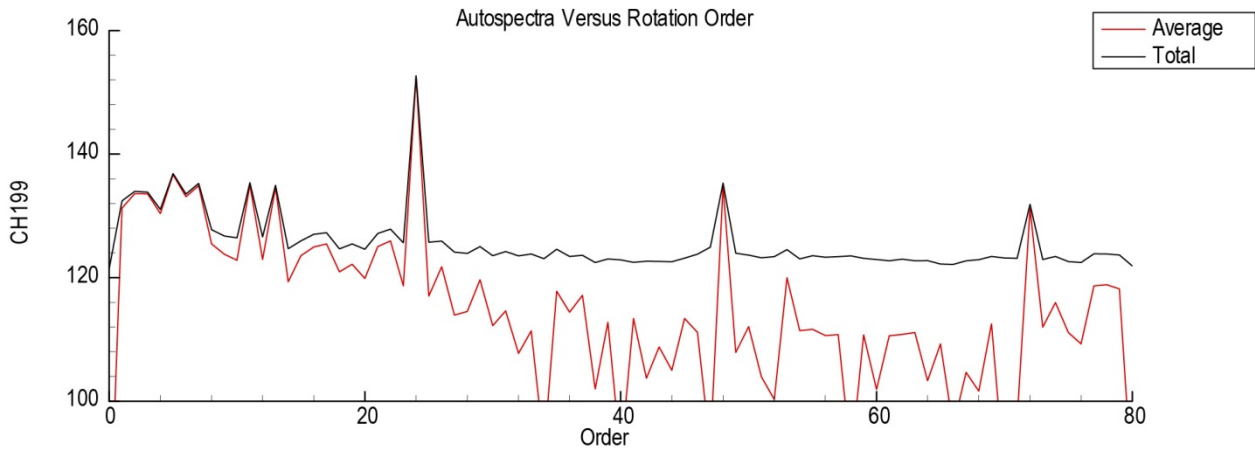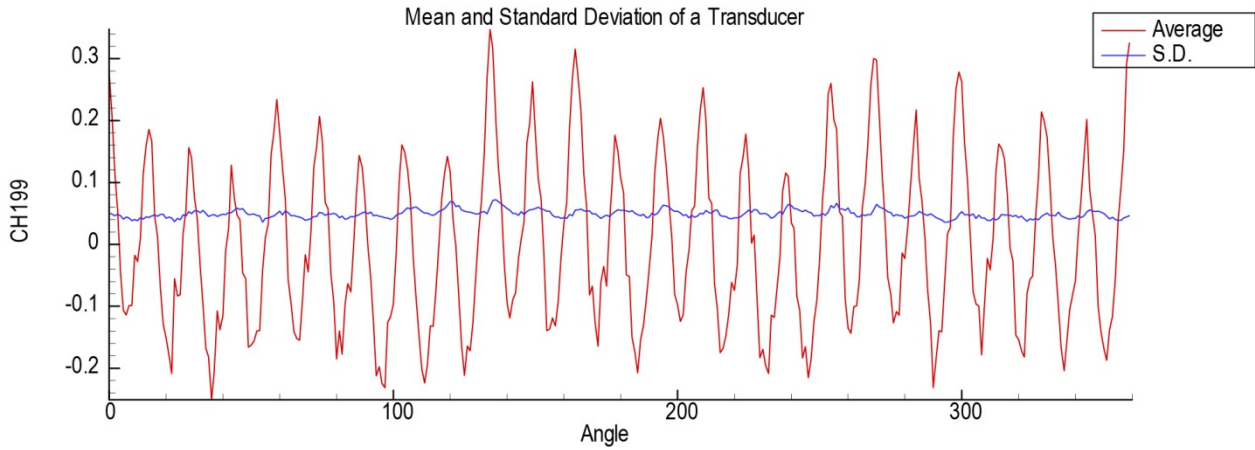
EVNRC Test Mode Ring Results
EVNRC2: BOM Trtd Inlet, HW Spool, 24B, 28V
(Run 11814, N1C=2200 rpm)
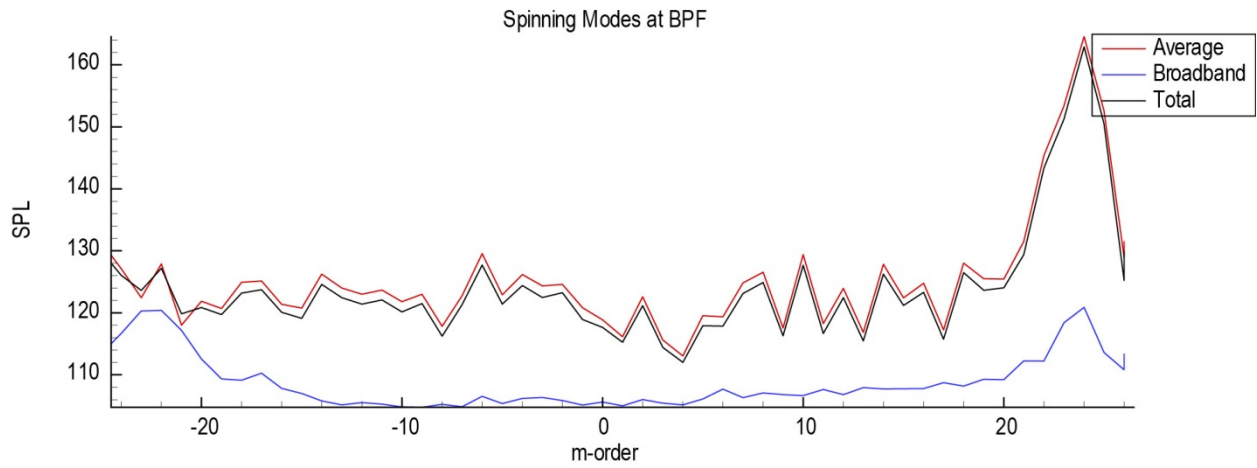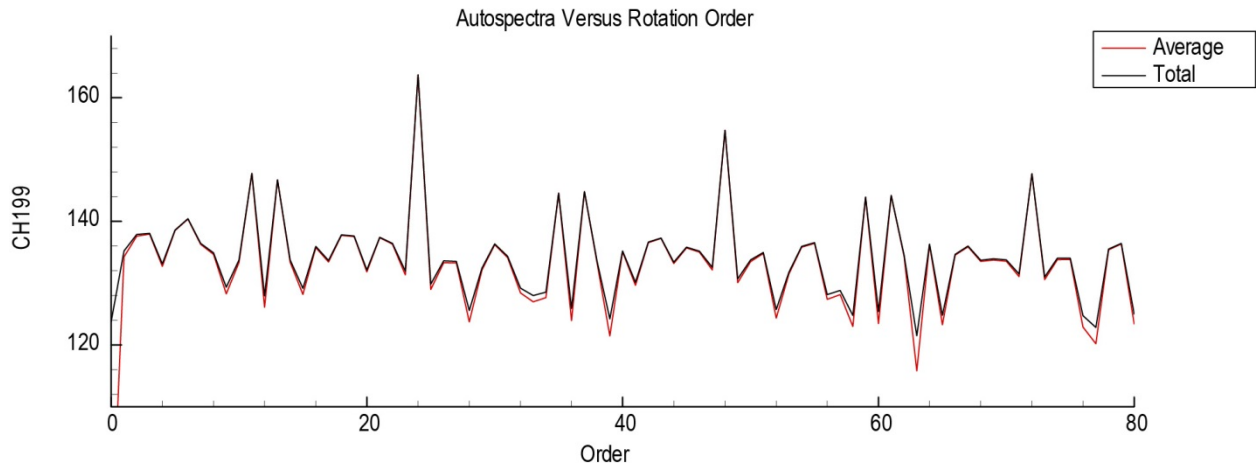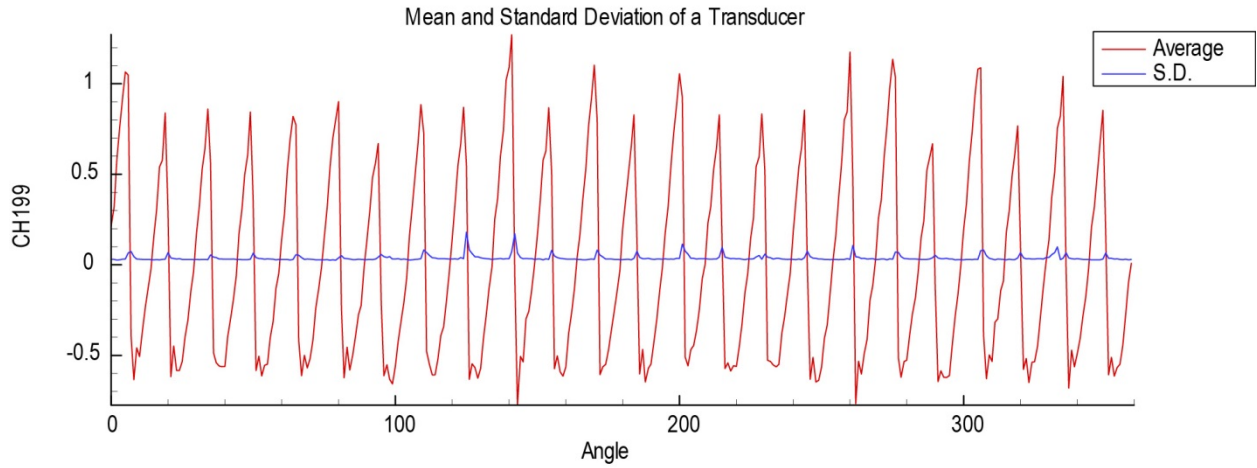
EVNRC Test Mode Ring Results
EVNRC2: BOM Trtd Inlet, HW Spool, 24B, 28V
(Run 11817, N1C=2450 rpm)
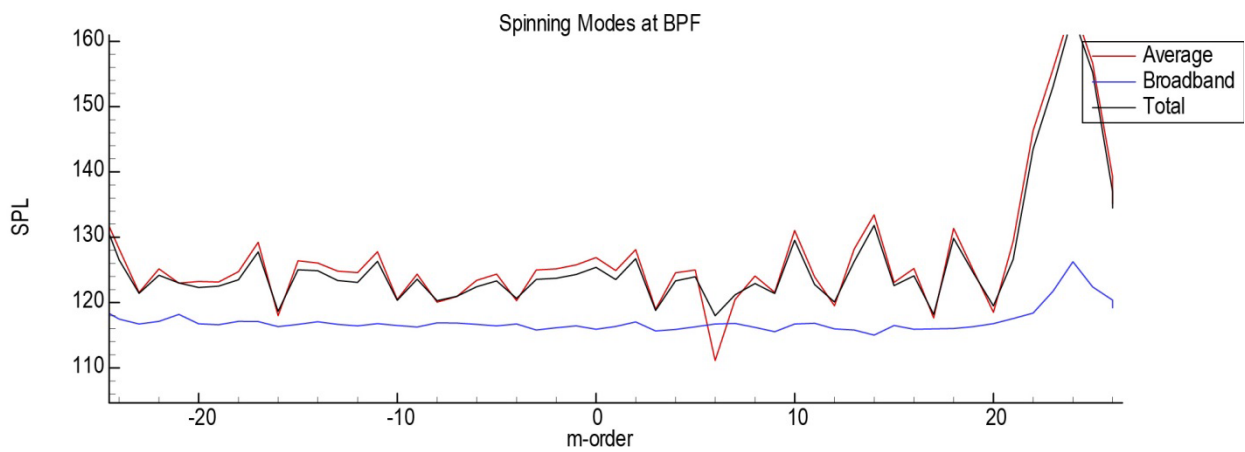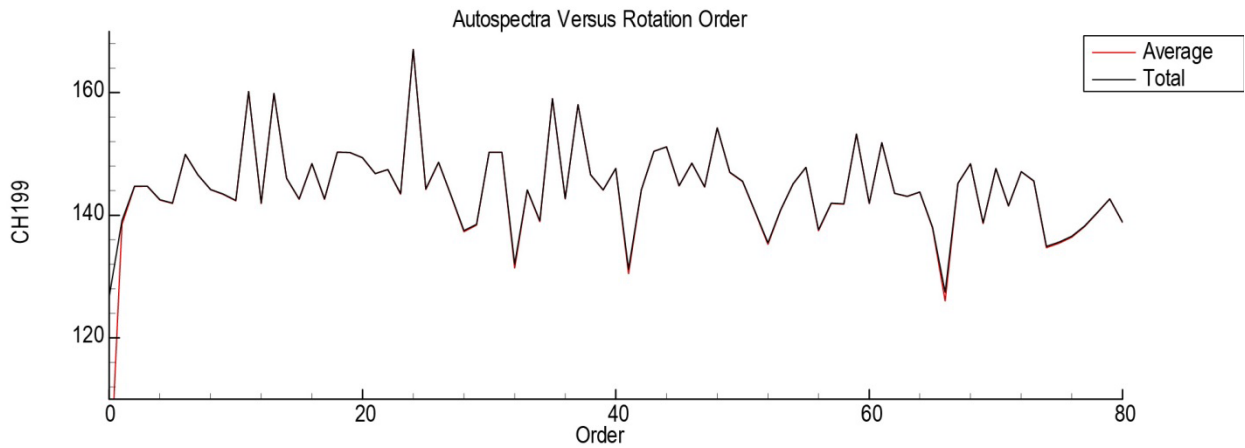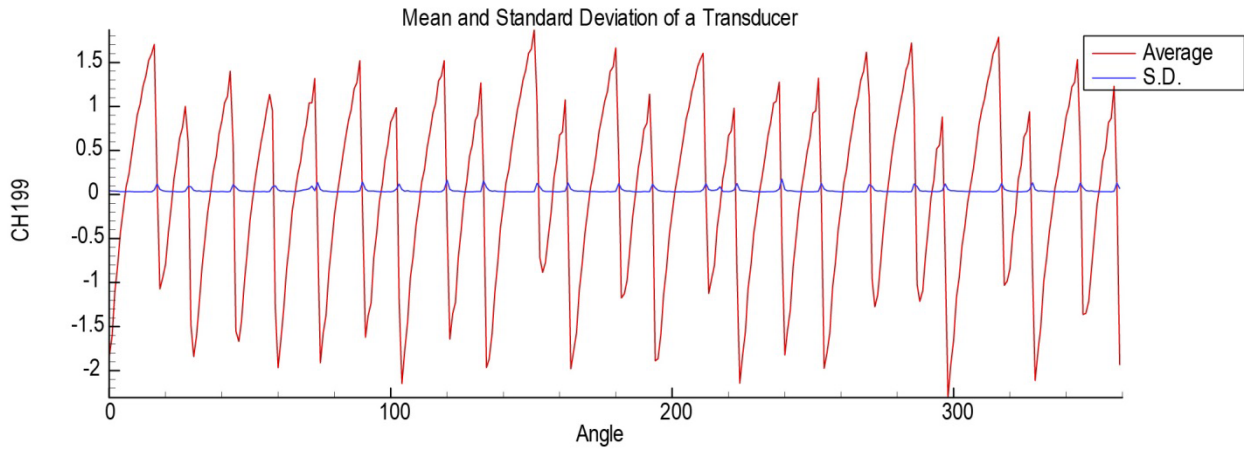
EVNRC Test Mode Ring Results
EVNRC2: BOM Trtd Inlet, HW Spool, 24B, 28V
(Run 11820, N1C=2700 rpm)

Mean and Standard Deviation of a Transducer

Autospectra Versus Rotation Order

Spinning Modes at BPF
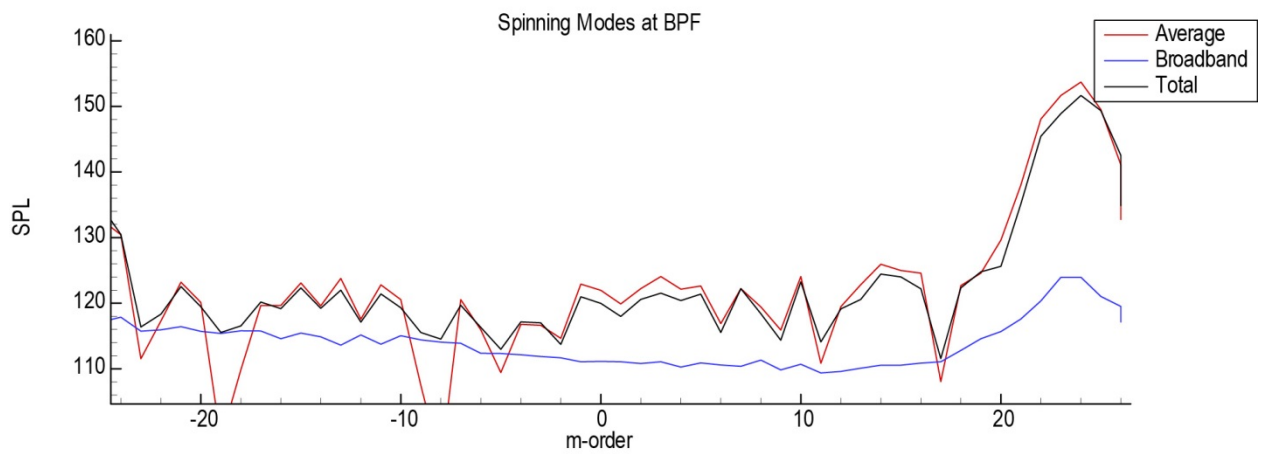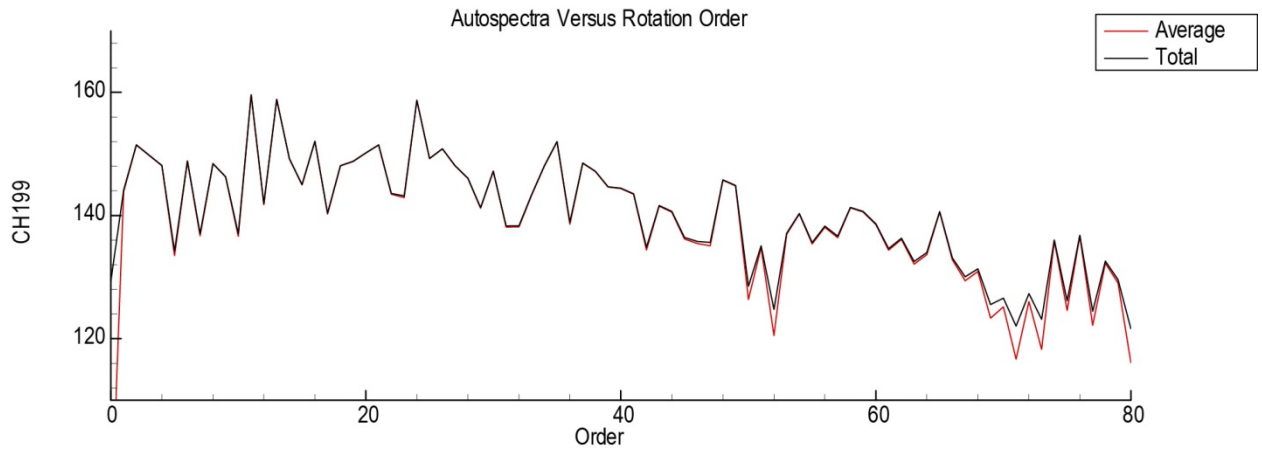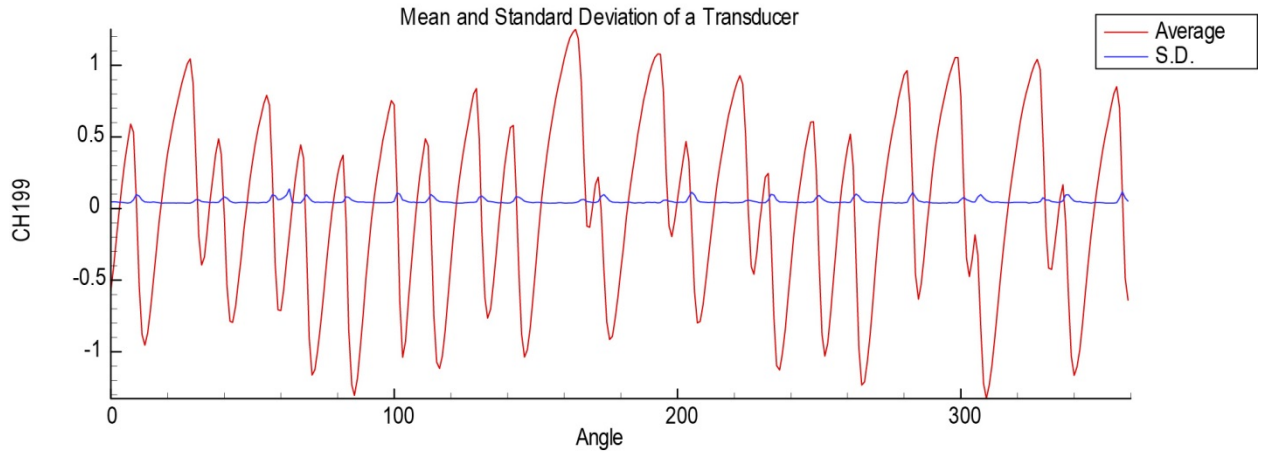
EVNRC Test Mode Ring Results
EVNRC2: BOM Trtd Inlet, HW Spool, 24B, 28V
(Run 11821, N1C = rpm)
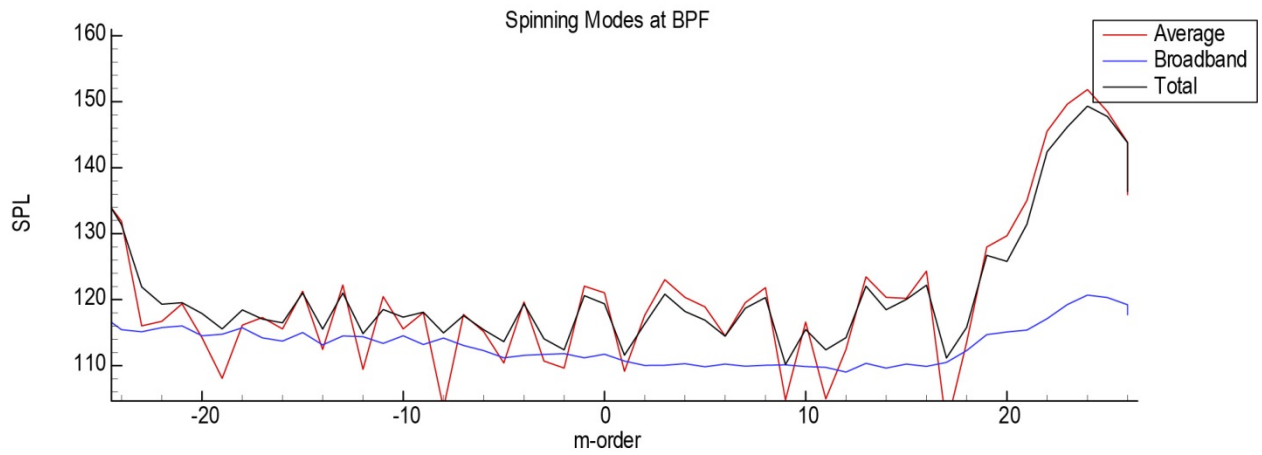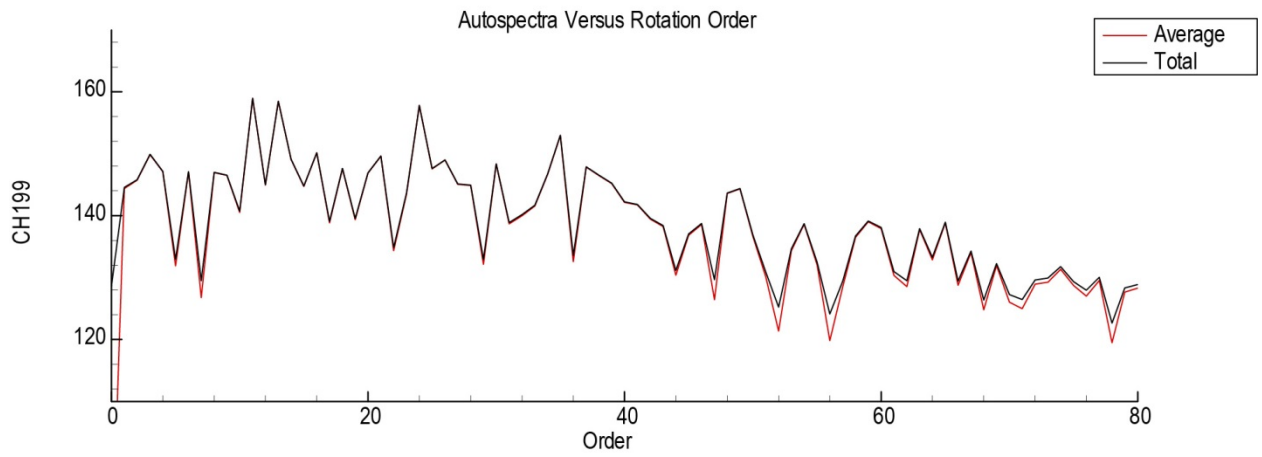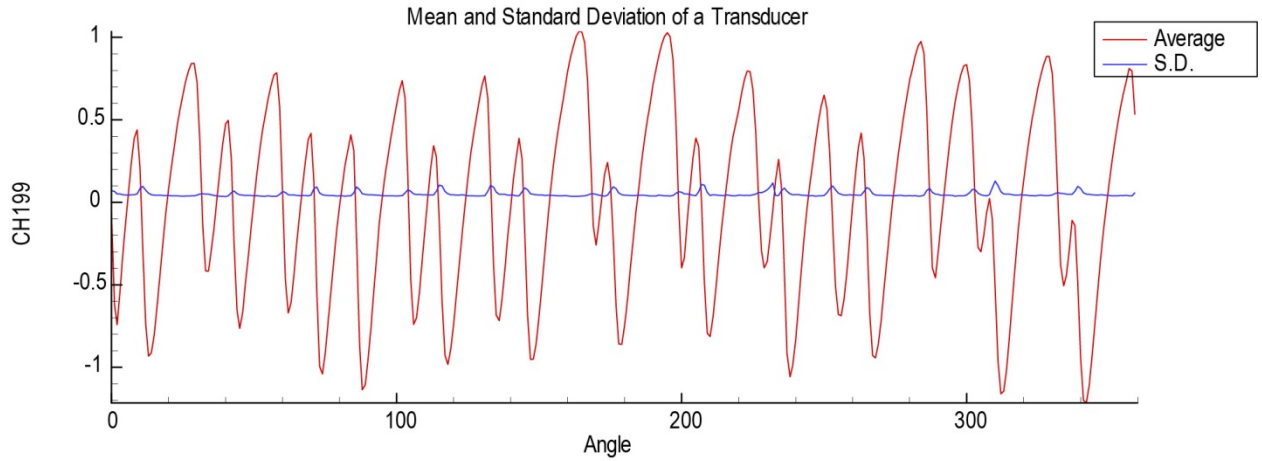
EVNRC Test Mode Ring Results
EVNRC3: BOM Trtd Inlet, HW Spool, 24B, 28V
(Run 11904, N1C= 580 rpm)

Mean and Standard Deviation of a Transducer

Autospectra Versus Rotation Order

Spinning Modes at BPF
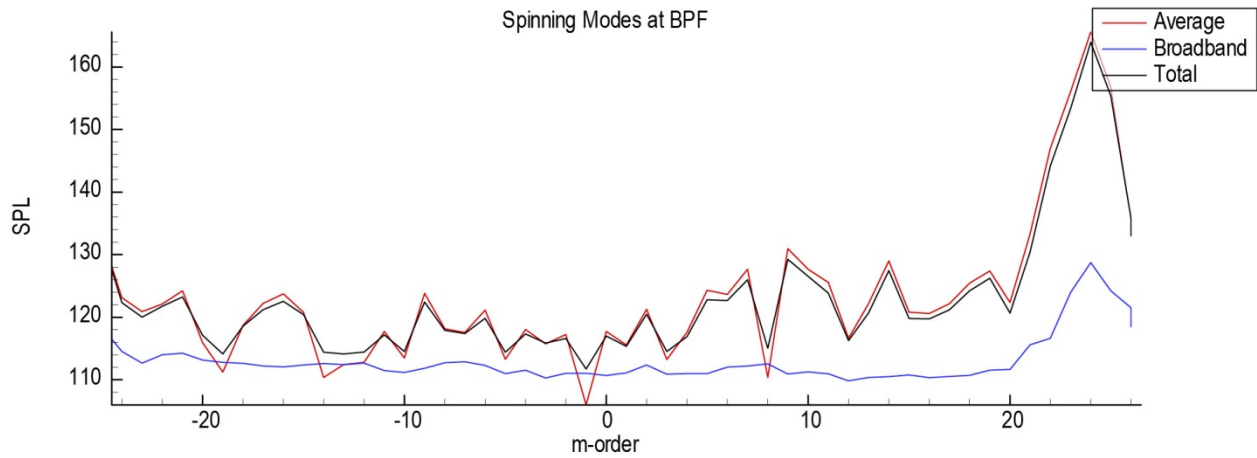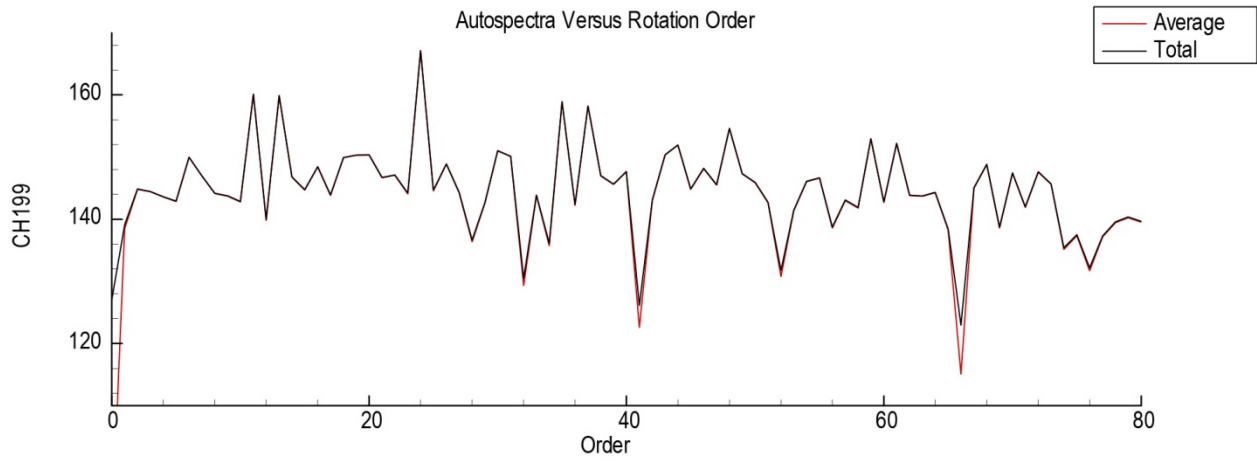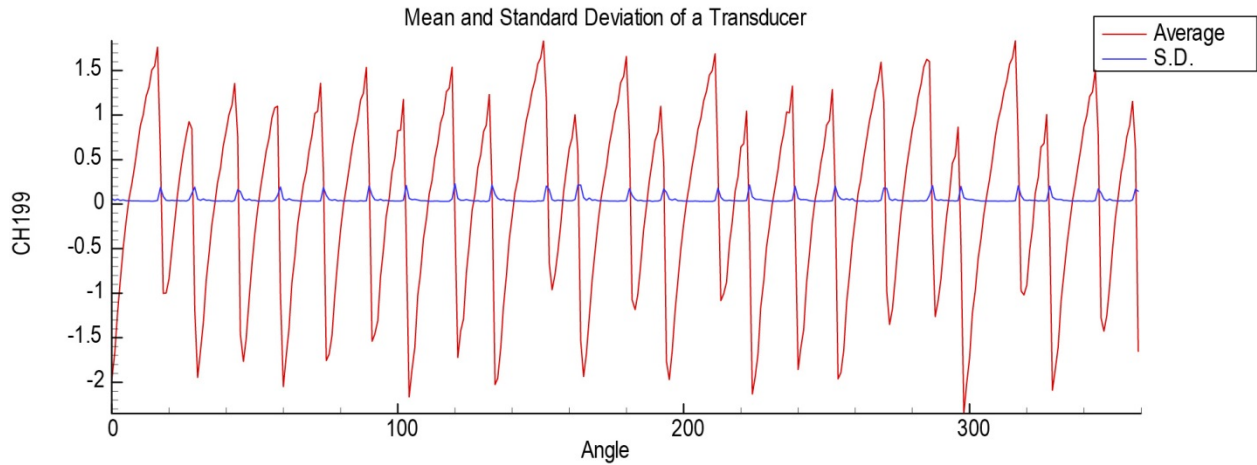
EVNRC Test Mode Ring Results
EVNRC3: BOM Trtd Inlet, HW Spool, 24B, 28V
(Run 11905, N1C=1620 rpm)

Mean and Standard Deviation of a Transducer
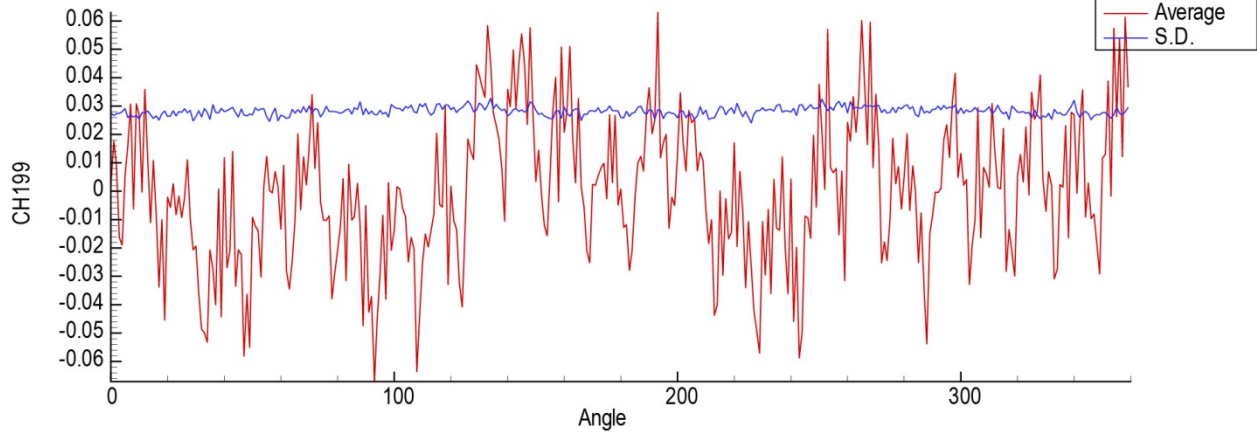
Autospectra Versus Rotation Order
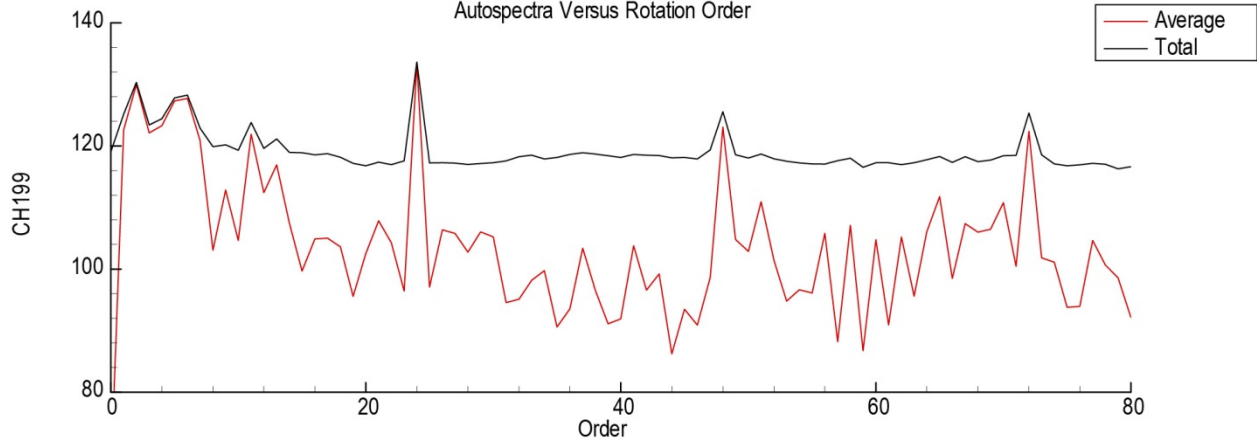
Spinning Modes at BPF

EVNRC Test Mode Ring Results
EVNRC3: BOM Trtd Inlet, HW Spool, 24B, 28V
(Run 11907, N1C=1800 rpm)

Mean and Standard Deviation of a Transducer
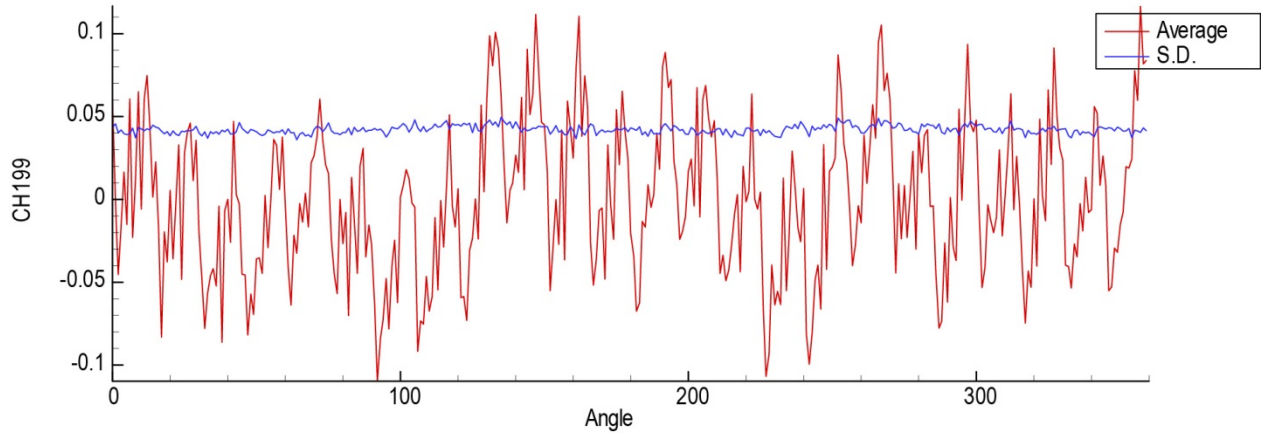
Autospectra Versus Rotation Order

Spinning Modes at BPF

EVNRC Test Mode Ring Results
EVNRC3: BOM Trtd Inlet, HW Spool, 24B, 28V
(Run 11909, N1C=2000 rpm)

Mean and Standard Deviation of a Transducer

Autospectra Versus Rotation Order

Spinning Modes at BPF

EVNRC Test Mode Ring Results
EVNRC3: BOM Trtd Inlet, HW Spool, 24B, 28V
(Run 11911, N1C=2200 rpm)

Mean and Standard Deviation of a Transducer

Autospectra Versus Rotation Order

Spinning Modes at BPF
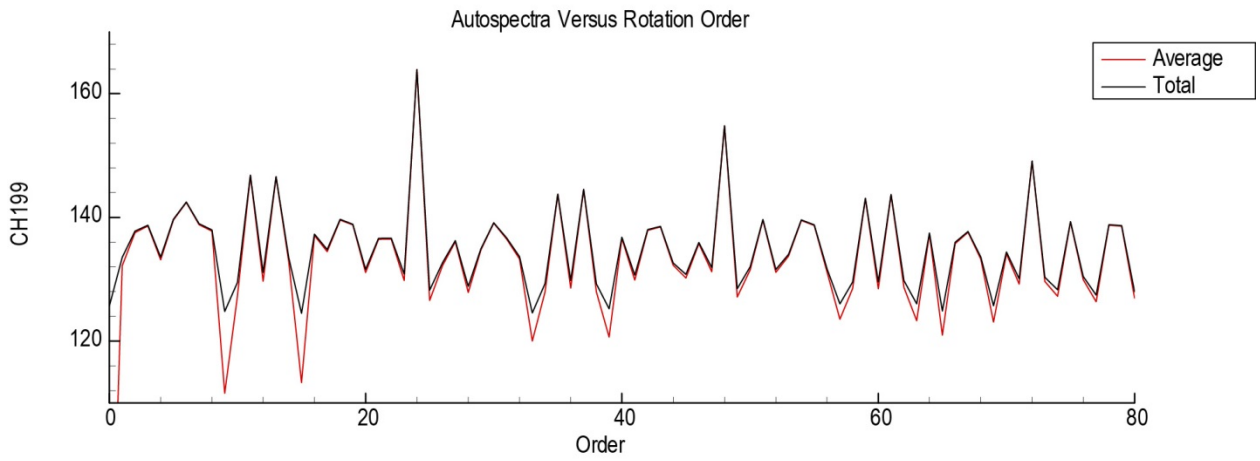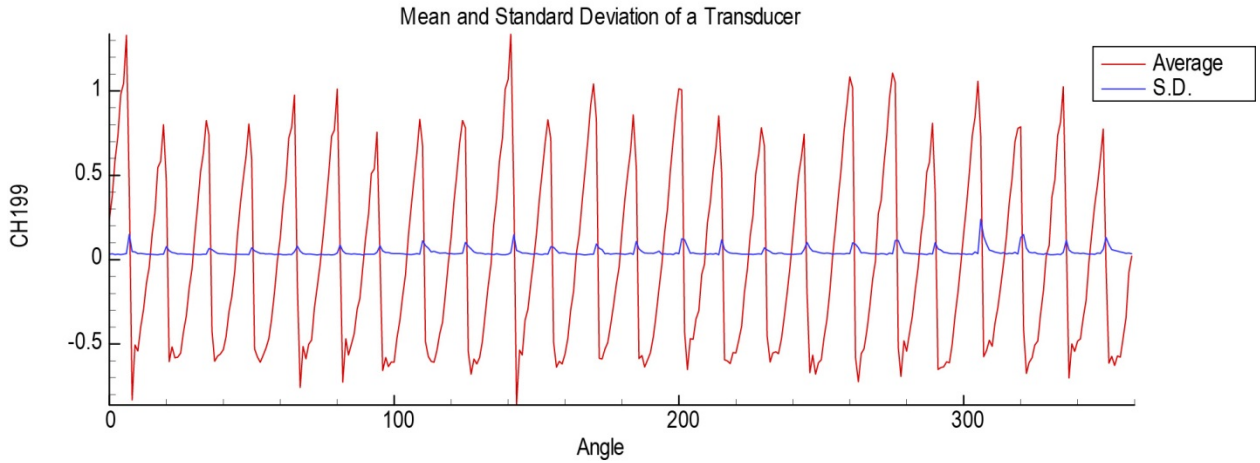
EVNRC Test Mode Ring Results
EVNRC3: BOM Trtd Inlet, HW Spool, 24B, 28V
(Run 11914, N1C=2450 rpm)

Mean and Standard Deviation of a Transducer

Autospectra Versus Rotation Order

Spinning Modes at BPF
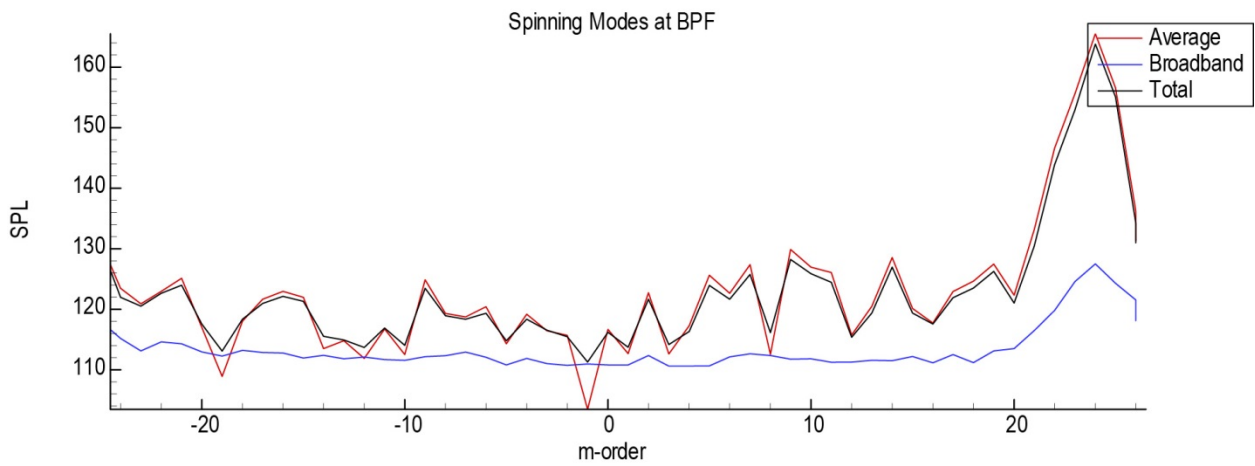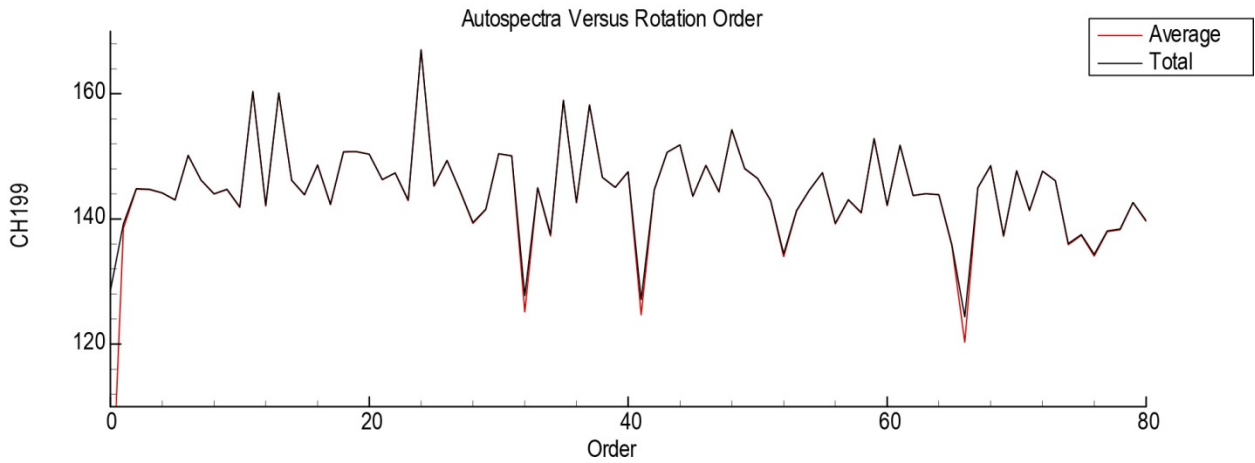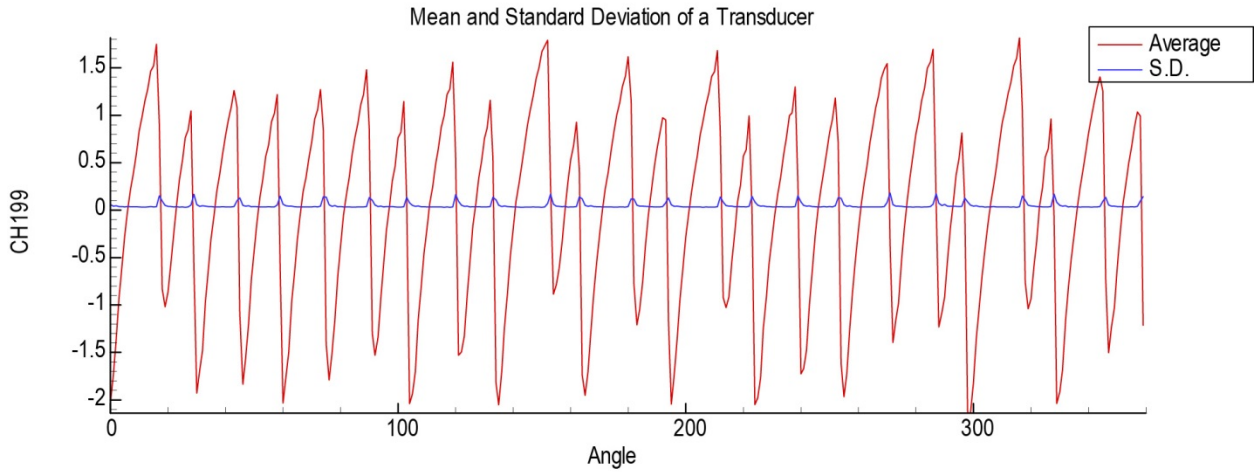
EVNRC Test Mode Ring Results
EVNRC3: BOM Trtd Inlet, HW Spool, 24B, 28V
(Run 11917, N1C=2700 rpm)

Mean and Standard Deviation of a Transducer

Autospectra Versus Rotation Order

Spinning Modes at BPF
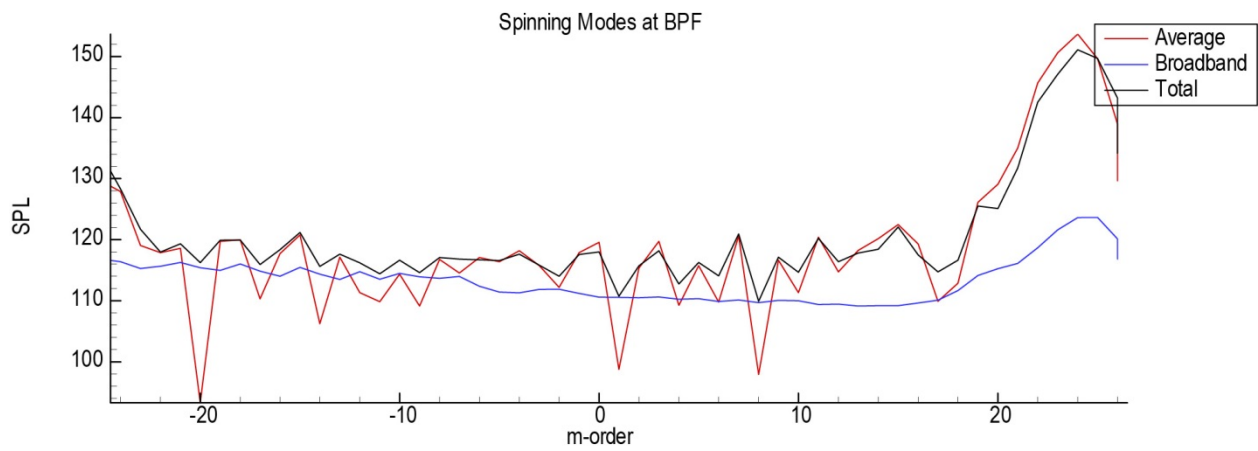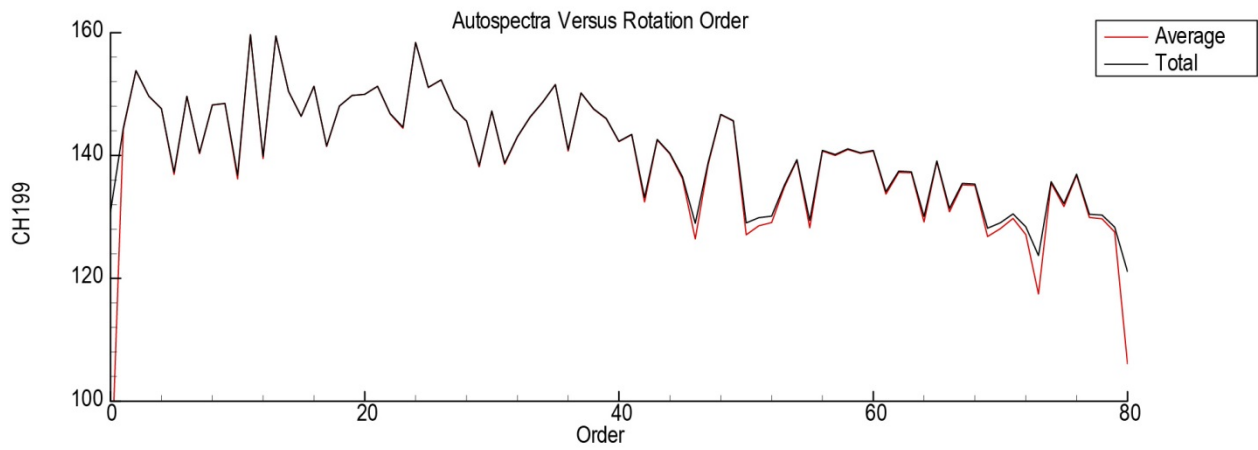
EVNRC Test Mode Ring Results
EVNRC4: Scarf HW Inlet, HW Spool, 24B, 60V
(Run 12005, N1C=1620 rpm)

Mean and Standard Deviation of a Transducer

Autospectra Versus Rotation Order

Spinning Modes at BPF

EVNRC Test Mode Ring Results
EVNRC4: Scarf HW Inlet, HW Spool, 24B, 60V
(Run 12007, N1C=1800 rpm)

Mean and Standard Deviation of a Transducer

Autospectra Versus Rotation Order

Spinning Modes at BPF

EVNRC Test Mode Ring Results
EVNRC4: Scarf HW Inlet, HW Spool, 24B, 60V
(Run 12009, N1C=2000 rpm)

Mean and Standard Deviation of a Transducer

Autospectra Versus Rotation Order

Spinning Modes at BPF

Appendix D.—P&W Data, Inlet Noise Study

D.1 Purpose of Study

The purpose of this study was to assess the validity of PW's source separation process for inlet and aft radiated noise. Inlet noise includes fan inlet tones, inlet broadband, LPC tones, sum tones, and extraneous noise.

D.2 Discussion

Inlet noise was separated from configurations 2 and 7 by PW's standard process. This inlet noise was then compared with barrier data (configurations 3 and 6), which shielded the microphone array from the aft noise. Since low frequency leakage (e.g., jet noise) could be expected around the barrier only the higher frequency portion of the barrier data, dominated by inlet-radiated noise, was examined.

D.3 Configuration Descriptions of Data Used in Inlet Noise Review

Configuration 2.—Run 16118, 24 fan blades, *28 fegv's*, hardwall tailpipe, *no barrier* walls, inlet components.

Configuration 3.—Run 16119, 24 fan blades, *28 fegv's*, hardwall tailpipe, *with barrier* walls.

Configuration 6.—Run 16121, 24 fan blades, *60 fegv's*, hardwall tailpipe, *with barrier* walls.

Configuration 7.—Run 16122, 24 fan blades, *60 fegv's*, hardwall tailpipe, *no barrier* walls, inlet components.

D.4 Directivity and Spectral Examples

Figure D.1, (top) PNL directivities at 1600 rpm for configurations 2 and 3 and (bottom) Figure D.2, configurations 6 and 7.
Figure D.3, (top) spectra at 110° at 1600 rpm for Configurations 2 and 3 and (Bottom) Figure D.4, configurations 6 and 7.
Figure D.5, (top) PNL directivities at 2400 rpm for configurations 2 and 3 and (bottom) Figure D.6, configurations 6 and 7.
Figure D.7, (top) spectra at 110° at 2400 rpm for configurations 2 and 3 and (bottom) Figure D.8, configurations 6 and 7.

D.4.1 Plot Symbol Legend

A   Separated inlet data that include inlet fan tones/broadband, lpc tones, sum tones, and extraneous inlet noise.
B   Barrier wall data where the farfield microphones are shielded from aft noise although there is low frequency leakage, particularly at the aft angles.
C   Total engine data. There are no walls used for this data and is used to demonstrate how effectively the walls blocked the aft engine noise.

D.5 Observations

For the two speeds considered in this study, representing a range from just below approach power to cutback power, the PNL directivities show excellent agreement between the wall data and separated data for both configurations. The spectral agreement is quite good especially considering that the inlet noise levels are roughly 15 dB below the total engine noise.

D.6 Conclusion

The P&W data analysis process is doing a good job of separating inlet and aft-radiated noise for the PW4098 engine for the conditions studied.
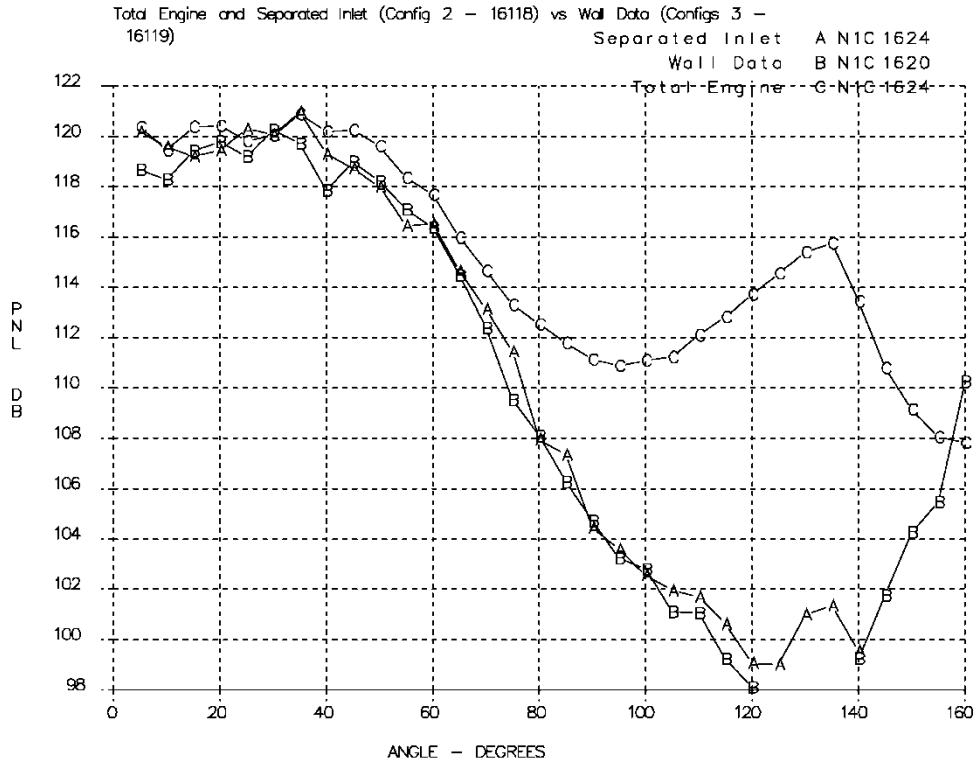
Figure D.1.—PNL—Configurations 2 and 3 at 1600 rpm.
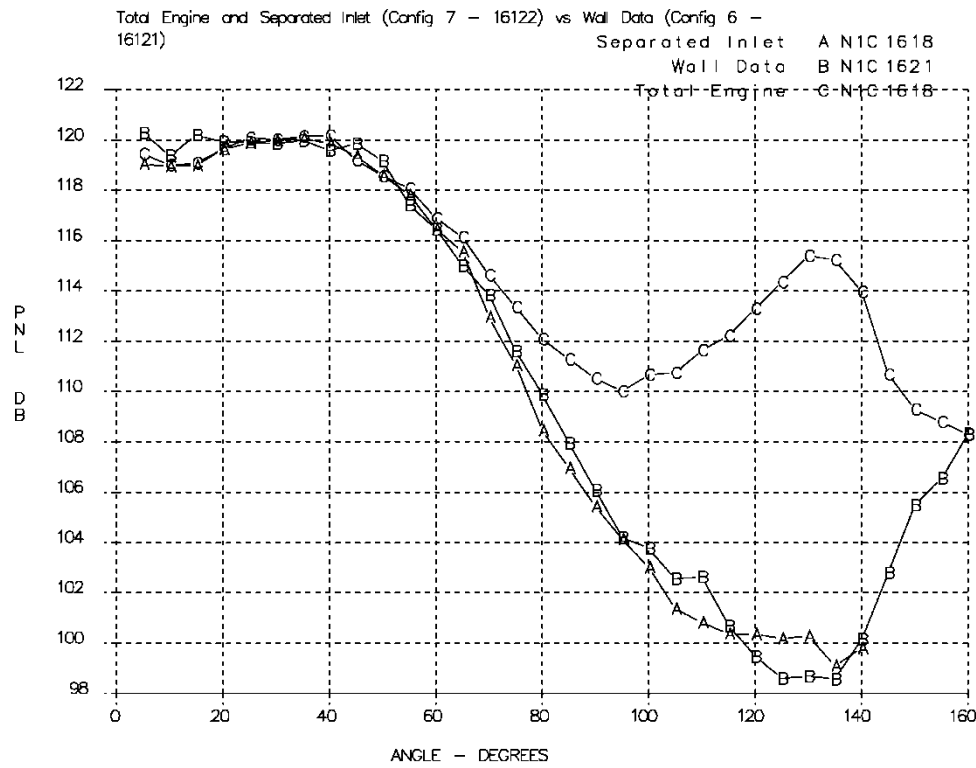
Figure D.2.—PNL—Configurations 6 and 7 at 1600 rpm.
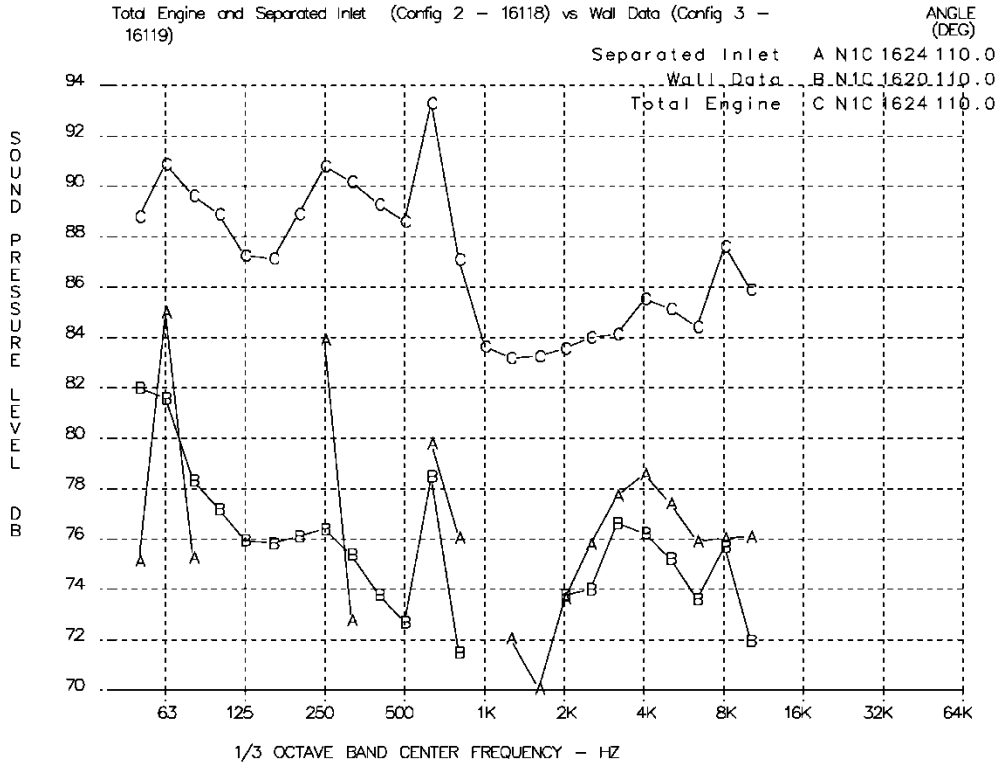
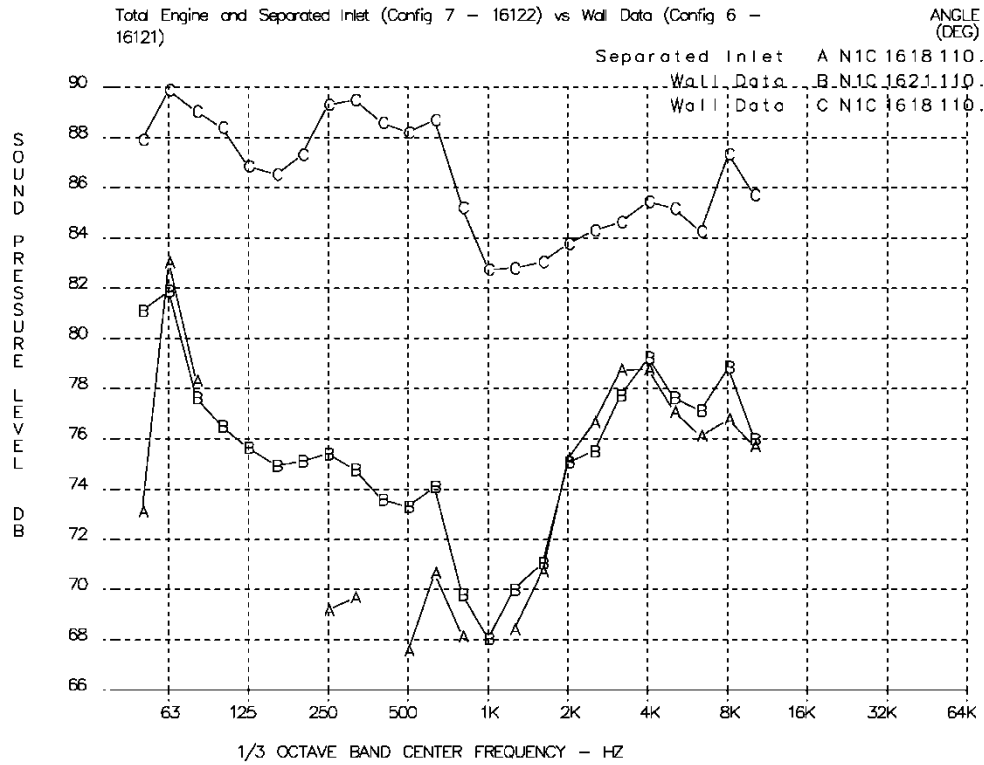Figure D.3.—An 110° Spectra—Configurations 2 and 3 at 1600 rpm.

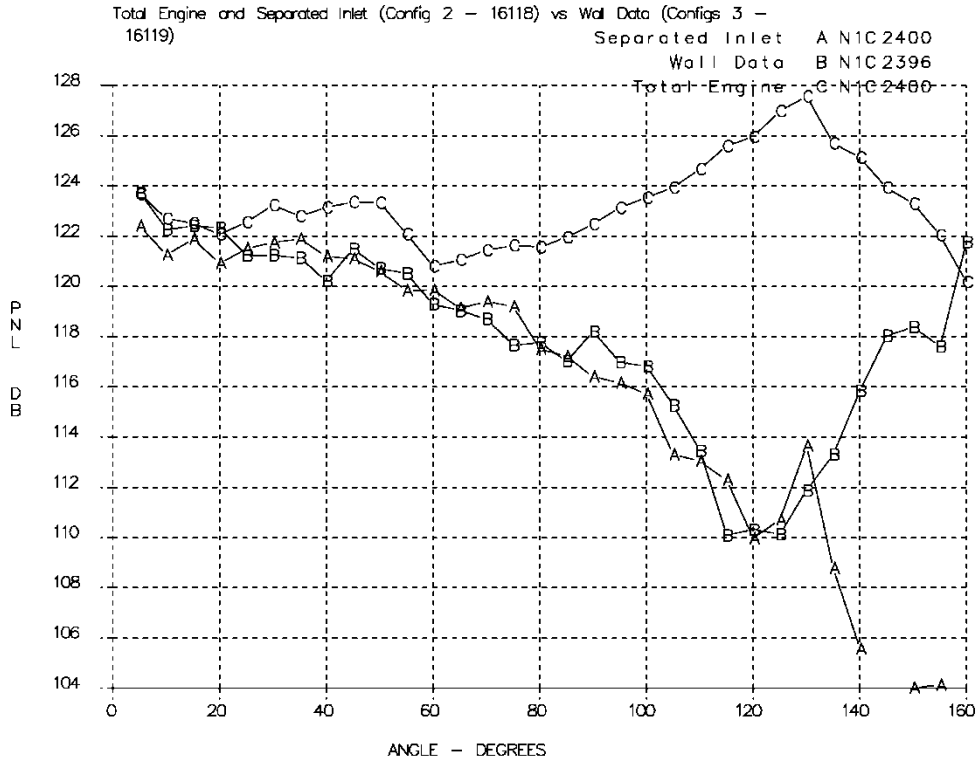Figure D.4.—An 110° Spectra—Configurations 6 and 7 at 1600 rpm

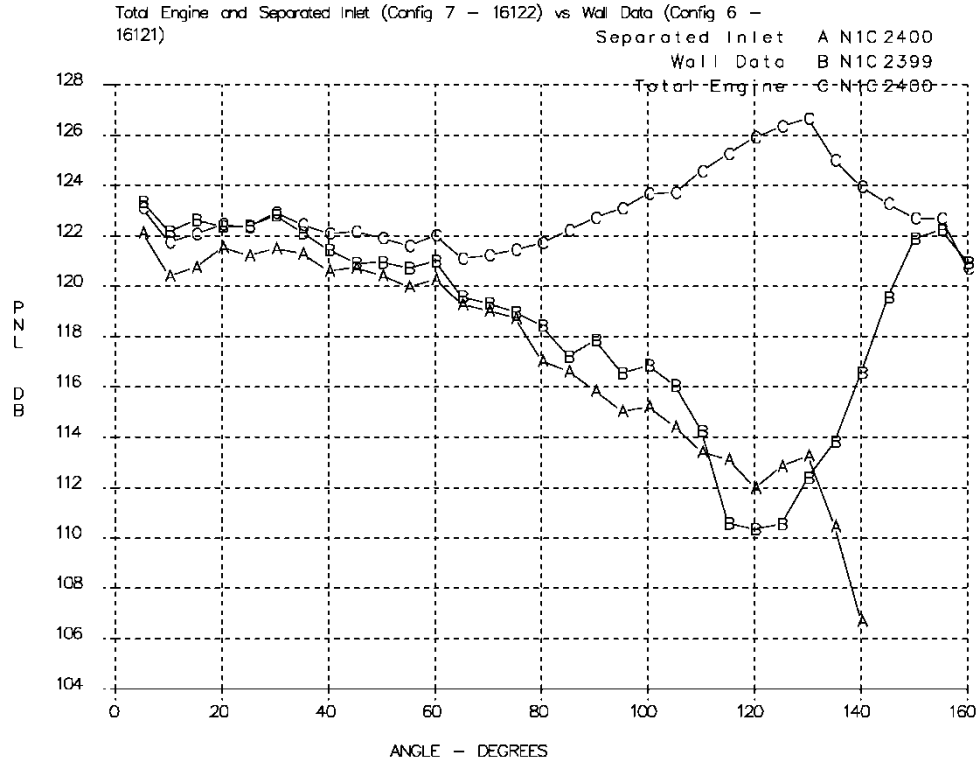Figure D.5.—PNL—Configurations 2 and 3 at 2400 rpm

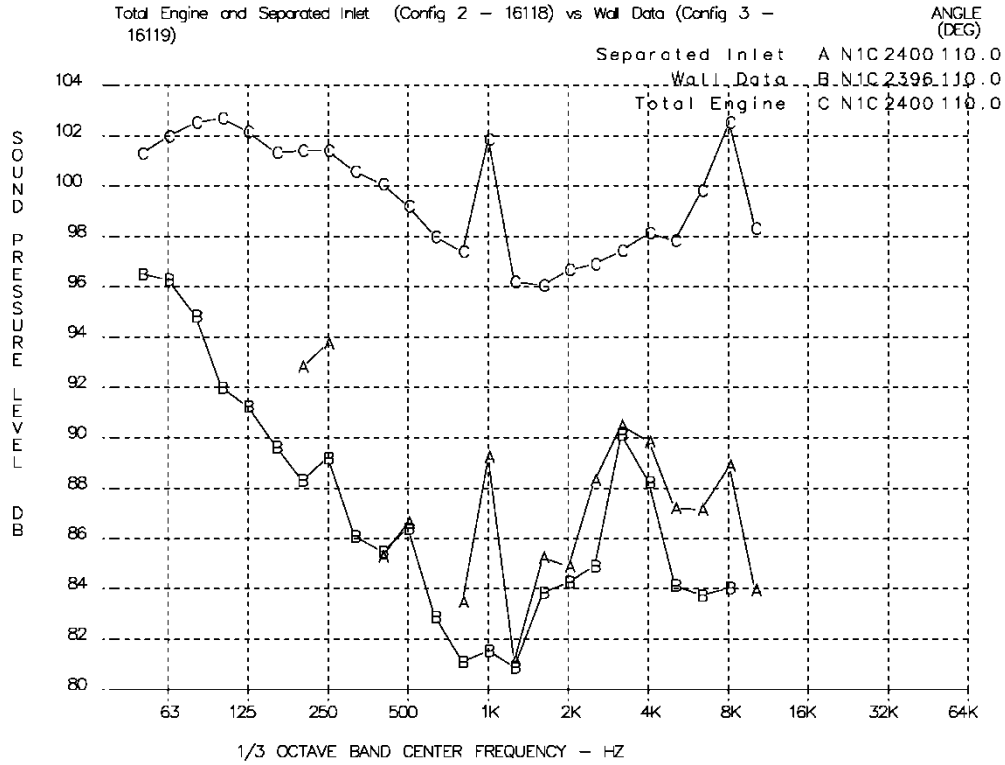Figure D.6.—PNL—Configurations 6 and 7 at 2400 rpm

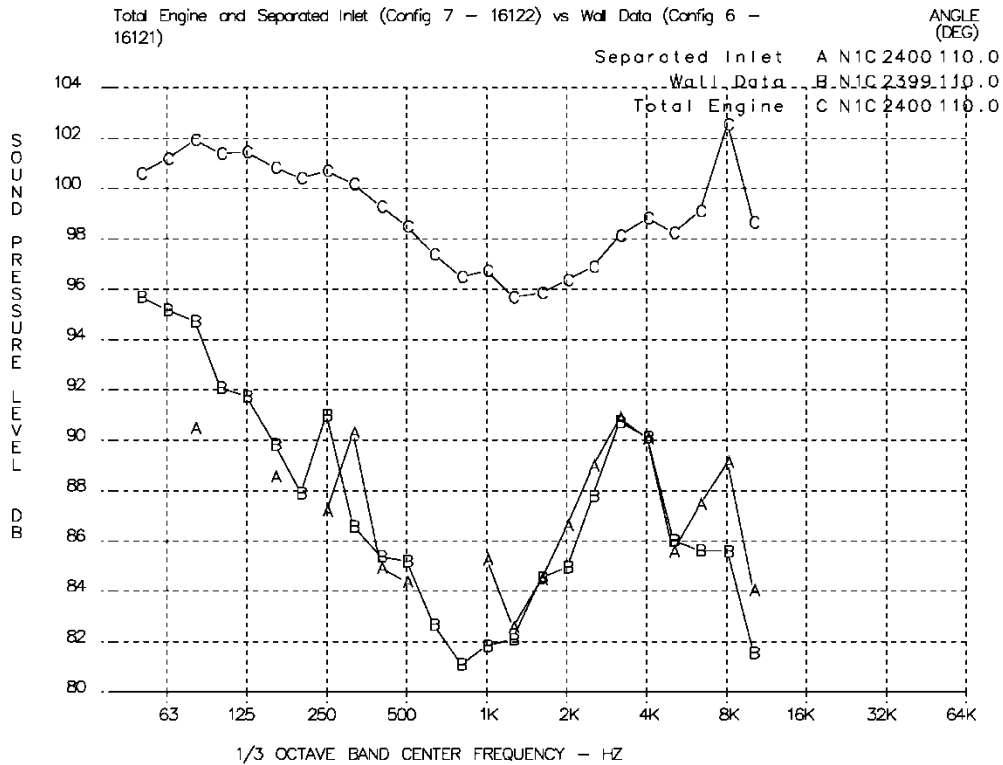Figure D.7.—An 110° Spectra—Configurations 2 and 3 at 2400 rpm

Figure D.8.—An 110° Spectra—Configurations 6 and 7 at 2400 rpm.

Appendix E.—P&W Data, Noise Component Sensitivity Study

E.1   Purpose

Determine the sensitivity of total EPNL to changes of (±) 1, 2, 5, and 10 dB of each noise component at approach, cutback, and sideline power levels and engine configurations 1, 2, 7, and 8.

E.2   Discussion

For each component at a given engine operating condition, specific dB amounts (ranging from 1 to 10) were added and taken away from each noise component at all angles and all frequencies, and subsequent EPNLs were calculated. Seven noise sources are included in this study as fan inlet tones, inlet broadband, aft fan tones, aft broadband, turbine, jet, and core.

The first figure on each page shows the ΔEPNdB versus ΔComponent curves. There are three important segments on these sensitivity curves. One segment is at the far left part of the curve, or the part where the most noise has been subtracted from a single component. The ΔEPNL value which corresponds to –10 dB from each component, represents nearly the asymptotic maximum benefit that could be achieved by completely eliminating a single noise component. The segment at the far right of the curve, where the most noise has been added to each component, will eventually approach an asymptotic slope of 1, since when any given noise component is high enough, a 1 dB increase in that component at all angles and all frequencies should result in an equal EPNdB increase in the total noise.

The center segment of the sensitivity curve is used to generate a parameter called the "*influence coefficient*" for each noise component. The second figure on each page shows a bar chart of these "influence coefficients". The influence coefficient is basically the change in total EPNL resulting from a 1 dB change in a specific component, with all other components held constant. These influence coefficient charts are very useful for determining which components most need to be the subject of further noise reduction efforts.   The bar charts shown in the second figure of each two-figure series include a breakdown of fan tones and broadband noise (inlet and aft) as well as the influence of turbine, jet, and core components.

Note that airframe noise was held constant for this sensitivity study.

E.3   Conclusions

In general, the sensitivity study revealed that inlet broadband noise was most influential on total EPNL at the approach condition for all engine configurations. Aft broadband noise at the cutback and sideline conditions was most influential on total EPNL for all engine conditions with two exceptions. These exceptions were both at cutback power for engine configurations 1 (22 fan blades/28 exit guide vanes) and 2 (24 blades/28 vanes) where the influence of the aft fan tones were more influential than the broadband (Figure E.5(b) and Figure E.6(b)). The reason for these exceptions is that fan BPF tones are cut-on with 28 vanes, and cut-off for the other configurations. Note that at the higher speeds, jet noise is also important.

Configuration 1 (16117GR008) APPROACH Sensitivity
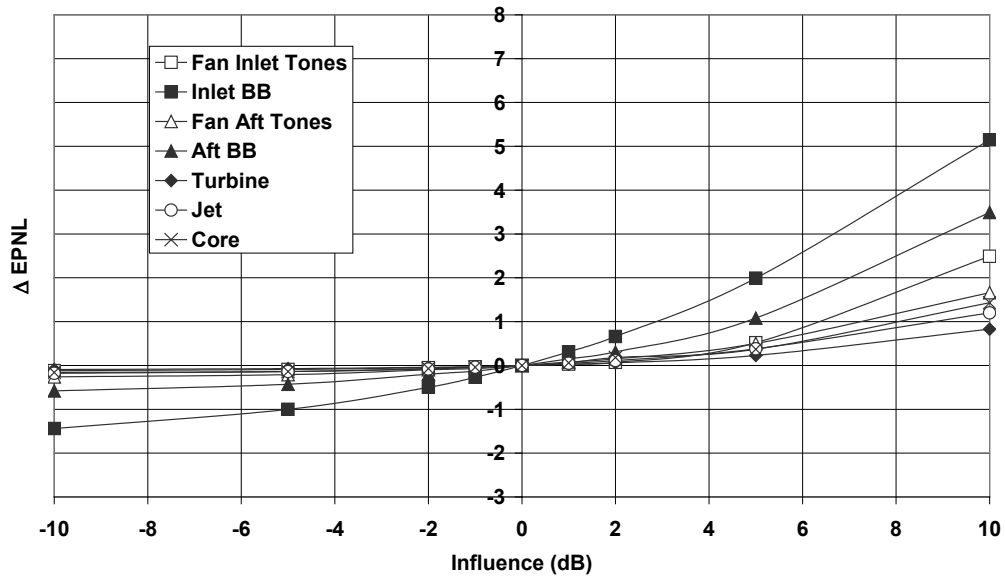

(a)
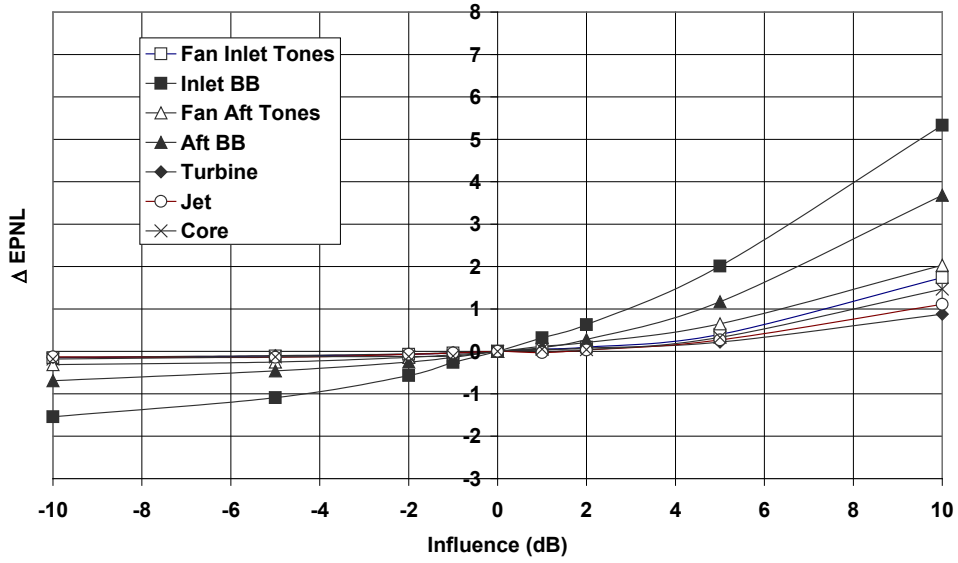
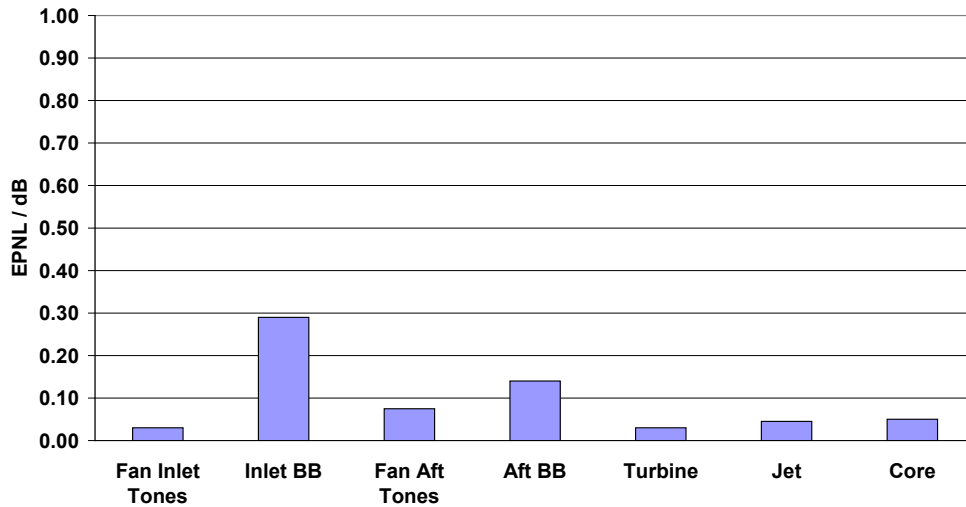**Configuration 1 (16117GR008) APPROACH Sensitivity Influence Coef's**
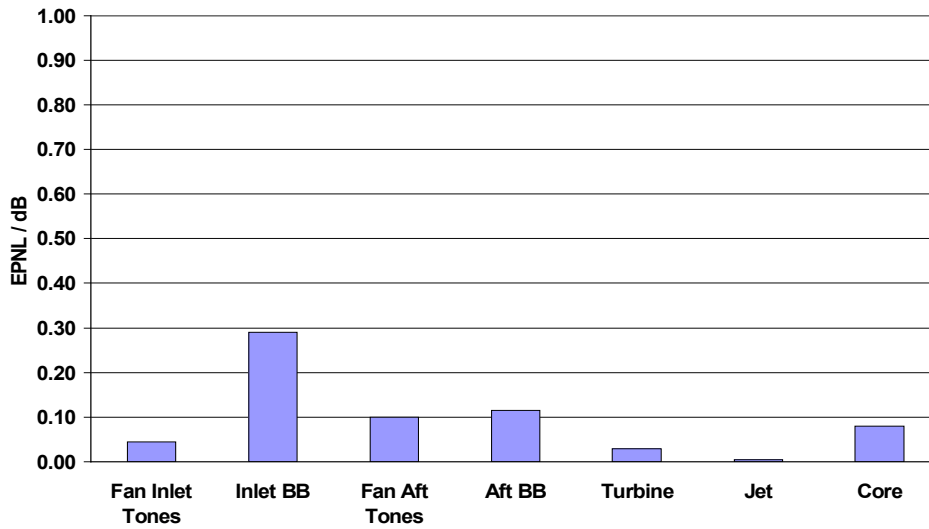
(b)

Figure E.1.—(a) Configuration 1, blades/vanes = 22/28, 1800 rpm, and (b) Configuration 1, blades/vanes = 22/28, 1800 rpm.
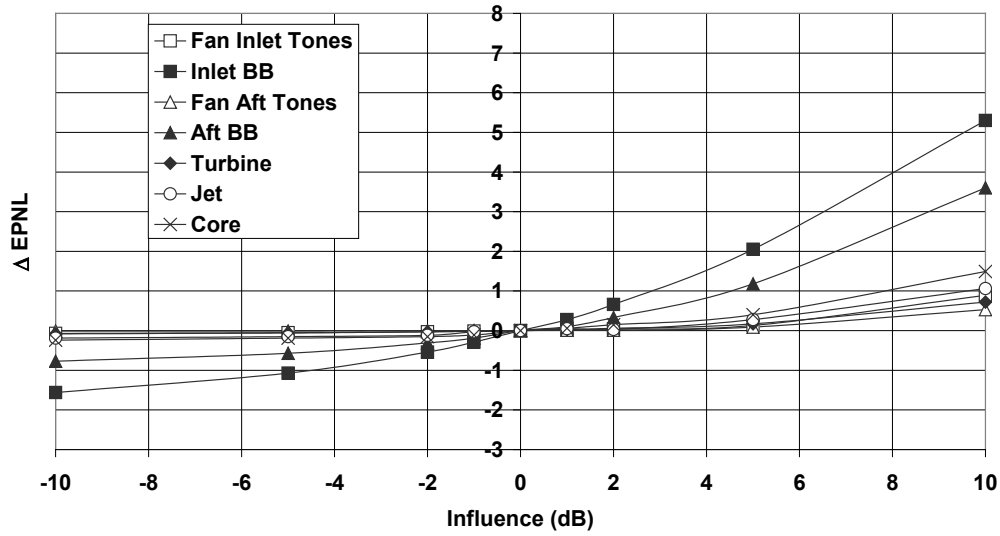
Configuration 2 (16118GR007) APPROACH Sensitivity

(a)

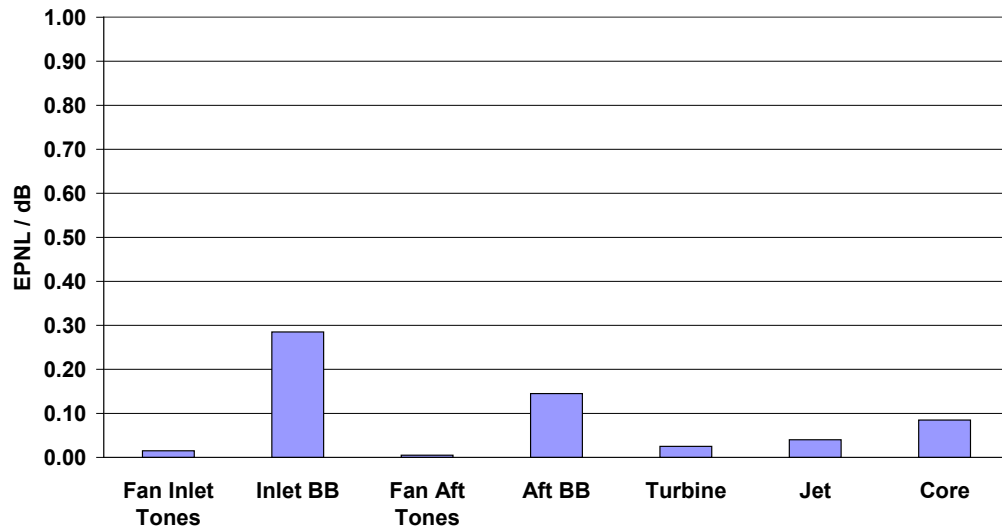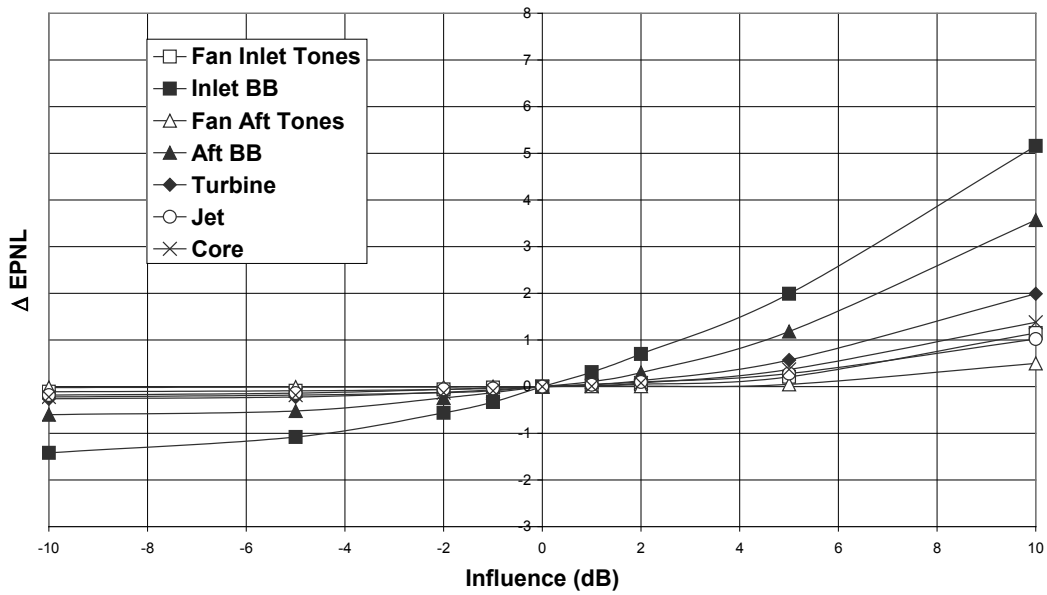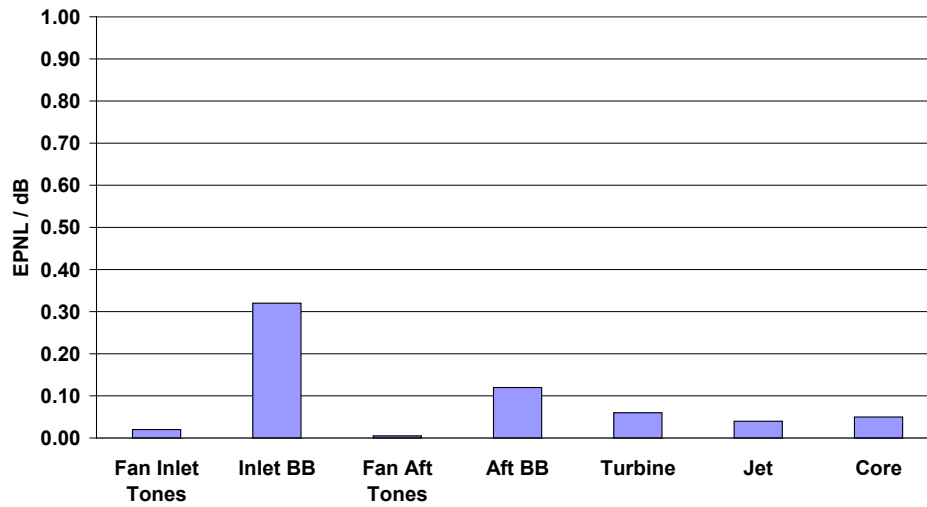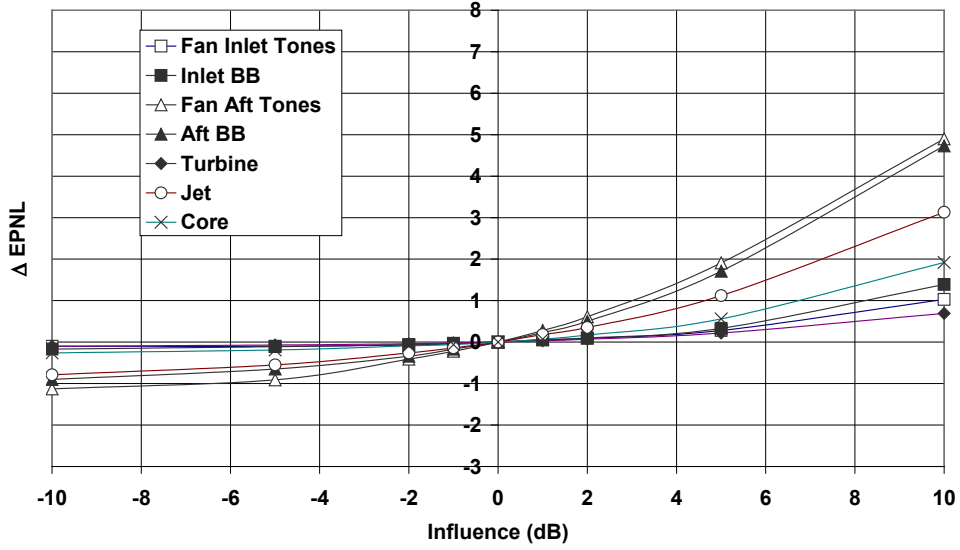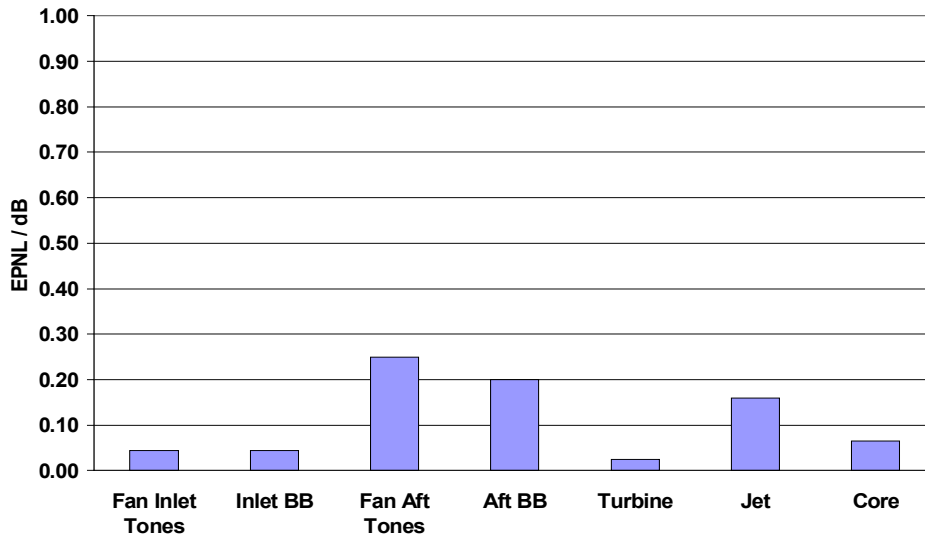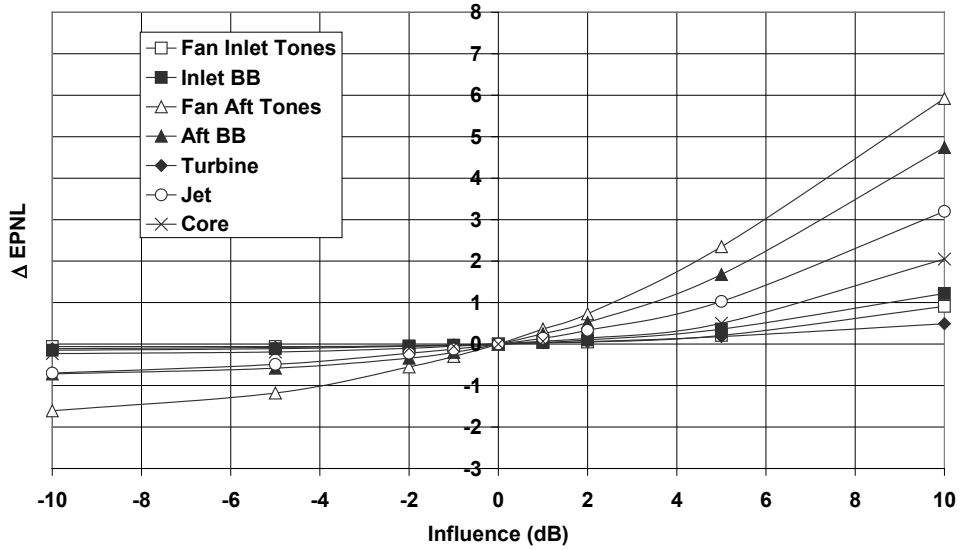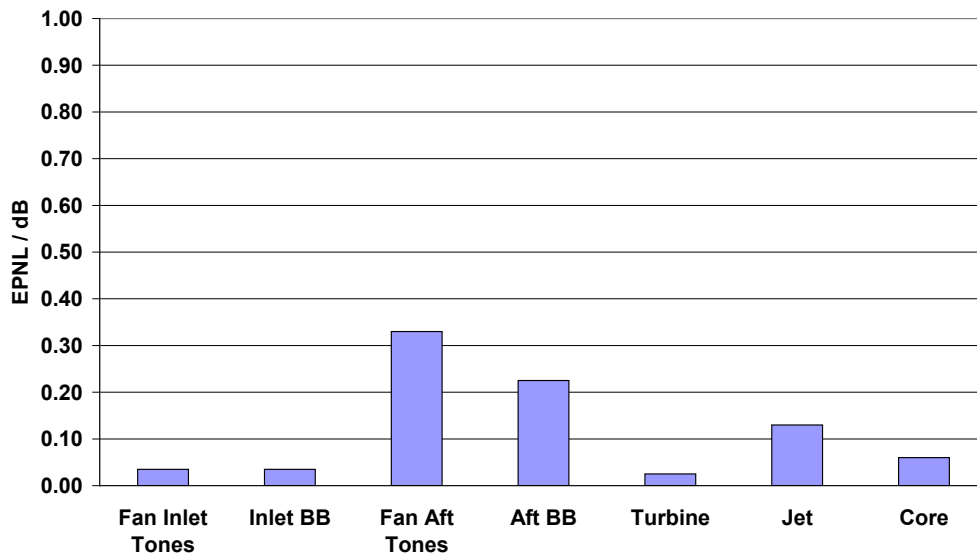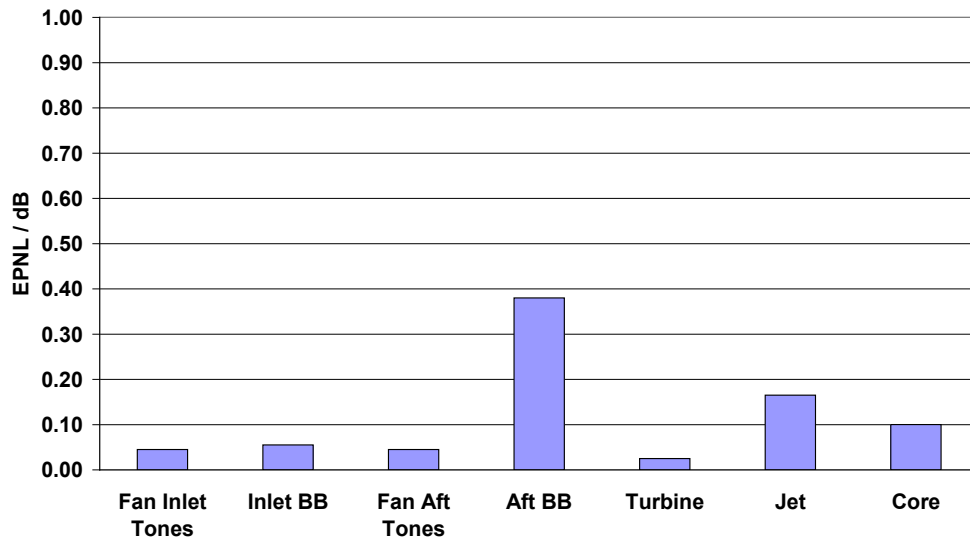**Configuration 2 (16118GR007) APPROACH Sensitivity Influence Coef's**

(b)

Figure E.2.—(a) Configuration 2, blades/vanes = 24/28, 1800 rpm,and (b) Configuration 2, blades/vanes = 24/28, 1800 rpm.

Configuration 7 (16122GR008) APPROACH Sensitivity
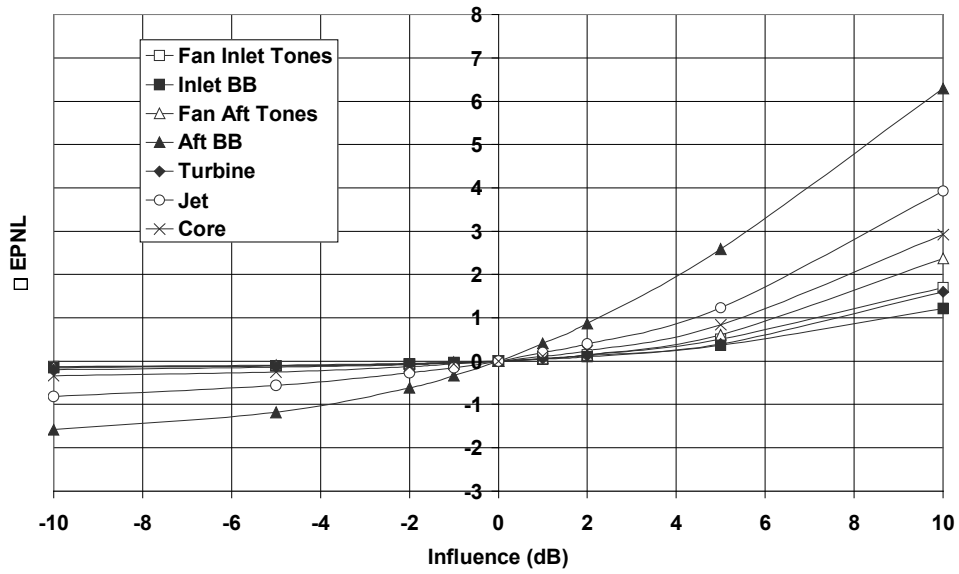

(a)

Configuration 7 (16122GR008) APPROACH Sensitivity Influence Coef's
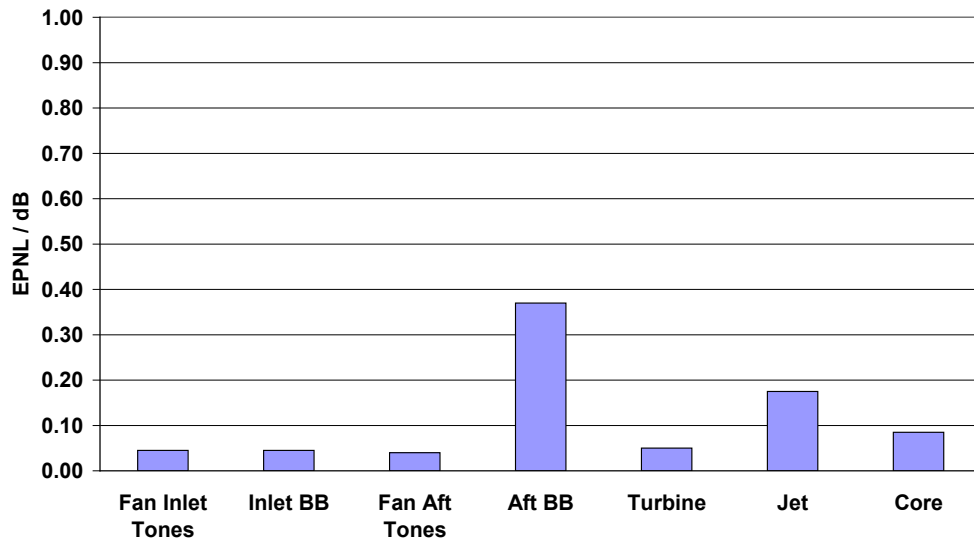

(b)

Figure E.3.—(a) Configuration 7, blades/vanes = 24/60, 1800 rpm, and (b) Configuration 7, blades/vanes = 24/60/, 1800 rpm.

Configuration 8 (16123GR007) APPROACH Sensitivity

(a)

Configuration 8 (16123GR007) APPROACH Sensitivity Influence Coef's

(b)

Figure E.4.—(a) Configuration 8, blades/vanes = 24/60, 1800 rpm, and (b) Configuration 8, blades/vanes = 24/60, 1800 rpm.

Configuration 1 (16117GR014) CUTBACK Sensitivity
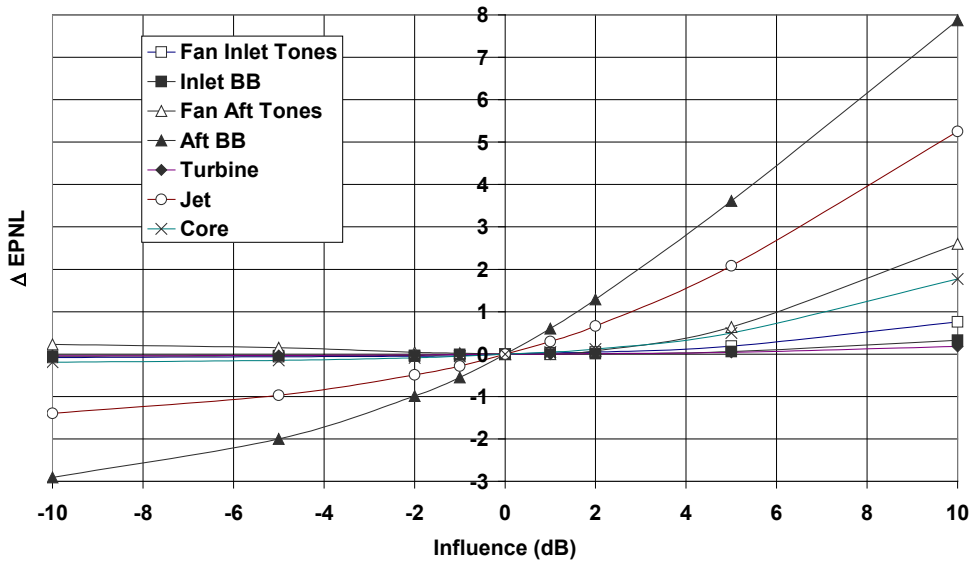

(a)

Configuration 1 (16117GR014) CUTBACK Sensitivity Influence Coef's

(b)

Figure E.5.—(a) Configuration 1, Blades/Vanes = 22/28, 2400 rpm, and (b) Configuration 1, Blades/Vanes = 22/28, 2400 rpm

Configuration 2 (16118GR013) CUTBACK Sensitivity

(a)

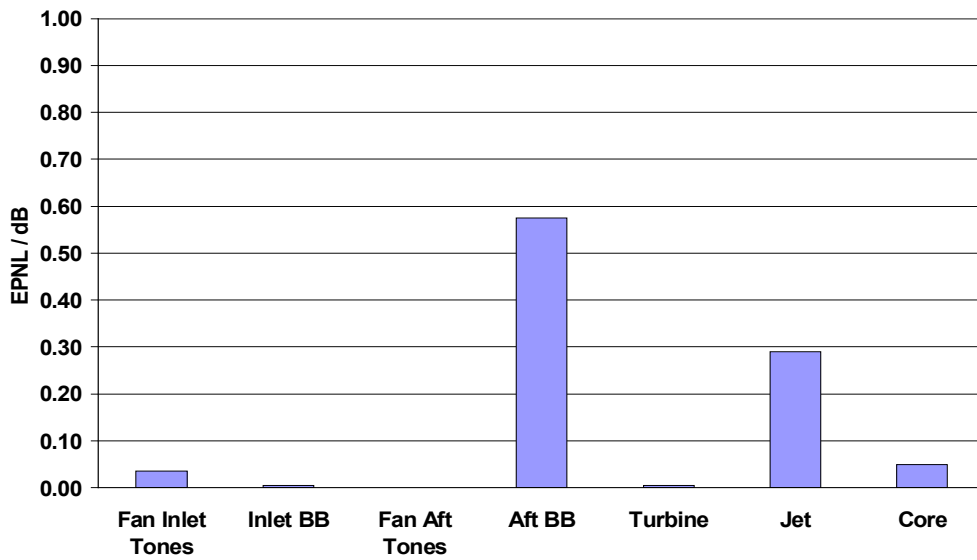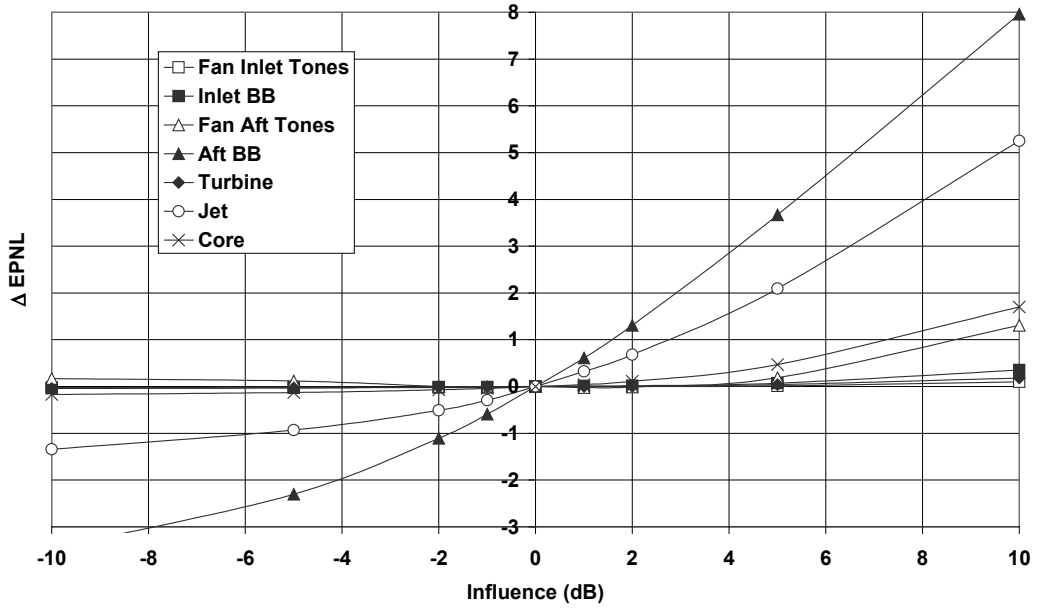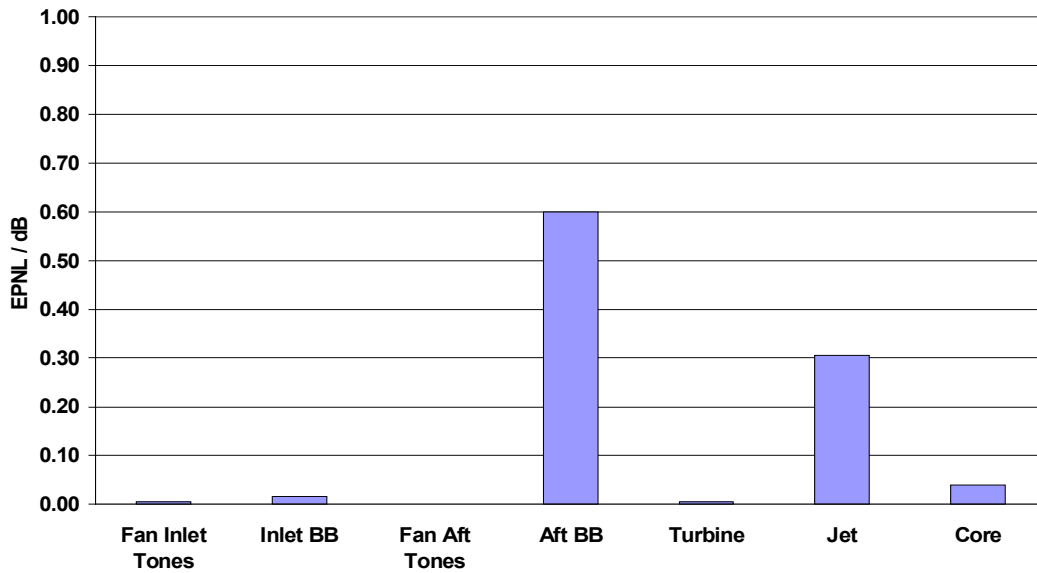## Configuration 2 (16118GR013) CUTBACK Sensitivity Influence Coef's

(b)

Figure E.6.—(a) Configuration 2, Blades/Vanes = 24/28, 2400 rpm, and (b) Configuration 2, Blades/Vanes = 24/60, 2400 rpm.

Configuration 7 (16122GR014) CUTBACK Sensitivity

(a)
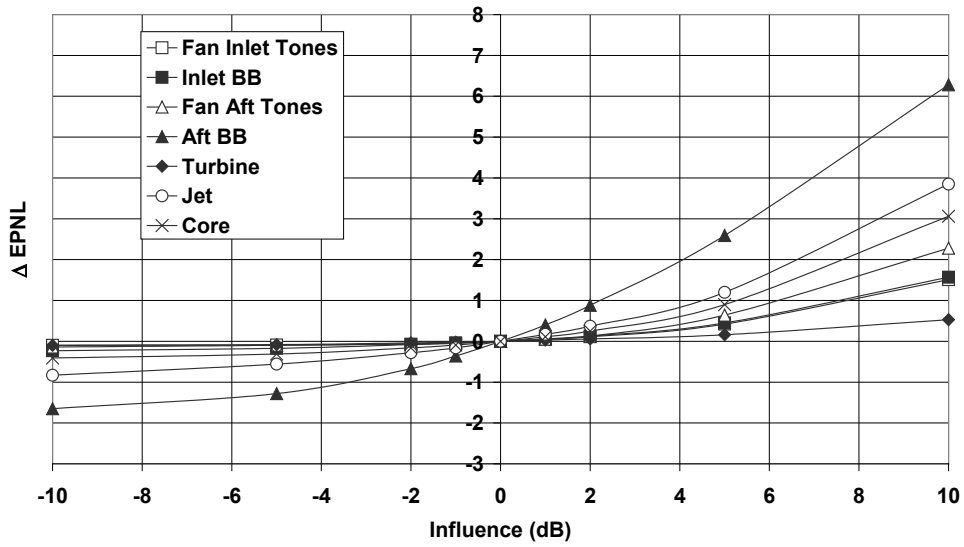
Configuration 7 (16122GR014) CUTBACK Sensitivity Influence Coef's

(b)

Figure E.7.—(a) Configuration 7, Blades/Vanes = 24/60, 2400 rpm, and (b) Configuration 7, Blades/Vanes = 24/60, 2400 rpm.

Configuration 8 (16123GR013) CUTBACK Sensitivity

(a)

Configuration 8 (16123GR013) CUTBACK Sensitivity Influence Coef's

(b)

Figure E.8.—(a) Configuration 8, blades/vanes = 24/60, 2400 rpm, and (b) Configuration 8, blades/vanes = 24/60, 2400 rpm.

Configuration 1 (16117GR018) SIDELINE Sensitivity

(a)

Configuration 1 (16117GR018) SIDELINE Sensitivity Influence Coef's

(b)

Figure E.9.—(a) Configuration 1, Blades/Vanes = 22/28, 2700 rpm, and (b) Configuration 1, Blades/Vanes = 22/28, 2700 rpm.

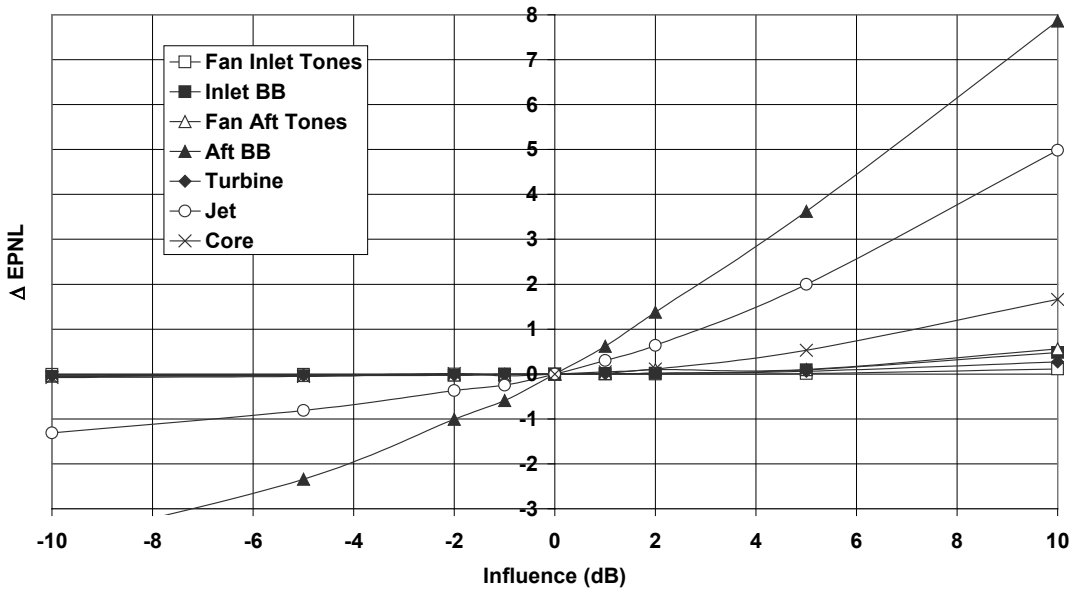## Configuration 2 (16118GR017) SIDELINE Sensitivity

(a)

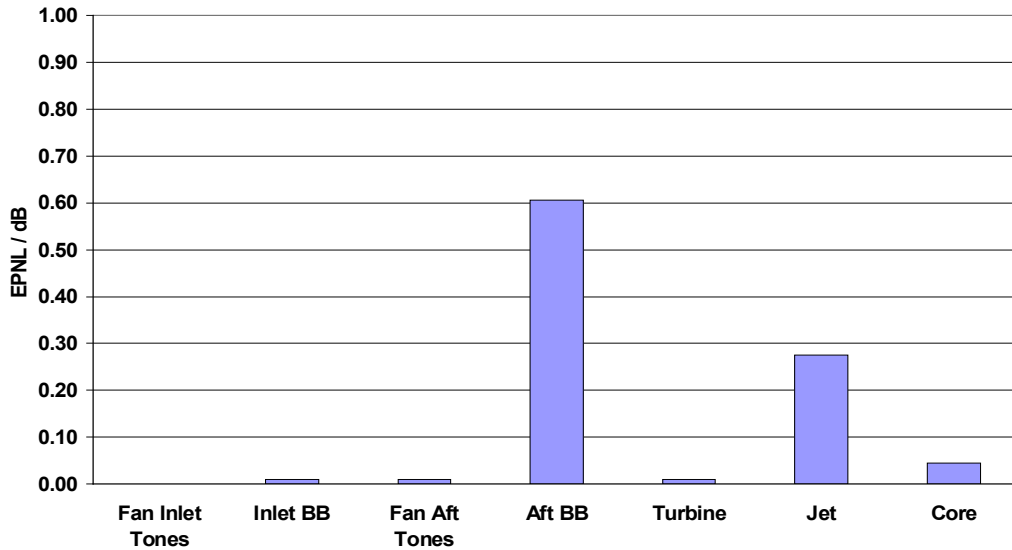## Configuration 2 (16118GR017) SIDELINE Sensitivity Influence Coef's

(b)

Figure E.10.—(a) Configuration 2, blades/vanes = 24/28, 2700 rpm, and (b) Configuration 2, blades/vanes = 24/28, 2700 rpm.
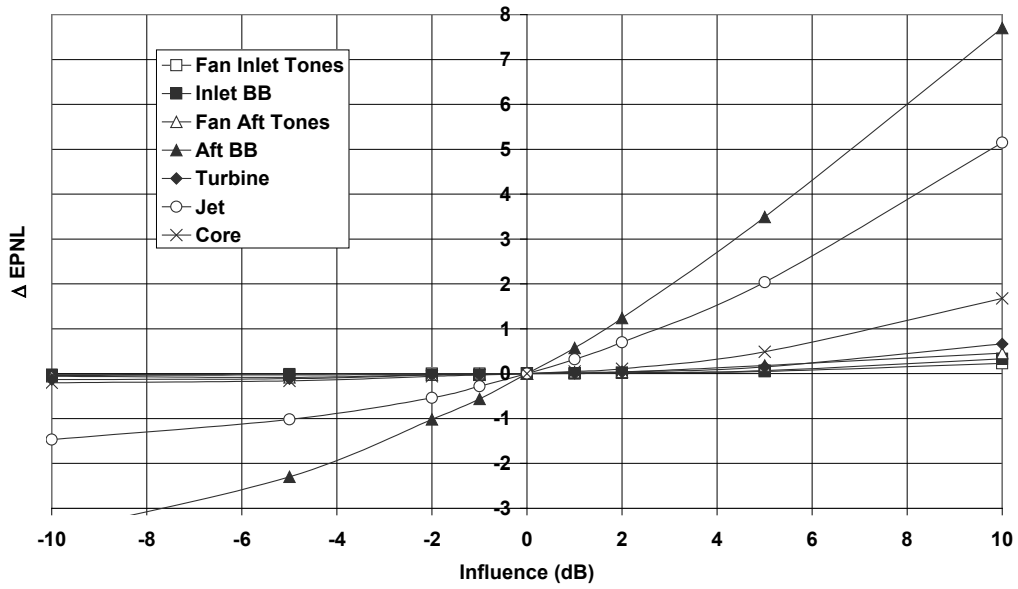
Configuration 7 (16122GR018) SIDELINE Sensitivity

(a)

Configuration 7 (16122GR018) SIDELINE Sensitivity Influence Coef's
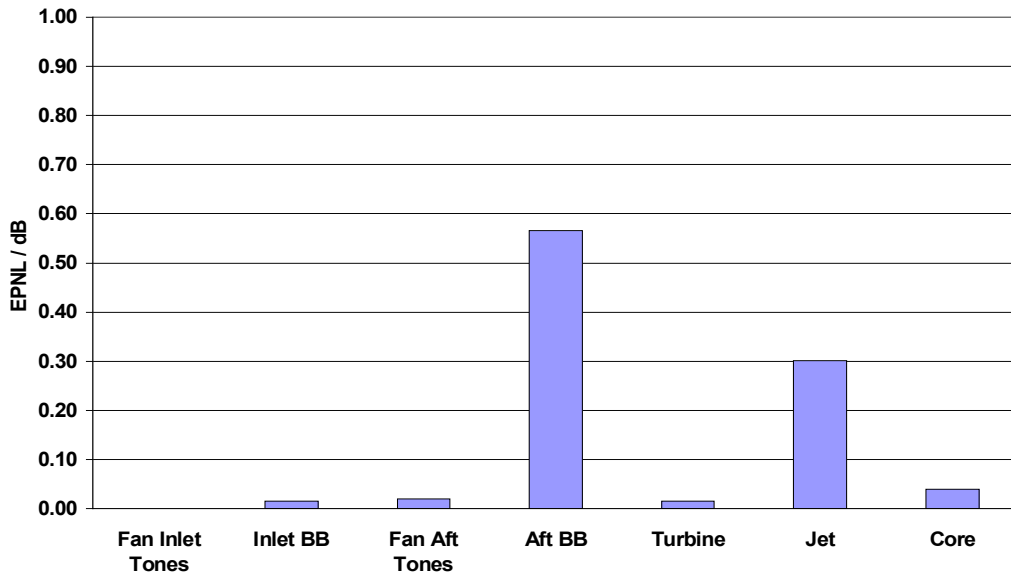

(b)

Figure E.11.—(a) Configuration 7, blades/vanes = 24/60, 2700 rpm, and (b) Configuration 7, blades/vanes = 24/60, 2700 rpm.

Configuration 8 (16123GR017) SIDELINE Sensitivity

(a)

Configuration 8 (16123GR017) SIDELINE Sensitivity Influence Coef's

(b)

Figure E.12.—(a) Configuration 8, blades/vanes = 24/60, 2700 rpm, and Configuration 8, blades/vanes = 24/60, 2700 rpm.

References

1. Mathews, D.C., Bock, L.A., Bielak, G.W., Dougherty, R.P., Premo, J.W., Scharpf, D.F., Yu, J., "Pratt & Whitney/Boeing Engine Validation of Noise Reduction Concepts", Final Report for NASA Contract NAS3-97144, Phase 1, NASA/CR—2014-218088.
2. Premo, J.W., "Fan Source Diagnostic Test—Wall Measured Circumferential Array Mode Results" AIAA-2002-2429, 8th AIAA/CEAS Aeroacoustics Conference, June 2002.
3. Ganz, Joppa, Patten, & Scharpf, "Boeing 18-Inch Fan Rig Test," NASA/CR—1998-208704, 1998.
4. Lan, J.H., "Turbofan Duct Propagation Model", NASA CR-2001-211245, 2001.
5. Envia, E. and Nallasamy, M., "Design Selection and Analysis of a Swept and Leaned Stator Concept," *Journal of Sound and Vibration*, Volume 228, Number 4, 1999, p.p. 793 – 836.
6. Topol, D. A., Tone Fan Noise Design/Prediction System, Volume I: System Description, CUP3D Technical Documentation and Manual for Code Developers," NASA/CR—1999-208882, March 1999.
7. Topol, D. A. and Eversman, W., Tone Fan Noise Design/Prediction System, Volume II: User Manual, TFaNS Vers. 1.4," NASA-CR-1999-208883, March 1999.
8. Topol, D. A., Tone Fan Noise Design/Prediction System, Volume III: Evaluation of System Codes," NASA/CR—1999-208884, March 1999.
9. Meyer, H. D., Source Methodology for Turbofan Noise Prediction (SOURCE3D Technical Documentation)," NASA-CR-1999-208877, March 1999.
10. Glegg, S. A. L., "Broadband Noise from Ducted Prop Fans," AIAA 93-4402, October 1993.
11. Glegg, S. A. L., "Airfoil Self Noise Generated in a Cascade," AIAA 96-1739, May 1996.
12. Glegg, S. A. L. and Jochault, C., "Broadband Self Noise from a Ducted Fan," May 1997.
13. Hobbs, D. E., et al., "Low Noise Research Fan Stage Design," NASA CR-195382, March 1995.
14. Neubert, R., Bock, L., Malmborg, E., Owen-Peer, W., "Advanced Low-Noise Research Fan Stage Design," Prepared under NASA Contract NAS3-26618, December 1996.
15. Woodward, R. P., Elliott, D. M., Hughes, C. E. and Berton, J. J., "Benefits of Swept and Leaned Stators for Fan Noise Reduction," AIAA-99-0497, January 1999.
16. Woodward, R. P., et al., "Fan Noise Source Diagnostic Test – Far Field Acoustic Results," AIAA 2002-2427, June 2002.

1. REPORT DATE (DD-MM-YYYY) 01-02-2014	2. REPORT TYPE Final Contractor Report	3. DATES COVERED (From - To)	
4. TITLE AND SUBTITLE Pratt & Whitney/Boeing Engine Validation of Noise Reduction Concepts Final Report for NASA Contract NAS3-97144, Phase 2		5a. CONTRACT NUMBER NAS3-97144	
		5b. GRANT NUMBER	
		5c. PROGRAM ELEMENT NUMBER	
6. AUTHOR(S) Bock, Larry, A.; Hauser, Joseph, E.; Mathews, Douglas, C.; Topol, David, A.; Bielak, Gerald, W.; Lan, Justin, H.; Premo, John, W.		5d. PROJECT NUMBER	
		5e. TASK NUMBER	
		5f. WORK UNIT NUMBER WBS 473452.02.03.07.06.01.02	
7. PERFORMING ORGANIZATION NAME(S) AND ADDRESS(ES) United Technologies Corporation, Pratt & Whitney 400 Main Street East Hartford, Connecticut 06108		8. PERFORMING ORGANIZATION REPORT NUMBER E-18794	
9. SPONSORING/MONITORING AGENCY NAME(S) AND ADDRESS(ES) National Aeronautics and Space Administration Washington, DC 20546-0001		10. SPONSORING/MONITOR'S ACRONYM(S) NASA	
		11. SPONSORING/MONITORING REPORT NUMBER NASA/CR-2014-218089	
12. DISTRIBUTION/AVAILABILITY STATEMENT Unclassified-Unlimited Subject Categories: 02 and 71 Available electronically at http://www.sti.nasa.gov This publication is available from the NASA Center for AeroSpace Information, 443-757-5802			
13. SUPPLEMENTARY NOTES			

14. ABSTRACT

This report presents results of the work completed in Phase 2 of the Engine Validation of Noise Reduction Concepts (EVNRC) contract. The purpose of the program is to validate, through engine testing, advanced noise reduction concepts aimed at reducing engine noise up to 6 EPNdB and improving nacelle suppression by 50 percent relative to 1992 technology. Phase 1 of the program is completed and is summarized in NASA/CR-2014-218088.

15. SUBJECT TERMS

Fans; Noise; Inlet aerodynamics

16. SECURITY CLASSIFICATION OF:			17. LIMITATION OF ABSTRACT	18. NUMBER OF PAGES	19a. NAME OF RESPONSIBLE PERSON STI Help Desk (email:help@sti.nasa.gov)
a. REPORT U	b. ABSTRACT U	c. THIS PAGE U	UU	252	19b. TELEPHONE NUMBER (include area code) 443-757-5802